Synthesis and Chemistry of Kinamycins and Related Antibiotics

by

Nan Chen

A thesis
presented to the University of Waterloo
in fulfillment of the
thesis requirement for the degree of
Doctor of Philosophy
in
Chemistry

Waterloo, Ontario, Canada, 2010

AUTHOR'S DECLARATION

I hereby declare that I am the sole author of this thesis. This is a true copy of the thesis, including any required final revisions, as accepted by my examiners.

I understand that my thesis may be made electronically available to the public.

Nan Chen

Abstract

The kinamycin antitumor antibiotics, discovered in Japan in the early 1970s as secondary metabolites of the soil bacterium *Streptomyces murayamaensis*, were at first believed to be derivatives of the *N*-cyanobenzo[*b*]carbazole ring system. In 1994, studies in this laboratory revealed that the initial structural assignment was incorrect. The true structures of the kinamycins are based on a novel diazobenzo[*b*]fluorene ring system, a fused 6-6-5-6 carbon skeleton bearing an unusually stable diazo moiety along with a *para*-quinone and other functionalities. Additionally, this group revised the structure of isoprekinamycin (IPK), a metabolite from *Streptomyces murayamaensis* previously considered to be a fully aromatized diazobenzo[*b*]fluorene. IPK was shown to be an isomeric diazobenzo[*a*]fluorene possessing a fused 6-5-6-6 carbon skeleton and incorporating an *ortho*-quinonediazide moiety. These observations stimulated much research elsewhere in regard to the synthesis and biological activity of these structurally novel natural products. Among the notable discoveries in other groups was the isolation and characterization of the lomaiviticins, metabolites of the marine bacterium *Micromonospora lomaivitiensis* that are dimeric diazobenzo[*b*]fluorene analogues, which are even more potent than the kinamycins as anticancer and antibacterial agents.

The present project was designed to develop new synthetic methods to improve access to the diazobenzo[*b*]fluorenes, with a focus on (1*R*,2*R*,3*R*,4*S*)-11-diazo-1,2,3,4,9-pentahydroxy-2-methyl-3,4-dihydro-1*H*-benzo[*b*]fluorene-5,10-(2*H*,11*H*)-dione, also called kinamycin F. The present project was also designed to carry out experimental and theoretical studies to gain insights into the structures and chemical properties of kinamycins, to better understand their biological properties and to identify how such properties might be optimized through specific structural alterations.

A synthetic study was carried out on 2-methyl-1,4-naphthoquinone as a model for a possible biomimetic generation of the highly oxygenated D-ring of the kinamycins as found in kinamycin F.

Epoxidation of the model quinone, followed by stereoselective reduction of both keto-carbonyl groups and ring opening of the epoxide with acetate as the nucleophile in a novel process involving tetramethylammonium triacetoxyborohydride provided (1*R**,2*R**,3*R**,4*S**)-2-methyl-1,2,3,4-tetrahydronaphthalene-1,2,3,4-tetraol in good yield. Comparison of the proton NMR characteristics of the model tetrol with those of the D-ring of kinamycins led to the conclusion that kinamycin F, unlike other kinamycins with some of their D-ring oxygen(s) bearing acyl groups, prefers a D-ring conformation in which the hydroxyl group that is nearest the diazo group is in a pseudo-equatorial orientation such that the C-O bond is approximately parallel with the diazo group. Ab initio molecular orbital calculations at the RHF 6-31G level led to the conclusion, supported by experimental measurements of diazo IR stretching frequencies, that the diazo group of kinamycin F has an enhanced diazonium ion character in this favoured conformation. This observation is of potential significance since the electrophilicity of the diazo group may play a role in the mode-of-action of the kinamycins, and since there is evidence to suggest that the other kinamycins may undergo conversion into kinamycin F in vivo before exerting their biological effect.

A strategy for applying the results of the model study to the total synthesis of kinamycin F is disclosed. In addition, the construction of 6-hydroxy-8-methoxy-3-methyl-7,12-dioxo-7,12-dihydrotetraphen-4-yl methanesulfonate from readily available starting materials is described and suggestions as to how this compound might serve as a key intermediate in the biomimetic synthesis of kinamycin F are provided. A critical analysis of this synthetic strategy to the kinamycins in contrast with several other approaches that have been reported by other groups during the course of this thesis research is presented. Additionally it is pointed out that this synthetic method could provide (1S,2R,3R,4R)-5-diazo-1,2,3,4,8-pentahydroxy-3-methyl-1,2,3,4-tetrahydrotetraphene-6,7,12(5H)-trione as a key intermediate, which might well represent a novel analogue of the kinamycins with potentially intrinsic anticancer and antibacterial activity of its own, since this compound possesses a

6-6-6-6 carbon skeleton containing an *ortho*-quinonediazide that could serve as an unique hybrid between the 6-6-5-6 diazobenzo[*b*]fluorene and the 6-5-6-6 diazobenzo[*a*]fluorene systems.

A semi-synthetic method for generating kinamycin F from other natural kinamycins by applying a modified Zemplen deacylation condition is reported. Electrospray mass spectrometry was employed to identify products from interaction of kinamycin F with glutathione on a very small scale. Kinamycin F was found to form a covalent adduct with this thiol that is ubiquitous in mammalian cells. A discussion of the potential biological significance of this process as well as possible interactions with other biologically important thiols in specific potential target proteins is provided.

A systematic ab initio molecular orbital analysis at the RHF 6-31 G level of the influence of substituents in the aromatic D-ring of isoprekinamycin was also carried out. The results have led to the suggestion of specific structural alterations that might be employed to fine tune the electrophilicity of the diazo group, which might affect the biological activity of such compounds.

Despite the very high potency of the lomaiviticins as anticancer and antibacterial agents, progress towards badly needed practical drugs in these areas has been frustrated by a lack of access to adequate quantities of these complex secondary metabolites either through in vitro fermentation or total synthesis at the moment. In the hope that a prediction of the three dimensional properties of the lomaiviticins might inspire the design and synthesis of simpler analogues with comparable biological activities, a systematic ab initio molecular orbital study at the RHF 6-31G level was undertaken. In the end, predictions of the most likely conformations of lomaiviticins A and B were achieved and are provided as potential starting points for medicinal chemists to design simpler but equally potent and much more accessible analogues.

Acknowledgements

Like always and the way it should be, the first, the biggest and the most sincerely “Thank you” should be devoted to my supervisor Dr. Gary I. Dmitrienko for numerous reasons, which I could only briefly mention so that this would not turn into a lengthy acknowledgement. When I look back at my fairly long stay at Waterloo, there are so many valuable memories and experience that always have Gary somewhere in the picture. Gary was the instructor of my very first graduate course at Waterloo, and he also served as my research committee member when I was a Master candidate (under the supervision of Dr. Monica Barra). My observation and communication with Gary convinced me that he would be the supervisor of my choice if I would like to continue my graduate (Ph.D.) studies at Waterloo in synthetic organic chemistry, which I did. I could not thank Gary enough for everything that he has done for me, from the great kinamycin project, the important financial support and his irreplaceable guidance to handle the research challenges, to his patient tolerance of my mistakes and failures over the years. I could only wish that I had worked harder and better to deserve his kindness and the opportunity of being his graduate student. Gary shall also be thanked for his extreme help to go through many versions of the very long drafts, which makes the thesis as readable as it is now.

Past and present members of the Dmitrienko group, Dr. Radoslaw Laufer, Mr. Justin Yiji Wu, Mr. Matthew Brown, Mr. Matthew Buck, Dr. Muhong Shang, Mr. Darryl Evanoff, Dr. Jeff Kent, Dr. Anthony Krismanich, Dr. Ahmad Ghavami, Dr. Wei Liu, Mr. Glenn Abbott, Mr. Jarrod Johnson, Mrs. Valerie Goodfellow, Mrs. Miriam Heynen, Dr. O. Adidayo and Dr. Laura Marrone, shall be thanked for their various help on the project and wonderful team work all the time. I am really lucky to meet and work with so many great colleagues that I could ask for no more. Undergraduate students who have participated in the kinamycin project, Herlina Lim, Raymond Chu and Janet Simons, shall also be acknowledged for their individual contributions.

All the committee members, Dr. Monica Barra, Dr. Mike Chong, Dr. Don Mackay and Dr. William Tam (University of Guelph), shall be thanked for their great help with not only the research projects (and thesis) along the way, but also their great guidance in many of the courses that I took with them. Many other professors of the Chemistry Department, particularly Dr. Thammaiah Viswanatha (who unfortunately passed away a while ago), Dr. Russell Rodrigo and Dr. Steve Forsey shall be thanked for their frequent and helpful discussions on many little issues of research.

The supporting staff of the Chemistry Department, from everyone in the ChemStore to the secretaries in the department office, has made my study at UW a very enjoyable process because of their excellent services. Ms. Jan Venne and Dr. Mike Ditty shall be acknowledged for their tremendous technical support on NMR experiments. I am also in debt to Dr. Nicholas Taylor (who sadly passed away more than a year ago) and Dr. Jalil Assoud for their superior service with X-ray. Dr. Richard Smith shall be greatly thanked for his work on not only the routine acquisition of mass spectra but also his particular help with the ESI-MS instrument, which built a significant part of this thesis. Collaboration on the kinamycin projects with Dr. Thorsten Dieckmann on NMR studies of kinamycin-DNA interaction and Dr. Brian Hasinoff (University of Manitoba) on biological studies of kinamycin F and isoprekinamycin shall also be greatly acknowledged.

Aside from scientific research, my personal experience at Waterloo has been indeed very wonderful because of the precious friendship and time together that many friends shared with me, for which I am so grateful. Last but not least, I would like to thank my parents for their greatest love and support ever since I was born.

Dedication

Dedicated to my dearest parents for their endless love and support.

Table of Contents

List of Figures

List of Schemes

List of Tables

List of Abbreviations

Δ	heating
μW	microwave
↑↓	reflux
[H]	reducing agent
[O]	oxidizing agent
A	absorbance
Ac	acetyl
AIBN	2,2-azobisisobutyronitrile
aq.	aqueous
Ar	aryl
ATCC	American Type Culture Collection (Manassas, VA, USA; www.atcc.org)
atm	atmosphere
ATP	adenosine triphosphate
a.u.	atomic unit (Hartree), 1 a.u. = 627.5095 kcal/mol
ax.	axial
Bn	benzyl
BIA	biochemical induction assay
BINAP	2,2′-bis(diphenylphosphino)-1,1′-binaphthyl
Boc	*tert*-butoxycarbonyl
br	broad
BSA	bovine serum albumin
t-Bu	*tert*-butyl
calc.	calculated

CAN	ceric ammonium nitrate
cat.	catalytic amount
CCDC	Cambridge Crystallographic Data Centre (Cambridge, UK)
CCRC	Culture Collection and Research Center (Hsinchu, Taiwan, R.O.C)
CDK	cyclin-dependent kinase
CHO	Chinese hamster ovary (cell)
CI	chemical ionization (mass spectrometry)
conc.	concentrated
m-CPBA	*m*-chloroperbenzoic acid
CSD	Cambridge Structural Database
Cy	cyclohexyl
CW	continuous wave
d	doublet
d	distance
dba	dibenzylideneacetone
DBU	1,8-diazabicyclo[5.4.0]undec-7-ene
DCE	dichloroethane
dd	doublet of doublets
D-DIPT	D(-)-diisopropyl tartrate
DDQ	2,3-dichloro-5,6-dicyano-1,4-benzoquinone
decomp.	decomposition
DIBAL	diisobutylaluminum hydride
DIPEA	diisopropylethylamine (Hünig's base)
DMA	*N*,*N*-dimethylacetamide

DMAP	4-*N*,*N*-dimethylaminopyridine
DMDO	dimethyldioxirane
DME	1,2-dimethoxyethane
DMF	*N*,*N*-dimethylformamide
DMSO	dimethylsulfoxide
DNA	deoxyribonucleic acid
DON	6-diazo-5-oxo-*L*-norleucine
dr	diastereomeric ratio
dTDP	deoxythymidine diphosphate
DTT	dithiothreitol
ee	enantiomeric excess
E_h	redox potential
EI	electron impact (mass spectrometry)
eq	equivalent
eq.	equatorial
ERO	epoxide ring opening
+/-ESI	(positive/negative) electrospray ionization
ESR	electron spin resonance
EPR	electron paramagnetic resonance
Et	ethyl
expt.	experimental
FT	Fourier transform
FVP	flash vacuum pyrolysis
g	gram

GGT	γ-glutamyl transpeptidase
GI_{50}	growth inhibitory activity
GSH	L-glutathione
GSSG	glutathione disulfide (oxidized form of GSH)
hr	hour
HOMO	highest occupied molecular orbital
HMBC	heteronuclear multiple bond correlation
HMDS	1,1,1,3,3,3-hexamethyldisilazane
HMPA	hexamethyl phosphoramide
HMQC	heteronuclear correlation through multiple quantum coherence
HPLC	high-performance liquid chromatography
HRMS	high resolution mass spectrum
HSAB	hard and soft acids and bases
Hz	Hertz
IC_{50}	half maximal (50%) inhibitory concentration
Im	imidazole
INA	incipient nucleophilic attack
IR	infra-red
ISP	International Streptomyces Project
J-MOD	J-modulated
KAT	kinamycin acetyltransferase
L	liter
LC	liquid chromatography
LD_{50}	half maximal (50%) lethal dose

LDA	lithium diisopropylamide
LRMS	low resolution mass spectrum
m	multiplet
Me	methyl
mg	milligram
MIC	minimum inhibitory concentration
min	minute
mL	milliliter
mp	melting point
MMA	methyl methacrylate
mmol	millimole
MO	molecular orbital
MOM	methoxymethyl
Ms	methanesulfonyl, mesyl
MS	mass spectrum
MW	molecular weight
MSA	methanesulfonic acid
$NADP^+$	nicotinamide adenine dinucleotide phosphate
NADPH	reduced form of nicotinamide adenine dinucleotide phosphate
NaHMDS	sodium bis(trimethylsilyl)amide
NBO	natural bond orbital
NBS	*N*-bromosuccinimide
ng	nanogram
NIS	*N*-iodosuccinimide

nM	nanomolar
NMR	nuclear magnetic resonance
NMO	*N*-methylmorpholine *N*-oxide
nOe	nuclear Overhauser effect
ORTEP	Oak Ridge (National Lab) Thermal Ellipsoid Program (Molecular Modeling)
PCC	pyridinium chlorochromate
PCM	Polarizable Continuum Model
PDB	protein data bank, http://www.rcsb.org/pdb/
PDC	pyridinium dichromate
Ph	phenyl
PKB	protein kinase B
PKS	polyketide synthase
PNB	*para*-nitrobenzyl
PNQ	pyrano-naphthoquinone
PPA	polyphosphoric acid
PTC	phase transfer catalyst
PTSA	*p*-toluenesulfonic acid
i-Pr	*iso*-propyl
Py	pyridine
R	conventional *R*-factor (X-ray)
R_w	Hamilton weighted *R*-factor (X-ray)
RHF	restricted Hartree-Fock
RNA	ribonucleic acid
rpm	revolutions per minute

rt	room temperature
s	singlet
sept	septet
STP	standard temperature and pressure
t	triplet
TBAF	tetra-*n*-butylammonium fluoride
TBDMS	*tert*-butyldimethylsilyl
TBS	*tert*-butyldimethylsilyl
TEBAC	triethylbenzyl ammonium chloride
Tf	trifluoromethanesulfonyl
TFA	trifluoroacetic acid
TFAA	trifluoroacetic anhydride
THF	tetrahydrofuran
TIPS	triisopropylsilyl
TLC	thin layer chromatography
TMS	tetramethylsilane (NMR) or trimethylsilyl (protecting group in synthesis)
TMSE	2-(trimethylsilyl)ethyl
Ts	*p*-toluenesulfonyl, tosyl
UDP	uridine 5'-diphosphate
UV-vis	ultraviolet-visible
VCD	vibrational circular dichroism
vdW	van der Waals
VOA	vibrational optical activity
ZPVE	zero point vibrational energy

Chapter 1

Introduction

1.1 Natural Products, Secondary Metabolites, Antibiotics and *Streptomyces*

By unrestricted definition in the widest sense, the term "natural products" refers to any organic substances that are obtained from natural living species such as microorganisms, plants and animals. In principle, natural products can be either the entire or partial organism (e.g., a bacterium/fungus or its extraction, a whole plant or its leaf/root/flower/seed, and an entire animal or its organs), as well as pure organic compounds isolated from such natural sources that are commonly known as metabolites.[1] However, modern chemistry has limited the term "natural products" to be used almost exclusively for the last case, referring to a large number of structurally varied small organic molecules produced by the living organisms, typically having a molecular weight (MW) less than 1500.[1] Most organic molecules in the natural product category are known as secondary metabolites, which are typically categorized based on their structural characteristics and/or biosynthetic origins. Secondary metabolites mainly include alkaloids, terpenoids, steroids, carbohydrates, glycosides, polyketides, phenolics, fatty acids, and some biopolymers such as non-life-essential DNA (deoxyribonucleic acid), RNA (ribonucleic acid), peptides and proteins.

On the other hand, certain naturally-occurring carbohydrates, amino acids, proteins and nucleic acids are common key intermediates and crucial products of metabolism for all living organisms, which are essential for life and therefore are classified as primary metabolites. Secondary metabolites are not directly involved in the normal growth or reproduction of the source organisms, unlike the primary ones, and the absence of secondary metabolites would not lead to immediate death of the organism. Such a situation, however, may still impair the organism's long-term survivability and

reproductivity, since, as a result of biological evolution of the organisms to accommodate the environment, secondary metabolites frequently act as either toxins against various biological threats (e.g., predators/parasites, diseases and interspecies competition), or promoters to facilitate the reproduction processes (e.g., colouring the organisms or producing distinct smells and flavours as commonly found within plants that lure insects for pollination).

Interest in natural products (secondary metabolites) mainly comes from the fact that many such compounds have broad and significant biological and pharmacological activities on living organisms, making them useful as medicines. Among thousands of secondary metabolites, chemical substances that are capable of inhibiting the growth of bacteria or other microorganisms are more commonly known as the antibiotics (antibacterial agents). The antibiotics may possess inhibitory activities either in vitro (i.e., in an artificial environment outside the living organism) or in vivo (i.e., within a living organism), and an antibiotic with high inhibitory activity but low toxicity in vivo would be extremely valuable in treating various bacterial infections. The most capable species to produce antibiotics are the various microorganisms including bacteria (particularly the *Actinomycetes*), fungi, algae, and in some cases sponges and soft corals, while plants are the second major source of antibiotics.[2] So far there are more than 16,500 natural antibiotics produced alone by various microorganisms that have been reported in the literature, not including thousands of semi-synthetic derivatives and synthetic analogues of these natural products, with about 90% of such antibiotics characterized and assigned with a molecular structure.[2]

As the most important and largest genus within the *Actinomycetes*, the *Streptomyces* are Gram-positive and aerobic bacteria but they seldom lead to human infections. The *Streptomyces* are typically found in soil that gives them the characteristic earthy odor and they play an essential role in soil ecology. More importantly, they can produce many clinically useful and scientifically important

antibiotics, such as streptomycin, tetracycline, mitomycin and vancomycin, as well as the kinamycins, which are the subject of this thesis.[3]

1.2 Overview of the Natural Kinamycin Antibiotics and Related Compounds

The entire family of the natural kinamycin antibiotics consists of a total of about 20 compounds (**1.1a**–**p**, **1.2a**–**b** and **1.3**–**1.5**, Figure 1-1 and Table 1-1) so far, which are only produced by certain species of *Streptomyces* or *Actinomycetes*. The kinamycins were found to be strongly active against Gram-positive bacteria but much less effective towards the Gram-negative ones, while some members have also demonstrated moderate to significant antitumor activities and other interesting biological activities as well (section 1.4.1). Interest in the kinamycins mainly arises from three aspects: (1) their structural novelty from a synthetic point of view; (2) the intriguing but poorly understood mode-of-action of their biological activities; and (3) the unique biosynthetic pathways.

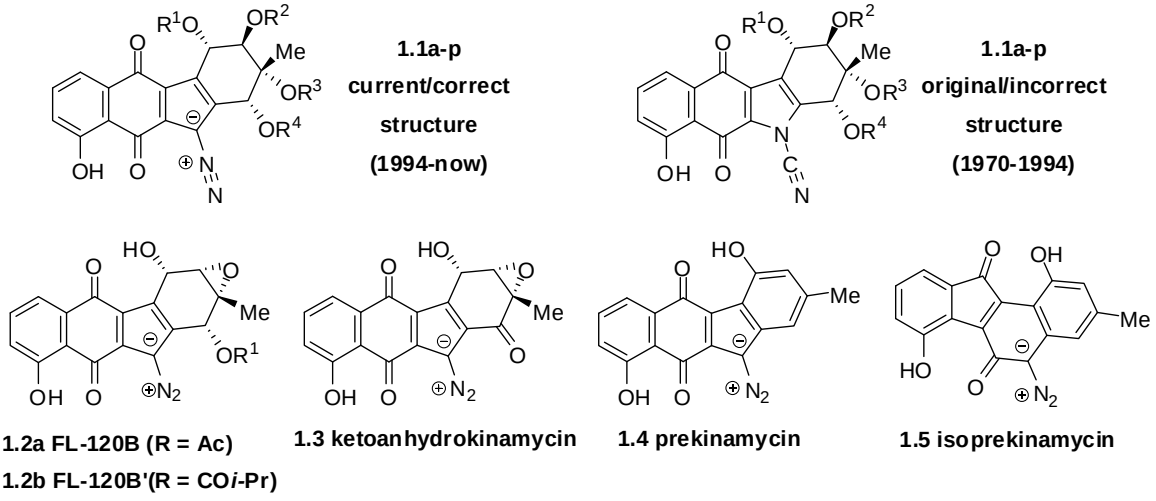

Figure 1-1. Structures of all known natural kinamycins (refer to Table 1-1 on next page for detailed name, variation of substituents and source *Streptomyces* of the kinamycins)

Table 1-1. Name, substituent variation and source *Streptomyces* for all known natural kinamycins.*

Name (year discovered)[Reference]	R^1	R^2	R^3	R^4	*Streptomyces*
kinamycin A **1.1a** (1970)[4]	H	Ac	Ac	Ac	a
kinamycin B **1.1b** (1970)[4]	H	H	Ac	H	a
kinamycin C **1.1c** (1970)[4]	Ac	Ac	H	Ac	a
kinamycin D **1.1d** (1970)[4]	H	Ac	H	Ac	a, b
kinamycin E **1.1e** (1989)[5,6]	H	H	H	Ac	a
kinamycin F **1.1f** (1989)[5,6]	H	H	H	H	a
kinamycin G **1.1g** (1989)[7]	Ac	Ac	CO*i*-Pr	Ac	c, d
kinamycin H **1.1h** (1989)[7]	Ac	Ac	H	CO*i*-Pr	c, d
kinamycin I **1.1i** (1992)[8]	Ac	CO*i*-Pr	H	CO*i*-Pr	d
kinamycin J **1.1j** (1973)**[9]	Ac	Ac	Ac	Ac	semi-synthetic
kinamycin K **1.1k** (1989)***[5,6]	H	Ac	H	H	a
kinamycin L **1.1l** (1992)****[8]	Ac	Ac	CO*i*-Pr	CO*i*-Pr	d
FL-120A **1.1m** (1994)[10,11]	H	Ac	CO*i*-Pr	Ac	b
FL-120C **1.1n** (1994)[10,11]	H	Ac	H	CO*i*-Pr	b
FL-120C' **1.1o** (1994)[10,11]	H	Ac	H	COEt	b
FL-120D' **1.1p** (1994)[10,11]	H	H	H	CO*i*-Pr	b
FL-120B **1.2a** (1994)[10,11]	Ac	-	-	-	b
FL-120B' **1.2b** (1994)[10,11]	CO*i*-Pr	-	-	-	b
ketoanhydrokinamycin **1.3** (1989)[5,6]	-	-	-	-	a
prekinamycin **1.4** (1994)*****[12,13]	-	-	-	-	e
isoprekinamycin **1.5** (1989)*****[5,6,14]	-	-	-	-	a

* Refer to Figure 1-1 for structures of kinamycins and the corresponding substituents; ** Compound **1.1j** was erroneously assigned as a natural kinamycin since 1997[15] until now (see next paragraph for details); *** This natural kinamycin **1.1k**, which will be called "kinamycin K" in this thesis, was never named officially even though it was isolated and characterized in 1989[5,6] (see next paragraph for details); **** It is possible that **1.1l** is another natural kinamycin that has not been officially named yet, which will be momentarily called "kinamycin L" in this thesis (see next paragraph for details); ***** In 1989,[5,6] the name and structure of prekinamycin (**1.4**) was assigned to an isolated purple metabolite from *Streptomyces* that was found to be in fact isoprekinamycin (**1.5**) in 2000,[14] while the real prekinamycin (**1.4**) was isolated in 1994[12] but only correctly characterized in 1996;[13] a. *murayamaensis* sp. nov. HATA *et* OHTANI (ATCC 21414) ; b. *chattanoogensis* subs. *taitungensis* subsp. nov. (strain IY2-13/CCRC 15124) ; c. *saccharothrix* (strain MI293-N4); d. unidentified *Actinomycete* (strain A83016); e. *murayamaensis* mutant MC2.

It should be noted that there are several old but still on-going mistakes in the literature regarding the names of natural kinamycins (footnotes of Table 1-1), which have never been pointed out and corrected until the writing of this thesis. First, Gould officially named compound **1.1j** as "kinamycin J" in his very thorough and detailed review of kinamycins published in 1997,[15] in which he referred to the original work of Smitka and co-workers in 1992[8] as the literature source of this presumed "natural" kinamycin. However, a more careful review of Smitka's original paper[8] indicates that no kinamycin J (**1.1j**) was isolated or identified back then. In fact, the molecule having the shown structure of kinamycin J (**1.1j**) was never found from nature (fermentation of bacteria), but it was first generated upon acylation of natural kinamycin A (**1.1a**) by Ōmura in 1973 (Scheme 1-1),[9] and more recently synthesized by the Nicolaou group in 2007.[16] Therefore, kinamycin J (**1.1j**) should be considered as a (semi-)synthetic derivative of natural kinamycins. Second, Gould isolated and fully characterized a unique natural kinamycin compound **1.1k** in 1989,[5,6] but interestingly, it was not even mentioned in his own 1997 review of kinamycins.[17] No one, including the discoverer, has ever provided the natural **1.1k** with an official kinamycin name, which will be called "kinamycin K" in this thesis. The last problem was caused by the Smitka group who isolated three natural kinamycins in 1992,[8] among which two had been unambiguously identified as kinamycin G (**1.1g**) and kinamycin I (**1.1i**). Smitka claimed[8] the third kinamycin to be the previously discovered kinamycin H (**1.1h**),[7] but the published chemical drawing for this "kinamycin H" was identical to the one shown in Table 1-1 for compound **1.1l**, which matched neither the real structure of kinamycin H (**1.1h**) nor the corresponding name of "3-*O*-isobutyrylkinamycin C" (common name for **1.1h**) used in his own paper.[8] This inconsistency would suggest two possibilities. First, the mistake could be nothing but a simple editorial error with the published chemical structure, although Smitka's paper provided no spectroscopic data of **1.1l** to prove such. Recent (June 2008) personal communications with Dr. Smitka regarding this issue unfortunately did not clarify the confusion either, due to the

inaccessibility of the original spectroscopic data at the moment. Therefore, a second possibility is that **1.1l** might be another natural kinamycin that has not been officially recognized yet, but only if the spectroscopic data of **1.1l** are different from **1.1h** and prove that the original chemical drawing of **1.1l** in Smitka's paper is correct.

There are several distinct structural features of the molecules, among which the most notable one is the existence of a very rare (for natural products) and unusually stable diazo functionality (>C=N^+=N^- ↔ >C^--N^+≡N). This *C*-diazo moiety was previously assigned as an *N*-cyano (>N-C≡N) group based on limited spectroscopic data (including a low quality X-ray of **1.1s**, Scheme 1-1) and misleading chemical evidence at the time of the initial discovery,[9,18,19] when the very first four members of the kinamycin antibiotics, kinamycins A, B, C and D (**1.1a-d**), were isolated from the fermentation broth of *Streptomyces murayamaensis* by Ōmura and Hata in 1970[4,20] and subsequently characterized in 1971.[18] This error in the kinamycin structure was finally discovered 23 years later, owing to the higher quality of X-ray evidence from the (+)-α-methylbutyrate of natural kinamycin D (**1.1v** in Scheme 1-1) from the Gould lab[21] and the simultaneous synthetic and spectroscopic work from the Dmitrienko lab.[22] The long-believed *N*-cyano structure for kinamycins was then revised to the current *C*-diazo assignment (see section 1.3.2 for details). In addition, prekinamycin (**1.4**) and isoprekinamycin (**1.5**) are indeed structural isomers with a difference in arrangement of their carbocyclic skeletons, which were not distinguished until 2000 when another structural revision of kinamycins (section 1.3.2) was suggested by the joint investigation of the Dmitrienko lab and the Proteau lab.[14]

Structures of some simple semi-synthetic derivatives of natural kinamycins, which were made in the process of their structure determination during the early stage of research in the area (section 1.3),[5,9,18,21] are shown in Scheme 1-1. These semi-synthetic compounds were typically named as derivatives of the corresponding mother kinamycin. It is interesting to note, in retrospect, that the

diazo group in these natural products survives the rather harsh (e.g., strong acidic) conditions engaged in some of the derivatizations, since most diazo compounds are unstable under such conditions. Later, some of these semi-synthetic derivatives were found to be natural kinamycins as well. For example, deacetylkinamycin C (**1.1f** in Scheme 1-1), derived in 1973 from kinamycin C (**1.1c**) upon basic hydrolysis,[9] is identical to natural kinamycin F (**1.1f** in Figure 1-1) that was isolated as a bacterial metabolite in 1989.[5] In addition, a few more synthetic derivatives of kinamycins were prepared in recent years when several total syntheses of the kinamycins were achieved (section 3.2).[16,23-26]

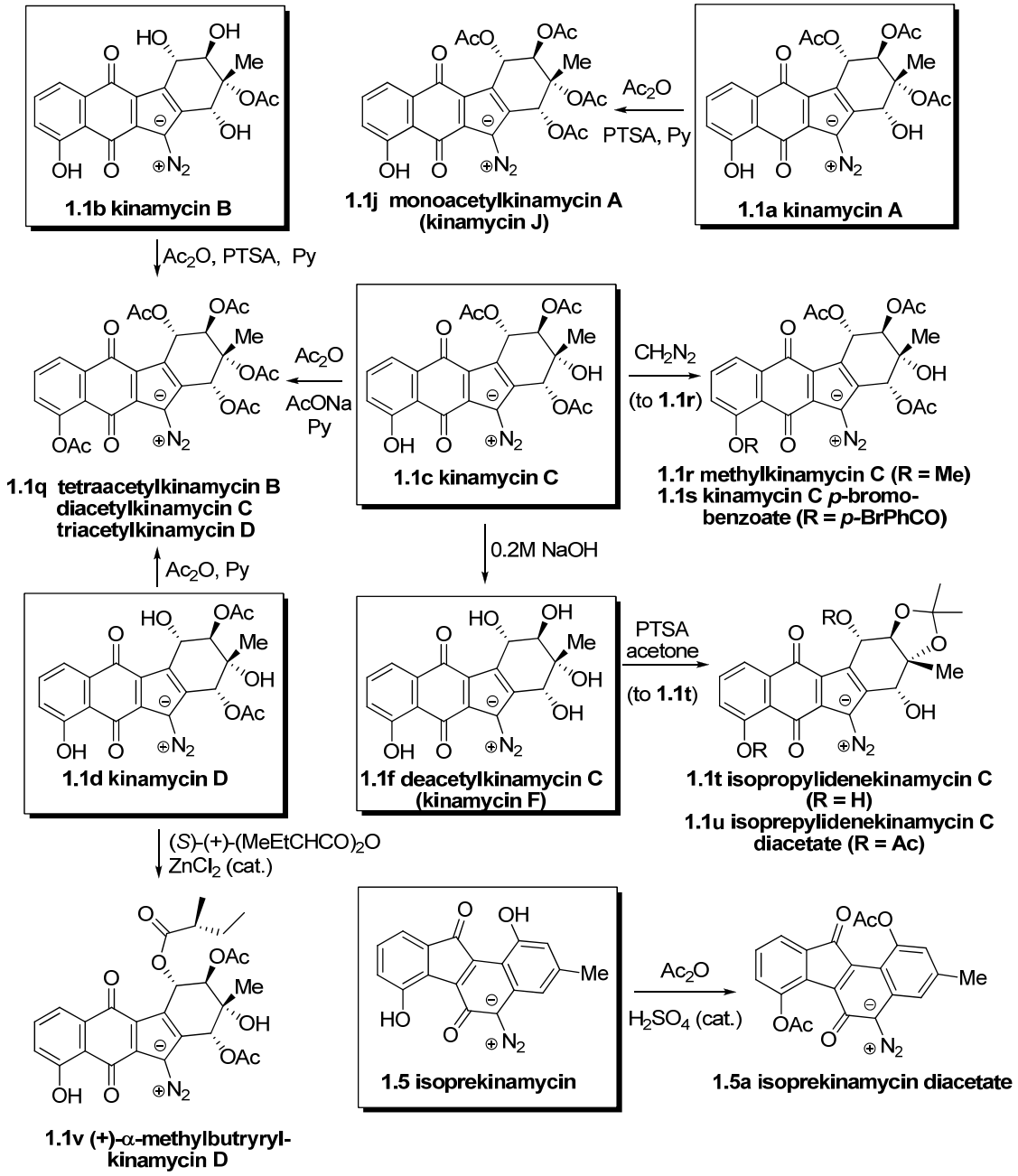

Scheme 1-1. Conversion of natural kinamycins (boxed) to some semi-synthetic derivatives.

Naturally-occurring diazo compounds are rare, and besides the kinamycins, there are only a handful of other examples reported in the literature. As summarized in Figure 1-2, other known

natural diazo compounds include several modified α-amino acids (e.g., 6-diazo-5-oxo-*L*-norleucine (DON, **1.6a**),[27,28] azaserine (**1.6b**),[29-35] alazopeptin (**1.6c**)[36] and its natural derivative OS-3256-B (no given structure)[37], duazomycin A (*N*-acetyl DON, **1.6d**) and B (**1.6e**),[38] *N*-(*L*-alanyl)azaserine (LL-D05139β, **1.6f**),[39] *O*-[(3*R*)-2-diazo-3-hydroxybutyryl]-*L*-serine (thrazarine/FR900840, **1.6g**)[40-44], cremeomycin (**1.7**),[45,46] SQ30957 (**1.8**),[47] lagunamycin (**1.9**),[48,49] SF2415A1, A2, and A3 (**1.10a**–**c**)[50,51] and lomaiviticin A (**1.11a**) and B (**1.11b**).[52] All these naturally-occurring diazo compounds were produced by certain strains of *Streptomyces* or *Actinomycetes* except **1.8**, which was isolated from a fungus, and in most cases they possess activity against various bacteria and tumor cells. The last two natural diazo compounds mentioned above are particularly noteworthy. Lomaiviticin A (**1.11a**) and B (**1.11b**) were isolated by He and collaborators from the fermentation broth of *Micromonospora lomaivitiensis* (*Actinomycete* strain *LL*-37I366).[52] In this case the bacterium was hosted by *Polysyncraton lithostrotum*, a Fijian marine ascidian that is more commonly known as a sea squirt, and these natural products were identified in an investigation that originally targeted the marine invertebrates as a possible source of enediyne-type anticancer agents.[52] Lomaiviticin A (**1.11a**) is a dimeric glycoside analogue of the kinamycins while lomaiviticin B (**1.11b**) is the bis-hemiketal formally derived from lomaiviticin A (**1.11a**). Both lomaiviticin A (**1.11a**) and B (**1.11b**) possess extremely potent activities with an ultra low level of IC_{50} of about 0.01–98 ng/mL against a very broad range of cancer cells and bacteria.[52]

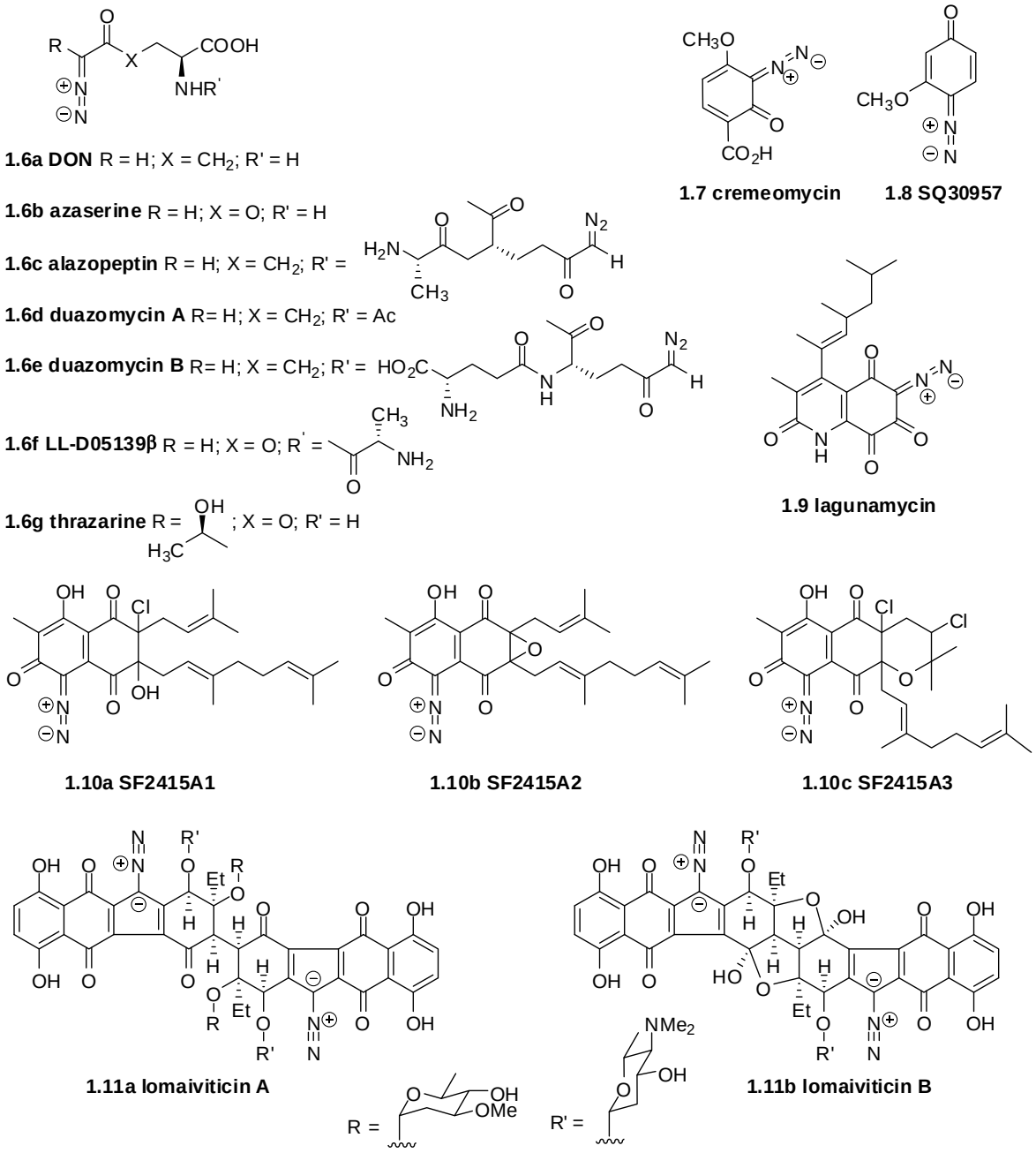

Figure 1-2. Other naturally-occurring diazo compounds besides kinamycins.

The second distinct structural feature of the kinamycins comes from their unusual skeletons (Figure 1-3). All kinamycins possess a carbocyclic skeleton containing three 6-membered rings and

one 5-membered ring, among which a typical fluorene core **1.12** with a fused 6-5-6 ring arrangement is common to all kinamycins. Depending on the relative orientation of the remaining 6-membered ring, the kinamycin skeleton can be defined as either a benzo[*a*]fluorene core **1.13a** or a benzo[*b*]fluorene core **1.13b**. The other possible isomeric benzo[*c*]fluorene core **1.13c** has never been found within the natural kinamycins. The four rings of the kinamycins are denoted as ring A, B, C and D consecutively, with the A-ring bearing a single –OH group in all natural kinamycins. The numbering system of the kinamycins, as suggested by Gould[14,21] and shown in Figure 1-3, follows the one employed for benzo[*a*]anthraquinone biosynthetic precursors[53] and that of *Chemical Abstracts*. All natural kinamycins except isoprekinamycin (**1.5**) possess the benzo[*b*]fluorene skeleton but with various substituents and different degrees of oxidation of their D-rings. Most kinamycins (**1.1a**–**p**, 15 out of 20) contain a saturated D-ring bearing four acyloxy and/or hydroxy substituents and three other kinamycins (**1.2a**, **1.2b** and **1.3**) have an epoxide within the saturated D-ring. In the case of prekinamycin (**1.4**), a fully aromatized D-ring is present. On the other hand, isoprekinamycin (**1.5**), a structural isomer of prekinamycin (**1.4**), is the only member of the kinamycin family that possesses the benzo[*a*]fluorene skeleton. Both the benzo[*b*]- and benzo[*a*]fluorene cores are very rare structures that occur within natural products, and only a few other examples are reported in the literature for each case (Figure 1-3), which includes momofulvenone A (**1.14a**) and B (**1.14b**)[54], stealthin A (**1.15a**), B (**1.15b**)[55] and C (**1.15c**)[17], kinobscurinone (**1.16a**)[56] and kinafluorenone (**1.16b**)[57,58], seongomycin (**1.17**),[59] cysfluoretin (**1.18**),[60] shikometabolin A (**1.19a**) and B (**1.19b**),[61,62] fluostatin A (**1.20a**), B (**1.20b**),[63] C (**1.14c**), D (**1.14d**) and E (**1.14e**).[64,65] Not only are all of these natural products closely related to the kinamycins in structure, but also they (except **1.19a**–**b**) are produced exclusively by certain species of *Streptomyces*. Among them, **1.15c** and **1.16a** were found to be key intermediates in the biosynthesis of kinamycins.

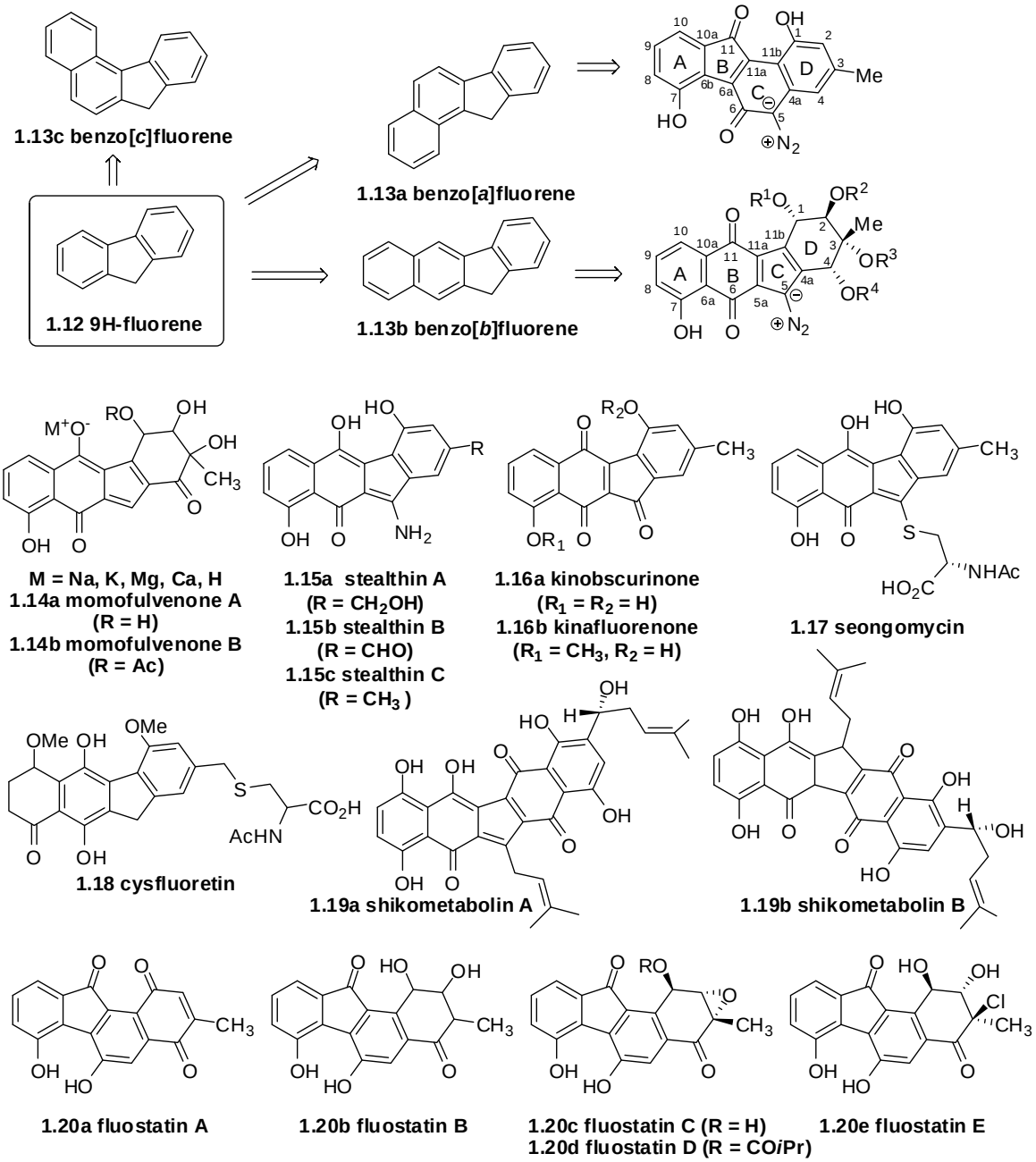

Figure 1-3. Natural products (besides kinamycins) possessing benzo[*b*]- and benzo[*a*]fluorene skeletons.*

* **1.16a**/**b** are shown in their oxidized quinone forms, but spectroscopic evidence suggested that they may actually co-exist in the corresponding hydroquinone or semiquinone radical forms as well. (57) Cone, M. C.; Melville, C. R.; Gore, M. P.; Gould, S. J. *J. Org. Chem.* **1993**, *58*, 1058-1061. (66) Gould, S. J.; Melville, C. R. *Tetrahedron Lett.* **1997**, *38*, 1473.

The significant bioactivity of the kinamycins, along with their unique structures, has made these antibiotics the focus of multi-disciplinary research. Since the initial discovery of kinamycins in 1970, many laboratories worldwide, including this research (Dmitrienko) group, have devoted much effort to various aspects of kinamycins over the past few decades, from isolation, structure characterization, and mechanism-of-action studies, to total synthesis.

1.3 Isolation, Characterization and Biosynthesis of the Kinamycins

In 1970, Ōmura, Hata, Ohtani and co-workers obtained a strain of *Streptomyces* from a soil sample collected in Murayama (Saitama-ken, Japan),[4] a small town situated in the north of Tokyo Metropolis' central area that became the city of Musashimurayama in the same year. Therefore, the bacteria strain was named as *Streptomyces murayamaensis* sp. nov. HATA *et* OHTANI, which was found to be capable of producing some orange crystalline antibiotics that were later identified and named as kinamycin A, B, C and D (**1.1a**–**d**).[4] Not long after its discovery, *Streptomyces murayamaensis* was patented and samples were deposited to the American Type Culture Collection (ATCC, Manassas, VA, USA; www.atcc.org) by Kyowa Fermentation Industrial Co., Ltd. under the registration number of ATCC 21414, which was then made available to the general scientific public. Until early 1989, *Streptomyces murayamaensis* (ATCC 21414) was the only bacterium known to produce the kinamycins. Later, the discovery of various kinamycins from *Streptomyces saccharothrix* (strain MI293-N4, 1989),[7] an unidentified *actinomycete* (strain A80316, 1992)[8] and *Streptomyces chattanoogensis* subsp. *taitungensis* (strain IY2-13/CCRC 15124, 1994)[11] significantly enlarged the source pool for the natural kinamycins. Although each *Streptomyces* mentioned above would produce unique natural kinamycins individually, some kinamycins were isolated and identified from more than one *Streptomyces* source. For example, kinamycin D (**1.1d**), initially obtained from *Streptomyces*

murayamaensis,[4] was also isolated much later from *Streptomyces chattanoogensis* subsp. *Taitungensis*.[11]

1.3.1 Production and Isolation of Natural Kinamycins

The initially discovered *Streptomyces murayamaensis*[4] (ATCC 21414) is the most frequently used bacterium to produce the valuable natural kinamycins through fermentation, which needs to be first grown on appropriate agar media prior to further use.[6] Fermentation of the *Streptomyces murayamaensis* is a rather complicated and very sensitive biological process, and the outcome is affected significantly by even small variations in experimental conditions (constituents of media and the conditions of cultivation), which were examined extensively by the Hata/Ōmura team[20,67] and the Gould group.[6] Organic extraction using benzene or toluene of the treated (acidified, concentrated, centrifuged and sonicated) fermentation broth followed by repetitive chromatographic separation would give the desired kinamycins usually in very low yields, along with isolation of other structurally and biosynthetically related metabolites such as dehydrorabelomycin (**1.21**) and murayaquinone (**1.22**).[6]

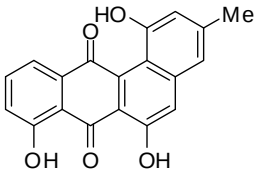

1.21 dehydroabelomycin

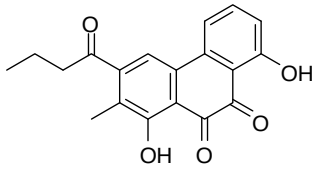

1.22 murayaquinone

Streptomyces capable of producing kinamycins have not been genetically engineered and optimized for such purpose, even though the genes in *Streptomyces murayamaensis* that are responsible for producing kinamycins were already identified, cloned and heterologously expressed by the Gould group in 1998,[58] and some similar genetic work was patented later on by the Diversa Co.

(CA, USA) in 2003.[68] In both studies, however, the gene(s) responsible for the formation of the kinamycin's diazo group were neither identified nor expressed.

1.3.2 Characterization and Structure Elucidation of the Kinamycins

1.3.2.1 Structural Determination and Revision of Kinamycins Containing the Benzo[*b*]fluorene-type Skeleton

After the isolation of kinamycin A, B, C and D (**1.1a**–**d**), Ōmura and co-workers carried out extensive spectroscopic characterization of these compounds by means of ^{1}H-NMR, mass spectrometry (MS), infrared (IR), UV-vis spectrometry and chemical derivatization and degradation. The bulk of the tetracyclic skeleton of kinamycins and major substituents and functional groups were assigned by following the common spectroscopic rules.[9,18] However, a linear triatomic moiety within the kinamycins containing two nitrogen and one carbon atoms (X-Y-Z, Figure 1-4), which has a corresponding strong IR absorption band at 2155 cm^{-1} (common to **1.1a**–**d**), remained mysterious. There are only three possible arrangements for this triatomic moiety, i.e. a *C*-diazo (>C=N^{+}=N^{-} ↔ >C^{-}-N^{+}≡N), an *N*-cyano (>N-C≡N) or an *N*-isonitrile (>N-N^{+}≡C^{-}). The possibility of a *C*-diazo group was never considered by Ōmura, likely because of the perceived instability of this functional group and the very few examples of diazo-containing natural products known at the time (**1.6a**–**d**, early 1970s). Qualitative chemical tests were used to distinguish between the *N*-cyano and the *N*-isonitrile groups due to the lack of further spectroscopic evidence. It was found that hydrolysis of kinamycin C (**1.1c**)[18] and deacetylkinamycin C (**1.1f**, kinamycin F)[9] in refluxing 30% aqueous KOH liberated ammonia but not formic acid,[18] and reaction of deacetylkinamycin C (**1.1f**, kinamycin F) under acidic conditions (refluxing 10% HCl-MeOH)[9] led to the apparent detection of ammonia but no formic acid. Since the cyano group would produce ammonia but not formic acid under either acidic or basic hydrolysis, and the isonitrile group would lead to formic acid but not ammonia either way, such

chemical observation would "suggest and confirm" the presence of an *N*-cyano group rather than an *N*-isonitrile group, when only considering these two options. Apparently this incorrect *N*-cyano structure of kinamycin also gave a modest fit to the X-ray crystallographic data (R = 8.9%) in the case of the *p*-bromobenzoate of kinamycin C (**1.1s** in Scheme 1-1), which established not only the absolute stereochemistry of the D-ring but also confirmed the relative orientation between the A-ring and D-ring.[19] However, the instrumental limitation of NMR spectroscopy in the early 1970s (i.e., most low field CW(continuous wave)-NMR instruments at the time were not capable of acquiring ^{13}C spectra) led to the lack of ^{13}C-NMR spectra of the kinamycins, which may have prevented assigning the incorrect *N*-cyano structure if such data had been available. Another possible contributing factor to this wrong structural assignment is likely the lack of spectroscopic data of other *N*-cyano compounds to compare with at the time when kinamycins were discovered. This proposed *N*-cyanobenzo[*b*]carbazole structure of kinamycins could reasonably explain most of the observed spectroscopic data and chemical behavior, therefore, it was believed to be correct for a long time until later studies discovered more conflicting and inconsistent observations in regards to this *N*-cyano structure.

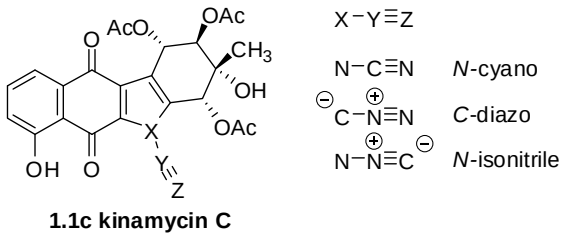

Figure 1-4. Possible arrangements of the triatomic moiety within kinamycins.

In the mid 1980s when Gould initiated biosynthetic studies on the kinamycins, he was able to observe and assign ^{13}C NMR resonances for all of the carbons of kinamycin D (**1.1d**) except the cyanamide carbon, which was expected to have a chemical shift of ca. 110–120 ppm.[69,70] Fortunately,

when Gould fed the *Streptomyces* with ^{15}N-labeled ammonium sulfate as the sole nitrogen source, a doubly-labeled [$^{15}N_2$]kinamycin D (**1.1d**) was produced. For the first time, this [$^{15}N_2$]kinamycin D enabled Gould to locate the "missing" NMR signal of the "cyanamide carbon" of kinamycins, which appeared as a doublet of doublets (dd, J = 21.2 Hz and 5.4 Hz) at chemical shift of 78.5 ppm due to the coupling between ^{13}C and the two adjacent ^{15}N atoms.[71] Further reexamination of previously recorded spectra of non-isotope-labeled natural kinamycin D (**1.1d**) revealed the presence of a very weak singlet at 78.5 ppm that was barely noticeable due to the nearby very strong solvent peak of $CDCl_3$ at 77 ppm and originally thought to be caused by impurities.[71] This newly discovered carbon signal at 78.5 ppm was then assigned to the "*N*-cyano carbon" despite its significant deviation from the expected chemical shift of 110–120 ppm. This dramatic difference of about 30 ppm was attributed to possible electronic effects of the indolequinone (within the original/incorrect structure of benzo[*b*]carbazole skeleton of kinamycins) on the cyanamide carbon.[71] However, literature data indicate that the ^{13}C atoms attached to diazo groups in some diazo compounds have chemical shifts in the 60–80 ppm region,[72] which matches the observed ^{13}C chemical shift of the "*N*-cyano carbon" of kinamycin D (78.5 ppm) much more closely than the ^{13}C chemical shifts of the *N*-cyano compounds. Such findings would suggest a necessary reconsideration of the previously ignored possibility of having a diazo functional group rather than the long-believed *N*-cyano moiety within the kinamycins. In the meantime (early to mid-1990s), other research groups had been working towards the total synthesis of kinamycins based on the incorrect benzo[*b*]carbazole skeleton, which led to the preparation of *N*-cyanoindoles (e.g., compound **1.23** and **1.24** in Scheme 1-2, made by the Dmitrienko lab) as well as other advanced intermediates containing both the *N*-cyano group and the benzo[*b*]carbazole skeleton.[73,74] The ^{13}C NMR chemical shifts of ca. 105–112 ppm for such *N*-cyano carbons match very well with the expected values, but poorly with the observed corresponding signal for kinamycins. In addition, such synthetic *N*-cyano compounds all have a characteristic IR band in

the region of ca. 2240–2250 cm^{-1} for their *N*-cyano moiety, while the IR band of the "*N*-cyano" in kinamycins appeared at ca. 2155 cm^{-1} (a difference of ca. 100 cm^{-1}). Among the available examples of *N*-cyano compounds, two literature reports are worthy of some additional comments. One work is the first synthetic route (Scheme 1-2a) towards the benzo[*b*]carbazole of prekinamycin (**1.4**), which was reported by Echavarren's group briefly in 1993[74] followed by a more detailed disclosure in 1997.[75] The other work was carried out by Mithani from the Dmitrienko lab, who reported another total synthesis of *N*-cyanobenzo[*b*]carbazole-based prekinamycin derivative **1.30** in 1994 (Scheme 1-2b).[22] Detailed spectroscopic analysis and comparison of **1.30** and a variety of other model *N*-cyano compounds with natural kinamycins clearly ruled out the possibility of kinamycin possessing the *N*-cyano group, and instead, a diazobenzo[*b*]fluorene quinone skeleton was proposed by the Dmitrienko lab as the final answer to the confusing structure of the kinamycins. Independent and simultaneous results, from a very careful and rigorous X-ray crystallographic study on the (+)-α-methylbutyrate of natural kinamycin D (**1.1v** in Scheme 1-1) performed by Gould's group, also led to the same conclusion.[21] Fitting of X-ray data of **1.1v** provided significantly better statistical *R* and R_w factors when the *C*-diazo group (R = 5.18%, R_w = 5.63%) is used for the triatomic linear structure rather than the other two possibilities, i.e. *N*-cyano group (R = 5.69%, R_w = 6.35%) and *N*-isonitrile group (R = 5.73%, R_w = 6.41%). The quality of Gould's X-ray data is superior when compared with Ōmura's X-ray result of the kinamycin C derivative **1.1s** that has a very large *R* of 8.9%, which made the corresponding conclusion more convincing and trustworthy.

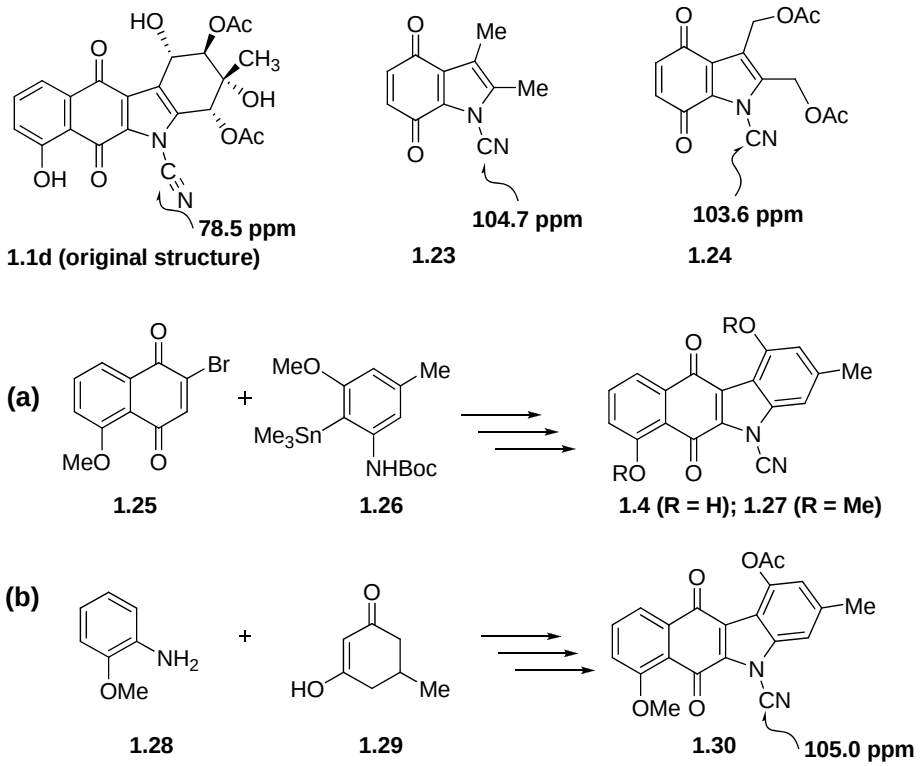

Scheme 1-2. NMR difference between the "*N*-cyano carbon" of kinamycin D (**1.1d**) and other *N*-cyano species and synthesis of the *N*-cyanobenzo[*b*]carbazoles by (a) Echavarren and (b) Dmitrienko.

This structure revision of kinamycins in 1994, from *N*-cyanobenzo[*b*]carbazoles to diazobenzo[*b*]fluorenes, has had a profound influence on many aspects of the chemistry and biochemistry of the kinamycin antibiotics. Not only did the synthetic strategies to kinamycins have to be redirected towards the very rare benzo[*b*]fluorene skeleton as well as the unique and potentially reactive diazo group, but also the previous knowledge and explanation of the biosynthesis and mechanism (mode-of-action) related to kinamycin's biological activities required reexamination.

1.3.2.2 Structural Determination and Revision of Isoprekinamycin - Kinamycin with a Benzo[*a*]fluorene-type Skeleton

In 1989, Gould's group isolated a purple solid metabolite, designated as compound "P1" in the original papers, from the bacterial fermentation broth of *Streptomyces murayamaensis*.[5,6] The corresponding name and structure of prekinamycin (**1.4** with the original *N*-cyanobenzo[*b*]carbazole skeleton) was then assigned to compound "P1" based on the spectroscopic data obtained. Evidence available at that time would suggest this so-called "prekinamycin" has the common *N*-cyanobenzo[*b*]carbazole skeleton but with an aromatized D-ring, which might be converted biosynthetically in a stepwise fashion into other kinamycins bearing the saturated D-ring with the necessary substituents.[5]

After the structural revision of kinamycins in 1994, the structure of this "prekinamycin" corresponding to compound "P1" was also updated accordingly (**1.4** changed from the incorrect *N*-cyanobenzo[*b*]carbazole to the correct diazobenzo[*b*]fluorene). This compound "P1" (isolated in 1989) was also known as "Cpd A" within Gould's group,[13] and its structure was not challenged until 1996, when Hauser and Zhou achieved the first total synthesis (section 1.5) of a product having the exact structure as the proposed prekinamycin (**1.4**).[76] The spectroscopic data of Hauser's synthetic prekinamycin, however, did not match the already reported literature values for the presumed natural "prekinamycin". Gould and co-workers then found that Hauser's synthetic prekinamycin indeed matched perfectly in all spectroscopic methods used (^{1}H-NMR, UV-vis and HPLC) with another metabolite, which had been previously observed from the extracts of *Streptomyces murayamaensis* mutant MC2 and designated as "Cpd B" in Gould's group but never characterized structurally.[12] As a result of this discovery, "Cpd A" lost the proposed name and structural assignment of prekinamycin (**1.4**) to "Cpd B". The true identity of "Cpd A" remained unclear until four years later, when joint studies by the Dmitrienko group and the Proteau group finally characterized the mysterious "Cpd A"

(compound "P1") as a structural isomer of prekinamycin (**1.4**, "Cpd B"). "Cpd A" was found to possess the rare diazobenzo[*a*]fluorene skeleton rather than the relatively common diazobenzo[*b*]fluorene skeleton among other kinamycins, therefore, "Cpd A" was named as isoprekinamycin (**1.5**, Scheme 1-1) afterwards.[14]

1.3.3 Biosynthesis of the Kinamycins

Experiments to explore the biosynthetic pathway to the kinamycins were carried out from the mid 1970s to the late 1990s. Initially, the Ōmura group used IR to suggest the origin of the "cyanamide carbon" of kinamycins. Later, Gould's group used extensive isotope labeling of precursors and NMR analysis to establish the biosynthetic pathways of kinamycins. Most studies on kinamycin biosynthesis were accomplished before the structural revision of kinamycins in 1994, which resulted in a reevaluation of the known biosynthetic mechanisms at the time, particularly in terms of intermediate metabolites involved. It was found that the new diazobenzo[*b*]fluorene structure for kinamycins was perfectly consistent with all the known results of biosynthetic studies, which were previously explained using the old and incorrect structure of *N*-cyanobenzo[*b*]carbazole. The corresponding results, reviewed thoroughly by Gould in 1997[15] and 1998,[58] now provide quite deep understanding in this regard.

1.3.3.1 Biosynthetic Origins of the Kinamycin Skeleton and D-ring Substituents

The biosynthetic origins of the kinamycins were determined by Gould and co-workers upon feeding *Streptomyces murayamaensis* with various isotope-labeled sodium acetates and metabolite intermediates (Scheme 1-3), and the derived isotope-containing kinamycin C (**1.1c**) and D (**1.1d**) were subjected to NMR spectroscopic analysis to locate the distribution of isotopic atoms.[5,53,70,71,77] Several fundamental conclusions were made based on these results (Scheme 1-3). The observed ^{13}C

enrichment (Scheme 1-3a/b/c) indicated that the entire skeleton of kinamycin was derived from acetate through a polyketide pathway and the origins of all carbons except the "cyanamide carbon" were identified. In addition, oxygen at C-1, C-6 and C-7 was derived from the acetate, oxygen at C-3, C-4 and C-11 came from the air (O_2) and the C-2 oxygen originated from water (Scheme 1-3c/d). In addition, the previously isolated dehydrorabelomycin (**1.21**) was confirmed to be a key biosynthetic intermediate for kinamycins (Scheme 1-3e/f).

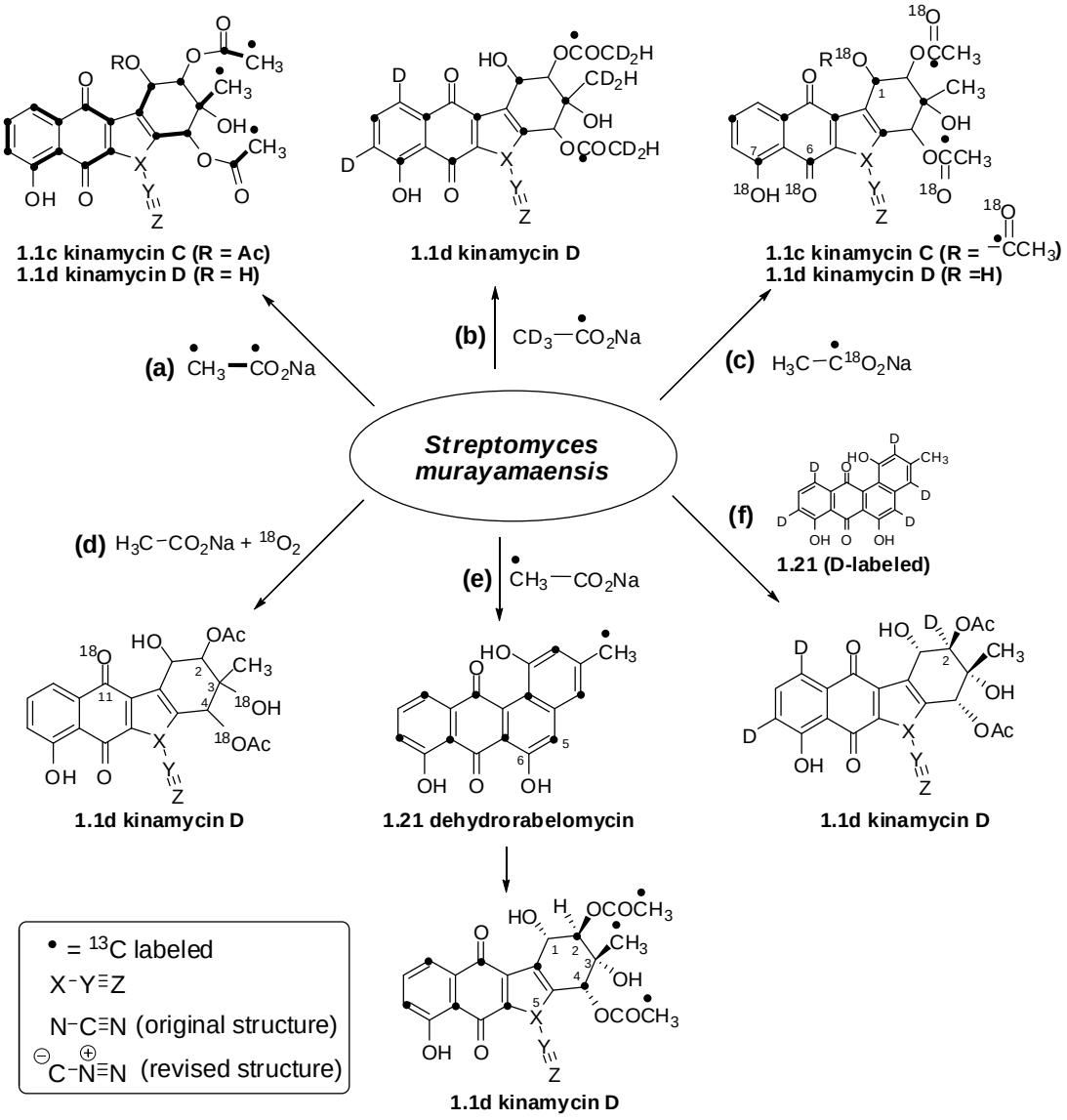

Scheme 1-3. Biosynthetic origins of carbon, oxygen and hydrogen atoms of kinamycins.

To tackle the biosynthetic origin of the "cyanamide carbon" (diazo carbon) of kinamycins, initial work was performed by Ōmura in 1976, who fed $CH_3{}^{13}COONa$ and $^{13}CH_3COONa$ to *Streptomyces murayamaensis*, and the derived kinamycin D (**1.1d**) were analyzed by IR spectroscopy.[78] An isotope-induced shift from 2155 to 2139 cm^{-1} of the IR peak, corresponding to the stretching frequency of the ^{13}C-N triple bond within the *N*-cyano group (now assigned to the diazo stretching), was only observed when $CH_3{}^{13}COONa$ was used but not in the case of $^{13}CH_3COONa$, suggesting the "cyanamide carbon" (>N-**C**≡N, now known as the diazo carbon >$\mathbf{C}^-$-N^+≡N) was derived from C-1 (carbonyl carbon) of the acetate.* Later, Gould and co-workers directly observed the "cyanamide carbon" within ^{13}C-labeled kinamycin D (**1.1d**) that were also produced by feeding bacteria with either $CH_3{}^{13}COONa$ or $^{13}CH_3COONa$.[71] However, the more convincing NMR evidence suggested the other alternative, i.e. the "cyanamide carbon" of kinamycins should be derived from C-2 (methyl carbon) of the acetate instead, since ^{13}C enrichment of the "cyanamide carbon" was only observed by NMR with kinamycin D (**1.1d**) derived from $^{13}CH_3COONa$ but not $CH_3{}^{13}COONa$.[71] Since the observed level of the isotope enrichment for this "cyanamide carbon" was similar to other carbons of the kinamycin skeleton, it was further proposed that the "cyanamide carbon" was derived from C-5 of dehydrorabelomycin (**1.22**) (Scheme 1-3e).[71]

Results of the above labeling studies also led to a plausible proposal for the oxidative elaboration of the D-ring of kinamycins as given by Scheme 1-4a, in which the lack of deuterium labeling at C-4 of the non-aromatic D-ring of kinamycin D (Scheme1-3b) would indicate first a hydroxylation occurred at C-4 of the precursor with an aromatic D-ring, and produced the hydroquinone **1.31** followed by oxidation to the epoxide **1.32**. The epoxide may then undergo stereospecific tautomerization to epoxyquinol **1.33** or **1.34**, and a stereospecific reduction of either **1.33** or **1.34**

* Preliminary computational results from this work indicated that this presumed "isotope-induced" diazo IR shift as observed by Ōmura must be caused by other reasons but not the claimed one.

would lead to the epoxy diol **1.35**. Finally, trans attack of water on the epoxy group of **1.35** at the less hindered C-2 position shall yield kinamycin with a fully oxygenated D-ring structure **1.36** having the correct stereochemistry and with each atom derived from the correct source as found by the labeling studies (Scheme 1-3).[77] This D-ring evolution mechanism was further supported by the later (1989–1994) isolation of minor metabolites such as ketoanhydrokinamycin (**1.3b**), prekinamycin (**1.4**), kinamycin F (**1.1f**) and kinamycin E (**1.1e**) from *Streptomyces murayamaensis* and its mutant (Scheme 1-4b).[5,6,12] In addition, Gould's group isolated an apparently large enzyme (MW > 669 kDa) from *Streptomyces murayamaensis* in 1996, which was responsible for two consecutive acetylations of kinamycin F (**1.1f**), first at C-4 leading to kinamycin E (**1.1e**) and then at C-2 leading to kinamycin D (**1.1d**). Therefore, the enzyme was named as kinamycin acetyltransferase I (KAT I),[79] but at least two more KATs were required by the minimum pathway to account for the remaining three other acetylation patterns on the kinamycin D-ring.[15] Furthermore, the isolation of stealthin C (**1.15c**) in 1997[17] as a minor metabolite from *Streptomyces murayamaensis* mutant MC2[12] by Gould's group, has provided deeper insight into the biosynthesis of kinamycins. Feeding of deuterium-labeled stealthin C (**1.15c**) to *Streptomyces murayamaensis* (not the mutant MC2 from which **1.15c** was produced) led to the corresponding deuterium-labeled kinamycin D (**1.1d**), which confirmed the role of stealthin C (**1.15c**) as a critical intermediate in kinamycin biosynthesis (Scheme 1-4c). Interestingly, feeding of synthetic compounds such as **1.37** that were essentially the same as **1.15c** except the difference in nitrogen substituents, led to no production of labeled kinamycin D (**1.1d**) (Scheme 1-4c).[17]

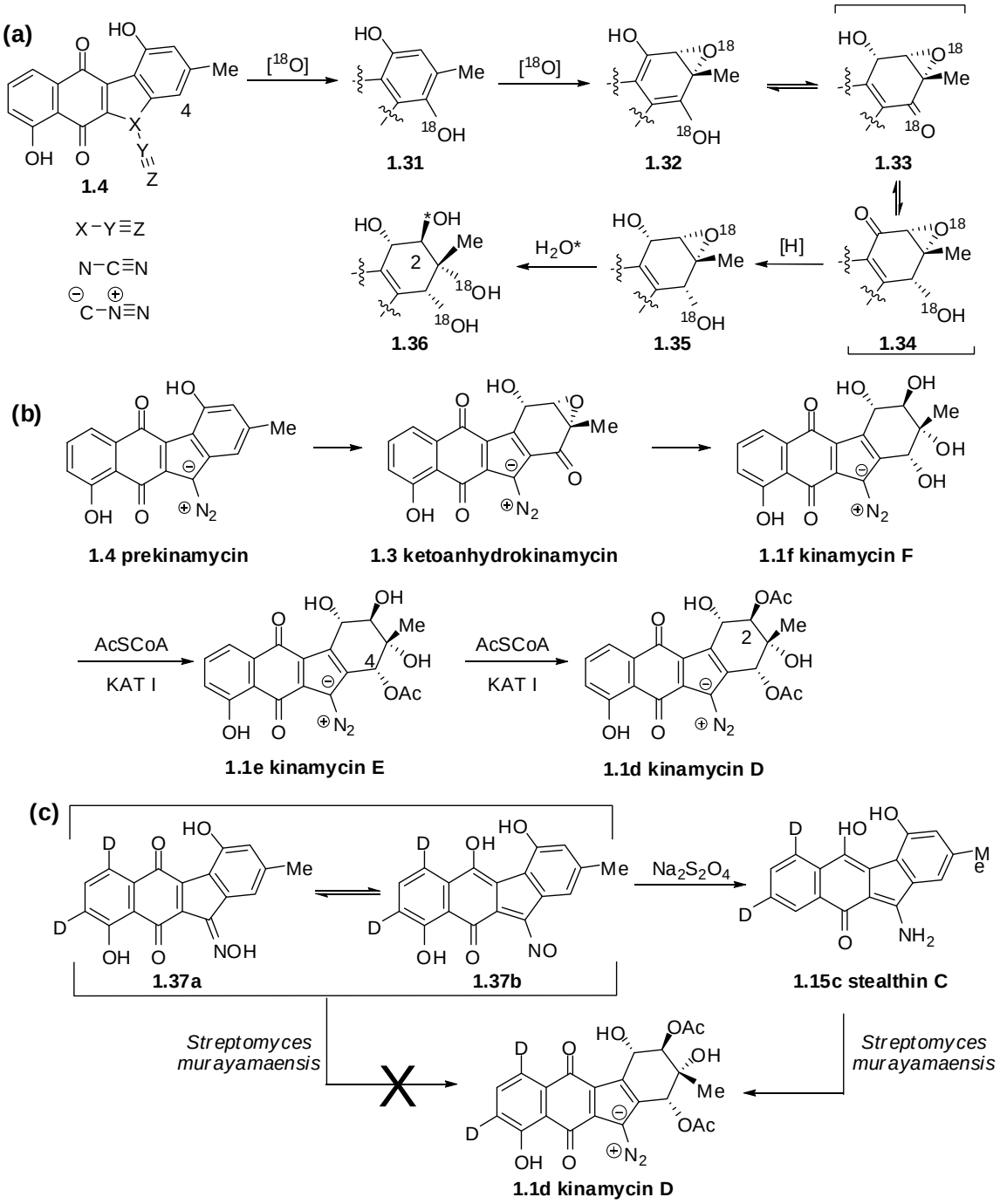

Scheme 1-4. (a) Proposed mechanism for the oxidative elaboration of kinamycin D-ring; (b) stepwise biosynthetic transformation sequence between kinamycins; and (c) experiments confirming stealthin C (**1.15c**) as a biosynthetic intermediate for kinamycins.

Later on, the understanding of kinamycin biosynthesis on the level of molecular biology was greatly promoted, after Gould's group successfully cloned the genomic DNA (genes) of *Streptomyces murayamaensis* and heterogeneously expressing the genes when the DNA was transferred into *Streptomyces lividinas* ZX7.[58] The genetic studies identified two clusters of polyketide synthase (PKS) genes, among which only one was responsible for producing the kinamycins through a decaketide intermediate **1.38a**, while the other was likely responsible for producing murayaquinone (**1.22**), a metabolite previously isolated from *Streptomyces murayamaensis*, through a different (but unknown) decaketide **1.38b** pathway (Scheme 1-5). Expression of the particular kinamycin gene cluster in *Streptomyces lividinas* ZX7, which was not complete but sufficient to biogenetically synthesize the benzo[*b*]fluorene skeleton of kinamycins, smoothly led to accumulation and identification of several known metabolites/intermediates of kinamycin biosynthesis such as dehydrorabelomycin (**1.21**), kinobscurinone (**1.16a**) and stealthin C (**1.15c**), as well as two shunt metabolites, namely kinafluorenone (**1.16b**) and seongomycin (**1.17**) (Scheme 1-5).[58] On the other hand, isolation of momofulvenone A (**1.14a**) and B (**1.14b**) from *Streptomyces diastatochromogenes* (strain Tü 2895) and the corresponding ^{13}C labeling experiments in 1995 indicated that these two species, whose counter ions vary depending on the salts used in the growing medium, were also involved in the same biosynthetic sequence as the kinamycins (Scheme 1-5).[54] All these biosynthetic studies have now led to a hypothetical and overall biosynthetic mechanism for kinamycins with the benzo[*b*]fluorene skeleton, as shown in Scheme 1-5.

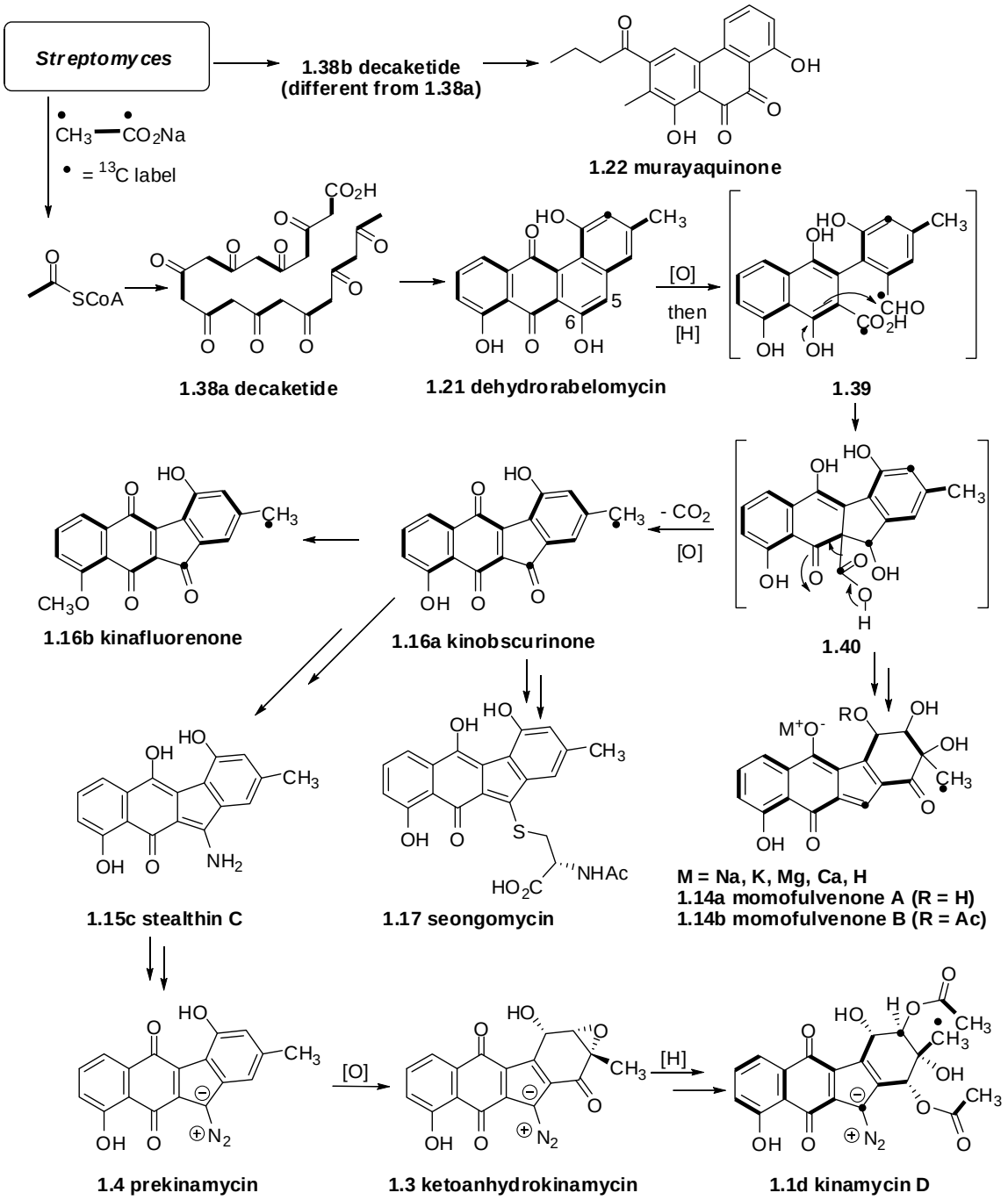

Scheme 1-5. Overall biosynthetic pathway for benzo[*b*]fluorene-type kinamycins.

The dehydrorabelomycin (**1.21**), derived from the polyketide precursor **1.38a** upon aromatization and decarboxylation, is the first key intermediate of the entire biosequence, which then undergoes an

oxidative ring opening at C-5 and C-6 followed by reduction of the quinone moiety leading to **1.39**. An electrophilic cyclization of **1.39** would afford structure **1.40** containing a benzo[*b*]fluorene skeleton for the first time. The dihydroquinone obtained from **1.40** upon decarboxylation (not shown in the scheme) would eventually lead to momofulvenones (**1.14a**–**b**) in *Streptomyces diastatochromogenes*, while in the case of *Streptomyces murayamaensis* this dihydroquinone would be further oxidized to kinobscurinone (**1.16a**), the second key intermediate of the kinamycin biosynthesis, which could be derivatized to other (shunt) metabolites such as kinafluorenone (**1.16b**), seongomycin (**1.17**) and most importantly stealthin C (**1.15c**), which now has an essential and critical amino group at C-5. The latter then may undergo an oxidative incorporation of the second nitrogen atom and produce prekinamycin (**1.4**), followed by stepwise oxidation, reduction and acetylation to alter the kinamycin D-ring. However, the genes and corresponding products responsible for the final step(s) in formation of the diazo group have not been identified.

Finally, co-production of both benzo[*a*]fluorene and benzo[*b*]fluorene types of kinamycins and their comparable stability (ab initio calculation predicted that **1.4** is more stable than **1.5** by ca. 2.4 kcal/mol) had led Dmitrienko and Proteau to propose a hypothesis of reversible interconversion between these two types of ring skeletons through a possible enzyme-catalyzed rearrangement (Scheme 1-6a).[14] Such a proposal was consistent with some unpublished isotopic labeling results from Gould's group of isoprekinamycin (**1.5**) (Scheme 1-6b), when *Streptomyces murayamaensis* was fed with $^{13}CH_3{}^{13}COONa$ (Scheme 1-6b).[80]

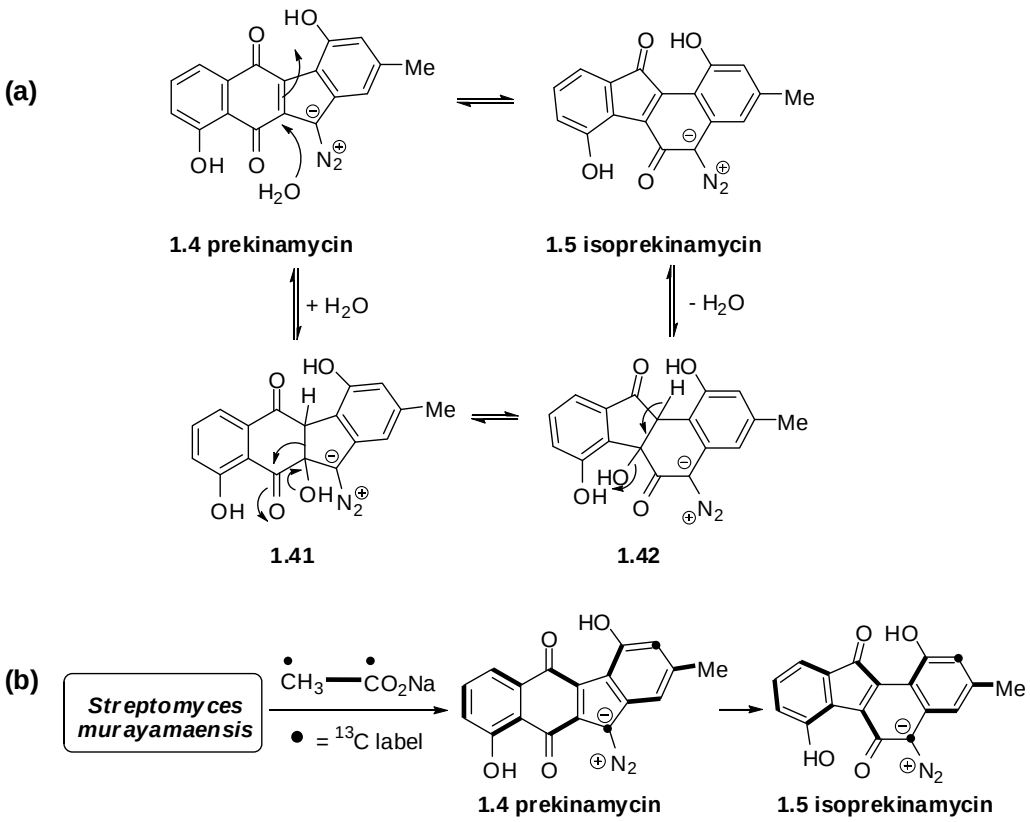

Scheme 1-6. (a) Proposed reversible interconversion between diazobenzo[*b*]fluorene and diazobenzo[*a*]fluorene skeletons and (b) isotope labeling results of benzo[*a*]fluorene-type kinamycin.

1.3.3.2 Biosynthetic Origins of the *C*-Diazo Moiety of Kinamycins

Although the bulk of the kinamycin biosynthetic mechanism as introduced in section 1.3.3.1 is quite well understood by now, there are still some unclear steps and conversions within this particular biosynthesis that deserve more detailed consideration and efforts, among which the most intriguing ones are the biosynthetic steps leading to the formation of the rare diazo group at C-5 of the kinamycins.

Early isotope labeling experiments carried out in Gould's lab in the late 1980s, by using $(^{15}NH_4)_2SO_4$ as the sole nitrogen source for *Streptomyces murayamaensis*, indicated that both nitrogen

atoms of the diazo group (believed to be the *N*-cyano group at that time) within kinamycins were incorporated with the ^{15}N isotope.[71] This observation suggested a stepwise incorporation of the two nitrogen atoms into the kinamycin structure, which is consistent with the later identification of the key biosynthetic intermediate stealthin C (**1.15c**), whose C-5 amino group was eventually transformed into the corresponding diazo group of kinamycins.

It is still not clear how the biosynthetic transformation from kinobscurinone (**1.16a**) to stealthin C (**1.15c**) (Scheme 1-5) is performed by the bacteria, but the cloned DNA from *Streptomyces murayamaensis* by Gould does contain the gene(s) responsible for introducing the first nitrogen of the eventual diazo group of the kinamycins.[58] Without identification of any possible amination substrates and intermediates, Gould proposed a likely but unproven hypothesis that kinobscurinone (**1.16a**) might exist in the corresponding quinone form **1.16a**, semi-quinone form (not shown) and hydroquinone form **1.46** at ambient temperature due to the rather small redox potential differences between such structures. In the presence of appropriate and necessary enzymes such as pyridoxal phosphate-dependent transaminase or glutamine-/ammonia-dependent transaminase among others, **1.16a** and its various redox forms may be converted biosynthetically to stealthin C (**1.15c**) through several possible pathways (Scheme 1-7).[58]

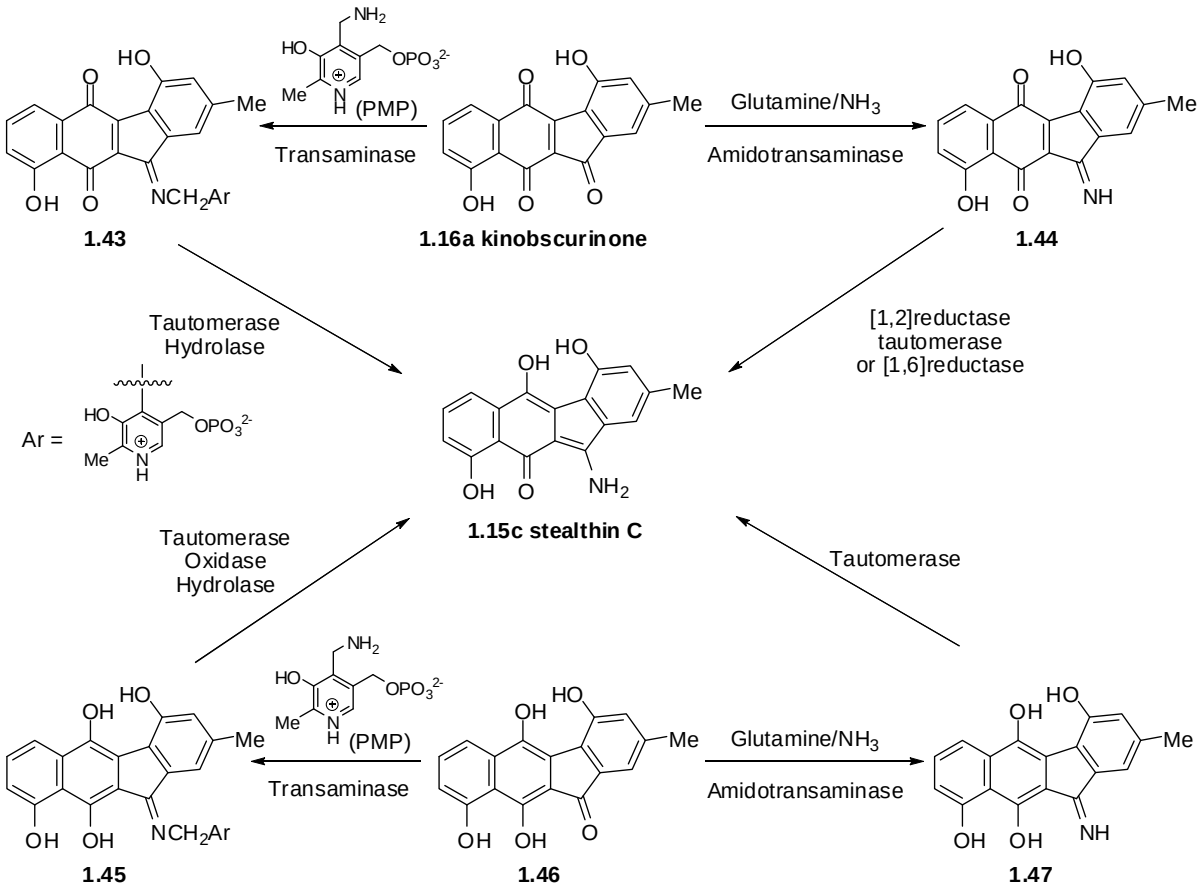

Scheme 1-7. Proposed biosynthetic conversions from kinobscurinone (**1.16a**) to stealthin C (**1.15c**).

Unfortunately, there are no experimental results observed so far that are related to the biosynthetic pathway leading to the introduction of the second nitrogen within the diazo moiety of kinamycins. Moreover, current knowledge about the biosynthetic formation of N-N bonds in nature is very limited despite the relatively wide existence of such functionalities.[81] There are a few examples in the literature indicating that the formation of natural N-N bonds could involve hydrazine intermediates,[81] and enzymes capable of oxidizing the arylhydrazine to aryldiazonium salts are known as well.[82,83] Therefore, in principle, the potential existence of a hydrazine intermediate in the kinamycin biosynthesis is possible but yet to be confirmed. Two such recent examples are valanimycin (**1.51**)

and agaritine (**1.52**). The former is an azoxy natural product isolated from *Streptomyces viridifaciens* MG456-hF10, and it is derived biosynthetically through oxidation of a hydrazine intermediate **1.50**, which is produced from the condensation of isobutylhydroxylamine (**1.48**) and serine (**1.49**) (Scheme 1-8a).[84] The later example of agaritine (**1.52**) is present abundantly in the most popular edible mushroom *Agaricus bisporus* in North America (more commonly known by the name of white/button/pizza mushroom), and biosynthetic studies (Scheme 1-8b) indicated that **1.52** could be initially hydrolyzed to the free hydrazine **1.53** by either mammalian or fungal enzymes such as γ–glutamyl transpeptidase (GGT), which was then consequently oxidized to the corresponding aryldiazonium salt **1.54**.[82,83,85]

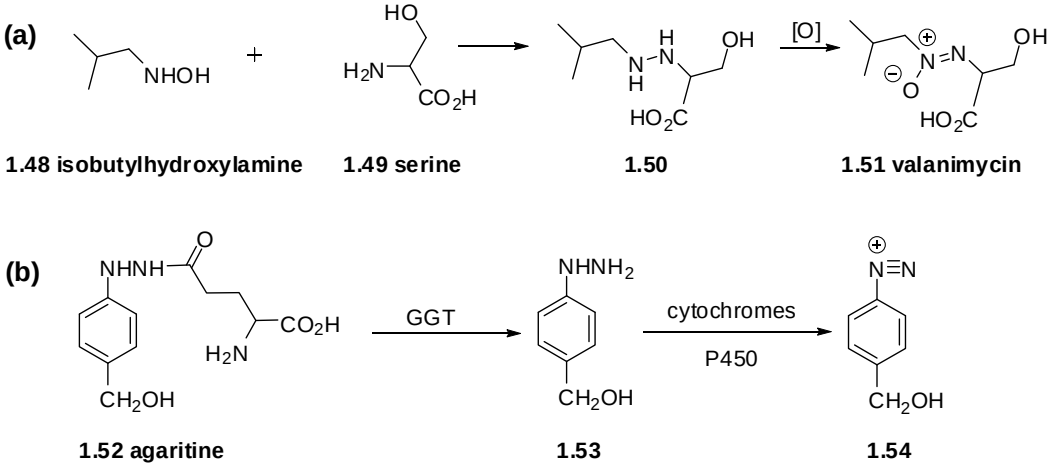

Scheme 1-8. Literature examples for formation of N-N bonds in nature via hydrazine intermediates.

On the other hand, the known behavior of soil bacteria to interconvert nitrate and ammonia through a complex series of redox reactions[86] with the radical byproduct of nitric oxide (NO) that can have various deleterious effects such as DNA damage in vivo,[87] has led to a reasonable speculation in the Dmitrienko lab, that *N*-nitrosation might be involved in the formation of the diazo group originating from the primary amine group of stealthin C (**1.15c**) (Scheme 1-9), since stealthins are

indeed very potent scavengers for trapping radicals to protect the microorganisms.[55] Hydrogen abstraction from the amino group of stealthin C (**1.15c**) could lead to the radical species such as **1.55** and **1.58**, and the following trapping of NO then gives the corresponding *N*-nitroso intermediates that may eventually lead to prekinamycin (**1.4**), the precursor for all other diazobenzo[*b*]fluorene type of kinamycins having non-aromatic D-rings. Experiments aimed at testing this hypothesis are planned.

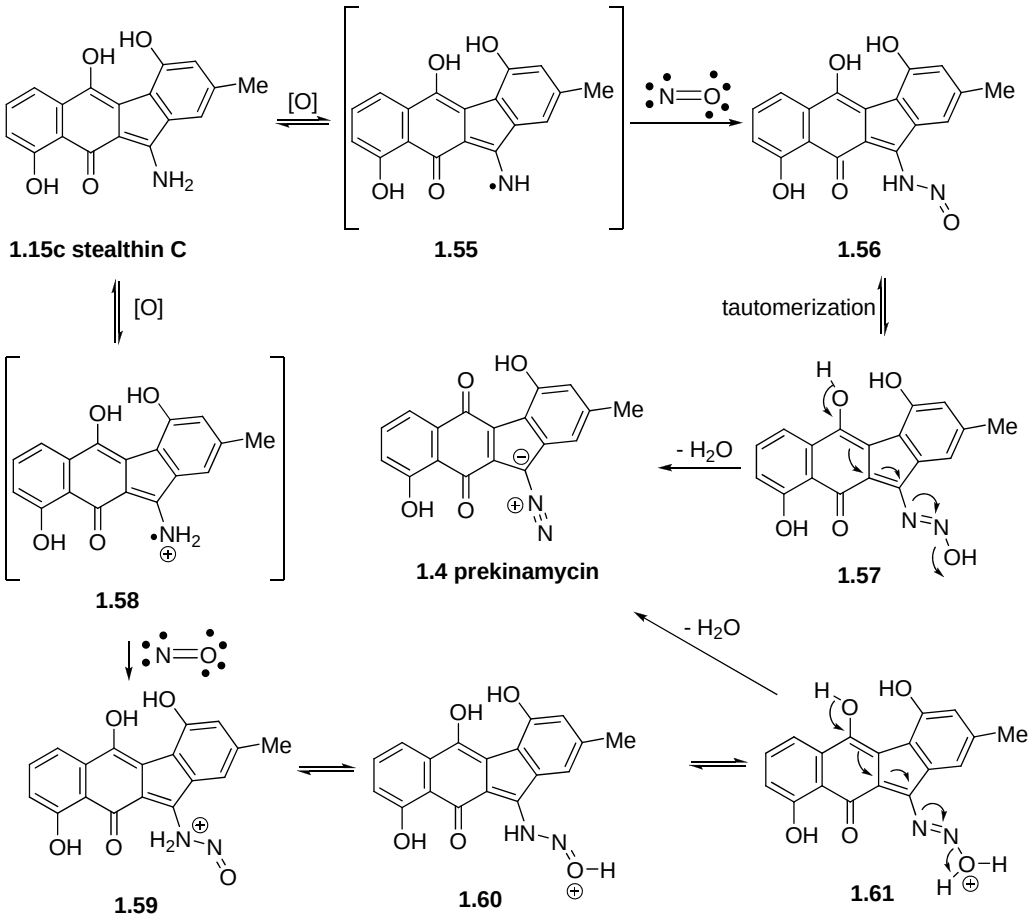

Scheme 1-9. Proposed mechanism by the Dmitrienko group for diazo formation in kinamycins through the nitric oxide (NO) trapping pathways.

1.4 Biological Activities and Speculation on the Mode-of-Action of the Kinamycins

1.4.1 Biological Activities of the Kinamycins and Lomaiviticins

The reported antimicrobial activities of natural and semi-synthetic kinamycins indicate that they are strongly active against Gram-positive bacteria but (much) less effective towards the Gram-negative ones.[4,6-10,18,52] Lomaiviticins (**1.11a/b**), the dimeric analogues of kinamycins, were found to be even more potent towards the Gram-positive bacteria. A detailed summary of the reported antimicrobial activities of all kinamycins in the literature is provided in the appendix section (Appendix A). As antibiotics, the intravenous acute toxicity (LD_{50}) of natural kinamycins in mice was found to be moderate in general. For kinamycin A–D (**1.1a**–**d**), LD_{50} is about 30-40 mg/kg each,[4] and for FL-120A (**1.1m**), FL-120B (**1.2a**) and FL-120C' (**1.1o**), LD_{50} is 35.36 mg/kg, > 50 mg/kg, and 6.97 mg/kg, respectively.[11] A lethal dose in mice of 0.5 mg per mouse was reported for kinamycin H (**1.1h**) but a reduction of the dose by half showed no toxicity.[7]

When compared with some common antibiotics such as streptomycin, mitomycin C and vancomycin, kinamycin D (**1.1d**) exhibits a moderate antimycoplasmal activity but with unknown mode-of-action.[88] In addition, kinamycin D (**1.1d**) possessed moderate antifungal activities at a concentration of 10–100 μg/mL against certain plant-pathogenic and agriculture-related fungi, comparable to other quinone-type antibiotics such as antimycin, nanaomycin A, oligomycin and ikutamycin.[89] This particular kinamycin also demonstrated significant herbicidal activity (30–80% inhibition of plant growth) against radish. Such antifungal and herbicidal activity of kinamycin D (**1.1d**) was considered to be effective through possible inhibition of the biosynthesis of cellulose.[89]

The other important biological activity of kinamycins, and lomaiviticins in particular, is their antitumor activity. Early antitumor tests of kinamycin C (**1.1c**) and D (**1.1d**) towards EHRLICH

ascites carcinoma and sarcoma-180 indicated that, **1.1c** showed some survival effect by intraperitoneal injection at 0.1 and 1 mg/kg, yet **1.1d** was found to have no tumor inhibition effect.[20] Later, kinamycin G (**1.1g**) and H (**1.1h**) were found to possess cytotoxicity against L1210 leukemia (IC_{50} **1.1g**: 0.72 μg/mL; **1.1h**: 0.38 μg/mL) and IMC carcinoma cells (IC_{50} **1.1g**: 0.88 μg/mL; **1.1h**: 0.72 μg/mL) in suspension culture, and cytotoxicity against LX-1 human lung carcinoma (IC_{50} **1.1g**: 0.542 μg/mL; **1.1h**: 0.790 μg/mL) and SC-6 human stomach carcinoma (IC_{50} **1.1g**: 2.50 μg/mL; **1.1h**: 0.760 μg/mL) in a clonogenic assay.[7] The dimeric diazobenzo[*b*]fluorenes of lomaiviticin A (**1.11a**) and B (**1.11b**) were found to possess very potent DNA-damaging activity (minimum induction concentration ≤ 0.1 ng/spot) in biochemical induction assay (BIA) and extreme cytotoxicity (0.01–98 ng/mL, equivalent to 0.007–72 nM) against a broad panel of cancer cell lines.[52] Moreover, the cytotoxicity profile of **1.11a** in a 24-cancer cell line panel was unique when compared with other known DNA-damaging anticancer drugs such as adriamycin and mitomycin C, indicating a different and still unknown mechanism of interaction with DNA. Studies also indicated that lomaiviticin A (**1.11a**) is capable of cleaving double-stranded DNA under reducing conditions.[52] The strong and broad anticancer activity of lomaiviticins, along with their unknown mode-of-action, have stimulated a great deal of research interests in the diazobenzo[*b*]fluorene systems. More recent work from the Dmitrienko lab in collaboration with the Hasinoff lab indicates that isoprekinamycin (**1.5**) significantly inhibits the growth of Chinese hamster ovary (CHO) cells (IC_{50} = 5.8 μM) and K562 human leukemia cells (IC_{50} = 6.4 μM), comparable to the clinically useful anticancer agent etoposide (CHO: IC_{50} = 1.4 μM; K562: IC_{50} = 3.4 μM).[25] In addition, during recent physical organic studies on prekinamycin (**1.4**) and simpler analogues, such compounds have been screened against a 60-cell human cancer panel and some of them demonstrated significant growth inhibitory activity (GI_{50}) against pancreas, breast, lung, colon and prostrate tumor cells at a concentration of ca. 0.41–7.3 μg/mL.[90]

1.4.2 Speculation of the Mode-of-Action of the Kinamycin Antibiotics

1.4.2.1 Proposed Mechanism for Kinamycins with the Original *N*-Cyanobenzo-[*b*]carbazole Structure

Prior to the structural revision of kinamycins in 1994, the original (incorrect) structure of *N*-cyanobenzo[*b*]carbazole for kinamycins had led Moore to first consider a close correlation between kinamycin C (**1.1c**) and mitomycin C (**1.62**) in the late 1970s.[91] Both compounds were believed to be indolequinones containing appropriate potential leaving groups, which might become more susceptible to displacement upon reduction of the quinone to a semi-quinone or hydroquinone. Mitomycin C (**1.62**) is a potent antineoplastic drug in clinical use for cancer chemotherapy, and it has been shown to function as a bisalkylating reagent that crosslinks DNA effectively, but only in the presence of either a reducing agent or under acidic (pH $\leq$ 5) conditions.[91-93] The reductive pathway of mitomycin C (**1.62**) is believed to follow the mechanism shown in Scheme 1-10a.[91-93]

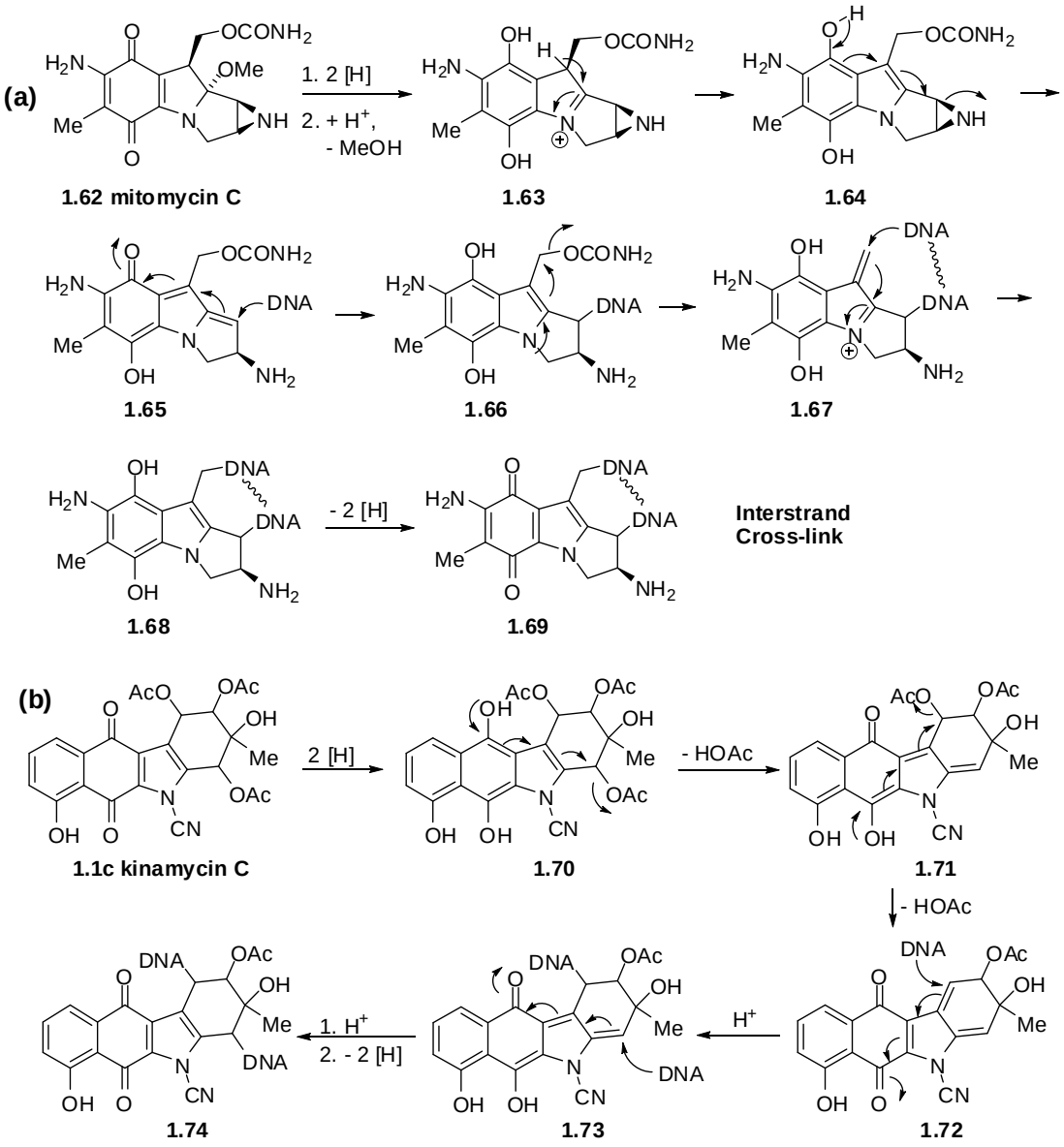

Scheme 1-10. Proposed mode-of-action of (a) mitomycin C (**1.62**) and (b) kinamycin C (**1.1c**) through two electron reductive activation.

Reduction of **1.62** to the corresponding hydroquinone **1.63** facilitates an acid-induced elimination of the angular methoxy group, and leads to the subsequent formation of the indole **1.64**. Ring-opening of the aziridine produces the quinone methide **1.65**, which is reactive towards nucleophilic attack by species such as deoxyguanosine of DNA. Further elimination of carbamate from **1.66** then affords a

Michael acceptor **1.67** capable of being attacked by DNA again. Although both DNA-alkylation steps (i.e., **1.65** to **1.66** and **1.67** to **1.68**) may be reversible, oxidation of **1.68** to the quinone **1.69** prevents the detachment of DNAs and therefore stabilizes the interstrand cross-link of DNAs. An analogous mechanism for kinamycin C (**1.1c**) was then proposed by Moore (Scheme 1-10b).[91,92] The in vivo reduction of **1.1c** may lead to the corresponding hydroquinone **1.70**, which then undergoes two consecutive eliminations of acetate groups off the D-ring and forms a double Michael acceptor **1.72** that can further interact with DNAs. In principle, Moore's hypothesis requires no participation of the "*N*-cyano/*C*-diazo" moiety of kinamycins, so its validity shall not be affected by the structural revision of kinamycins. However, once the kinamycins were shown to be diazobenzo[*b*]fluorenes and not *N*-cyanobenzo[*b*]carbazoles in 1994, their diazo moieties became the focus of speculation concerning the possible mechanism(s) involved in the anticancer and antibacterial activity.

Shortly before the discovery of the diazo moiety within kinamycins, the isolation and identification of kinafluorenone (**1.16b**) from a mutagenic strain (MC1) of *Streptomyces murayamaensis* led to some surprising observations. Both the natural **1.16b** and its synthetic triacetate derivate **1.16c** possess the benzo[*b*]fluorene skeleton but lack the *C*-diazo moiety (considered as the *N*-cyano group at the time), whose structures were unambiguously established based on spectroscopic evidence and single crystal X-ray studies of **1.16c**.[57] Kinafluorenone (**1.16b**) showed no detectable antibiotic activity against *Bacillus subtilis* (ATCC 6633), which is very sensitive to the kinamycins (MIC = 0.01–0.39 μg/mL).[57] In addition, **1.16c** also showed no detectable antibiotic activity, even at a fairly high concentration of 64 μg/mL, against many bacteria that were known to be inhibited by kinamycins at (much) lower concentrations.[57] This observation would indicate that, the presence of a diazo functionality within a benzo[*b*]fluorene skeleton, is very likely involved and essential in the biological activity of the diazobenzo[*b*]fluorenes of kinamycins.

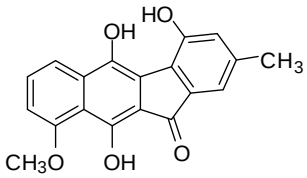

1.16b

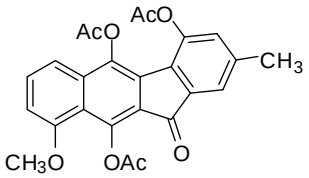

1.16c

1.4.2.2 Role of Diazo and Diazonium Moiety in Biological Activities

Cleavage of single and double stranded DNA upon exposure to simple (*para*-substituted) phenyldiazonium salts has been observed but with no substitution effect.[94,95] It is generally believed that the aryl radicals, generated in situ from the corresponding diazonium salts, are the active species that cause the DNA cleavage[94,95] and are responsible for their genotoxicity.[96] The exact pathway leading to the aryl radicals from the aryldiazonium ions in aqueous solution is still not very clear; however, both an inner-sphere and an outer-sphere electron transfer mechanisms are commonly considered (Scheme 1-11).[97-99] The inner-sphere path involves no apparent reductant but an electron donor (Nu^-) with high oxidation potentials (e.g., ^-OH), which adds to the electrophilic diazonium ion ($Ar\text{-}N_2^+$) and forms a transient species **1.75** of Ar-N=N-Nu(OH). It then either directly dissociates in a homolytic manner to produce the corresponding aryl radical Ar• along with the hydroxyl radical HO•, or reacts further in its anionic form **1.89** with another molecule of the diazonium ion to form a dimer **1.90**, still affording the same Ar• upon the loss of an arylazoxy radical **1.78** and N_2. The outer-sphere mechanism would apply if there exists an appropriate and readily oxidizible (by the diazonium ion) reductant, which could directly transfer an electron to the diazonium ion resulting in the formation of aryl diazenyl radical Ar-N=N• (**1.79**) that further decomposes to the Ar• upon the loss of N_2.

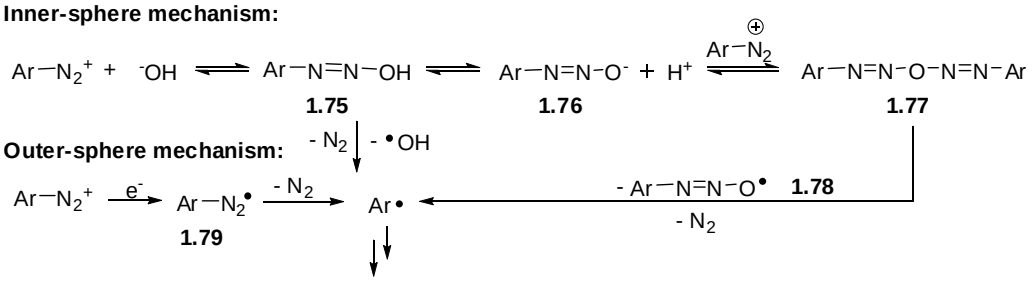

Scheme 1-11. Two mechanisms for the formation of aryl radicals from aryldiazonium salts.

Early model studies by Stock and co-workers on reactions of aryldiazonium salts with the purine units of DNA such as adenine, guanine and their derivatives revealed details on how the diazo compounds may interact with DNA.[100,101] Adenine (**1.80a**) and its derivates such as adenosine (**1.80b**) and 5'-adenylic acid (**1.80c**) react readily with aryldiazonium salts under basic conditions, and the corresponding purine-based C6-triazene **1.81a–c** were obtained as the initial and isolated products (Scheme 1-12).[100] The triazenes (**1.81a** as an example) decomposed either quickly at room temperature under acidic conditions (pH 3) by following the typical acid-catalyzed triazene degradation mechanism, or very slowly (3 days) even at elevated temperature (60–100 °C) under basic conditions (pH 10) and yielded C8-aryladenines **1.90** via a free radical mechanism. The free-radical mechanism, however, was proposed to involve initially a heterolytic and acid-catalyzed cleavage of the triazene **1.81a** leading back to the adenine (**1.80a**) and the aryl diazonium ion **1.83**. The latter could exist in equilibrium with **1.82** and **1.84** that eventually lead to the aryl radicals **1.86** and **1.87** through the aforementioned inner-sphere mechanism. Further radical substitution and hydrogen abstraction would give the final C8-arylated product **1.89** causing the irreversible DNA damage.

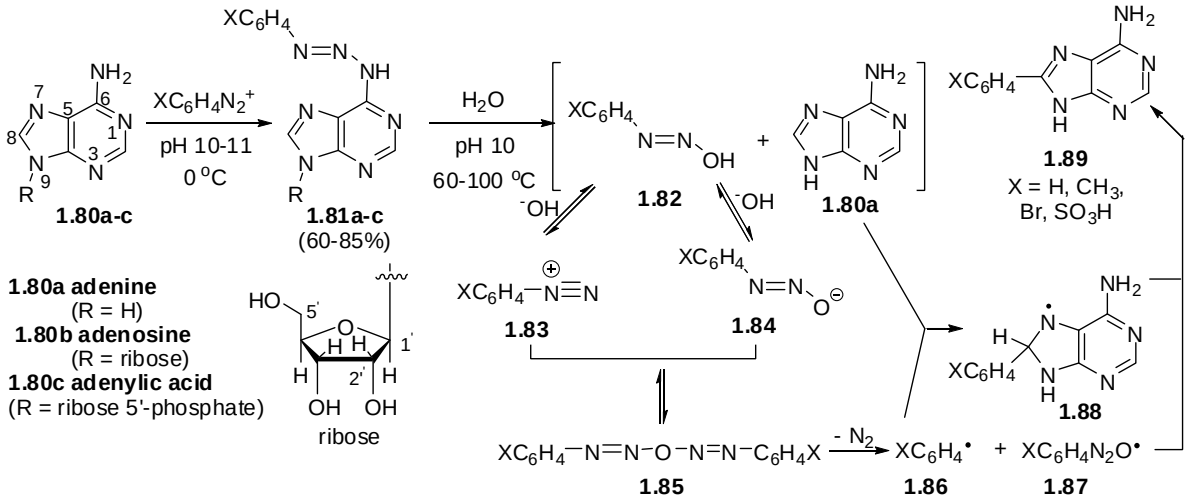

Scheme 1-12. Stock's proposed mechanism for reactions of aryldiazonium ions with adenines.

On the other hand, guanine (**1.90a**) and its derivatives such as guanosine (**1.90b**) and 5'-guanylic acid (**1.90c**) demonstrated more complex results when reacting with aryldiazonium salts at pH 10–11 (Scheme 1-13). The corresponding DNA cleavage mechanism, however, was believed to still follow the same radical pathway involving triazene intermediates (Scheme 1-12).[101] Guanine (**1.90a**) led to quick (15 min) formation of C8-arylazoguanines **1.91** at low temperature (0 °C), which could survive both very acidic (pH 1) and harsh basic conditions (pH 10, 24 hr, 90–100 °C), yet it was easily reduced to the corresponding amines of **1.92** and **1.93**. Even at slightly higher temperature (25 °C), guanosine (**1.90b**) still reacted much more slowly (24 hr) with the diazonium salts than guanine (**1.90a**), but in this case the C8-arylguanosines **1.94** were obtained as the final product with concurrent production of N_2. The 5'-guanylic acid (**1.90c**) reacted even more slowly with the diazonium salts than **1.90b**, and under the same conditions (24 hr, 25 °C) it only afforded the C2-triazenes **1.95** in low yield. Heating of the reaction, however, caused radical arylation at C8 to occur to a certain extent to generate **1.96** instead. The observed difference in the reactivity among guanine (**1.90a**) and its derivatives **1.90b/c**, as well as the adenines **1.80a**–**c**, were explained in terms of the

relative nucleophilicities of the C6 (of **1.80**) and C2 (of **1.90**) amino groups, and the relative tendency to undergo an electrophilic reaction at the C8 positions of such purines, which would be significantly retarded due to unfavorable polar (inductive) and steric effects if a sugar such as ribose and ribose-5'-phosphate is present at the adjacent N9.[101] A later study also showed that 4-carbamoyl-benzenediazonium chloride can form a C2-triazene with the deoxyguanine bases of DNA (i.e., dGMP, deoxyguanosine monophosphate), whose structure was confirmed by both NMR and mass spectrometry.[102] Spectroscopic evidence for the involvement of a DNA-triazene adduct, both in vitro and in vivo, through the reaction of benzenediazonium ion (formed in situ from *N*-nitroso-*N*-methylaniline) and DNA has also been reported.[103]

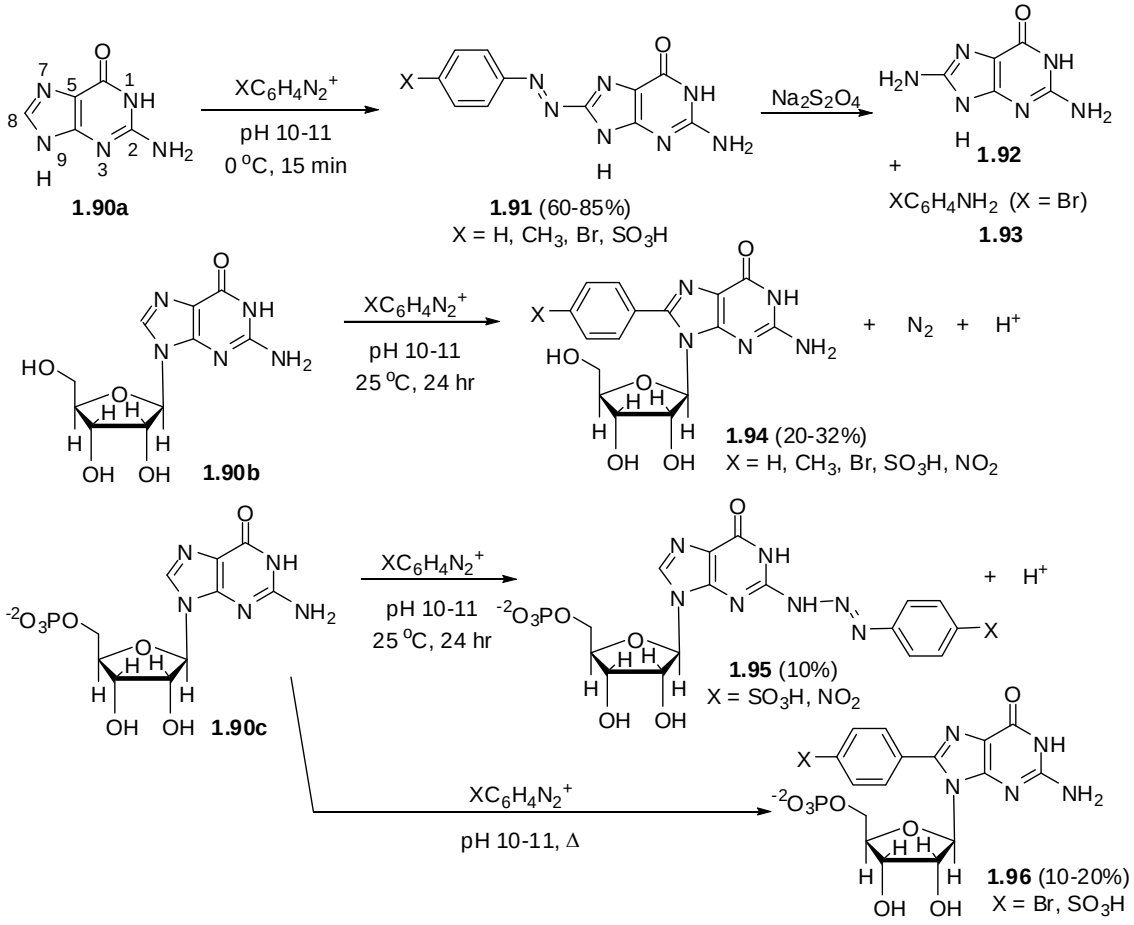

Scheme 1-13. Product distribution of reactions between aryldiazonium ions and guanines.

Further in vitro and in vivo studies on the reactions of arenediazonium ions *p*-X-$C_6H_5N_2^+$ (**1.97**, X = CH_3, CH_2OH, CH_2OCH_3, CO_2H) with DNA bases, nucleosides, DNAs and cells by the Gannett group agreed well with Stock's proposal (Scheme 1-12) in general, but with some new discoveries (Scheme 1-14).[99,104-106] Both aryldiazonium ions **1.97** and the corresponding aryl radicals **1.98** generated upon either chemical or metabolic reduction of **1.97** are genotoxic and mutagenic. The dominant bioactive species, however, is determined by the reduction potential of the diazonium ion, i.e. a diazonium ion with a low reduction potential (difficult to reduce) is more important than the corresponding radical and vice versa.[104] Reaction of the aryldiazonium ions with adenine and/or guanine leads to the formation of either isolated or detectable triazenes **1.98**, which decompose at both physiological and elevated temperatures (25–75 °C) in weak basic (pH 7.4) aqueous buffers.[105] Triazene decomposition leads to not only the aryl radicals but also reactive hydroxyl radicals, as characterized by their ESR (electron spin resonance) spectra.[99,104-106] The possibility that these concurrent oxygen radicals participate in the DNA damage was ruled out based on observations from competitive inhibition experiments.[106] The aryl radicals, most likely generated by concurrent multiple routes, including but not limited to stepwise acid-catalyzed decomposition of triazenes (**1.99** to **1.98** via **1.103**), homolytic radical cleavage (**1.99** to **1.98** via **1.100**), and direct diazo reduction (**1.97** to **1.98**), then give the corresponding DNA adducts upon arylation at C8 of adenines (cf. **1.102**) and guanines (cf. **1.107**), ultimately resulting in the DNA damage.

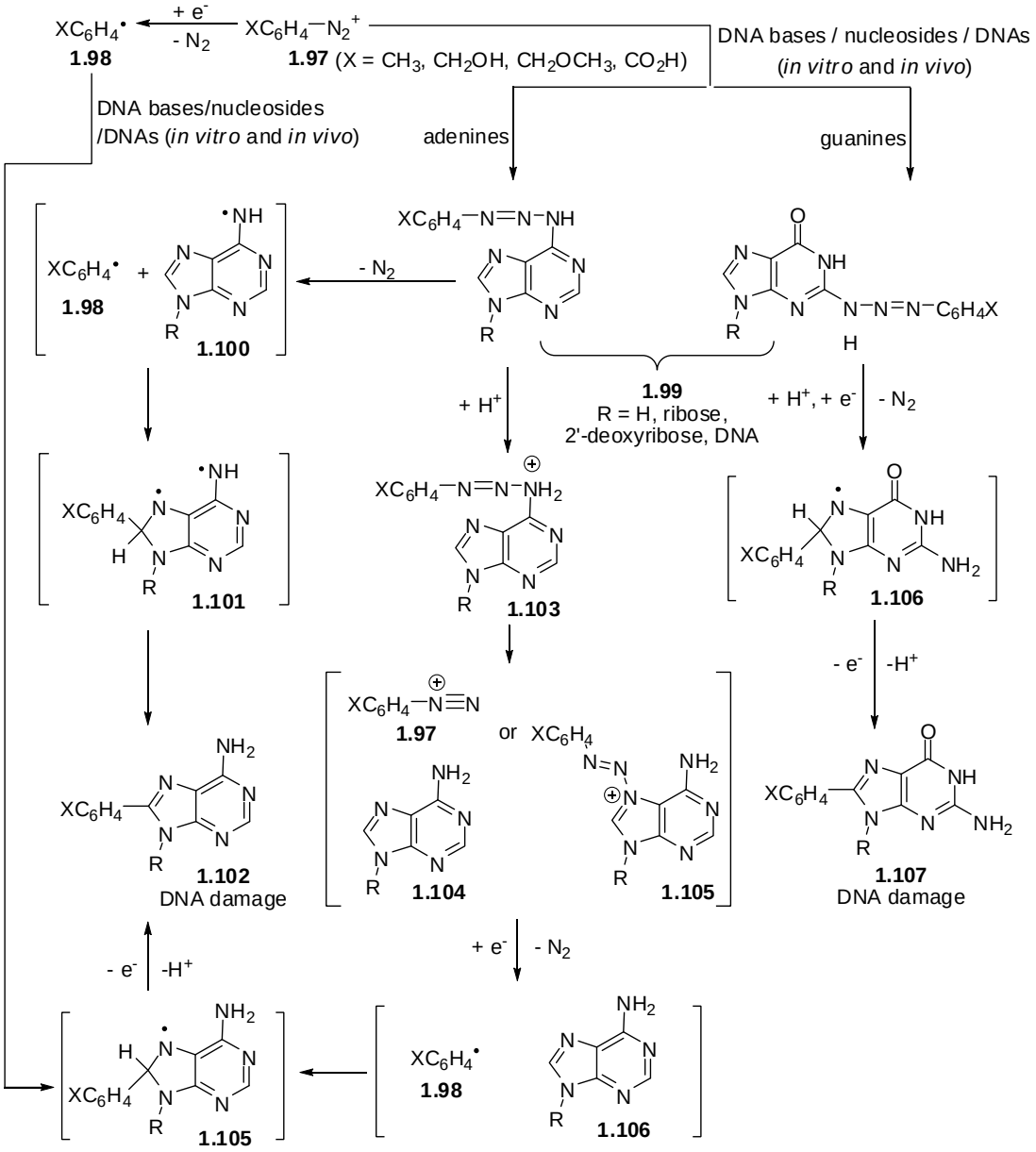

Scheme 1-14. Proposed mechanism by Gannett for DNA damage caused by aryldiazonium ions.

In the meantime, Kikugawa and coworkers carried out a series of biological and mechanistic studies on some mutagenic diazo compounds, most of which are carcinogenic and capable of cleaving single-strand DNA in vitro under physiological conditions. Such examples include 3-diazo-*N*-

nitrosobamethan,[107,108] diazo-*N*-nitrosoetilefrin,[109] *o*- and *p*-diazoquinones,[110-112] fluorene-2-diazonium salt,[113,114] 5-diazouracil,[115] 4-(hydroxymethyl)benzenediazonium salt (**1.54**),[116,117] and 6-diazo-5-oxo-*L*-norleucine (DON, **1.6a**).[118] The observed biological activities were not affected by molecular oxygen but inhibited by common hydrogen donors, nucleophiles and reductants such as alcohols, phenols, azide and thiols,[114,115,118] amino acids and proteins,[119] even unsaturated fatty acids and lipoprotein.[120] Despite the structural diversity involved in these diazo compounds, their mode-of-action was confirmed by ESR experiments to rely on the carbon-centered radicals generated in situ from the corresponding diazo compounds but not the concurrently produced oxygen radicals, consistent with Gannett's observations. The carbon radicals would react with not only purines (free or within DNA) still at C8 but also pyrimidine bases (free or within DNA). In addition, diazo-initiated bond breakage of phosphodiester of DNA was also observed and attributed to the action of the carbon radicals as well.

Soon after the structural revision of the kinamycins from the *N*-cyanobenzo[*b*]carbazole to the diazobenzo[*b*]fluorenes, Jebaratnam's group reported some initial evidence suggesting the possible diazo involvement in the bioactivity of kinamycins when 9-diazofluorene (**1.109**) was used as a simple model compound.[121] It was found that **1.109** did not induce any DNA cleavage either alone (no cleavage at pH 4–7 and cleavage observed at pH < 4 was caused by acid rather than **1.109**) or in the presence of Cu_2Cl_2 (i.e., Cu^+). However, in the presence of an oxidant such as cupric acetate $Cu(OAc)_2$, **1.109** led to successful DNA cleavage while the Cu(II) salt itself did not cleave DNA (Scheme 1-15). These results were rationalized as an one-electron oxidation of **1.109** with Cu^{2+} followed by loss of N_2 to produce a corresponding carbon radical **1.110**, which was suggested to be the active species that initiates DNA cleavage, likely by hydrogen atom abstraction from DNA.[121]

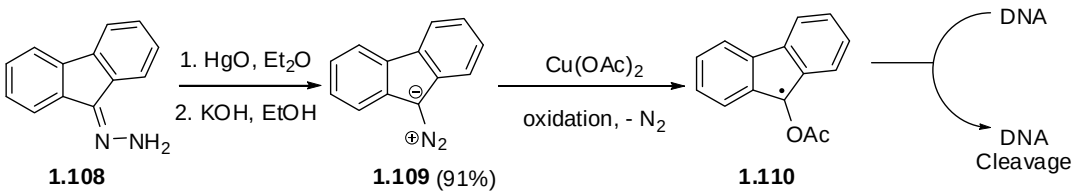

Scheme 1-15. Proposed mode-of-action involving the diazo moiety of the kinamycin model compound 9-diazofluorene (**1.109**).

A few years later, Zaleski and co-workers reported that bis(9-diazo-4,5-diazafluorene)copper(II) nitrate (**1.111**, X = NO_3^-) was able to cleave DNA upon exposure to visible light ($\lambda \geq 455$ nm) under anaerobic conditions in near-neutral buffers (Scheme 1-16).[122] Interestingly, the corresponding free ligand **1.112**, even though containing the diazo group, was found to be significantly less effective in DNA cleavage under the same conditions (Scheme 1-16). It was proposed that photolysis of the diazo species led to N_2 expulsion and formation of the corresponding radical cation **1.113** (from **1.111**) or carbene **1.114** (from **1.112**) that initiates DNA damage.[123]

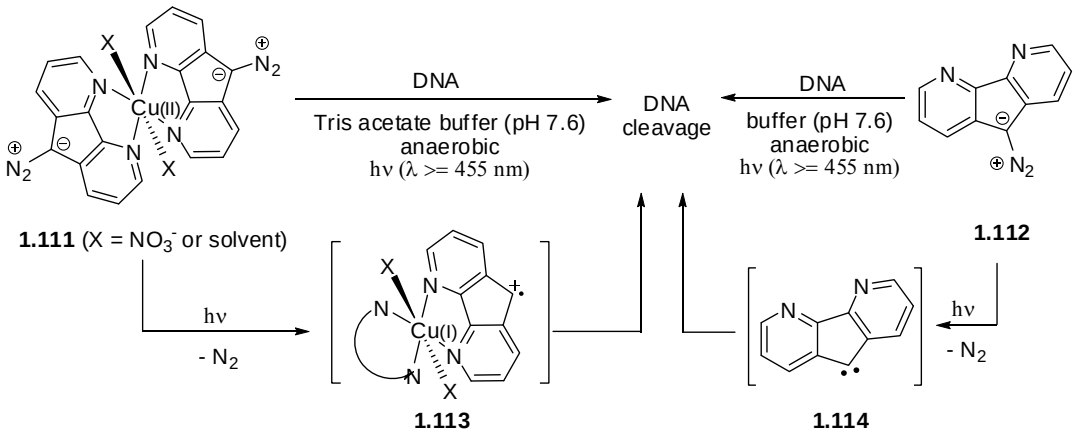

Scheme 1-16. Photolytic DNA cleavage by diazofluorene-type compounds.

The involvement of either carbon radical, radical cation or carbene as diazo-derived active intermediates in the above two mechanisms, presented to have relevance to the possible mode-of-action of the kinamycins, resembles the previous knowledge of how the simple diazo(nium) species interact with DNA. However, both Jebaratnam's and Zaleski's hypotheses require the mandatory presence of either an oxidant (Cu^{2+} in both cases) or the condition of photolysis to facilitate the transformation of the kinamycin-like diazo compound to the active species. Such artificial conditions are barely available (i.e., Cu^{2+} is less commonly available in biosystems as oxidant) or even unnecessary (e.g., light) in the actual biological systems where the bioactivities of kinamycins were observed. Therefore, both mechanisms (particularly the Zaleski model) are of questionable value. These considerations led to a logical suggestion by the Dmitrienko group that the diazo moieties of kinamycins are probably diazonium-like and electrophilic to a significant extent, and that similar chemical behaviour analogous to that exhibited by aryl diazonium ion as described above may occur with these natural diazobenzo[*a*]fluorenes and diazobenzo[*b*]fluorenes.[80,124] Reactivities of diazonium and diazo species with various organic and inorganic nucleophiles have been well studied and documented ever since the discovery of the first diazo compound in 1858.[97,125-128] Among the numerous examples, reactions such as azo coupling, thiol-addition and amine-addition are of particular importance, since such reactions might be involved in the bioactivity and modes-of-action of the diazo compounds such as the kinamycins. Experimental and computational evidence from the Dmitrienko lab, which are to be described in the following section, are in good agreement with such a proposal.

1.4.2.3 Mechanistic Studies of Kinamycins in the Dmitrienko Lab

It is known in the literature that o*rtho*- (**1.115**) and *para*-hydroxy aryldiazonium salts can be readily deprotonated even under acidic conditions to produce the corresponding *o*- (**1.117**) and *p*-

quinonediazides (Figure 1-5).[80] X-ray crystallographic data of some simple diazo compounds (Figure 1-5) clearly indicate a concomitant decrease of the bond order for the C-N linkage with the increasing N-N triple bond character in the order of diazoketone **1.118** < substituted *o*-quinonediazide **1.119** < substituted *p*-quinonediazide **1.120** < diazonium salt **1.121**, suggesting that the chemical reactivity of the diazo group within quinonediazides would typically fall in between those from diazoketones and aryl diazonium salts. Quinodiazides can undergo azo coupling with phenols in both weakly acidic and alkaline solution, but *ortho*-quinodiazides are less reactive than their *para*-isomers and even less so than diazonium salts for such reactions, which may require the use of strong and activated nucleophiles. The presence of electron withdrawing groups on the quinodiazide nucleus would accelerate the corresponding azo coupling reactions, since the diazonium character is enhanced when the negative charge on the diazo carbon is stabilized by the electron withdrawing factor(s). Moreover, DNA cleavage by quinonediazides has also been reported.[110-112] In this regard, kinamycins such as the isoprekinamycin (**1.5**) could be recognized as a structure incorporating a 1,2-naphthoquinone-1-diazide (**1.122**), which may demonstrate similar chemical properties and behaviour as mentioned above. A likely correlation between the biological activities of kinamycins and their corresponding diazo reactivities should be considered.

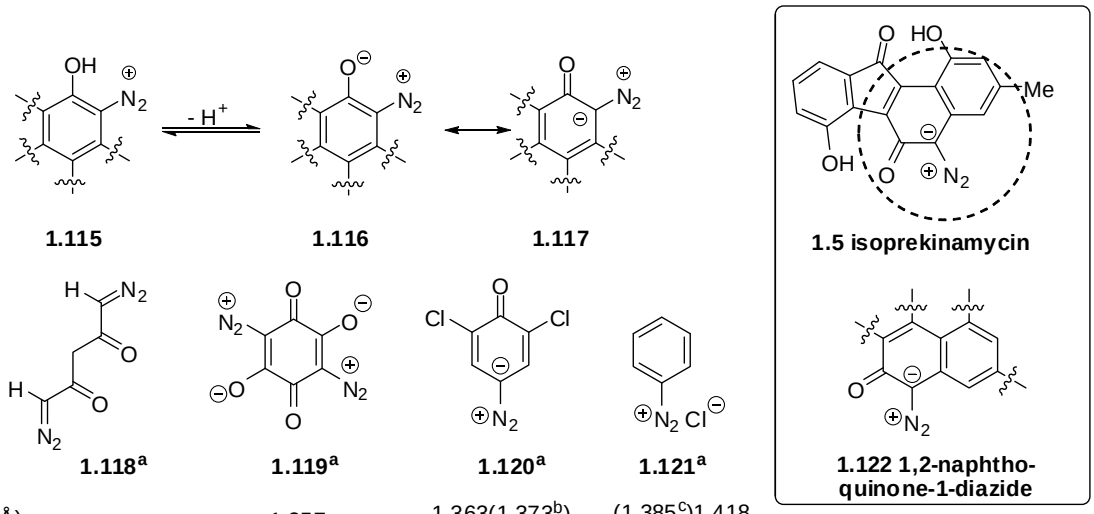

	1.118[a]	1.119[a]	1.120[a]	1.121[a]
$d_{C\text{-}N}$ (Å)	1.313	1.357	1.363(1.373[b])	(1.385[c])1.418
$d_{N\text{-}N}$ (Å)	1.114	1.106	1.104(1.095[b])	(1.099[c])1.093

a. Bond lengths were measured directly from the corresponding .cif file of the compound deposited in the CCDC database; b. Two different geometries of **1.120** co-exist in the same crystal; c.**1.121** co-crystallized with acetic acid.

Figure 1-5. Properties of the diazo group within some diazo compounds.

In 2002, Laufer from the Dmitrienko lab synthesized a model compound **1.123** (Scheme 1-17), possessing the same benzo[*a*]fluorene skeleton and the essential *o*-quinonediazide moiety as in the natural isoprekinamycin (**1.5**) but lacking its A-ring and D-ring substituents.[80,124] Attempts to rearrange the benzo[*a*]fluorene frame of **1.123** to the isomeric benzo[*b*]fluorene of **1.124** failed under both basic and acidic conditions (Scheme 1-17), but **1.123** survived the acidic conditions intact and it was converted to a hydrodediazoniation product **1.127** exclusively under the basic conditions. This led to the conclusion that the hypothetical interconversion equilibrium between the diazobenzo[*a*]fluorene and the diazobenzo[*b*]fluorene structures (Scheme 1-6a), if it occurs in vivo, would be an enzyme-catalyzed rather than a spontaneous chemical transformation. In addition, the known base-induced hydrodediazoniation of aryldiazonium species[129,130] would suggest a plausible mechanism (Scheme 1-17) for the conversion of **1.123** to **1.127**. A diazohydroxide intermediate **1.125** may be obtained upon nucleophilic attack of the diazo moiety of **1.123** by the HO^-, which

subsequently decomposes to an aryl radical **1.126** that undergoes hydrogen abstraction from a solvent molecule (THF or EtOH) to afford **1.127**. Such an observation would suggest substantial diazonium-like character of the diazo moiety within isoprekinamycin (**1.5**).

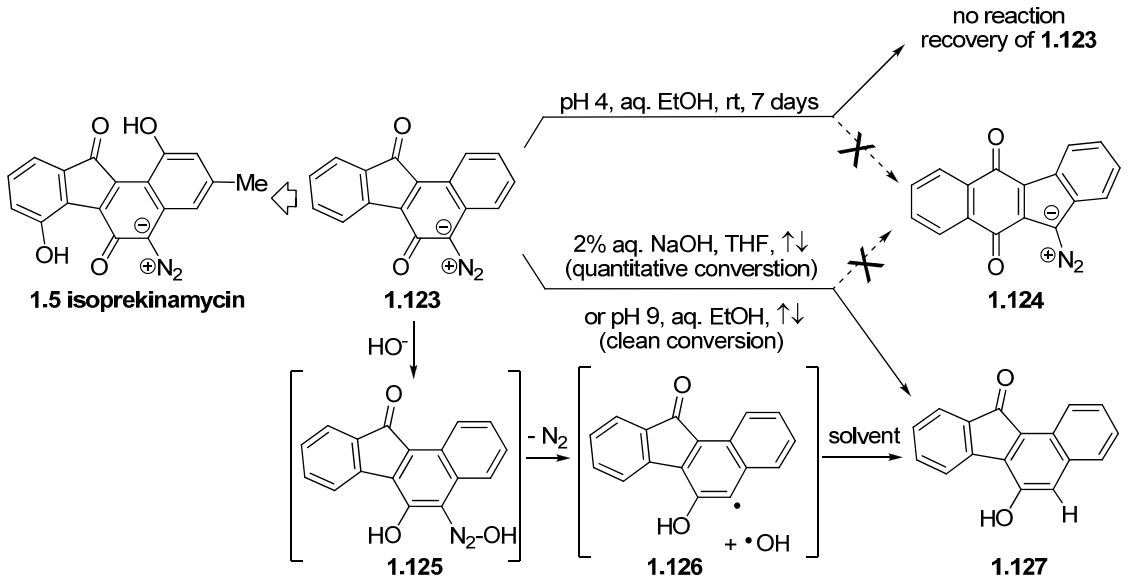

Scheme 1-17. Attempted rearrangement of an isoprekinamycin model compound **1.123** to the corresponding diazobenzo[*b*]fluorene structure **1.124**.

Further proof of the diazonium ion character within kinamycins was obtained when isoprekinamycin (**1.5**) and **1.123** were subjected to azo-coupling reaction with β-naphthol (**1.128**) under very mild basic conditions (Scheme 1-18).[80,124] When reacted individually with **1.128**, **1.5** afforded a 1:2 mixture of the corresponding azo-coupling product **1.129** and a hydrodediazoniation product **1.130** (Scheme 1-18a), while **1.123** gave only the azo-coupling product **1.134a** under the same conditions (Scheme 1-18b). This observed difference in reaction outcome would indicate that **1.5**, likely due to its higher diazonium (electrophilic) ion character, has a higher reactivity than **1.123**. Naphthoxide **1.131** generated upon deprotonation of **1.128** is an ambident nucleophile with both the C2-oxygen and the C1-carbon available for further reactions. According to the "hard and soft acids

and bases" (HSAB) theory,[131] the C2-oxygen is a hard nucleophile (Lewis base) while the C1-carbon is a soft one, since the former bears more negative charge than the latter. The terminal nitrogen of the diazo moiety in **1.5**, on the other hand, bears significant positive charge, which makes it a hard electrophile (Lewis acid), as indicated by its LUMO coefficients obtained from MO calculation. So when **1.5** reacts with **1.131**, the competition between a hard-hard interaction (path A, Scheme 1-18a) and a soft-hard interaction (path B, Scheme 1-18a) is expected. Since hard acid prefers to react with hard base and vise versa, preference of path A is predicted by the HSAB theory and the corresponding product **1.132** then may undergo a hydrodediazoniation to afford **1.130** as the final major product, likely via the mechanism outlined in Scheme 1-17. On the contrary, theoretical calculation by means of NBO (natural bond orbital) population analysis indicated that the terminal nitrogen of the diazo group in **1.123** is significantly less positive and therefore softer than that in **1.5**.[80] This prediction is consistent with the result that the reaction of **1.123** and **1.128** only led to **1.134a** as the only/major product (Scheme 1-18b), which should be derived from the preferred soft-soft interaction (path B) in this case. When a 1:1 mixture of **1.5** and **1.123** was subjected to the azo coupling conditions, TLC (thin layer chromatography) and ^{1}H-NMR evidence indicated a significantly preferential consumption of **1.5** over **1.123**. This observation suggests a strong correlation between the diazonium ion characters of kinamycins and their reactivities. Another parallel competition experiment was carried out by simultaneously treating **1.5** and **1.123** with **1.128** under exactly identical and strictly controlled conditions but in separate flasks, and both reactions were monitored until the complete consumption of the diazo compounds (Scheme 1-18c). Isoprekinamycin (**1.5**) was found to be much more reactive than its simpler analogue **1.123**, as demonstrated by the shorter reaction time and lower reaction temperature needed to complete the azo-coupling. Moreover, unpublished results from Laufer also indicated that under the same conditions, isoprekinamycin (**1.5**) reacted with guanosine triacetate and kinamycin D (**1.1d**) reacted with β-

naphthol (**1.128**).[80] Complete consumption of the kinamycins due to reactions with the nucleophiles were observed in both cases.

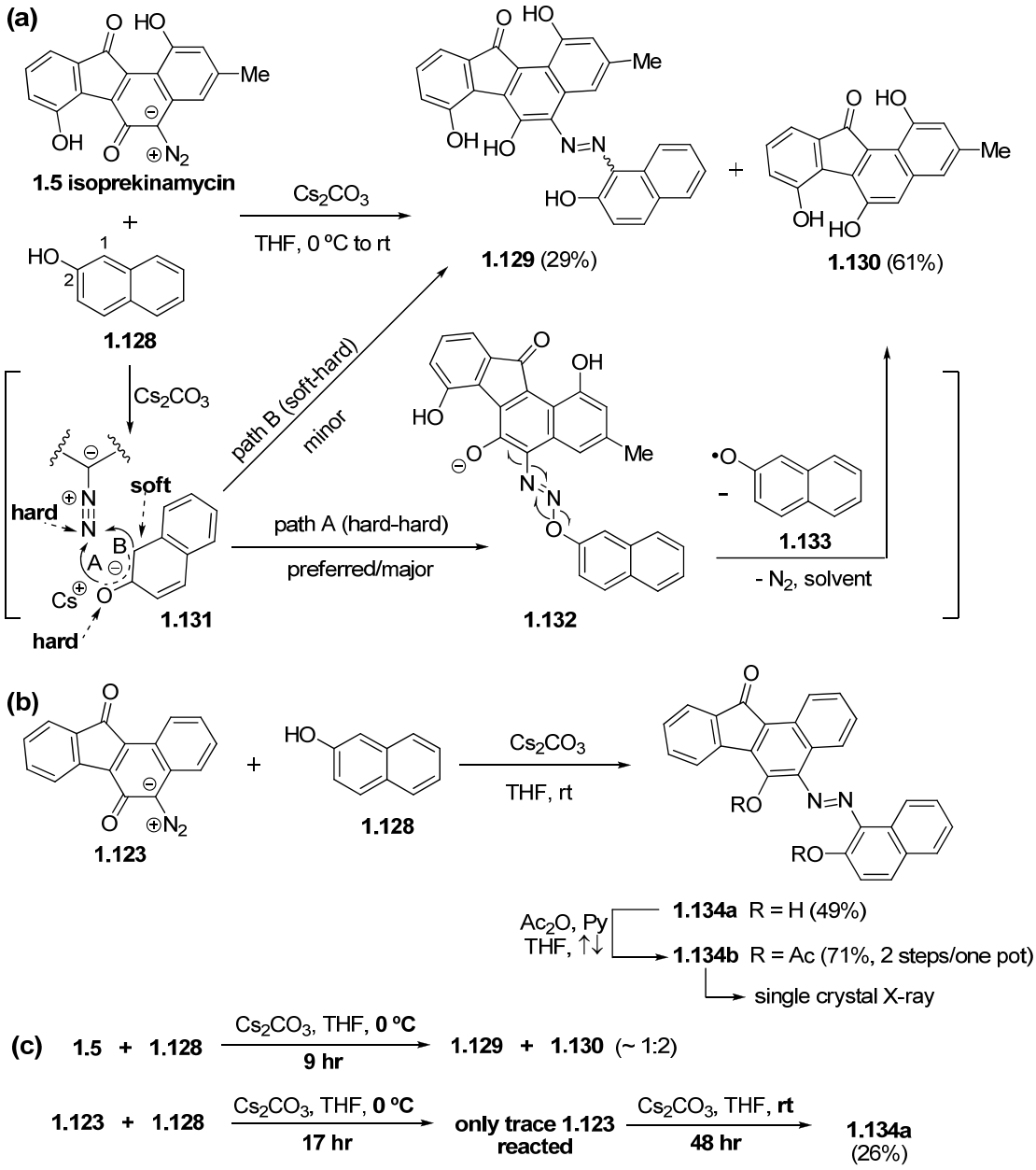

Scheme 1-18. Comparison of diazo reactivity and electrophilicity of isoprekinamycin (**1.5**) and model compound **1.123** via azo-coupling reactions with β-naphthol (**1.128**).

To account for the observed difference in chemical behaviour of isoprekinamycin (**1.5**) and the model compound **1.123** from a structural point of view, Laufer also carried out extensive ab initio MO (molecular orbital) calculations on kinamycins and related structures,[80,124] with a focus on the diazo IR stretching frequency and the N-N bond length. Such properties were found to be a suitable indication for the corresponding diazonium ion character. Comparison of the computational results with available experimental values showed satisfying consistency, and a clear tendency of increasing diazo IR frequency and diazonium ion character with concurrent decreasing N-N bond length (Table 1-2), in the order of 9-diazofluorene (**1.109**) < 2,1-napthoquinodiazide (**1.122**) < isoprekinamycin model **1.123** < isoprekinamycin (**1.5**) < kinamycin B (**1.1b**) < lomaiviticin A model **1.138** < $PhN_2^+Cl^-$ (**1.121**), matches roughly the increasing biological activities in essentially the same order, i.e. isoprekinamycin (**1.5**) < kinamycin B (**1.1b**) < lomaiviticin A (**1.11a**). It is clear, however, that many factors other than diazonium ion character may also influence the biological activity of kinamycins and their analogues.

Table 1-2. Calculated diazo frequencies and N-N bond lengths of various kinamycin structures.[a]

Compound	Calculated $\nu_{N\equiv N}$ (cm^{-1})	Experimental $\nu_{N\equiv N}$ (cm^{-1})	Calculated $d_{N\equiv N}$ (Å)	Experimental $d_{N\equiv N}$ (Å)
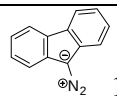 **1.109**	1906	2000 (KBr)	1.133	1.126
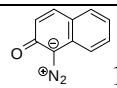 **1.122**	2056		1.111	
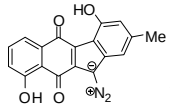 **1.4**	2058	2119 (film)	1.111	
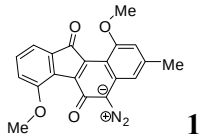 **1.135**	2079	2113 (CH_2Cl_2 solution)	1.109	
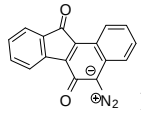 **1.123**	2087	2105 (film)	1.108	
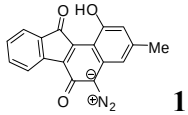 **1.136**	2101		1.107	
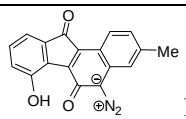 **1.137**	2125		1.105	
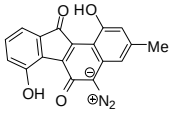 **1.5**	2139	2162 (film)	1.103	1.104
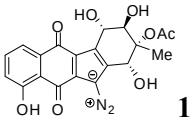 **1.1b**	2188	2155 (KBr)	1.099	**1.1s**: 1.080[b] 1.115[b]
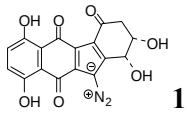 **1.138**	2212		1.097	
$PhN_2^+Cl^-$ **1.121**	2212	2260	1.100	1.099

a. All MO calculations were performed at the RHF/6-31G//6-31G level. Although the calculated absolute IR frequencies for diazo groups may differ significantly from the experimental values, the computed difference in IR frequency ($\Delta\nu$) as a result of structural change matches the observed experimental $\Delta\nu$ fairly well. For example, experimental $\Delta\nu$ (**1.5 - 1.123**) = 57 cm^{-1}, and the corresponding computed $\Delta\nu$ (**1.5 - 1.123**) = 52 cm^{-1};
b. Two different diazo bond lengths co-exist in the crystal of **1.1s** (refer to Scheme 1-2 for structure of **1.1s**).

The diazonium ion character of isoprekinamycin (**1.5**) is significantly enhanced by not only the electron-withdrawing keto group on its B-ring, as evident by comparison of the diazo IR frequency of **1.123** and **1.5** with that of **1.122**, but also the intramolecular hydrogen bonding (H-bonding) interactions, as evident by comparison of diazo IR of **1.123**, **1.136**, **1.137** and **1.5**.[80,124] The presence of strong intramolecular H-bond(s) within natural kinamycins, both the diazobenzo[*a*]- and diazobenzo[*b*]fluorene type, is well known since all A-ring and D-ring phenolic protons of kinamycins have characteristic down-field NMR chemical shifts of ca. 11–13 ppm.[5,9,76] As a comparison, typical phenolic protons without inter-/intramolecular H-bonding interactions exhibit chemical shifts of only ca. 4–7.5 ppm.[132] Therefore, the diazonium ion character of **1.5** is greatly enhanced by the presence of double intramolecular H-bonding interactions (Scheme 1-19), which delocalize the negative charge from the diazo carbon in the quinonediazide structure and stabilize the negative charge on the oxygen atom as in the phenolic diazonium form.[80,124] This theoretical model provided a reasonable rationale for the observed difference in reactivities between isoprekinamycin (**1.5**) and the analogue **1.123**. The observed much lower diazo IR frequencies of isoprekinamycin diacetate **1.5a** (2119 cm^{-1})[5] and isoprekinamycin dimethyl ether **1.135** (2113 cm^{-1}) than that of the mother compound **1.5** (2162 cm^{-1}),[5] both of which lack the intramolecular H-bonding interactions, are entirely consistent with the discussion above.

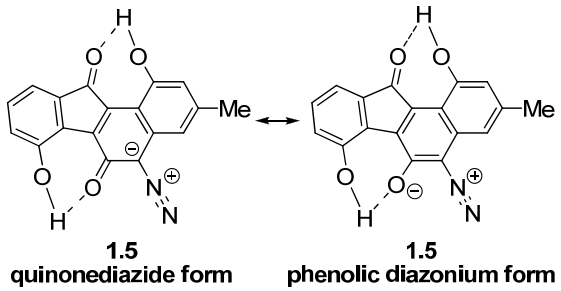

Scheme 1-19. Intramolecular H-bonding model for isoprekinamycin (**1.5**).

The significant structural influence on the diazonium ion character of the diazo moiety within kinamycins, as indicated by the above structure-activity studies, led the Dmitrienko group to propose, at the time, that kinamycins (and lomaiviticins) may react with DNA in a manner similar to that of the aryl diazonium salts as discussed in section 1.4.2.2.[80] The purine units of DNA (adenine-based **1.139** and guanine-based **1.140**) may react with the diazo group of kinamycins to form the corresponding triazenes (**1.141** and **1.142**) initially (Scheme 1-20a), followed by dediazotization with loss of N_2 (**1.141** as an example) to yield the kinamycin-derived radical **1.143** and purine-derived radical **1.144**. Such radicals can react further through complex sequences, such as possible depurination via **1.145** and C8-arylation to form **1.150**, ultimately leading to DNA damage. It was also realized that the structural features such as in the case of isoprekinamycin (**1.5**) that enhance diazonium ion character and, hence, the electrophilicity of the diazo group, also enhance the electron affinity. This might favour a reductive pathway to radical **1.151** via the electron transfer in vivo (Scheme 1-20b).[80]

The speculations concerning the mechanism of action of the kinamycins outlined above represent the state of thinking in the field when the present research project was initiated. Since then other speculations based on model chemical studies as well as biochemical and whole cell experiments have provided additional thoughts on the subject. These more recent results are presented and discussed in Chapter 4 of this thesis.

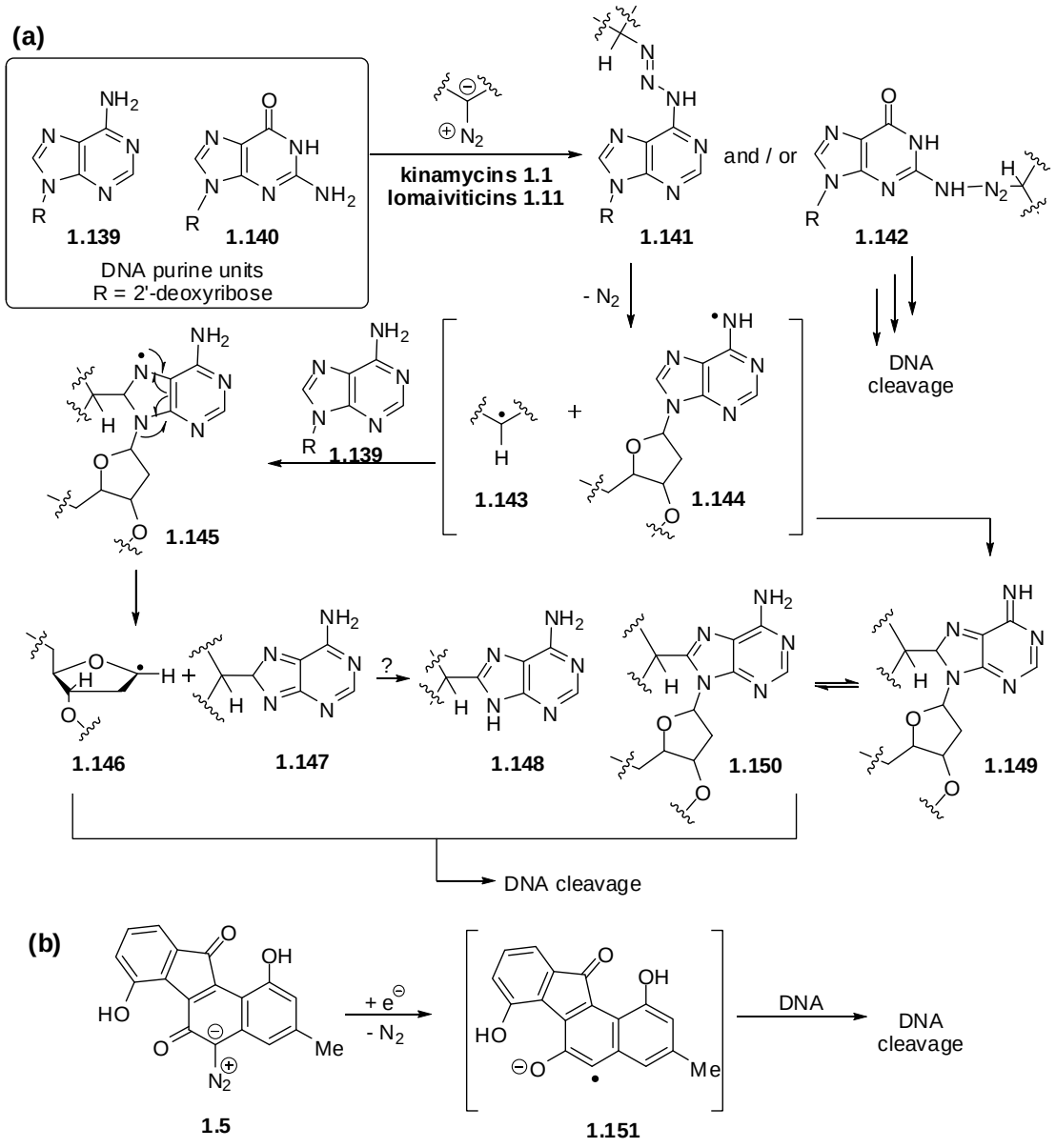

Scheme 1-20. Possible mechanisms proposed by the Dmitrienko group for DNA cleavage by kinamycins (a) via triazene intermediates; (b) through diazo reduction.

1.5 Reported Syntheses of Kinamycins and Related Compounds

Natural products such as the kinamycins possessing unique structural features and potent biological activities are ideal targets for synthetic organic chemists. However, the isolation and characterization of kinamycins as the *N*-cyanobenzo[*b*]carbazole in the early 1970s did not trigger enough synthetic interest in this type of compounds for almost twenty years. Efforts towards the synthesis of kinamycins started to appear beginning in 1990, when the Dmitrienko group first prepared some *N*-cyanoindoles as model compounds for kinamycins,[73] still considered to be *N*-cyanobenzo[*b*]carbazoles at the time. The structural revision of kinamycins in 1994 revealed the presence of the very rare naturally-occurring benzo[*b*]fluorene skeleton and diazo moiety, which evoked significant interest in these unusual natural antibiotics. Since then, a number of related synthetic studies have been reported. The major details of these synthetic results will be discussed in Chapters 2 and 3, which present the synthetic efforts towards the kinamycins from this project. Only literature studies prior to the beginning of this thesis project will be introduced in the following section.

1.5.1 Synthetic Efforts towards the *N*-cyanobenzo[*b*]carbazole System

Two major synthetic works towards the *N*-cyanobenzo[*b*]carbazole structure of kinamycins, one by Echavarren (1993)[74] and one by Dmitrienko (1994)[22] have already been briefly mentioned earlier (Scheme 1-2, Section 1.3.2.1). Other examples of the synthesis of the benzo[*b*]carbazoles include reports by Dmitrienko (1990),[73] Sugimone (1991),[133] Murphy (1992),[134] and more recently by Xu (2006).[135] Although the *N*-cyanobenzo[*b*]carbazole structure no longer applies and most synthetic efforts were redirected towards the diazobenzo[*b*]fluorene of kinamycins since 1994, the importance of the former structure can not be completely ignored. The appropriate *N*-cyanobenzo[*b*]carbazoles may serve as the isomeric species of the corresponding kinamycins for the studies of mechanism of

action, and benzo[*b*]carbazole compounds were found to possess versatile and significant biological activities of their own.[136-138]

1.5.2 Synthetic Efforts towards the Diazobenzo[*b*]- and Diazobenzo[*a*]fluorenes

The very rare structure of benzo[*b*]fluorene within natural products was first discovered with stealthin A (**1.15a**) and B (**1.15b**) in 1992,[55] and the structural revision of kinamycins from *N*-cyanobenzo[*b*]carbazole to diazobenzo[*b*]fluorene in 1994[21,22] further stimulated synthetic interest in kinamycins due to such structural novelty and their biological activities. Prior to the discovery of benzo[*b*]- and benzo[*a*]fluorenes within the natural products, the wide environmental occurrence of such ring systems as natural compounds (not "natural products" by definition) in oil, gasoline and combustion products is well known. There are a few synthetic examples of fluorenes,[139] benzo[*b*]fluorenes[140-143] and benzo[*a*]fluorenes[142,143] in the literature prior to 1990, however, none of these methods has been applied to synthetic efforts towards the kinamycins. Outlined here are some of the known approaches to the benzo[*b*]fluorene structures related to kinamycins that had been developed when the present project began.

In general, retrosynthetic analysis of the generic benzo[*b*]fluorene structure **1.152** of kinamycins would suggest mainly three possible ways of disconnection at B- and/or C-ring as shown in Scheme 1-21, which covers most known syntheses of benzo[*b*]fluorene structures related to the kinamycins:

(i) Disconnection (a) of **1.152** requires the use of a substituted naphthyl compound such as **1.153a** or **1.153b** as the AB-ring precursor and an appropriate aryl species such as **1.154a** or **1.154b** as the corresponding D-ring precursor. Initial cross-coupling or addition reaction of **1.153a** and **1.154a** (or **1.153b** and **1.154b**) would afford the corresponding biaryl product, whose subsequent intramolecular (Friedel-Crafts, anionic/cationic or

metal-catalyzed cross-coupling) cyclization would then lead to the desired fluorene skeleton.

(ii) Disconnection (b) involves a base-induced double condensation between either an *o*-phthalyldicarbonyl species **1.155a** and a substituted 1-indanone **1.156a** or a phthalide **1.155b** and a substituted 1-indenone **1.156b**.

(iii) Disconnection (c) leads to a polyenyne intermediate **1.157** that can undergo a thermal biradical cyclization to form the benzo[*b*]fluorene core, while **1.157** itself could be derived from simple aromatic precursors such as **1.158** and **1.159**.

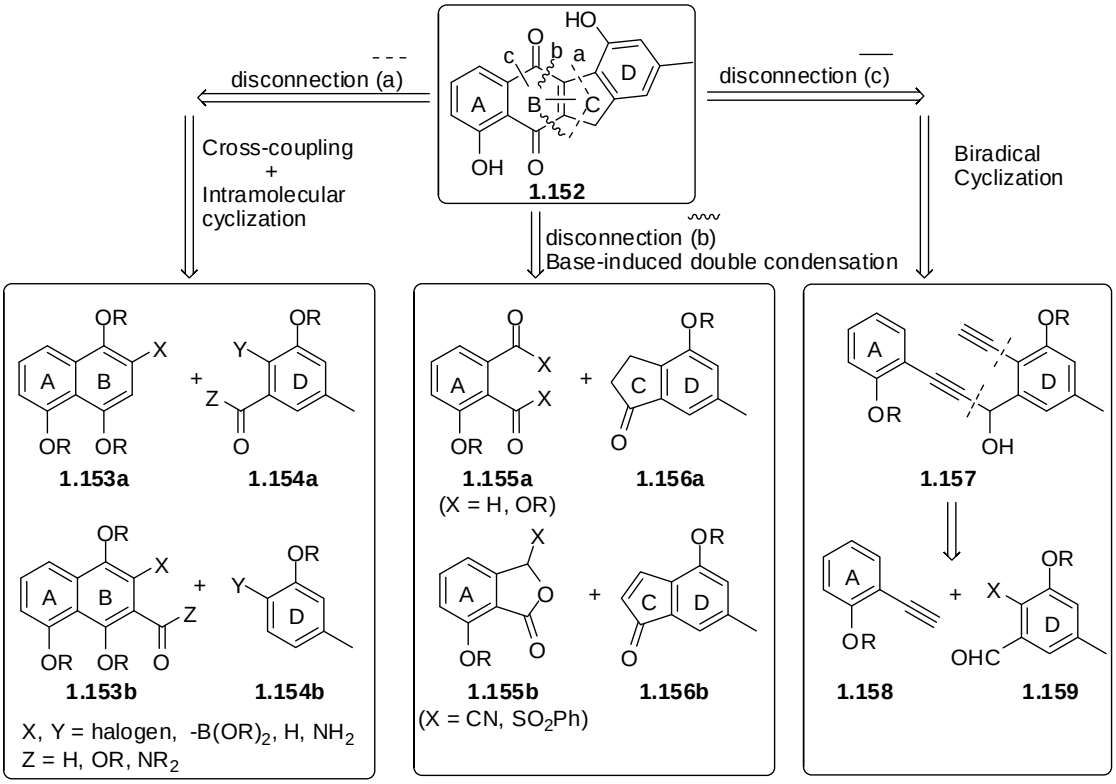

Scheme 1-21. Retrosynthetic analysis of the generic benzo[*b*]fluorene structure **1.152** of kinamycins.

Among all naturally-occurring benzo[*b*]fluorenes, kinobscurinone (**1.16a**) was the first one synthesized. In 1995, Gould first prepared **1.16a** by demethylation and oxidation of tri-*O*-methylkinafluorenone (**1.165**),[56] and the latter was initially and incidentally prepared as a very minor side product from **1.164** through an anionic cyclization also by Gould during his total synthesis of phenanthroviridin aglycon (**1.167**) in early 1990s (Scheme 1-22a).[144,145] Later in 1997 during the total synthesis of stealthin C (**1.15c**), Gould prepared the key intermediate **1.165** more efficiently through an improved anionic cyclization of **1.163b** and an intramolecular Friedel-Crafts cyclization of **1.168** (Scheme 1-22a).[17] Around the same time in 1997, another synthetic route to **1.165** was achieved by the Snieckus group via a Suzuki coupling between **1.169** and **1.170**, the subsequent directed-metalation of **1.171** and cyclization of **1.174** as the key steps (Scheme 1-22b).[146]

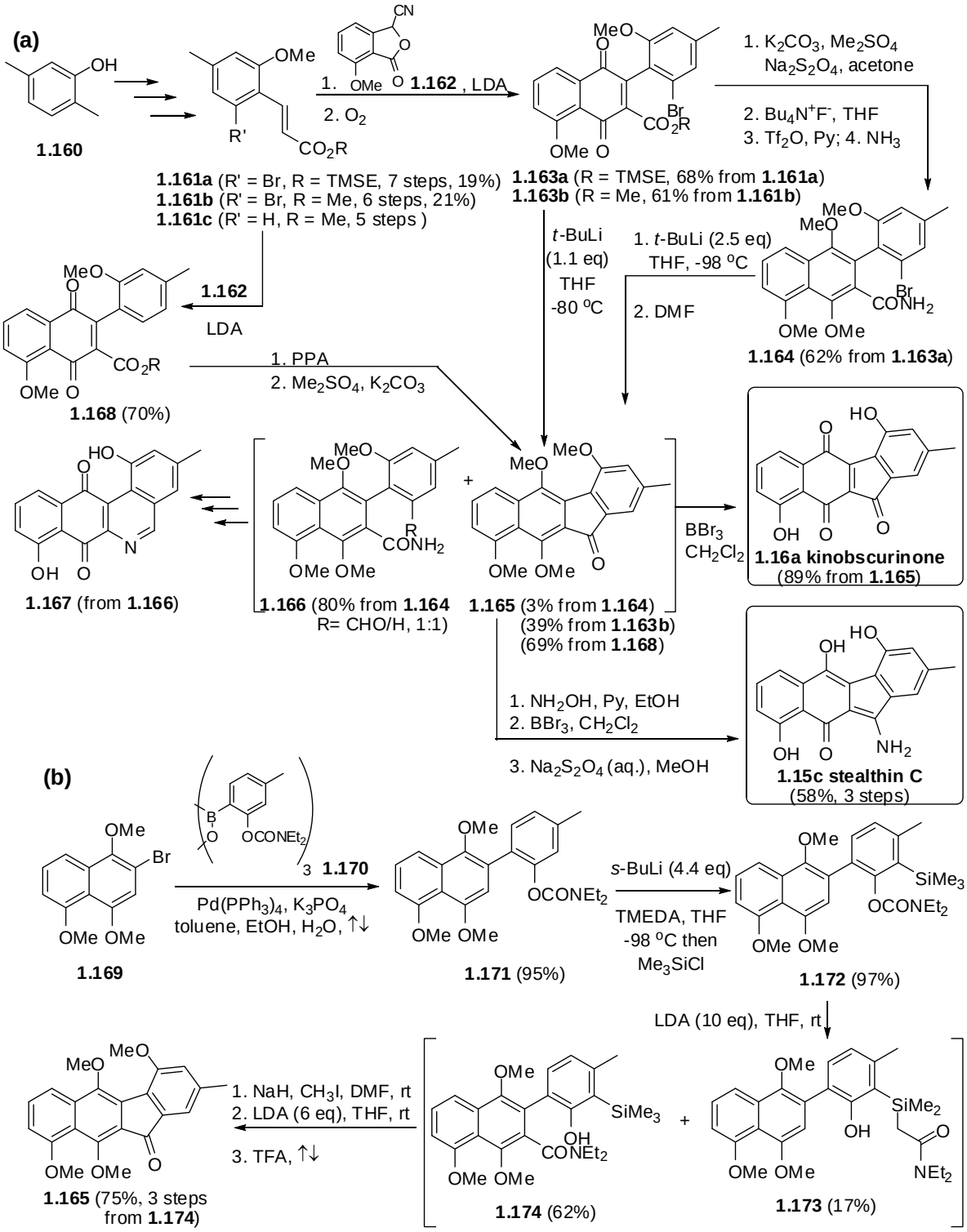

Scheme 1-22. Total synthesis of kinobscurinone (**1.16a**) and stealthin C (**1.15c**).

In addition, the above protocol of Suzuki coupling followed by intramolecular Friedel-Crafts cyclization was also used by Kamikawa and co-workers in 1998 to complete the total synthesis of dimethyl stealthin A (**1.180**) and dimethyl stealthin C (**1.181**) (Scheme 1-23), which also involved the same key intermediate **1.165**.[147]

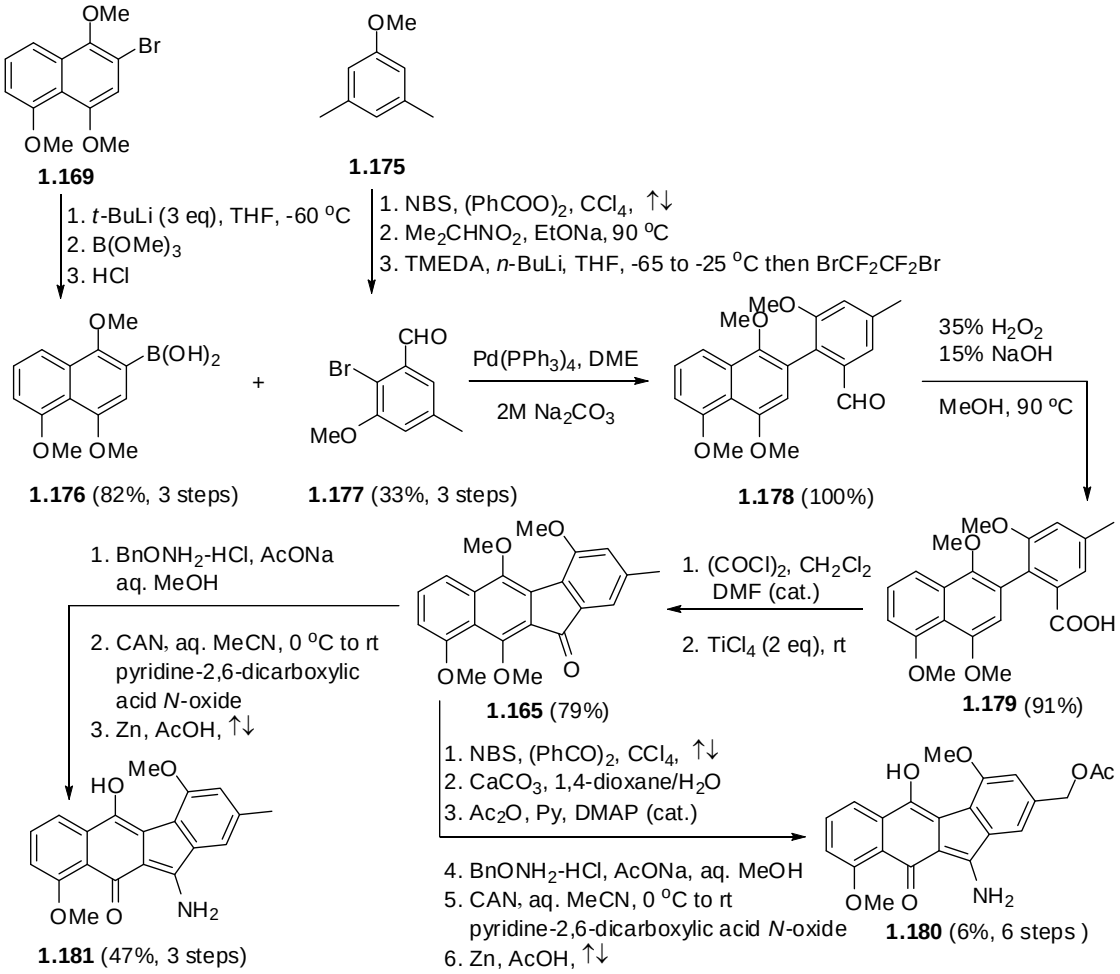

Scheme 1-23. Total synthesis of dimethyl stealthin A (**1.180**) and dimethyl stealthin C (**1.181**).

There are two other known synthetic procedures that can be regarded as a slightly modified version of the above protocol (i.e., disconnection (a) of Scheme 1-21). The first work was reported by Jebaratnam also in 1997, who prepared two prekinamycin analogues **1.186a** and **1.186b** (Scheme

1-24a).[148] The synthesis involved first an anionic addition of an aryl bromide **1.182** to acetanthranil (**1.183**), after which the formed biaryl amide **1.184** underwent an intramolecular Pschorr reaction through an in situ diazonium ion intermediate, leading to ring closure and the benzo[*b*]fluorenone of **1.185** followed by straight diazo transformation at C5. The second route was disclosed in 2000 by Jones and Qabaja (Scheme 1-24b), in which the initial intermolecular addition of aryl lithium species to substituted phenyl aldehyde followed by oxidation afforded the biaryl ketone **1.188**, then a Pd(II)-catalyzed intramolecular cross-coupling/cyclization of **1.188** under microwave conditions produced the key intermediate **1.165** in moderate yield.[149,150]

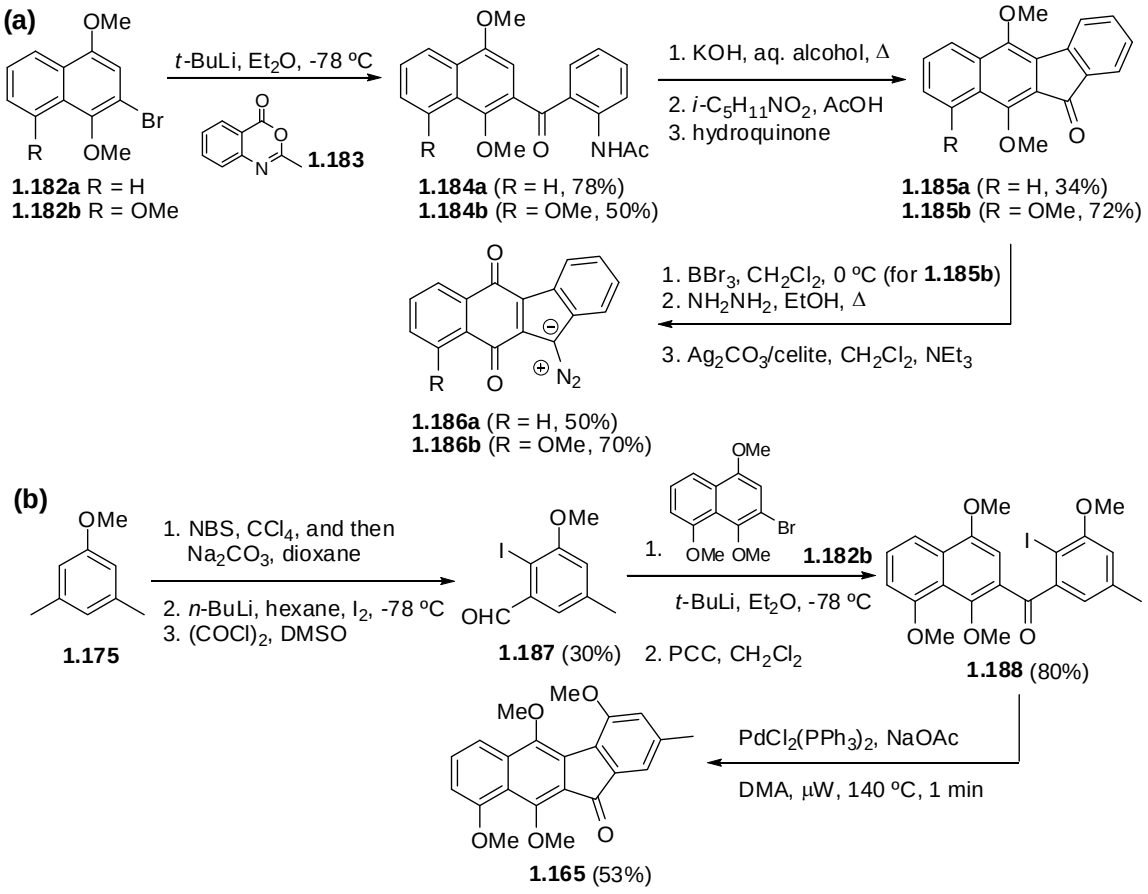

Scheme 1-24. Synthesis of (a) prekinamycin analogues **1.186** and (b) kinafluorenone derivative **1.165**.

The first attempt to construct the benzo[*b*]fluorenes of kinamycins via based-induced double condensation (i.e., disconnection (b) of Scheme 1-21) was reported by Mal and co-workers in 1996 by using either the 1-indenone (**1.190**), generated upon flash vacuum pyrolysis (FVP) of **1.189**, or α,β-unsaturated ketone **1.194** to react with the phthalide sulfone **1.191** in the presence of a strong base (Scheme 1-25a),[151] through the well established Hauser annulation[152] pathway. Shortly afterwards in the same year, Hauser also used his very own annulation methodology[152] to accomplish the first total synthesis of prekinamycin (**1.4**) and its dimethyl derivative **1.4a** starting from a substituted 1-indenone **1.197** (Scheme 1-25b).[76]

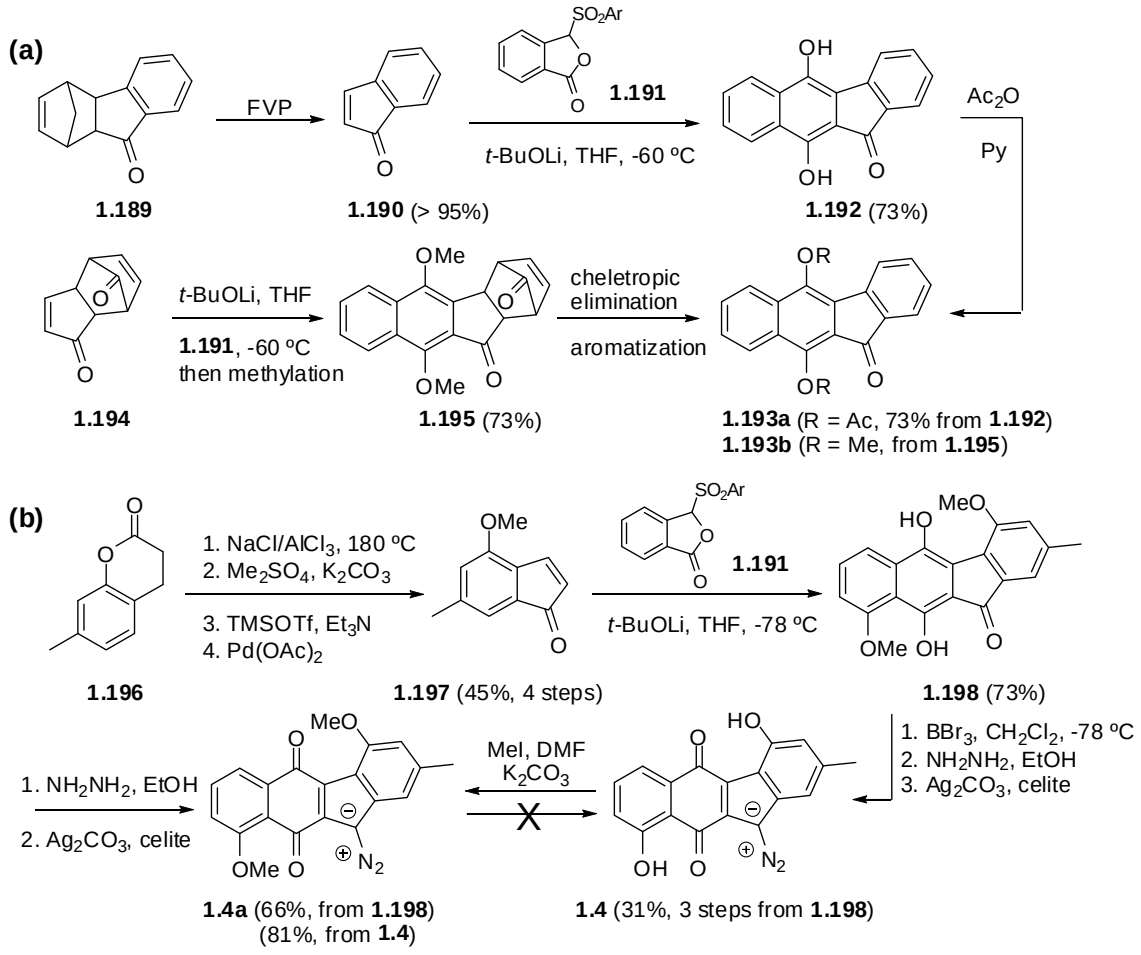

Scheme 1-25. Synthesis of (diazo)benzo[*b*]fluorenes via base-induced double condensation.

As more recent developments that are to be discussed in Chapter 3, the Birman lab employed another base-induced double condensation to build the benzo[*b*]fluorenes and complete the second total synthesis of prekinamycin (**1.4**) in 2007.[153] At the same time, Estevez's group combined an initial base-induced aldol condensation with a subsequent intramolecular Pd(II)-catalyzed cyclization to derive the benzo[*b*]fluorenone skeleton.[154]

The last synthetic efforts towards the benzo[*b*]fluorene skeleton of kinamycins to be described in this chapter are from the Echavarren group and the Dominguez/Saa lab (1997–2001). Such syntheses of the benzo[*b*]fluorenes all employed a very sophisticated thermal biradical cyclization of conjugated polyenyne systems (i.e., disconnection (c) of Scheme 1-21) as the key step. Examples include enyne-allene **1.203** (Scheme 1-26a)[75], benzotriyne **1.207** and benzodiyne **1.211** (Scheme 1-26b)[155] as well as benzoynones **1.214** (Scheme 1-26c)[156]. In the last case (Scheme 1-26c), unexpected benzo[*a*]fluorenes **1.221** were formed concurrently with the desired benzo[*b*]fluorenes **1.217**, possibly through an electrocyclic ring opening-closing sequence. As unique and interesting as this chemistry appears, it is obviously not attractive to be adopted for efficient synthesis of kinamycins and analogues.

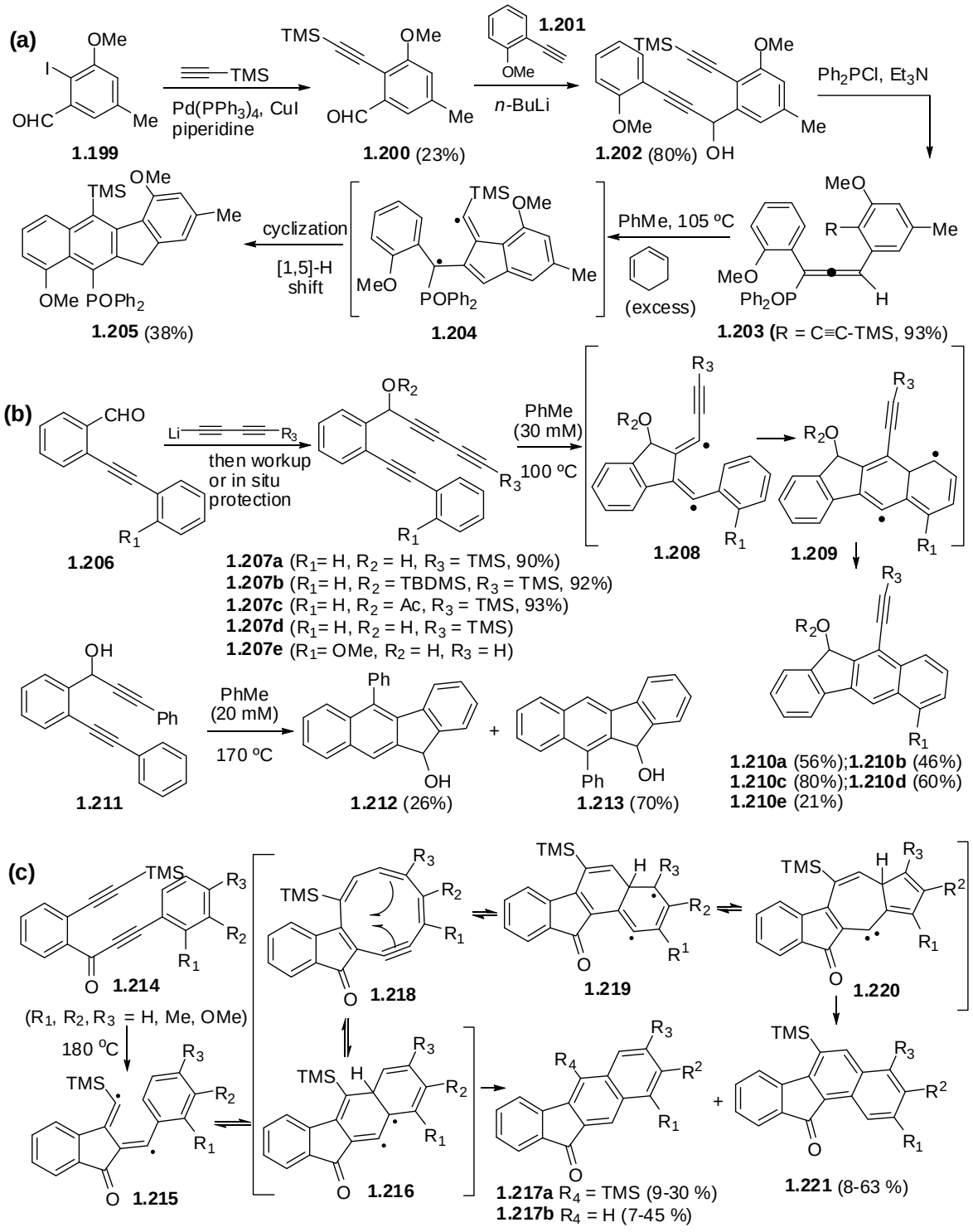

Scheme 1-26. Synthesis of benzo[*b*]fluorenes via thermal biradical cyclization of polyenynes.

There were no complete syntheses of the kinamycins or isoprekinamycin reported in the literature when the present thesis project was initiated, other than the total synthesis of prekinamycin (**1.4**) by Hauser and Zhou in 1996 (Scheme 1-25b).[76] During the course of this work, however, there have been a number of very recent developments in kinamycin total synthesis and model studies towards the lomaiviticins, including the first total synthesis of kinamycin C (**1.1c**) by Porco and Lei (2006),[23] total synthesis of (±)-methyl kinamycin C by Kumamoto and Ishikawa (2007),[24] the second total synthesis of kinamycin C (**1.1c**) by Nicolaou's group (2007)[16] and a most recent total synthesis of kinamycin F (**1.1f**) by Herzon's group (2010),[26] as well as syntheses of model structures for the dimeric diazobenzo[*b*]fluorene of lomaiviticins (**1.11**) by Nicolaou's group (2006[157] and 2009[158]) and Shair's group (2008)[159]. As for the diazobenzo[*a*]fluorene of isoprekinamycin (**1.5**), the delay in its correct structural identification until 2000 limited the synthetic efforts towards this compound. The Dmitrienko group is the first and only one so far that has successfully achieved the total synthesis of isoprekinamycin (**1.5**) (2007),[25] based on a series of continuous synthetic efforts from this lab over the years.[80,124,160,161] In addition, synthesis of the only other known naturally-occurring benzo[*a*]fluorene compounds besides **1.5**, i.e. the fluostatins (**1.20a**–**e**), has been reported by Danishefsky and Yu (2008), who prepared fluostatins C (**1.20c**) and E (**1.20e**).[162] Details of all this recent synthetic progress on kinamycins and related structures are presented and discussed in Chapter 3.

Chapter 2

A Simple Biogenetically-Inspired Synthesis of a Ring-D Model of Kinamycin F: Insights into the Conformation of Ring-D

2.1 Synthetic vs Natural Biopathway towards the D-Ring of Kinamycins

The highly oxygenated non-aromatic D-ring of the diazobenzo[*b*]fluorene type kinamycins (**1.1a**–**p**) seems to be one of the major structural features that complicate the synthetic work towards such "apparently simple" molecules. When the present project that aimed at total synthesis of kinamycin F (**1.1f**) was undertaken, there were no reports of the total synthesis of any of the kinamycins other than the fully aromatized prekinamycin (**1.4**). During the course of the project, however, four methods for total synthesis of the kinamycins[16,23,24,26] were reported. They are described and contrasted with the present synthetic strategies towards kinamycins in Chapter 3.

Among the known synthetic methods to address the challenging kinamycin D-ring, the very first one, which was also the only available one in the literature until the work described in this chapter was completed in the Dmitrienko lab, was a strategy reported by Kumamoto and Ishikawa in 2000 (Scheme 2-1).[163] A more detailed disclosure of this route was published a year later by the same group.[164]

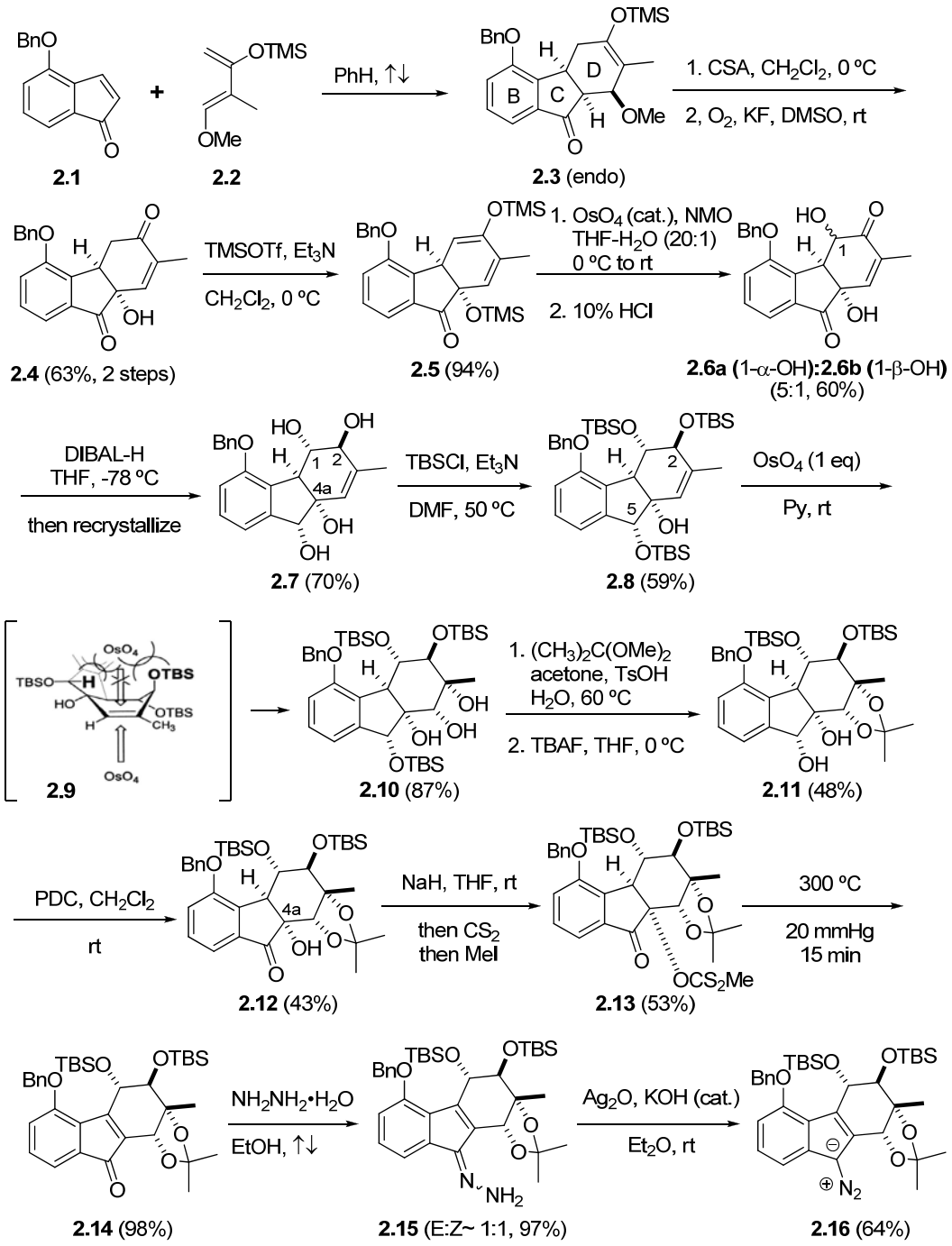

Scheme 2-1. Non-stereoselective construction of kinamycin D-ring by Kumamoto and Ishikawa.

The success of this rather ingenious strategy towards the kinamycin D-ring, with some significant limitations, relies on the following key aspects. First, the desired D-ring skeleton was constructed from a regioselective Diels-Alder reaction between indenone **2.1** and a Danishefsky-type diene **2.2**. Unfortunately the corresponding endo cycloaddition product **2.3** was obtained as a racemic mixture, and the entire route as well as the final stereochemical outcome suffered from this intrinsic deficiency. Second, due to the fact that the D-ring of **2.3** has no appropriate oxygen substituents as found in the kinamycins, extensive efforts had to be made to create new unsaturation within the D-ring through oxidation and enolization (**2.3** to **2.5**), followed by dihydroxylation (**2.5** to **2.6**) and reduction (**2.6** to **2.7**) to introduce the two essential oxygen substituents at C1 and C2 with the correct relative stereochemical relationship, and the desired stereoisomer had to be isolated by recrystallization. However, such chemical transformations also introduced an unwanted –OH (C4a of **2.7**) that had to be removed later on. Third, installation of the remaining two oxygen substituents of the D-ring was achieved by first appropriate protection of the –OHs of **2.7** and then a (second) dihydroxylation. Protection of the –OHs of **2.7** by small group (such as acetonide) led to undesired stereoselectivity during the dihydroxylation, so the much bulkier TBS groups were used instead. As a result of the significant steric hindrance introduced by the TBS ethers, the D-ring of **2.8** possessed a possible boat-like conformation with the bulky C1 and C2-OTBS groups in diaxial orientation to minimize steric repulsion, as indicated by NMR evidence. Thus, dihydroxylation of **2.8** would occur from the preferred side since its concave face was severely shielded by axial C2-OTBS group and C5-H (as shown by structure **2.9**); however, the use of a stoichiometric amount of the very expensive and toxic OsO_4 became unavoidable in this case. It is at the stage of compound **2.10** that the required four oxygen substituents on the D-ring were all installed with the relative stereochemistry matching the natural kinamycins, as confirmed by a single crystal X-ray structure analysis of **2.11**. Fourth, removal of the unwanted –OH at C4a of **2.12** was carried out by means of an elimination reaction of the

corresponding xanthate **2.13** through a high temperature pyrolysis under vacuum, yielding the enone **2.14** that was transformed to the final 9-diazotetrahydrofluorene **2.16** to serve as a model compound for the BCD-rings of the kinamycins. Overall, this route was quite lengthy and complicated, consisting a total of 12 steps (not including the extra steps needed to prepare **2.1** and **2.2**) and an overall yield of only 0.8%. In terms of the efficiency towards oxygenation of the D-ring, it took 8 steps (from **2.1** to **2.11**, ~ 12% yield) to furnish the structural requirement. In addition, some fairly harsh conditions that were needed (e.g., 300 °C to effect β-elimination of **2.13** to **2.14**) suggested that this route might not be practical for the total synthesis of kinamycins. Eventually, however, this route was adopted and modified, yet with no improvement of simplicity (number of steps) and overall yield, for the total synthesis of racemic (±)-methyl kinamycin C several years later (see Chapter 3).[24]

On the other hand, the challenge of the kinamycin D-ring was considered in a quite different manner by the Dmitrienko group, which has been exploring the possibility that the problem of stereo- and regioselective construction of the kinamycin D-ring might be overcome in a relatively much simpler way, by means of a synthesis that mimics (in part) the currently accepted biogenetic transformation pathway to natural kinamycins (Scheme 1-4, section 1.3.3.1). As a logical extension of such knowledge (Scheme 2-2a), a precursor that possesses a suitable aromatic D-ring such as **2.20** might be oxidized to the corresponding *p*-quinone **2.21**, followed by (asymmetric) epoxidation and subsequently a (stereoselective) reduction of the ketone groups to generate the epoxy diol **2.23** (Scheme 2-2b). A regioselective ring opening by an oxygen-centered nucleophile might occur at the less hindered C2-epoxy carbon of **2.23** from the backside, under appropriate conditions, leading to the construction of the complete D-ring with desired stereochemistry and substituents in only a few very simple and straightforward steps (Scheme 2-2b). It was also realized that the existence of a fully aromatized ABC-ring, or at least an aromatic C-ring for the model studies, could be essential for the success of this proposed strategy, since a non-aromatized ABC-ring might cause unnecessary

complications in such synthesis. For example, the critical epoxidation step from **2.21** to **2.22** might be facing the selectivity and competition issue between the two C=C double bonds of **2.21** if its C-ring is non-aromatic. Therefore, it was decided that it could be better to have a simple and stable aromatic system (i.e., a benzene ring) to represent the ABC-ring of the benzo[*b*]fluorene skeleton of kinamycins in the model study, so that efforts could be focused on the development of new chemistry related to the D-ring structure.

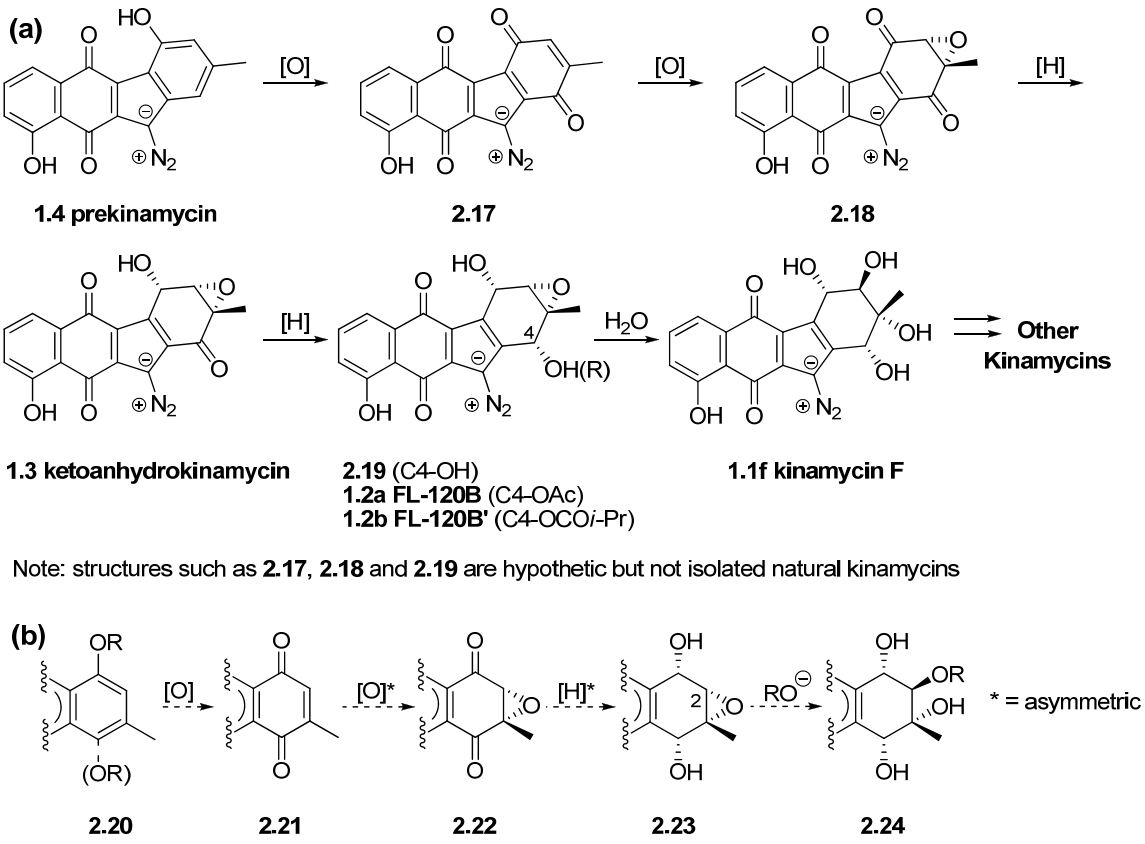

Scheme 2-2. (a) Biosynthetic pathway to the D-ring of the kinamycins in *Streptomyces*; and (b) proposed biomimetic model synthesis of the kinamycin D-ring by the Dmitrienko group.

2.2 A Simple Biogenetically-Inspired Synthesis of a Ring-D Model of Kinamycin F

Based on the proposal (Scheme 2-2b) to carry out synthetic work in a manner mimicking the extremely simple and effective biopathway of kinamycins (Scheme 2-2a), a model study for the stereoselective elaboration of the D-ring of kinamycin in only three steps from an appropriate *para*-quinone, analogous to the (possible) biogenetic intermediate **2.17**, was performed successfully after extensive attempts.[165] It should be pointed out that while the chemistry discussed in this chapter was being developed in the Dmitrienko group, the only literature work available at the time on the synthesis of the kinamycin D-ring was that from Kumamoto and Ishikawa's early results (Scheme 2-1).[163,164] After the completion of work described herein (but published at a much later time), Porco and Lei (2006) released a total synthesis of natural (-)-kinamycin C (**1.1c**), whose D-ring (absolute) stereochemistry was built from scratch starting from an achiral precursor.[23] Later on in 2007, Nicolaou's group developed another total synthesis of kinamycin C (**1.1c**); however, the required absolute stereochemistry of the D-ring originated from a chiral precursor this time.[16] Yet none of the above three methods was able to offer the same simplicity and efficiency to construct the kinamycin D-ring as the Dmitrienko strategy.

The commercially available 2-methyl-1,4-naphthoquinone (**2.25**, Vitamin K_3), which contains a simple and stable benzene ring while possessing the essential *para*-quinone moiety with a methyl substituent as required by the proposed model studies, served well for the purpose and thus was chosen as the starting material. Nucleophilic Weitz-Scheffer epoxidation of **2.25** with 30% hydrogen peroxide under mild basic conditions (aqueous Na_2CO_3 solution)[166] afforded the corresponding epoxy diketone **2.27** smoothly in 77% yield. Although various potential strategies for ensuring reduction of **2.27** with the desired stereoselectivity (i.e., the reduced diol hydroxyl groups must be *syn* to the epoxy oxygen) were envisaged, $NaBH_4$ was considered to be a good choice in this case due to the following

two reasons: (i) The mild but efficient reducing ability of $NaBH_4$ towards α,β-epoxy ketone[167] shall be able to carry out the desired reaction but to avoid or minimize other possible side reactions such as reductive epoxide ring opening. (ii) It is also known in the literature that $NaBH_4$ can reduce ketones in the presence of diazo groups,[127] which could benefit future total synthesis of kinamycins and any related intermediates that may have diazo group present in the structure. In practice, direct reduction of **2.27** with only one mol-equivalent of $NaBH_4$ in MeOH was complete within only a few minutes at ambient temperature, and the reaction provided the epoxydiol **2.28** with very high diastereoselectivity and in quantitative yield.

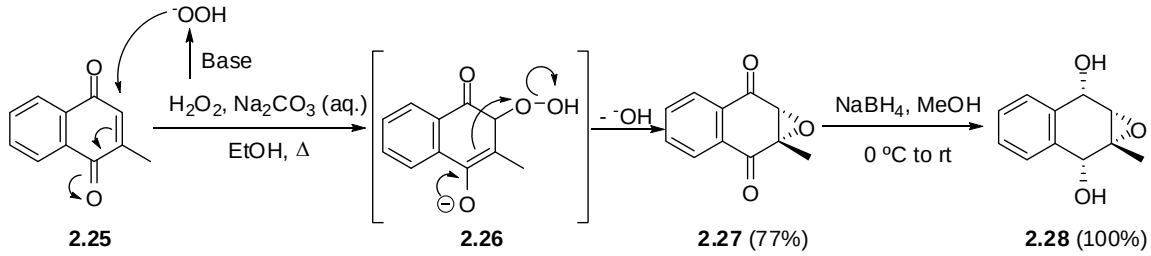

Scheme 2-3. Synthesis of the model epoxy diol **2.28** from the model *para*-quinone **2.25**.

The epoxydiol **2.28** was obtained exclusively as the (racemic) diastereoisomer shown in the structure, which has the two newly formed hydroxyl groups *cis* to the epoxy oxygen. This stereochemistry of **2.28** was assigned and established unambiguously based on various spectroscopic (NMR and X-ray) evidence from several ester derivatives (Scheme 2-4). Previous work in the Dmitrienko lab showed that it was possible to convert the epoxydiol **2.28** to the corresponding diacetate **2.29** in 86% yield upon simple acetylation.[168] The difference NOE NMR studies of **2.29** suggested that not only all three non-aromatic ring hydrogens but also the methyl group are present on the same side of the ring (see Scheme 2-4).[168] Unfortunately no single crystal of **2.29** could be grown for the purpose of X-ray analysis to further confirm this initial discovery of stereochemistry

based on NMR evidence, since **2.29** exists as an oil at room temperature. However, the epoxydiol **2.28** was, later on in this study, transformed to the corresponding bis(3,5-dinitrobenzoate) ester **2.30** in 73% yield (Scheme 2-4), which turned out to be a very stable solid (mp > 260°C). To ultimately determine the stereochemistry of the saturated 6-membered ring within **2.28** (and **2.30**), various efforts had been made to grow single crystals of **2.30**. Attempts with common pure organic solvents or by vapor/liquid diffusion techniques all failed except in one case. Slow diffusion of Et_2O vapor into a concentrated solution of **2.30** in DMSO-d6 (a previous NMR sample) produced single crystals of marginal quality for X-ray diffraction crystallography studies. For the first time, the single crystal X-ray results of **2.30** (ORTEP plot in Scheme 2-4, details of X-ray are provided in Appendix B) provided unambiguous confirmation of the stereochemistry of **2.28**/**2.30**. However, due to the poor quality of the single crystal used, it was noticed that one benzylic carbon atom in the obtained ORTEP plot of **2.30** was significantly distorted (as marked in Scheme 2-4). Even though such a severe crystal defect of **2.30** does not alter the conclusion concerning the stereochemistry of interest, it was felt necessary to further prepare some other derivative(s) of the epoxydiol **2.28**, in the hope that better X-ray results might be achieved. In practice, the diisobutyryl ester **2.31** was prepared from **2.28** in 64% yield by acylation with *i*-butyryl chloride (Scheme 2-4). The ester **2.44** crystallized easily from several solvents including Et_2O, EtOAc, acetone, benzene, THF and $CDCl_3$, all yielding good quality single crystals suitable for X-ray studies. The corresponding ORTEP plot of **2.31** is also shown in Scheme 2-4 (details of X-ray are provided in Appendix C), which once again confirmed the expected stereochemistry of the epoxydiol **2.28**.

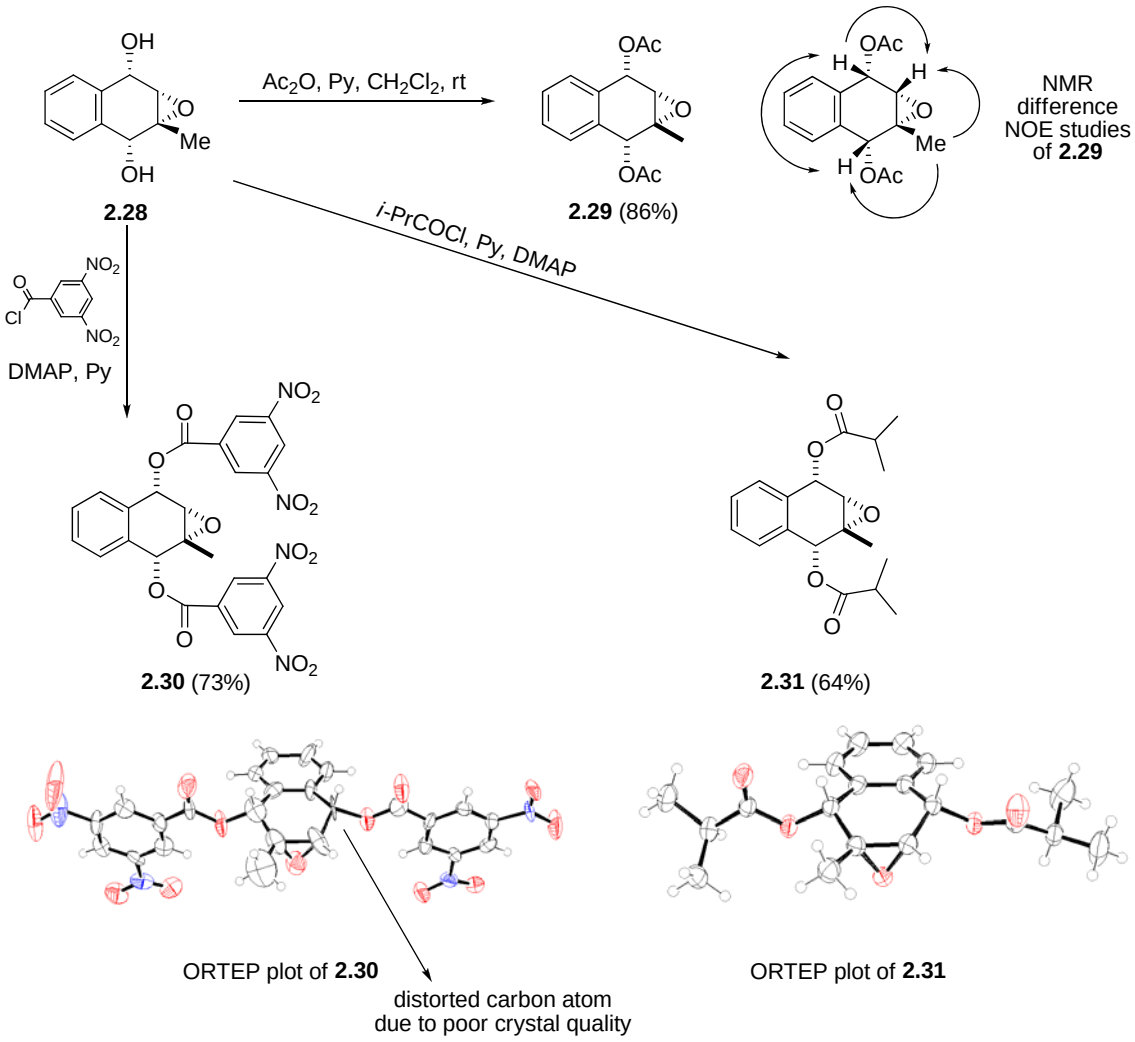

Scheme 2-4. Synthesis of various ester derivatives of epoxy diol **2.28**.

The observed high stereoselectivity in the reduction of **2.27** by $NaBH_4$ was quite surprising but could be explained partially by the hypothesis that solvation of the epoxy oxygen of **2.27** with MeOH (reaction solvent) by means of hydrogen bonding interactions would cause a large steric barrier (Scheme 2-5a), if the nucleophilic hydride approached the carbonyl groups from the side *syn* to the epoxy oxygen.[165] Therefore, the observed stereochemical outcome of the epoxydiol **2.28** is a direct

result of hydride reduction occurring from the less hindered side of the planar non-aromatic ring. To further explore the role and importance of H-bonding in this proposed mechanism, reduction of the epoxy diketone **2.27** by $NaBH_4$ was also carried out in other alcoholic solvent including EtOH, *i*PrOH and *t*BuOH, and in the last case of *t*BuOH the reduction was carried out at both room (~ 21 °C) and elevated temperature (60 °C). The desired stereoselectivity and quantitative yield of the diketone reduction were retained in all cases examined, indicating the benefit of using an alcoholic solvent. Interestingly, it seems that the existence of an aromatic (benzene) ring that fuses with the non-aromatic cyclohexane ring in the molecule of **2.27** might also contribute, to a certain extent, to the observed stereoselectivity. Reported reduction by $NaBH_4$ of simpler epoxy ketones (Scheme 2-5b) such as 2,3-epoxy-4-hydroxycyclohexanone (**2.32**),[169] (alkyl-substituted) 2,3-epoxy-cyclohexanones **2.35**[170] and 2,3-epoxy-cyclohexanone (**2.38**),[171] in either alcoholic or non-alcoholic solvents, always yielded a mixture of two corresponding alcohols (i.e., –OH derived from the ketone either *cis* or *trans* to the epoxide) in comparable amounts (~ 1:1). Further exploration of the literature led to a work on the $NaBH_4$ reduction of Vitamin K_1 epoxide **2.41**,[172] which has a long aliphatic side chain replacing the epoxy proton of **2.27** (Vitamin K_3 epoxide) but otherwise identical.[173] It was found that reduction of the two carbonyl groups of **2.41** proceeds in a stepwise and competitive manner (Scheme 2-5c), and despite the unclear stereochemistry of the final product, the corresponding epoxydiol **2.42** was also obtained as a single species rather than a mixture of four possible diastereomers, similar to the observed reduction of **2.27** by $NaBH_4$.[172]

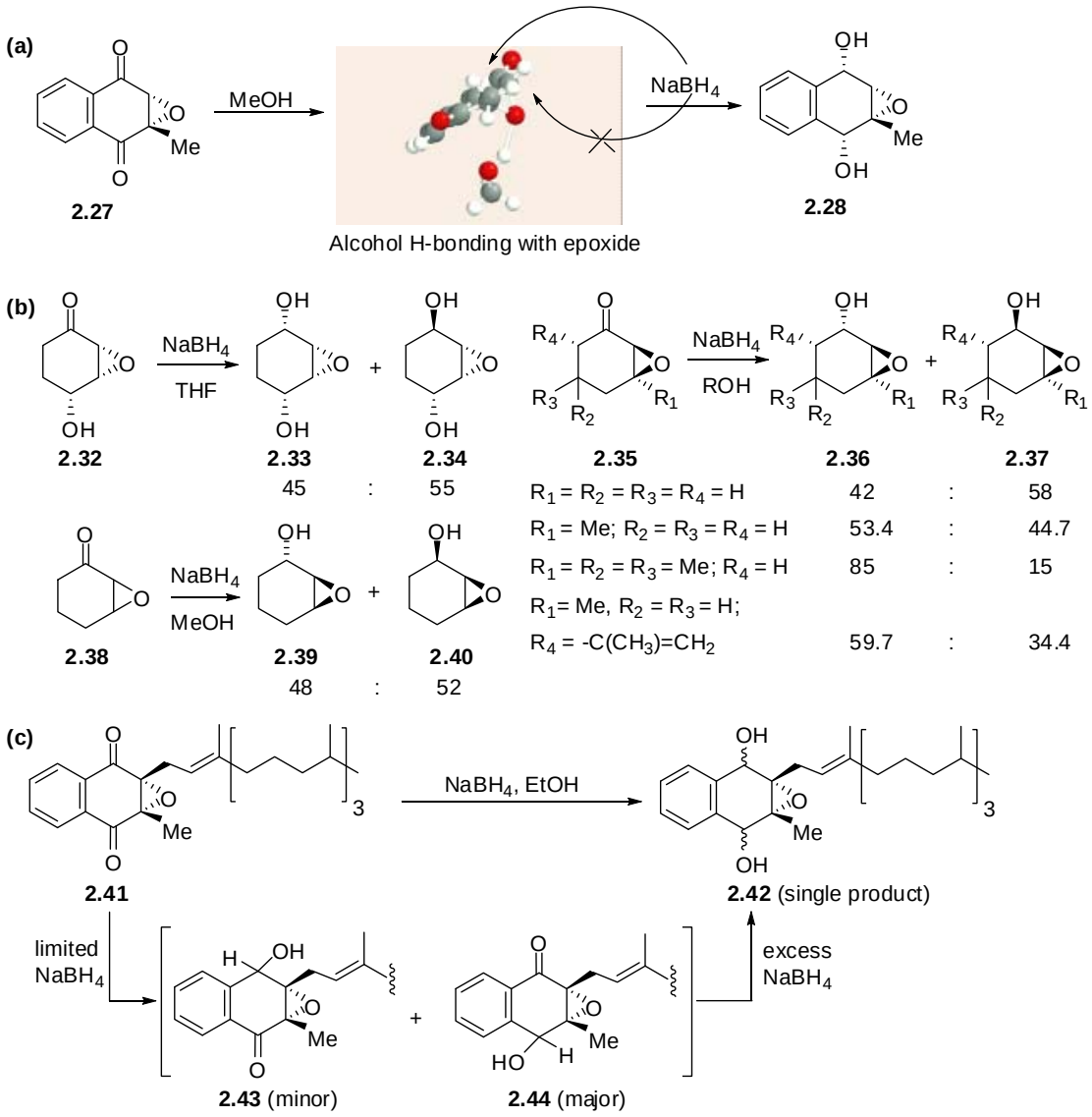

Scheme 2-5. (a) Proposed H-bonding model for the observed stereoselectivity on reduction of **2.27**; (b) literature examples of non-stereoselective reduction of cyclic epoxy ketones by $NaBH_4$; (c) literature example of reduction of Vitamin K_1 epoxide **2.41**.

With the epoxydiol **2.28** possessing the desired stereochemistry readily available in multigram quantities at hand, the next key step was to tackle the epoxide ring opening (ERO) reaction of **2.28** or its ester derivatives by an appropriate nucleophile (i.e., with a negatively charged or neutral oxygen

atom being the nucleophilic site) in a regio- (at the less hindered C2 epoxy carbon) and stereoselective (backside attack) manner. The general strategy of the ring opening reaction of epoxides relies heavily on the participation of a suitable protic or Lewis acid catalyst,[174] particularly in the cases requiring regio- and stereoselectivity, unless the nucleophilicity of the attacking reagent is very strong (e.g., thiol-type nucleophiles[175,176] or HO^-/RO^- at elevated temperature[177-179]). There are many examples in the literature regarding the regioselective ERO of (cyclic) epoxides, epoxy ketones and epoxy alcohols that possess structural similarities to compounds **2.28**–**2.31**, and some of the reported protic and Lewis acid catalysts for such ERO reactions include simple inorganic/organic proton acids (such as HCl,[180] HBr,[181], HI[182] H_2SO_4,[183,184] $HClO_4$,[185,186] HOAc,[187,188] HOAc/alumina,[189] Cl_3CCO_2H[190]), inorganic/organic metal salts (such as $AlCl_3$,[191] Al(TFA)(*i*PrO)$_2$,[192] $AlPO_4/Al_2O_3$,[193] $BF_3{\cdot}Et_2O$,[194] $BiCl_3$,[195] $CeCl_3$,[196] $CuSO_4$,[197] CsF,[198] $FeCl_3/SiO_2$,[199] $Fe(ClO_4)_3$,[200] $Fe(TFA)_3$,[201] $MgSO_4$,[202] $MgBr_2$,[166,203] MgI_2,[204] $NbCl_5$,[205] $TiCl_3(OTf)/TiO(TFA)_2$,[206] $Me_3SiCl/DMSO$[207]) and enzymes.[208] Such regioselective ERO might also be achieved through an one-electron oxidation process in the presence of a nucleophile and an oxidizing reagent, such as Ce(IV) salts,[209,210] DDQ[211] and I_2.[212] Previous work in the Dmitrienko group found that the epoxy diacetate **2.29** was unable to undergo the ERO under several literature conditions[168] and later attempts with **2.28** in this study following some other reported procedures, which are summarized in Table 2-1, also failed. Either no reaction occurred with mild conditions (Trial 1, 3 and 4), or extensive decomposition was observed when harsher (acidic or basic) conditions were applied (Trial 2 and 5).

Table 2-1. Summary of failed attempts on ERO reactions of **2.28** and **2.29**.

Trial	Starting Material	Reagents and Conditions[Reference]	Obtained Product(s)
1[a]	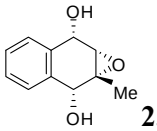 **2.28**	NaOAc, $MgSO_4$, MeOH ↑↓[202]	Complete recovery of **2.28**
2[a]	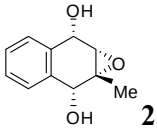 **2.28**	NaOAc, HOAc Δ (90°C), 4 hr[187]	ERO and elimination led to **2.25** as the only product
3[b]	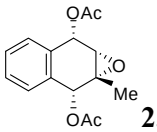 **2.29**	KOAc, Aliquat 336, CH_3CN rt, 72 hr[213]	Complete recovery of **2.29**
4[b]	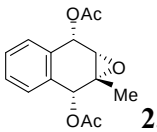 **2.29**	H_2O, Dioxane Δ (100 °C), 18 hr[168]	Complete recovery of **2.29**
5[b]	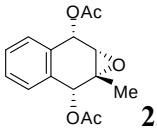 **2.29**	NaOMe, MeOH ↑↓[214]	Complex mixture Not characterized

a. This work; b. From M. B. Carriere's MS.c. Dissertation.[168]

After the above unsuccessful attempts on the nucleophilic ERO of **2.28** and **2.29** to mimic the putative biosynthetic conversion of **2.19** to kinamycin F (**1.1f**) (Scheme 2-2), it was eventually found that the desired stereo- and regioselective ring opening of the epoxydiol **2.28** could be achieved in good yield (76%) by using $Me_4NBH(OAc)_3$ in refluxing dry THF with excess NaOAc as the external nucleophile (Scheme 2-6). Under such conditions, a mixture of two triol acetates **2.45a** and **2.45b** (a pair of regioisomers) in a ratio of approximately 1:1 was obtained. The structures were assigned based on extensive NMR spectroscopic analysis including ^1H, ^{13}C, HMQC, HMBC and difference

NOE (Scheme 2-6) analysis. Honda and Mizutani had previously used this boron reagent to induce ring opening of both acyclic and cyclic 2,3-epoxy alcohols such as **2.50** (Scheme 2-6) but not of epoxy diols.[215] In the case of 2,3-epoxycyclohexanols, it was found that the ERO reaction succeeds only if the alcohol and epoxide are *syn* to each other, and that ring opening occurs upon nucleophilic attack at C3 by the acetoxy anion (released from the boron reagent) or other added external nucleophiles.[215] Interestingly, it was also noted in Honda's original work that if the alcohol possesses an *anti* correlation to the epoxide, the corresponding ERO reaction would lead to the formation of a reduction product, in which the $Me_4NBH(OAc)_3$ acts as a nucleophilic hydride source rather than a Lewis acid catalyst.[215] This had led to the suggestion that the ERO reaction induced by $Me_4NBH(OAc)_3$ occurs by a mechanism analogous to that proposed by Sharpless and co-workers for ring-opening of 2,3-epoxy alcohols (**2.53** in Scheme 2-6),[216] 2,3-epoxy acids and 2,3-epoxy amides (**2.54** in Scheme 2-6)[217] with $Ti(O\text{-}i\text{-}Pr)_4$.[215]

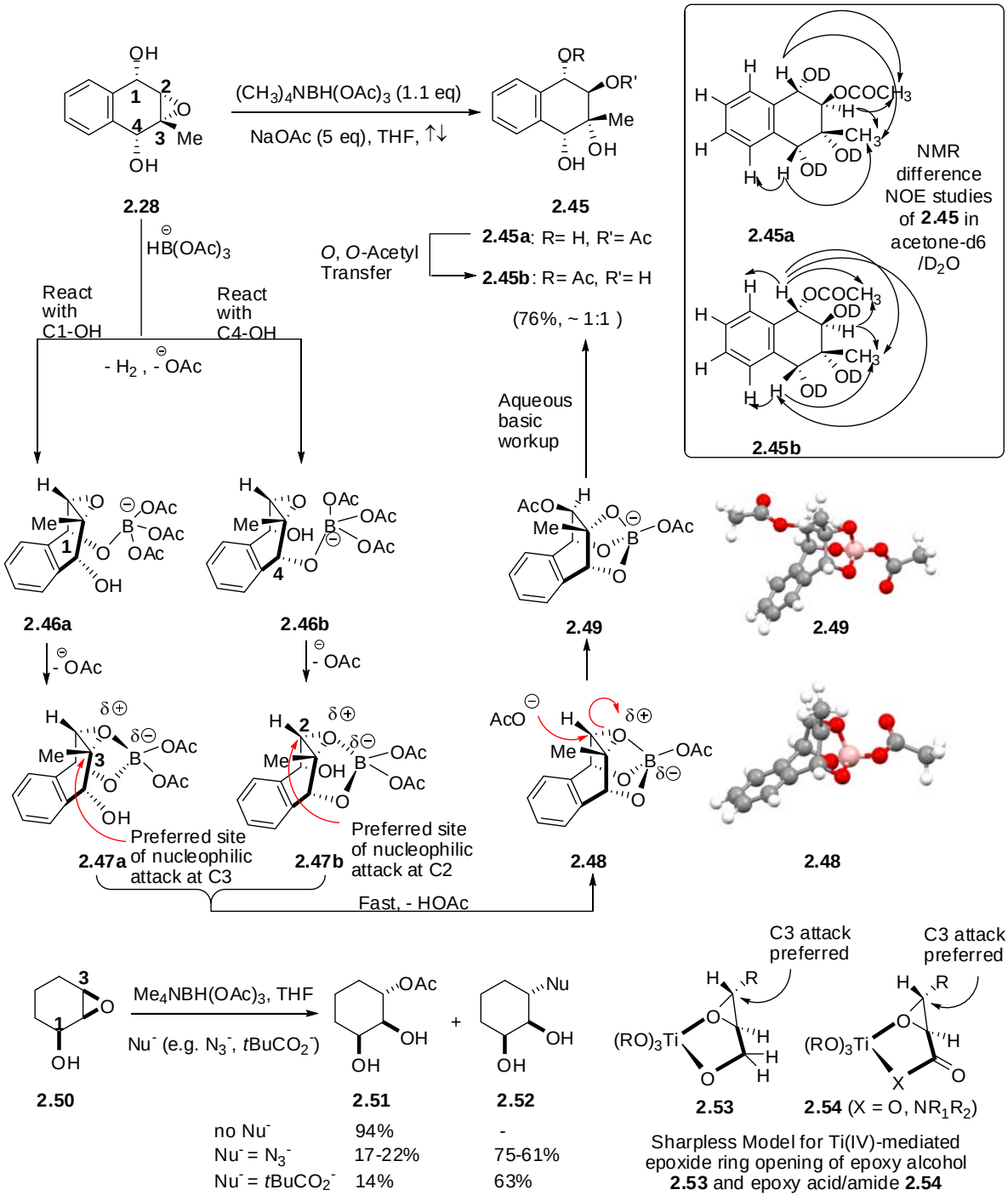

Scheme 2-6. Proposed mechanism for the observed regio- and stereoselective ring opening of the epoxydiol **2.28** in the presence of $Me_4NBH(OAc)_3$ and related literature examples.

Essentially, the boronic reagent $Me_4NBH(OAc)_3$ is thought to react initially with the alcohol to provide a Lewis acid, tethered to the alcohol oxygen atom. Further complexation intramolecularly with the epoxy oxygen atom helps to induce the epoxide ring opening by a nucleophile. For epoxydiol **2.28**, either -OH group at C1 and C4 might react with $Me_4NBH(OAc)_3$ to form a corresponding distinct adduct **2.47a** or **2.47b** respectively (Scheme 2-6), at the same time releasing an acetoxy anion and hydrogen gas. The literature precedents would predict ring opening with rupture of the epoxide C-O bond at C3 for adduct **2.47a**, but with rupture of the C-O bond at C2 for adduct **2.47b**. Since the accessibility of the reagent to the two alcohol groups in **2.28** is expected to be comparable, the high degree of regioselectivity observed in this epoxide ring opening step is somewhat surprising. It is suspected that the initial adducts, **2.47a** and **2.47b**, do not directly undergo epoxide ring opening. Instead, both species may react further and quickly to form the same cyclic complex **2.48** in which the boron serves as a Lewis acid intramolecularly and binds to all three oxygen atoms that exist on the same side of the non-aromatic ring, to assist with the epoxide ring opening by the nucleophile from a back-side attack at the sterically less crowded C2 position to give **2.49**. The corresponding computation models of **2.48** and **2.49**, generated by ab initio MO calculations at RHF/6-31G//6-31G level, are shown in Scheme 2-6. Aqueous basic workup then initially provides **2.45a**, which equilibrates with **2.45b** through a facile *O, O*-acetyl transfer that is very likely to occur under the basic workup conditions involved. Such migration behavior of acyl groups is well-known in the literature (e.g., **2.55** to **2.58**, Scheme 2-7).[218]

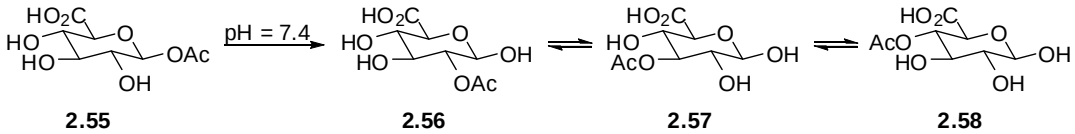

2.55 **2.56** **2.57** **2.58**

Scheme 2-7. Literature example of acyl migration under mild basic conditions.

It should be pointed out that the ring-opening of **2.28** can also be achieved smoothly in the absence of NaOAc but with a slightly lower yield (*ca.* 50–60%), and the nucleophile (i.e., the acetoxy anion AcO^-) required by the ERO reaction must be provided and released from $Me_4NBH(OAc)_3$ when forming the boronic adducts in this case. Since $Me_4NBH(OAc)_3$ is also known to be an excellent reducing agent for ketones,[219] it was thought to be worthy to attempt a possible one-pot (double) ketone reduction and ERO of the epoxy diketone **2.27** with $Me_4NBH(OAc)_3$. Unfortunately, the attempted reaction in THF only afforded a very complicated mixture (not characterized) instead of the desired product of **2.45**.

The two regioisomers of the triol acetates **2.45a** and **2.45b** (~ 1:1) of the ring-opening product **2.45** were readily separated by flash column chromatography, even though the separation was not necessary for the subsequent derivatization steps. The triol acetates **2.45** (as a mixture) were further deacylated and afforded the corresponding tetrol **2.59** under several basic conditions (Scheme 2-8). Deacetylation of the triol acetates **2.45** was initially achieved by either reduction with $LiAlH_4$ in anhydrous THF or a simple basic hydrolysis (aqueous NaOH solution), although low yields and difficult isolation of the pure tetrol **2.59** were encountered in both cases (56% crude for $LiAlH_4$ reduction and 25% crude for NaOH hydrolysis). Fortunately, a further attempt at the deacylation reaction of **2.45** (mixture) under the Zemplen conditions (catalytic amount of NaOMe in MeOH) followed by a workup using a proton resin instead of an aqueous acid,[220] a method that is widely used in sugar chemistry for deacylation purposes, was capable of generating **2.59** as a single product in near quantitative (98%) yield. Moreover, peracetylation of the tetrol **2.59** was first carried out with AcOH in the presence of $Sc(OTf)_3$ as a Lewis acid catalyst, since literature work indicates that this is a mild but efficient method for acetylation of all kinds of alcohols including the sterically hindered ones.[221] However, under such conditions, only partial (and random) acetylation of the tetrol **2.59** occurred at ambient temperature, while decomposition of the tetrol dominated when the acetylation

was attempted at elevated temperature. The tetra-acetate **2.60** was eventually prepared in 83% yield by acetylation of **2.59** with acetic anhydride in the presence of a large excess of DMAP (Scheme 2-8). The same product was also obtained when a mixture of the triol acetates **2.45** was acetylated under identical conditions. Such derivatization of **2.45** indicates that a global chemical transformation of the four oxygenated-substituents on the non-aromatic D-ring (of kinamycins) is likely to be feasible, which may be of value in future total syntheses of kinamycins as well, since **2.59** has an identical D-ring as the one in kinamycin F (**1.1f**) and **2.60** has one identical to that of kinamycin J (**1.1j**).

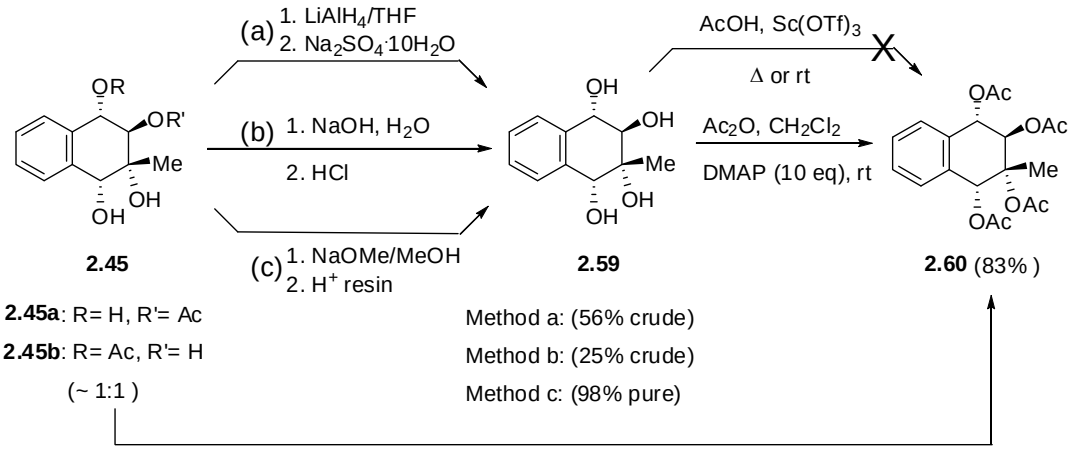

Scheme 2-8. Derivatization of the triol acetates **2.45**.

In summary, the proposed model study to construct the D-ring of the kinamycins in a biomimetic fashion (Scheme 2-2) was successfully achieved in only three simple steps with readily available and low-cost commercial reagents and an overall yield of 59%, starting from the *para*-quinone **2.25** and involving epoxidation, reduction and epoxide ring opening to give the triol acetates **2.45**. The essential and required four oxygenated-substituents for the D-ring of the kinamycins are all installed in the correct relative stereochemical manner, demonstrating the power and particularly the efficiency of this biogenetically-inspired synthetic sequence. A comparison of this strategy with other procedures that have been since appeared in the literature is provided in Chapter 3.

The use of $Me_4NBH(OAc)_3$ in the ERO reaction provides more flexibility for various chemical transformations of the epoxide functionality within the epoxydiol **2.28**, since, in principle, other nucleophiles such as halogens (e.g., Br^- and I^-) might also be introduced to the non-aromatic ring through the ERO reaction. Using $Me_4NBH(OAc)_3$ as the ring-opening promoter, initial ERO attempts on **2.28** with NaBr as the external nucleophile, however, led to a complex mixture of products (not characterized). With the more nucleophilic I^-, the corresponding iodohydrin **2.61** was generated as expected in 90% yield (Scheme 2-9). Since coupling reagents and conditions suitable for the dimerization of iodocyclohexane **2.63**,[222] 2-iodocyclohexanone **2.65**[223] and some rather complicated α-iodoketones **2.67**[224] are known in the literature (Scheme 2-9), the possibility that the obtained iodohydrin **2.61** might be converted into the corresponding dimer **2.62** is worthy of consideration, which is structurally closely related to lomaiviticin A (**1.11a**), a dimeric diazobenzo[*b*]fluorene. Alternatively, proper protection of the hydroxy groups within **2.61** can lead to substrates such as **2.69**, which may undergo a possible base-induced elimination to give the corresponding enolate **2.70** followed by a hydrolysis/deprotection to yield **2.71** (Scheme 2-9). This compound possesses a saturated cyclohexyl ring with very minor variation(s) of the ring substituents that is similar to the D-ring of lomaiviticin A (**1.11a**). Such potential synthetic applications with the structure of **2.62** could open doors to construction of simple analogues of the biologically potent dimeric diazobenzo[*b*]fluorene of lomaiviticins.

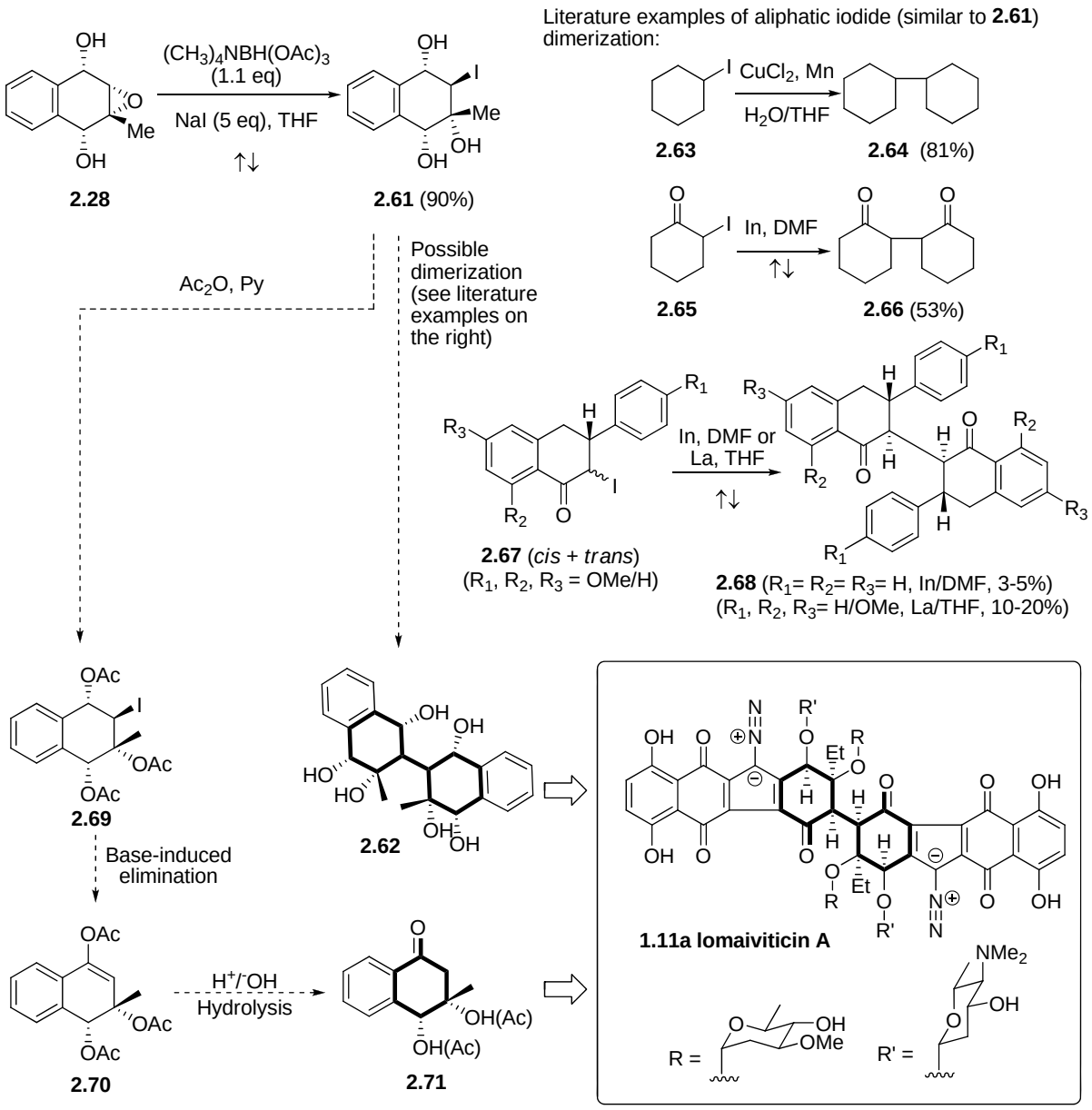

Scheme 2-9. ERO reaction of **2.28** by halogen nucleophile in the presence of $Me_4NBH(OAc)_3$ and the potential synthetic applications of **2.61** as a model compound.

Last but not least, there are some additional comments on the above model study that are worth further discussion. Even though epoxidation of the quinone **2.25** was not carried out in a

stereoselective manner in this study, there are some literature examples regarding the asymmetric epoxidation of such α,β-unsaturated ketones including **2.25**, which normally involves the use of an appropriate chiral catalyst to control the stereochemical outcome along with an epoxidation reagent for the chemical transformation (or the direct use of a chiral epoxidation reagent to complete the two tasks simultaneously). Early work in this area showed that asymmetric epoxidation of **2.25** affords the corresponding epoxide **2.27** with fair to good yields but only with low to moderate *ee* (either enantiomer is available), depending on the chiral catalysts/peroxides used, such as chiral phase-transfer catalysts (PTC) of quaternary ammonium salts derived from quinidine (72–94% yield, 1–34% *ee*),[225,226] cinchonine (53–63% yield, 10–18% *ee*),[227] and quinine (60–70% yield, ~5% *ee*),[228,229] chiral sugar hydroperoxides (71% yield, 45% *ee*),[230] α-/β-cyclodextrin (33–100% yield, 0–24% *ee*)[231] and bovine serum albumin (BSA, 20–34% yield, 20–47% *ee*).[232-234] On the other hand, if the methyl group on the quinone moiety of **2.25** is replaced by sterically bulkier substituents such as long alkyl chain (C_8), *i*-Pr, cyclohexyl and aryl groups (Ph/Ar), the observed stereoselectivity of epoxidation immediately increases to a (much) higher and reasonable level of *ee* (64–100% *ee*).[225,226,235,236] Introducing substituents onto the benzene ring of **2.25** also slightly increases the *ee* of the obtained epoxide under the same stereoselective epoxidation conditions.[228]

More interestingly, recent progress regarding the asymmetric epoxidation of **2.25** indicates that (Scheme 2-10),[237] in the presence of some readily available *Cinchona* alkaloids (e.g., quinidine **2.75** and quinine **2.76**)-based chiral PTCs such as **2.72**–**2.74**, and a careful choice of epoxidation conditions (NaOCl as a mild peroxidation reagent, low reaction temperature and an appropriate binary solvent system of chlorobenzene/water), stereoselective epoxidation of **2.25** could produce either enantiomer of the corresponding epoxide (**2.27a**/**2.27b** in Scheme 2-10) with significantly improved *ee* (67–85%) and good yields (73–92%). Note that the enantiomer **2.27a** possesses the identical absolute stereochemistry as the D-ring of the proposed kinamycin biointermediate **2.18** as

shown in Scheme 2-2. The stereoselectivity achieved in epoxidation of such a flat and near-symmetric naphthoquinone was explained by the difference in steric interactions in the intermediate chlorooxy enolate (**2.77**)-PTC (e.g., **2.72**) ion pair depending on the enantiomer of **2.77** and the chiral PTC involved, which was formed through possible hydrogen bonding, Coulombic interaction and π-π stacking (Scheme 2-10). This new development makes the model synthetic strategy described in this chapter more attractive and valuable towards being applied to the enantioselective total synthesis of kinamycins and related antibiotics.

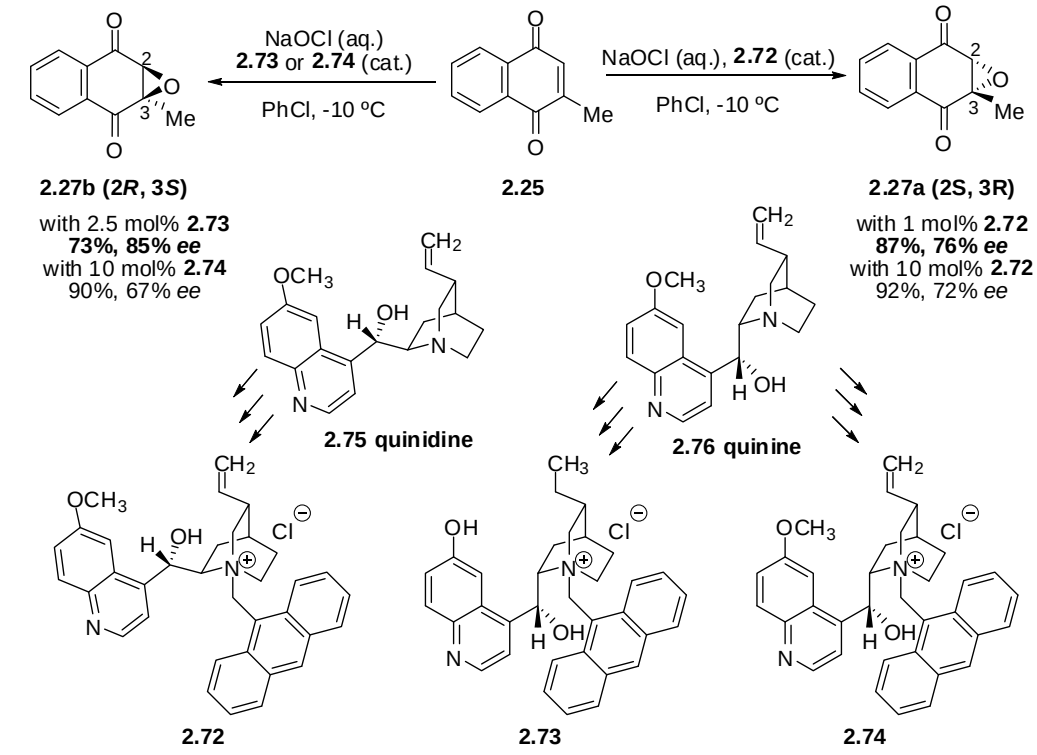

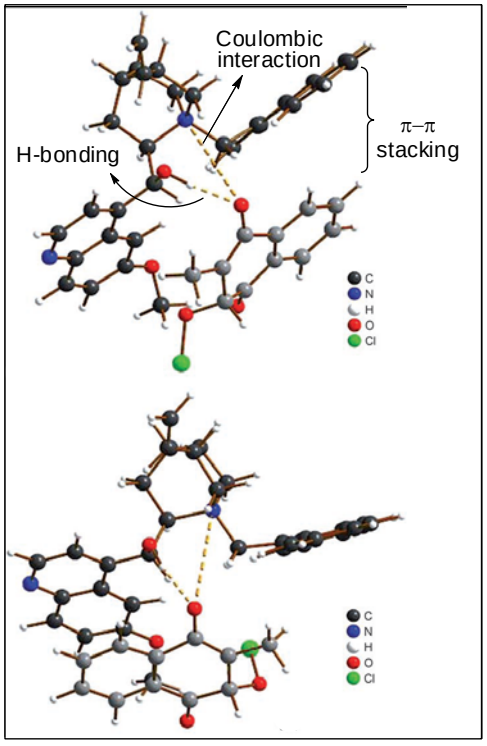

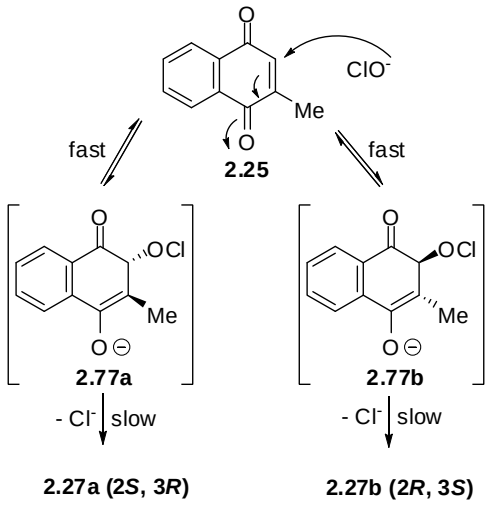

Left: computation model for the ion pair of the epoxidation intermediate chlorooxy enolate (**2.77**) and chiral PTC (**2.72**). The top enantiomeric ion pair (**2.77a**-**2.62**) is predicted to be more stable than the bottom one (**2.77b**-**2.72**) by ca. 3.5 kJ/mol.

Scheme 2-10. Proposed mechanism for the improved asymmetric epoxidation of **2.25**.

2.3 Conformational Analysis of the D-Ring of Kinamycin F and Model Compounds

While reviewing NMR spectroscopic data of the natural kinamycins presented in the literature, it was noted that the reported D-ring H1-H2 coupling constant for kinamycin F (**1.1f**) was unusually small (J = 3.4 Hz in DMSO-d6)[9] for such a vicinal H-H coupling, presumablely pseudo axial-axial, as one would normally expect (8–10 Hz).[132] This coupling constant is also inconsistent with those of other natural kinamycins and their synthetic derivatives, as listed in Table 2-2, which are all about 7–9 Hz (in $CDCl_3$) regardless of the various substituents on their D-rings. Therefore, it was first thought that the significant difference in the reported coupling constants between kinamycin F (**1.1f**) and other kinamycins could very likely be due to a simple error of observation or even just a typographical error in the literature. In addition, the model compound **2.59** that possesses exactly the same (relative) stereochemistry and substituents of the D-ring as kinamycin F (**1.1f**), also shows a typical vicinal H1-H2 coupling constant of 6.9 Hz in DMSO-d6. Literature examples of some other similar cyclic polyalcohols such as **2.78** and **2.79** give coupling constants around the same range (ca. 7.8–9.9 Hz, Table 2-2) as well. One might also consider the fact that the use of DMSO-d6 (for kinamycin F) instead of $CDCl_3$ (for other kinamycins) as NMR solvent could affect the observed coupling constant to a certain extent; however, it is generally believed that "vicinal H-H coupling constants exhibit a negligible solvent dependence in the absence of solvent-induced changes in conformational populations".[238] In fact, the model tetrol **2.59** served as a good example (Table 2-2, J = 6.9 Hz in DMSO-d6 and J = 7.0 Hz in $CDCl_3$) in support of this conclusion. Thus, it was possible that the unusually small coupling constant of **1.1f**, if it was not a mistake, would indicate that kinamycin F (**1.1f**) may adopt a quite different conformation than other kinamycins.

Table 2-2. Literature $J_{H\text{-}H}$ of some natural kinamycins, derivatives and related model compounds.

Natural Kinamycin	$J_{H^1\text{–}H^2}$ (Hz) in $CDCl_3$	Natural Kinamycin (* Synthetic derivatives)	$J_{H^1\text{–}H^2}$ (Hz) in $CDCl_3$
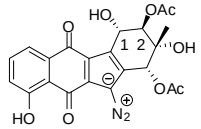 **1.1a** kinamycin A	**8.5**[9]	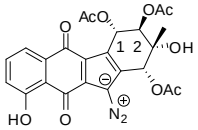 **1.1c** kinamycin C	**7.2**[9,16]
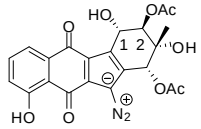 **1.1d** kinamycin D	**8.0**[9] **8.1**[5] **7.9**[10]	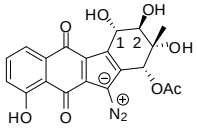 **1.1e** kinamycin E	**7.9**[5]
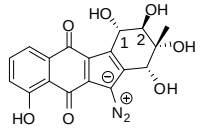 **1.1f** kinamycin F	**(DMSO-d6)** **3.4**[9]	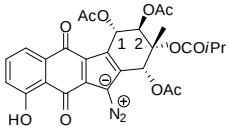 **1.1g** kinamycin G	**7.0**[7]
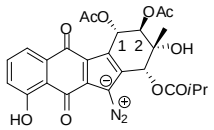 **1.1h** kinamycin H	**7.0**[7]	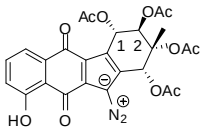 **1.1j*** kinamycin J	**7.5**[9] **6.6**[16]
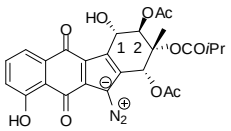 **1.1m** FL120-A	**8.1**[10]	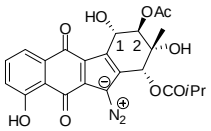 **1.1n** FL120-C	**8.1**[10]

Table 2-2. (continued).

Natural Kinamycin (* Synthetic derivatives)	$J_{H^1-H^2}$ (Hz) in $CDCl_3$	Natural Kinamycin (* Synthetic derivatives)	$J_{H^1-H^2}$ (Hz) in $CDCl_3$
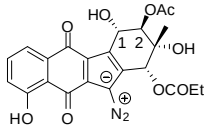 **1.1o** FL-120C'	**8.1**[10]	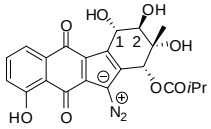 **1.1p** FL-120D'	**7.8**[10]
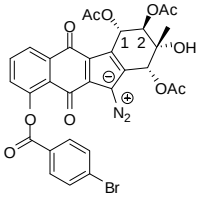 **1.1s***	**7.8**[9]	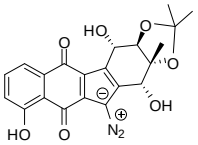 **1.1t***	**9.0**[9,18]
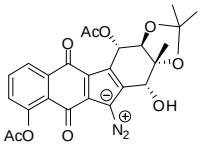 **1.1u***	**9.0**[9,18]	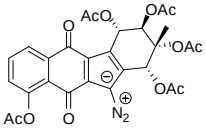 **1.1q***	**6.0**[9]
Model Compound	J_{H-H} (Hz)	Model Compound	J_{H-H} (Hz)
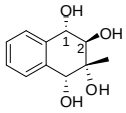 **2.59**	**($CDCl_3$)** H^1-H^2**: 7.0**	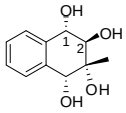 **2.59**	**(DMSO-d6)** H^1-H^2**: 6.9**
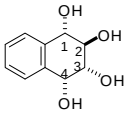 **2.78**	**(CD_3OD)**[239] H^1-H^2**: 8.0** H^2-H^3**: 9.9** H^3-H^4**: 3.7**	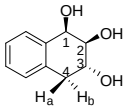 **2.79**	**(Pyridine-d5)**[240] H^1-H^2**: 3.8** H^2-H^3**: 7.8** $H^3-H_a^4$**: 6.3** $H^3-H_b^4$**: 8.8**

In order to clarify this confusing discovery, it was decided to carry out our own first-hand NMR spectroscopy experiments, since the only literature NMR data of kinamycin F (**1.1f**) available at the time was acquired by Ōmura on a 100 MHz CW-NMR spectrometer more than 30 years ago.[9] A small amount of natural kinamycin D (**1.1d**) had been isolated and purified from the fermentation broth of *Streptomyces* by V. Goodfellow and Dr. O. Adidayo in the Dmitrienko lab. Kinamycin F (**1.1f**) was prepared in quantitative yield from the isolated **1.1d** upon the Zemplen deacylation reaction (Scheme 2-11) by this work, and the same result was obtained when natural kinamycin A (**1.1a**) was subjected to identical conditions. The stability and survival of the diazo moiety of the kinamycins under such strong basic and nucleophilic conditions is noteworthy.

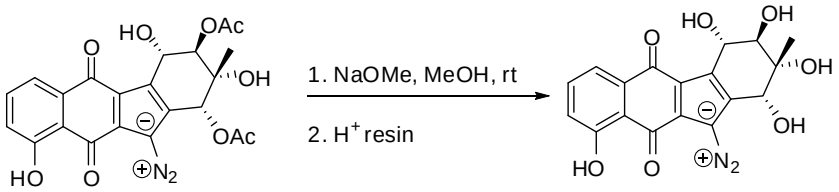

1.1d kinamycin D **1.1f** kinamycin F (100%)

Scheme 2-11. Preparation of kinamycin F (**1.1f**) from natural kinamycin D (**1.1d**).

The ^{1}H-NMR spectrum of kinamycin F (**1.1f**) in DMSO-d6, acquired on a 300 MHz FT-NMR spectrometer, gave a very small H1-H2 coupling constant of only 2.7 Hz. This observation indeed matched the suspected literature value of 3.4 Hz for **1.1f** in DMSO-d6 very well as reported by Ōmura.[9] To exclude the influence of solvent, a proton NMR spectrum of kinamycin F (**1.1f**) was also acquired in $CDCl_3$ and an even more surprising observation was revealed this time, as the H1-H2 coupling constant of interest became 6.0 Hz! Although this new value was closer to those coupling constants observed with other kinamycins (i.e., 7–9 Hz, Table 2-2), it was still noticeably smaller. There is no doubt that some significant conformational change of D-ring of kinamycin F (**1.1f**) occurred simply due to the change of solvent. To further investigate this quite unusual and totally unexpected solvent effect, a series of NMR experiments in various NMR solvents were performed

with kinamycin F (**1.1f**), kinamycin D (**1.1d**) and some model compounds (i.e., **2.59**, **2.60** and **2.45**). The corresponding results of the observed vicinal H1-H2 coupling constants are summarized in Table 2-3. Among all the compounds examined, clearly kinamycin F (**1.1f**) is the only one that shows a solvent dependency of the observed coupling constant, and it is also the only species that gives a much smaller H-H coupling constant than usual under certain circumstances.

Table 2-3. Measured $J_{H^1-H^2}$ of some natural kinamycins and model compounds in various solvents.

Natural kinamycins or model compounds	$J_{H^1-H^2}$ (Hz)				
	$CDCl_3$	CD_3CN	CD_3OD	Acetone-d6	DMSO-d6
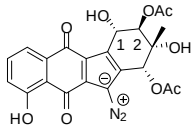 **1.1d** kinamycin D	**8.1**[a]	-	**8.0**[b]	**8.0**[b]	**7.5**[a]
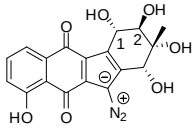 **1.1f** kinamycin F	**6.0**[b,c]	**4.5**[b,d,e]	**4.2**[a] (CD_3OD/D_2O = 1:1) **5.0**[b]	**3.0**[b] (Acetone-d6/CD_3OD = 5:1) **4.0**[b]	**2.7**[a]
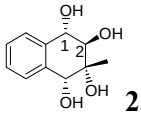 **2.59**	**7.0**[b]	-	**7.5**[b]	-	**6.9**[a] (Pyridine-d5) **7.2**[a]
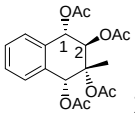 **2.60**	**7.2**[a]	-	-	-	**6.0**[a]
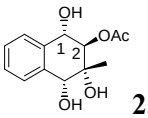 **2.45a**	-	-	-	**7.2**[a]	**8.3**[a,f]
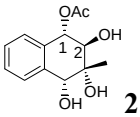 **2.45b**	-	-	-	**8.4**[a]	**7.8**[a,f]

a. 300 MHz FT-NMR; b. 500 MHz FT-NMR; c. After the publication of this work in 2008,[165] the most recent total synthesis of kinamycin F (**1.1f**) by the Herzon group (section 3.2) released in early 2010,[26] reported an almost identical value ($J_{H^1-H^2}$ = 6.1 Hz in $CDCl_3$ on a 500 MHz NMR); d. D_2O was present in the NMR sample; e. The Nicolaou group synthesized kinamycin F (**1.1f**) in 2007 (section 3.2) and reported its NMR data in CD_3CN acquired on a 600 MHz NMR.[16] The reported δ values, however, are all "wrong" (~ 0.2 ppm higher than the actual ones) due to the mistakenly used calibration standard and no H^1-H^2 coupling was observed; f. The NMR sample used a mixture of **2.45a** and **2.45b** (~1:1).

The ^{1}H-NMR spectra of the triol acetates, **2.45a** and **2.45b**, and the tetra-acetate **2.60** reveal that the observed coupling constants ($J_{H^1–H^2}$ = 6.0–8.3 Hz in DMSO-d6) are consistent with the predominance, in each case, of a half-chair conformation in which the C1 and C2 hydroxy or acetoxy groups are in pseudo-equatorial orientations, so that the H1 and H2 would exist in such an orientation (both pseudo-axial) that the dihedral angle of H1-C1-C2-H2 is large enough to give a "normal" coupling constant. The comparable magnitude of $J_{H^1–H^2}$ reported for those natural kinamycins as listed in Table 2-2 except kinamycin F (**1.1f**) is likewise consistent with such a conformational preference for their D-rings. X-ray crystallographic studies of the C7-O-*p*-bromobenzoate derivative of kinamycin C **1.1s**[19] and of the C1-O-*S*-2-methylbutyrate derivative of kinamycin D **1.1v**[21] suggest that this conformational preference persists in the solid state as well. The observed $J_{H^1–H^2}$ for the tetrol **2.59** (6.9 Hz in DMSO-d6 and 7.0 Hz in $CDCl_3$) and tetra-acetate **2.60** (6.0 Hz in DMSO-d6 and 7.2 Hz in $CDCl_3$) was also consistent with a similar conformational preference regardless of the solvent. It was surprising to find, however, that $J_{H^1–H^2}$ for the fully deacylated kinamycin F (**1.1f**), in DMSO-d6 was just 2.7 Hz. The gradual change of the coupling constant from 6 Hz to 2.7 Hz, as observed with kinamycin F (**1.1f**) when gradually changing the NMR solvent from the less polar $CDCl_3$ to more polar DMSO-d6, would suggest that kinamycin F (**1.1f**), unlike the model **2.59** and other kinamycins, exhibits a different (opposite) conformational preference for its D-ring. Kinamycin F (**1.1f**), particularly in the polar solvents, has an unusual preference for a half chair conformation where the C1-OH and C2-OH groups are pseudo-axial (Scheme 2-12, conformer **A**), and consequently the H1 and H2 would exist in pseudo-equatorial orientation having a rather small dihedral angle of H1-C1-C2-H2 and $J_{H^1–H^2}$. This conclusion is especially interesting given the recent suggestion that the kinamycin F (**1.1f**) may represent the bioactive form of the other kinamycins.[241] Further study on this phenomenon provided more supportive evidence from ab initio MO calculation of **1.1f** in both gas phase and solution phase and experimental IR observations, and details of the

corresponding results will be discussed in Chapter 4. Although various attempts have been made to grow single crystals of kinamycin F (**1.1f**) in the hope of obtaining further physical evidence, no success has been achieved so far.

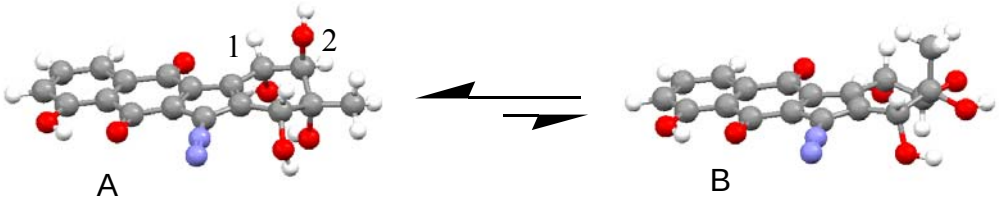

Scheme 2-12. Calculated two energy minimum conformations of kinamycin F (**1.1f**) in which the conformation A is preferred.

2.4 Conclusion

In summary, a new and biomimetic strategy for constructing the highly oxygenated and stereospecific D-ring of kinamycin F (**1.1f**), in four steps from a D-ring quinone precursor and 57% overall yield, has been demonstrated in a model study using 2-methyl-1,4-naphthylquinone (**2.25**) as the starting material. Additionally, spectroscopic analysis as well as ab initio molecular orbital calculations have led to the conclusion that kinamycin F (**1.1f**), unlike the other kinamycins, prefers a D-ring conformation in which the C4-OH group is in a pseudo-equatorial orientation. Enhanced diazonium ion character is predicted for this preferred conformation (see Chapter 4) and may influence the biological activity of kinamycin F (**1.1f**). These observations have now appeared in print.[165]

2.5 Experimental Details

2.5.1 General Information

Materials and Methods. All reactions were carried out in flame and oven-dried glassware under an argon or nitrogen atmosphere, unless otherwise specified. All solvents were reagent grade. Anhydrous tetrahydrofuran (THF) was freshly distilled from sodium/benzophenone under nitrogen prior to use. Deionized water was supplied by a Biolab vertical series reverse osmosis system. All commercial reagents were purchased from either Aldrich Chemical Co. or BDH Inc., and were used as received unless otherwise indicated. Reactions were magnetically stirred and monitored by thin layer chromatography (TLC) with Merck pre-coated silica gel plates (silica gel 60 F_{254} on aluminum sheet). Flash column chromatography was carried out using the Merck silica gel (70–230 or 230–400 mesh) or the SiliCycle silica gel (60 Å). All reported yields refer to chromatographically and spectroscopically pure compounds, unless otherwise specified.

Characterization Methods. ^{1}H NMR spectra were recorded on a Brüker AVANCE500 (500 MHz), Brüker AVANCE300 (300 MHz), Brüker AC300 (300 MHz) or Brüker AC200 (200 MHz) NMR spectrometer. ^{13}C NMR spectra were broad band decoupled and recorded on a Brüker AVANCE500 (125.8 MHz), Brüker AVANCE300 (75.5 MHz), Brüker AC300 (75.5 MHz) or Brüker AC200 (50 MHz) NMR spectrometer using the carbon signal of the deuterated solvent as the internal standard. HMQC, HMBC and difference NOE experiments were performed on the Brüker AVANCE500 spectrometer. The following abbreviations are used for NMR peak multiplicities: s, singlet; d, doublet; t, triplet; q, quartet; dd, doublet of doublets; dt, doublet of triplets; m, multiplet; br, broad; w, weak. Chemical shifts are reported in parts per million (ppm) relative to either TMS (δ 0.0), chloroform (δ 7.26), DMSO (δ 2.50) or acetone (δ 2.05) for ^{1}H NMR, and either chloroform (δ 77.16), DMSO (δ 39.52) or acetone (δ 29.84) for ^{13}C NMR.[242] Infrared spectra (IR) were recorded on

a Perkin-Elmer spectrum RX I FT-IR spectrometer as KBr discs or thin films on NaCl plates, as indicated in each individual case. High resolution mass spectra (HRMS) and low resolution mass spectra (LRMS), obtained via electron impact (EI) and/or chemical ionization (CI), were measured by the McMaster Regional Centre for Mass Spectrometry (Department of Chemistry, McMaster University, Hamilton, Ontario, Canada) or by the WATSPEC Mass Spectrometry Facility (Department of Chemistry, University of Waterloo, Waterloo, Ontario, Canada). Elemental/combustion analysis was performed by M-H-W Laboratories (Phoenix, Arizona, USA). Melting points were determined on a MEL-TEMP melting point apparatus and were uncorrected.

2.5.2 Detailed Experimental Procedures

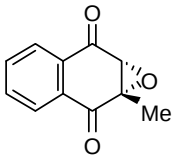

2,3-Epoxy-2-methyl-1,4-naphthoquinone 2.27: The commercial 2-methyl-1,4-naphthoquinone **2.25** (98%, 5.005 g, 28.5 mmol) was dissolved completely in ethanol (20 mL) upon heating the solution to about 70 °C under an air atmosphere. The solution was then cooled to about 50 °C and aqueous hydrogen peroxide solution (30%, 10 mL) was added dropwise during a period of 20 min. Then aqueous sodium carbonate solution (2.5 g of Na_2CO_3 dissolved in 10 mL of deionized water) was added dropwise during a period of 15 min in order to avoid a rapid increase of the solution temperature. A large amount of gas bubbles were generated during the addition of the Na_2CO_3 solution, and the yellow color of the quinone solution gradually disappeared. The almost colorless reaction solution was kept stirring for another 5 min after the addition of base, during which some white solid precipitated from the solution. Upon addition of deionized water (250 mL), a large amount of white solid precipitated from the solution. The white solid was collected by vacuum

filtration and washed thoroughly with H_2O (25 mL). The product was further dried overnight under vacuum to yield a fine white power (4.112 g, 21.9 mmol, 77% yield) as the desired pure compound. (Note: the epoxidation is quite exothermic so precaution to control the speed of addition of the base and reaction temperature is necessary when working on larger scales). IR (KBr) 1701, 1595, 1337, 1298, 1250, 1194 cm^{-1}; ^1H NMR (300 MHz, $CDCl_3$) δ 8.05–7.89 (m, 2 H), 7.80–7.68 (m, 2 H), 3.85 (s, 1 H), 1.72 (s, 3 H); ^{13}C NMR (75 MHz, $CDCl_3$) δ 192.0, 191.9, 134.7, 134.5, 132.2, 132.1, 127.6, 126.9, 61.6, 61.5, 14.8; HRMS (EI) *m/z* 188.0470 [M^+; calculated for $C_{11}H_8O_3$: 188.0473]; mp 93.5–94.5 °C (lit.[166] 94.5–95.5 °C).

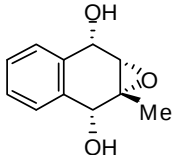

2,3-Epoxy-1,4-hydroxy-2-methyl-1,2,3,4-tetrahydronaphthalene 2.28: 2,3-Epoxy-3-methyl-1,4-naphthoquinone **2.27** (0.376 g, 2.0 mmol) was dissolved in methanol (30 mL) and the solution was cooled to about 0 °C with an ice bath. Sodium borohydride (0.0767 g, 2.0 mmol) was added to the solution in one portion under stirring and then the ice bath was removed. The solution was stirred for another 10 min and the temperature of the solution raised to ca. 18 °C. The solvent was then removed *in vacuo* at room temperature and the remaining white solid was mixed with saturated aqueous NH_4Cl solution (250 mL). The obtained aqueous solution was extracted thoroughly with ethyl acetate (6 × 80 mL), and the combined organic phase was dried over Na_2SO_4 and concentrated *in vacuo*. The epoxy diol **2.28** was obtained quantitatively as a white powder (0.388 g, 2.0 mmol, 100% yield). IR (KBr) 3295, 1508, 1420, 1348, 1186, 1118, 1094, 1042, 1009 cm^{-1}; ^1H NMR (200 MHz, DMSO-d6) δ 7.52–7.37 (m, 2 H), 7.30–7.18 (m, 2 H), 5.84–5.72 (m, 2 H), 4.80 (d, J = 7.0 Hz, 1 H), 4.65 (d, J = 8.5 Hz, 1 H), 3.33 (d, J = 1.5 Hz, 1 H), 1.47 (s, 3 H); ^{13}C NMR (50 MHz, DMSO-d6/D_2O) δ 136.5, 135.7,

126.89, 126.85, 125.5, 125.4, 68.7, 65.8, 61.9, 59.4, 19.2; HRMS (EI) *m/z* 192.0789 [M^+; calculated for $C_{11}H_{12}O_3$: 192.0786]; mp 148–153 °C (decomp.).

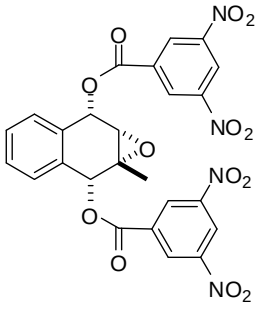

2,3-Epoxy-1,4-hydroxy-2-methyl-1,2,3,4-tetrahydronaphthalene bis(3,5-dinitrobenzoate ester) 2.30: The commercially available 3,5-dinitrobenzoyl chloride (98+%, 1.180 g, 5.0 mmol) was mixed with a catalytic amount of 4-dimethylaminopyridine (DMAP, 0.0131 g, 0.11 mmol). Pyridine (10 mL) was added to the above solid mixture and the resulting solution was stirred under a N_2 atmosphere in an ice bath. The epoxy diol **2.28** (0.240 g, 1.25 mmol) was dissolved in pyridine (2 mL) and the obtained orange-red solution was added dropwise to the acid chloride/pyridine solution during a period of 5 min. The flask containing the epoxy diol-pyridine solution was further washed with pyridine (3 × 1 mL), which was also transferred into the reaction flask. The clear yellow reaction solution was stirred at ambient temperature for 10 hr, with the observation that the solution gradually turned very turbid and the color of the reaction mixture became brown-red at the end. The reaction was quenched by pouring the mixture into previously cooled H_2O (20 mL) in an ice bath and the obtained aqueous mixture was further stirred for 5 min, and was then extracted with CH_2Cl_2 (3 × 40 mL). The organic phases were thoroughly washed with saturated aqueous $CuSO_4$ solution (3 × 60 mL), H_2O (2 × 60 mL) and 5% aqueous $NaHCO_3$ solution (5 × 60 mL). The CH_2Cl_2 solution was dried over Na_2SO_4 and the solvent was removed *in vacuo*. A light brown powder was obtained as the crude product (0.673 g). Recrystallization of the crude product in organic solvents such as ethanol, toluene, CH_2Cl_2 and acetone all failed due to the low solubility of the product. However, it was found

that acetone could efficiently wash off the colored impurities from the crude product. Therefore, the crude product was washed with a minimal amount of acetone under slightly reduced pressure, yielding some pale gray powder as the pure final product (0.526 g, 0.9 mmol, 73% yield). IR (KBr) 3449, 3089, 1730, 1630, 1546, 1459, 1347, 1269, 1163, 1122, 1076 cm^{-1}; ^{1}H NMR (500 MHz, DMSO-d6) δ 9.13 (dt, *J* = 2.0, 0.5 Hz, 1 H), 9.12 (dt, *J* = 2.0, 0.5 Hz, 1 H), 9.05 (dd, *J* = 2.0, ~0.5 Hz, 2 H), 9.03 (dd, *J* = 2.0, ~0.5 Hz, 2 H), 7.45–7.37 (m, 3 H), 7.29 (d, *J* = 8.5 Hz, 1 H), 6.79 (s, 1 H), 6.75 (s, 1 H), 3.95 (d, *J* = 2.0 Hz, 1 H), 1.53 (s, 3 H); ^{13}C NMR (75 MHz, DMSO-d6) δ 162.8, 162.6, 148.5, 148.4, 132.4, 131.8, 131.0, 130.2, 129.4, 129.2, 128.3, 125.8, 125.4, 123.0, 122.9, 73.6, 71.0, 57.9, 57.7, 18.4; HRMS (CI) *m/z* 580.0773 [M^{+}; calculated for $C_{25}H_{16}N_4O_{13}$: 580.0714], 598.1039 [$(M+NH_4)^{+}$; calculated for $C_{25}H_{20}N_5O_{13}$: 598.1058]; mp > 260 °C.

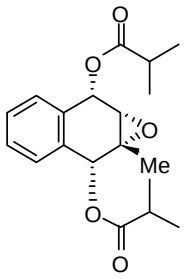

2,3-Epoxy-1,4-hydroxy-2-methyl-1,2,3,4-tetrahydronaphthalene Diisobutyryl ester 2.31: The epoxy diol **2.28** (0.385 g, 2.0 mmol) was mixed with a catalytic amount of DMAP (0.0506 g, 0.41 mmol), followed by the addition of pyridine (20 mL). Then isobutyryl chloride (98%, 0.86 mL, 8.0 mmol) was added dropwise through a syringe during a period of 0.5 min to the above reaction mixture, and the resulting solution was stirred under the air atmosphere for 24 hr at ambient temperature. The reaction was quenched by dilution with H_2O (20 mL) and the obtained solution was further stirred for 15 min, during which a large amount of white precipitate formed. The precipitate was filtered and washed with H_2O (20 mL) and it was then re-dissolved in CH_2Cl_2 (50 mL). The CH_2Cl_2 solution was washed with saturated aqueous $CuSO_4$ solution (1 × 50 mL) and H_2O (1 × 50

mL). The organic solution was dried over Na_2SO_4 and the solvent was removed *in vacuo,* yielding a white solid as the pure product (0.426 g, 1.27 mmol, 64% yield). IR (KBr) 2980, 2933, 1735, 1496, 1448, 1437, 1388, 1355, 1187, 1146, 1103 cm^{-1}; ^1H NMR (300 MHz, $CDCl_3$) δ 7.40–7.20 (m, 3 H), 7.10–7.00 (m, 1 H), 6.32 (s, 1 H), 6.22 (s, 1 H), 3.57 (s, 1H), 2.90–2.70 (m, 2 H), 1.49 (s, 3 H), 1.40–1.30 (m, 12 H); ^{13}C NMR (75 MHz, $CDCl_3$) δ 177.1, 177.0, 131.4, 130.4, 128.19, 128.12, 125.7, 125.5, 70.3, 68.3, 58.5, 57.6, 34.3, 19.26, 19.20, 18.99, 18.78; LRMS (CI) *m/z* 350.2 $[(M+NH_4)^+$; calculated for $C_{19}H_{28}NO_5$: 350.4]; mp 120–120.5 °C.

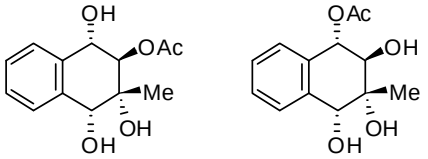

Triol acetates 2.45: The epoxy diol **2.28** (0.963 g, 5.00 mmol) was mixed with NaOAc (99%, 2.072 g, 25.0 mmol) and the commercial $Me_4NBH(OAc)_3$ (95%, 1.525 g, 5.50 mmol) in a flame- and oven-dried round bottom flask, followed by addition of anhydrous THF (50 mL). A large amount of gas bubbles were generated at the beginning and the reaction mixture was heated to reflux in an oil bath for 6 hr under an argon atmosphere. The reaction mixture was further stirred for 1 hr without heating until the solution cooled gradually to room temperature. The reaction was quenched by the addition of saturated aqueous $NaHCO_3$ solution (50 mL) and the mixture was further stirred for 10 min. Another 50 mL of H_2O was added to completely dissolve the remaining NaOAc powder. The aqueous solution was then extracted thoroughly with CH_2Cl_2 (8 × 100 mL) and the organic phase was dried over Na_2SO_4 and concentrated *in vacuo*. The crude epoxide ring-opening product was obtained as a slightly yellow foamy solid (0.809 g). Some more crude product was successfully recovered from the aqueous phase in the previous extraction step: the aqueous phase was concentrated to dryness and the remaining solid residue was stirred with 2 L of CH_2Cl_2, and the CH_2Cl_2 solution was then dried over Na_2SO_4, leading to another 0.180 g of the crude product upon removal of the solvent. The combined

crude product (0.989 g) was further purified by charcoal decolorization in CH_2Cl_2 and some off-white foamy solid (0.956 g, 3.79 mmol, 76% yield) was obtained as the final pure product, which consists of two regioisomers of the triol acetates **2.45a** and **2.45b** in an approximate ratio of 1:1, as determined by NMR. This "pure" mixture is directly suitable for the next Zemplen deacylation and peracetylation reaction. If the pure form of each of the regioisomers is desired, flash column chromatography using a mixture of EtOAc and hexanes (3:1, v/v) as the eluent could be performed directly with the crude product, without the need of charcoal decolorization. The separated two pure triol acetates were then subjected to extensive NMR spectroscopy studies, including ^{1}H, ^{13}C, difference NOE, HMBC and HMQC, to establish the stereochemistry assigned.

Mixture of **2.45a** and **2.45b** (~ 1:1): IR (KBr) 3423, 1736, 1720, 1376, 1255, 1096, 1025 cm^{-1}; IR (film) 3396, 2936, 1716, 1491, 1456, 1374, 1252, 1097, 1024 cm^{-1}.

Regioisomer **2.45a**: IR (film) 3392, 1719, 1375, 1251, 1094, 1037 cm^{-1}; ^{1}H NMR (300 MHz, acetone-d6) δ 7.57 (d, *J* = 7.8 Hz, 1 H), 7.50–7.20 (m, 3 H), 5.45 (d, *J* = 7.5 Hz, 1 H), 4.72 (d, *J* = 6.3 Hz, 1 H), 4.70–4.55 (m, 2 H), 4.47 (d, *J* = 4.4 Hz, 1 H), 3.78 (s, 1 H), 2.08 (s, 3H), 1.11 (s, 3 H); ^{1}H NMR (500 MHz, acetone-d6/D_2O) δ 7.56 (d, *J* = 8.0 Hz, 1 H), 7.40 (d, *J* = 7.0 Hz, 1 H), 7.36–7.27 (m, 2 H), 5.44 (d, *J* = 8.0 Hz, 1 H), 4.56 (d, *J* = 7.5 Hz, 1 H), 4.46 (s, 1 H), 2.08 (s, 3 H), 1.11 (s, 3 H); ^{13}C NMR (125 MHz, acetone-d6/D_2O) δ 171.4, 138.1, 137.0, 130.5, 128.86, 128.85, 128.5, 77.7, 76.0, 73.1, 71.1, 21.2, 19.6; HRMS (EI) *m/z* 235.0956 [$(M\text{-}OH)^+$; calculated for $C_{13}H_{15}O_4$: 235.0970]; HRMS (CI) *m/z* 235.0989 [$(M\text{-}OH)^+$; calculated for $C_{13}H_{15}O_4$: 235.0970], 252.1258 [$(M+NH_4\text{-}H_2O)^+$; calculated for $C_{13}H_{18}NO_4$: 252.1236], 253.1130 [$(M+H)^+$; calculated for $C_{13}H_{17}O_5$: 253.1076]; mp 153–155 °C; Elemental/combustion analysis: calculated for $C_{13}H_{16}O_5$: C 61.90, H 6.39; found: C 61.89, H 6.48.

Regioisomer **2.45b**: IR (film) 3415, 2926, 1725, 1644, 1493, 1457, 1374, 1246, 1099, 1027 cm^{-1}; ^1H NMR (300 MHz, acetone-d6) δ 7.50–7.10 (m, 4 H), 5.89 (d, *J* = 8.1 Hz, 1 H), 4.49 (s, 1 H), 4.38 (d, *J* = 4.5 Hz, 1 H), 4.30–4.15 (m, 1 H), 3.91 (s, 1 H), 2.14 (s, 3 H), 1.11 (s, 3 H); ^1H NMR (500 MHz, acetone-d6/D_2O) δ 7.43–7.38 (m, 1 H), 7.34–7.28 (m, 2 H), 7.19–7.14 (m, 1 H), 5.88 (d, *J* = 8.5 Hz, 1 H), 4.49 (s, 1 H), 4.20 (d, *J* = 8.5 Hz, 1 H), 2.14 (s, 3 H), 1.10 (s, 3 H); ^{13}C NMR (125 MHz, acetone-d6/D_2O) δ 171.8, 137.9, 134.9, 131.3, 129.0, 128.9, 128.0, 76.0, 75.1, 73.6, 73.0, 21.2, 18.7; HRMS (EI) *m/z* 234.0895 [$(M-H_2O)^+$; calculated for $C_{13}H_{14}O_4$: 234.0892]; HRMS (CI) *m/z* 235.1003 [$(M-OH)^+$; calculated for $C_{13}H_{15}O_4$: 235.0970], 252.1256 [$(M+NH_4-H_2O)^+$; calculated for $C_{13}H_{18}NO_4$: 252.1236], 253.1064 [$(M+H)^+$; calculated for $C_{13}H_{17}O_5$: 253.1076]; mp 45–48 °C.

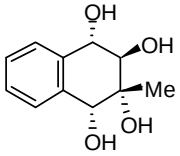

Tetrol **2.59**:

Method (a) Reductive deacylation of triol acetates **2.45** by $LiAlH_4$:

A mixture of the two triol acetates **2.45** (0.10 g, 0.4 mmol) was dissolved in anhydrous THF (5 mL) under argon atmosphere and the solution was cooled in an ice bath. A commercial THF solution of $LiAlH_4$ (1.0 M, 2 mL, 2 mmol) was added dropwise to the reaction flask through a syringe during a period of 5 min. The reaction solution was warmed to ambient temperature by removing the ice bath and further stirred for 0.5 h, followed by the addition of $Na_2SO_4 \cdot 10H_2O$ (0.66 g, 2 mmol) in two portions to quench the reaction. The reaction mixture was further stirred with ethyl acetate (200 mL) for 2 h and then filtered under reduced pressure through a Büchner funnel preloaded with a layer of celite (~ 2 cm thick). The solid residue in the funnel was thoroughly washed with ethyl acetate (200 mL). The combined ethyl acetate solution was concentrated *in vacuo* and a yellow oil was obtained as

the crude product (0.05 g, 59% crude yield), which solidified upon drying under vacuum overnight. A repeated reaction with larger amounts of **2.45** (0.16 g, 0.65 mmol) produced a crude yield of 56%. NMR spectroscopy indicated that the major component of crude product was indeed the desired product but various purification processes turned out to be quite difficult and inefficient. See the section of "Method (c)" for spectroscopic data of the produced tetrol **2.59**.

Method (b) Deacylation of triol acetates **2.45** by simple basic hydrolysis:

A freshly prepared NaOH solution (7.6 mL, 0.1975 M, 1.5 mmol) was added in one portion to a mixture of the two triol acetates **2.45** (0.05 g, 0.2 mmol) and the reaction mixture was stirred at room temperature for 2 h under argon atmosphere. The reaction mixture was then cooled in an ice bath and the excess NaOH was neutralized by adding 0.5 M HCl solution (3 mL) dropwise until the pH of the reaction mixture reached about 6 (as indicated by pH paper). The aqueous solution was extracted with CH_2Cl_2 (4 × 20 mL). The organic phase was dried over Na_2SO_4 and concentrated *in vacuo*, yielding a white solid as the crude product (0.009 g, 0.04 mmol, 25% crude yield). See the section of "Method (c)" for spectroscopic data of the produced tetrol **2.59**.

Method (c) Zemplen deacylation of triol acetates **2.45**

A fresh MeOH solution of NaOMe (1 M) was prepared by completely reacting sodium metal (0.23 g, 10 mmol) with small amount of methanol (~ 4 mL) first. The final volume of this NaOMe/MeOH solution was adjusted to 10.0 mL in a volumetric flask. A mixture of the two triol acetates **2.45a** and **2.45b** (~1:1, 0.470 g, 1.86 mmol) was dissolved in methanol (18.8 mL). The previously prepared 1 M NaOMe/MeOH solution (5.0 mL, 5 mmol) was added dropwise to the reaction mixture and the solution was stirred at room temperature for 1 h under the air atmosphere. The reaction was quenched

by the addition of about 10 g of a weak acidic ion (H^+) exchange resin (CGC-271, 200–400 mesh, chromatographic grade, weak acid, carboxylic, methylacrylate, 2.5% XL with a total exchange capacity of 9.6% meq/g). The mixture was stirred for 5 min until the pH of the solution reached around 6, as indicated by wet pH paper. Vacuum filtration gave a light yellow filtrate and the ion exchange resin was further washed with MeOH (100 mL). The combined MeOH filtrate yielded a white (slightly yellow) foamy solid upon concentration *in vacuo*, which was then subjected to a charcoal decolorization in acetone. The obtained almost colorless acetone solution of the product gave a white foamy solid (0.385 g, 1.83 mmol, 98% yield) upon removal of the solvent, which was proven by NMR spectroscopy to be the desired tetrol **2.59**. The compound **2.59** should be stored in a dessicator since it is slightly hydroscopic in its solid state. IR (film) 3390, 2925, 2855, 1645, 1458, 1378, 1262, 1099, 1024 cm^{-1}; ^1H NMR (300 MHz, DMSO-d6) δ 7.44 (d, *J* = 6.9 Hz, 1 H), 7.36–7.20 (m, 3 H), 5.28 (d, *J* = 6.6 Hz, 1 H), 5.00 (d, *J* = 5.1 Hz, 1 H), 4.87 (s, 1 H), 4.41 (s, 1 H), 4.29 (d, *J* = 3.9 Hz, 1 H), 4.21 (t, *J* = 6.3 Hz, 1 H), 3.77 (d, *J* = 6.6 Hz, 1 H), 1.00 (s, 3 H); ^{13}C NMR (75 MHz, DMSO-d6) δ 138.2, 137.1, 129.0, 128.0, 127.3, 127.0, 74.4, 74.0, 72.7, 72.0, 20.1; HRMS (EI) *m/z* 192.0781 [$(M-H_2O)^+$; calculated for $C_{11}H_{12}O_3$: 192.0786], 174.0674 [$(M-2H_2O)^+$; calculated for $C_{11}H_{10}O_2$: 174.0681]; HRMS (CI) *m/z* 210.1122 [$(M+NH_4-H_2O)^+$; calculated for $C_{11}H_{16}NO_3$: 210.1130], 228.1214 [$(M+NH_4)^+$; calculated for $C_{11}H_{18}NO_4$: 228.1236].

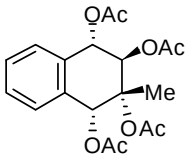

Tetra-acetate 2.60: The tetrol **2.59** (0.053 g, 0.25 mmol) and *N*, *N*-dimethylaminopyridine (DMAP, 99%, 0.307 g, 2.5 mmol) were dissolved in CH_2Cl_2 (5 mL), resulting in a faint red-brown solution. Acetic anhydride (99.4%, 0.24 mL, 2.5 mmol) was added dropwise during a period of 3 min at room temperature under stirring, which caused the faint red-brown color of the solution to immediately turn

to light yellow. The yellow reaction mixture was then stirred for 12 hr at room temperature under air atmosphere. MeOH (10 mL) was then added and the reaction mixture was further stirred for 20 min to quench the excess acetic anhydride. Upon removal of the solvent, some yellow-orange solid was obtained and it was then mixed with dilute HCl (2 M, 30 mL), followed by extraction with Et_2O (3 × 50 mL). The obtained light yellow organic phase was dried over Na_2SO_4 and concentrated *in vacuo*. A slightly yellow foamy solid was obtained as the crude product (0.085 g). The yellow color of the crude product was completely removed by charcoal decolorization in Et_2O. The pure product was obtained as a snow-white foamy solid (0.080 g, 0.21 mmol, 83% yield). IR (film) 3474, 2992, 2939, 1750, 1374, 1256, 1227 1043, 1023 cm^{-1}; ^1H NMR (300 MHz, DMSO-d6) δ 7.47–7.24 (m, 4 H), 6.48 (s, 1 H), 5.96 (d, *J* = 6.0 Hz, 1 H), 5.85 (d, *J* = 6.0 Hz, 1 H), 2.13 (s, 3 H), 2.10 (s, 3 H), 2.08 (s, 3 H), 1.93 (s, 3 H), 1.50 (s, 3 H); ^1H NMR (300 MHz, $CDCl_3$) δ 7.55–7.50 (m, 1 H), 7.42–7.35 (m, 2 H), 7.23-7.20 (m, 1 H), 6.78 (s, 1 H), 6.14 (d, *J* = 7.2 Hz, 1 H), 5.94 (d, *J* = 7.2 Hz, 1 H), 2.16 (s, 3 H), 2.14 (s, 3 H), 2.10 (s, 3 H), 1.99 (s, 3 H), 1.58 (s, 3 H); ^{13}C NMR (75 MHz, $CDCl_3$) δ 171.0, 170.1, 169.9, 169.7, 132.9, 132.7, 130.7, 129.8, 129.4, 128.7, 128.1, 80.5, 72.7, 72.6, 71.5, 22.0, 21.2, 21.1, 16.4; HRMS (EI) *m/z* 319.1180 [$(M\text{-}OAc)^+$; calculated for $C_{17}H_{19}O_6$: 319.1182]**.**

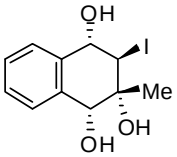

Iodohydrin 2.61: The epoxy diol **2.28** (0.096 g, 0.5 mmol), $Me_4NBH(OAc)_3$ (95%, 0.15 g, 0.55 mmol) and sodium iodide (98%, 0.383 g, 2.5 mmol) were mixed and dissolved in anhydrous THF (5 mL). The reaction solution was heated to reflux in an oil bath for 6 h under an argon atmosphere. A large amount of gas bubbles was generated at the beginning and the color of the solution turned from clear to yellow. The reaction mixture was further stirred for 1 hr without heating until it cooled gradually to the ambient temperature, followed by the addition of saturated aqueous $NaHCO_3$ solution

(10 mL) and further stirring for 10 min. The solution was then stirred with 10% aqueous $Na_2S_2O_3$ solution (10 mL) for 5 min. After thorough extraction with CH_2Cl_2 (6 × 25 mL), the obtained organic phase was dried over Na_2SO_4 and concentrated *in vacuo*. A red shiny flake was obtained as the pure product (0.145 g, 0.45 mmol, 90% yield). IR (KBr) 3400, 1017 cm^{-1}; ^1H NMR (500 MHz, acetone-d6) δ 7.59 (d, *J* = 7.5 Hz, 1 H), 7.41–7.29 (m, 3 H), 4.97 (d, *J* = 8.0 Hz, 1 H), 4.84–4.79 (m, 1 H), 4.75 (d, *J* = 9.0 Hz, 1 H), 4.67 (d, *J* = 5.5 Hz, 1 H), 4.61 (d, *J* = 5.0 Hz, 1 H), 4.24 (s, 1 H), 1.20 (s, 3 H); ^{13}C NMR (125 MHz, acetone-d6) δ 130.8, 129.1, 128.9, 128.7, 75.9, 75.8, 74.6, 74.5, 50.6, 23.4; HRMS (CI) *m/z* 320.0169 $[(M+NH_4-H_2O)^+$; calculated for $C_{11}H_{15}INO_2$: 320.0148], 338.0301 $[(M+NH_4)^+$; calculated for $C_{11}H_{17}INO_3$: 338.0253]**.**

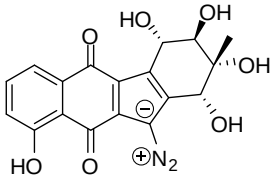

Kinamycin F 1.1f: A NaOMe-MeOH solution (1 M) was prepared by dissolving the commercial NaOMe (95% pure, 0.5687 g, 0.01 mol) in MeOH (HPLC grade, 10.00 mL) in a volumetric flask. Pure natural kinamycin D (**1.1d**) (0.0087 g, 0.0191 mmol), isolated from bacteria fermentation broth, was dissolved in MeOH (3 mL) and the reaction flask was completely covered with aluminum foil to avoid exposure to light. Then the previously prepared NaOMe-MeOH solution (1 M, 0.1 mL, 0.1 mmol) was added dropwise through a syringe under stirring to the bright orange yellow kinamycin D-MeOH solution, whose color turned immediately to very dark purple. The reaction mixture was then stirred at room temperature for 1 hr to complete the deacetylation. To a white slurry of ion (H^+) exchange resin (3 g, CGC-271, 200–400 mesh, chromatographic grade, weak acid, carboxylic, methylacrylate, 2.5% XL with a total exchange capacity of 9.6% meq/g) in MeOH (10 mL) under stirring, the dark purple reaction mixture was added dropwise and further stirred for 5 min, and the

slurry turned to dark orange red. The slurry was filtered under reduced pressure and the remaining resin was washed with copious amount of MeOH (ca. 40 mL) until it looked snow-white. The crude product was obtained as some a brown red solid (thin film) upon removal of solvent, which was further purified on a small dry silica gel column (3 cm x 2.5 cm) with acetone as the eluent. Pure kinamycin F (**1.1f**) was obtained as a dark brown-red fine powder quantitatively (0.0071 g, 0.0192 mmol, 100% yield). IR (KBr) 3438, 2142, 1622, 1456, 1238, 1158, 1087 cm^{-1}; IR (MeOH film) 3468, 2137, 1620, 1458, 1087 cm^{-1}; ^1H NMR (300 MHz, DMSO-d6) δ 12.31 (s, disappear after D_2O exchange, 1 H), 7.68 (t, *J* = 8.1 Hz, 1 H), 7.58 (d, *J* = 6.9 Hz, 1 H), 7.26 (d, *J* = 8.1Hz, 1 H), 5.43 (d, *J* = 9.3 Hz, disappears after D_2O exchange, 1 H), 5.38 (d, *J* = 4.2 Hz, disappears after D_2O exchange, 1 H), 5.01 (s, disappears after D_2O exchange, 1 H), 4.99 (d, *J* = 9.0 Hz, disappears after D_2O exchange, 1 H), 4.73 (br dd; after D_2O exchange, d, *J* = 2.7 Hz; 1 H), 4.64 (d, *J* = 9.0 Hz; after D_2O exchange, s; 1 H), 3.74 (br t; after D_2O exchange, d, *J* = 2.1 Hz, 1 H), 1.28 (s, 3 H); HRMS (+ESI-MS, in 1:1 (v/v) CH_3CN/H_2O with sucrose and LiOAc as additives) *m/z* 377.0962 [$(M+Li)^+$; calculated for $C_{18}H_{14}N_2O_7Li$: 377.0961; $(sucrose+Li)^+$ with a known *m/z* of 349.1322 was used as the internal standard].

Chapter 3

Synthetic Attempts towards the Kinamycin Antibiotics and Analogues

3.1 Synthetic Work towards the Kinamycin Benzo[*b*]fluorene Skeleton

The Dmitrienko lab is among a few research groups that have been involved in synthetic studies aimed at the kinamycins antibiotics and related structures since the late 1980s, and work in this lab has led to several important publications regarding the various aspects of the chemistry of the kinamycins over the years.[14,22,25,73,124,165,241,243,244] Prior to the start of this research project, Laufer from the Dmitrienko group had proposed and partially developed two synthetic strategies towards the benzo[*b*]fluorene skeleton of kinamycins (Scheme 3-1a),[80] which were based on even earlier results by Mithani[245] and Carrière[168] also from the Dmitrienko lab. The benzo[*b*]fluorene structure **3.1** could be constructed (Scheme 3-1a) via either (i) an intramolecular Jacobson-Torssell coupling of **3.2** (i.e., arylation/alkylation of *p*-quinone with free radicals derived from the corresponding carboxylic acid under strong oxidative conditions[246,247]), which itself can be prepared from an intermolecular Jacobson-Torssell coupling of the halogenated juglone **3.3** and a substituted homophthalic acid **3.4** or (ii) a Ni(0)-catalyzed intramolecular coupling of **3.7**, which could be conceivably prepared through an intermolecular Jacobson-Torssell coupling of **3.3** and substituted *o*-halophenylacetic acid **3.6**. In fact, initial success to synthesize model compounds such as **3.10**[168] and **3.13**[80] (Scheme 3-1b) was achieved by following the above retrosynthetic proposals.

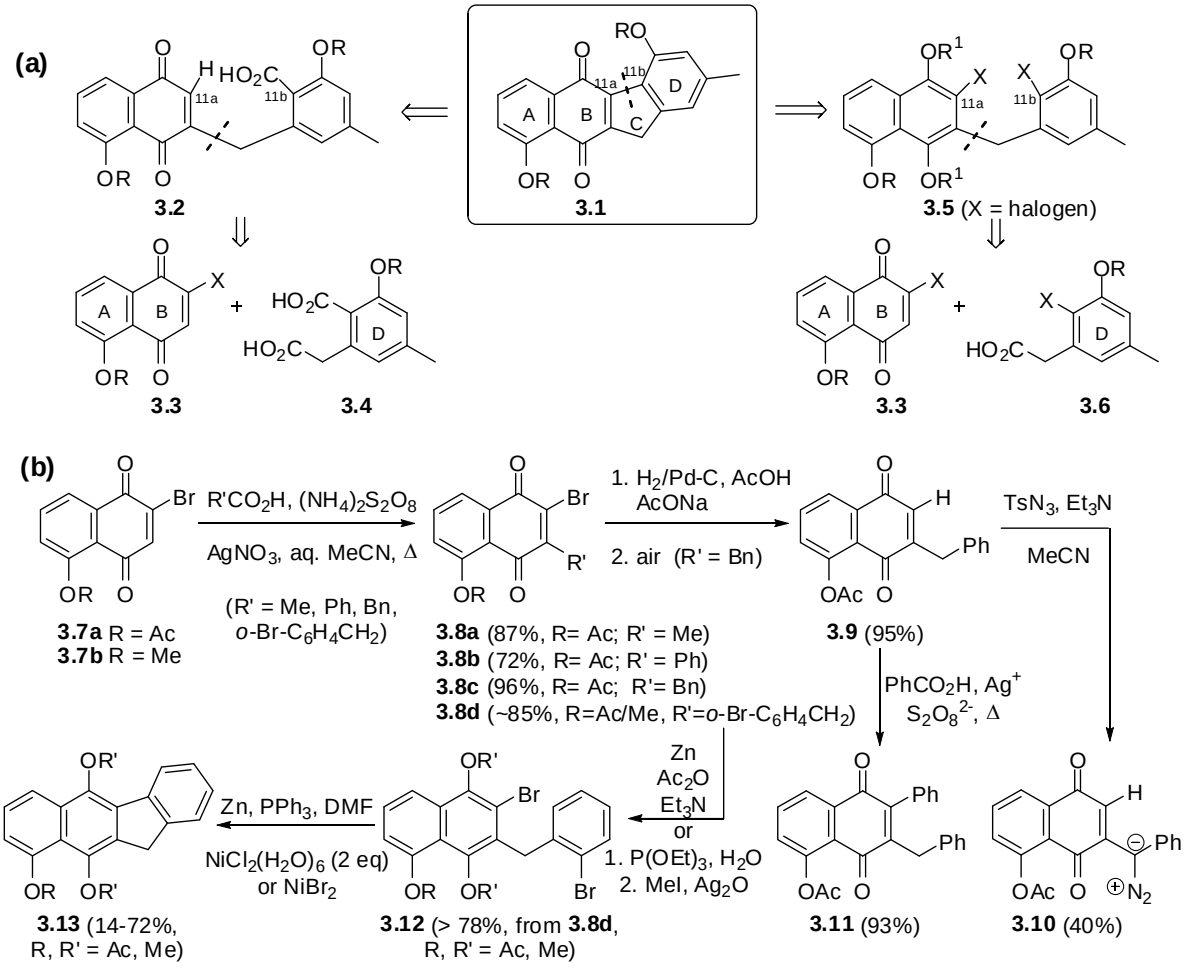

Scheme 3-1. (a) Original retrosyntheses of the benzo[*b*]fluorene skeleton by the Dmitrienko lab; (b) synthesis of kinamycin model compounds based on retrosyntheses in (a).

However, both strategies suffered from their own deficiencies at certain steps when being applied towards the total synthesis of prekinamycin (**1.4**) (Scheme 3-2).[80] For example, the key intramolecular Ni(0)-catalyzed cyclization of **3.16** to form the benzo[*b*]fluorene skeleton experienced a low yield of only 27% (Scheme 3-2a) even after extensive optimization. In addition, the apparently simple D-ring precursors involved, such as **3.15** (Scheme 3-2a) and **3.20** (Scheme 3-2b), had to be prepared through complex sequences that also encountered some difficult chemical transformations with low yields. As

a continuation of these available yet unpublished results, initial synthetic efforts of this thesis project were made to repeat and attempt the incomplete synthetic route outlined (with dashed arrow) in Scheme 3-2b, which required the preparation of **3.19** in fairly large quantities as an essential starting material to begin with. Unfortunately, large scale preparation of **3.19** turned out to be problematic and yields were significantly lower than the small scale ones (64–94%). Another issue with these two synthetic paths is that, even though the desired diazo transfer reactions at C5 of benzo[*b*]fluorenes was carried out successfully in the case of model compound **3.26** (Scheme 3-2c), the same chemical derivatization at C5 of **3.17** and simpler analogues (i.e., without A-ring and/or D-ring substituents of **3.17**) were found to be very difficult.[80] These results led to some further reconsideration of the original retrosynthetic plans within the Dmitrienko group. An alternative synthetic approach was proposed in order to avoid the above challenges, and the corresponding experimental results will be discussed next in detail.

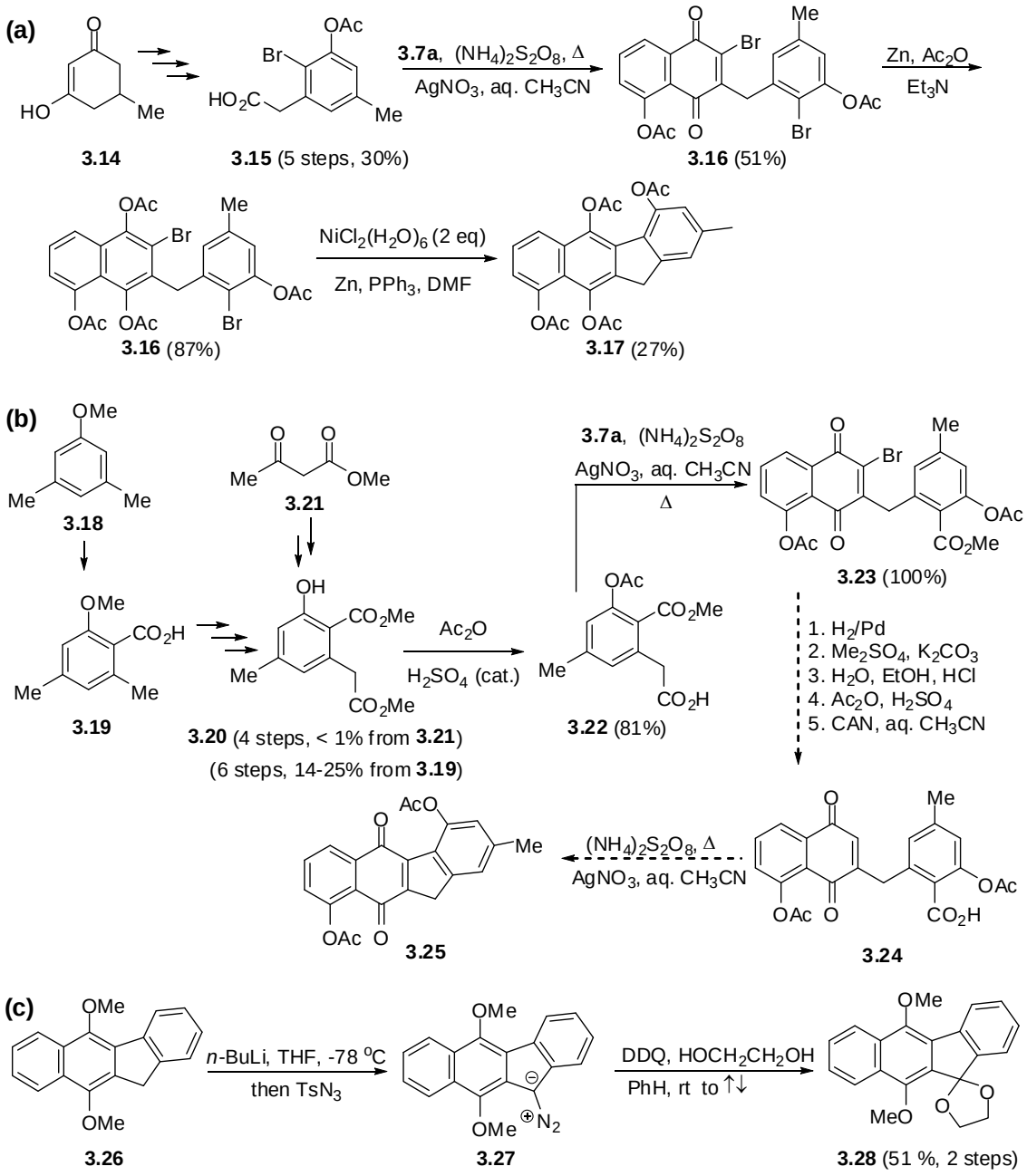

Scheme 3-2. Synthetic attempts towards the benzo[*b*]fluorene of prekinamycin (**1.4**) based on retrosynthetic plans of Scheme 3-1a.

3.1.1 New Retrosynthesis of the Benzo[*b*]fluorene System

The proposed new synthetic strategy towards the benzo[*b*]fluorene skeleton of the kinamycins is based on the new retrosynthetic analysis as illustrated in Scheme 3-3. Initial disconnection still occurs at C5 of the generic diazobenzo[*b*]fluorene structure **3.29** of kinamycin. Introduction of the diazo moiety to the benzo[*b*]fluorenone precursor **3.30**, either through a diazo transfer with **3.30a** similar to the previous model study (Scheme 3-2c) or a conversion of C5-ketone **3.30b** to the corresponding hydrazone followed by oxidation, should provide the target kinamycins. The fluorene **3.30a** or the fluorenone **3.30b** might be derived from appropriate reduction or oxidation of the corresponding alcohol (not shown), which originates from decarboxylation of the α-hydroxy carboxylic acid **3.31**. The challenge of constructing the essential but rare 6-6-5-6 benzo[*b*]fluorene skeleton of **3.31** (and kinamycins), is then transformed into an easier synthetic task with many literature precedents, which aims at a precursor possessing a much more common 6-6-6-6 aglycon core. Contraction of the C-ring upon disconnection at the C5-C6 bond of two candidates, either the *o*-quinonediazide **3.32** or the *ortho*-quinone **3.33**, through either a Wolff rearrangement (for **3.32**) or a base-induced rearrangement (for **3.33**), should be able to achieve the goal. Both **3.32** and **3.33** might be prepared from the same precursor **3.34**, except that the former requires a diazo transfer at C5 of **3.34** while the latter demands a selective C-ring oxidation. By taking advantage of the newly developed biomimetic and highly efficient elaboration of kinamycin D-ring (Chapter 2), the non-aromatic and oxygenated D-ring of **3.34**, analogous to those found in the kinamycins, might be synthesized from the quinone precursor **3.35** through a sequence of asymmetric epoxidation, stereoselective reduction and regio-/stereoselective epoxide ring opening. Obviously the D-ring quinone of **3.35** is a result of regioselective oxidation of the fully aromatized **3.36**, as long as appropriate ABC-ring phenol protecting groups are present. Then the 6-6-6-6 aglycon skeleton of **3.36** would be formed via an intramolecular Friedel-Crafts cyclization of the biaryl species **3.37**, which is obviously a product from

the Suzuki coupling of AB-ring precursor **3.38** and D-ring precursor **3.39**. In general, either of **3.38** and **3.39** can be prepared in the form of a boronate or boronic acid, while the remaining one would be the corresponding aryl halide.

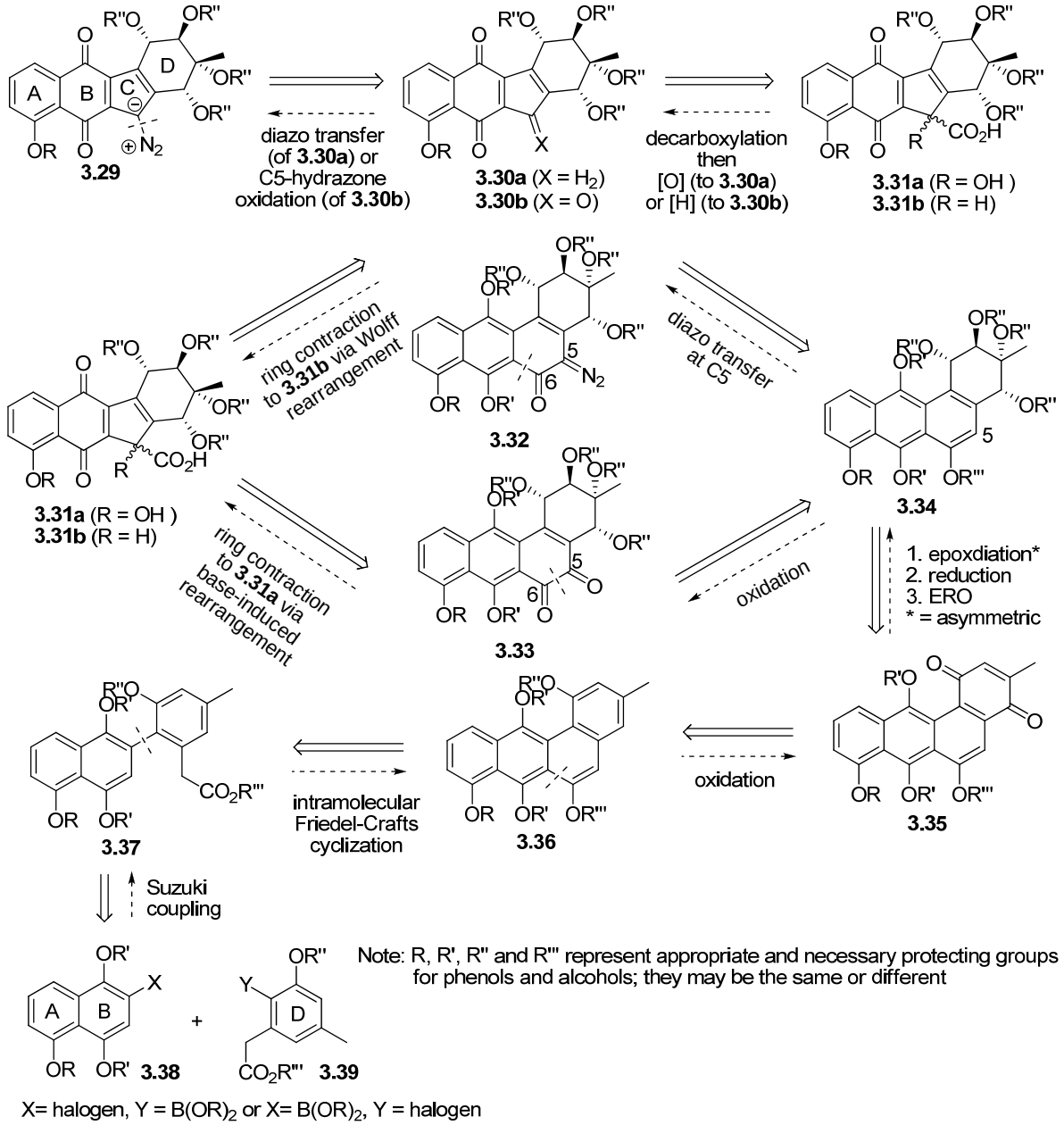

Scheme 3-3. New retrosynthetic analysis of the diazobenzo[*b*]fluorenes of kinamycins.

In regard to the proposed ring contraction step (i.e., **3.32**/**3.33** to **3.31**), the century-old Wolff rearrangement approach involving an α-diazoketone (or *o*-quinonediazide **3.32** in this case) has been well documented and thoroughly reviewed,[248] as the literature examples under either thermal conditions (e.g., **3.44** to **3.45**[249,250]), photolysis (e.g., **3.40** to **3.41**[251,252] and **3.44** to **3.46**[249,250]) or even microwave conditions (e.g., **3.42** to **3.43**[253]) shown in Scheme 3-4a. On the other hand, the proposed ring contraction of **3.33** through the base-induced rearrangement is strongly supported by a fairly recent (2006) literature report from the Mal group (Scheme 3-4b),[254] which was not available when the above route was proposed in the Dmitrienko group. The α-hydroxy carboxylic acids **3.52** possessing a 6-6-5-6 benzo[*b*]fluorene skeleton of kinamycins were prepared in good yields by a simple base (KOH)-induced ring contraction (a.k.a benzil-benzilic acid rearrangement[255]) of the corresponding 6-6-6-6 aglycon precursors **3.51**, which in turn were synthesized by using the Hauser annulation[152] of **3.47** (an equivalent to those indenones in Hauser annulation) and **3.48-3.50** (synthons equivalent to phthalides in Hauser annulation).[254]

The above synthetic strategy towards kinamycin involves many well-studied reactions at various key steps; on the other hand, it also utilizes the new biomimetic route for the elaboration of D-ring (Chapter 2). A bonus advantage of this route is that the intermediate α-diazoketone **3.32** with the 6-6-6-6 aglycon skeleton, if successfully prepared, is in fact a novel analogue of the 6-6-5-6 diazobenzo[*b*]fluorene and 6-5-6-6 diazobenzo[*a*]fluorene type kinamycins. Analogue **3.32** may itself have useful biological activity and may be of value for studies on the mode-of-action and influence of structures on the biological activities of these unusual diazo-containing antibiotics.

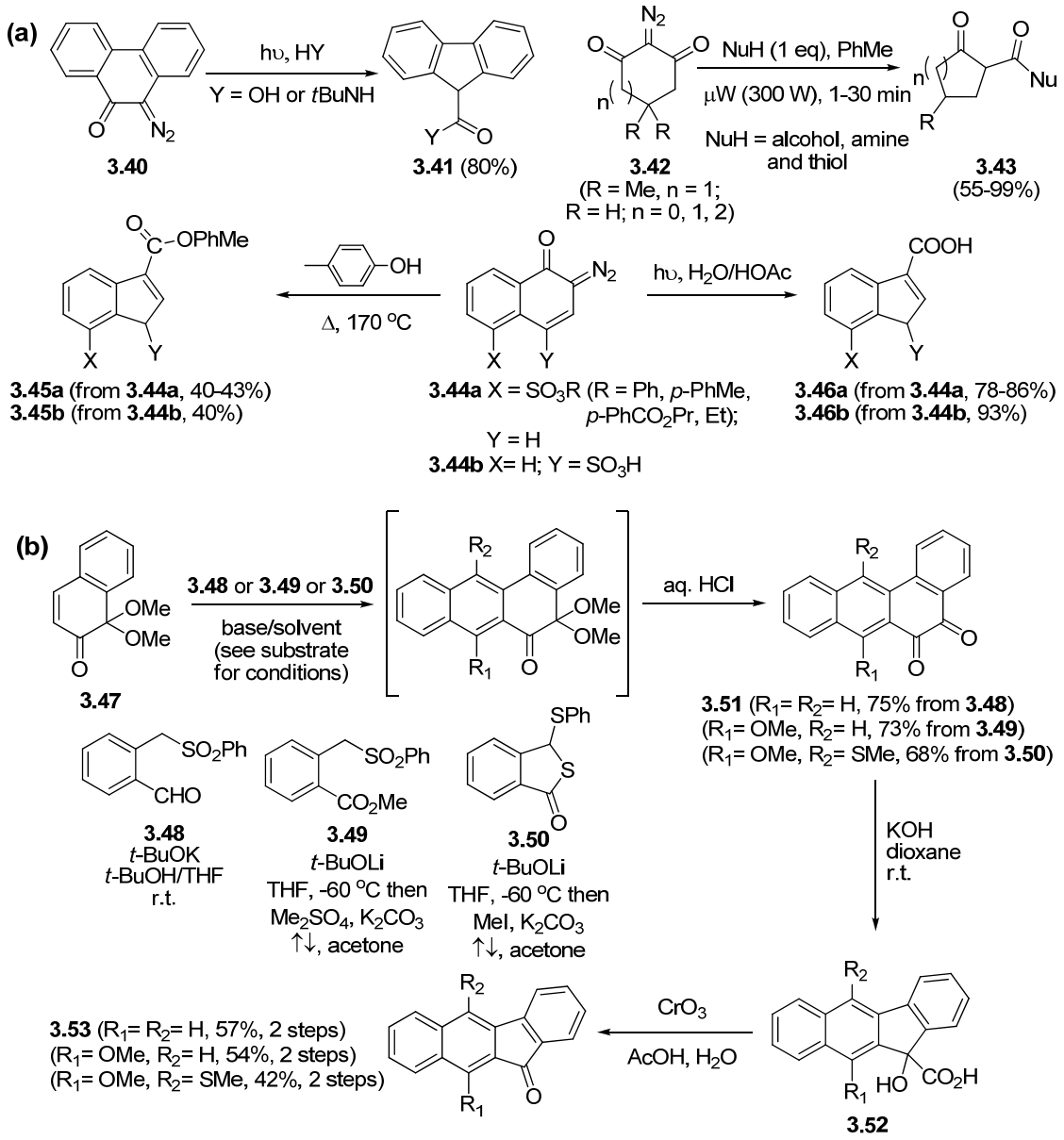

Scheme 3-4. Literature examples of ring contraction through (a) Wolff rearrangement and (b) base-induced rearrangement related to the benzo[*b*]fluorene skeleton of kinamycins.

3.1.2 Synthetic Work on the Kinamycin AB-Ring Precursor

The proposed kinamycin AB-ring precursor **3.38** (Scheme 3-3), either in the form of an aryl boronic acid/boronate or aryl halide, is a naphthol-based compound that can be easily prepared

through a few simple chemical transformations (Scheme 3-5), starting from the commercially available and inexpensive 1,5-dihydroxynaphthalene (**3.54**). There are several literature procedures describing the synthesis of similar compounds such as **3.56**,[256] **3.58**[257] and **3.59**[258] (Scheme 3-5). The naphthol **3.54** could be smoothly acetylated with acetic anhydride to the corresponding diacetoxy derivative **3.55**, which was then brominated with NBS in hot (55-65 °C) aqueous acetic acid leading to the key intermediate of bromojuglone **3.7a** for the reported several transformations. The one-pot bromination and oxidation from **3.55** to **3.7a**, which was originally developed by Grunwell and Heinzman,[259] required a minimum of 3 equivalents of NBS (relative to **3.55**) to complete the reaction, but the use of 4 equivalents of NBS offered better yields in practice. Therefore, Grunwell proposed the mechanism as shown in Scheme 3-5b to explain such experimental observations, where the nature of the electrophilic brominating agent was not specified.[259] It was later argued by Jung and Hagenah that the actual brominating reagent was likely the molecular bromine (Br_2) derived from NBS in situ.[260] Jung and Hagenah isolated a tribromo species **3.69** as an intermediate when the reaction was carried out at a lower temperature of 45 °C, which was converted back to the bromojuglone **3.7a** quantitatively upon further heating in aqueous acetic acid at 65 °C (Scheme 3-5c).[260] The same results were also independently observed later by Mithani from the Dmitrienko lab.[245] Thus, Jung proposed a different mechanism (Scheme 3-5c).[260] An unstable 5-acetoxy-2,3,4-tribromo-3,4-dihydronaphthalene-1(2*H*)-one (**3.67**) was believed to be the initial bromination product, whose subsequent dehydrobromination led to the dibromonaphthol **3.68** that further reacted with NBS to afford **3.69**. Jung also suggested the possibility that a direct electrophilic bromodeacetylation of **3.55** yielding a monobromophenol followed by a rapid and second bromination leading to **3.68** might exist as well.[260]

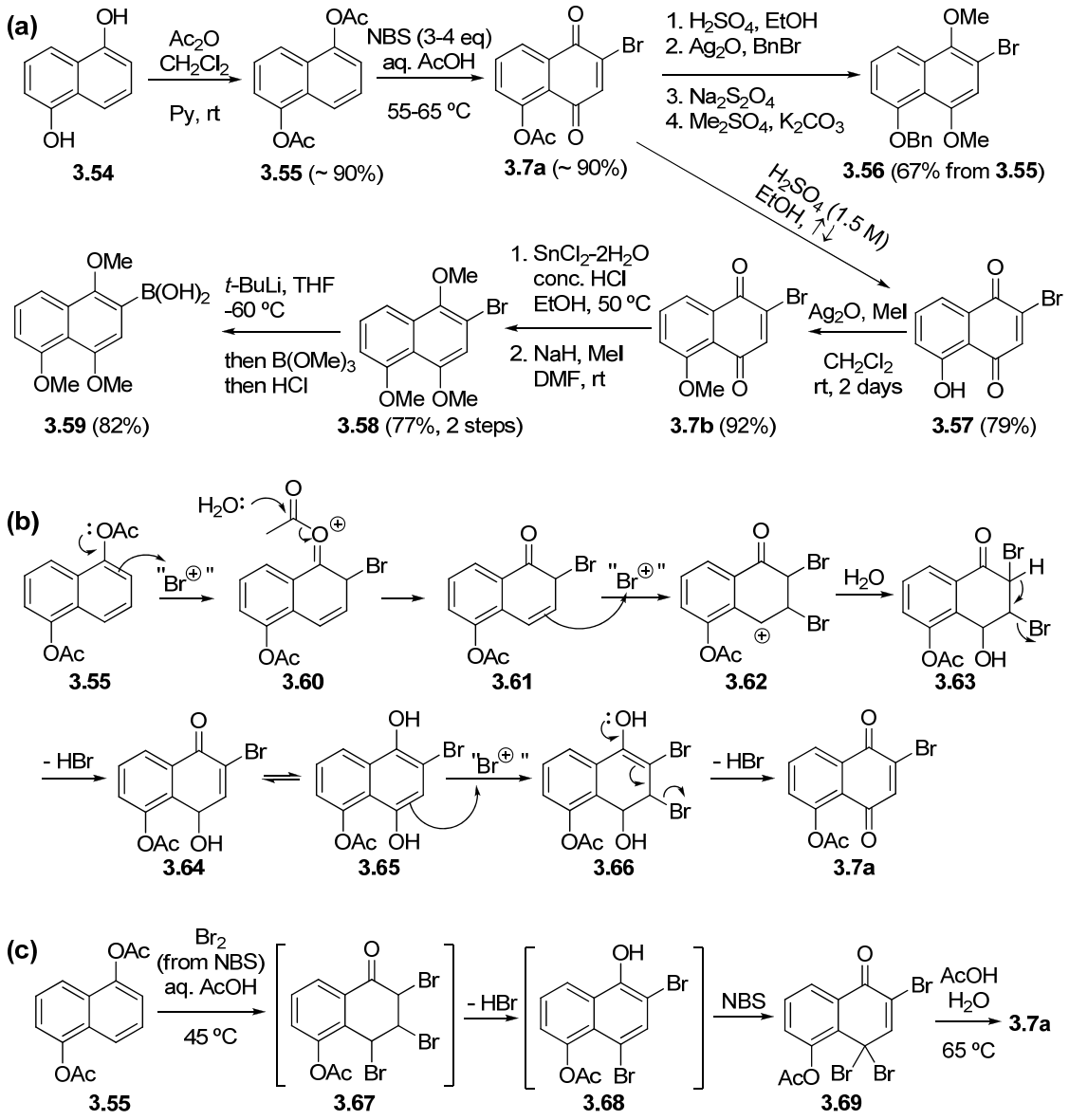

Scheme 3-5. (a) Several reported syntheses of compounds suitable as AB-ring precursor **3.38**; (b) proposed mechanism of NBS bromination of **3.55** by Grunwell and (c) by Jung.

This project was started with the above literature knowledge at hand as well as some previous results within the Dmitrienko group. Initially, the bromojuglone **3.7a** was prepared in large quantities (10-20 gram/batch), and excellent yields of both large scale acetylation of **3.54** (98%) and

bromination/oxidation of **3.55** (85%) were smoothly achieved (Scheme 3-6) by following the literature procedures but with modifications to accommodate the large quantities of various reagents used. It was interesting to notice that, during the large scale bromination of **3.55**, generation of Br_2 (red vapour) in situ from NBS in hot aqueous acetic acid became experimentally visible, and the presence of Br_2 was further confirmed by the qualitative chemical test (i.e., KI-starch paper immediately turned blue upon contacting the reaction vapour). This observation is supportive of the mechanism proposed by Jung (Scheme 3-5c) for this reaction in which Br_2 was considered to act as the real brominating species, although no physical/chemical evidence was provided in that report.

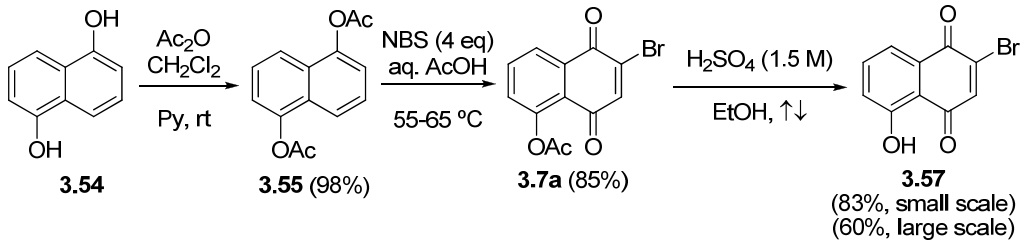

Scheme 3-6. Synthesis of the bromojuglone **3.7a** (this work).

The bromojuglone **3.7a** was then deacetylated with dilute aqueous H_2SO_4 (1.5 M) in refluxing ethanol (Scheme 3-6) by following the same literature precedent (**3.7a** to **3.57**, Scheme 3-5a).[258] This simple acid-catalyzed hydrolysis of the ester proceeded with no problems when carried out on a small scale (83% yield with 3 mmol of **3.7a**). Larger scale reaction (20 mmol starting material), however, only led to a moderate yield of 60% for the desired phenol **3.57**. On the other hand, the literature procedure (Scheme 3-5a) requires fairly long reaction time (i.e., 2 days) and an excessive use of the quite expensive Ag_2O for the next methylation step of **3.57** leading to **3.7b**, and the latter also needs two additional steps before being converted to the aryl bromide **3.58**.[258] Thus, it was felt necessary to explore the possibility of a quicker and easier chemical transformation, from the bromojuglone **3.7a**

to the corresponding deacetylated and reduced naphthol form of **3.70** (Scheme 3-7), which could then be permethylated to form **3.58**.

Based on the known results (Scheme 3-5a) that (i) the ester hydrolysis of **3.7a** can be achieved under an aqueous acidic condition (dilute aq. H_2SO_4, refluxing EtOH); and (ii) the reduction of the bromoquinone **3.7b** to the corresponding dihydroxyphenol by $SnCl_2{\cdot}2H_2O$ also involved a similar acidic medium (conc. HCl, EtOH, 50 °C), it was thought that the combination of an acid (either H_2SO_4 or HCl) and a reductant (such as $SnCl_2{\cdot}2H_2O$) might be able to simultaneously complete the ester hydrolysis and quinone reduction of **3.7a**. In fact, an initial one-pot hydrolysis/reduction attempt of **3.7a** was made by using (excess) $SnCl_2{\bullet}2H_2O$ in refluxing MeOH with a catalytic amount of conc. H_2SO_4 (Scheme 3-7), and satisfying results as originally expected were obtained. After 7 hours of reaction under such conditions, the desired product **3.70** was isolated in 85% yield in fairly pure form. Without any further purification, the naphthol bromide **3.70** was directly subjected to a permethylation reaction using MeI and powdered KOH in DMSO, which had been reported as a very simple and economical methylation (alkylation) method for all types of phenols, alcohols, amides and acids, as long as other substituents within the molecule can survive such strong basic condition.[261] The corresponding trimethyl-protected species **3.58** was obtained in 71% yield after only one hour of reaction. This modification provides a more economical and efficient synthesis of **3.58** from **3.7a** (2 steps, 60% yield) than the literature procedure (4 steps, 56% yield). Another significant advantage was that the methylation conditions used could tolerate the presence of water/moisture and air fairly well; thus no precaution had to be made to use particularly dry solvent and reagents (commercial ACS grade DMSO and MeI were used directly). While the literature methylation procedure involving MeI, NaH and DMF (Scheme 3-5a) required the preparation otherwise, and a trial with **3.70** under these conditions experienced problems such as very low yield and difficult separation/purification of the desired product **3.58**. In addition, a few attempts were also made in hope to achieve the one-pot

deacetylation and reduction of **3.7a** under basic conditions in the presence of a quinone reductant (e.g., $KOH/Na_2S_2O_4$), followed by the methylation with MeI/KOH/DMSO, but unfortunately all efforts led to complex and inseparable mixtures instead of the desired **3.58**.

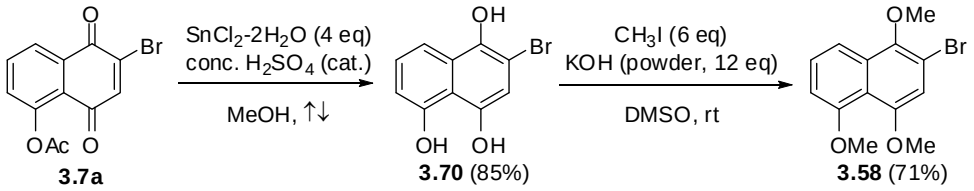

Scheme 3-7. Simplified synthesis of the aryl bromide **3.58** from the bromojuglone **3.7a**.

After the above simple synthesis of **3.58**, it was also found that, when the reaction solvent was switched from pure MeOH to a $MeOH/H_2O$ (1:1, v/v) mixture for the one-pot hydrolysis/reduction of **3.7a** and followed by methylation (MeI/KOH/DMSO), a fully methyl-protected but debrominated naphtholether **3.71** was obtained as the only product (75% yield, 2 steps) instead of **3.58** (Scheme 3-8). The unexpected dehalogenation was probably due to a possible higher reducing ability of the Sn(II) salt in the more aqueous environment. Interestingly, when the deacetylated bromojuglone **3.57** was subjected to the $SnCl_2$-reduction in the presence of conc. HCl in refluxing EtOH, conditions that were very similar to the first step of the literature conversion of **3.7b** to **3.58** (Scheme 3-5a), and followed the same methylation treatment (Scheme 3-8), the expected product **3.58** was still obtained but with a fairly low yield of only 40%. A new dimeric species **3.68**, as suggested by its proton NMR, was also isolated in comparable quantities (39% yield). It should be pointed out that, even though the deacetylated bromojuglone **3.57** was not used to synthesize the desired aryl bromide **3.58** in this project due to the availability of a more efficient route (i.e., **3.7a** to **3.58**), a compound like **3.57** could serve as a suitable intermediate if different phenol protecting groups on A- and B-ring of the precursor **3.38** are desired. The A-ring phenol of **3.57** can easily be protected with the first type of

protecting group, and the B-ring quinone could then be reduced to the hydroquinone followed by protection with a second type of protecting group. Such flexibility may offer better chemo- and regio-selectivity during the later chemical transformations (such as selective deprotection or oxidation) towards kinamycins. This is clearly indicated by the literature example of **3.56** shown in Scheme 3-5a, prepared in 4 steps from **3.7a**, in which the A-ring phenol is masked as an –OBn ether while the B-ring phenols are protected as methyl ethers.

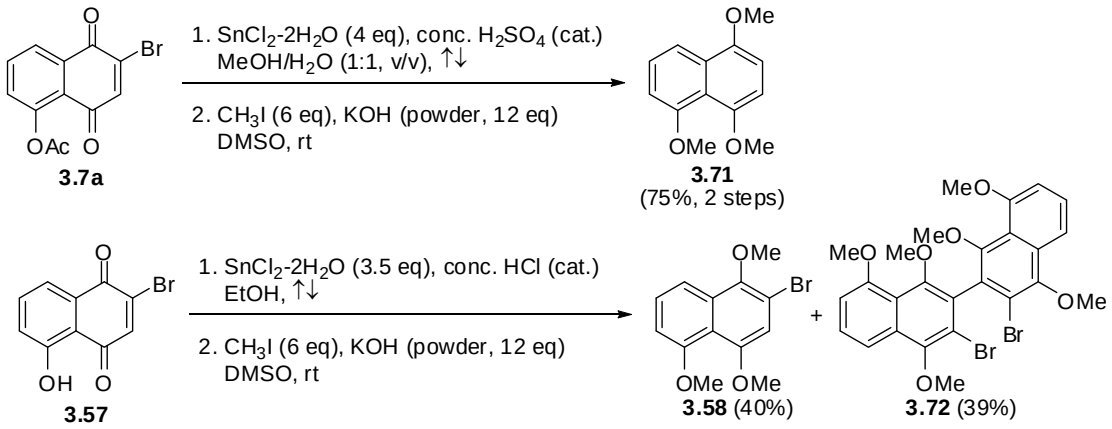

Scheme 3-8. Attempted one-pot reduction/methylation of bromojuglones under modified conditions.

With the aryl bromide **3.58** readily available in the lab, the next step was a simple and classical conversion of an aryl bromide to the corresponding boronic acid through a lithium-halogen exchange, followed by quenching with trimethyl borate and an acidic hydrolysis. Even though the literature work had already showed a good result to convert **3.58** to **3.59** (Scheme 3-5a, 82% yield), the use of the relatively expensive and highly pyrophoric *t*-BuLi make the procedure less attractive. Therefore, the desired chemical transformation was attempted by following some other literature examples and it was eventually achieved by using the much cheaper and safer *n*-BuLi, and the desired boronic acid was prepared in an adequate yield of 70% (Scheme 3-9). The boronic acid **3.59** as the AB-ring precursor was then ready to be coupled with the D-ring precursor (section 3.1.3). One benefit of

making the AB-ring precursor rather than the D-ring precursor as the boronic acid is that compound **3.59** is very stable under the strong basic and nucleophilic conditions, due to its aromaticity and simple functional groups. Conversely, the D-ring precursor might complicate the synthesis of its corresponding boronic acid, since it contains some other (sensitive) functional groups that may not survive the chemical transformation.

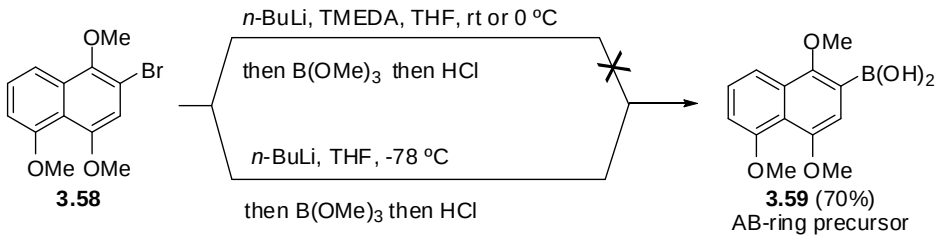

Scheme 3-9. Synthesis of the AB-ring boronic acid precursor **3.59**.

3.1.3 Synthetic Work on the Kinamycin D-Ring Precursors

The kinamycin D-ring precursor having the general structure of **3.39** was proposed at the beginning of the project (Scheme 3-3), and such a structure should be easily prepared, in principle, according to the simple retrosynthetic analysis as shown in Scheme 3-10, starting from the commercially available 3,5-dimethylanisole (**3.18**).

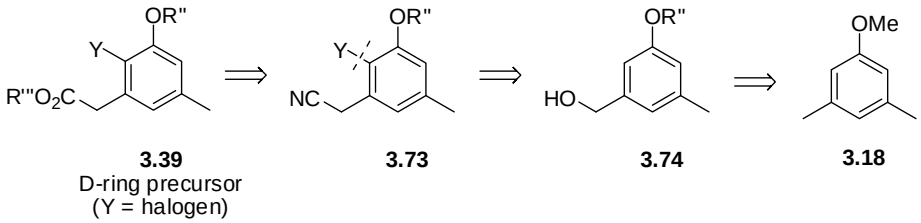

Scheme 3-10. Retrosynthetic analysis of the D-ring precursor **3.39**.

In practice, when **3.18** was subjected to a classical benzylic radical bromination with NBS initiated by $(PhCOO)_2$, the reaction produced a complex mixture including the desired product **3.75** (expected

radical monobromination occurred on the methyl group of **3.18**) but also other unwanted side products such as **3.76** and **3.77**, as well as unreacted starting material (Scheme 3-11), even though literature work claimed that such transformation from **3.18** to **3.75** under identical conditions could be achieved in 68% yield.[147] Careful and extensive optimization of experimental conditions carried out in the Dmitrienko group (this work and other projects that also required **3.75** as starting material[161]), such as the use of a different batch of NBS, purification of the radical initiator $(PhCOO)_2$, switching the reaction solvent (from CCl_4 to benzene) and carrying out the bromination either thermally (refluxing solvent) or photolytically, unfortunately all failed to provide a clean reaction with an acceptable yield of the desired benzyl bromide **3.75**. Extra difficulties were encountered during the separation and purification of reaction products. In another bromination attempt on **3.18**, NBS in glacial acetic acid[262-265] was able to smoothly afford the monobromination product **3.76** in 80% yield (Scheme 3-11). The halogen substitution occurred on the electron rich benzene ring of **3.18** rather than the expected methyl group, likely through an electrophilic aromatic substitution mechanism. Despite the apparently simple but very unsatisfying bromination step, the crude mixture of bromination products (i.e., **3.75** + **3.76** + **3.77** + **3.18**) was directly used for the next hydrolysis reaction with $CaCO_3$ in refluxing dioxane and water (Scheme 3-11).[149,150,266,267] After very tedious column separation, two benzylic alcohols **3.78** and **3.79** were isolated as the major products of hydrolysis but with very low yields (23% and 7%, respectively). The suitable benzylic alcohol **3.78** then underwent a directed metalation and a halogen was able to be introduced at the *ortho* position of the methoxy group, leading to the aryl iodide **3.80** in 62% yield (Scheme 3-11). Even though the aryl iodide **3.80** did not have the exact structure as the proposed D-ring precursor such as **3.81**, it could in principle undergo the Suzuki coupling with the available AB-ring boronic acid precursor **3.59**. A trial of the Suzuki coupling between **3.80** and **3.59** under the conditions reported for a similar literature example (Suzuki coupling of **1.176** and **1.177** leading to **1.178**, Scheme 1-23, section 1.5),[147] however,

failed to give the desired biaryl product **3.82** (Scheme 3-11) and a very complex mixture was obtained instead. The failure of the Suzuki coupling was presumably due to the steric crowdedness of the aryl iodide **3.80**, in which the iodine atom located at a concave site in between the two *ortho* substituents of methoxy group and benzyl alcohol group. Such steric hindrance was expected to be even more severe if the benzyl alcohol group (Ar-CH_2OH) within **3.80** was further converted to the even bulkier ester group (Ar-CH_2CO_2R) of **3.81**, which had the proposed structure of D-ring precursor **3.39** (Scheme 3-11). In addition, the encountered but totally unexpected huge difficulties and low efficiency to prepare **3.78** as described above made the D-ring precursor(s) such as **3.80** and **3.81** very unattractive, and the proposal of a new and better D-ring precursor became an urgent task.

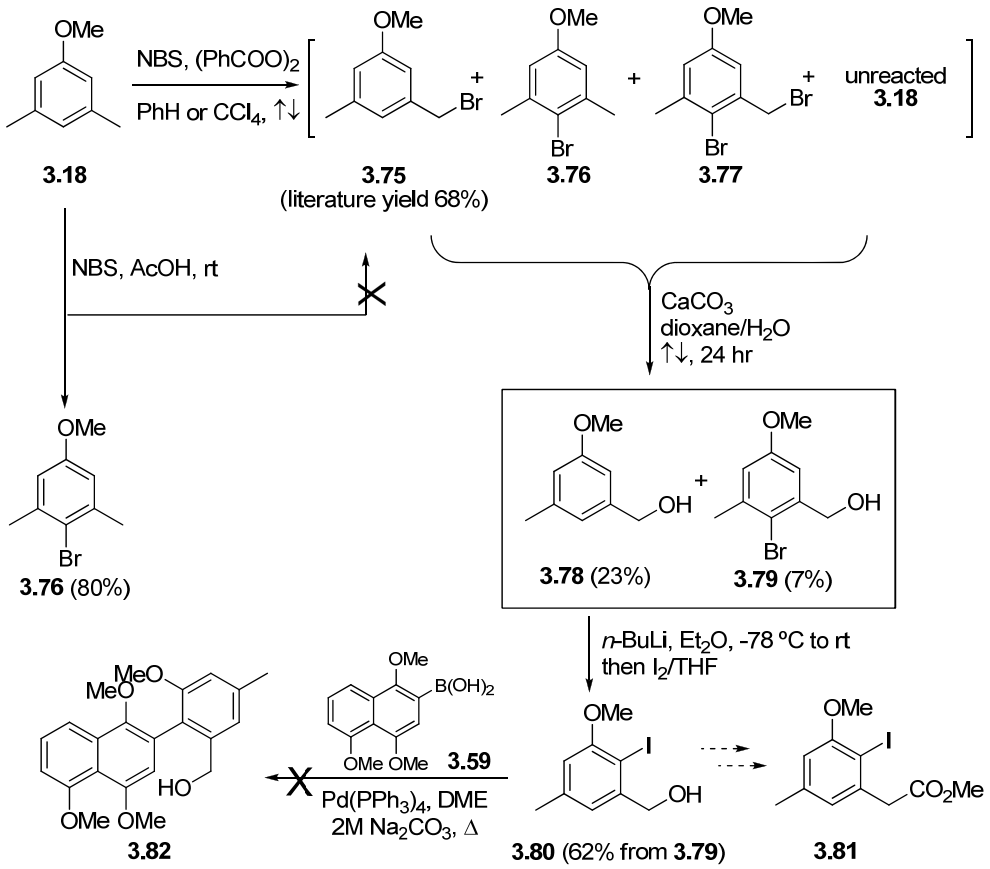

Scheme 3-11. Synthesis of the aryl iodide **3.80** and its attempted Suzuki coupling with **3.59**.

As indicated by the retrosynthesis (Scheme 3-3), the presence of an alkoxy group (i.e., a protected phenol) on the D-ring precursor is essential, since this functional group will be used for later oxidation of the D-ring to form a quinone in order to elaborate the non-aromatic D-ring of kinamycins. However, if the location of the hydroxyl (or alkoxyl) group of the original D-ring precursor **3.39** is switched to its *para* site (Scheme 3-12), the corresponding structure of **3.83** would be a synthetic equivalent to **3.39**, but with the obvious benefit of leaving the halogen atom more exposed and readily available for Suzuki coupling than that of **3.39** as a result of such structural revision. Then this new D-ring precursor **3.83** may follow the retrosynthetic path as outlined in Scheme 3-12, and its synthetic origin can be traced back to a very simple and readily available compound, 3-methylsalicylic acid (**3.86**).

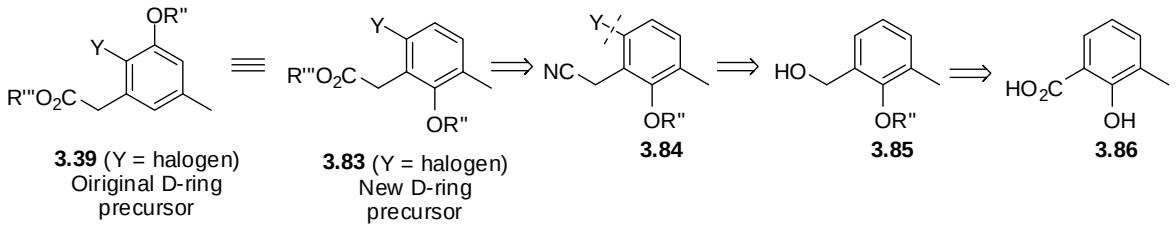

Scheme 3-12. Proposal of the new D-ring precursor **3.83** and its retrosynthetic analysis.

Initial synthetic attempts with **3.86** were carried out by an in situ borane reduction ($NaBH_4$, H_2SO_4)[268] of the carboxylic acid and the corresponding benzyl alcohol **3.87** was obtained in 87% yield (Scheme 3-13). This newly formed benzyl alcohol group within **3.87** was used as the directing species for a possible *ortho*-metalation with *n*-BuLi, so that an iodine atom might be introduced at this particular position (i.e., compound **3.88**). Reaction of **3.87** under such conditions, however, produced a complex mixture that could not be clearly identified. The failure might be due to the presence of an unprotected phenol in **3.87** that may be sensitive to the oxidative capability of I_2. On

the other hand, the desired *ortho*-metalation on the benzene ring of **3.87** might also be difficult, since **3.87** had to exist as a very unstable species of a trivalent anion since its phenol and benzyl alcohol groups would immediately deprotonate upon treatment with the strong base *n*-BuLi. Therefore, it was decided to at least protect the free phenol of **3.86** in order to minimize the possible difficulties mentioned above. A biphasic double methylation of **3.86** took place smoothly in the presence of a quaternary ammonium phase transfer catalyst (Scheme 3-13),[269] leading to **3.89** in 91% yield that had the phenol protected as a methyl ether while the carboxylic acid was also transformed into the corresponding methyl ester. The methyl ester **3.89** was then reduced by $LiAlH_4$ to the corresponding benzyl alcohol **3.90** in 82% yield, which now had a methyl-protected phenol. Directed *ortho*-metalation of **3.90** was attempted under the same conditions as before; unfortunately the outcome of the reaction was still a complex mixture instead of the desired aryl iodide **3.91**. A possible explanation to this failure was that the aryl methyl group in **3.87** (and **3.90** as well) might be more easily deprotonated by *n*-BuLi than the aromatic C-H thus complicating the reaction, since the pKa of a benzyl methyl proton is about two magnitudes more acidic in general than a typical benzene proton.[270] Such a prediction would also suggest that a milder regioselective halogenation condition should be employed.

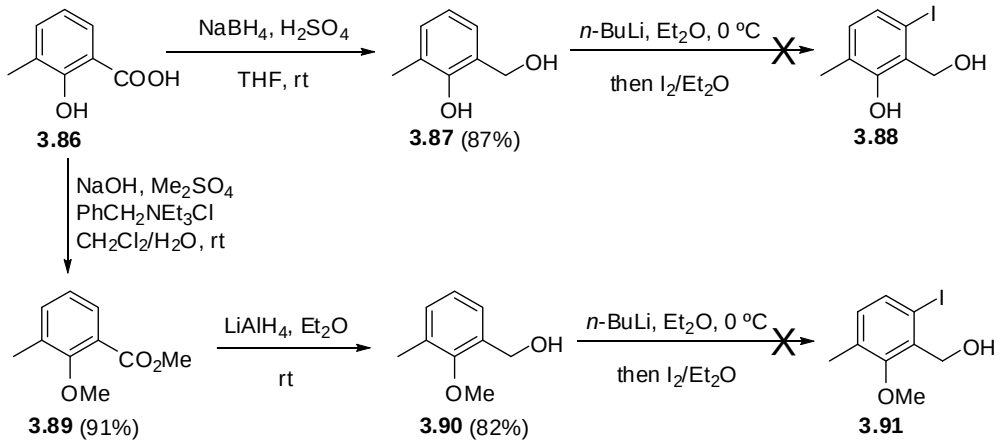

Scheme 3-13. Attempted syntheses of the new D-ring precursor(s) such as **3.88** and **3.91**.

After further exploration of the literature, it was found that Kodama and co-workers had patented a regioselective halogenation of aromatic carboxylic acids and amides by using the carboxylic acid functionality as an *ortho*-directing group in the presence of a Pd catalyst.[271] For example, the *o*-toluic acid (**3.92**) was able to provide exclusively the 2-iodo-6-methylbenzoic acid (**3.93**) under the two conditions shown in Scheme 3-14a.[271] Initially, **3.86** was subjected to one of these patented *ortho*-iodination conditions (i.e., $Pd(OAc)_2/I_2/H_5IO_6$/aq. AcOH)[271] and another literature procedure using HgO/I_2[272] as the iodination reagents (Scheme 3-14b). In both cases the halogenation occurred smoothly leading to **3.94** in good yields with iodination occurring at the undesired *para* position of the –OH group rather than desired *ortho* position of the carboxylic acid group. Thus, the halogenation via an electrophilic aromatic substitution, favoured by the presence of the very strong *ortho, para*-directing OH group proceeded much more rapidly than the Pd-catalyzed halogenation with the carboxylic acid acting as a directing group. These results clearly indicated that the free phenol within **3.86** must be protected and deactivated, so that the iodination can be regioselectively controlled by the carboxylic acid group. The first obvious choice was to acetylate the phenol since the acetoxy group is only a moderate *ortho, para*-directing group. Even though the acetoxy ester **3.95** could be prepared from **3.86** in good yield (69%) by following several literature conditions such as the one shown in Scheme 3-14b, this transformation suffered from a very difficult removal of a significant amount of unreacted starting material from the desired product. In addition, an *ortho*-iodination attempt with **3.95** (containing ~20% of **3.86**) using the other patented *ortho*-iodination condition (i.e., $Pd(OAc)_2$/NIS (*N*-iodosuccinimide)/DMF) did not give the expected iodoacid **3.96** but a near-complete recovery of the starting material **3.95** (Scheme 3-14b).

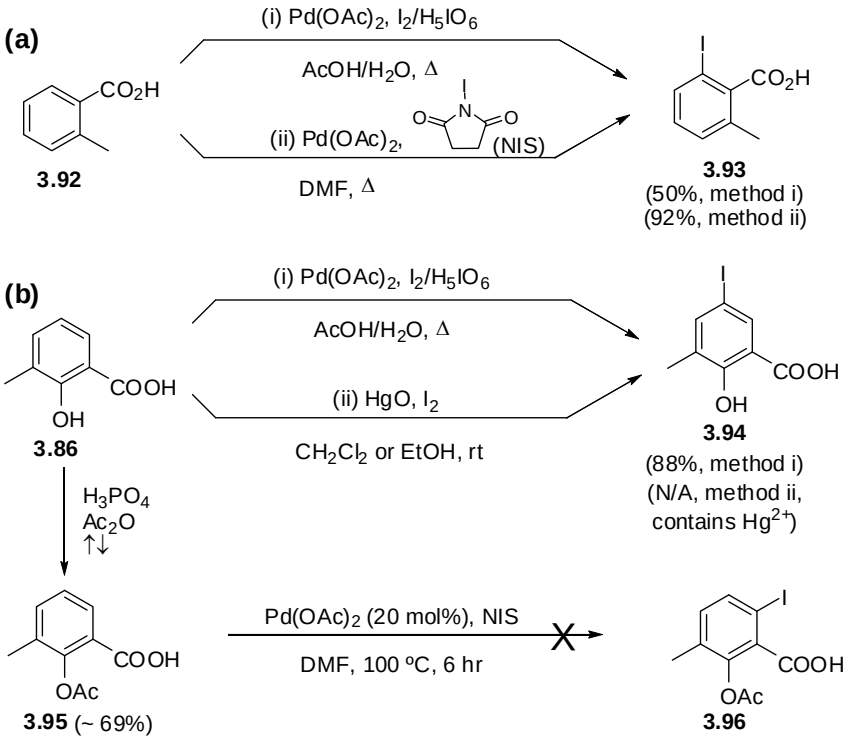

Scheme 3-14. (a) Literature example of Pd-catalyzed *ortho*-iodination of substituted benzoic acid; (b) attempted Pd(II)-catalyzed *ortho*- iodination of **3.86** and **3.95**.

After more careful consideration, it was thought that mesylation of the phenol **3.86** might be a better solution mainly for two reasons. First the –OMs group is known to be a deactivating and *meta*-directing substituent for electrophilic aromatic substitution. This characteristic would significantly help the desired iodination to occur *ortho* to the carboxylic acid group, since this position would be *meta* to the –OMs group. Second, the mesyl group is a very stable protecting species for phenols under various (strong acidic, oxidative, reductive and high temperature) conditions[273] yet it can be readily removed under strong basic/nucleophilic conditions (such as warm aq. base ($NaOH/KOH/Na_2CO_3$) solution,[274-277] NaOEt/EtOH/reflux,[278,279] $CH_3SNa/NaOH$[273] or LDA/THF/-78 °C[280]).

Initially, the mesylation of **3.86** was carried out with MsCl in the presence of a typical base; however, the use of common bases including NaOH, KOH, NaOEt, pyridine and NEt_3 all failed to produce the desired mesylate **3.97** in any meaningful yields, while the use of NaH in DMF was able to afford **3.97** but in a very poor yield of only 24% (Scheme 3-15a). Finally, mesylation of **3.86** was accomplished in 94% yield in THF with CaO as the appropriate base (Scheme 3-15a), and addition of a small amount of water was found to significantly accelerate the initiation of the mesylation reaction. This success was probably due to not only the strong basicity of $CaO/Ca(OH)_2$, but also and more importantly the divalent capability of Ca^{2+} that could form a complex of **3.99** with the salicyclic acid to ensure a complete deprotonation of the phenol (Scheme 3-15a). The mesylate **3.97** was then subjected to the two $Pd(OAc)_2$-catalyzed *ortho*-iodination conditions (Scheme 3-15a): although the starting mesylate was essentially recovered with only about 10% conversion to the expected monoiodination product when I_2/H_5IO_6 in aqueous acetic acid was used as the iodination reagent, the use of NIS in DMF afforded the desired aryl iodomesylate **3.100** in good yields. The experimental conditions for this iodination were further optimized in various aspects and it was found that (i) an ideal loading of the $Pd(OAc)_2$ catalyst of about 10–15 mol% would ensure complete iodination, but the halogenation could occur with as little as only 2% Pd catalyst loading; (ii) DMF is the solvent of choice and no iodination occurred at all when (refluxing) THF was used, while the use of (refluxing) AcOH also showed very limited conversion (~ 20%) of **3.97** even after extended reaction times; (iii) the ideal reaction temperature in DMF was around 100–120 °C while refluxing DMF (bp 153°C) would cause a severe decrease of the yield. The mechanism for this carboxylic acid-directed regioselective iodination was not discussed in the original patent, but likely it involved a mechanism (Scheme 3-15b) similar to the one that was proposed for the Pd(II)-catalyzed *ortho* halogenation of substituted benzoic acids by IOAc, in which the carboxylate would bind and direct the Pd(II) to its *ortho* position where the C-H bond was activated towards the halogenation.[281]

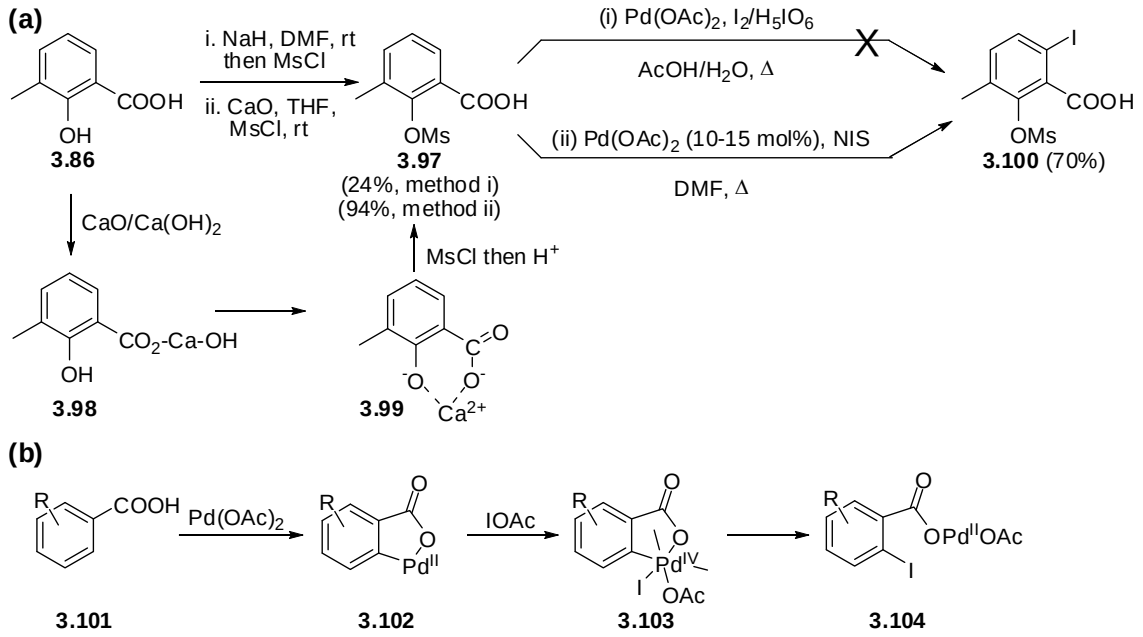

Scheme 3-15. (a) Pd(II)-catalyzed *ortho*-iodination of the mesylbenzoic acid **3.97**; (b) proposed literature mechanism for Pd(II)-catalyzed *ortho*-iodination of substituted benzoic acids.

The key intermediate **3.100** now had all the main structural features of the proposed new D-ring precursor **3.83**, except that the carboxylic acid group of **3.100** would require some further chemical transformations (Scheme 3-16). Reduction of the carboxylic acid group within **3.100** was problematic at the beginning and it was found that the reaction would barely occur if less than 3 equivalents of borane, regardless of the borane source (either direct or generated in situ), were used. This was probably due to the presence of the –OMs group in the molecule, whose multiple oxygen atoms might bind to the Lewis-acidic borane reductant. In practice, the reduction of **3.95** was eventually carried out with a large excess of BH_3 (10 equivalents) and the corresponding benzyl alcohol **3.105** was prepared in 77% yield (Scheme 3-16). The initial attempt on the benzylic bromination of **3.105** was made with conc. HBr, but no substitution product was obtained and the starting material was completely recovered. However, the desired bromo substitution of **3.105** was achieved quantitatively

with excess CBr_4/PPh_3 (6 equivalents), and the corresponding benzyl bromide **3.101** was further converted quantitatively to the benzyl cyanide **3.107** with NaCN in DMSO (Scheme 3-16). In principle, the benzyl cyanide **3.107** could be transformed into the corresponding carboxylic ester **3.108** by a simple acid-catalyzed hydrolysis and esterfication reaction (Scheme 3-16), but this conversion was not further carried out since **3.107** itself was already a suitable and probably a better D-ring precursor than **3.108**. The smaller benzyl cyano group of **3.107**, relative to the benzyl acetyl ester group of **3.108**, might benefit the subsequent Suzuki coupling with the AB-ring precursor.

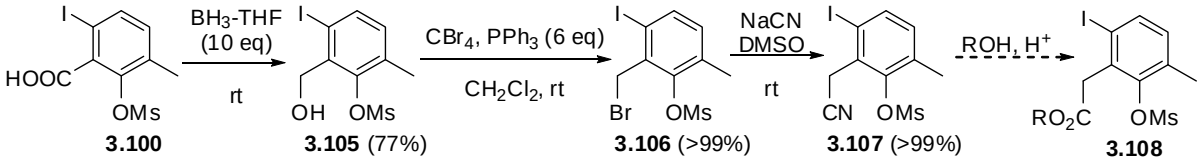

Scheme 3-16. Synthesis of the benzyl cyanide **3.107** as the D-ring precursor.

3.1.4 Coupling of the Kinamycin AB- and D-Ring Precursors and the Following Steps

With both the AB-ring boronic acid precursor **3.59** and the D-ring aryl iodide precursor **3.107** readily available, the next step was obviously the critical Suzuki coupling between these two compounds as planned in the retrosynthesis (Scheme 3-3). Under a slight modification of the literature Suzuki coupling conditions that were developed by Snieckus and co-workers (coupling of aryl bromide **1.169** and aryl boroxine **1.170**, Scheme 1-22, section 1.5) for their synthesis towards the benzo[*b*]fluorene system,[146] the expected Suzuki coupling of **3.59** and **3.107** (Scheme 3-17) yielded the desired biaryl product **3.109** in excellent yields (91–98% depending on the reaction scale). However, another attempt of the Suzuki coupling of **3.59** and **3.107** under a ligand-free and aerobic condition (i.e., $Pd(OAc)_2$/NaOEt/EtOH/air) by following a literature example[282] in the hope of further simplifying the coupling reaction failed.

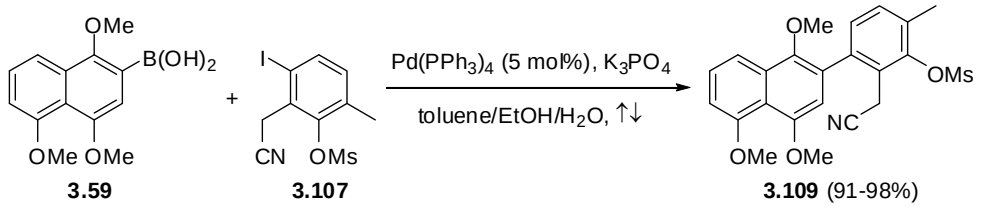

Scheme 3-17. Suzuki coupling of the AB-ring precursor **3.59** and the D-ring precursor **3.107**.

The cyano group of the biaryl species **3.109** was then on the route to be hydrolyzed to the corresponding carboxylic acid **3.110** (Scheme 3-18); yet such an apparently simple functional group conversion was found to be a lot more challenging than one would expect. A series of hydrolysis attempts on the benzyl cyanide **3.109**, under either typical acidic or basic conditions as summarized in Table 3-1, all failed to afford the desired acid **3.110** but some interesting results were obtained.

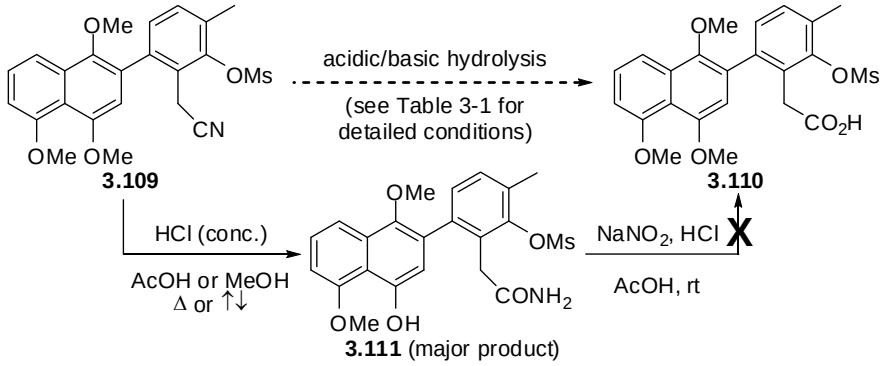

Scheme 3-18. Various attempted acidic/basic hydrolysis (Table 3-1) of the cyanide **3.109**.

Table 3-1. Detailed experimental conditions and results for the hydrolysis of **3.109** (Scheme 3-18).

Trial	Reagents and Conditions[Reference]	Products and Results
1	H_2SO_4 (conc.)/AcOH/H_2O/rt	No reaction, recovery of **3.109**
2	H_2SO_4 (conc.)/AcOH/H_2O/↑↓	Complex mixture that contains no acid but small amount of cyclized product(s)
3	HCl (conc.)/MeOH/rt	No reaction, recovery of **3.109**
4	HCl (conc.)/AcOH (1:1)/↑↓	**3.111** (major product)
5	HCl (conc.)/AcOH (1:1)/70–80 °C	
6	HCl (conc.)/MeOH/↑↓	
7	H_3PO_4 (conc.)/AcOH/H_2O/rt	No reaction, recovery of **3.109**
8	H_3PO_4 (conc.)/AcOH/H_2O/70–80 °C	No reaction, recovery of **3.109**
9	Amberlite IR-120/MeOH/H_2O/↑↓[283]	No reaction, recovery of **3.109**
10	Amberlite IR-120/AcOH/H_2O/↑↓	No reaction, recovery of **3.109**
11	H_2O_2/NaOH/↑↓[284]	Complex mixture: no hydrolysis of –CN at all but complete loss of –Ms
12	KOH/MeOH/↑↓[285]	Complex mixture: no hydrolysis of –CN at all but complete loss of –Ms

First, hydrolysis of **3.109** under mild acidic conditions (i.e., strong acids at ambient temperature or weak acids at ambient/elevated temperature, trial 1, 3 and 7–10, Table 3-1) led only to a complete recovery of the starting material. This was likely due to the presence of the bulky substituted naphthyl group and mesylate group, both *ortho* to the benzyl cyanide moiety, which retarded the nucleophilic attack on the cyano by H_2O. Second, under some harsh acidic conditions (i.e., strong acids at elevated temperature) but depending on the acid involved, the substrate behaved quite differently. For example, when H_2SO_4 was used as the acid catalyst (trial 2, Table 3-1), although the product was obtained as a complex mixture that contained no desired acid **3.110** at all, crude NMR indicated that there existed a small amount of a cyclized species. This observation seemed to be consistent with the known literature results that biaryl benzyl cyanides such as **3.112** could cyclize in conc. H_2SO_4 (with no

solvent) to give the corresponding aniline **3.113** (Scheme 3-19a).[286,287] On the other hand, when conc. HCl was used for the hydrolysis (trial 4–6, Table 3-1), the major product isolated from these reactions was an amide **3.111** from a partial hydrolysis of the cyanide, but containing also a partially demethylated B-ring (Scheme 3-18). The demethylation of the B-ring in these cases was unexpected, but it could be explained by the proposed possible mechanism shown in Scheme 3-19b. Manipulation of the solvent, reaction temperature and time could not push the amide **3.111** to be further hydrolyzed under these acidic conditions to the desired acid **3.110** at all. Attempts to convert the amide to the acid via an acyl-diazonium intermediate under the conditions (i.e., $NaNO_2$/HCl/AcOH) similar to literature examples did not succeed either and gave a complex mixture (Scheme 3-18).[288,289] This was probably due to the very electron-rich AB-ring of **3.111** that, instead of the amide moiety, could react readily and probably preferably with the strong electrophile (NO^+) generated in the reaction. Third, hydrolysis of **3.109** under either oxidative or normal basic conditions (trial 11–12, Table 3-1) also did not convert the cyano moiety to the desired carboxylic acid group or even to the intermediate stage of an amide, but a complete loss of the D-ring mesyl protecting group was observed in both cases. The in situ generated (D-ring) phenol upon demesylation was probably not stable under such conditions, thus led to a complex mixture as the final products. Even though the last two trials did not offer the expected chemical outcome, at least they provided some applicable conditions that might be useful for the later deprotection/removal of the mesyl group.

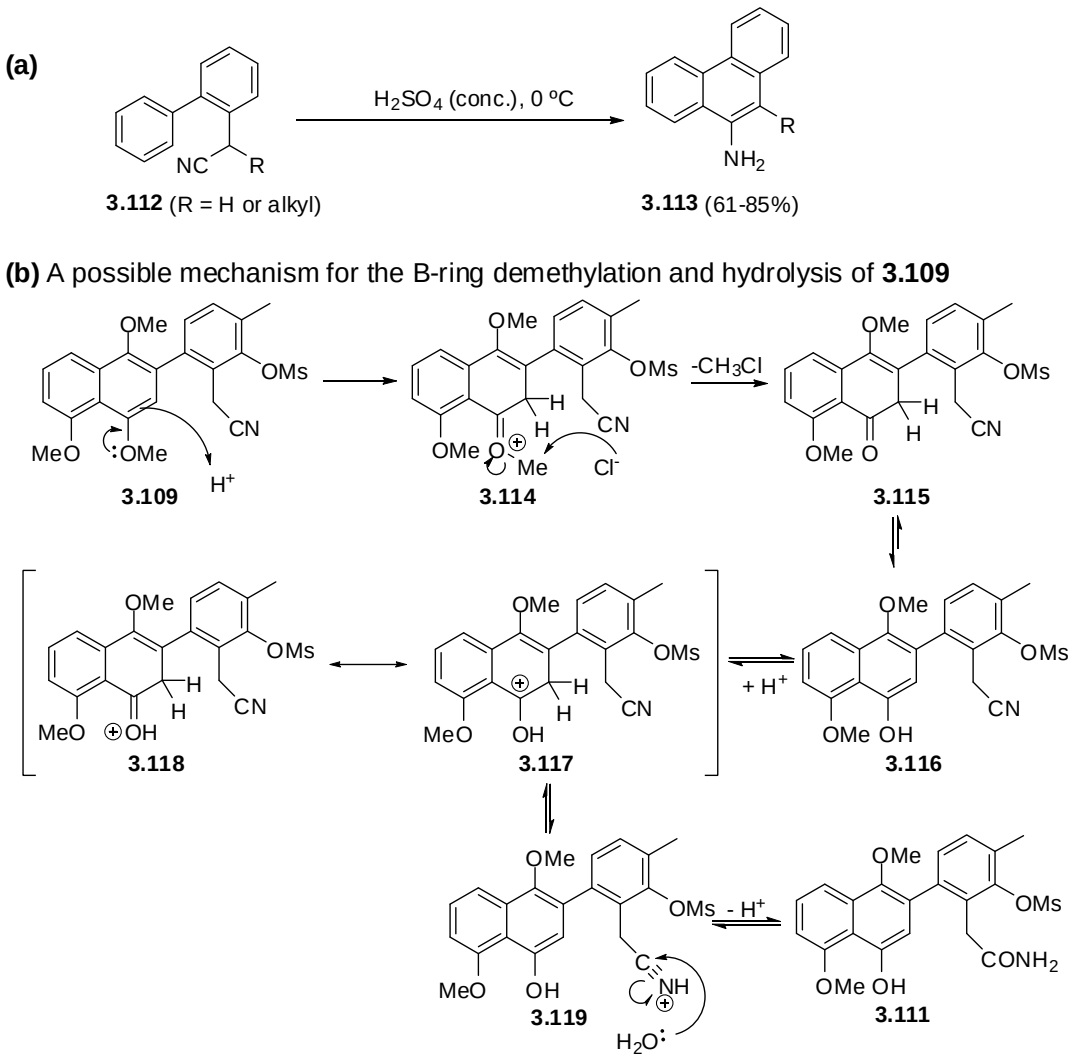

Scheme 3-19. (a) Literature example of benzyl cyanide cyclization in conc. H_2SO_4 and (b) a possible mechanism for the partial demethylation and cyano hydrolysis of **3.109** under acidic (HCl) conditions.

All these failures to obtain the desired acid **3.110** from the cyanide **3.109** had led to the consideration that, it might be necessary to prepare either the corresponding acid (or the ester) of the D-ring precursor **3.102** upon conversion of its cyano group prior to the Suzuki coupling, which then can couple with **3.55** to prepare the corresponding biaryl species with the required carboxylic acid (or ester) functionality preinstalled and thus eliminate the need of a difficult cyano hydrolysis as

encountered in the case of **3.109**. Just before efforts were about to be redirected to such an alternative plan, a literature work using chlorotrimethylsilane (TMSCl) in alcohol solvents to convert nitriles to the corresponding esters was discovered.[290] This method involves HCl generated in situ as the acid catalyst for the solvolysis of the nitrile. The HCl originates from the reaction of TMSCl and the first equivalent of alcohol, and a second equivalent of the alcohol acts as the nucleophile to produce an iminium salt from the HCl-activated nitrile that was further hydrolyzed to the ester during the aqueous workup stage of the reaction (Scheme 3-20).[290] It was decided to carry out one more trial with the biaryl benzyl cyanide **3.109** under such conditions to see if the corresponding ester **3.120** could be obtained or not. Based on the encountered difficulties to hydrolyze the cyano group of **3.109** as described above, consideration and modification of the literature procedure in the following two aspects were applied. First, the original literature procedure only required one equivalent of TMSCl and two equivalents of alcohol relative to the nitrile used,[290] while a large excess of both reagents that were still kept in a 1:2 ratio were used in the case of **3.109** in the hope that the desired but difficult conversion might be forced to a completion. Second, even though various simple alcohols such as methanol, ethanol and isopropanol were all found to be quite effective to prepare the corresponding esters from the nitriles (69–92% yields),[290] the very crowded space environment around the benzyl cyano group of **3.109** would probably benefit the most from the use of methanol, the smallest alcoholic nucleophile available.

$$TMSCl + ROH \rightarrow HCl + TMSOR$$

$$R'CN + HCl + ROH \rightarrow R'\text{-}C(OR)=N^{+}H_2Cl^{-}$$

$$R'\text{-}C(OR)=N^{+}H_2Cl^{-} + H_2O \text{ (workup)} \rightarrow R'COOR + NH_4Cl$$

Scheme 3-20. Plausible literature mechanism for the conversion of nitrile to ester by TMSCl/alcohol.

In practice, a solution of **3.109** was heated at reflux in a large excess of TMSCl/MeOH (1:2) mixture and followed by an aqueous workup as described in the literature work (i.e., saturated aq. $NaHCO_3$ solution). It was gratifying to find that the expected and desired methyl ester **3.120** was isolated in 60% yield along with a corresponding amide **3.121** in 28% yield (Scheme 3-21 and Table 3-2), and no demethylation (of B-ring) at all occurred with either product this time. Inspired by this initial success but not very satisfied with the product distribution (i.e., significant amount of unwanted amide **3.121**), the aqueous workup condition was further explored to see if there was any room for improvement. In fact, it was found that the ratio between the methyl ester **3.120** and the amide **3.121** varied significantly depending on the acidity of the workup condition used, as summarized in Table 3-2. The best result (83% isolated yield of **3.120** and 16% isolated yield of **3.121**) was achieved with 10% HCl as the workup medium. The competition between the formation of both **3.120** and **3.121** (Scheme 3-21), starting from the same iminium salt intermediate **3.122**, is probably a reflection of the competition between the $–NH_2$ and –OMe in their protonated forms as the leaving groups (i.e., $–N^+H_3$ within **3.123** and $–O^+$(H)Me within **3.124**). The presence of excess acid during the workup stage would favour keeping the intermediate in the $–NH_2$ protonated form and thus leading to the preferential formation of the ester **3.120**. Such a result would also suggest that the B-ring demethylation previously observed for **3.109**, when it was hydrolyzed in aqueous HCl in refluxing MeOH or heated AcOH (Scheme 3-19 and Table 3-1), might be partially due to the presence of water during the reaction in these cases, and this conclusion was further supported by the following experimental observations. The literature work indicated that the solvolysis of the nitriles by the alcohols with TMSCl can be also successfully carried out in the presence of water,[290] therefore an attempt with **3.109** in a solvent mixture such as $MeOH/H_2O$ would be worthwhile if the corresponding acid **3.110** instead of the methyl ester **3.120** could be directly prepared, since the acid would serve as a better candidate than the ester for the subsequent intramolecular cyclization step.

However, a trial with **3.109** in a refluxing mixture of TMSCl/MeOH/H_2O (1:1:1, in large excess relative to **3.109**) followed by an acidic workup did not yield the preferred acid **3.110** but a complex mixture (Scheme 3-21). Even though the mixture could not be well separated and fully characterized, NMR evidence indicated that the products in this case were still a mixture of a methyl ester **3.125** and an amide **3.126** but both with a (partially) demethylated B-ring, along with other unidentified by-products.

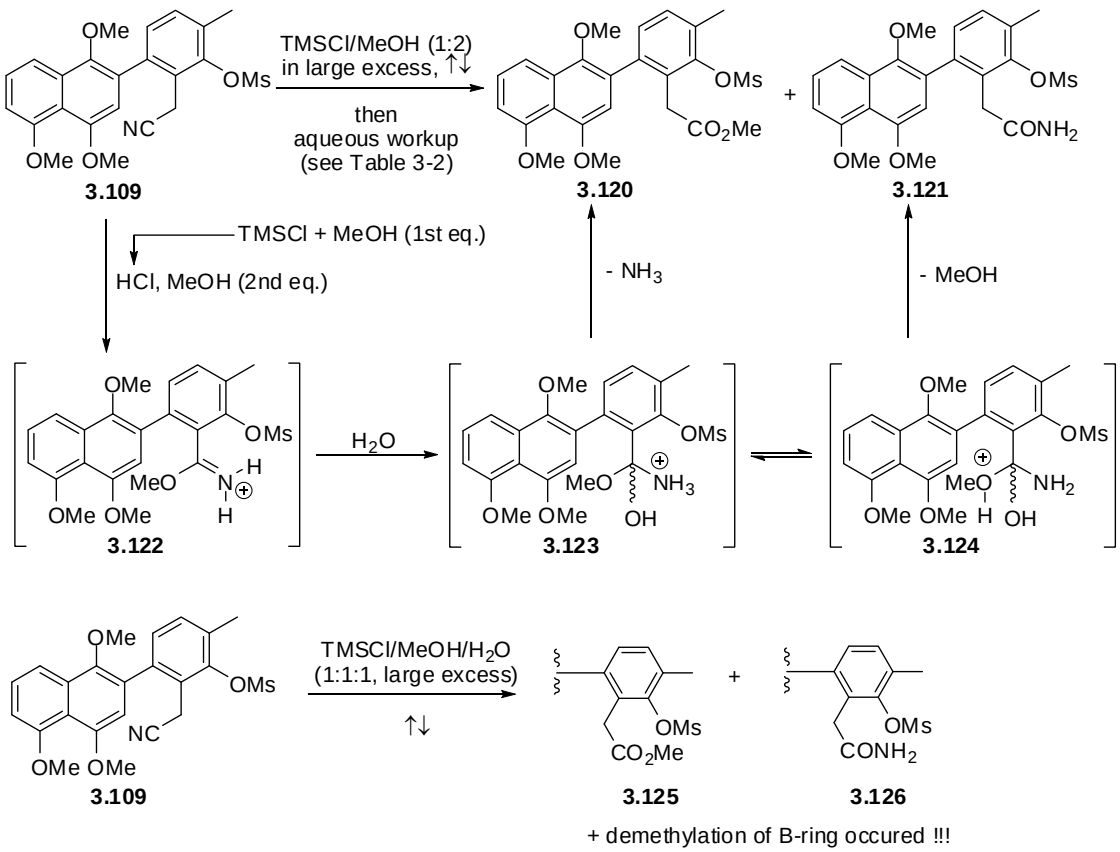

Scheme 3-21. Products and mechanism of the solvolysis of **3.109** (refer to Table 3-2).

Table 3-2. Detailed workup conditions and results for the solvolysis of **3.109** (Scheme 3-21).

Workup conditions	**3.120** (Isolated yield)	**3.121** (Isolated yield)
saturated aq. $NaHCO_3$ solution	60%	28%
H_2O + Na_2CO_3 powder	68%	21%
H_2O only*	66%	29%
10% HCl aq. solution	83%	16%

* This is indeed an acidic workup due to the presence of large excess HCl (generated from the large excess of TMSCl/MeOH).

Further efforts were made to hydrolyze the methyl ester **3.120** into the corresponding carboxylic acid **3.110** (Scheme 3-22) by following quite a few literature conditions as summarized in Table 5-3. Even though such an ester hydrolysis could be carried out under either acidic or basic conditions, for practical reasons all attempts were made under mild basic conditions (Table 5-3). This precaution of using no strong acidic or basic conditions was to avoid some of the possible side reactions that may occur with **3.120** due to its structural and electronic characters, based on the previous experience with the very similar biaryl species such as **3.109**. For example, the use of HCl may cause a very possible B-ring demethylation; on the other hand, strong basic conditions at elevated temperature would likely cleave the mesyl group that was to be kept as the phenol protecting group at the moment. However, despite the various and carefully selected mild basic hydrolysis conditions attempted (Table 5-3), some difficulties were encountered once again for such an apparently simple functional group transformation, which was still very likely due to the enormous steric hindrance around the ester moiety from the two neighbouring bulky groups. In most cases the methyl ester **3.120** was found to be inert towards the mild basic hydrolysis, while in the case when ester hydrolysis did occur (trial 2), the low conversion percentage (< 10%) and slow rate (3 days) were not acceptable from a practical point of view, and demesylation still occurred concurrently with the ester hydrolysis, although both to a very small extent, even at such mild conditions (trial 4).

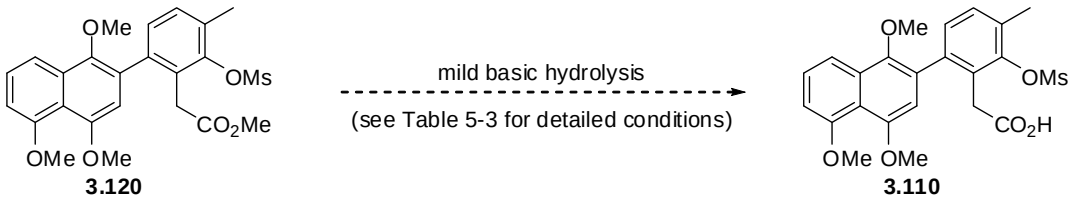

Scheme 3-22. Mild basic hydrolysis (Table 3-3) of ester **3.120**.

Table 3-3. Detailed experimental conditions and results for the hydrolysis of **3.120** (Scheme 3-22).

Trial	Reagents and Conditions[Reference]	Products and Results
1	Mg/MeOH/rt then H_3O^+[291]	No reaction, recovery of **3.120**
2	Na_2CO_3/MeOH/H_2O/rt/4 hr – 3 days[292]	Mainly recovered **3.120**, only small percentage (< 10%) of ester hydrolyzed after 3 days
3	LiOH/H_2O_2/THF-H_2O/0 °C then H_3O^+	No reaction, recovery of **3.120**
4	KOH/MeOH/H_2O/rt then H_3O^+	Mainly recovered **3.120** + 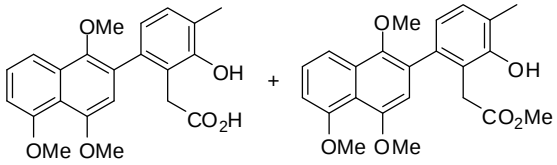 **3.127** (minor) **3.128** (minor)

The difficulties to prepare the carboxylic acid **3.110** from the methyl ester **3.120**, which was the required precursor for the next intramolecular Friedel-Crafts cyclization step as planned (Scheme 3-3), had led to the search of possible conditions that might be suitable for the direct and intramolecular cyclization of the ester **3.120**. Generally speaking, esters are known to be much less active towards the electrophilic aromatic substitution reactions when compared to other carbonyl compounds, especially the acid halides and carboxylic acids. Non-aromatic esters are barely known or used as acylation reagents. In fact, intermolecular aromatic substitution by simple esters under the typical Friedel-Crafts conditions, i.e. $AlCl_3$ as the Lewis acid catalyst with simple aromatic hydrocarbons

such as benzene as the nucleophile, has been shown to give aromatic alkylation products rather than acylation products.[293] When the ester group co-exists with other carbonyl functionalities such as an aldehyde, the latter would preferentially undergo the intramolecular cyclization.[294] Most known literature examples of ester intramolecular aromatic cyclization involve the benzoate type of esters (Ar-(C=O)-OR) rather than the benzyl esters (Ar-CH_2-(C=O)-OR), since the conjugation of the ester moiety with an aromatic ring would significantly enhance its reactivity yet cyclization reactions of such activated esters would still require the use of a very strong Lewis acid catalyst.[295] Unfortunately the prepared intermediate ester **3.120** belongs to the latter and less active type. It was noticed that, however, a literature work claimed that a styrene-methyl methacrylate (MMA) based polymer was able to undergo an intramolecular Friedel-Crafts cyclization between the benzene ring of the styrene unit and the ester group of the MMA unit when the polymer was heated (60 °C) in dichloroethane with $SnCl_4$ as the catalyst.[296] However, repeated reaction of **3.120** under the same conditions, even at a slightly higher temperature (i.e., refluxing dichloroethane, 84 °C) and extended longer reaction time than the literature example, still recovered mainly the unreacted **3.120** instead of yielding the expected cyclization product **3.129** (Scheme 3-23). On the other hand, a trial attempt was also made by subjecting the ester **3.120** to methanesulfonic acid CH_3SO_3H (MSA) in CH_2Cl_2[294] at ambient temperature (Scheme 3-23) to check the (cyclization) reactivity of **3.120** under such conditions. MSA is one of the commonly used acid catalysts for acylation of aromatic systems by carbonyl compounds (mostly carboxylic acids), particularly for the intramolecular type, as indicated by many available literature precedents.[294,297-300] Not surprisingly, the less active ester (than acid) was once again essentially recovered after 24 hr of reaction with no evidence for the formation of **3.129**.

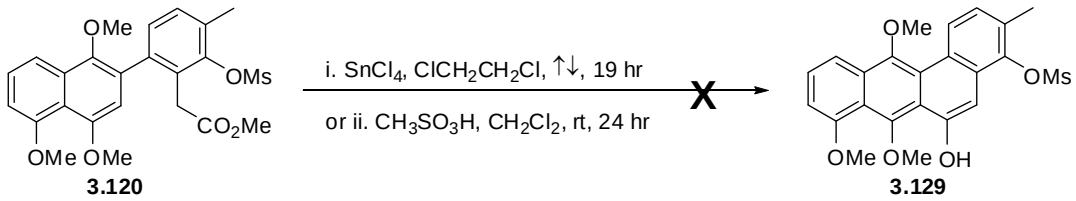

Scheme 3-23. Attempted direct intramolecular cyclization/acylation of the ester **3.120**.

Breakthrough of this apparent deadend was made after accidentally coming across an old literature procedure developed by Loev back in the 1960s, which showed that simple alkyl or aryl (including heterocyclic) carboxylic esters could be readily hydrolyzed to the corresponding acid by heating with MSA in conc. formic acid (or acetic acid).[301] It was felt that this condition might provide a better chance of success on the troublesome hydrolysis of methyl ester **3.120** (Scheme 3-22). In addition, if the carboxylic acid **3.110** could be generated from the ester **3.120** under such conditions (MSA + HCOOH), then it was also possible that **3.110** might even undergo an in situ intramolecular cyclization to afford **3.129** due to the presence of MSA (Scheme 3-24), which is an excellent catalyst capable of promoting intramolecular cyclization of carboxylic acids. Therefore, an initial attempt was made by refluxing **3.120** with excess MSA in conc. formic acid for 3 hr (Table 3-4, trial 1). Although the obtained crude products were quite messy and still contained a large amount of unreacted **3.120**, NMR evidence did show that several chemical transformations including cyclization, partial A/B-ring demethylation and even oxidation (reaction carried out under air atmosphere) had occurred experimentally. When **3.120** was heated in the mixture of MSA and conc. formic acid for extended time (12–16 hr, Table 3-4, trial 2), compound **3.130** having the structure as shown (rather than **3.129**) was surprisingly isolated as the major product from the reaction in about 44% yield. Even though the ring closure of the in situ generated carboxylic acid (from **3.120**) through an intramolecular Friedel-Crafts cyclization had been predicted, and the formation of the B-ring quinone was very likely a

spontaneous air-oxidation of the corresponding phenol (from demethylation of the phenol methyl ether) since the reaction was carried out under air atmosphere, but the complete demethylation on both A- and B-ring (especially the former) was beyond expectation. MSA is not a typical *O*-demethylation reagent[273] and the very few examples where *O*-demethylation did occur with MSA required the presence of a strong nucleophile such as methionine[302] or NaI,[303] which had no equivalent species in this case. Hypothetically, the very strong acidity of MSA (pK_a < -1) and the electron-rich character of the AB-ring of **3.120** are two likely factors that would definitely contribute to the observed demethylation. Formation of **3.130** was a surprising but very pleasant result since the desired 6-6-6-6 carbon skeleton as planned in the retrosynthesis (cf. structures **3.32**–**3.35** in Scheme 3-3) was now achieved. However, **3.130** did have some issues that needed to be addressed. First, it was found experimentally that the solubility of **3.130** in various common organic solvents (polar or non-polar) was extremely low, which probably would make future chemical transformations of this compound difficult, especially at large scales. Such physical behaviour might be due to the presence of strong intramolecular hydrogen bonding between the A-/C-ring phenols and the B-ring quinone carbonyl group, which is evident from the characteristic large downfield NMR chemical shifts of the phenolic protons as a result of such H-bonding interactions, and similar phenomenon is known for compounds such as isoprekinamycin (**1.5**). Second, the two phenol functionalities within **3.129** (i.e., the A-ring phenol from *O*-demethylation and C-ring phenol from ring closure), if not properly differentiated, may compete with each other and complicate the later oxidation step that was planned to occur (preferably) at the C-ring to generate the corresponding *ortho*-quinone needed for further ring contraction reaction. Last, the relatively low yield of 44% obviously had room for improvement. The first two trials with **3.120** in MSA/HCOOH all involved the fairly harsh condition of refluxing; therefore, a milder attempt was explored (Table 3-4, trial 3). A large portion of **3.120** survived in the MSA/HCOOH mixture at ambient temperature after 40 hr but partial demethylation of AB-ring did

take place as indicated by the NMR of the crude products, which was further stirred in a hot (60–70 °C) MSA/HCOOH mixture for 2 days, leading to a 1:1 mixture of **3.130** and **3.131** as the major products, and the latter compound **3.131** was in fact an A-ring methylated derivative of **3.130**. Such result would suggest that compound **3.130** was an in situ demethylated product of **3.131** under such conditions during extended reaction time or at elevated temperature, and this conclusion was further confirmed by the latter experiments (Table 3-5).

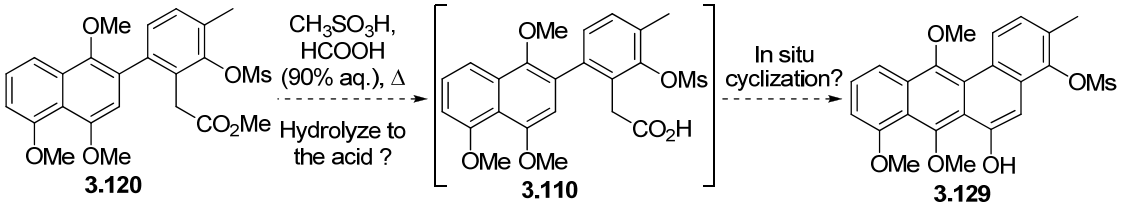

Scheme 3-24. MSA-catalyzed hydrolysis and in situ cyclization (Table 3-4) of **3.120**.

Table 3-4. Detailed experimental conditions and results for the MSA-catalyzed hydrolysis and cyclization of **3.120** (Scheme 3-22).

Trial	Reagents and Conditions	Products and Results
1	CH_3SO_3H/HCOOH (90% aq.)/air/↑↓ 3 hr	Complex mixture: cyclization/demethylation/oxidation
2	CH_3SO_3H/HCOOH (90% aq.)/air/↑↓ 12–16 hr	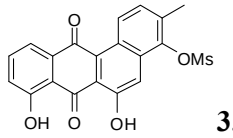 **3.130** (~ 44% yield)
3	CH_3SO_3H/HCOOH (90% aq.)/air first 40 hr @ rt then 48 hr @ 60–70 ºC	rt: mainly unreacted **3.120** but partial demethylation of AB-ring was observed! 60–70 ºC: two major products (~ 1:1) 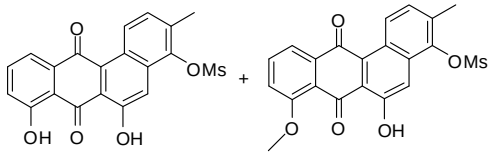 **3.130** **3.131**

The newly produced **3.131** solved two issues mentioned above, first the solubility concern since **3.131** was found to be quite soluble in various organic solvents, and second the (regio-)selectivity issue as the A-ring of **3.131** had a methoxy group (a protected phenol) while the C-ring existed as a free phenol, which had a much higher reactivity towards oxidation than the former. The only disadvantage was that the efficiency for the conversion from **3.120** to the desired cyclization product **3.131** was not high enough, since half of the ester was transformed into the unwanted **3.130** and the reaction time (2 days) was less than satisfying although bearable. In order to find out the best conditions to prepare **3.131** not only with good yield but also at a reasonable rate, attempts were made by trying to cyclize the methyl ester **3.120** in neat MSA with variation of other conditions (Scheme 3-25 and Table 3-5). It was very delightful to find that the desired cyclization product **3.131** was the

major species from the reaction, along with a small amount of the (A-ring) demethylated **3.130** and, in some cases, the unreacted starting ester **3.120**. To the best of our knowledge, there is no reported example in the literature that directly and intramolecularly cyclizes a benzyl type of ester without converting it to the corresponding carboxylic acid first. It could be clearly seen from the several trials (Table 3-5) that reaction temperature played a significant role in determining the conversion percentage and final product distribution, and a maximum yield of 80% of **3.131** was obtained when the reaction was carried out at 40–45 °C in neat MSA for 6 hr (Table 3-5, trial 3). As a control experiment (Table 3-5, trial 5), cyclization was also performed in a (1:1) mixture of MSA and CH_2Cl_2, which was previously reported as a more efficient condition for such cyclization than neat MSA,[294] but the result indicated otherwise.

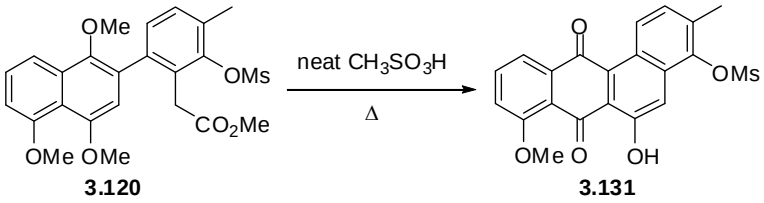

3.120 **3.131**

Scheme 3-25. MSA-catalyzed direct cyclization of **3.120** (Table 3-5).

Table 3-5. Detailed experimental conditions and results for the MSA-catalyzed cyclization of **3.120** (Scheme 3-25).

Trial	Reaction conditions	Molar ratio of products		
		3.120 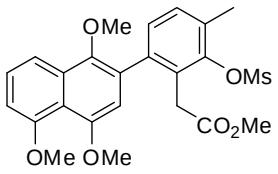	**3.131** 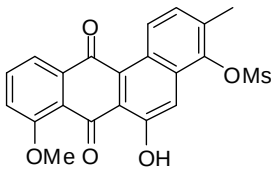	**3.130** 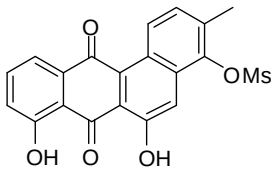
1	neat MSA/N_2 60–70 ºC/1 hr then rt/8 hr	4[a]	4[a]	1[a]
2	neat MSA/N_2 60–65 ºC/4 hr	0	2	1
3	neat MSA/N_2 40–45 ºC/6 hr	0	major (80% isolated yield)	very minor
4	neat MSA/air 45–50 ºC/4.5 hr	0	major (70% isolated yield)	very minor
5	MSA-CH_2Cl_2 (1:1), air/↑↓/8hr	major[a]	1 (minor)[a]	1 (minor)[a]

a. Estimated based on NMR spectra of crude product.

Due to time limitations, no further experiments to convert **3.131** into the kinamycins and their analogues were carried out in this thesis work. However, the successful and concise preparation of compound **3.131** had provided some quite promising results to achieve the ultimate goal. It is expected that, by following the synthetic plan as outlined in Scheme 3-26, total synthesis of kinamycin derivatives such as **3.140** may be accomplished if given more time. In fact, as a continuation of this work, Janet Simons of the Dmitrienko group was able to carry on some of the proposed synthesis as planned. Compound **3.141b** bearing a protected C-ring phenol but an exposed

D-ring phenol for further elaboration, which corresponds to the proposed intermediate structure of **3.133**, was successfully prepared in good yield from **3.131** (Scheme 3-26).[304]

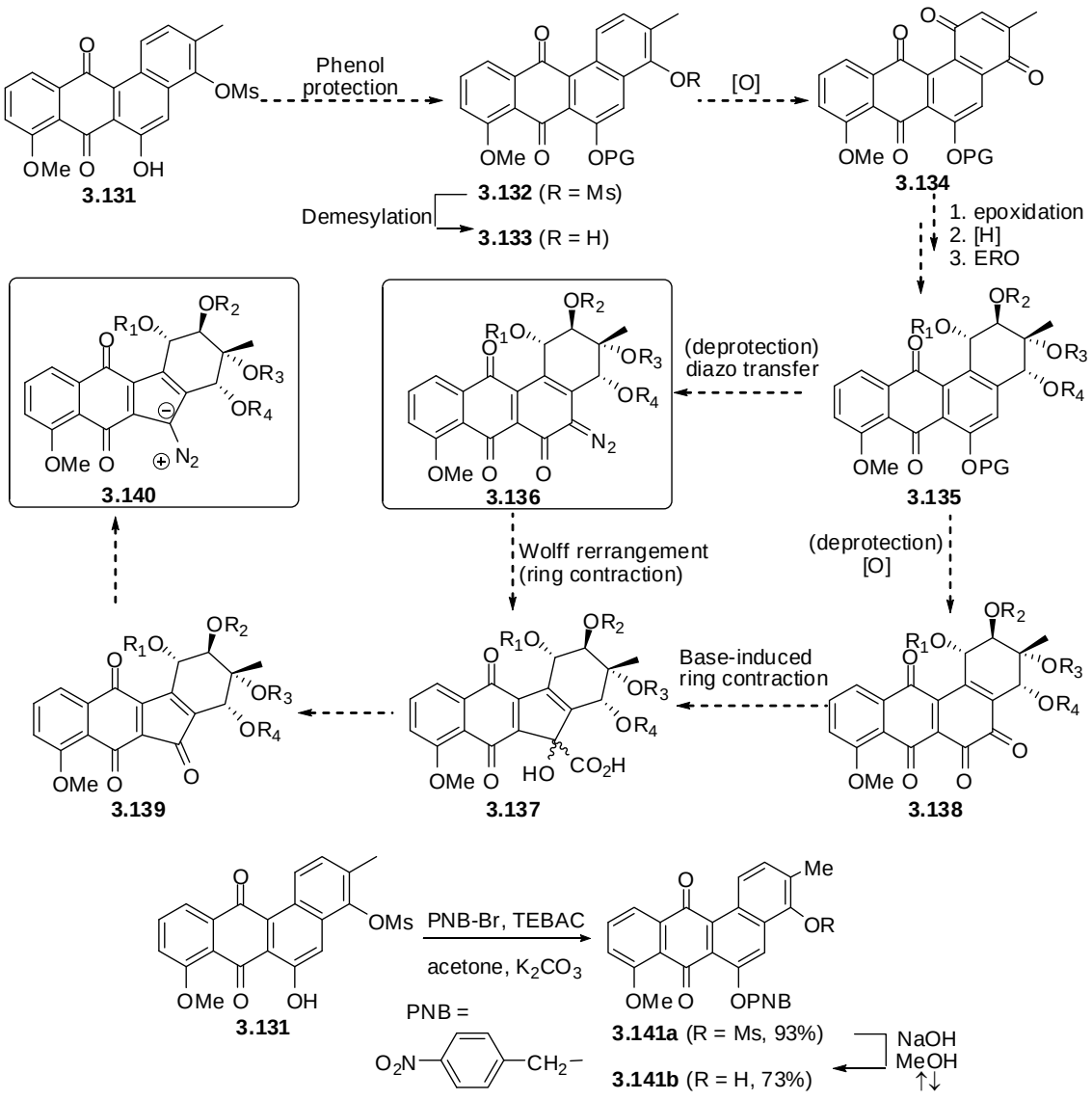

Scheme 3-26. Synthetic plan towards kinamycins from the intermediate **3.131** and some recent progress (from **3.131** to **3.141b**) made by Janet Simons according to the plan.

During the course of this project, there appeared a few literature reports concerning the total synthesis of the kinamycins, particularly the diazobenzo[*b*]fluorene type that covers the majority of the natural kinamycin antibiotics. These recent literature examples will be discussed and compared with the current results and the corresponding future synthetic plan next.

3.2 Recent Literature Concerning The Total Syntheses of Kinamycins

The above synthetic strategy towards the kinamycins, i.e. section 2.2 describing a biomimetic elaboration of the kinamycin's D-ring and section 3.1 describing the construction towards the benzo[*b*]fluorene skeleton, was generated at a time when there were no reports of successful synthesis of these natural products. Thus, the synthetic plan was not influenced by any conscious effort to improve upon strategies developed in other laboratories. Although the present synthetic effort towards the kinamycins is not complete, it is worthwhile to contrast this approach with successful synthetic methods that have been reported by other laboratories during the course of this research project. In particular, it is of potential value to examine the synthetic approaches critically to determine if the biogenetically inspired synthetic strategy offers any advantages over other methods in order to decide if further work to complete the synthesis via the biomimetic method is worthwhile.

Since the biomimetic approach of this thesis work towards the kinamycins has not been completed, it is necessary to make some educated guesses as to the total number of synthetic steps that will be involved in this strategy, before comparison can be made with the literature approaches to be discussed next. To summarize, thus far, the preparation of the advanced aromatic 6-6-6-6 fused ring system of **3.131** requires a linear sequence of only three steps with an overall yield of 65% (Scheme 3-27), starting from the corresponding AB-ring precursor **3.59** and D-ring precursor **3.107**. Either precursor can be very easily prepared, with good overall yields and in large scales (if needed),

from commercially available and relatively inexpensive materials/reagents. Precursor **3.59** can be derived from **3.54** in five steps with an overall yield of 35%, while **3.107** can be obtained from **3.86** in also five steps with an overall yield of 51% (Scheme 3-27). Therefore, the longest linear sequence to prepare the intermediate **3.131** involves eight steps, from either the naphthol **3.54** or the methylsalicylic acid **3.86** (Scheme 3-27). The remaining steps require **3.131** to undergo *O*-protection of the C-ring phenol, demesylation and the subsequent D-ring oxidation to the *p*-quinone of **3.134**, to which the model chemistry for ring D-elaboration might be applied (Scheme 3-26). Ideally, the ring D-elaboration of **3.134** should require only three steps (epoxidation, reduction and epoxide ring opening as demonstrated by the model D-ring synthesis described in Chapter 2) to yield the intermediate **3.135** (Scheme 3-26), although it is possible that conversion of the B-ring quinone to an *O*-protected hydroquinone may be necessary if the redox manipulation in the D-ring is interfered with by the B-ring quinone. To provide the benzo[*b*]fluorene ring system of the kinamycins as in **3.137** via ring contraction of **3.135** (Scheme 3-26), two possible routes are available and both involve two steps. Conversion of **3.137** to the target diazobenzo[*b*]fluorene system would then be done in two more steps using established methods for decarboxylative diazotransfer reactions (Scheme 3-26). Thus, the present state of the biomimetic approach may be ten steps away from kinamycin F (**1.1f**). This would mean that a total synthesis of the kinamycins might be achievable in approximately 18 steps from the commercially available naphthol **3.54** and/or methylsalicylic acid **3.86**.

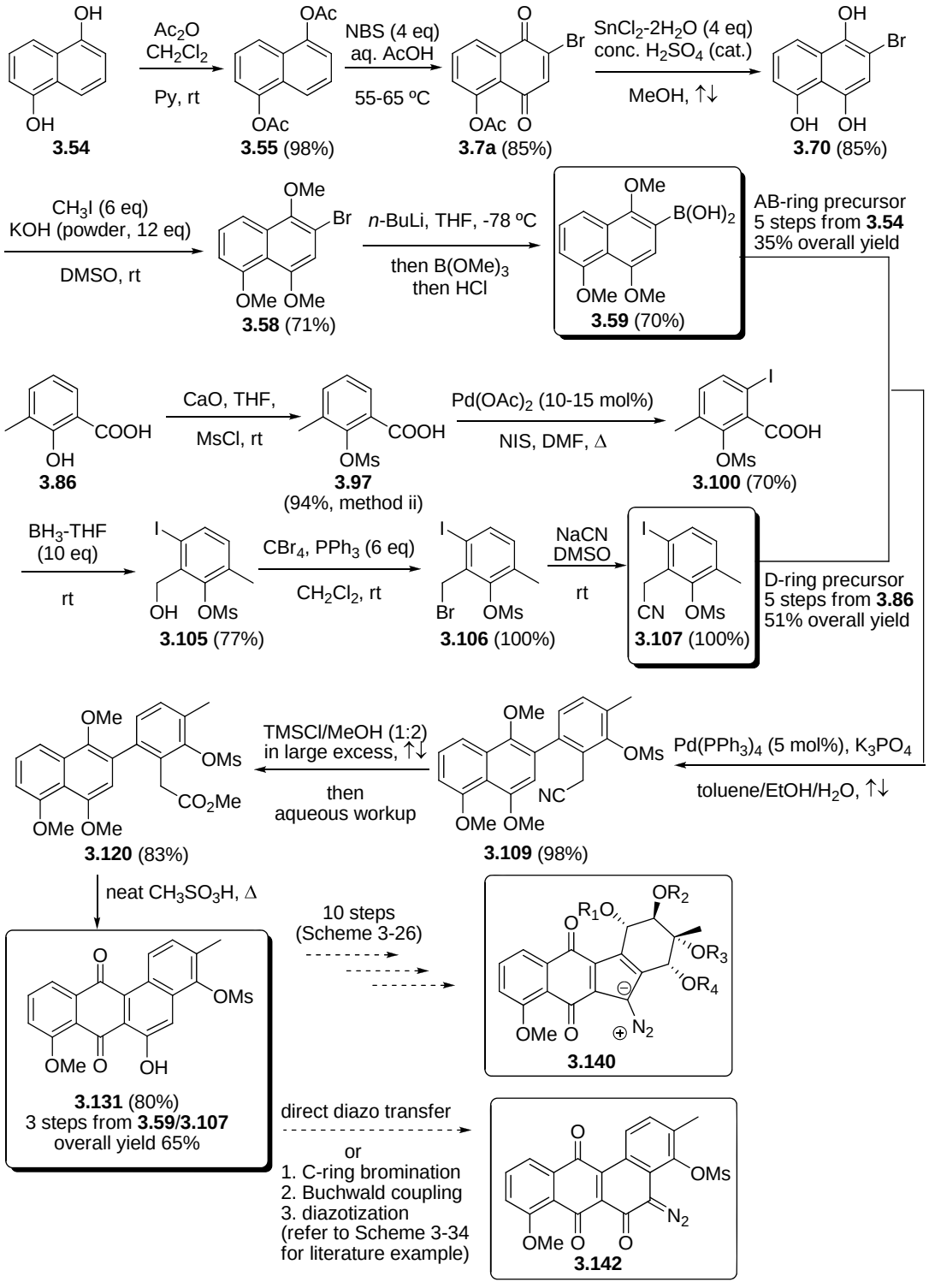

Scheme 3-27. Summary of the current synthetic efforts towards the kinamycins.

It is important to realize that the Wolff rearrangement approach to ring contraction would involve the formation of an *o*-quinodiazide intermediate **3.136** (Scheme 3-26). This intermediate diazo species **3.136** with a 6-6-6-6 carbon skeleton is potentially very interesting in its own right, since it is a hybrid of the isoprekinamycins (diazobenzo[*a*]fluorenes with 6-5-6-6 skeletons) and kinamycins (diazobenzo[*b*]fluorenes with 6-6-5-6 skeletons) systems. Thus, it is in itself an interesting structural analogue of the kinamycins that might possess useful anticancer and antibacterial activity and is, on its own, a worthy synthetic target. This potentially bioactive compound might be accessed in eight steps from the phenol intermediate **3.131** that has been successfully prepared in this study. In fact, if such diazo analogues with a 6-6-6-6 skeleton are of certain values as expected, a much quicker and easier access to a fully aromatized **3.142** from **3.131** is quite possible (Scheme 3-27), either through a direct diazo transfer reaction of **3.131** or by taking advantage of some synthetic conditions previously developed by the Dmitrienko group.

Although all of the synthetic work done in this project on the kinamycin D-ring has been carried out with racemic compounds, the recent developments in regard to asymmetric epoxidation of quinones suggests that the method could be adapted to provide highly enantiomerically enriched end products, as discussed in Chapter 2. Thus, this approach has the potential to yield kinamycin F (**1.1f**) in 18 synthetic steps in optically active form from the commercially available compounds as well as to provide the novel kinamycin analogue **3.136** as an intermediate.

3.2.1 Literature Total Synthesis of the Diazobenzo[*b*]fluorene type of Kinamycins

For prekinamycin (**1.4**), the fully aromatized diazobenzo[*b*]fluorene, other than the previously introduced total synthesis by Hauser and Zhou in 1996 (section 1.5.2, Scheme 1-25b)[76] and some even earlier and related work by Mal and co-workers (section 1.5.2, Scheme 1-25a)[151], two recent (both published in 2007) reports have appeared in the literature,[153,154] which will be only very briefly

described here since the targets of the thesis project are diazobenzo[*b*]fluorenes possessing non-aromatic D-rings. As a further development of the base-induced double condensation to build the benzo[*b*]fluorenes (Scheme 1-21), Birman and co-workers synthesized prekinamycin (**1.4**) and its unsubstituted analogue **3.147** via an indanone dianion **3.144** annulation with phthalate diesters **3.145** (Scheme 3-28a).[153] In the case of the double condensation between **3.144b** and the unsymmetrical phthalate diester **3.145b**, the observed regioselectivity of the product **3.146b** matches the natural product **1.4**. The condensation was governed by the electronic nature of the indanone dianion **3.144b** (β-position is more active/electron-rich than α-position) and diester **3.145b** (ester *meta* to the methoxy group is more active/electron-deficient than the *ortho* ester). Interestingly, another work by Estevez's group employed the combination of an initial base-induced aldol condensation between 1-tetralone (**3.148**) and an *ortho*-halogenated benzaldehyde **3.149**, followed by a subsequent intramolecular Pd(II)-catalyzed cyclization and spontaneous benzylic oxidation to derive the benzo[*b*]fluorenone skeleton of **3.154** (Scheme 3-28b).[154]

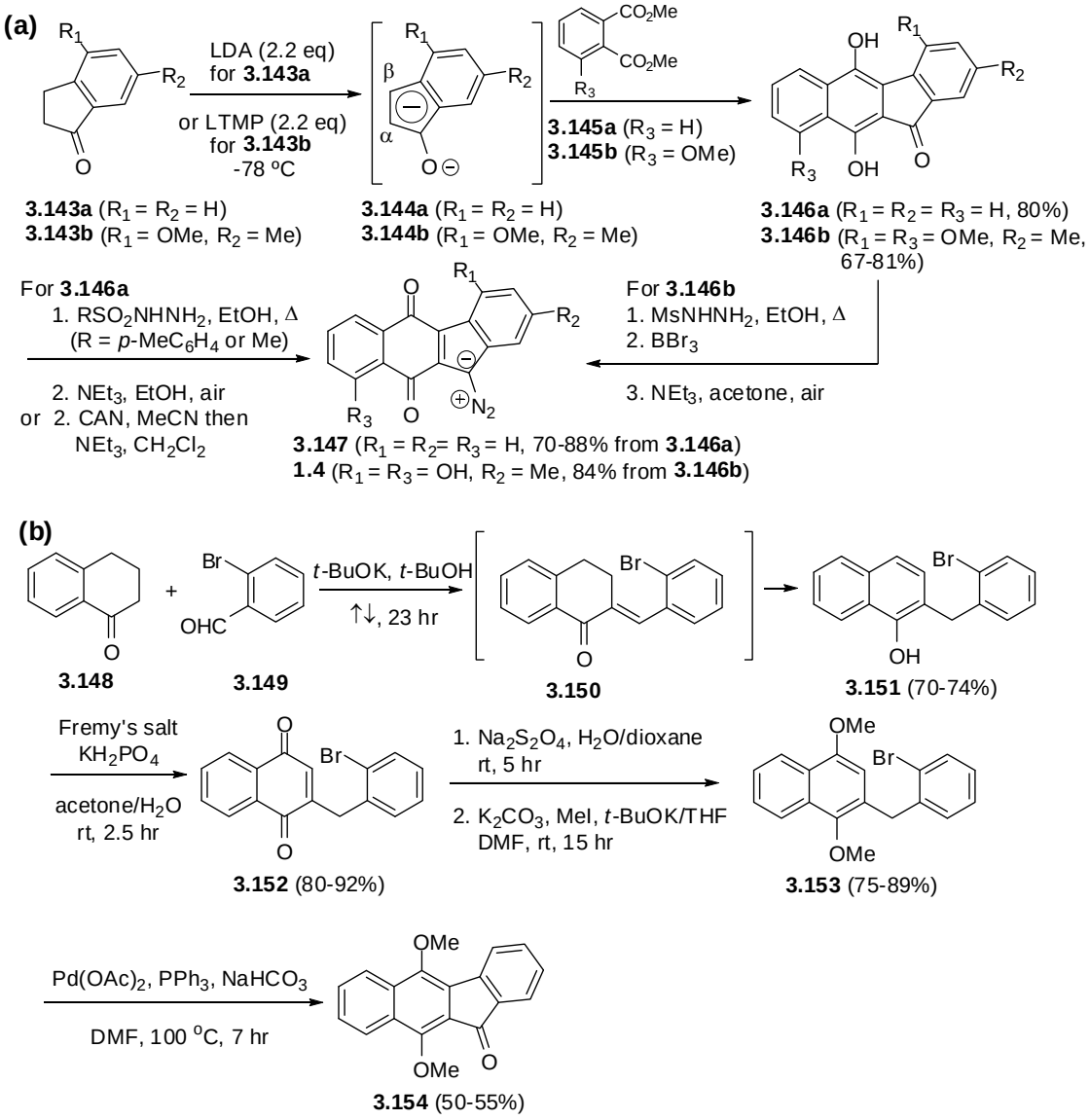

Scheme 3-28. (a) Total synthesis of prekinamycin (**1.4**) via base-induced double condensation by Birman's group and (b) synthesis of benzo[*b*]fluorenone via base-induced condensation and intramolecular cross coupling by Estevez's group.

For the diazobenzo[*b*]fluorene type of kinamycins possessing a non-aromatic D-ring, four related total syntheses have been reported so far starting from 2006. The first is from the group of John

Porco, who successfully prepared the kinamycin C (**1.1c**) for the first time since the discovery of these natural diazobenzofluorenes.[23] As shown in Scheme 3-29, starting from an achiral bromoquinone monoketal **3.156**, the Porco approach constructed the kinamycin D-ring stereoselectively via a hydroxyl-directed asymmetric nucleophilic epoxidation of **3.156** as the key step to control the subsequent stereochemical outcome. The good enantioselectivity (90% *ee*) of the epoxidation under a modified tartrate-mediated condition achieved with **3.157** is noteworthy. Then a Pd-catalyzed cross coupling of the D-ring fragment **3.158** and the AB-ring precursor **3.159** led to coupling product **3.160**. A stereoselective ketone reduction, followed by a regioselective, stereospecific and nucleophilic epoxide ring opening of **3.160** afforded an unsaturated (D-)ring within **3.161** that possesses the same absolute stereochemistry as the D-ring of kinamycins. Further chemical transformations afforded a carboxylic acid **3.162**, which underwent an intramolecular Friedel-Crafts cyclization to yield the benzo[*b*]fluorenone skeleton. The subsequent introduction of the diazo group by oxidation of a hydrazone intermeidate furnished the enantioselective total synthesis of kinamycin C (**1.1c**).

The establishment of the absolute stereochemistry and substitution pattern for kinamycin D-ring in Porco's procedure was well designed and achieved, but it took 14 steps to complete this task (along with other useful transformations though), i.e. 7 steps to prepare the asymmetric epoxide **3.157** from **3.155**, and another 7 steps to **3.161** from **3.155**. Overall, the Porco synthesis of kinamycin C (**1.1c**) involves a 23 step linear sequence from 2,5-dihydroxy-6-bromobenzaldehyde (**3.155**), which is referred to as a readily available starting material even though it is not commercially available. Compound **3.155** has to be generated by a one-step bromination of commercially available 2,5-dihydroxybenzaldehyde, an apparently very simple but expensive starting material (yet it can be prepared through a few additional steps). In addition, the AB-ring precursor **3.159** has to be prepared from a bromojuglone **3.188** (refer to Scheme 3-32) through three additional steps, and this simple

juglone itself is not commercially available and requires additional synthesis from other materials. By contrast, the biomimetic approach of this work only requires three steps to establish the D-ring stereochemistry/substituents and an overall 18 steps to the target molecule. Thus, in terms of the number of synthetic operations involved, the biomimetic approach of this work has the potential to be competitive with the Porco synthesis.

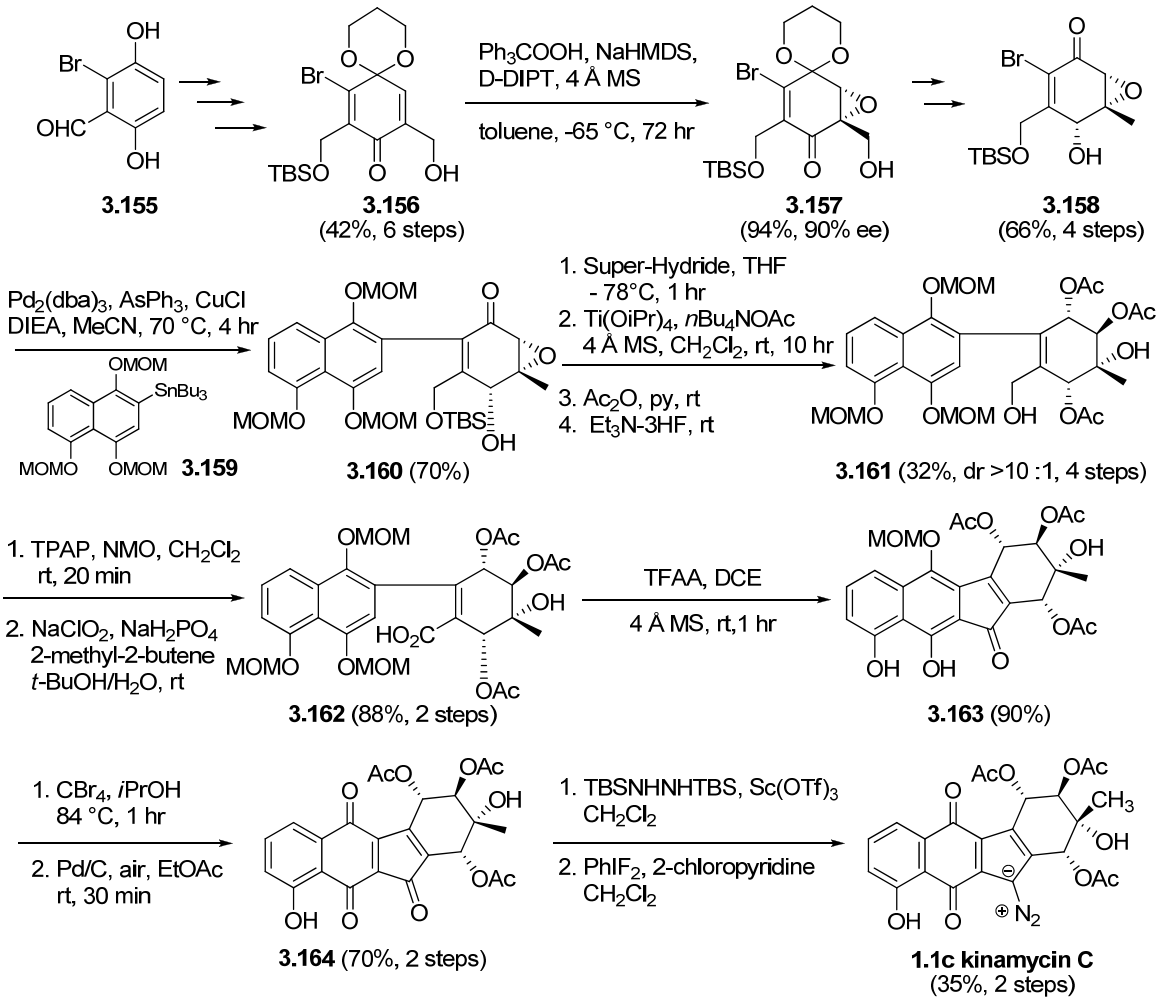

Scheme 3-29. Total synthesis of kinamycin C (**1.1c**) by the Porco group.

In 2007, a group of researchers led by Kumamoto and Ishikawa reported a total synthesis of racemic (±)-methyl kinamycin C **3.176**, which was based on a unique strategy of using a Diels-Alder

reaction between an ABC-ring (indenone type) precursor **3.169** and a Danishefsky-type diene **3.166** to form the D-ring skeleton of kinamycins (Scheme 3-30c).[24] This route was developed from their earlier synthetic model studies to construct the kinamycin BCD-ring (Scheme 3-30a)[163] and ABCD-ring (Scheme 3-30b),[258] and the former model synthesis has been discussed in greater details previously (Scheme 2-1, section 2.1). As a continuation of their previous efforts to prepare the kinamycin ABC-ring precursor **3.169** (Scheme 3-30b), Kumamoto and Ishikawa reported some interesting results in 2008 (Scheme 3-31).[305] Regioselective Diels-Alder reaction of the quinones and quinone ketals **3.178** with diene **3.179** (Scheme 3-31a) led to **3.180** and also an unexpected propellane **3.181**, while the ring opening reaction of another Diels-Alder product **3.183** gave the unexpected **3.184** rather than **3.185** (Scheme 3-31b). However, both **3.180** and **3.184** may serve as possible precursors for the synthesis of regioisomeric kinamycin analogues of the natural products by employing the Kumamoto/Ishikawa's approach.

Since, in this synthetic approach, the first chiral centres are introduced via a Diels-Alder reaction, it is possible that the method might be modified to take advantage of effective chiral catalysts for this process so that the method might provide an asymmetric synthesis of the kinamycins. However, the lengthy and rather complicated 26 steps to produce the racemic *O*-methyl kinamycin C **3.176** from the naphthol **3.54** (and the Danishefsky-type diene **3.166** has to be prepared by some additional steps), which is also one of the starting material used in this study, suggest that the current biomimetic approach, if completed, is likely to be competitive with the Kumamoto/Ishikawa's approach.

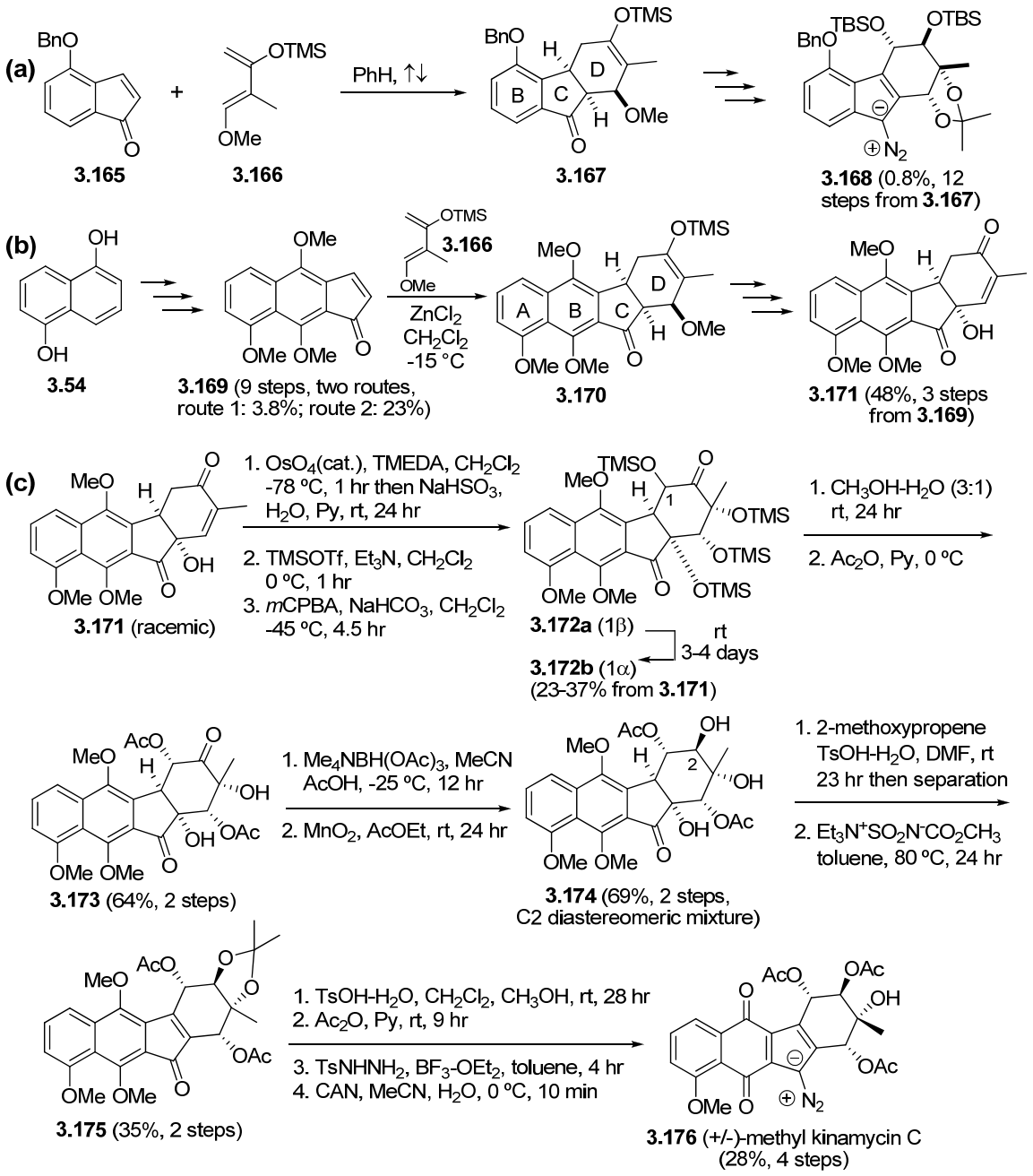

Scheme 3-30. Total synthesis of (±)-methyl kinamycin C **3.176** by the Kumamoto/Ishikawa group.

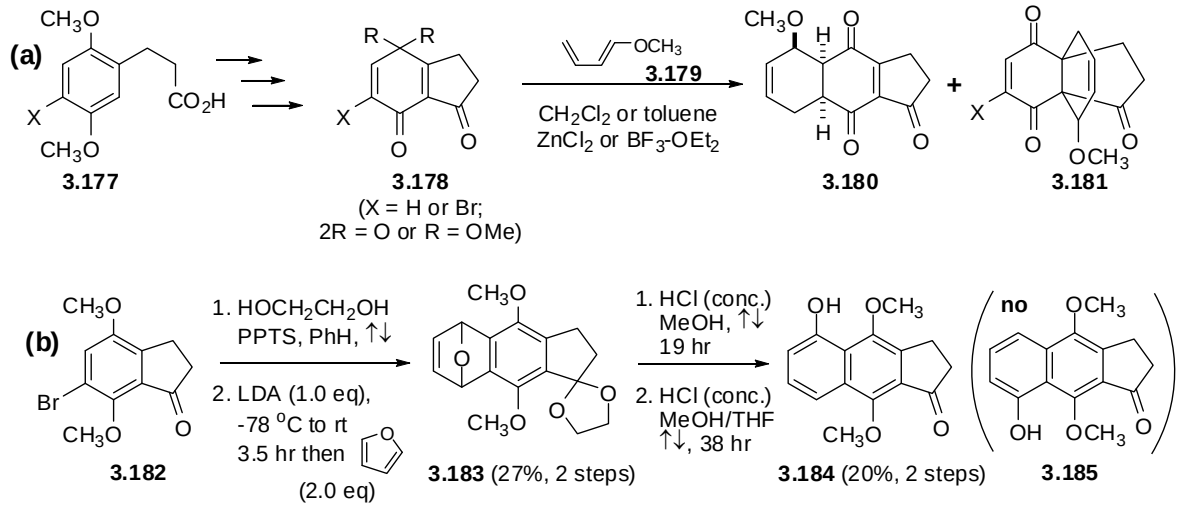

Scheme 3-31.Synthesis of kinamycin ABC-ring precursor analogues through Diels-Alder reactions by the Kumamoto/Ishikawa group.

Later in 2007, Nicolaou and co-workers published the second total synthesis of kinamycin C (**1.1c**) (Scheme 3-32).[16] The D-ring iodo-enone precursor **3.187** was prepared from a chiral α,β-unsaturated cyclohexanone **3.186**, and the consequent modified Ullman coupling of **3.187** with a naphthylbromoaldehyde **3.189** as the corresponding AB-ring precursor gave the coupling product **3.190**, which was then cyclized through a benzoin-type reaction to form the crucial benzo[*b*]fluorene skeleton found in **3.192**. Further chemical transformations finished the installation of the remaining D-ring C1-OH stereoselectively first, and then the introduction of diazo group to the benzo[*b*]fluorenone structure, eventually leading to kinamycin C (**1.1c**), F (**1.1f**) and J (**1.1j**). Two years later, this synthetic strategy was modified and used again by the Nicolaou group in their synthesis of the monomeric diazobenzo[*b*]fluorene unit of the lomaiviticin aglycon **3.197** (Scheme 3-32).[158]

Nicolaou's procedure showed some improved efficiency in constructing the D-ring stereochemistry/substituent (i.e., 11 steps from **3.186** to **3.193**, along with other useful

transformations) when compared to the previous approach by the Porco group and the Kumamoto/Ishikawa group. In the Nicolaou synthesis, the longest linear sequence involves five steps from the chiral enone **3.186** to the iodo-enone **3.187** followed by 13 additional steps to get to kinamycin C (**1.1c**) or J (**1.1j**). The critical chiral building block of enone **3.186**, despite being reported as readily available, requires an additional four steps for preparation from an achiral and commercially available starting material (and surprisingly no yield is reported), while the other precursor **3.189** also requires an additional five steps from the commercially unavailable bromojuglone **3.188**. The projected 18 step sequence for synthesis of kinamycin F (**1.1f**) via the biomimetic strategy has the potential to compare relatively well in regard to efficiency with the Nicolaou approach.

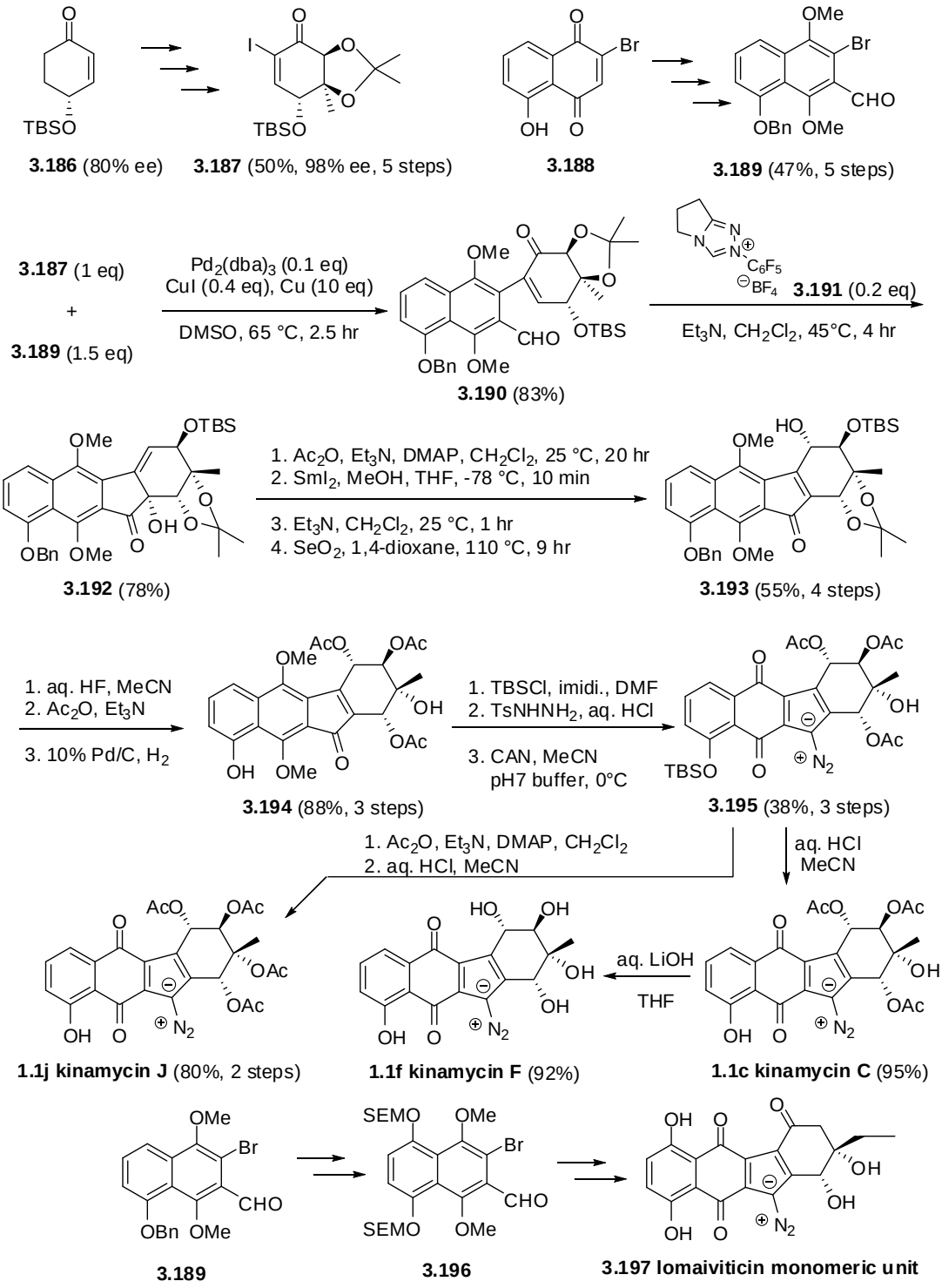

Scheme 3-32. Total synthesis of kinamycin C (**1.1c**) by the Nicolaou group.

The latest addition to the total syntheses of kinamycin was reported by Herzon's group in early 2010 (Scheme 3-33) and offers a more concise route to the diazobenzo[*b*]fluorene type of kinamycin antibiotics. The regioselective asymmetric dihydroxylation of **3.199** leading to the (protected) chiral vicinal diol **3.200** set up the foundation to control the stereochemistry of kinamycin D-ring, although the complete installation of necessary D-ring substituents in the correct stereochemical manner is only achieved at the very end of the total synthesis (after the second last step).

Due to the wisely designed synthetic route, the longest linear sequence within this approach is only 12 steps from the aromatic silyl ether **3.198** (the precursor **3.205** requires three additional steps to prepare). The current biomimetic approach would be less effective (in terms of number of steps) than this latest method by the Herzon group.

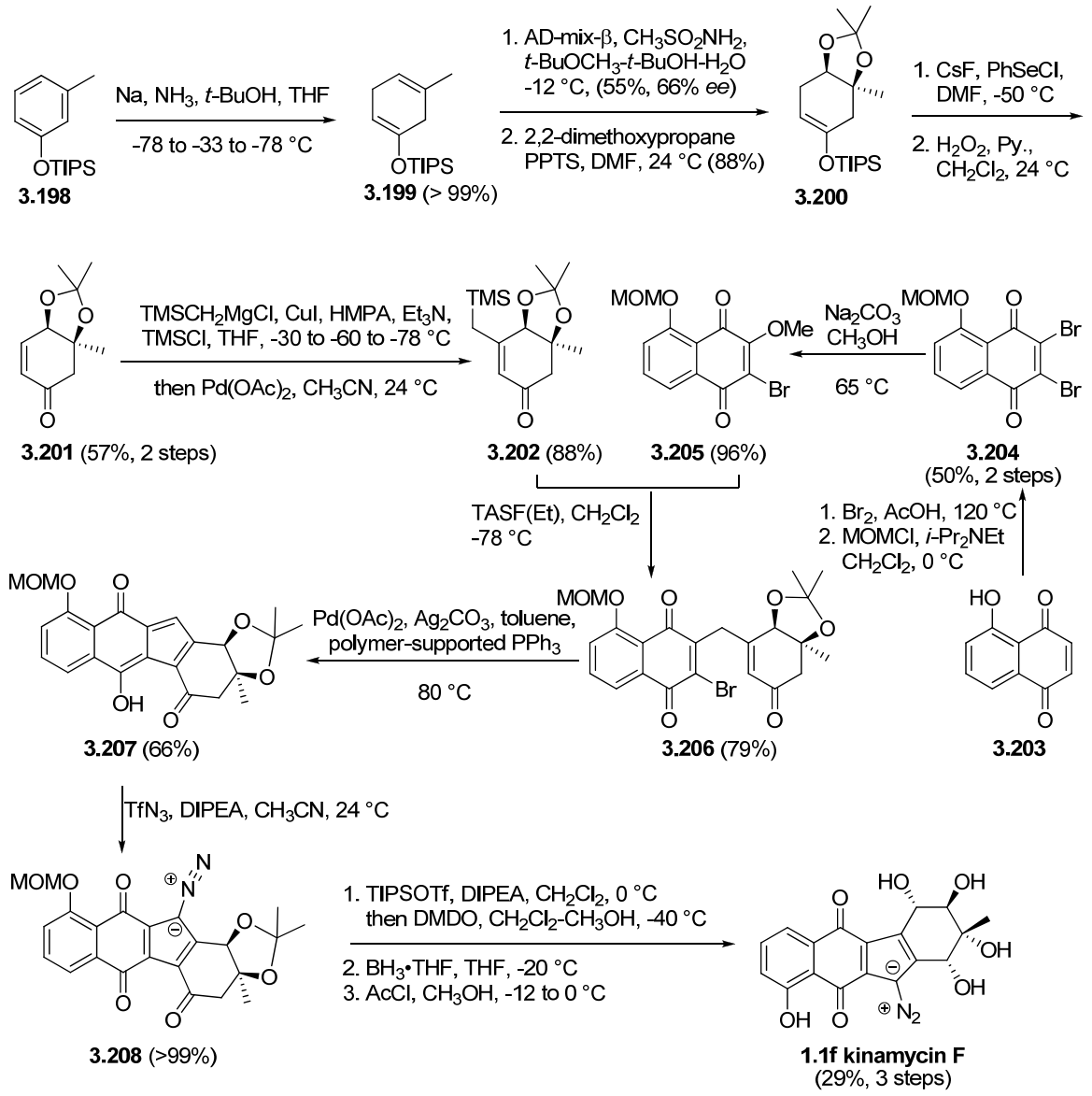

Scheme 3-33. Total synthesis of kinamycin F (**1.1f**) by the Herzon group.

In conclusion, the biomimetic approach developed by this project has the potential to be competitive with the existing approaches to the total synthesis of the kinamycins. The biomimetic approach may, however, provide access to some unique and very interesting diazo analogues for anticancer and antibacterial screening (e.g., **3.136** in Scheme 3-26 and **3.142** in Scheme 3-27), that are

not accessible by any of the other methods. The current work involves neither complicated operations/conditions nor expensive reagents/materials for chemical transformations thus far, and the remaining steps (Scheme 3-26) are also not expected to be very different in this aspect either. Therefore, this method might be well developed to be a practical method to prepare the kinamycins and analogues. Thus, it is reasonable to suggest that, despite the appearance of four reported total syntheses of the kinamycin system during the course of this research project, it is judged that the biomimetic approach has sufficient merit to warrant further work to complete the synthesis of kinamycin F (**1.1f**) via this strategy.

Finally, synthetic efforts towards some dimeric model structures for the dimeric diazobenzo[*b*]fluorene of lomaiviticins (**1.11**) such as **3.209**, **3.210** and **3.211** also appeared in the literature lately. Such synthetic results will not be discussed here since they are of less relevance to the synthesis of the diazobenzo[*b*]fluorene of the kinamycins, but details can be found from reports by the Nicolaou group published in 2006 (for **3.209** and **3.210**)[157] and the Shair group released in 2008 (for **3.211**)[159].

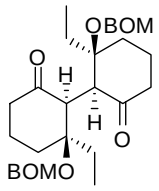

3.209
lomaiviticin A core

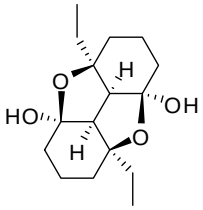

3.210
lomaiviticin B core

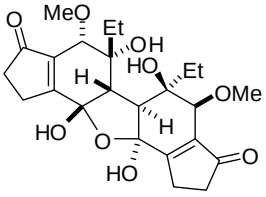

3.211
lomaiviticin A core

3.2.2 Total Synthesis of the Diazobenzo[*a*]fluorene type of Kinamycins by the Dmitrienko Group

Even though isoprekinamycin (**1.5**) was isolated in 1989,[5,6] its true structure of diazobenzo[*a*]fluorene was not characterized correctly until 2000.[14] The delay in structural

identification had limited the synthetic efforts towards this compound. Apparently, the Dmitrienko group is the only one that has succeeded in achieving the total synthesis of isoprekinamycin (**1.5**) and its analogues. Although the diazobenzo[*a*]fluorene antibiotics were not the main focus of this thesis project, it is necessary to briefly introduce the synthetic efforts from the Dmitrienko group towards this molecule (by others but not this thesis work). In fact, the availability of isoprekinamycin (**1.5**) in the Dmitrienko lab (initially through bacteria fermentation and later on by means of total synthesis) and a few synthetic analogues have also led to some very intriguing discoveries and a series of computational studies of this type of molecule by this project, which will be described and discussed in Chapter 5.

In 2002, Laufer from the Dmitrienko group finished the synthesis of a simple analogue **1.123** of isoprekinamycin (**1.5**), which possesses the exact diazobenzo[*a*]fluorene skeleton as the natural product but without any substituents on either the A-ring or D-ring (Scheme 3-34a).[124] The synthesis started with a Suzuki coupling between the boronic acid **3.212** and aryl bromide **3.213** to afford the biaryl **3.214**, which was then brominated with NBS to a biaryl bromide **3.215**. Anionic cyclization of either **3.214** or **3.215** afforded **3.216** having the desired benzo[*a*]fluorene skeleton for the target molecule, and demethylation of **3.216** gave **3.217**. Although the skeleton was constructed fairly easily, introducing the diazo group to **3.217** was found to be quite difficult presumably due to the presence of the electron-withdrawing keto group on the B-ring, which prevented the desired diazo transfer or even simple bromination to occur at C-5 of **3.217**. The problem was solved by reducing the keto group of **3.216** and the corresponding alcohol from reduction was protected as a silylether **3.218**. Then the simple bromination at C-5 of **3.218** occurred smoothly with NBS in DMF, and the consequent palladium-catalyzed amination of **3.219** with benzylamine not only introduced the essential nitrogen substituent at C-5 but also resulted in desilylation and oxidation to give the ketone **3.220** (along with minor amount of **3.221**). Debenzylation of the amine by hydrogenolysis produced **3.221,** and

diazotization and demethylation of **3.221** occurred simultaneously under the typical diazotization conditions to afford the final product **1.123**. Alternatively, **1.123** was also synthesized through a shorter and more efficient route (Scheme 3-34b) by using the naphthyl methoxyether **3.222** (to generate the boronic ester in situ) and the aryl bromide **3.223** for the Suzuki coupling, the obtained biaryl **3.224** was brominated with NBS smoothly and then underwent a Friedel-Crafts cyclization in high yield, which avoided the previous problems involved in the anionic cyclization route. The produced bromoketone **3.226** was then subjected to the same amination, debenzylation and diazotization conditions to finish the synthesis.

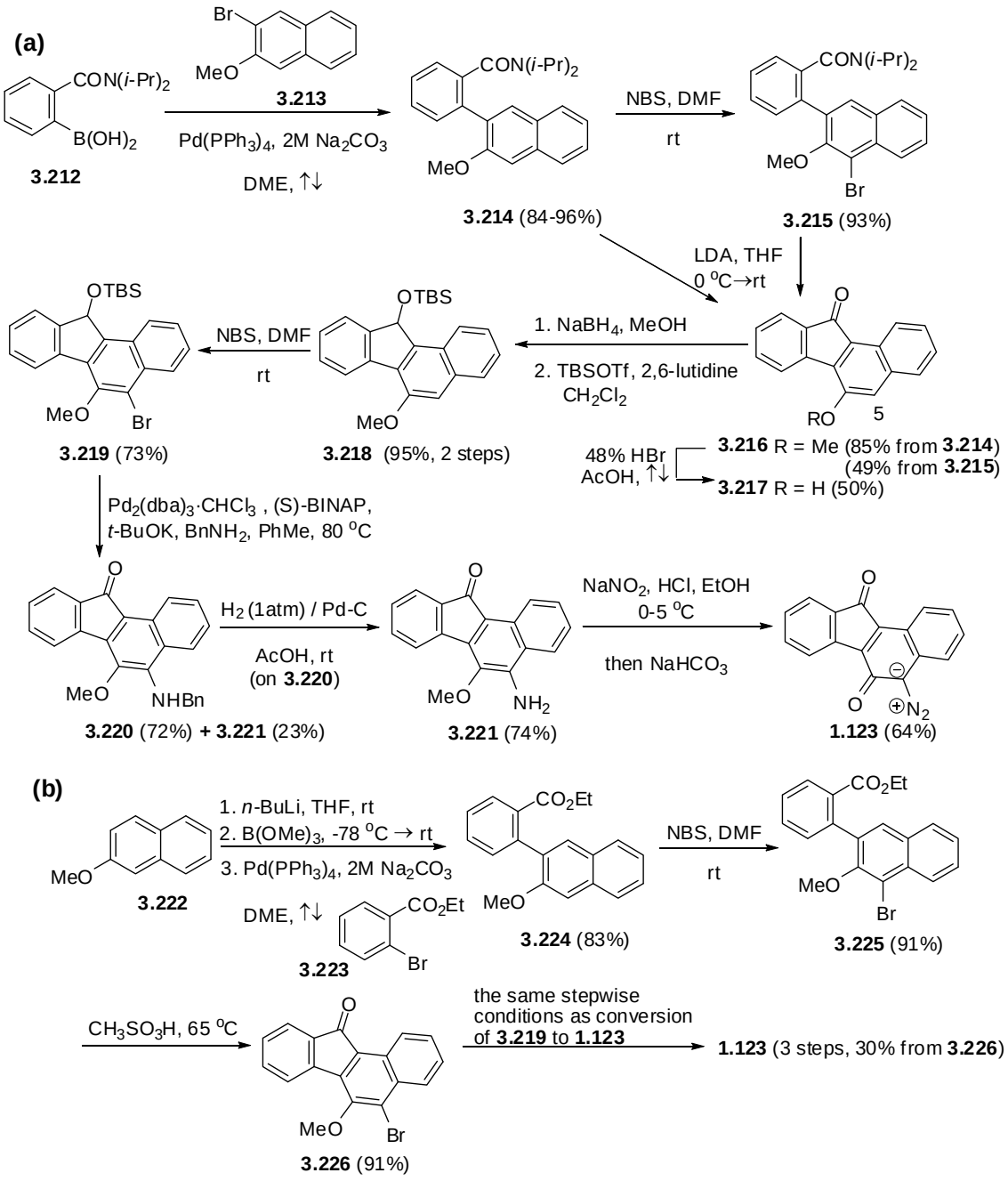

Scheme 3-34. Total synthesis of isoprekinamycin analogue **1.123** by Laufer.

Despite Laufer's initial success, later on, Buck and Liu from the Dmitrienko group had to unfortunately use a different approach to achieve the total synthesis of another analogue **3.236** of

isoprekinamycin (**1.5**), which possesses an A-ring methoxy group but still no D-ring substituents.[25] The necessary change of the synthetic methodology was a result of some unforeseen difficulties on the critical ring closure step by following Laufer's procedure (Scheme 3-34) when an additional methoxy group was introduced to the starting materials (unpublished results from this lab), which was hoped to eventually become the A-ring methoxy group of **3.236**.[80] The new synthetic path towards **3.236** is given in Scheme 3-35, in which the Suzuki coupling of **3.229** (AB-ring precursor) and **3.230** (D-ring precursor) under non-basic conditions generated the crucial biaryl **3.231** in excellent yield, which then underwent an intramolecular Dieckman-like reaction to carry out the desired ring closure and afforded the benzo[*a*]fluorenenitrile **3.232**. The cyano group of **3.232** was then gradually transformed by hydrolysis (to amide **3.233**), modified Hoffman rearrangement (to carbamate **3.234**) and saponification (to amine **3.235**). The aryl amine **3.235** was finally diazotized to provide the isoprekinamycin model compound **3.236**.

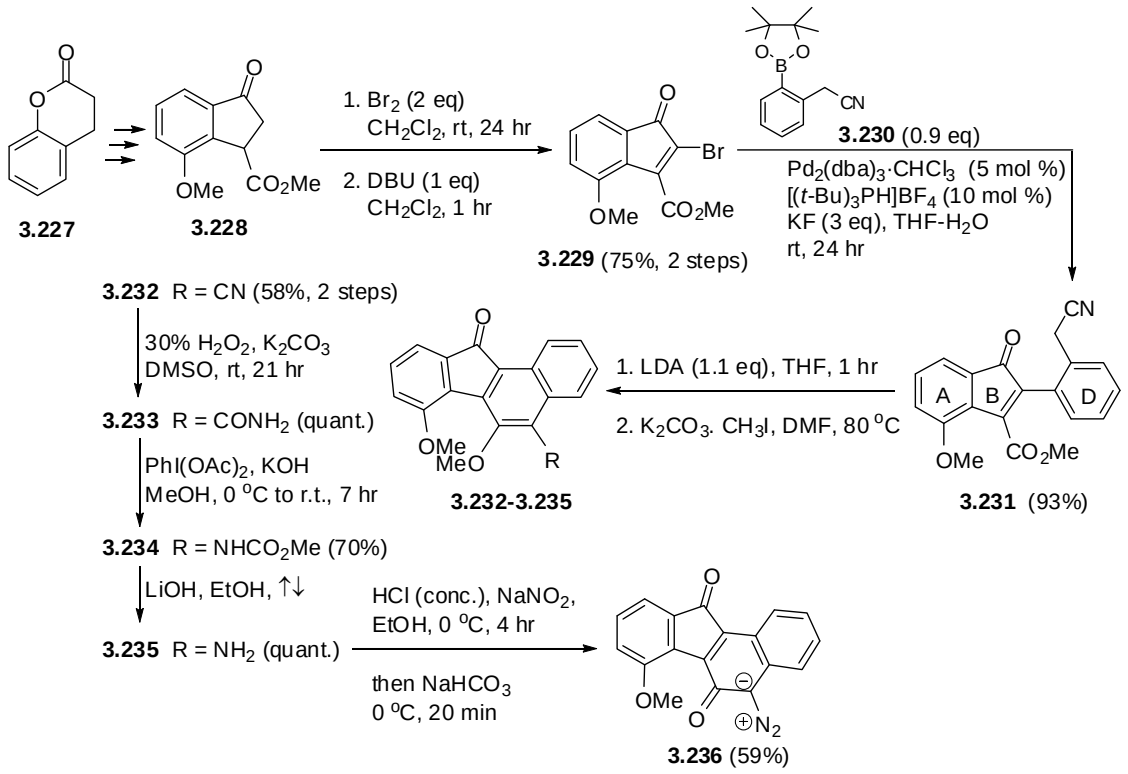

Scheme 3-35. Total synthesis of isoprekinamycin analogue **3.236**.

The above successful strategy was then applied to the total synthesis of isoprekinamycin (**1.5**) (Scheme 3-36), starting from the Suzuki coupling of an arylboronate **3.238** as the appropriate D-ring precursor with bromide **3.239**.[25] However, the subsequent anionic cyclization of the biaryl **3.240** under the previously successful condition (i.e., LDA/THF/-78 °C for **3.231**, Scheme 3-35) failed to yield the desired Claisen product **3.241**, instead, an aldol product **3.242** was obtained almost exclusively. Reduction of the B-ring keto group of **3.240** with borohydride followed by cyclization (not shown in the scheme) could suppress the undesired **3.242** to a certain extent (not completely) but at the cost of low yield of the desired **3.241**. Eventually it was found that low temperature reduction of **3.240** with a mixture of *n*-butyllithium and DIBAL gave the reduced trialkylaluminate **3.243**, which was further treated with LDA in situ to perform the expected cyclization, leading to a mixture

of **3.245** and **3.241** (formed by partial air oxidation of **3.245**). Methylation of this mixture without separation followed by a (oxidative) hydrolysis of the cyano group produced the amide **3.246** (and the B-ring hydroxyl group of **3.245** was concurrently oxidized to the ketone). Isoprekinamycin dimethylether **1.135** was obtained after transformation of **3.246** under the previous Hoffman rearrangement, hydrolysis and diazotization conditions, which gave the target molecule of isoprekinamycin (**1.5**) upon demethylation with BCl_3.

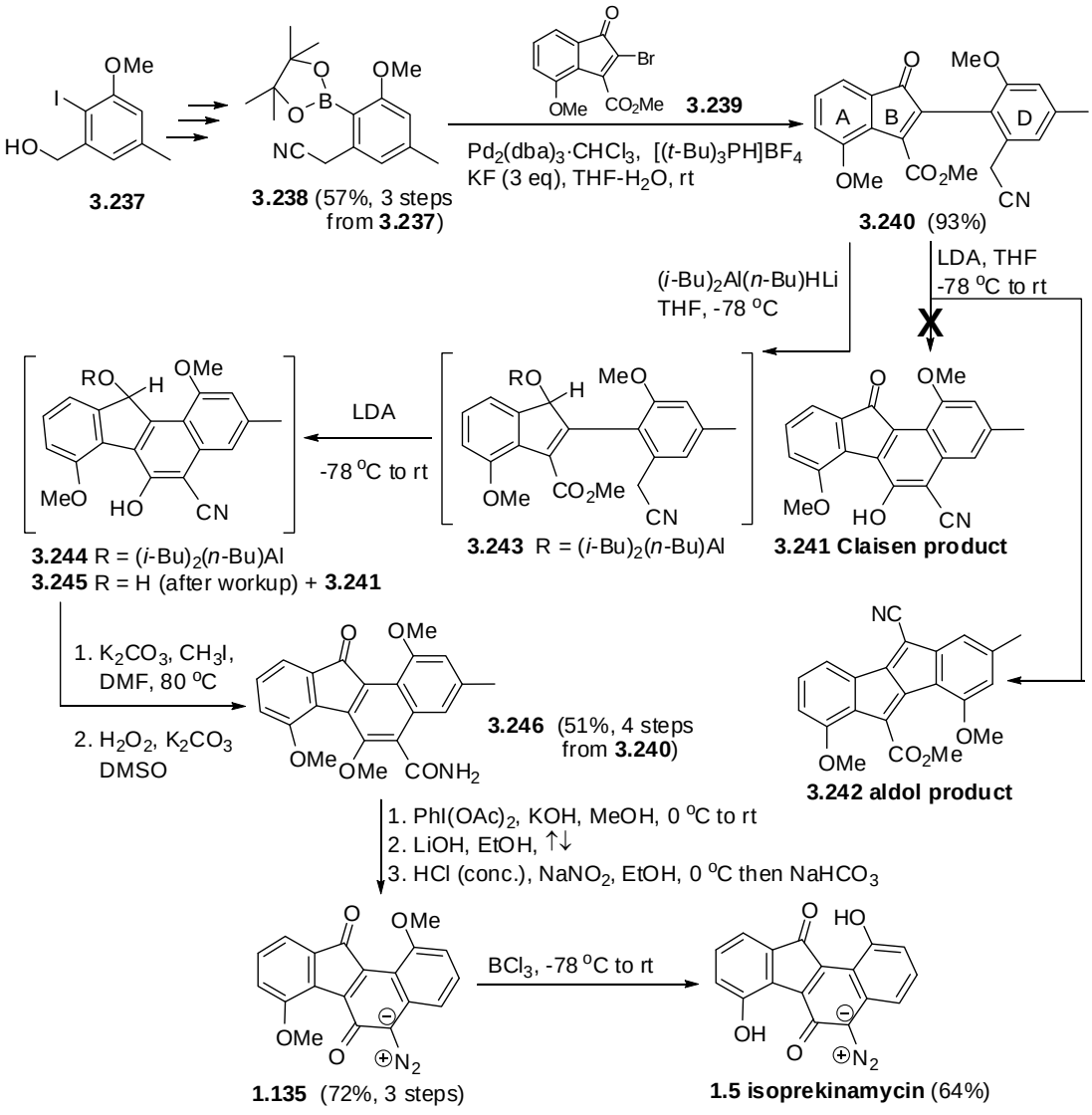

Scheme 3-36. Total synthesis of isoprekinamycin (**1.5**).

Besides the successful and first total synthesis of isoprekinamycin (**1.5**) by the Dmitrienko lab in 2007, the only other synthetic work towards the natural benzo[*a*]fluorene structures in the literature was reported recently (2008) by Danishefsky and co-worker with their total synthesis of fluostatin C (**1.20c**) and E (**1.20e**).[162] The reported synthesis was rather complicated and of less value to be applied as a general method for the synthesis of diazobenzo[*b*]fluorene analogues of kinamycin, when compared with the above two synthetic strategies developed by the Dmitrienko group, but the manuscript showed some interesting chemistry yet details will not be introduced here.

3.3 Conclusion

In summary, an efficient method has been developed for the synthesis of a tetraphene derivative 6-hydroxy-8-methoxy-3-methyl-7,12-dioxo-7,12-dihydrotetraphen-4-yl methanesulfonate (**3.131**), a 6-6-6-6 ring system that is to serve as a substrate for the ring-D oxygenation chemistry that is described in Chapter 2. The method provides **3.131** in only three steps with an overall yield of 65% from the two corresponding precursors **3.59** and **3.107**, and each of the latter two intermediate can be easily prepared from commercial starting material in five steps with an overall yield of 35% and 51%, respectively. A strategy for the conversion of **3.131** into kinamycin F (**1.1f**) is described, and the possibility arises that a key *o*-quinodiazide intermediate **3.136** in the process may possess interesting biological activity similar to those of the kinamycins. Actual comparison of the formulated plan to convert **3.131** to kinamycin F (**1.1f**) with total syntheses of kinamycins recently reported by other groups suggests that this approach might be competitive with the reported synthetic procedures by the Porco group,[23] the Kumamoto/Ishikawa group[24] and the Nicolaou group,[16] but may not be as efficient as that reported most recently by the Herzon group.[26]

3.4 Experimental Details

3.4.1 General Information

Materials and Methods. See section 2.5.1.

Characterization Methods. See section 2.5.1. For some of the well documented compounds (mainly the simple AB-ring starting materials) prepared during the synthesis, only NMR but not all (other) spectroscopic identification methods were used, since the NMR data (and comparison with literature values) were judged to be adequate to characterize the compounds and to estimate their purity.

3.4.2 Detailed Experimental Procedures

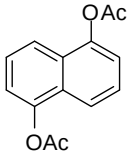

1,5-Diacetoxynapthalene 3.55: Commercial 1,5-dihydroxynaphthalene **3.54** (97%, 24.7719 g, 150 mmol) was mixed with CH_2Cl_2 (400 mL), followed by addition of pyridine (30.6 mL, 375 mmol). The obtained dark black reaction mixture was cooled in an ice bath for 10 min and then acetic anhydride (35.8 mL, 375 mmol) was added dropwise during a period of 10 min. The ice bath was then removed and the mixture was stirred at ambient temperature for 18 hr. The organic solvent was removed under reduced pressure and the remaining sticky black residue was mixed and shaken vigorously with deionized water (400 mL), and then filtered under reduced pressure followed by washing of the solid product (in the filtration funnel) with a large amount of water (300 mL). The obtained brown crystalline solid was dried under vacuum (oil pump) overnight. It was proved to be the diacetate **3.50** (35.9430 g, 147.2 mmol, 98% yield) and judged by NMR to be of good purity despite the discouraging color, since very pure **3.50** looks off white. The color of the "crude" **3.50** can be removed, if desired, by either recrystallization (EtOAc/hexanes) or washing with small amount of

MeOH under (slightly) reduced pressure. However, such treatment is not necessary for the next reaction. ^{1}H NMR (300 MHz, $CDCl_3$): δ 7.78 (d, *J* = 8.4 Hz, 2 H), 7.50 (m, 2H), 7.29 (d, *J* = 7.5 Hz, 1H), 2.47 (s, 6H); ^{13}C NMR (75 MHz, $CDCl_3$) δ 169.2, 146.7, 128.1, 126.0, 119.3, 118.8, 21.0.

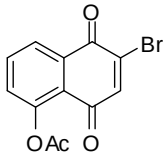

2-Bromo-5-acetoxynaphthoquinone 3.7a: 1,5-Diacetoxynaphthalene **3.55** (12.2227 g, 50 mmol) was dissolved in glacial acetic acid (150 mL) under gentle heating. The warm solution of **3.55** was then added slowly during a period of 5 min to a mixture of commercial NBS (99%, 35.9630 g, 200 mmol), glacial acetic acid (150 mL) and deionized water (200 mL) under stirring. The obtained aqueous mixture was then heated in an oil bath at a controlled temperature in between 65–70 °C for 90 min, during which the reaction flask was equipped with a water condenser to minimize the escape of Br_2 vapour that was generated in situ from the reaction mixture. There are several noteworthy experimental observations. First, the color of the reaction mixture turned from the grey-yellow at the beginning to brown-red after about 20 min of heating. Second, formation of the brown-red Br_2 vapour was physically visible during the reaction, which was further confirmed by a positive chemical test with wet KI-starch paper. Third, the actual temperature of the reaction solution was ca. 15 °C (at the beginning of reaction) to 5 °C (at the end of reaction) lower than the bath temperature (65–70 °C). The oil bath was then removed and the solution was slightly cooled before it was poured into water (1 L), which produced large quantities of yellow precipitate. The precipitate was filtered and washed with water (500 mL) under reduced pressure, and then recrystallized from EtOH[*]. The final product **3.7a** was obtained as a bright orange solid (12.5154 g, 42.4 mmol, 85% yield). ^{1}H NMR (300 MHz,

[*] The recrystallized **3.10** requires a long period of drying (at least overnight) under vaccum (oil pump) to completely remove the residual solvent of EtOH

$CDCl_3$): δ 8.14 (d, *J* = 7.8 Hz, 1H), 7.77 (t, *J* = 7.8 Hz, 1H), 7.42 (d, *J* = 7.8 Hz, 1H), 7.39 (s, 1H), 2.46 (s, 3H); ^{13}C NMR (75 MHz, $CDCl_3$) δ 181.0, 177.5, 169.3, 149.9, 141.5, 138.6, 135.1, 132.6, 130.4, 126.5, 123.2, 21.2.

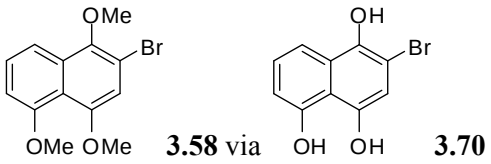

3.58 via **3.70**

2-Bromo-1,4,5-trimethoxynaphthalene 3.58: 2-Bromo-5-acetoxynaphthoquinone **3.7a** (0.5915 g, 2.0 mmol) was mixed with MeOH (ACS grade, 20 mL) and stirred. Then $SnCl_2•2H_2O$ powder (1.8065 g, 8.0 mmol) was added in one portion to the **3.7a**-MeOH suspension followed by dropwise addition of conc. H_2SO_4 (~ 18 M, 1mL, 18 mmol). Initially, the yellow suspension quickly turned brown upon addition of the acid, but it gradually turned again to light yellow within the next few minutes. The reaction mixture was then heated at reflux for 7 hr. The mixture was filtered to remove large amount of solid residue and the filtrate was then diluted with H_2O (50 mL). The aqueous solution was extracted with Et_2O (100 mL x 3), and the organic extract was washed with H_2O (20 mL x 3) and brine (50 mL). The pH of the last aqueous phase (brine) after the wash was ca. 6. The Et_2O solution was then dried over Na_2SO_4 and concentrated, and the remaining grey-yellow solid residue was dried under vacuum (oil pump) for a few hours. This grey-yellow solid was confirmed by ^1H-NMR (in DMSO-d6) to be compound **3.70**, which was pure enough (0.4305 g, 85% yield from **3.58**) to undergo the next methylation step without any further treatment.

^1H NMR (300 MHz, DMSO-d6): δ 10.84 (s, 1H), 10.76 (s, 1H), 9.05 (s, 1H), 7.57 (d, *J* = 8.4 Hz, 1H), 7.32 (m, 1H), 6.80 (d, *J* = 7.5 Hz, 1H), 6.80 (s, 1H). The three one proton signals at δ = 10.84, 10.76 and 9.05 ppm all disappeared after adding D_2O to the NMR sample.

Powdered KOH (85%, 1.1178 g, 16.9 mmol) was mixed with DMSO (4 mL) and stirred for 5 min. Then compound **3.70** (0.3605 g, 1.41 mmol) was added to the above KOH-DMSO suspension in one portion followed by immediate dropwise addition of MeI (99.9%, d = 2.28, 0.53 mL, 8.43 mmol). The mixture was stirred at room temperature under an air atmosphere for 30 min and a slight exothermic reaction was noticed at the beginning during the addition of MeI. The reaction mixture was filtered through a thin layer of celite to remove the remaining KOH powder and the celite was washed with approximately 5 mL of DMSO. The dark black DMSO filtrate was then diluted with H_2O (90 mL) and neutralized by slowly adding conc. H_2SO_4 under stirring, until the pH of the aqueous solution reached about 2–3. The now acidic aqueous solution was extracted with CH_2Cl_2 (100 mL x 4) and the combined organic phase was dried over $MgSO_4$ and concentrated. The remaining solid residue was further purified by flash column chromatography with hexanes:EtOAc (10:1, v/v) as eluent. The trimethylated aryl bromide **3.58** was obtained as a yellow solid (0.2954 g, 70% yield from **3.70**). ^{1}H NMR (300 MHz, $CDCl_3$): δ 7.69 (dd, *J* = 8.4 Hz, 0.9 Hz, 1H), 7.44 (t, *J* = 8.1 Hz, 1H), 6.91 (s, 1H), 6.90 (d, *J* = 8.1 Hz, 1H), 3.97 (s, 3H), 3.94 (s, 3H), 3.92 (s, 3H).

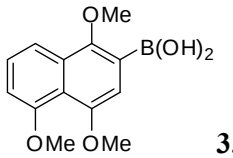

3.59

1,4,5-Trimethoxynaphthalen-2-ylboronic acid 3.59: 2-Bromo-1,4,5-trimethoxynaphthalene **3.58** (0.4717 g, 1.59 mmol) was dissolved in anhydrous THF (8 mL) in a flame-dried flask, and the resultant brown yellow solution was stirred in an acetone/dry ice bath (-78 °C) for 0.5 hr under N_2. Commercial *n*-BuLi in hexane (1.38 M, 1.21 mL, 1.67 mmol) was then added dropwise to the brown yellow solution of **3.54** during a period of 10 min followed by further stirring at -78 °C for 0.5 hr. Commercial $B(OMe)_3$ (98+%, d = 0.915, 0.55 mL, 4.75 mmol) was then added dropwise by syringe to the reaction mixture during a period of 5 min followed by a further stirring at -78 °C for 0.5 hr. The

dry ice bath was removed and the reaction mixture was allowed to warm to room temperature. The mixture was then stirred with 10% HCl (2 mL) for 5 min, diluted with deionized water (20 mL) and extracted with Et_2O (40 mL x 3). The combined organic phase was dried over $MgSO_4$ and concentrated, leading to some brown-yellow solid as the crude product, which was further purified by flash column chromatography on silica gel using CH_2Cl_2 as the eluent. Pure boronic acid **3.59** (0.1956 g, 0.75 mmol, 77% yield based on reacted starting material) was isolated along with the debrominated compound **3.71** (0.1367 g, 0.63 mmol). ^{1}H NMR (300 MHz, $CDCl_3$): δ 7.67 (dd, *J* = 8.1 Hz, 0.9 Hz, 1H), 7.46 (t, *J* = 8.1 Hz, 1H), 7.16 (s, 1H), 6.95 (d, *J* = 7.8 Hz, 1H), 4.00 (s, 3H), 3.99 (s, 3H), 3.95 (s, 3H).

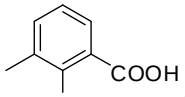

3.97

3-Methyl-2-(methylsulfonyloxy)benzoic acid 3.97: 3-Methylsalicylic acid **3.86** (98%, 15.5282 g, 100 mmol) was dissolved in THF (100 mL). CaO powder (14.0253g, 250 mmol) was added in one portion to the THF solution, followed by dropwise addition of MsCl (99.5+%, d =1.474, 9.4 mL, 120.4 mmol) during a period of 10 min under stirring. Another 50 mL of THF was added to the reaction mixture to help stir the slurry. After about 30 min of mixing all reagents, a significant and spontaneous exothermic reaction[*] took place. Occasional manual stirring with a glass rod became necessary since the slurry of the reaction mixture gradually turned thicker and stickier as the reaction proceeded, during which another 50 mL of THF was added gradually to compensate for the loss of solvent as a result of the exothermic reaction (a condenser was not installed so that manual stirring of the sticky reaction mixture with a glass rod could be performed). After about 10 min of the

[*] The exothermic reaction can be accelerated by the addition of a small amount of water (a few drops) after mixing all reagents. If the reaction is to be carried out at an even larger scale, extra precaution of this exothermic process is needed.

exothermic reaction, the white slurry of reaction mixture turned into some very sticky semi-solid. Another 150 mL of THF was added to the reaction mixture and it was left to stand at room temperature for another 10 hr. The reaction was worked up by slowly adding conc. HCl (45 mL) and the resultant solution that was adjusted to pH ca. 1 was further stirred for 30 min. The aqueous reaction mixture was then extracted with EtOAc (200 mL x 3). The combined organic phase was dried over anhydrous Na_2SO_4 and concentrated to afford the crude mesylate **3.97** that contained a small amount of unreacted **3.86**. The starting material was removed by washing the crude product with a small amount of Et_2O under slightly reduced pressure until the filtrate (Et_2O) looked completely colorless. The pure mesylate **3.97** was obtained as a white solid (21.7298 g, 94.4 mmol, 94.4%). IR (CH_2Cl_2 film) 3028, 1691, 1606, 1586, 1466, 1412, 1337, 1299, 1207, 1190, 1171, 1144, 1088, 976, 871, 770, 700 cm^{-1}; ^1H NMR (300 MHz, $CDCl_3$): δ 7.87 (d, *J* = 7.7 Hz, 1H), 7.50 (d, *J* = 7.6 Hz, 1H), 7.29 (t, *J* = 7.7 Hz, 1H), 3.34 (s, 3 H), 2.47 (s, 3 H); ^{13}C NMR (75 MHz, $CDCl_3$): δ 170.2, 146.2, 136.8, 134.3, 130.1, 126.9, 124.4, 39.4, 17.4; high resolution mass spectrum (EI) *m/z* 230.0244 [M^+; calculated for $C_9H_{10}O_5S$: 230.0249].

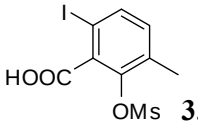

3.100

6-Iodo-3-methyl-2-(methylsulfonyloxy)benzoic acid 3.100: 3-Methyl-2-(methylsulfonyloxy)-benzoic acid **3.97** (11.5149 g, 50 mmol) was dissolved in DMF (ACS grade, 25 mL), followed by the addition of $Pd(OAc)_2$ powder (98%, 1.7181 g, 7.5 mmol, 15% catalyst loading). The resultant brown solution was stirred for 5 min and then NIS powder (98+%, 12.6305 g, 55 mmol) was added in one portion. The reaction mixture was heated up in an oil bath at 120 ºC for 24 hr and then filtered through a thick layer of silica gel in a sintered glass funnel (5cm x 7cm) and washed with ether (4 L). The ether filtrate was concentrated to ca. 700 mL and then washed with H_2O (200 mL x 6). The

organic phase was dried over Na_2SO_4 and concentrated and the residue was recrystallized from THF to afford **3.100** as a white (slightly yellow) solid (12.5274 g, 70%). IR (CH_2Cl_2 film): 3038, 2939, 1712, 1593, 1563, 1455, 1360, 1251, 1190, 1150, 1117, 973, 887, 816, 793, 728 cm^{-1};^{1}H NMR (300 MHz, $CDCl_3$): δ 11.32 (s, 1H), 7.69 (d, *J* = 8.1 Hz, 1H), 7.06 (d, *J* = 8.1 Hz, 1H), 3.29 (s, 3H), 2.39 (s, 3H); ^{13}C NMR (75.5 MHz, $CDCl_3$): δ 170.4, 144.7, 138.2, 134.7, 134.0, 133.5, 88.9, 39.6, 17.6; high resolution mass spectrum (EI) *m/z* 355.9218 [M^+; calculated for $C_9H_9IO_5S$: 355.9215].

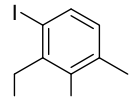

3.105

2-(Hydroxymethyl)-3-iodo-6-methylphenyl methanesulfonate 3.105: A fresh commercial 1M BH_3-THF solution (200 mL, 200 mmol) was added to the solid of 6-iodo-3-methyl-2-(methylsulfonyloxy)benzoic acid **3.100** (7.1662 g, 20.1 mmol) under stirring. The first 30 mL was added slowly as large amounts of gas was generated during the addition of BH_3-THF solution. The remaining 170 mL of BH_3-THF solution was added all at once. The obtained light yellow reaction solution, which turned completely colorless after 12 hr, was then stirred under N_2 at room temperature for 24 hr. The large excess of borane was quenched by slowly adding H_2O (10 mL) to the solution until it no longer bubbled, and the reaction mixture was washed with 10% aqueous Na_2CO_3 solution (200 mL). The THF solution, which separated from the aqueous phase when washed with the basic solution, was kept aside. The remaining aqueous (basic) phase was extracted with Et_2O (200 mL x 2) and the Et_2O phases were combined with the previously separated THF solution. The combined organic phases were washed with H_2O (100 mL) and then loaded onto a layer of silica gel (5cm x 7cm) in a sintered glass funnel. The silica gel was further washed with Et_2O (200 mL), the obtained filtrates were concentrated and the remaining solid was further dried under vacuum (oil pump) for a few hours. The benzyl alcohol **3.105** was obtained as a white solid (5.3196 g, 15.5 mmol, 77%). IR

(CH_2Cl_2 film) 3386, 3022, 2935, 1591, 1564, 1455, 1383, 1362, 1185, 1153, 1114, 1034, 1006, 974, 876, 810, 793 cm^{-1}; ^1H NMR (300 MHz, $CDCl_3$) δ 7.72 (d, *J* = 8.1 Hz, 1 H), 6.96 (d, *J* = 8.1 Hz, 1 H), 4.78 (d, *J* = 6.9 Hz, 2 H), 3.40 (s, 3 H), 2.65 (t, *J* = 6.9 Hz, 1 H), 2.37 (s, 3H); ^{13}C NMR (75 MHz, $CDCl_3$) δ 145.9, 138.6, 136.8, 133.6, 133.2, 98.3, 64.0, 38.8, 17.6; high resolution mass spectrum (EI) *m/z* 341.9429 [M^+; calculated for $C_9H_{11}IO_4S$: 341.9423].

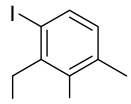

3.106

2-(Bromomethyl)-3-iodo-6-methylphenyl methanesulfonate 3.106: 2-(Hydroxymethyl)-3-iodo-6-methylphenyl methanesulfonate **3.105** (0.2773 g, 0.81 mmol) was dissolved in CH_2Cl_2 (HPLC grade, 5 mL) followed by addition of CBr_4 powder (98%, 1.6746 g, 5 mmol) in one portion. The resultant colorless solution was stirred for 5 min at room temperature under an air atmosphere until all solid dissolved. Then PPh_3 pellet (99%, 1.3268 g, 5 mmol) was added in one portion but slowly to the CH_2Cl_2 solution, which immediately turned to yellow and started to boil (the boiling only lasted for a few seconds and no cooling was necessary). The reaction flask was then loosely capped and the solution was further stirred at ambient temperature for 0.5 hr. The product was isolated from the reaction mixture by loading the yellow CH_2Cl_2 solution onto a thick layer of dry silica gel (6 cm tall x 5 cm wide) in a sintered glass funnel, followed by washing the silica gel with CH_2Cl_2 (distilled, 300 mL) under slightly reduced pressure. The resultant colorless CH_2Cl_2 solution was concentrated and the product was further dried under vacuum (oil pump) for a few more hours. The benzyl bromide **3.106** was obtained as a white solid (0.3275 g, 0.0809 mmol, 99.8% yield). IR (CH_2Cl_2 film) 3022, 2935, 1591, 1560, 1455, 1356, 1264, 1222, 1189, 1158, 1137, 1100 cm^{-1}; ^1H NMR (300 MHz, $CDCl_3$) δ 7.71 (d, *J* = 8.1 Hz, 1 H), 6.94 (d, *J* = 8.1 Hz, 1 H), 4.81 (s, 2 H), 3.43 (s, 3 H), 2.37 (s, 3H);

^{13}C NMR (75 MHz, $CDCl_3$) δ 145.7, 138.7, 134.7, 134.0, 133.6, 98.3, 39.6, 34.1, 17.8; high resolution mass spectrum (EI) *m/z* 403.8584 [M^+; calculated for $C_9H_{10}BrIO_3S$: 403.8579].

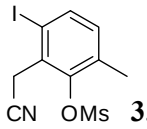

3.107

2-(Cyanomethyl)-3-iodo-6-methylphenyl methanesulfonate 3.107: 2-(Bromomethyl)-3-iodo-6-methylphenyl methanesulfonate **3.106** (0.0406 g, 0.1 mmol) was dissolved in a minimal amount of DMSO (ACS grade, 0.5 mL) and NaCN powder (98.1%, 0.0106 g, 0.21 mmol) was added to the DMSO solution, which immediately turned from very light yellow to dark pink (slightly reddish). The reaction solution was further stirred at room temperature for 15 min although the reaction seemed to be completed within 10 min as indicated by TLC. The DMSO solution was then diluted with H_2O (50 mL) and the resultant white turbid aqueous solution was extracted with Et_2O[*] (50 mL x 2). The combined Et_2O solution was dried over Na_2SO_4 and concentrated, and the remaining white (slightly yellow) solid was further dried under vacuum (oil pump) for a few hours that was proved by NMR to be the pure benzyl cyanide **3.107** (0.0353 g, 0.1 mmol, 100%). IR (CH_2Cl_2 film) 3039, 3030, 2981, 2940, 2249, 1726, 1593, 1565, 1457, 1410, 1351, 1263, 1200, 1185, 1155, 1114 cm^{-1}; ^{1}H NMR (300 MHz, $CDCl_3$) δ 7.73 (d, *J* = 8.1 Hz, 1 H), 7.00 (d, *J* = 8.1 Hz, 1 H), 4.11 (s, 2 H), 3.41 (s, 3 H), 2.38 (s, 3H); ^{13}C NMR (75 MHz, $CDCl_3$) δ 145.3, 138.7, 134.4, 133.5, 128.9, 116.3, 97.4, 39.2, 26.0, 17.6; high resolution mass spectrum (EI) *m/z* 350.9433 [M^+; calculated for $C_{10}H_{10}INO_3S$: 350.9426].

[*] The solubility of **3.107** in Et_2O was found to be quite limited as ~ 35 mg of **3.107** was not able to completely dissolve in 3 mL of Et_2O, but CH_2Cl_2 was found to be a good solvent for **3.107**. Therefore a larger scale of reaction could benefit from using CH_2Cl_2 as the extraction solvent.

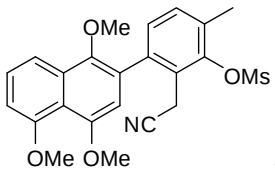

3.109

2-(Cyanomethyl)-6-methyl-3-(1,4,5-trimethoxynaphthalen-2-yl)phenyl methanesulfonate 3.109: A mixture of 1,4,5-trimethoxynaphthalen-2-ylboronic acid **3.59** (0.0655 g, 0.25 mmol), 2-(cyanomethyl)-3-iodo-6-methylphenyl methanesulfonate **3.107** (0.0808 g, 0.23 mmol) and K_3PO_4 (0.1100 g, 0.5 mmol) was dissolved by stepwise addition of toluene (5 mL), EtOH (1.5 mL) and deionized H_2O (0.5 mL). The resultant yellow solution was then deoxygenated through three freeze-thaw cycles under a nitrogen atmosphere. During the last freeze-thaw process and prior to the melting of the frozen mixture, the catalyst $Pd(PPh_3)_4$ (0.0145 g, 0.0125 mmol) was added to the reaction mixture. The reaction mixture was then stirred and heated to reflux in an oil bath under N_2 for 6 hr. The reaction solution was cooled to ambient temperature and diluted with saturated aqueous NH_4Cl solution (10 mL) and H_2O (10 mL). The resultant aqueous mixture was then extracted with EtOAc (40 mL x 3). The light yellow organic phase was dried over Na_2SO_4 and concentrated, and the remaining crude product was purified by flash chromatography with EtOAc:hexanes (3:1, v/v) as the eluent (repeat of the same column purification is necessary to achieve a better separation result with the impurities and by-products), which appears as a light yellow foamy solid (0.0999 g, 0.226 mmol, 98% yield). When working on a larger scale of the Suzuki coupling reaction (1 mmol of each coupling compound), the purification can be greatly simplified by carrying out the following procedure: the crude product was dissolved in a small amount of CH_2Cl_2 and this solution was loaded onto a large amount of dry silica gel (5 cm x 5 cm) in a sintered glass funnel, which was flushed under reduced pressure first with a large amount of CH_2Cl_2 (400 mL, to remove grease and some non-polar by-products) followed by acetone (400 mL). The light yellow acetone fraction was concentrated and the remaining solid was dissolved in a minimal amount of Et_2O. The Et_2O solution of the product

was subjected to the second silica gel "column" (i.e., 5 cm x 5 cm dry silica gel in sintered glass funnel) purification by washing the silica gel with enough amount of Et_2O until the yellow band on the silica gel completely came off. Removal of the solvent Et_2O leads to pure biaryl product **3.109** that is suitable for further reactions. IR (CH_2Cl_2 film) 2936, 2842, 2251, 1597, 1582, 1494, 1459, 1375, 1350, 1266, 1235, 1191, 1153, 1126, 1079, 1059, 1004 cm^{-1}; ^1H NMR (300 MHz, $CDCl_3$) δ 7.77 (d, J = 8.4 Hz, 1 H), 7.47 (m, 1 H), 7.36 (d, *J* = 8.1 Hz, 1 H), 7.36 (d, *J* = 8.1 Hz, 1 H), 7.33 (d, *J* = 7.8 Hz, 1 H), 6.95 (d, *J* = 7.8 Hz, 1 H), 6.65 (s, 1 H), 4.00 (s, 3 H), 3.92–3.96 (m, 4H, $-SO_2CH_3$ overlapped with one half of AB quartet from $ArCH_2$-CN), 3.78 (d, *J* = 17.4 Hz, 1 H), 3.45 (s, 3 H), 2.51 (s, 3H); ^{13}C NMR (75 MHz, $CDCl_3$) δ 157.5, 153.8, 146.5, 146.0, 138.4, 132.8, 131.5, 129.5, 127.4, 127.2, 124.7, 118.4, 117.8, 115.1, 107.9, 107.4, 61.3, 60.4, 56.8, 56.6, 39.0, 18.1, 17.6; high resolution mass spectrum (EI) *m/z* 441.1241 [M^+; calculated for $C_{23}H_{23}NO_6S$: 441.1246].

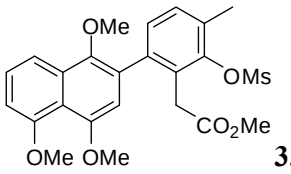

3.120 and

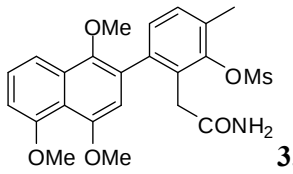

3.121

Methyl 2-(3-methyl-2-(methylsulfonyloxy)-6-(1,4,5-trimethoxynaphthalen-2-yl)phenyl)acetate 3.120: The solid of 2-(cyanomethyl)-6-methyl-3-(1,4,5-trimethoxynaphthalen-2-yl)phenyl methanesulfonate **3.109** (0.0787 g, 0.18 mmol) was quickly mixed with TMSCl (5.0 mL, 38.6 mmol) and MeOH (4.0 mL, 98.8 mmol), and the mixture was then stirred and heated in an oil bath with a condenser attached to the reaction flask. The reaction mixture was heated at reflux for 24 hr and the solution was then cooled to room temperature. Under vigorous stirring, 10% HCl (5 mL) was added dropwise to the reaction mixture, leading to the formation of a large amount of precipitate. Then MeOH (5 mL) was added and the mixture was further stirred for 2 hr. The aqueous reaction mixture was then extracted with CH_2Cl_2 (50 mL x 2) and the organic phases were combined and dried over

anhydrous Na_2SO_4. A dark brown yellow solid was obtained as the crude product upon removal of solvent, which contained mainly the desired methyl ester **3.120** but with small amount of unwanted amide **3.121**. Repeated flash column purification (2 times) with pure EtOAc as eluent successfully separated **3.120** (0.0711 g, 0.15 mmol, 83% yield) from **3.121** (0.0128 g, 0.028 mmol, 16% yield).

For **3.120**: ^{1}H NMR (300 MHz, $CDCl_3$) δ 7.74 (d, *J* = 7.6 Hz, 1H), 7.45 (dd, *J* = 7.8 Hz, 8.2 Hz, 1H), 7.39 (d, *J* = 8.1 Hz, 1H), 7.15 (d, *J* = 8.1 Hz, 1H), 6.91 (s, 1H), 6.64 (d, *J* = 8.2 Hz, 1H), 3.91 (s, 3H), 3.89 (s, 3H), 3.88 (s, 3H), 3.81 (d, *J* = 16.1 Hz, 1H), 3.73 (d, *J* = 15.7 Hz, 1H), 3.67 (s, 3H), 3.51 (s, 3H), 2.47 (s, 3H); ^{13}C NMR (75 MHz, $CDCl_3$) δ 171.6, 157.4, 153.1, 147.1, 146.7, 139.0, 131.8, 131.6, 130.6, 129.3, 128.4, 128.2, 127.1, 118.2, 115.2, 108.7, 107.2, 61.3, 60.4, 56.8, 56.6, 51.8, 39.0, 34.7.

For **3.121**: ^{1}H NMR (300 MHz, $CDCl_3$) δ 7.68 (d, *J* = 8.1 Hz, 1 H), 7.47 (t, *J* = 7.8 Hz, 1 H), 7.27 (m, 2 H), 6.94 (d, *J* = 7.5 Hz, 1 H), 6.64 (s, 1H), 6.19 (br, 1H), 5.27 (br, 1H), 4.00 (s, 3H), 3.92 (s, 3H), 3.56 (s, 3H), 3.46 (s, 3H), 2.52 (s, 3H).

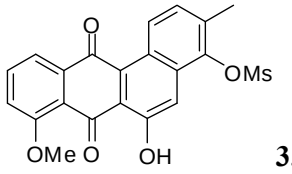

3.131 and

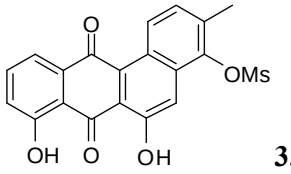

3.130

6-Hydroxy-8-methoxy-3-methyl-7,12-dioxo-7,12-dihydrotetraphen-4-yl methanesulfonate 3.131:

The solid of methyl 2-(3-methyl-2-(methylsulfonyloxy)-6-(1,4,5-trimethoxynaphthalen-2-yl)phenyl)acetate **3.120** (0.0028 g, 0.0059 mmol) was mixed with neat MSA (1.0 mL), and the resultant yellow solution was stirred under N_2 atmosphere in a heated oil bath with the bath temperature carefully controlled between 40–45 °C. The solution turned to dark brown-red (slightly purple) after a few minutes of heating. After 6 hr of reaction, the reaction mixture was cooled and diluted with CH_2Cl_2 (60 mL). Then the dark organic phase was washed with H_2O (10 mL x 3), which

was further stirred with $CaCO_3$ and Na_2SO_4 powder and then filtered. The resultant orange-yellow filtrate was concentrated to afford a dark brown solid residue as the crude product, which was further purified by flash column chromatography with Et_2O as eluent. The desired cyclization product **3.131** was isolated as a dark red solid (0.0020 g, 0.0048 mmol, 81% yield). When the MSA-catalyzed cyclization of **3.120** was carried out in refluxing conc. formic acid for extended time, the isolated major product (~ 44% yield) from this harsher condition was **3.130**, which is an A-ring demethylated **3.131**.

For **3.131**: ^{1}H NMR (300 MHz, $CDCl_3$): δ 9.23 (d, *J* = 7.9 Hz, 1H), 7.94 (dd, *J* = 8.2 Hz, 7.6 Hz, 1H), 7.89 (d, *J* = 8.2 Hz, 1H), 7.84 (s, 1H), 7.35 (d, *J* = 7.6 Hz, 1H), 6.99 (d, *J* = 7.9 Hz, 1H), 4.08 (s, 3H), 3.41 (s, 3H), 2.57 (s, 3H).

For **3.130**: ^{1}H NMR (300 MHz, $CDCl_3$): δ 12.06 (s, 1H), 11.83 (s, 1H), 9.35 (d, *J* = 9.6 Hz, 1H), 7.96 (s, 1H), 7.83 (dd, *J* = 7.8 Hz, 1.2 Hz, 1H), 7.73 (m, 1H), 7.42 (d, *J* = 9 Hz, 1H), (dd, *J* = 8.1 Hz, 0.9 Hz, 1H), 3.43 (s, 3H), 2.58 (s, 3H).

Chapter 4

Chemistry of Kinamycin F: Studies on the Mode-of-Action of the Diazobenzo[*b*]fluorene Type of Antibiotics

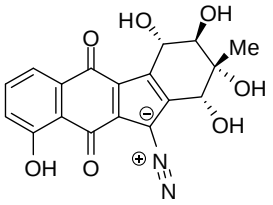

1.1f kinamycin F

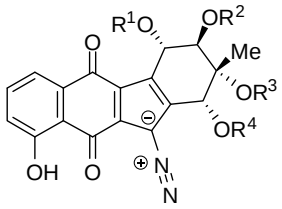

1.1a-d kinamycin A-D

	R^1	R^2	R^3	R^4
1.1a kinamycin A	H	Ac	Ac	Ac
1.1b kinamycin B	H	H	Ac	H
1.1c kinamycin C	Ac	Ac	H	Ac
1.1d kinamycin D	H	Ac	H	Ac

Kinamycin F (**1.1f**), the diazobenzo[*b*]fluorene with a fully deacylated D-ring, received no significant attention prior to this work, even though this substrate seems to possess better antibacterial activity in general (Appendix A) than the other more well-studied kinamycins such as kinamycin A–D (**1.1a**–**d**). During the course of this thesis project, the Dmitrienko group established a collaboration with the Hasinoff group (University of Manitoba) to perform some in-depth biological studies of these rare diazobenzofluorene antibiotics. Kinamycin F (**1.1f**) that had been prepared in the present project from other natural kinamycins, and isoprekinamycin (**1.5**) that had been either isolated or synthesized,[25] as well as some isolated natural kinamycins A, C and D (**1.1a**/**c**/**d**) in the Dmitrienko group were provided to the Hasinoff group. Some very interesting but previously unknown bioactivities of these compounds were discovered.[25,241,244] These results triggered further consideration and significant interest to study the corresponding mechanisms for the kinamycins (this work), as to be discussed in this Chapter 4 and later in Chapter 5. For simplification purposes, the chemical name of "kinamycin X (X = A–F)" will be abbreviated as "kinX (X = A–F)" throughout this chapter.

4.1 Kinamycin F: the Unique Diazobenzo[*b*]fluorene Antibiotic

The kinF (**1.1f**) used in the mechanistic studies was prepared quantitatively from natural kinD (**1.1d**) under Zemplen deacylation conditions (NaOMe/MeOH), as introduced earlier (Scheme 2-12). The latter along with natural kinA (**1.1a**) and kinC (**1.1c**) were isolated from the fermentation broth of *Streptomyces murayamanesis* by V. Goodfellow and Dr. O. Adidayo in this laboratory. Collaborative in vitro biological studies in the Hasinoff laboratory on these natural diazobenzo[*b*]fluorene type kinamycins led to a few novel discoveries, which can be summarized as follows.[241,244]

First, both kinA (**1.1a**) and kinC (**1.1c**) potently inhibited cancer cell growth and the latter species could induce a rapid apoptotic response in human Leukemia K562 cells.[244] Second, kinA (**1.1a**) displayed an unusual and delayed G_1/S cell cycle block in synchronized Chinese hamster ovary (CHO) cells only upon entry to a second cell cycle, which might be due to a slow deacetylation of kinA (**1.1a**) to kinF (**1.1f**) by intracellular esterases.[244] The observed similar IC_{50} of the kinA (**1.1a**), kinC (**1.1c**) and kinF (**1.1f**) towards the Leukemia K562 cells (i.e., 0.31, 0.37 and 0.33 μM respectively) is consistent with the suggestion that the completely-deacylated kinF (**1.1f**) might be the real bioactive form of all other natural diazobenzo[*b*]fluorene-type kinamycins, which metabolize to kinF (**1.1f**) prior to performing their biological activities.[244] Third, both kinA (**1.1a**) and kinC (**1.1c**) demonstrated inhibitory activities towards the DNA topoisomerase IIα that contains protein sulfhydryl (-SH) groups. However, such inhibition experienced a substantial reduction when the kinamycins were pre-incubated with a high concentration (> 1 mM) of L-glutathione (GSH, **4.1**). The GSH (**4.1**) is a widely-occurring thiol-containing tripeptide (γ-L-Glu-L-Cys-Gly) that exists intracellularly in various cells at fairly high concentration (typically ~ 5 mM), and protects the cells by scavenging harmful electrophiles (as a nucleophile) and oxidants (as a reductant).[306] This

observation would suggest the very likely participation of the sulfhydryl groups, present in both the DNA topoisomerase IIα and GSH (**4.1**), in the corresponding mechanism of action of the kinamycins.

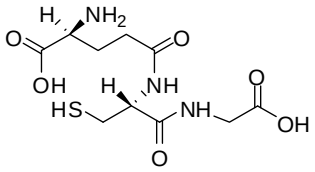

4.1 L-glutathione (GSH)

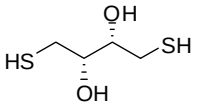

4.2 dithiothreitol (DTT)

Under physiological conditions, reactions between natural kinamycins and GSH (**4.1**) or other similar sulfur-based reductant/nucleophile such as the dithiothreitol (DTT, **4.2**) were observed, as indicated by the corresponding UV-vis spectra.[241] In particular, in the presence of GSH (**4.1**) or DTT (**4.2**), kinF (**1.1f**) was found to be capable of not only breaking the single-strand DNA (in K562 cells) but also cleaving some double-strand DNA (i.e., nicking of *pBR322* plasmid DNA) as well.[241] The involvement of the reductant GSH in the activation of kinF (**1.1f**) leading to significant DNA cleavage was quite important, and this finding was in good agreement with two other studies indicating that other natural diazoparaquinones such as lomaiviticin A (**1.11a**)[52] and kinD (**1.1d**)[307] are able to cleave DNA under similar reducing conditions. However, pure kinF (**1.1f**) itself, even in the absence of a thiol, was found to be still capable of inducing certain amount of nicking of *pBR322* plasmid DNA under physiological conditions, although only if a relatively high concentration of kinF (**1.1f**) was used.[241]

The above observations, particularly the last two, are of significant meaning in regard to kinamycins and related analogues (e.g., lomaiviticins) as potentially useful and novel antitumor antibiotics, since cleavage of double-strand DNAs is generally much more lethal towards the target cells than that of the single-strand DNAs. The only other known classes of effective double-strand DNA scavengers as anticancer drugs in current clinical trials[308,309] are the glycopeptide antibiotic

bleomycins **4.3**[310-312] and the well-known enediynes (e.g., **4.4**–**4.7**).[309,313,314] The latter are characterized by the presence of a nine- or ten-membered carbon ring containing two triple bonds separated by a double bond (i.e., the enediyne moiety), which is the active site for its biological activities and commonly considered as the "warhead" against target cells. Naturally occurring enediynes include three different types of compounds, (i) the chromoproteins[315] such as the neocarzinostatin **4.4**,[316] which is in fact a complex consisting of a 1:1 non-covalently bonded mixture of a very unstable enediynes chromophore (in its neat form) that was recently synthesized,[317] and a carrier polypeptide/apoprotein[318] that stabilizes and delivers the chromophore, (ii) the multisulfide-based calicheamicins **4.5**[319] and esperamicins **4.6**,[320] which are two of the most potent antitumor agents known to human by far, and (iii) the anthracycline-based dynemicins **4.7**.[321,322]

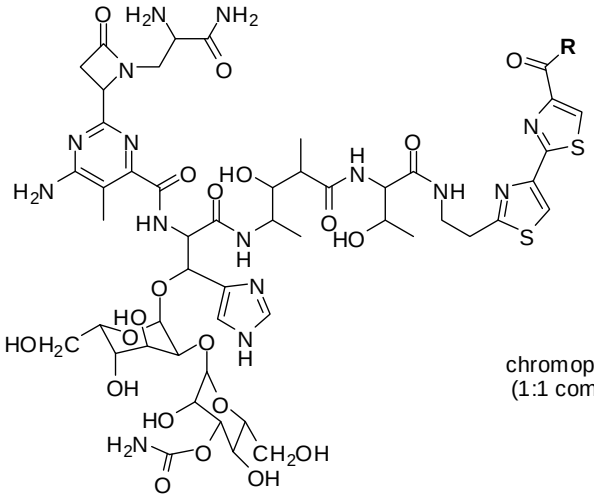

4.3a bleomycin A_2 (R = -NH-$(CH_2)_3$-$S^+(CH_3)_2X^-$)
4.3b bleomycin B_2 (R = -NH-$(CH_2)_4$-NH-C(=NH)-NH_2)

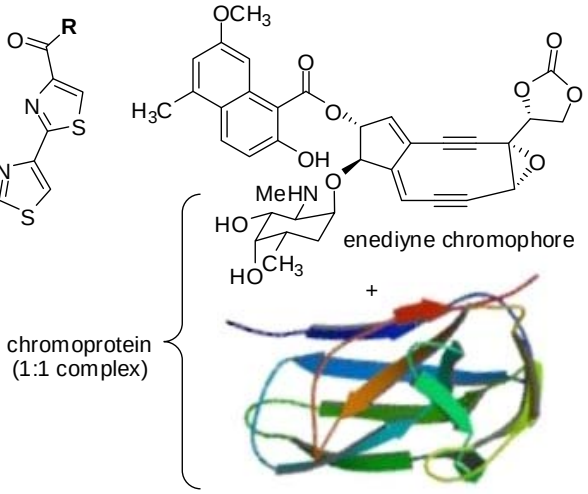

4.4 neocarzinostatin

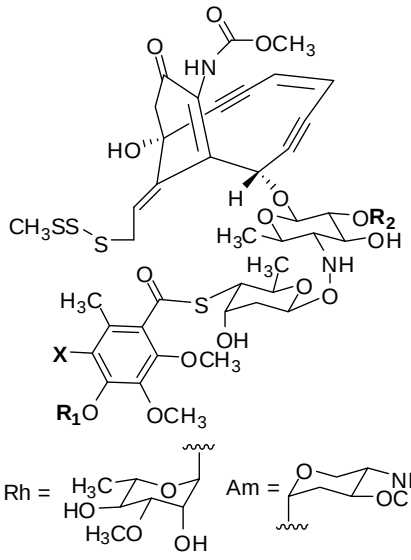

Rh =
Am =

4.5 calicheamicins

Calicheamicin	X	R_1	R_2	R_3
β_1^{Br}	Br	Rh	Am	*i*Pr
γ_1^{Br}	Br	Rh	Am	Et
α_2^{I}	I	H	Am	Et
α_3^{I}	I	Rh	H	-
β_1^{I}	I	Rh	Am	*i*Pr
γ_1^{I}	I	Rh	Am	Et
δ_1^{I}	I	Rh	Am	Me

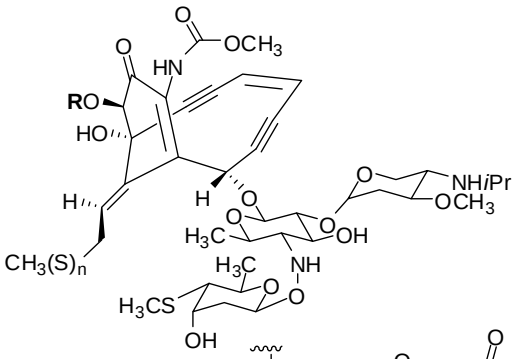

4.6a esperamicin A_1 (n = 3, R = 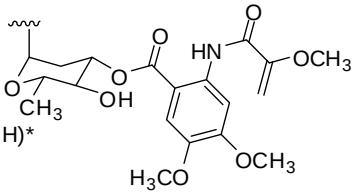)
4.6b esperamicin P (n = 4, R =)
4.6c esperamicin C (n = 3, R = H)*
* hydrolysis product of **4.6a**

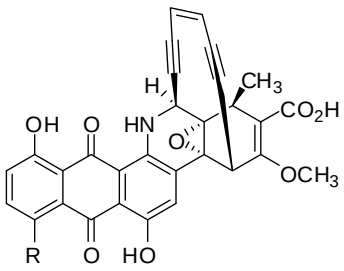

4.7a dynemicin A (R = OH)
4.7b deoxydynemicin A (R = H)

Regardless of the structural variation, all enediynes follow the common mechanism as shown in Scheme 4-1a.[308,309,313-315,323] The enediyne molecule first binds to the minor groove of DNA loosely, followed by a critical activation at a specific triggering site that then allows the originally locked and inactive enediyne warhead to adopt a new and appropriate geometry and consequently aromatize via the Bergman reaction.[324] This leads to the production of a highly active diradical species **4.9**, which is capable of abstracting hydrogen atoms from DNA to initiate a complex reaction sequence and ultimately resulting in DNA cleavage. Binding of enediynes to DNA, however, is performed in different ways depending on the non-enediyne part of the molecule. For example, the carbohydrate portion within **4.5**/**4.6** acts as the binding and delivery mechanism, while the planar naphthoate of **4.4** and the anthraquinone of **4.7** would intercalate into the minor groove of DNA. Interestingly, participation of thiols such as GSH (**4.1**) in the observed potent anticancer activity has been reported for all three types of enediynes, but the role of GSH (**4.1**) in the mode-of-action depends on the enediyne involved (Scheme 4-1b and 4-1c). In the case of the multisulfide-based and chromoprotein type of enediynes, the GSH (**4.1**) acts as a nucleophilic activator (Scheme 4-1b). The GSH (**4.1**), however, serves as an initial reductive activator in the case of dynemicins (Scheme 4-1c), and the resulting hydroquinone moiety within **4.13** undergoes an intramolecular nucleophilic ERO reaction, followed by a further nucleophilic activation by water to offer the required and activated enediyne **4.15**.

Even though the cleavage of DNA by kinF (**1.1f**) in the presence of GSH (**4.1**) or DTT (**4.2**) had been observed, the exact species and detailed mechanism(s) involved in these newly discovered biological activities were not clear. It would be of great interest to examine the possibilities of thiol-activation of kinamycins as discussed above for the enediyne system. Chemical exploration of such reactions was expected to shed some light onto the corresponding mysterious pathway.

(a) General mechanism-of-action of DNA cleavage by enediyne

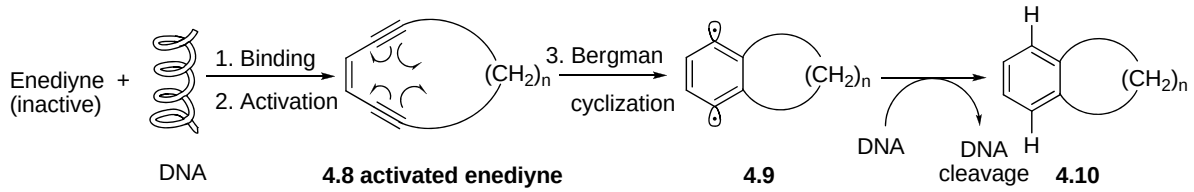

(b) Nucleophilic activation of enediyne (calicheamicins/esperamicins/chromoproteins) by GSH

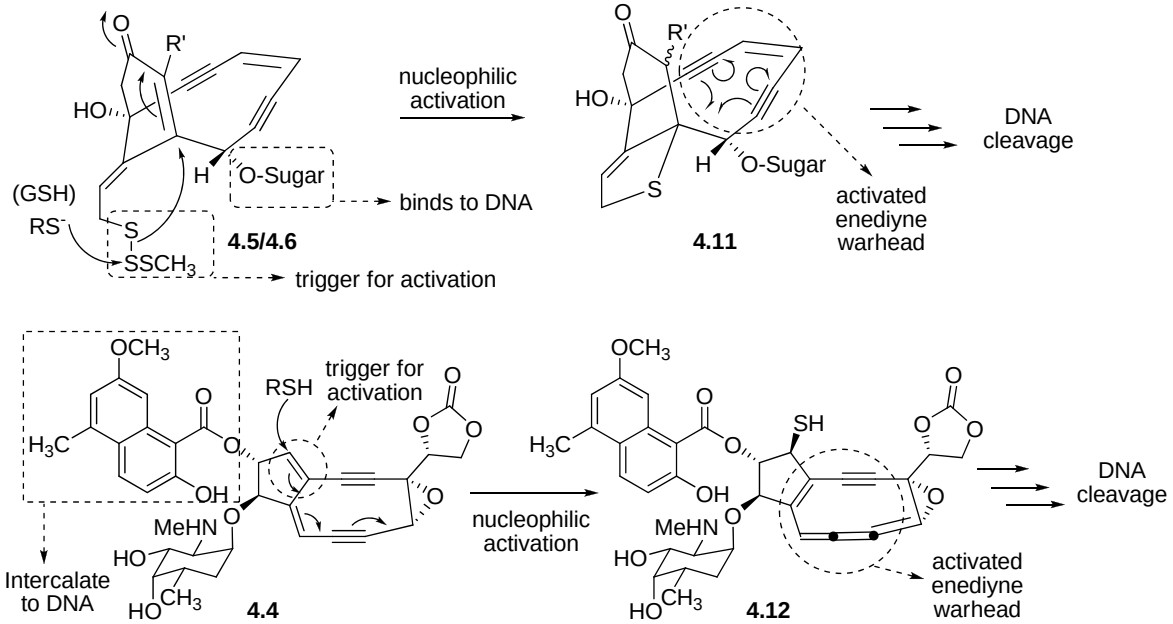

(c) Reductive activation of enediyne (dynemicins) by GSH

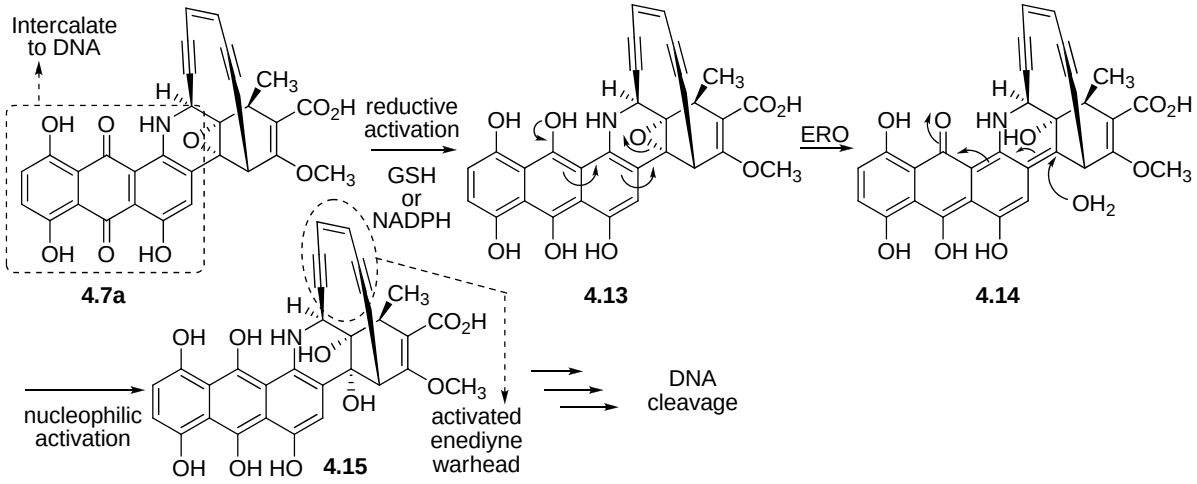

Scheme 4-1. Thiol-activated mechanisms for DNA cleavage by enediynes.

4.2 Mechanistic Study of Kinamycin F by Means of ESI-MS

4.2.1 Reactions of Thiols with Kinamycin F

When considering kinF (**1.1f**) from a structural point of view, the presence of a diazo group (C-ring), a paraquinone (B-ring) and a phenolic functional group (A-ring) could all contribute significantly to its bioactivities. On the other hand, the non-aromatic D-ring of kinF (**1.1f**) with the four hydroxyl groups seems to be of less importance chemically towards the bioactivity at first glance (see section 4.3 for further discussion). The existence of this sugar-like and highly hydrophilic D-ring, however, would at least make the substrate more water-soluble than other kinamycins especially under physiological aqueous conditions, which may in turn enhance the bioactivity. Then the ultimate question regarding the mechanism-of-action of the kinamycins is obvious: the diazo moiety vs the quinone moiety, which one (or maybe the combination of both) is the real player behind the actions?

Reactions of thiol compounds with either quinones[325-327] or diazonium salts[328-331] are known. In the latter case, simple organic (both alkyl and aryl) thiols[328,331] and some biologically significant ones[329,330] such as GSH (**4.1**), cysteine (**4.16**) and its *N*-acetyl derivative **4.17** (*N*-Ac-cys) could react with aromatic diazonium salts to form the corresponding thiolethers or diazosulfides (Scheme 4-2a), depending on the reactivity of the thiols and the stability of the corresponding diazo-thiol adducts. The generally higher reactivity (or instability) of the diazo moiety than that of the quinone had led to the proposal in the Dmitrienko group that, in the case of kinamycins where both functional groups co-exist (kinF (**1.1f**) as an example), the sulfhydryl group of GSH (**4.1**) would probably undergo a preferable nucleophilic addition to the terminal nitrogen of the diazo moiety (Scheme 4-2b). This should generate initially a kinF-GSH adduct **4.18** that can tautomerize in between the semiquinone-diazene form (HR–N=N–S–R') and the corresponding quinone-diazane form (R=N–NH–S–R'). The intermediate **4.18** in its semiquinone-diazene form should be capable of losing N_2 to form a sp^2

carbon-centred radical such as **4.19**, which might lead to attack on and cleavage of DNA. One goal of this mechanistic project was to look for evidence for this type of nucleophilic activation process, and an ideal result would be the successful detection and characterization (or even isolation if possible) of the proposed kinamycin-thiol adducts such as **4.18** by appropriate spectroscopic methods.

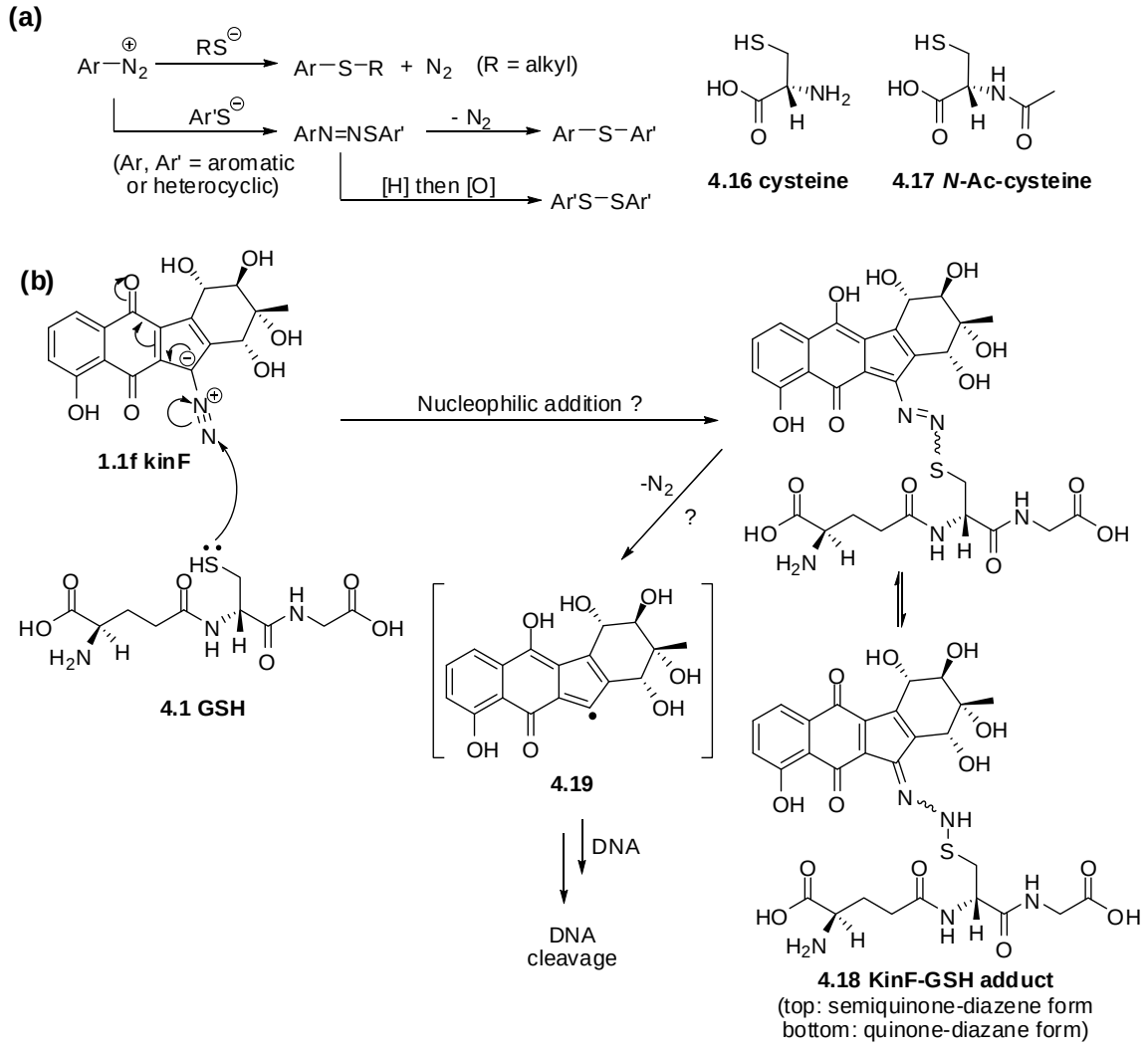

Scheme 4-2. (a) Literature examples of nucleophilic addition of thiols to aromatic diazonium salts; (b) proposed nucleophilic GSH-activation mechanism for DNA cleavage by kinF (**1.1f**).

As the initial attempt to verify the above proposed mechanism of action (Scheme 4-2b), *N*-Ac-cys (**4.17**) was used as a simpler thiol analogue of GSH (**4.1**) to react with kinF (**1.1f**) in MeOD-d4 at room temperature. The corresponding NMR spectra, when monitored as a function of time, indicated that no reaction occurred between these two compounds even after extended time (a few days) of mixing, and the only observed chemical change was the air oxidation of **4.17** to the corresponding disulfide. KinF (**1.1f**) was apparently very stable under such conditions. The failure to observe the expected formation of the kinamycin-thiol adduct suggests that the neutral thiol of **4.17** (pKa($-SH_{\mathbf{4.17}}$) = 9.52;[332] pKa($-CO_2H_{\mathbf{4.17}}$) ~ 5) is not sufficiently nucleophilic to react with the diazo group of kinF (**1.1f**). In the absence of a base or buffer to maintain a high enough (near neutral or weakly basic) pH, generation of the much more nucleophilic sulfide anion (RS^-) would be negligible. This observation also suggested that, to ensure a smooth occurrence of the desired reaction between kinF (**1.1f**) and the thiol such as GSH (**4.1**, pKa ($-SH_{GSH}$) = 8.63[332]/8.66[333]), the later mechanistic studies should be carried out at relatively high pHs.

There are several other significant challenges to be considered prior to any further mechanistic studies. First, the supply of natural kinamycins through bacteria fermentation in the Dmitrienko laboratory was quite limited and only a few milligrams of kinF (**1.1f**) were available at the time. Therefore, the series of mechanistic studies could only be carried out on micro-scale, which would significantly increase the difficulties to identify the products, particularly by NMR that requires substantial amount of material. Second, the studies had to deal with a complex multi-component system, since the reaction would involve at least two substrates (i.e., kinF and a thiol), two solvents (both water and an appropriate organic co-solvent for kinF) and some buffer species (to control a proper pH). The situation could become more complicated due to possible side reactions such as (air) oxidation of the thiol to the disulfide. Even the purest commercial thiols still contain a certain amount of the corresponding disulfides. Last but not least, the choice of the organic co-solvent would be quite

critical, so that both the kinamycin solubility requirement and the compatibility with the analytical methods used for compound characterization had to be satisfied.

It was found earlier in this project (Chapter 2) that, attempts with common EI (electron impact) or CI (chemical ionization) methods to acquire the mass spectra of kinF (**1.1f**) simply failed, and no molecular ion of kinF (**1.1f**) $[kinF]^{+\bullet}$ ($C_{18}H_{14}N_2O_7^{+\bullet}$, *m/z*: 370.0801) could be observed. Instead, mass spectra of kinF (**1.1f**) could be obtained only by +ESI (positive electrospray ionization) mass spectrometry in the presence of either proton or metal ion such as Li^+, with 1:1 (v/v) $MeCN/H_2O$ as the solvent. The only other literature mass data of kinF (**1.1f**) was later reported by Nicolaou using exactly the same (+ESI) ionization method.[16] In fact, +ESI mass was used previously in this project to confirm the prepared kinF (**1.1f**) via the high-resolution mass spectra of $[kinF + Li]^+$ in 1:1 (v/v) $MeCN/H_2O$. The kinF (**1.1f**) molecule binds with the available cations (H^+ or Li^+) and the corresponding ionic species, i.e. $[kinF + H]^+$ ($C_{18}H_{15}N_2O_7$, *m/z*: 371.0879 and $[kinF + Li]^+$ ($C_{18}H_{14}N_2O_7Li^+$, *m/z*: 377.0961), were smoothly detected in the +ESI mass spectra (Figure 4-1a and 4-1b), which further fragmented as observed in the corresponding MSMS spectra (Figure 4-1c and 4-1d). In the meantime, formation of other non-covalent bonded ionic cluster species such as $[kinF + kinF + H]^+$ ($C_{36}H_{29}N_4O_{14}^+$, *m/z*: 741.1680), $[kinF + kinF + Li]^+$ ($C_{36}H_{28}N_4O_{14}Li^+$, *m/z*: 747.1762) and $[kinF + Na]^+$ ($C_{18}H_{14}N_2O_7Na^+$, *m/z*: 393.0699) were also observed (Figure 4-1a and 4-1b). The last ionic species was formed by complexation of kinF (**4.1**) with Na^+ ions, which most likely originate from "environmental contamination" such as the common glassware used in the laboratory.[334]

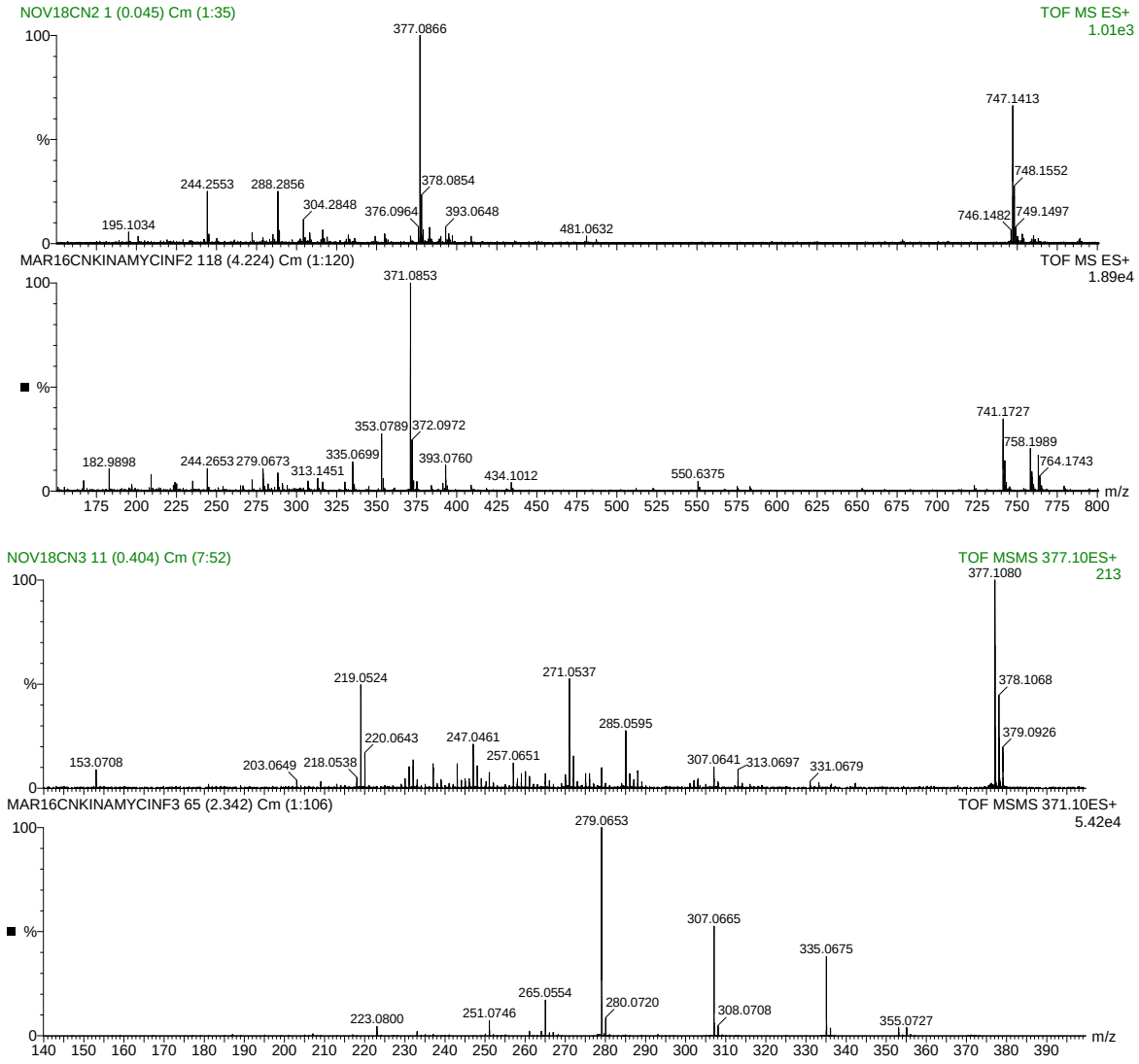

Figure 4-1. +ESI-MS of kinF (**1.1f**) in 1:1 MeCN/H_2O (from top to bottom, a–d): (a) MS of kinF + LiOAc; (b) MS of kinF + 0.2% HCOOH; (c) MSMS of $[kinF + Li]^+$; (d) MSMS of $[kinF + H]^+$.

On the other hand, quick tests of GSH (**4.1**) in 1:1 (v/v) MeCN/H_2O indicated that this thiol also responds very well and similarly with +ESI-MS spectroscopy (Figure 4-2). Ionic species including $[GSH + H]^+$ ($C_{10}H_{18}N_3O_6S^+$, *m/z*: 308.0916), $[GSH + Li]^+$ ($C_{10}H_{17}N_3O_6SLi^+$, *m/z*: 314.0998), $[GSH + Na]^+$ ($C_{10}H_{17}N_3O_6SNa^+$, *m/z*: 330.0736), $[GSH + GSH + H]^+$ ($C_{20}H_{35}N_6O_{12}S_2^+$, *m/z*: 615.1754), $[GSH + GSH + Li]^+$ ($C_{20}H_{34}N_6O_{12}S_2Li^+$, *m/z*: 621.1836) and $[GSH + GSH + Na]^+$ ($C_{20}H_{34}N_6O_{12}S_2Na^+$, *m/z*:

637.1574) were clearly observed. However, as predicted earlier, the presence of the disulfide GSSG (oxidized dimer form of GSH) in the commercial GSH (Sigma®, purity ≥ 98%) used in this study was noticed as well. The GSSG was detected (Figure 4-2) as the corresponding protonated form [GSSG + H]$^+$ ($C_{20}H_{33}N_6O_{12}S_2^+$, *m/z*: 613.1598) and Na^+-complex [GSSG + Na]$^+$ ($C_{20}H_{32}N_6O_{12}S_2Na^+$, *m/z*: 635.1417).

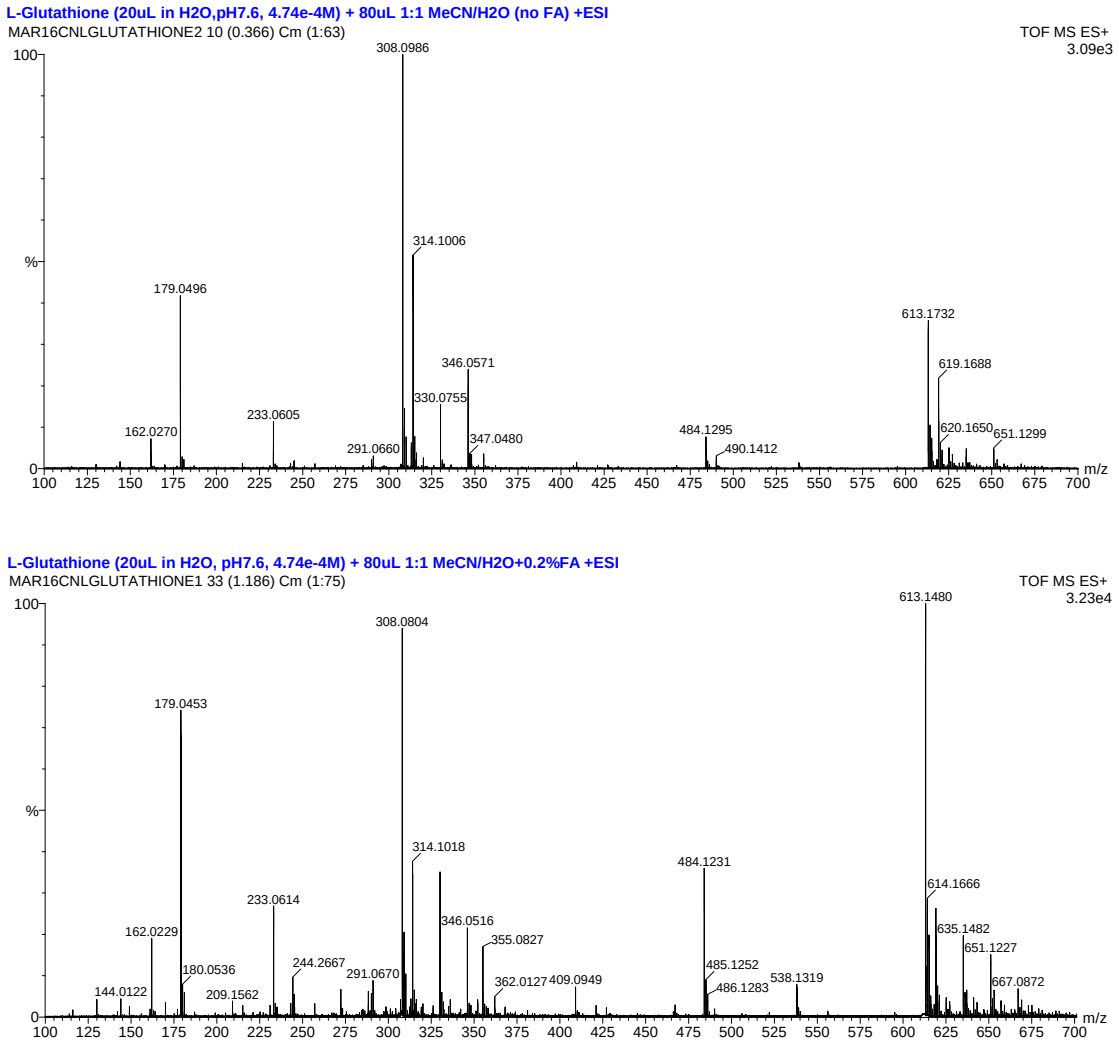

Figure 4-2. +ESI-MS of GSH (**4.1**) in 1:1 (v/v) MeCN/H_2O (pH of the aqueous GSH solution was adjusted to 7.60 with LiOH before adding MeCN): (top) GSH alone; (bottom) GSH + 0.2% HCOOH.

Based on these preliminary results, +ESI-MS was considered a suitable spectroscopic method to characterize the products from the reactions of interest between kinF (**1.1f**) and thiols. The high resolution and ultra sensitivity of mass spectrometry would allow the use of very small quantities of kinF (**1.1f**), and its fast response speed would be particularly beneficial if the produced kinF-thiol adduct is an unstable and short-lived species. To mimic the biological studies of the known GSH-promoted cleavage of DNA by kinF (**1.1f**) that were carried out under physiological conditions (i.e., 37 °C, pH 7.6, 0–400 μM kinF, 5 mM GSH),[241] mechanistic studies on the reactions between kinF (**1.1f**) and thiols were also designed and performed under very similar conditions (Table 4-1). It should be pointed out that the use of bases such as LiOH or NaOH provided not only the required (near) physiological pH for the reaction, but also the metal ions (Li^+ or Na^+) that are essential to the ionization of various species of interest in the +ESI-MS studies, since most of them could bind with the metal ions. On the other hand, acidification of the mass samples with dilute formic acid (HCOOH) also greatly promotes the +ESI mass response due to the significant protonation of the neutral species. Acetonitrile was chosen as the organic co-solvent due to its compatibility with not only ESI-MS but also HPLC (to be used for the separation of kinF-thiol reaction products), as well as the good solubility of kinF (**1.1f**) in this polar solvent. In most cases the kinF-thiol reaction was controlled at either ambient (23 °C) or physiological temperature (37 °C), but a few lower temperatures (i.e., 4 ºC and -10 ºC) were also attempted. To minimize any possible photolytic process of the diazoquinone of kinF (**1.1f**) or the likely kinF-thiol adducts, all reactions were carried out and examined without exposure to light. As the control experiments and for comparison purpose, beside GSH (**4.1**), other thiol and sulfur-containing species such as the *N*-acetyl-cysteine (**4.17**) and GSSG were also employed. The mechanistic studies were carried out by following the general experimental procedure as described in section 4.7.

Table 4-1. Experimental conditions for the reactions between kinF (**1.1f**) and thiols.

Sample No.[a]	[kinF] (mM) : [thiol] (mM)[b]	Base[c]	T (°C)[d]	Reaction Time
KINFGSH0	0.027 : 0.0139 (1.94:1)	LiOH	23	10/20/30/45/60/75/90/300 min
KINFGSH1	0.027 : 0.0139 (1.94:1)	LiOH	-10	24 hr
KINFGSH2	0.027 : 0.0139 (1.94:1)	LiOH	4	24 hr
KINFGSH3	0.027 : 0.0139 (1.94:1)	LiOH	23	24 hr
KINFGSH4	0.027 : 0.0139 (1.94:1)	LiOH	37	24 hr
KINFGSH5	0.027 : 1.21 (1:44.8)	LiOH	23	50/120/250 min, 50 hr
KINFGSH6	0.0513 : 0.121 (1:2.36)	LiOH	23	10/20/30/60/90 /160 min, 44 hr
KINFGSH7	0.1323 : 0.121 (1.09:1)	LiOH	23	10/90 min, 43 hr
KINFGSH8	0.054 : 0.00968 (5.58:1)	LiOH	23	10 min
KINFGSH9	0.027 : 1.21 (1:44.8)	LiOH	37	53 hr
KINFGSH10	0.027 : 0.02975 (1:1.1)	NaOH	37	12 hr
KINFGSH11	0.027 : 0.119 (1:4.4)	NaOH	37	12 hr
KINFGSH12[e]	0.0675 : 0.0705 (1:1.04)	LiOH	23	-
KINFGSH13	0.135 : 0.141 (1:1.04)	LiOH	23	15 min/2 hr
KINFGSSG1	0.027 : 1.12 (1:41.5)	LiOH	23	70/230 min, 50 hr
KINFGSSG2	0.027 : 1.12 (1:41.5)	LiOH	23	70/230 min, 50 hr
KINFGSSG3	0.027 : 1.12 (1:41.5)	LiOH	37	53 hr
KINFCYS1	0.027 : 0.02975 (1:1.1)	NaOH	37	12 hr
KINFCYS2	0.027 : 0.119 (1:4.4)	NaOH	37	12 hr

a. GSH = L-glutathione (**4.1**), GSSG = oxidized dimer form of GSH (a disulfide), KINF = kinamycin F (**1.1f**), CYS= *N*-acetyl-L-cysteine (**4.17**); b. Concentration refers to the final value of the substrate in the reaction solution (1:1 MeCN/H_2O); c. pHs of the aqueous thiol solutions were adjusted to the physiological value of 7.60 with the base (either LiOH or NaOH as listed) prior to the mixing with the kinF-MeCN solution (see section 4.7 for details); d. ± 1 °C; e. Excess 0.2% HCOOH in MeCN-H_2O (1:1) was added to both substrates individually prior to the mixing, and the mixed sample was directly subjected to the +ESI-MS analysis.

After the quite extensive and systematic +ESI-MS studies of the reaction between kinF (**1.1f**) and the thiols, some interesting results were obtained. They are summarized and interpreted as follows.

(i) Initial attempt (sample KINFGSH0, Table 4-1) was made by mixing kinF (**1.1f**) with GSH (**4.1**) in a ratio of ~ 2:1 in 1:1 (v/v) MeCN/H_2O (pH 7.6), and the reaction was monitored closely by +ESI-MS as a function of time (10–300 min, Figure 4-3). It should be noted that observed mass peaks with *m/z* around or smaller than 300 are of very little value to the mechanistic interpretation, since such peaks, particularly those with high nominal masses (e.g., *m/z* ~ 288.3, 272.3, 244.3), mainly come from the background.

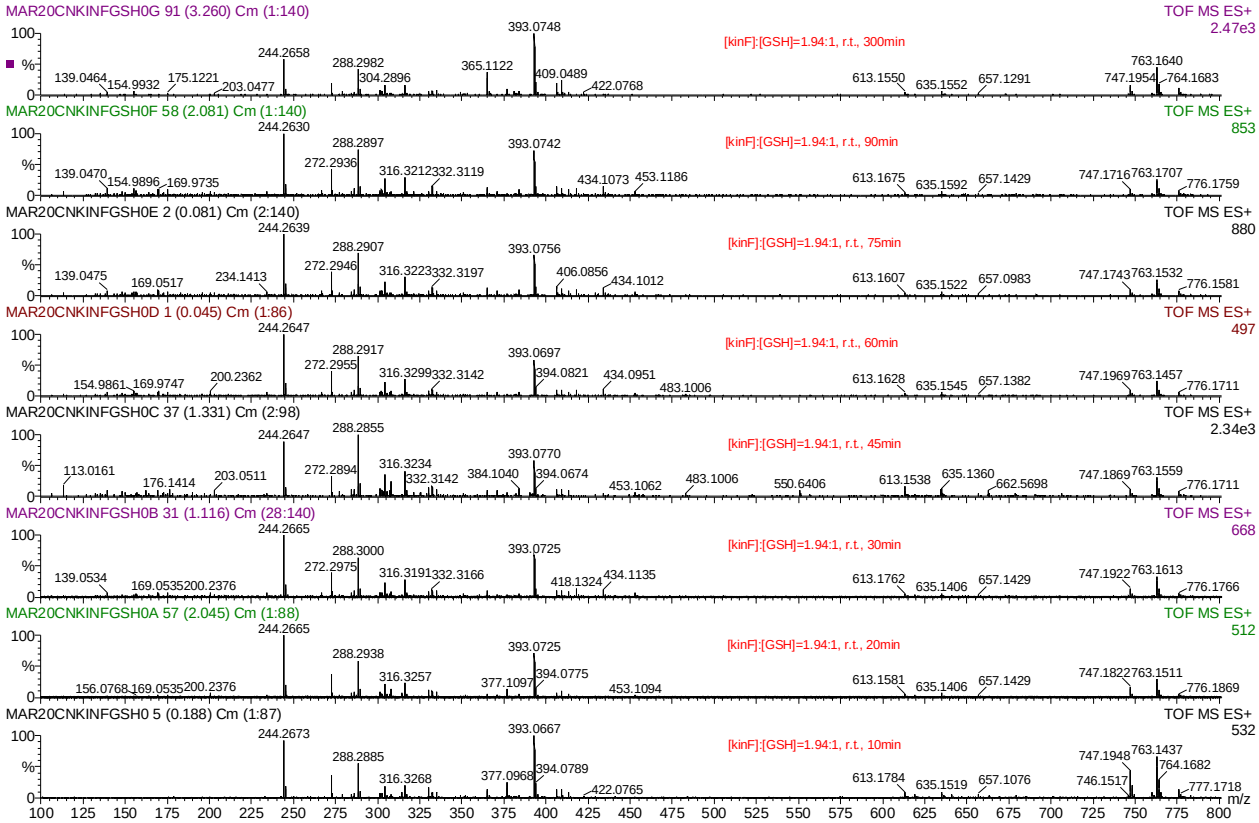

Figure 4-3. Time-resolved (as labeled on each MS spectrum) +ESI-MS spectra of the reaction mixture of kinF (**1.1f**) and GSH (**4.1**) (sample KINFGSH0, Table 4-1).

With no acidification of the reaction sample, no mass peak(s) that might directly correspond to the proposed kinF-GSH adduct **4.18** was observed. For example, a mass peak with *m/z* ~ 678.17 was expected for the protonated kinF-GSH adduct [**4.18** + H]$^+$ and *m/z* ~ 684.18 was expected for the Li$^+$-complex of the kinF-GSH adduct [**4.18**+ Li]$^+$. Consumption of kinF (**1.1f**), however, was clearly indicated by the time-dependent decreasing intensities of several characteristic kinF-based mass peaks (Figure 4-3), e.g. the [kinF + Li]$^+$ with *m/z* ~ 377.1 and [kinF + kinF + Li]$^+$ with *m/z* ~ 747.2. At the same time, these mass spectra also suggested a possible tighter binding of kinF (**1.1f**) with Na$^+$ than Li$^+$, as indicated by the common presence of a fairly strong [kinF + Na]$^+$ mass peaks (*m/z* ~ 393.1) and a slightly weaker [kinF + kinF + Na]$^+$ mass peak (*m/z* ~ 763.2) (Figure 4-3, all spectra), since only a trace amount of environmental Na$^+$ was available in this case while Li$^+$ was present in much larger excess. In the presence of excess kinF (**1.1f**), the thiol (GSH) was found to react with the diazobenzo[*b*]fluorene completely and very quickly (< 10 min), since no mass peak that corresponds to the [GSH + H]$^+$ ion (*m/z* ~ 308.1) could be detected only 10 min after mixing the two reagents (Figure 4-3, bottom spectrum). As a comparison, this [GSH + H]$^+$ ion (*m/z* ~ 308.1) was clearly observed with GSH (**4.1**) alone in 1:1 (v/v) MeCN/H_2O even at pH 7.6 (Figure 4-2a). The observed disappearing rate of GSH (**4.1**) was also much faster than that of the air-oxidation of this thiol, which normally takes at least hours or even days to occur to a noticeable extent under mild (physiological) conditions in the absence of a catalyst.[335,336] These results would imply not only a fairly rapid reaction occurred between the kinF (**1.1f**) and GSH (**4.1**), but also the formation of an initial product that was rather unstable and reactive. Whether this initial product was the proposed adduct **4.18** or not, however, required further exploration and evidence.

In addition, several reaction samples of kinF (**1.1f**) and GSH (**4.1**) having a ratio of ~ 2:1 were incubated at various temperatures (-10 to 37 °C, sample KINFGSH1–4, Table 4-1) for extended time (i.e., 24 hr). At the end of the reaction, small amounts of these samples were directly subjected to

+ESI-MS analysis, while the remaining mixtures were further treated by HPLC separation (see section 4.7 for experimental details) in the hope that this might lead to the isolation of either the possible initial nucleophilic adduct such as **4.18** or any further products that may be derived from it. Despite the many chromatographic fractions obtained and examined, +ESI-MS led to no meaningful data that could be correlated to the proposed structure of **4.18**. However, regardless of the incubation temperature, direct MS analysis (Figure 4-4) did indicate the complete consumption of the limiting reagent GSH (**4.1**), as suggested by the total absence of the characteristic peak of $[GSH + H]^+$ (*m/z* ~ 308.1). This observation was consistent with the earlier interpretation that a fast reaction between kinF (**1.1f**) and GSH (**4.1**) would lead to an unstable product.

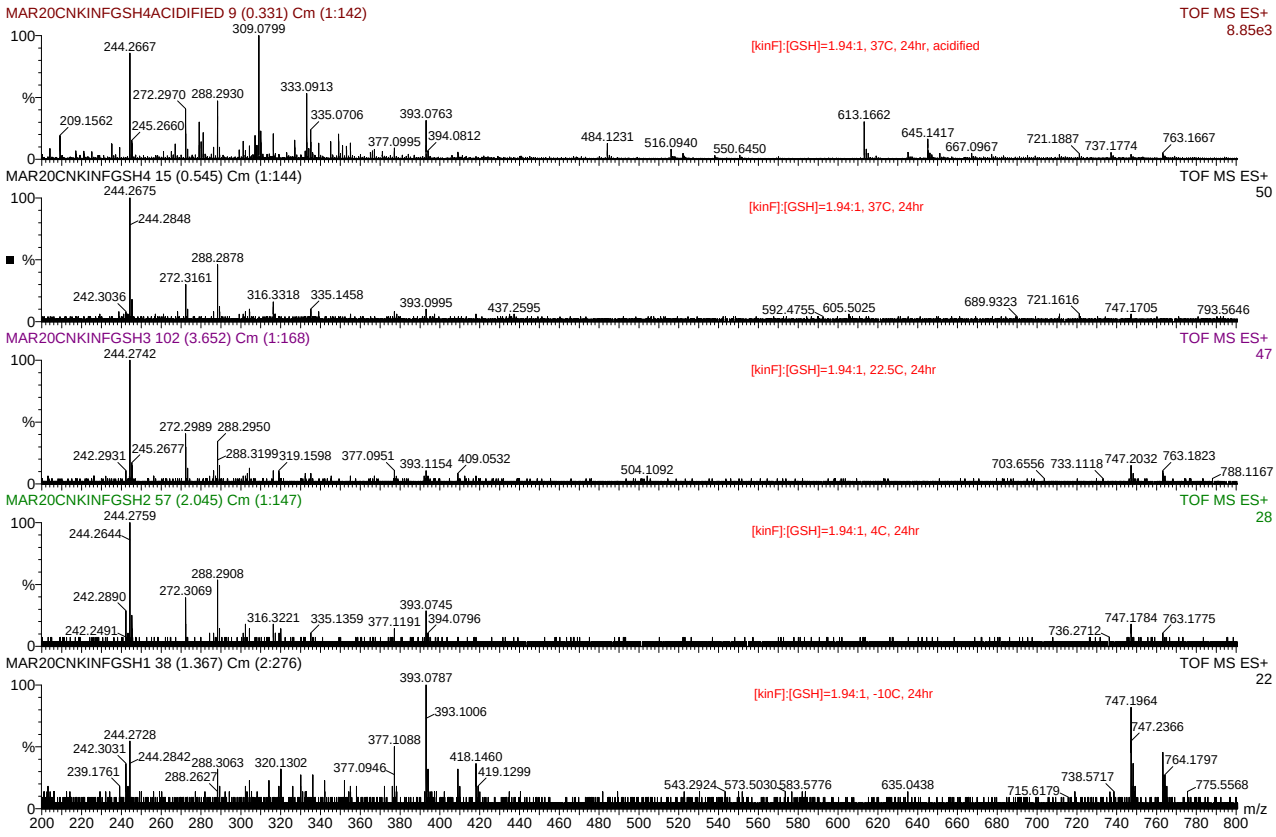

Figure 4-4. +ESI-MS spectra of the reaction mixtures of kinF (**1.1f**) and GSH (**4.1**) incubated for 24 hr at different temperatures (as labeled on each spectrum, samples KINFGSH1–4, Table 4-1).

When GSH (**4.1**) was used in (large) excess relative to kinF (**1.1f**) (sample KINFGSH5, 6, 9 and 11, Table 4-1), detection of GSH- and GSSG-derived ion species dominated the obtained mass spectra, and observation of those kinF-related ions became quite difficult (Figure 4-5). Again no evidence for the proposed kinF-GSH adduct **4.18** was obtained, but quick (< 10 min) and complete consumption of kinF (**1.1f**) under such conditions was still evident. This was indicated by the complete absence of the characteristic peaks of $[kinF + Li]^+$ (*m/z* ~ 377.1) and $[kinF + Na]^+$ (*m/z* ~ 393.1) only 10 min after mixing these two reagents (Figure 4-5, bottom spectrum), which matched very well the earlier observation that the GSH (**4.1**) was used up within 10 min when kinF (**1.1f**) presented in excess (Figure 4-3, bottom spectrum). However, it seemed that when GSH (**4.1**) was used in only slightly excess (e.g., sample KINFGSH6, [kinF]:[GSH] = 1:2.36), a small amount of the cluster ion species of kinF (**1.1f**) such as the $[kinF + kinF + Li]^+$ (*m/z* ~ 747.2) could survive the conditions even after extended reaction time (Figure 4-5, all spectra).

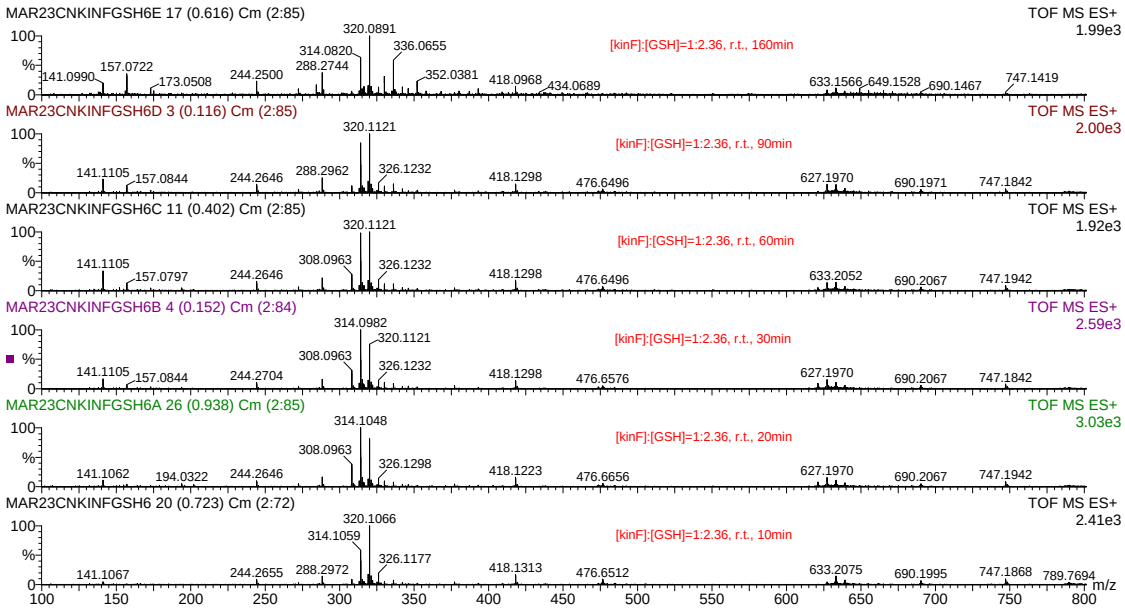

Figure 4-5. Time-resolved (as labeled on each spectrum) +ESI-MS spectra of the reaction mixture of kinF (**1.1f**) and GSH (**4.1**) (sample KINFGSH6, Table 4-1).

Despite the failure to observe the mass species that correspond to the proposed kinF-GSH adduct **4.18**, the above experiments did once again confirm the occurrence of a fast reaction between GSH (**4.1**) and kinF (**1.1f**) under the near physiological conditions.

(ii) Further investigation on the interactions of kinF (**1.1f**) and GSH (**4.1**) in solution eventually led to the observation of two different types of mass species, both of which possessed a *m/z* of ca. 678.18 as expected for the protonated form of the proposed kinF-GSH adduct **4.18**. Despite the identical molecular masses of these two ion species (Note: the observed *m/z* for these two ions did have a small difference of ± 0.01 or less, which was due to the resolution limit and normal fluctuation of the mass detector's response), they showed completely different mass behaviours.

The first type of ion with an observed *m/z* of ca. 678.18 was a stable and non-covalent cluster species (a complex) $[kinF + GSH + H]^+$ ($C_{28}H_{32}N_5O_{13}S$, *m/z*: 678.1717), which consists of one molecule of kinF ($C_{18}H_{14}N_2O_7$, Exact Mass = 370.0801), one molecule of GSH ($C_{10}H_{17}N_3O_6S$, Exact Mass = 307.0838) and one proton (H^+, Exact Mass = 1.0078). This cluster ion species could be easily generated from kinF (**1.1f**) and GSH (**4.1**) when stock solutions of both substrates were diluted individually with excess formic acid prior to the mixing (sample KINFGSH12, Table 4-1). Based on the previous NMR finding that the reaction between kinF (**1.1f**) and thiol **4.17** would not occur under weakly acidic conditions (in MeOD-d4 with no buffer, pKa ($COOH_{\mathbf{4.17}}$) ~ 5), the much stronger formic acid (pKa = 3.75) in large excess would ensure a more complete blockage of reaction between kinF (**1.1f**) and GSH (**4.1**) from occurring. The corresponding +ESI mass spectra of this acidified mixture of kinF (**1.1f**) and GSH (**4.1**) in 1:1 MeCN/H_2O (Figure 4-6, top two spectra, same sample but different mass collision energy) showed a small but real mass peak with a *m/z* of ca. 678.18, which synchronously diminished and eventually disappeared upon gradual dilution (up to 1:10) of the same sample (Figure 4-6, bottom spectrum). On the contrary, other major ion species observed in the same mass spectra were barely affected by the dilution except that their absolute signal intensities did

decrease as expected (Figure 4-6, middle spectrum of regular sample vs bottom spectrum of diluted sample). The observed concentration dependence of this ion species (*m/z* ~ 678.18) was a good indication that it was a loose binding complex formed by the physical interaction of kinF (**1.1f**), GSH (**4.1**) and proton, rather than the protonated form of the expected and (chemically) covalent bonded kinF-GSH adduct **4.18**.

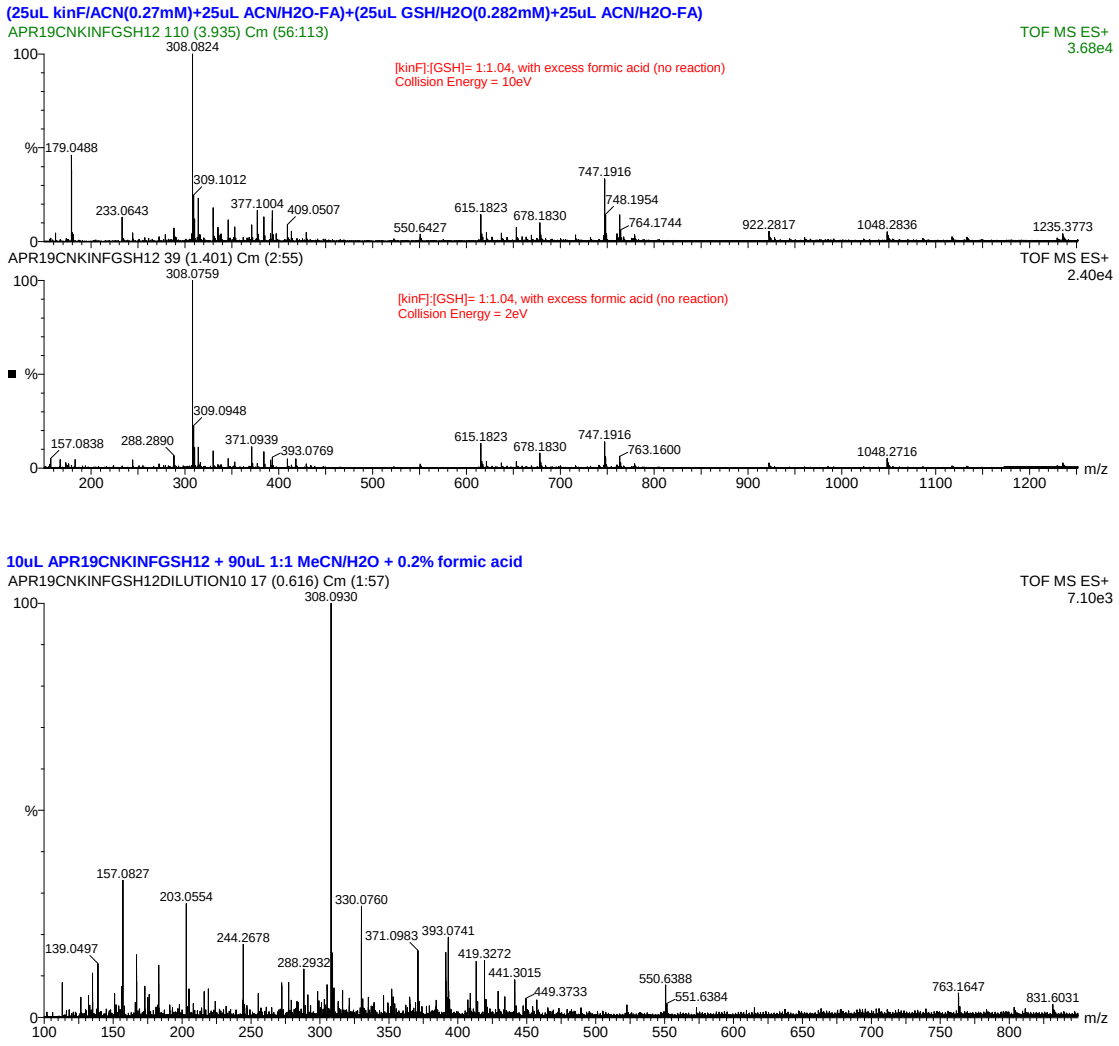

Figure 4-6. +ESI-MS spectra of the cluster ion $[kinF + GSH + H]^+$ with *m/z* ~ 678.18 (sample KINFGSH12, Table 4-1). Top spectrum: collision energy = 10 eV; Middle spectrum: collision energy = 2 eV; Bottom spectrum: 1:10 dilution of the sample with collision energy = 2 eV.

More evidently, the corresponding MSMS spectra of the above mass peak with *m/z* of ca. 678.18 (Figure 4-7) clearly indicated that, upon stepwise increasing the mass collision energy from 2 eV to 35 eV, the mass signal at *m/z* of ca. 678.18 gradually decreased with a concurrent occurrence of a mass peak at *m/z* of ca. 308.1 via the loss of a neutral fragment.

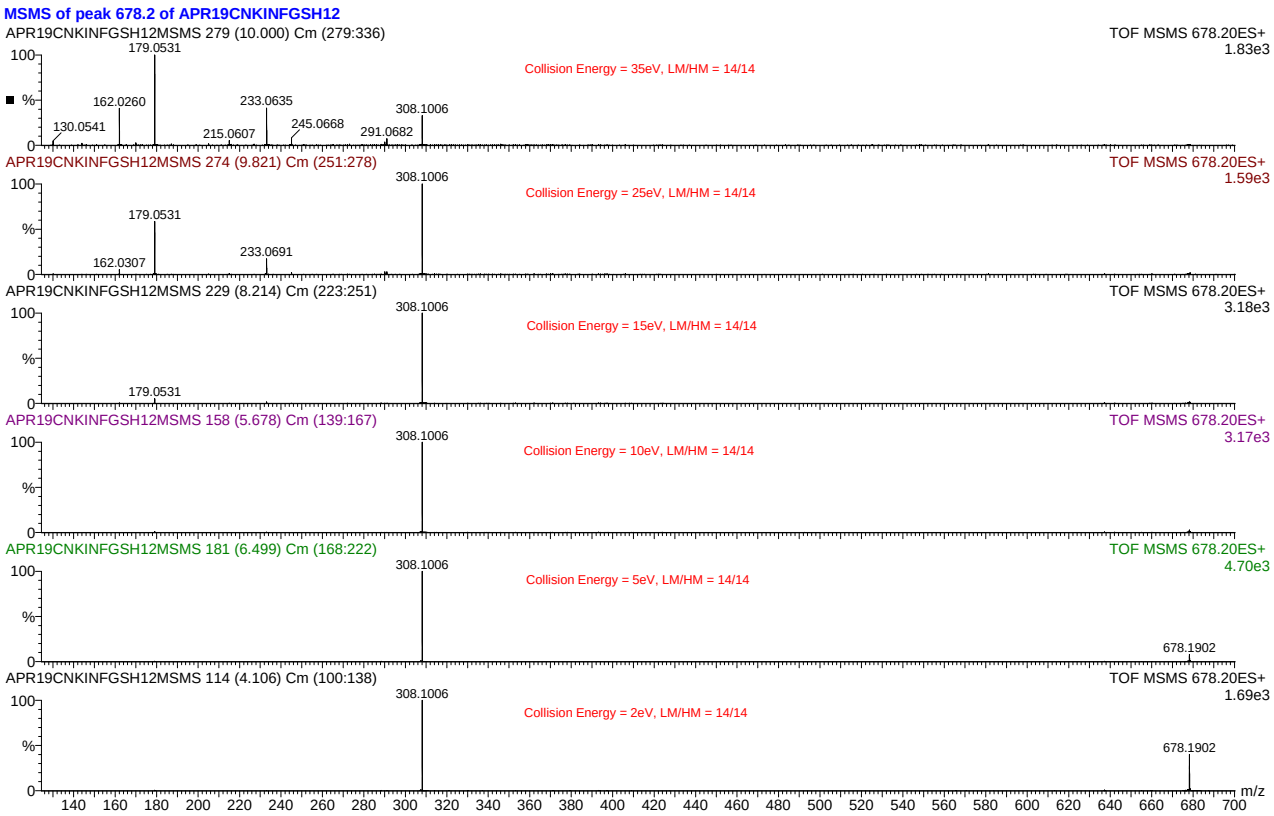

Figure 4-7. +ESI-MSMS of mass peak with *m/z* of ca. 678.18 that corresponds to the cluster ion species of $[kinF + GSH + H]^+$ under different mass collision energies (as labeled on each spectrum).

The only reasonable interpretation for the above observation was that the cluster ion species $[kinF + GSH + H]^+$ (*m/z* ~ 678.18) loses a neutral kinF (**1.1f**) molecule (mass ~ 370.08) and produces the $[GSH + H]^+$ ion **4.20** (*m/z* ~ 308.1). This conclusion was further confirmed by the observed major mass fragment species with *m/z* of ca. 291.07, 233.06, 179.05, 162.03 and 130.05 (Figure 4-7, top spectrum), which not only matched the previously observed mass spectra of $[GSH + H]^+$ **4.20** (Figure

4-2) but also could be well explained from the structural point of view by following the fragmentation pattern as shown in Figure 4-8a. Other observed minor mass fragments with *m/z* of ca. 245.07 and 215.06 under the high collision energy were more likely derived from the neutral kinF (**1.1f**) fragment. The possibility that the above mass peak with *m/z* of ca. 678.18 corresponds to the protonated form of the proposed kinF-GSH adduct [**4.18** + H]$^+$ was further ruled out by making analogy to the known mass behaviour of the etoposide-GSH adduct **4.21** (Figure 4-8b).[337] Under the MALDI/ESI mass conditions, protonated **4.21** could lose various small portion(s) of the molecule, either from the etoposide part (e.g., the carbohydrate) or the GSH part as well as the combination of both possibilities, to produce the corresponding mass ion species. Similarly, some mass fragments with *m/z* values in between 308.1 and 678.18 due to partial fragmentation of either the GSH- or kinF-structure within [**4.18** + H]$^+$ were highly expected. However, no such ion species (308.1 < *m/z* < 678.18) were observed in this case (Figure 4-7). In addition, exactly the same ion species (with *m/z* ~ 678.18 and identical mass behaviour as above) were also found with some other samples studied (i.e., KINFGSH7 and 8), but only when these samples were acidified with 0.2% formic acid in 1:1 MeCN/H_2O shortly (i.e., 10 min) after mixing kinF (**1.1f**) and GSH (**4.1**). Longer incubation time (≥ 90 min) of these samples, however, led to a complete disappearance of the mass peak at *m/z* of ca. 678.18 even if they were acidified at the time of examination, as a result of the complete consumption of the limiting reagent (either kinF or GSH). The observation suggested that, with no doubt, this type of mass species with *m/z* of ca. 678.18 requires the mandatory co-existence of free and available kinF (**1.1f**), GSH (**4.1**) and proton, hence consistent with the proposed cluster ion structure of [kinF + GSH + H]$^+$.

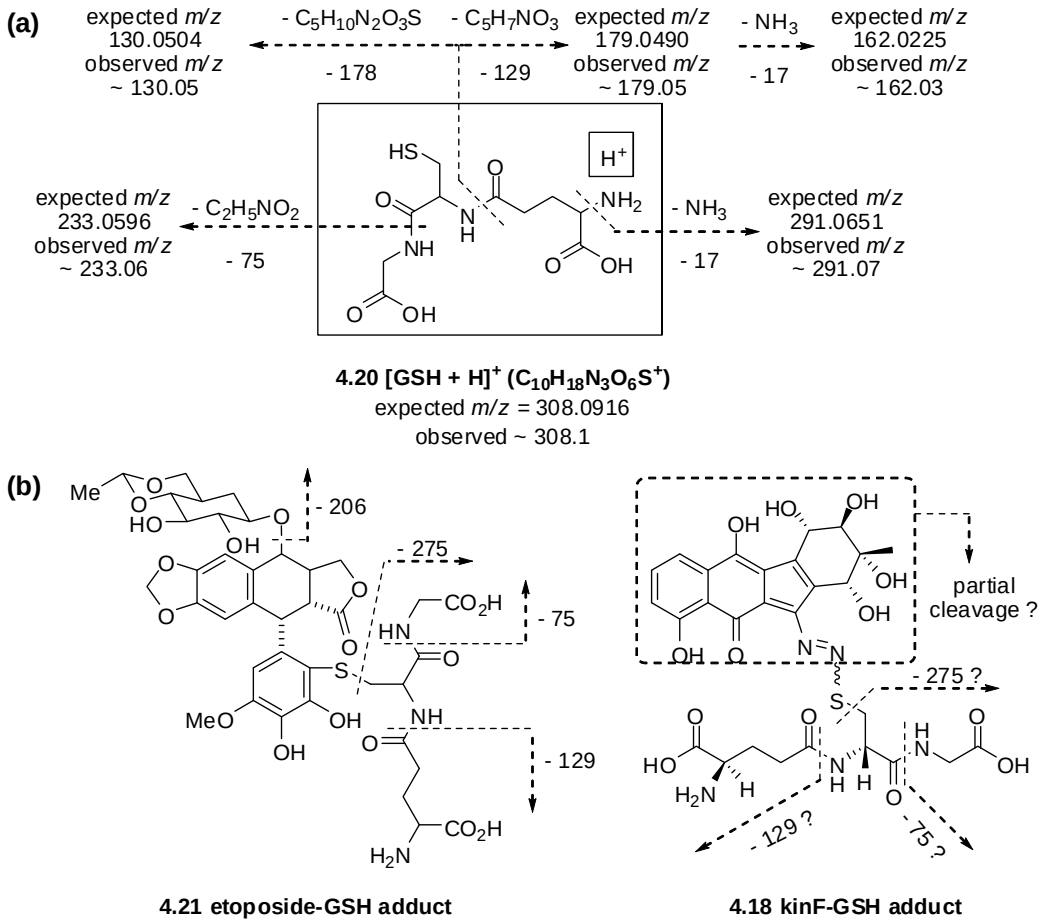

Figure 4-8. Mass fragmentation pattern of (a) $[GSH + H]^+$ **4.20**; (b) protonated etoposide-GSH adduct **4.21** (literature result) and kinF-GSH adduct **4.18** (expected).

Interestingly, another different type of ion also having a *m/z* of ca. 678.18 was observed in the case of sample KINFGSH13 (Table 4-1), but only as a transient and unstable species. This new mass peak (*m/z* ~ 678.18) was detected upon acidification of the sample (KINFGSH13) with formic acid shortly (i.e., 15 min) after mixing the kinF (**1.1f**) and GSH (**4.1**) (Figure 4-9a and 4-9c); however, it completely disappeared when the same reaction sample was acidified and checked again only 2 hr later. This was totally different from the previously observed cluster ion species $[kinF + GSH + H]^+$ with *m/z* ~ 678.18 that could stay steady for at least days under normal conditions. In addition,

attempts by means of -ESI-MS (negative ESI) using aqueous ammonia as the base were also made with this sample after extended time of reaction (55–57 hr). The obtained quite messy and complicated spectra, however, showed no ion species that might be correlated to the corresponding deprotonated form of the proposed kinF-GSH adduct [**4.18** – H]$^-$.

This new and unstable ion species with *m/z* of ca. 678.18 seemed to be quite sensitive to the mass collision energy applied. For example, at 2 eV of collision energy, the mass peak at ca. 678.18 was barely noticeable as it was buried with nearby noises having comparable intensities (Figure 4-9b and 4-9d). The use of higher collision energy of 10 eV, however, clearly showed a weak but real mass signal at ca. 678.18 (Figure 4-9a and 4-9c). This was contrary to the previous mass peak of the cluster ion species [kinF + GSH + H]$^+$ (*m/z* ~ 678.18), which could be easily detected regardless of the collision energy used (Figure 4-6). What really differentiated this new mass signal at 678.18 from the previous one came from the corresponding MSMS spectra under different mass collision energies (Figure 4-10). A series of new mass peaks with *m/z* in between 308.1 and 678.18 (i.e., *m/z* ~ 660.1, 549.1, 420.0 and 339.1), which had been predicted but not observed earlier for the expected mass behaviour of the protonated kinF-GSH adduct [**4.18** + H]$^+$ (Figure 4-8b), started to appear in the obtained mass spectra. Another very interesting discovery was the observation of a concurrent (and even stronger) mass peak with a *m/z* of ca. 677.1 (Figure 4-9 and 4-10, see later text for detailed discussion) along with the expected mass peak at ca. 678.18. In the mean time, protonated **4.1** [GSH + H]$^+$ (*m/z* ~ 308.1) and the corresponding mass fragments (*m/z* ~ 233.1 and 179.1) were also observed in such MS (Figure 4-9) and MSMS (Figure 4-10) spectra. This last observation would suggest that the observed mass peak at *m/z* of ca. 678.18 consisted of two different species. In fact, one is the previously observed cluster ion [kinF + GSH + H]$^+$ (thus it gave the [GSH + H]$^+$ (*m/z* ~ 308.1) and the corresponding daughter fragments, cf. Figure 4-6 and 4-7) while the other one is more likely the protonated form of the proposed kinF-GSH adduct [**4.18** + H]$^+$.

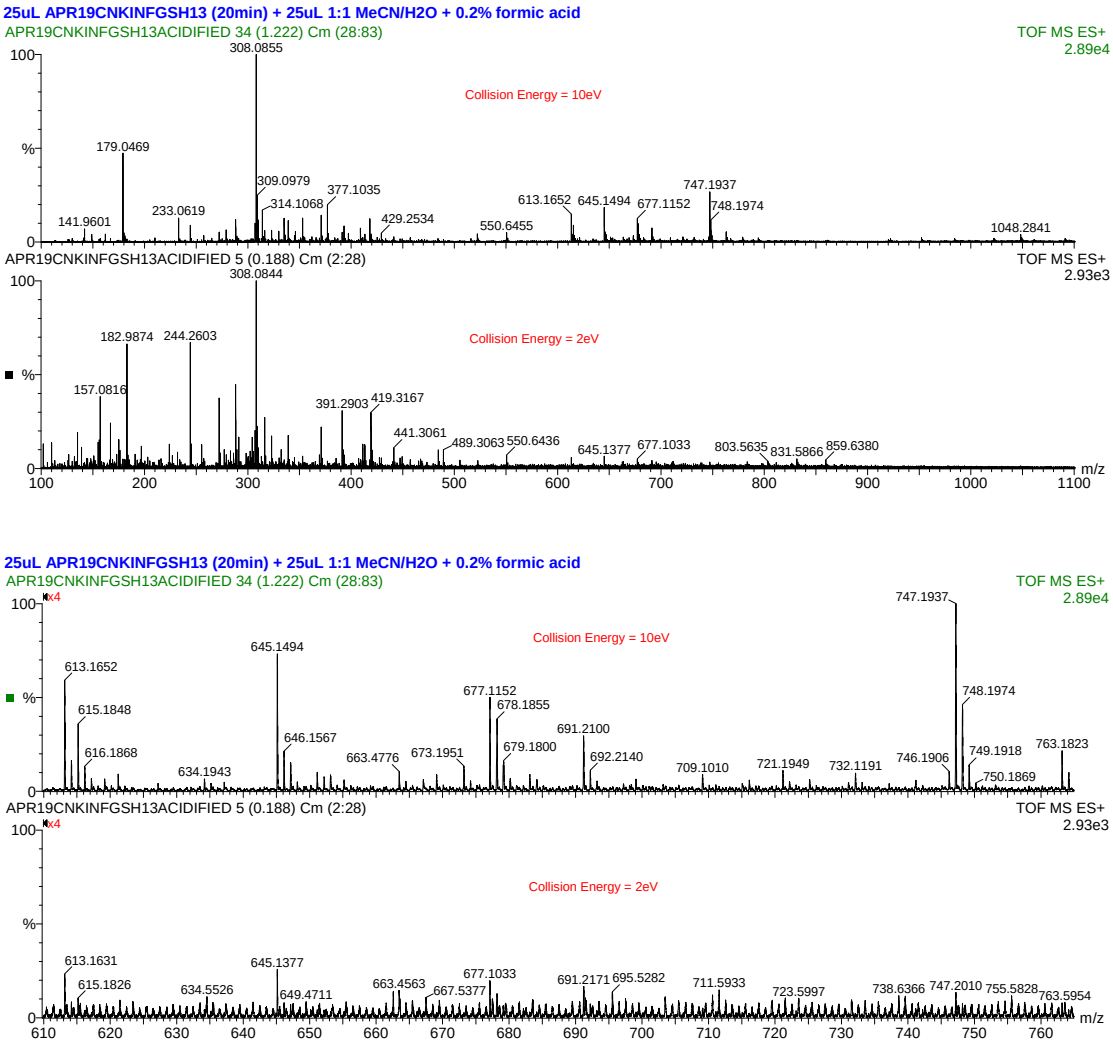

Figure 4-9. +ESI-MS spectra of a new (non-cluster) type of ion species with *m/z* of ca. 678.18 (sample KINFGSH13, Table 4-1, acidified after 20 min of mixing) under different mass collision energies (from top to bottom, a–d): (a) 10 eV; (b) 2 eV; (c) 4x zoom-in of spectrum (a) ; (d) 4x zoom-in of spectrum (b).

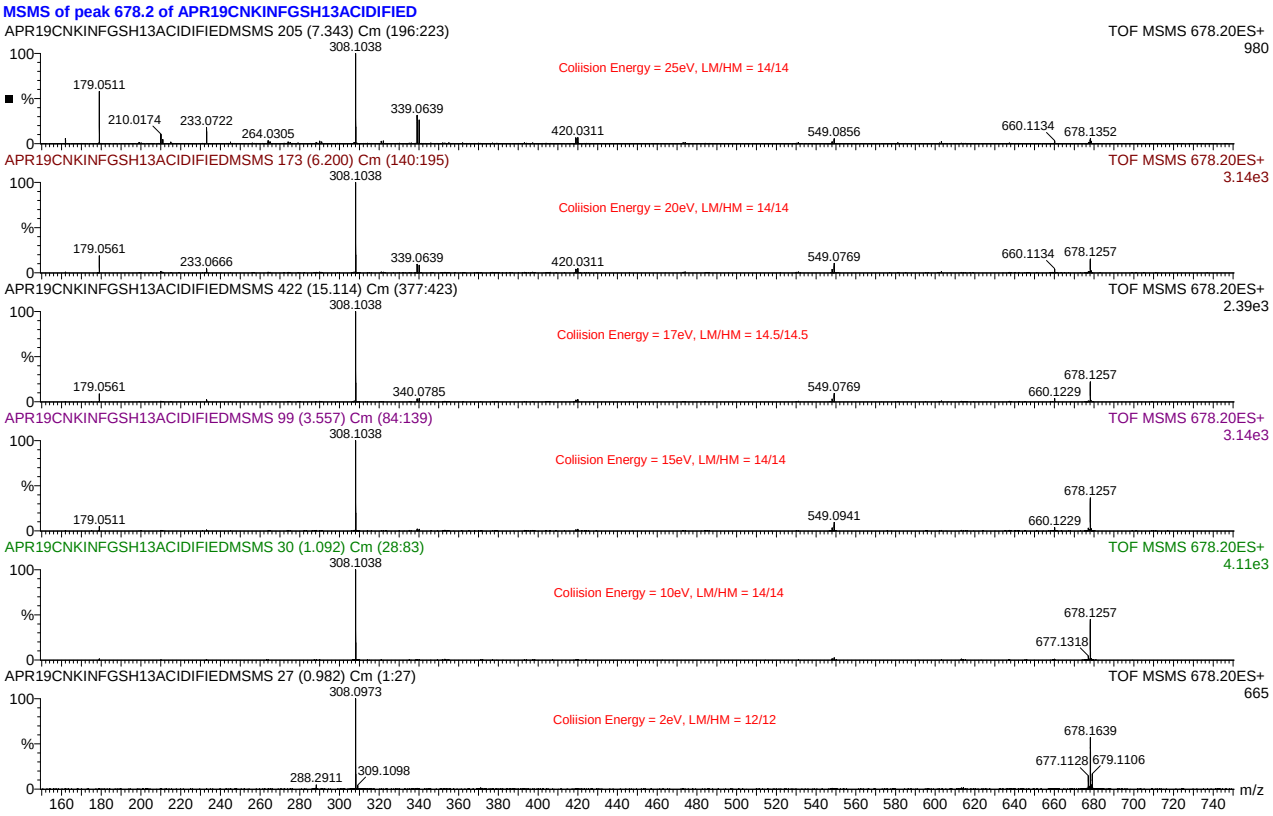

Figure 4-10. +ESI-MSMS of the new (non-cluster) ion species with *m/z* of ca. 678.18 under different mass collision energies (as labeled on each spectrum).

It was further found that the quality of the observed MSMS spectra of this new ion species (*m/z* ~ 678.18) was altered to a noticeable extent (Figure 4-11) by only small variation of the mass analyzer parameters of LM (low mass) and HM (high mass) resolution. The LM/HM are control parameters with calculated arbitrary values, which are used in the mass spectrometer controlling software that could alter the resolution of ions at the low and high mass range of the quadrupole (i.e., the detector of the mass spectrometer used in this study).[338] If the LM/HM resolution are set too low (e.g., 5), then isotope peaks may merge with the main peak (loss of resolving power) despite the increased signal intensity, on the other hand, high values of LM/HM (e.g., 20) would cause the quadrupole to over-resolve but with poor sensitivity.[338] The factory default settings of both LM and HM resolution for the

+ESI-MS instrument were 14, and it seemed that changing these values to 15/16 (Figure 4-11, top two spectra) could afford a slightly better resolution while maintaining a reasonable level of sensitivity (intensity of the signals).

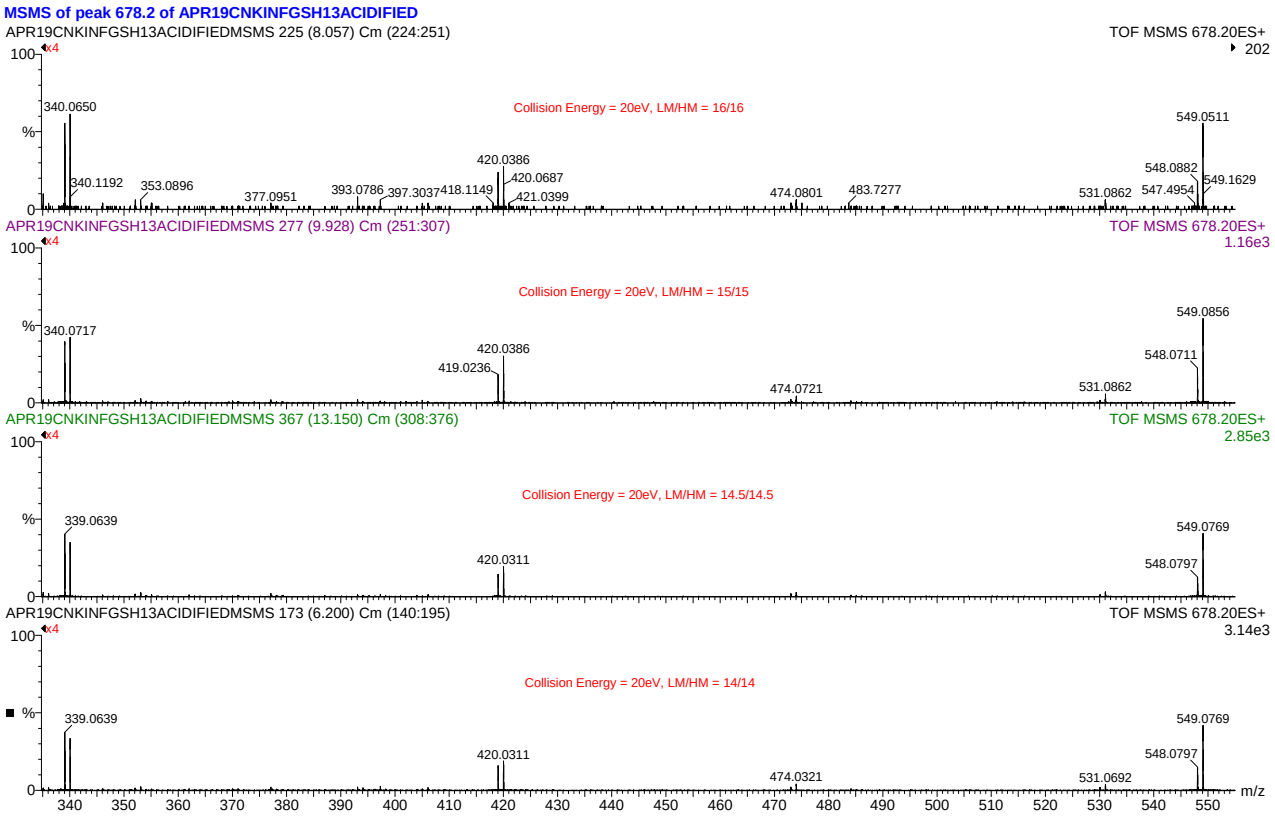

Figure 4-11. Optimization of the +ESI-MSMS spectra (only 330 < *m/z* < 560 were shown) of the new (non-cluster) ion species with *m/z* of ca. 678.18 under fixed collision energy (20 eV) but variable LM/HM (as labeled on each spectrum).

Further MSMS spectra with different mass collision energies and, when necessary, slightly different LH/MH parameters were also acquired with the mass peaks at 549.1 (Figure 4-12) and 339.1 (Figure 4-13), in order to follow the evolution of these important intermediate ion species and to determine the correlations between the observed mass fragments. In the case of the mass peak at 549.1, the MSMS spectra (Figure 4-12) were quite weak and messy, and the mass signals around

549.1 was found to be consist of several mass peaks with very close *m/z* values in fact (Figure 4-12). However, it seemed that at least the fragments with *m/z* of ca. 531.1, 459.0 and 420.0 (Figure 4-12c–4-12e) could be reasonably considered to be derived from the particular ion with *m/z* of ca. 549.1.

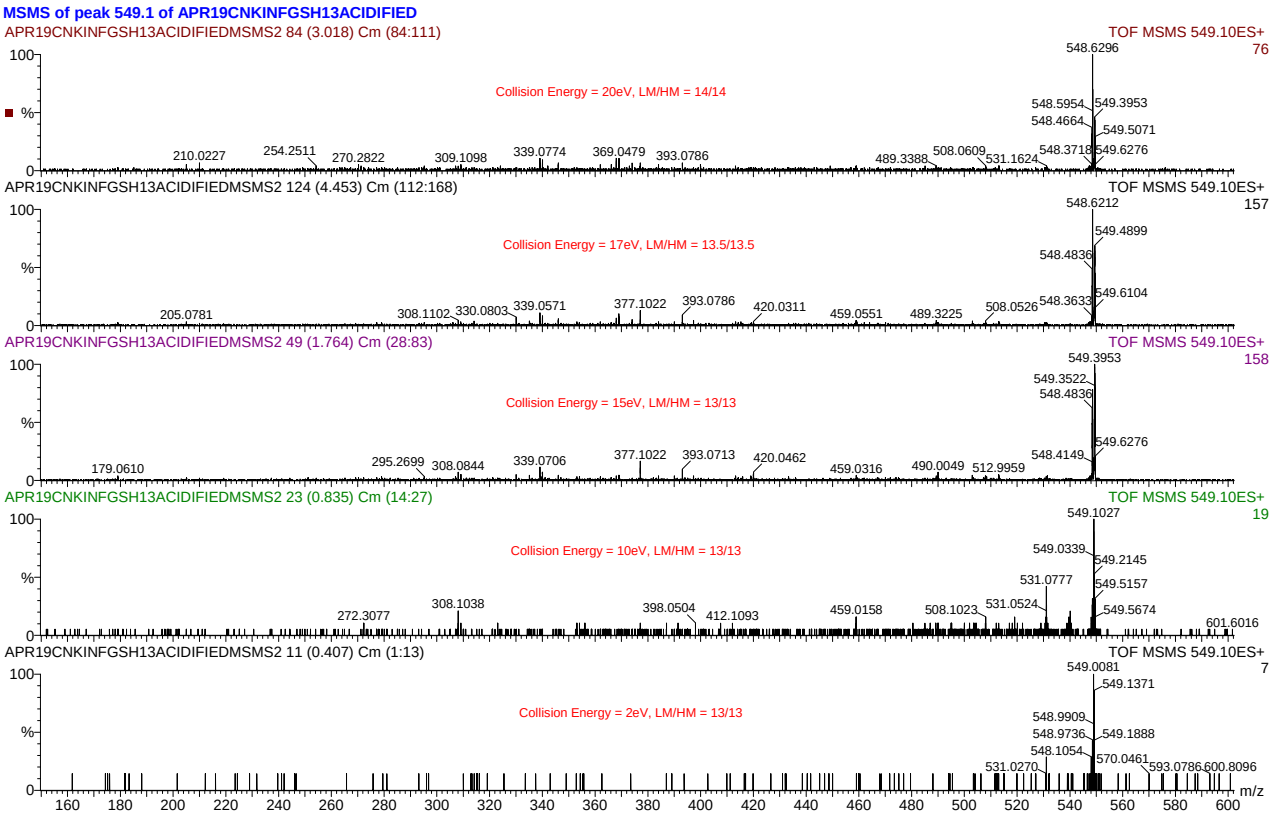

Figure 4-12. +ESI-MSMS spectra of the mass peak with *m/z* of ca. 549.1 under different mass collision energies and settings of LM/HM (as labeled on each spectrum, from top to bottom, a–e).

In the case of mass peak at 339.1, the corresponding MSMS spectra (Figure 4-13) looked much better than the previous case; however, there were still a few other ions with *m/z* values close to 339.1 co-existing with the ion species of interest. The fairly clean MSMS spectra indicated that fragments with *m/z* of ca. 322.0, 264.0, 243.1 and 210.0 were very likely the daughter species originated from the fragmentation of the parent ion with *m/z* of ca. 339.1.

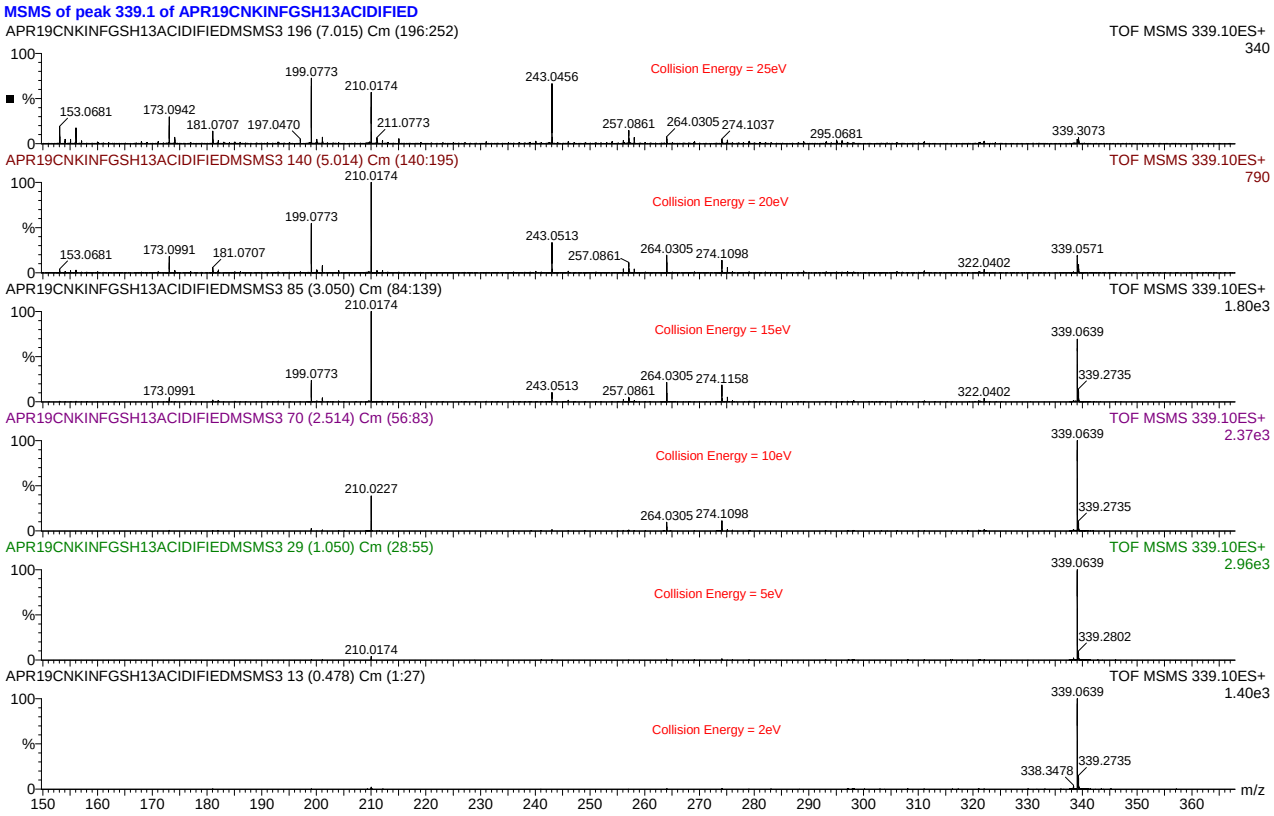

Figure 4-13. +ESI-MSMS spectra of the mass peak with *m/z* of ca. 339.1 under different mass collision energies (as labeled on each spectrum).

A plausible mass fragmentation mechanism (part I: Scheme 4-3; part II: Scheme 4-4) was proposed, in which this new but unstable ion species with *m/z* of ca. 678.18 was assigned to the protonated kinF-GSH adduct [**4.18** + H]$^+$, to reasonablely explain most of the observed mass fragments above (Figure 4-11, 4-12 and 4-13). It should be noted that the stereochemistry of the D-ring of kinF (**1.1f**) was ignored in the proposed mechanism, and structures shown in the square brackets were postulated (but not observed) mass fragmentation intermediates.

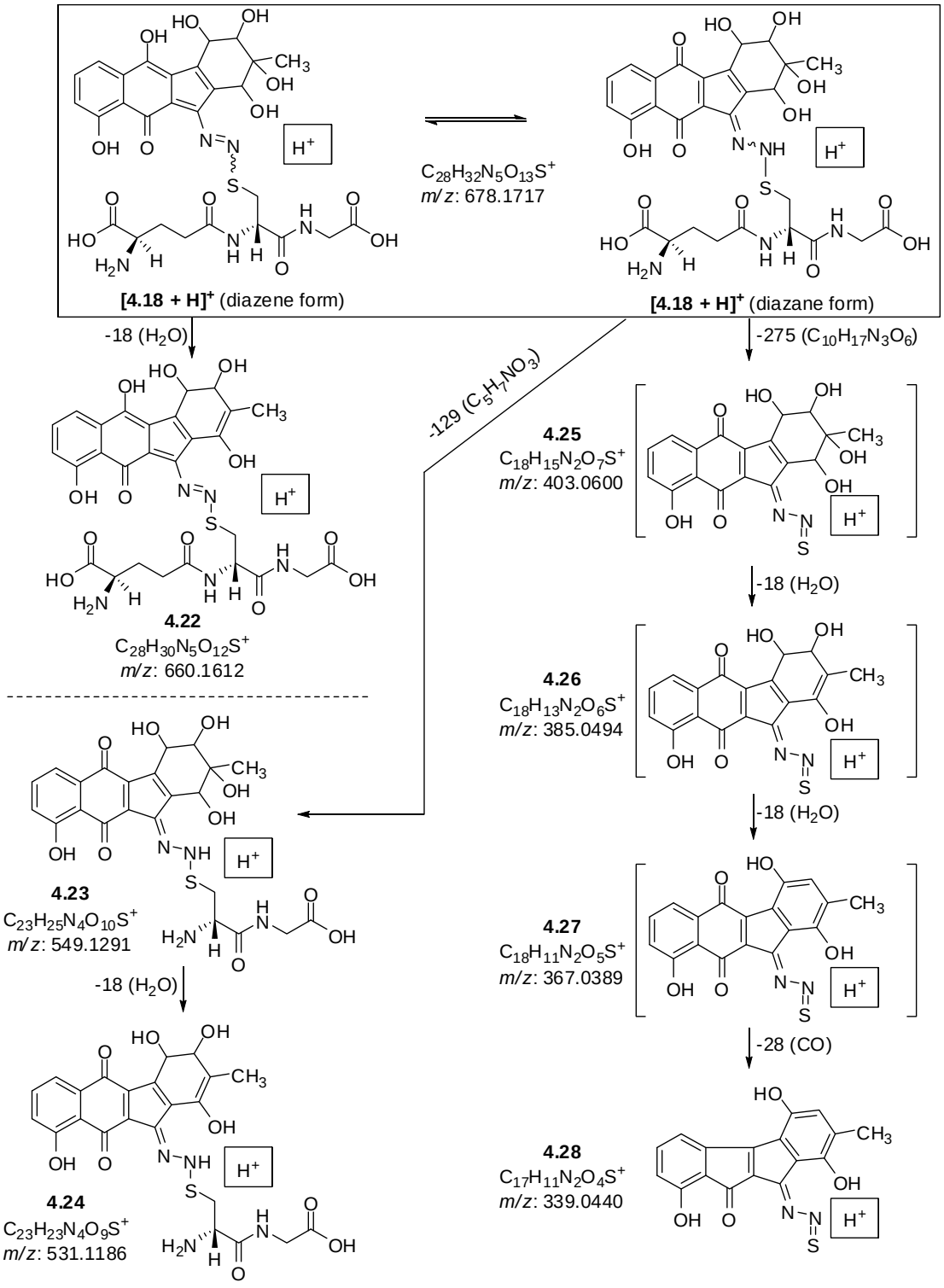

Scheme 4-3. Proposed fragmentation mechanism (part I) for the protonated kinF-GSH adduct **4.18**.

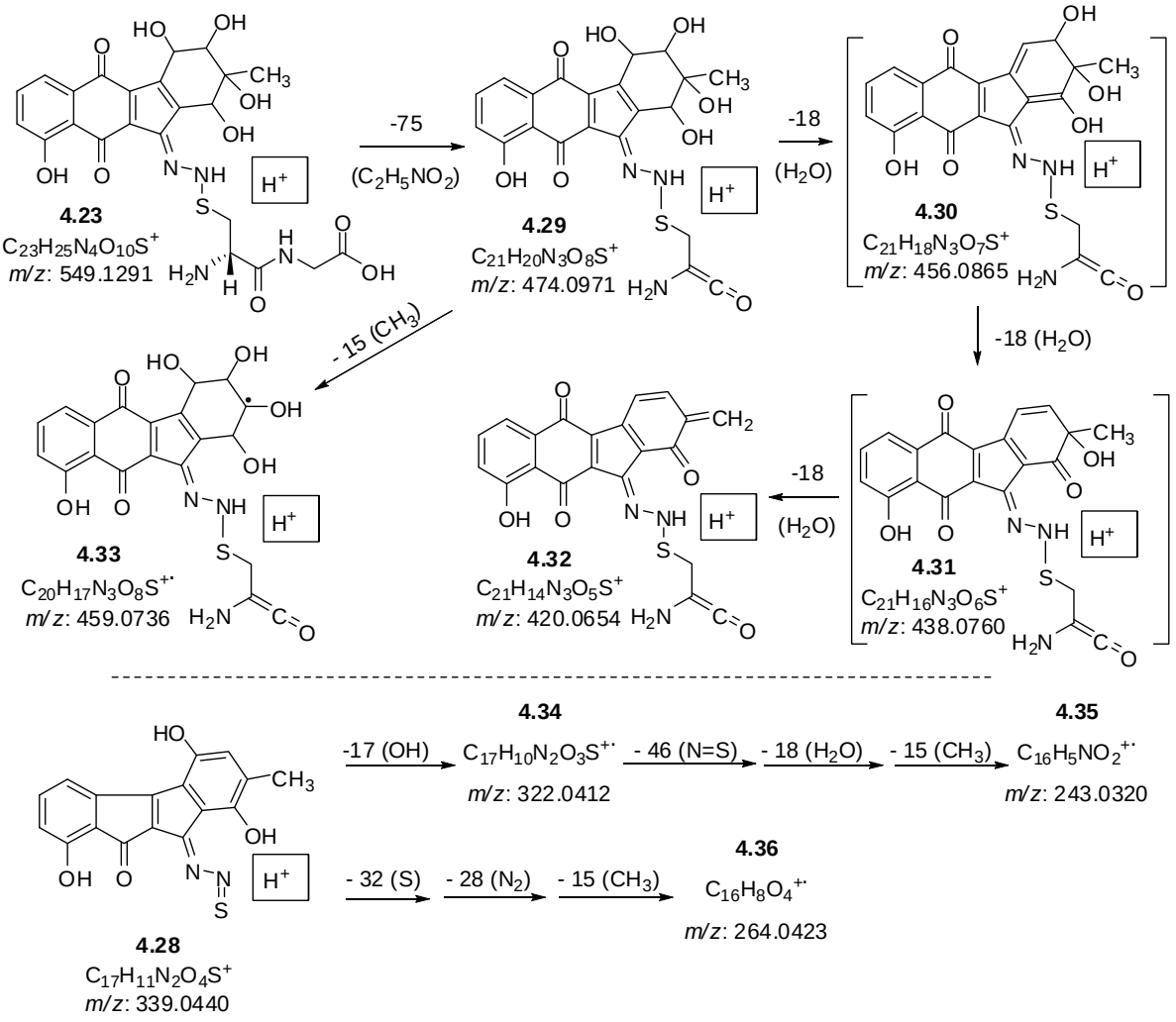

Scheme 4-4. Proposed fragmentation mechanism (part II) for the protonated kinF-GSH adduct **4.18**.

Even though the final conclusion shall not be established solely on such mass results without further (spectroscopic) evidence, the observed mass and chemical behaviour were very supportive of the proposal (Scheme 4-2b) that the kinF-GSH adduct **4.18** was the initial and unstable product from nucleophilic attack on kinF (**1.1f**) by GSH (**4.1**). Its decomposition might then initiate the cleavage of the DNA in the biological studies. Furthermore, the observation of mass peak with *m/z* of ca. 677.1 (Figure 4-9 and 4-10) was surprising and worthy of some additional comments. Correlation of this signal (*m/z* ~ 677.1) to the molecular ion of the proposed kinF-GSH adduct **4.18** ($C_{28}H_{31}N_5O_{13}S^{+\bullet}$, *m/z*:

677.1639) would be entirely consistent with the assignment of the concurrent mass peak with *m/z* of ca. 678.18 to the protonated kinF-GSH adduct [**4.18** + H]$^+$. It should be pointed out that, even though charge formation in ESI-MS occurs commonly as a result of either acid-base reaction or coordination with metal cations (which is also the basis for this mechanistic study), formation of (radical) molecular ions due to the direct loss of one or two electron(s) from the neutral species under the ESI-MS conditions are not rare.[339]

On the other hand, it was also realized that the obtained mass results did have certain flaws that limit the logical interpretation of the data. Due to the complexity of the multi-component reaction system involved and the resolution limit of the instrumentation, monitoring of a pure and single ion species on the mass spectrometer is practically impossible. Even in the case of MSMS studies on an ion of interest with a particular *m/z*, the reality was that a few other ions with very close *m/z* (some were due to isotopic distribution of the ion species while others may simply come from the accidental formation of clusters/ions with very similar *m/z*) would normally co-exist and fragment at the same time, causing the observed mass spectra to be more complicated than it should be. Therefore, the obtained mass fragments were not necessarily always related with the species of interest. For example, observation of the characteristic mass peak (*m/z* ~ 308.1) for the ion of [GSH + H]$^+$ in the MSMS spectra of the new and unstable ion species with *m/z* of ca. 678.18 would indicate that, the starting source ions contains not only the protonated kinF-GSH adduct [**4.18** + H]$^+$ but also certain amount of the cluster ion of [kinF + GSH + H]$^+$, since only the latter species is capable of producing the ion of [GSH + H]$^+$.

Another issue is that the observed nominal mass(es) taking account of the mass defect does not match perfectly with the proposed structures. For instance, the protonated kinF-GSH adduct [**4.18** + H]$^+$ shall have a *m/z* of 678.1717 ($C_{28}H_{32}N_5O_{13}S^+$), while the observed values for mass peaks that were considered to be [**4.18** + H]$^+$ varied in between 678.1257 (cf. Figure 4-10) and 678.1855 (cf.

Figure 4-9). The apparent difference between the theoretical and experimental values (i.e., $|\Delta(m/z)| \sim 0.014–0.046$) was quite huge when judged by the typical mass spectrometry standard, since acceptable *m/z* difference is generally expected to be observed only on the fourth or the third (at most) digit after the decimal point. However, such apparently "large" mass discrepancy was mainly due to the detection limit and fluctuation of the mass spectrometer, as well as the lack of an appropriate internal standard to calibrate the *m/z* values. This kind of situation was quite common, for example, in the case of MSMS of the mass peaks at ca. 678.1 that were regarded as the [**4.18** + H]$^+$, the same ion was observed with several different *m/z* values (i.e., 678.1639, 678.1257 and 678.1352, Figure 4-10) under almost identical mass conditions. Another two such examples are the ion species [kinF + KinF + Li]$^+$ and [GSSG + H]$^+$. Even under apparently identical mass conditions, the former ion ($C_{36}H_{28}N_4O_{14}Li^+$, expected *m/z*: 747.1762) was observed with several *m/z* values in between 747.1776 and 747.1969 (Figure 4-4, $|\Delta(m/z)| \sim 0.0014–0.021$), and the latter one ($C_{20}H_{33}N_6O_{12}S_2^+$, expected *m/z*: 613.1598) was detected with different *m/z* values of 613.1732 and 613.1480 (Figure 4-2, $|\Delta(m/z)| \sim 0.012–0.013$). Therefore, the observed "large" inconsistency of *m/z* between the theoretical and experimental values for mass peaks at ca. 678.18, which were considered to correspond to the [**4.18** + H]$^+$, are still more or less within the instrumentation limit.

(iii) Mixing of kinF (**1.1f**) with a large excess disulfide GSSG (sample KINFGSSG1–3, Table 4-1) under identical conditions (1:1 MeCN/H_2O, pH 7.6) revealed the crucial and irreplaceable role of the sulfhydryl (-SH) group when thiols react with kinF (**1.1f**). The lack of the –SH moiety within GSSG, which is the oxidized sulfur-coupled dimeric form of GSH (**4.1**), led to no reaction at all with kinF (**1.1f**) even after long time of incubation at ambient temperature (i.e., 50 hr @ 23 °C). Both compounds behaved individually on the +ESI-MS as if the other one did not exist, and no obvious mass evidence was found for the formation of possible cluster ion species such as [GSSG + kinF + H]$^+$, [GSSG + kinF + Li]$^+$ or [GSSG + kinF + Na]$^+$. However, incubation of kinF (**1.1f**) with large

excess of GSSG at higher temperature of 37 °C for 53 hr (sample KINFGSSG3, Table 4-1) led to no detection of kinF (**1.1f**) or related ion species at the end. Since the commercial GSSG (Sigma®, Grade II with 5–6% EtOH) did contain a trace amount of GSH as indicated by its label of content as well as the corresponding +ESI-MS spectra (not shown), a large excess of GSSG would imply the co-existence of a significant amount of GSH (**4.1**). Therefore, it was not surprising that the very limited amount of kinF (**1.1f**) was completely consumed (by GSH but not GSSG) over long time, particularly at elevated temperature. Once again this observation confirmed the occurrence of a reaction between the thiol (GSH) and kinF (**1.1f**).

(iv) When the simple thiol *N*-acetyl-L-cysteine **4.17** was used in excess to react with kinF (**1.1f**) (sample KINFCYS1–2, Table 4-1), the experimental findings were somehow unexpected. Even after 12 hr of reaction of excess **4.17** with kinF (**1.1f**) (~ 4:1) at 37 °C, the corresponding mass spectra still indicated the presence of significant amount of unreacted kinF (**1.1f**), as characterized by either the $[kinF + Na]^+$ mass peak (*m/z* ~ 393.1, Figure 4-14, both spectra) or the $[kinF + H]^+$ mass peak (*m/z* ~ 371.1, Figure 4-14, bottom spectrum from acidified reaction sample). At the same time, the acidified mass sample (Figure 4-14, bottom spectrum) also afforded an interesting mass peak with *m/z* of ca. 556.1, which could be either the very likely non-covalent cluster ion of $[kinF + \mathbf{4.17} + Na]^+$ or the other possible Na^+-binding form of the kinF-**4.17** adduct $[kinF\text{-}\mathbf{4.17} + Na]^+$. Similar to the kinF-GSH adduct **4.18**, the possible kinF-**4.17** adduct was expected to have the sulfur atom from **4.17** chemically bonded to the terminal nitrogen of the diazo moiety of kinF (**1.1f**).

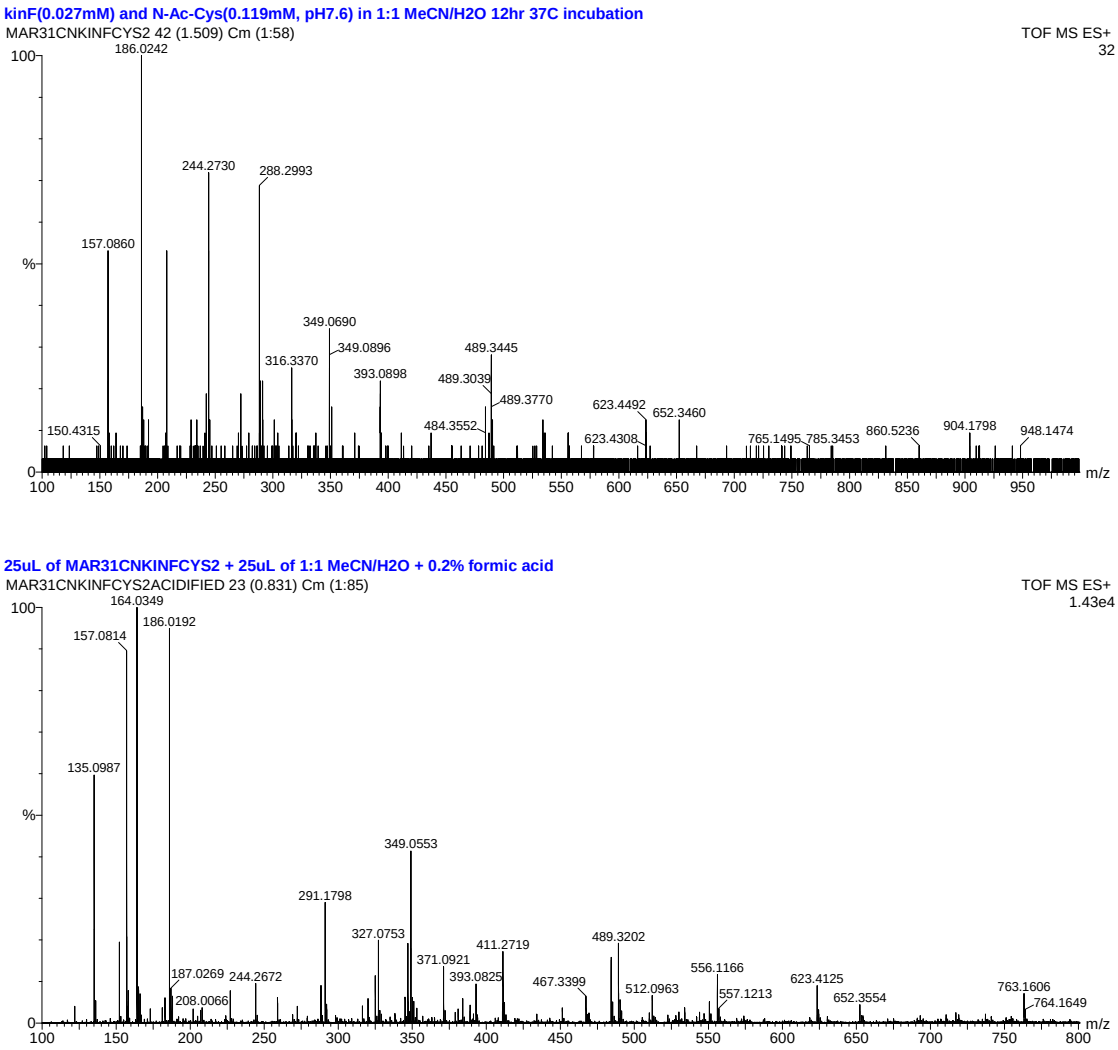

Figure 4-14. +ESI-MS spectra of an ion species with *m/z* of ca. 556.1 observed with kinF (**1.1f**) and **4.17** in 1:1 MeCN/H_2O (sample KINFCYS2, 12 hr at 37 °C, Table 4-1). Top spectrum: reaction sample with no formic acid; bottom spectrum: reaction sample acidified with 0.2% HCOOH.

The consequent MSMS spectra of mass peak at 556.1 under different mass collision energies (2–35 eV, Figure 4-15) clearly indicated that this ion species only led to two major mass fragments with *m/z* of ca. 393.1 and 365.1 even under fairly high collision energy. The only reasonable structural interpretation of such mass results was that the mass peak at 393.1 is due to the $[kinF + Na]^+$ ($C_{18}H_{14}N_2O_7Na^+$, *m/z*: 393.0699) and the mass peak at 365.1 is a fragment ($C_{17}H_{14}N_2O_6Na^+$, *m/z*:

365.0750) derived from [kinF + Na]$^+$ upon the loss of a neutral CO or N_2 (mass = 28) fragment. Therefore, the observed mass peak at 556.1 could only correspond to the non-covalent cluster ion of [kinF + **4.17** + Na]$^+$ but not the Na$^+$-binding form of the kinF-**4.17** adduct [kinF-**4.17** + Na]$^+$.

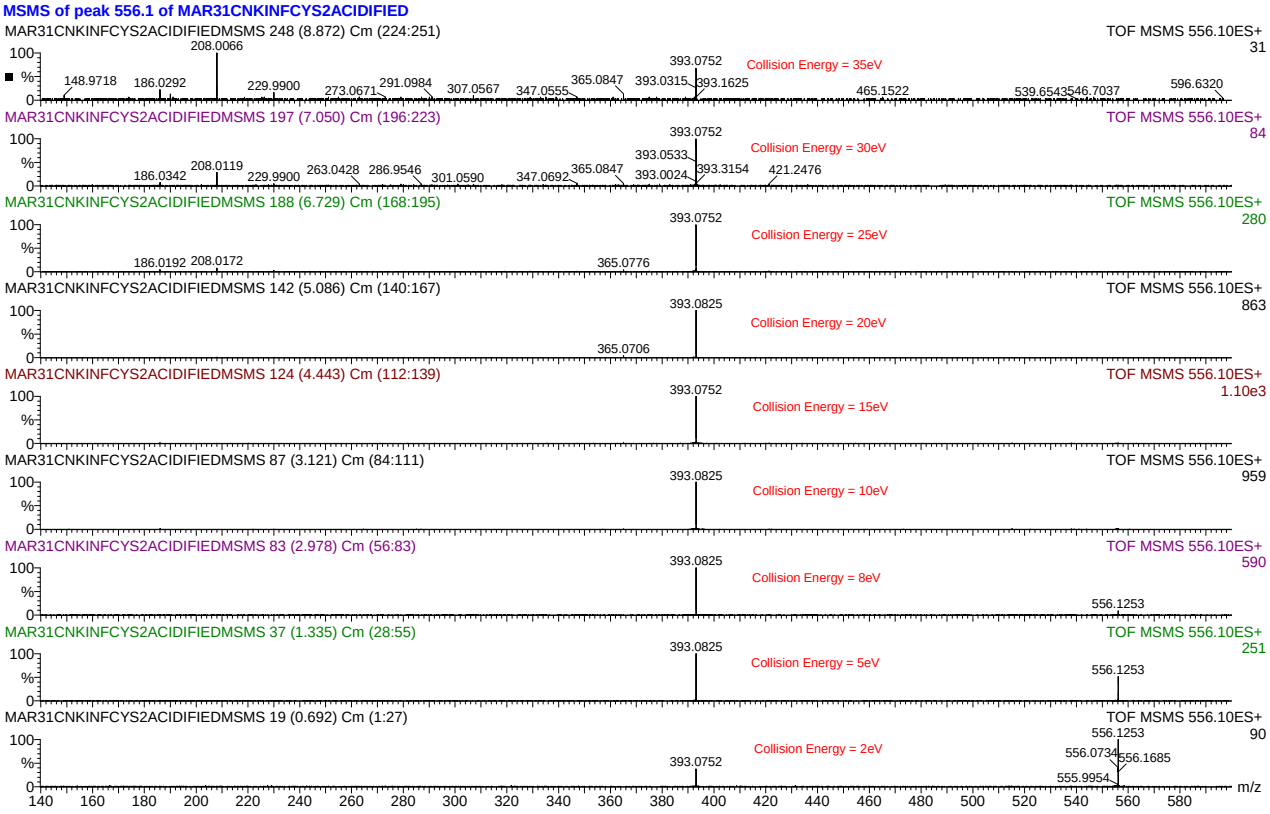

Figure 4-15. +ESI-MSMS spectra of mass peak with *m/z* of ca. 556.1 under different mass collision energies (as labeled on each spectrum).

The previously observed smooth reaction between GSH (**4.1**) and kinF (**1.1f**), which was quite fast and complete (i.e., reaction accomplished within 10–20 min and limiting reagent of either kinF or GSH would be entirely consumed by the other reagent in excess), no longer applied in the case of **4.17** and kinF (**1.1f**). Such observation can be explained by the known fact that, when thiols act as potent nucleophilic agents, the reaction rates would depend on and are inversely proportional to the acidity of the sulfhydryl moiety (i.e., its ability to dissociate to the corresponding thiolate anion).[306]

Despite the quite similar spatial and stereochemical environments for the sulfhydryl (-SH) groups within GSH (**4.1**) and **4.17**, their pKa values ($pKa(-SH)_{\mathbf{4.17}}$ = 9.52 vs $pKa(-SH)_{GSH}$ = 8.63) would suggest that **4.17** is significantly less reactive towards the diazo moiety of kinF (**1.1f**) when compared with GSH (**4.1**) under the conditions involved (i.e., pH 7.6), therefore leading to the observed incomplete reaction even after long time.

For the first time, the above mechanistic studies using +ESI-MS has provided some direct and convincing evidence to indicate that, under the (near) physiological conditions and in the presence of an appropriate and bio-significant substrate such as GSH (**4.1**), nucleophilic addition to the diazo moiety of the kinamycins is the very first key step involved in the mode-of-action of these unique antibiotics. Therefore, exploration of other natural and synthetic diazobenzofluorene analogues with higher diazonium ion character is a promising direction of study, which is expected to be able to provide new candidates with even stronger biological activity.

4.2.2 Potential Significance of the Reaction of Kinamycin F with Thiols

Recent collaborative studies by the Dmitrienko and the Hasinoff groups on the biological properties of kinF (**1.1f**) have revealed that treatment of human K562 leukemia cells with kinF (**1.1f**) induced erythroid differentiation, a rapid apoptotic response, induction of caspase-3/7 activities and a delayed cell cycle progression through the S and G2/M phases.[340] These observed effects by kinF (**1.1f**) were correlated with its selective reduction of levels of cyclin D3 protein, which plays a key role in cell cycle progression and acts by binding primarily to cyclin-dependent kinase 6 (CDK-6). The reduction in levels of cyclin D3 protein by kinF (**1.1f**) appeared to be mediated at the level of transcription, rather than by affecting the stability of either cyclin D3 protein or mRNA, thus making the cyclin D3 a potential target of kinF (**1.1f**). [340]

There is currently a great deal of interest in the discovery of small molecules that are selective inhibitors of specific kinases as potential anticancer agents.[341] Many compounds that inhibit kinases do so by binding to the ATP binding site, thus leading to a lack of specificity among the 500 or so known human kinases and undesired toxic side effects. A very interesting discovery reported recently by researchers at the Wyeth labs relates to the selective inhibition of the key human kinase called AKT, also known as protein kinase B (PKB).[342,343] AKT/PKB belongs to the AGC super family of serine/threonine protein kinases and is a key regulator of various growth factors and hormones leading to activation of proteins involved in proliferation, metabolism, growth and survival.[344] That work has attracted the attention of this laboratory in the context of the possible mode-of-action of kinF (**1.1f**), since one of the expected consequence of inhibiting PKB/AKT is a diminution in the level of cyclin D3.

The Wyeth group screened numerous natural products as potential selective inhibitors of PKB/AKT and have discovered that lactoquinomycin (**4.37a**), a polyketide-derived pyrano-naphthoquinone (PNQ) type antibiotic discovered in the 1970's, is an effective and selective inhibitor for this kinase.[342] By synthesizing simplified analogues such as **4.37b**–**f** and in vitro cytotoxicity measurements with the breast cancer cell line MDA468, the Wyeth group has shown that neither the amino sugar component nor the phenolic OH group of **4.37a** is essential for its PKB/AKT inhibition and anticancer activity, but the lactone functionality is vital.[343] Further study of the interaction of simpler synthetic PNQ lactone analogues **4.37f** with the protein (AKT-2, an isoform of AKT) revealed that, as evident from the corresponding LC/ESI-MS spectrometry results, such compound covalently modify the cysteine sulfhydryl group of AKT-2 to form a mono-adduct at C297 and a bis-adduct at C297 and C311 in a 1:1 ratio, leading to > 90% loss of enzymatic activity.[343] A hypothetical mechanism for this process involving a PNQ-based quinone methide **4.40** as the key intermediate has been proposed (Scheme 4-5).[343] It should be noted that the kinase AKT-1, shown in the mechanism

(Scheme 4-5), is another isoform of AKT and has two cysteine residues of C296 and C310 corresponding to the C297 and C311 of AKT-2.

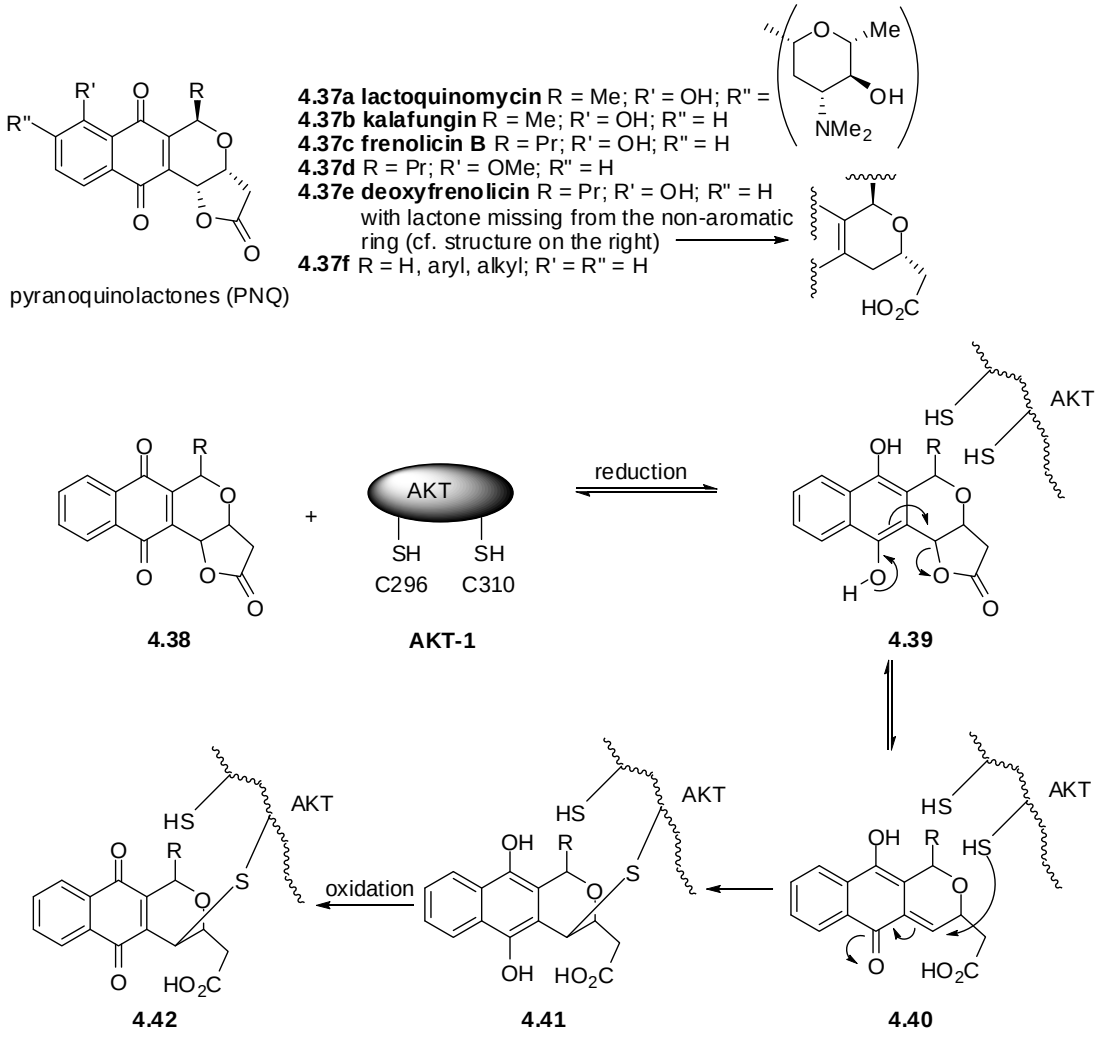

Scheme 4-5. Proposed mechanism for the inhibition of AKT by PNQ lactones in the literature.

In the context of the search for a mode-of-action for the kinamycins and isoprekinamycin, these observations suggest that such diazobenzo[*b*]- and diazobenzo[*a*]fluorene natural products might act at the same kinase target. The experimental observations in regard to covalent adduct formation with GSH (**4.1**) and kinF (**1.1f**) raise the possibility that, similar to the PNQ lactones (Scheme 4-5), a process such as that shown below might occur between the sulfhydryl groups within PKB/AKT and

the kinamycins (Scheme 4-6): nucleophilic attack of the sulfur towards the diazo moiety leads to the adduct **4.43**, whose subsequent homolytic cleavage upon the loss of N_2 followed by recombination of the corresponding vinyl radical **4.44** and the sulfur radical **4.45** might lead to a more stable adduct **4.46** (path (a), Scheme 4-6); alternatively, another reaction mode is also worth considering (path (b), Scheme 4-6), in which the initial adduct **4.43** might undergo an intramolecular conjugate addition of another cysteine sulfhydryl group to the enone system followed by the expulsion of N_2 and a thiolate. However, it should be noted that an analogous pathway (b) is unlikely in the case of isoprekinamycin (**1.5**), since the corresponding initial adduct **4.50** in that case would possess an aromatic C-ring that can not act as a Michael acceptor in the second nucleophilic attack, while the diazobenzo[*b*]fluorene type kinamycins could form a quinone methide (such as **4.47**) in their cases to proceed further. Thus, the mechanism involving addition to the diazo group followed by homolysis and radical recombination (i.e., path (a) in Scheme 4-6) might be more feasible for isoprekinamycin (**1.5**).

Efforts to explore these possibilities with recombinant human PKB/AKT using ESI-MS experiments, similar to those described earlier for adduct formation between kinF (**1.1f**) and GSH (**4.1**), are currently in progress in the Dmitrienko group.

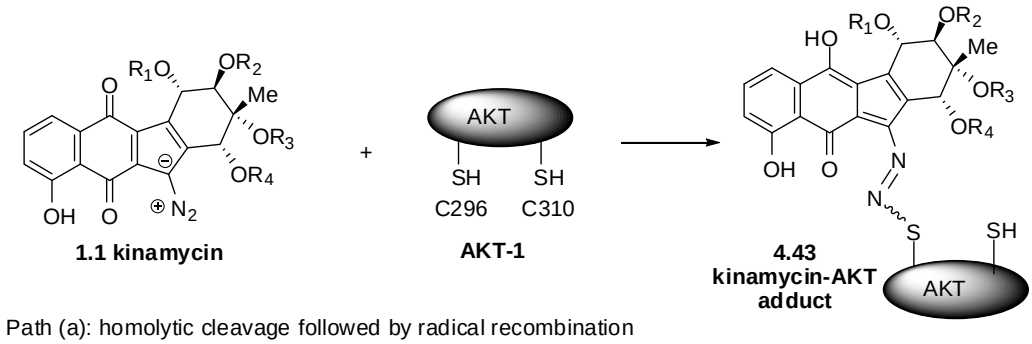

Path (a): homolytic cleavage followed by radical recombination

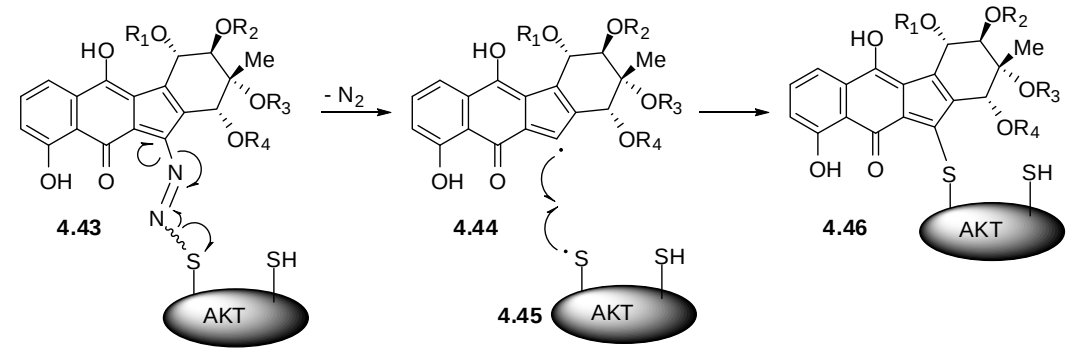

Path (b): intramolecular conjugate addition followed by elimination

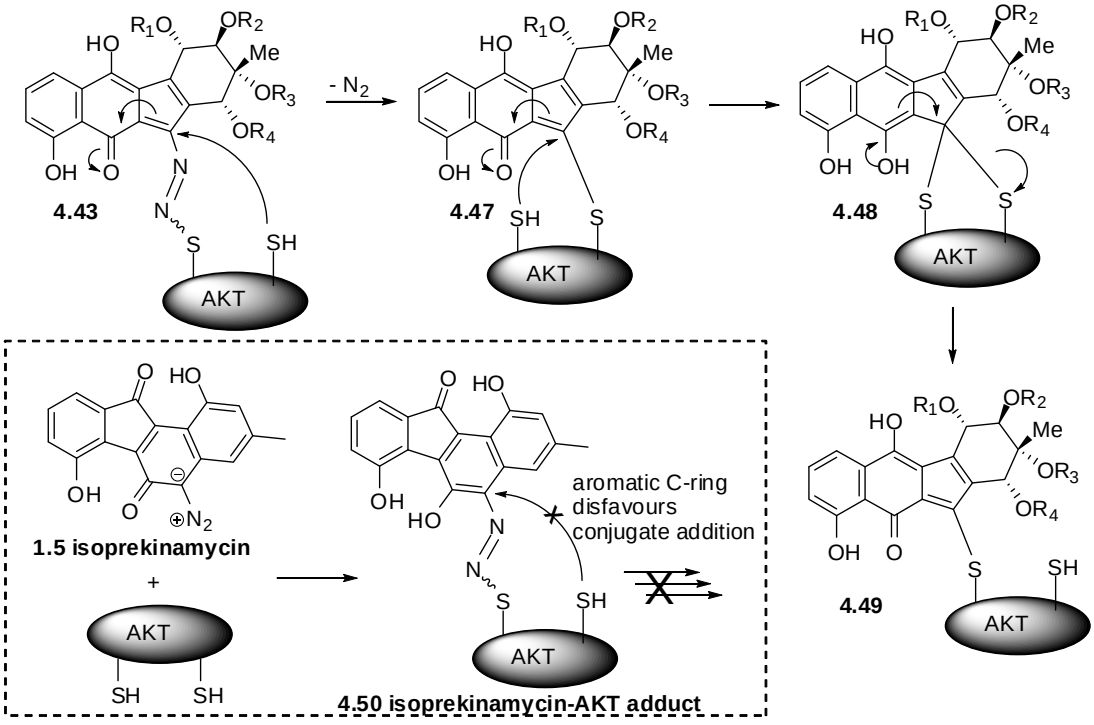

Scheme 4-6. Proposed mode-of-action for possible inhibition of PKB/AKT by the kinamycins.

A side by side comparison of the computed (optimized) conformations of prekinamycin (**1.4**, a diazobenzo[*b*]fluorene), kalafungin (**4.37b**, a simplified version of lactoquinomycin) and isoprekinamycin (**1.5**, a diazobenzo[*a*]fluorene) is shown in Figure 4-16. A "Tube" format instead of the "Ball and Stick" style to display the conformation is used for clarity. It is very intriguing to notice the overall conformational similarity among them, since the lactone moiety locks the non-aromatic ring of **4.37b** and forces it to adopt a fairly flat conformation. In addition, the diazo group within the kinamycins could serve as a suitable alternative (Scheme 4-6) to the lactone moiety, which acts as the critical leaving group during the formation of the quinone methide key intermediate for the mode-of-action of lactoquinomycin (Scheme 4-5). Such observations and speculations suggest that, it seems to be reasonable to consider the possibility that kinamycins might have affinity for the same biological receptors (the kinase) as the PNQ lactones.

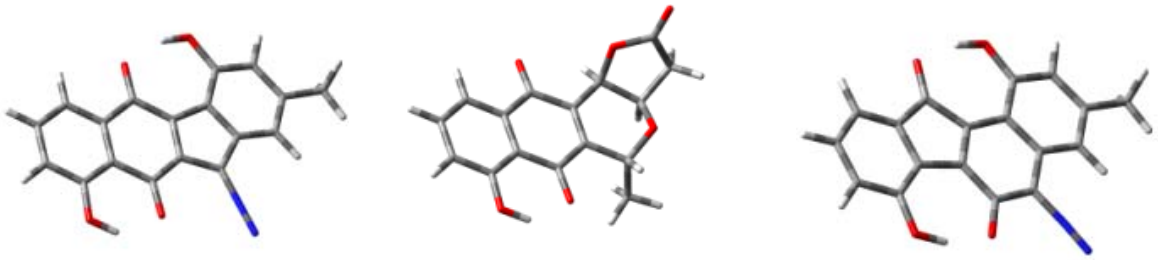

1.4 prekinamycin **4.37b kalafungin** **1.5 isoprekinamycin**

Figure 4-16. Comparison of optimized conformations at RHF/6-31G level of prekinamycin (**1.4**), kalafungin (**4.37b**) and isoprekinamycin (**1.5**, from X-ray, see Chapter 5 for more details).

4.2.3 Recent Literature Work on the Mode-of-action of Kinamycins

Other than the few and already introduced mechanistic studies on the mode-of-action of kinamycins prior to the start of this project (section 1.4.2), several new reports in this regard have appeared in the literature during the course of this thesis research project. It is necessary to summarize these recent developments in the field and compare with results presented above (section 4.2.1).

In late 2005, Feldman and Eastman published some preliminary results on the possible mode-of-action of prekinamycin (**1.4**),[345] a diazobenzo[*b*]fluorene type kinamycin (considered as a diazoparaquinone by Feldman), followed by a more detailed disclosure in the following year.[346] By using the literature observation that cleavage of double stranded DNA by lomaiviticin A (**1.11a**) was performed under reducing conditions as an argument,[52] Feldman proposed a mechanism involving one-electron reduction of the quinone moiety of kinamycins to a reactive semi-quinone followed by non-obligatory protonation as the initial key step (Scheme 4-7).[345,346] The radical (anion) species **4.52a**, generated upon reduction of the generic kinamycin-type diazoparaquinone structure **4.51**, may also be represented by the corresponding resonance forms **4.52b** and **4.52c**. Feldman further assumed that C-5 in **4.52** is "pyramidalized sufficiently to permit adequate overlap between the enol (enolate) orbitals and $\sigma^*_{C\text{-}N}$"[345] to allow the consequent rapid loss (β-elimination) of N_2 and afford the sp^2 C-5 radical **4.53**, which then may perform hydrogen abstraction from DNA if the radical stays in the close proximity of DNA. In addition, Feldman also proposed that the diazoparaquinone/DNA interaction may even go beyond simple hydrogen abstraction to damage DNA further (Scheme 4-7).[346] The possible quinone methide **4.54**, derived from **4.53** upon hydrogen abstraction from DNA, was considered to have a hydroxymethylacylfulvene (**4.55**) subunit. This may act as the key electrophilic pharmacophore upon nucleophilic attack by the DNA bases such as guanosine unit **4.56** with its N-7 as the nucleophilic site, resulting in DNA damage. Alternatively, radical addition of DNA• with quinone methide **4.54** could afford a covalent adduct **4.58** that eventually leads to the same result of DNA damage.

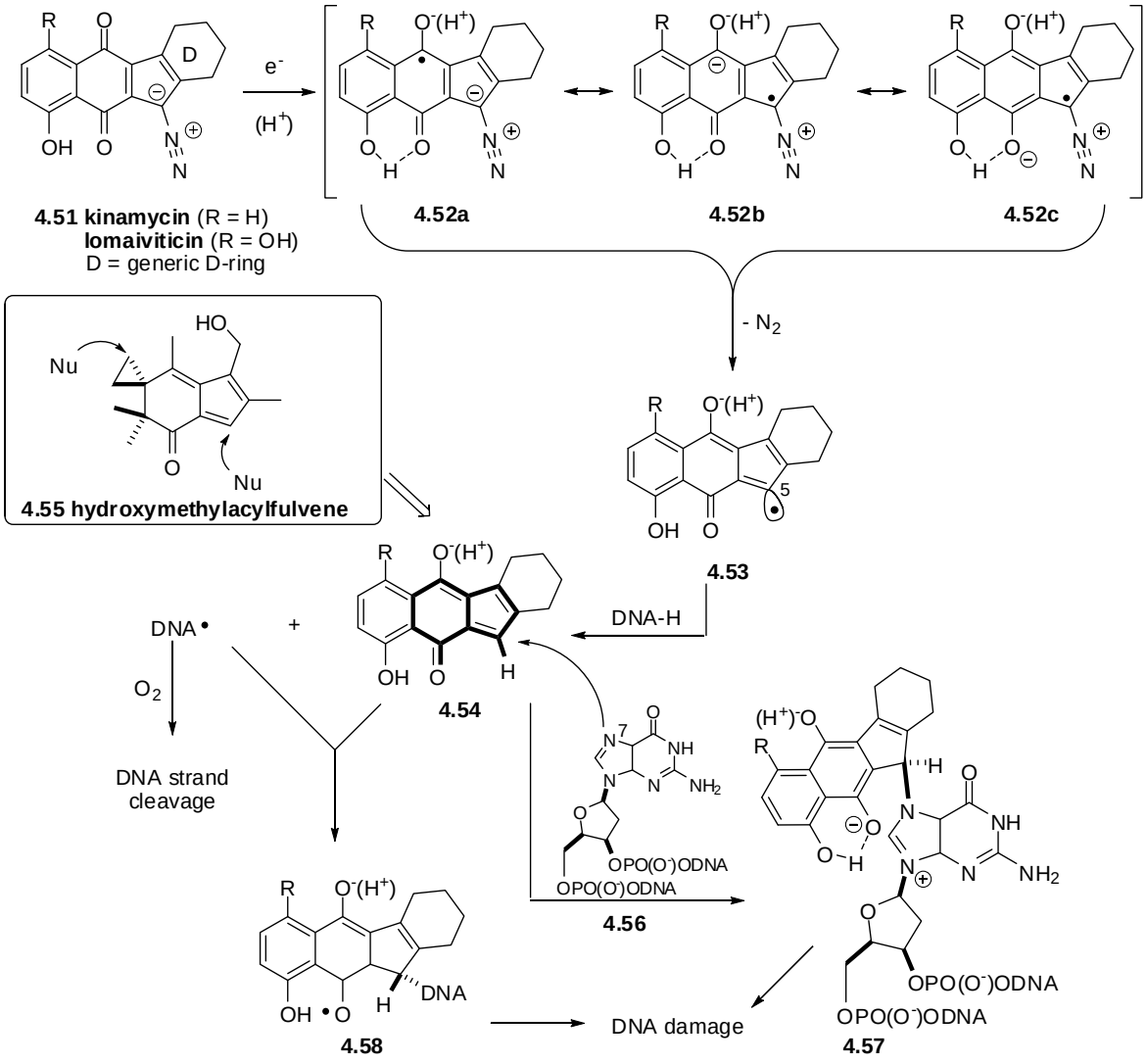

Scheme 4-7. Proposed mechanism for kinamycins based on one electron reduction pathway.

Within the above hypothesis by the Feldman group (Scheme 4-7), transformations from **4.53** and beyond are completely theoretical speculations without any experimental evidence. Formation of the proposed C-5 radicals **4.53** from prekinamycin (**1.4**) and its dimethyl (**1.4a**) and diacetyl (**1.4b**) derivatives (Scheme 4-8), however, was observed when such kinamycins were heated at 80 °C in an aromatic solvent (benzene or arene **4.65**) in the presence of Bu_3SnH (as one electron reductant) and 2,2-azobisisobutyronitrile (AIBN, as appropriate initiator). Control experiments indicated that the

smooth occurrence of this reaction required the mandatory co-existence of heat, the tinhydride and AIBN, but light was found to be not necessary. On the other hand, non-aromatic solvents including THF, 1,4-dioxane, CCl_4, CH_3CN, EtOH and $CHCl_3$ only led to unreacted starting kinamycins even if other essential conditions were complied with, suggesting that the sp^2 radical **4.53** is either promoted to form or stabilized by π-complexation in aromatic solvents. Formation of the critical radical species **4.62** from the prekinamycin dimethylether **1.4a** (Scheme 4-8), which is the same type as **4.53** in Scheme 4-7, was evident from the obtained final products of **4.60a**–**c**, **4.61**, **4.67**, **4.69**, **4.70** and **4.71**, which all had a new substituent (e.g., -Ph, -Ar, -SePH, -SBn and -D) introduced at C-5 depending on the available reagent(s) (i.e., benzene, substituted arenes, thiols and tinhydride) in the system that participated in the radical reaction. The concurrent isolation of the minor product of dimer **4.64**, whose formation might undergo several possible pathways such as direct radical dimerization of **4.62,** radical addition between **4.62** and **4.63** followed by oxidation, or hetero Diels-Alder dimerization of **4.63** followed by oxidation, seemed to be difficult to explain if a radical mechanism was not involved (Scheme 4-8). The proposed radical mechanism also fit with the observed kinetic data, product distributions and Hammett correlation when substituted arenes **4.65** and isotope-labeled tinhydride/thiols were used in such reactions (Scheme 4-8).[345,346]

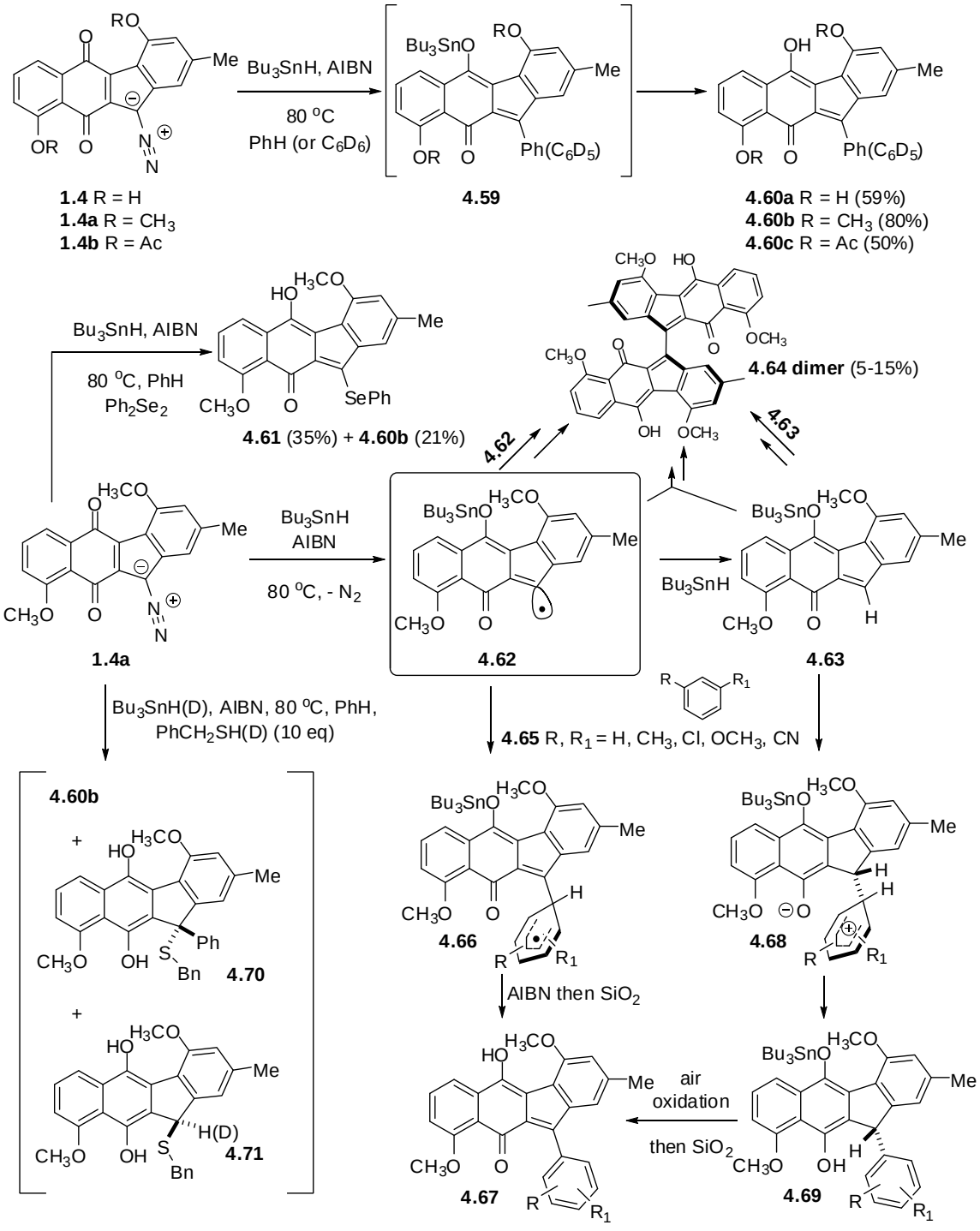

Scheme 4-8. Products and possible reductive radical mechanism for prekinamycin (**1.4**) and its derivatives in the presence of Bu_3SnH (one electron reductant) and AIBN (initiator).

Feldman's work provided observations of some interesting chemical behavior of the diazobenzo[*b*]fluorene type kinamycins under a (rare) reducing condition, and an alternative possibility for the mode-of-action of kinamycins. However, even Feldman himself admitted that the conditions involved in his studies were far from the physiological conditions under which the bioactivities of kinamycins were observed and measured.[346] The use of tinhydride as a reducing agent in the presence of radical initiator such as AIBN is by no means to have any bio-significance or even chemical-significance related to the known in vitro and in vivo bioactivity studies of the kinamycins, not to mention the unrealistically high temperature and non-aqueous aromatic solvent involved that are essential for the observed chemistry and proposed mechanism. Therefore, the breadth of Feldman's conclusion is rather limited, and its validity for the actual mechanism of kinamycins is questionable.

Around the same time when Feldman's mechanism was published, Arya reviewed the known mechanistic studies on diazo and diazonium DNA cleavage agents at the time (prior to 2006 but not including Feldman's results), with a focus on kinamycins.[347] In this review, Arya proposed two other theoretically possible mechanisms for the kinamycins but with no experimental evidence to support the proposals. The first one (Scheme 4-9a) involves an initial protonation of the kinamycin at C-5 of the diazobenzo[*b*]fluorene skeleton as the triggering step, perhaps after its binding with DNA, and the obtained kinamycin diazonium ion **4.72** can lose N_2 either heterolytically to produce the corresponding carbocation **4.73**, or homolytically and reductively to give the resonance stabilized radical (**4.74** ↔ **4.75**). Then the vinyloxy radical **4.75** can react further to cause DNA cleavage. Protonation at C-5 of kinamycin is obviously the core of this proposed mechanism, but one can easily argue that, at least in theory, such C-5 protonation should be strongly disfavoured or easily prohibited since it would destroy the aromaticity of the C-ring. It is also true that the kinamycins exhibit a high degree of stability towards acids experimentally, and hence it seems highly unlikely that protonation

is a key step in the mode-of-action as suggested by Ayra. For example, the Dmitrienko group recently isolated the kinamycins in very good yield from bacteria fermentation broth that were adjusted to pH 2 (unpublished results by V. Goodfellow), and it was also found that kinamycins are very stable even in the presence of excess trifluoroacetic acid (unpublished results by Dr. A. Ghavami). Reported derivatization and synthesis of the kinamycins in the literature also show that these compounds, particularly the C5-diazo moiety, could tolerate and survive various strong acids such as PTSA (*p*-toluenesulfonic acid) (Scheme 1-1),[9] sulfuric acid (Scheme 1-1)[5] and HCl (Scheme 3-32 and 3-33).[16,26]

Ayra's second mechanism involves a photolytic decomposition of the kinamycin, which shall produce the corresponding carbene **4.77** that may induce DNA cleavage (Scheme 4-9a). In addition, **4.77** may also rearrange to the vinylic carbon radical **4.78** that might be capable of DNA cleavage as well. Until now there are no direct reports in the literature regarding the photochemical behaviour of kinamycins. However, in accordance to Arya's photolytic proposal, the Zaleski group recently carried out some photochemistry work with (2-diazo-3-oxo-tetraphenylchorinato)M(II) (**4.80**, M = Ni, Zn, Cu) that were claimed as model compounds for natural kinamycins and to be potentially useful in photodynamic therapy (PDT) for tumors. Photolysis of **4.80** was found to involve singlet carbenes as the reactive intermediates to form the corresponding Wolff rearrangement products **4.81** and dimers **4.82** (Scheme 4-9b).[348] The photochemical mechanism by Arya and the related work by Zaleski are also of very little value to clarify the real mode-of-action of these antibiotics, since the known biological activities of kinamycins require no light at all. As an added support for this argument, experimental observation by the mechanistic study of this thesis work has found that, exposure of a mixture of kinF (**1.1f**) and GSH (**4.1**) in aqueous acetonitrile to normal room/day light, even for hours, does not alter the reaction outcome when compared with the same sample that has been stored in the dark (see section 4.7 for experimental details).

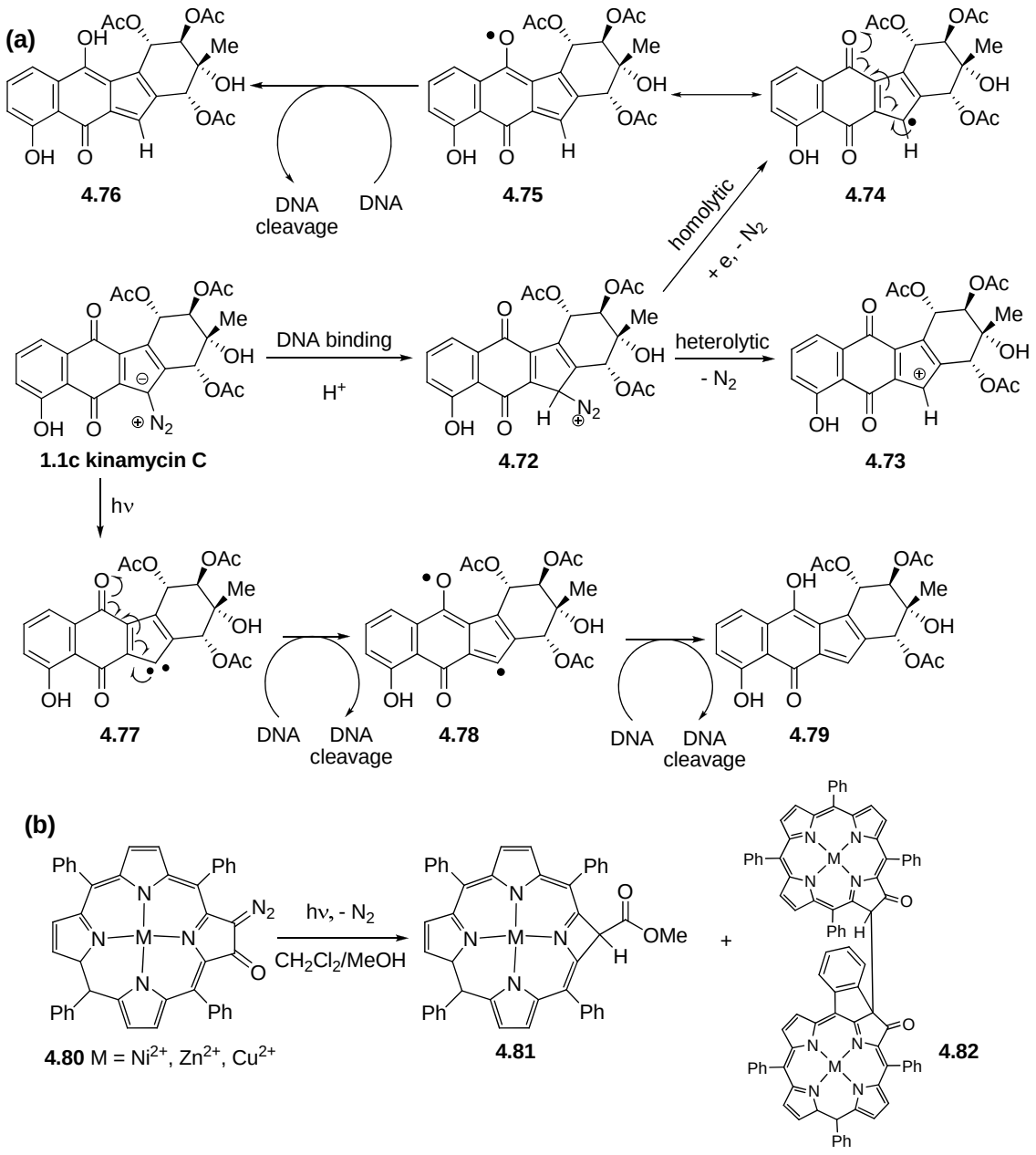

Scheme 4-9. (a) Two possible mechanisms proposed by Ayra for the mode-of-action of kinamycins; (b) photochemical reaction of diazo-oxochlorin (as kinamycin model compounds) involving a carbene.

Also in 2006, Melander and co-workers synthesized some simple analogues of 9-diazofluorene (**1.109**), including 1-substituted (**4.83a**–**d**), 4-substituted (**4.84a**–**d**) and 1,4-

disubstituted-9-diazofluorenes (**4.85a**–**b**), as model compounds for natural kinamycins.[349] Biological tests to cleave supercoiled DNA with these diazofluorenes and natural kinD (**1.1d**) (Scheme 4-10a) indicated that, under physiological conditions, DNA cleavage was only observed with such diazo compounds in the presence of an appropriate promoter (in most cases) such as dithiothreitol (DTT, **4.2**), and apparently the DNA cleavage was fairly slow (2 days). Among the analogues tested, 1-methoxy-9-diazofluorene (**4.83b**) was found to be the most active one and its activity towards DNA cleavage was comparable to (in fact slightly higher than) the natural kinD (**1.1d**).[349] However, no mechanism was provided for the observed bioactivities of these diazofluorene model compounds at the time. Two year later, the Melander group released some additional results regarding the DNA cleavage by natural kinD (**1.1d**) in the presence of either DTT (**4.2**) or GSH (**4.1**) as a promoter, and increasing in temperature was found to significantly accelerate the DNA cleavage by the kinamycin (accomplished within 24 hr at physiological temperature vs 2 days at room temperature).[307] Since sulfides such as DTT (**4.2**) are well-known sources for $2e^-$ reduction, Melander proposed a corresponding mechanism in which the first key step is a two electron reduction of kinD (**1.1d**) by the thiol (DTT or GSH) leading to the formation of a diazodihydroxyquinone **4.86** (Scheme 4-10b).[307] Further conversion of **4.86** leading to the ultimate DNA cleavage could undergo two different pathways as proposed by Melander (Scheme 4-10b). The first route borrowed an idea from the published Dmitrienko mechanism (Scheme 1-28) involving a nucleophilic attack on the diazo group of **4.86**, then the corresponding azo adduct **4.87** underwent a homolytic cleavage to generate a carbon radical **4.88** that is responsible for DNA cleavage; the second route showed certain similarities to Arya's mechanism (Scheme 4-9a) with protonation at C-5 of **4.86** as the key step, followed by the spontaneous decomposition of the diazo group of **4.89** to generate an *ortho*-quinone methide **4.90**, which could also act as an alkylating agent for DNA. This two electron reductive mechanism for kinamycins seemed to be supported (only) by some very limited MO calculations on a simplified

diazobenzo[*b*]fluorene model structure (i.e., **1.1d** without all D-ring substituents) and its reduced dihydroxyquinone form.[307] Despite the physiological conditions used in Melander's study, no chemical or biological evidence was reported in this work for the existence or involvement of **4.86** or any other derivatives within the proposed mechanism, thus leaving its credibility in doubt.[307]

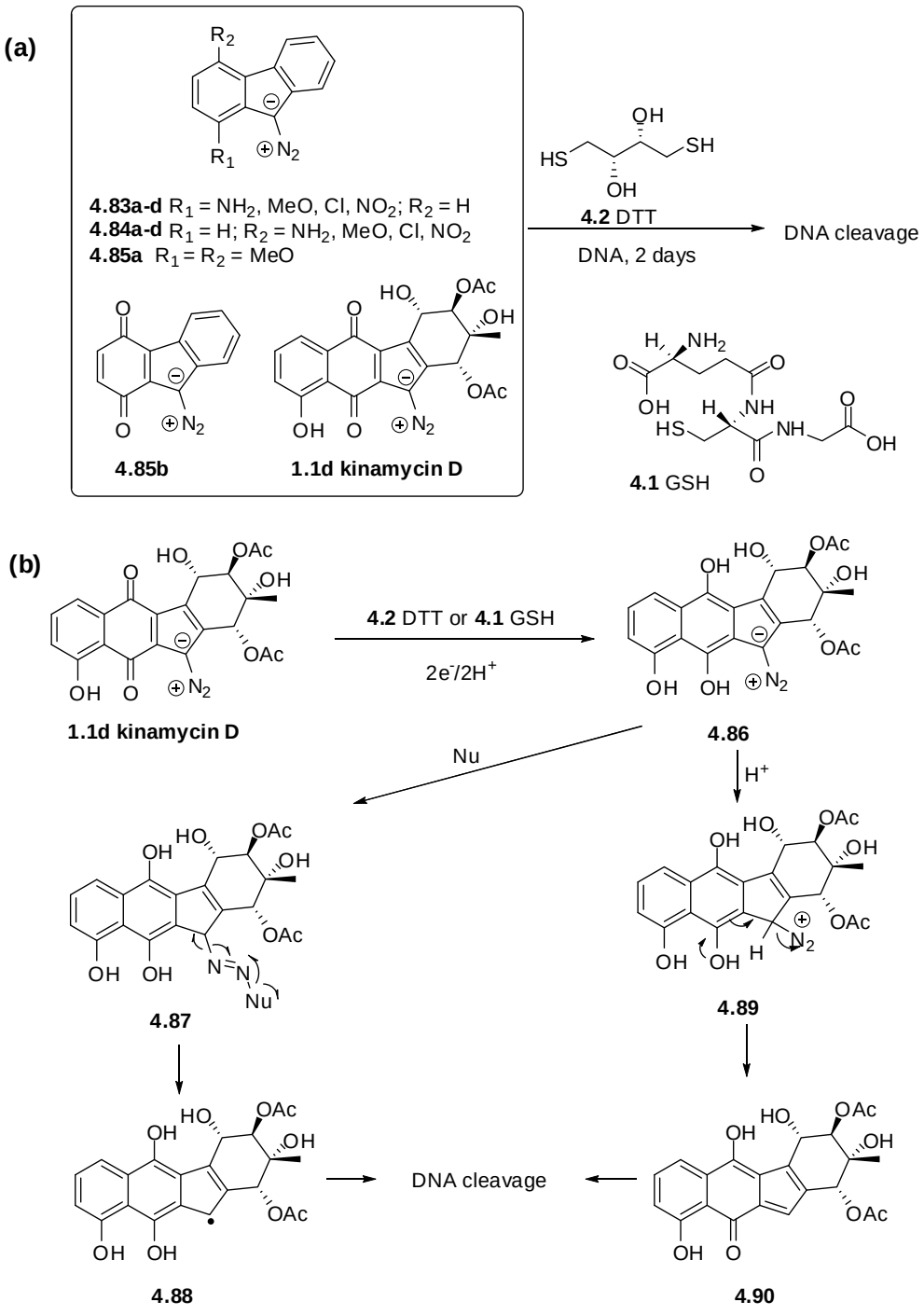

Scheme 4-10. (a) Observed DNA cleavage by diazofluorenes in the presence of DTT (**4.2**); (b) proposed two electron reductive DNA cleavage mechanisms for kinamycins by Melander.

Very recently (2009), Skibo and Khdour carried out physical organic chemistry experiments aimed at identifying the possible mode-of-action of prekinamycin (**1.4**), a diazobenzo[*b*]fluorene with a fully aromatized D-ring, via the two electron reduction that might occur in vivo (Scheme 4-11).[90] It was proposed that, reduction of the B-ring quinone of **1.4** to the corresponding dihydroxyquinone of **4.91** followed by protonation and dediazoniation, both at C-5, leads to the formation of **4.93**, an *ortho*-quinone methide intermediate. Compound **4.93** could equilibrate with its keto tautomer **4.94**, which is a deazotized quinone, but only the former species is capable of trapping a nucleophile and thus considered to be responsible for the biological activity of kinamycins. In fact, one can easily realize that this mode-of-action is essentially the same as the previous mechanistic proposal by Melander for kinD (**1.1d**) (Scheme 4-10b, **4.86** to **4.90** via **4.89**), a diazobenzo[*b*]fluorene with a non-aromatic D-ring.

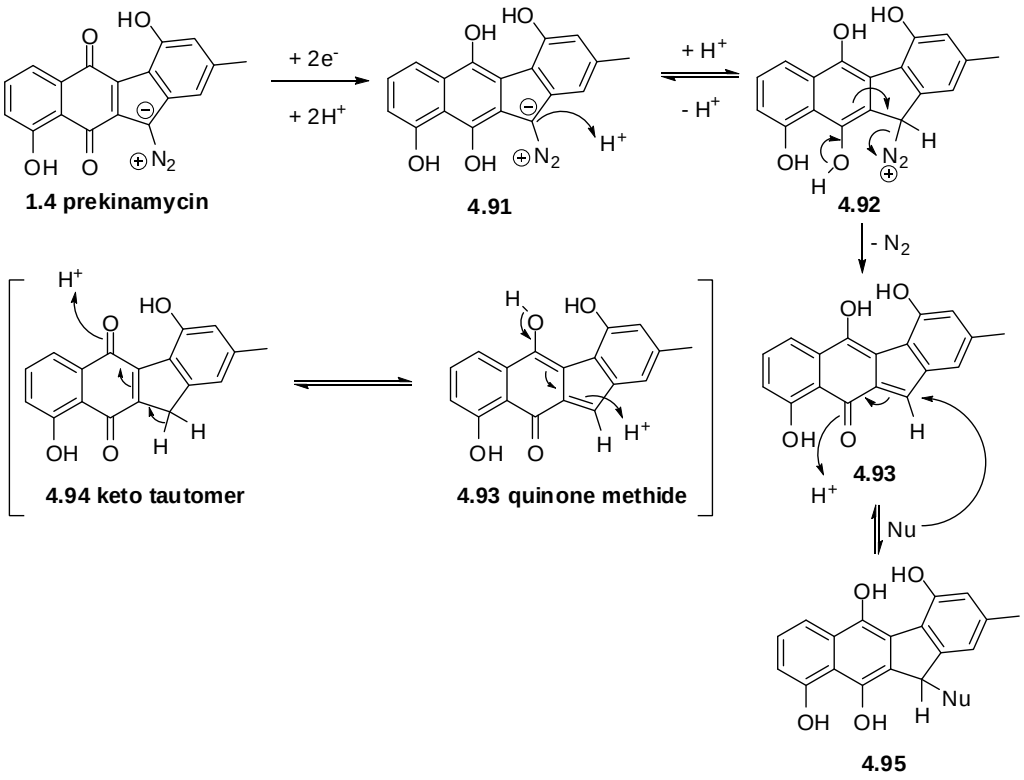

Scheme 4-11. Proposed two electron reduction mechanism for prekinamycin (**1.4**) by Skibo.

In particular, the Skibo group prepared a number of prekinamycin analogues including **1.4a** and **4.96a–d** with the C-5 diazo carbon atom enriched with ^{13}C, and subjected these compounds to catalytic hydrogenation (H_2/Pd-C in anaerobic and aqueous DMSO buffer, pH 7.2–9.4) to mimic the possible two electron reduction in vivo (Scheme 4-12).[90]

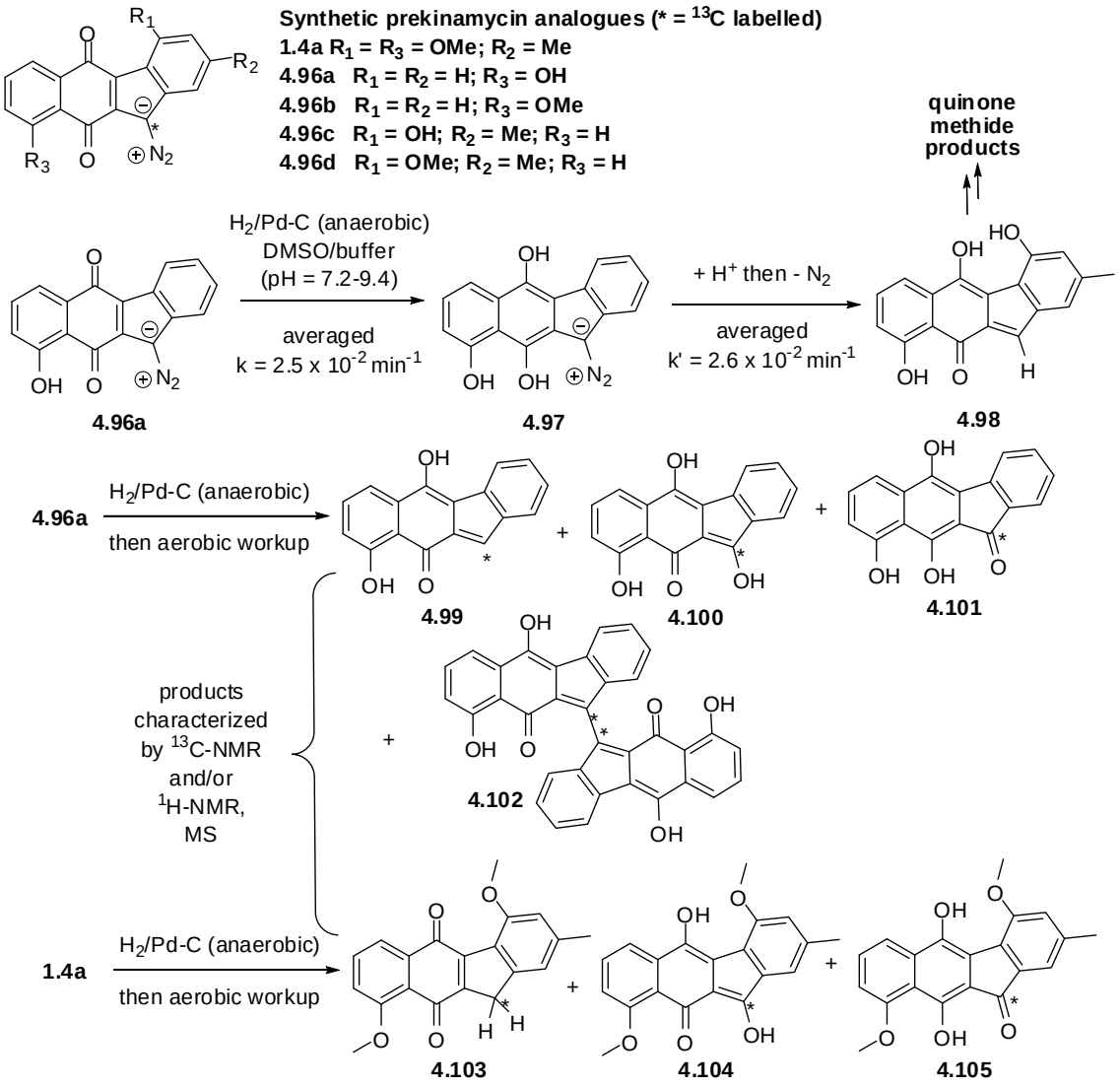

Scheme 4-12. Experimental results by Skibo and co-worker in support of the proposed two electron reduction mechanism for the kinamycins.

The above evidence from kinetic data, UV-vis spectroscopy and product analysis allowed Skibo and Khdour to detect certain intermediates that are reactive and possibly electrophilic, and such observations were suggested to be consistent with the proposed mechanism as shown in Scheme 4-11. It was postulated further, based on some rough MO calculations (only at the HF/3-21G level), that those prekinamycin analogues that favour the quinone methide tautomer over the keto tautomer are more likely to act as electrophiles with DNA bases as nucleophilic partners in conjugate addition reactions, thus having higher bioactivity. Such alkylated DNA was then suggested to be unstable with respect to an elimination reaction that ultimately effects cleavage of the DNA-backbone, thus rationalizing anticancer and antimicrobial activity on the basis of bioreductive activation of the prekinamycin system in vivo to create electrophilic species that can alkylate DNA leading eventually to sufficient damage to induce cell death.

There are a number of interesting, but somewhat troubling, aspects to the proposal by the Skibo group in regard to the mode-of-action of prekinamycin (**1.4**) and, by implication, of the kinamycins (**1.1**–**1.3**), the lomaiviticins (**1.11**) and isoprekinamycin (**1.5**). In the case of isoprekinamycin (**1.5**), hydrodediazoniation following Skibo's pathway would yield an aromatic system (cf. structure **4.50** in Scheme 4-6) rather than an *ortho*-quinone methide so that such a mechanism can not be operative. Thus, to accept the Skibo proposal for biological activity, one needs to assume that, isoprekinamycin (**1.5**) and prekinamycin (**1.4**) must act by different mechanisms despite their high structural similarity.

The Skibo mechanism also invoked an unusually high basicity for the oxygen atom of the ketone carbonyl group (pKa of approximately 6–7), wherein the non-protonated *ortho*-quinone methide such as **4.106** was argued to be unreactive as an electrophile and must first be *O*-protonated to form a cation **4.107** (Scheme 4-13a), which was proposed to be the reactive alkylating agent for DNA or other biological targets. On the other hand, Skibo also predicted a pKa > 8 for the enolic OH to

explain the lack of reactivity of the quinone methide **4.106** observed at pH > 9, and the corresponding enolate **4.108** was considered electron-rich enough to resist nucleophilic attack (Scheme 4-13a). Why such a carbonyl group would be so basic is not only unclear (Skibo offered no explanation at all) but also confusing, since protonated carbonyl species (>C=O^+–H) typically have negative pKa values suggesting such carbonyl oxygens are generally very weak bases. Interestingly, in the case of the natural product momofulvenones **1.14** incorporating an *ortho*-quinone methide system of the same type invoked by the Skibo group, the enolic OH is so acidic that the compounds actually exist in the corresponding conjugated base form at physiological pHs (Scheme 4-13b).[54] Such known experimental observations disfavour Skibo's argument of the unusually high basicity of the carbonyl oxygen and the relatively low acidity of the enol for the quinone methide. Likewise, the presence of the keto group in the D-ring of the lomaiviticin A (**1.11a**) may cause the corresponding *ortho*-quinone methide **4.109**, generated from **1.11a** by following the Skibo's mechanism, to exist in its deprotonated form (i.e., **4.110**) at pH 7 (Scheme 4-13c), similar to the momofulvenones (Scheme 4-13b). This enolate **4.110** would also make such system unable to function as an electrophile, if following Skibo's judgment for the same type of species of **4.108**. Therefore, the Skibo mechanism for the mode-of-action of prekinamycin (**1.4**) is not suitable to be the mode-of-action for the lomaiviticins, which are known to be very potent anticancer agents.

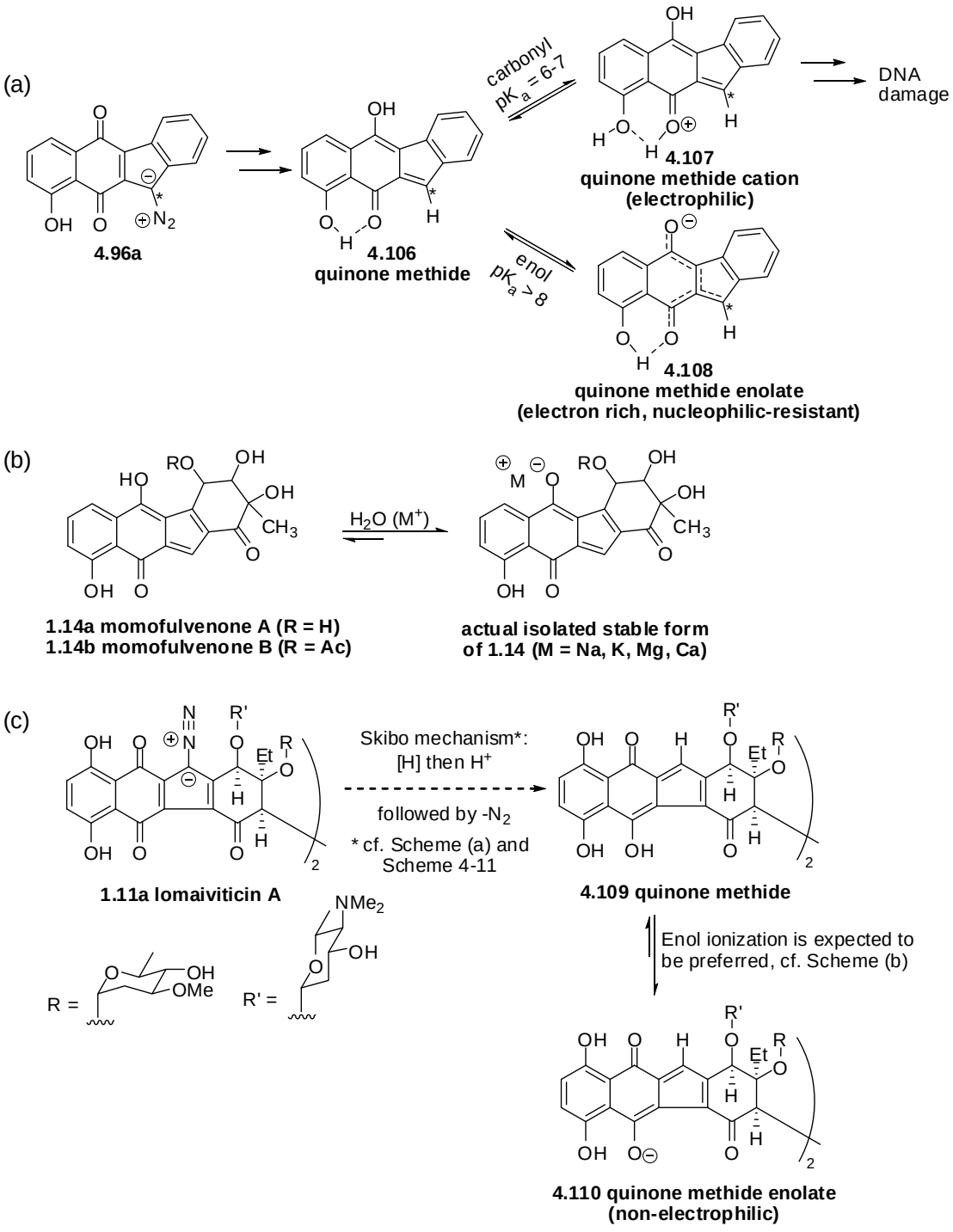

Scheme 4-13. (a) Skibo's argument on the pKa of carbonyl oxygen and phenolic OH of the quinone methide; (b) known acid-base equilibrium of momofulvenones (**1.14**) favouring the enolate; and (c) possible acid-base equilibrium of the quinone methide generated from lomaiviticin A (**1.11a**).

Finally, Skibo's study used H_2/Pd-C in aqueous (DMSO) buffer as the reducing agent for kinamycins in the absence of oxygen (air). Strictly speaking, even though such experimental conditions are probably better choices than Feldman's totally abiological conditions (tinhydride/AIBN/aromatic solvent/high temperature/anaerobic), they are still not ideal imitations of the biological studies of kinamycins that were carried out under not only physiological but also (mostly) aerobic conditions. The limited reducing power of H_2, as judged by its redox potential (i.e., $E_h(H_2/H^+, STP) = 0$ V), is significantly weaker than bio-significant reducing agents such as thiols or NADPH. The common aerobic condition, on the other hand, is in fact rather oxidative due to the presence of O_2 (i.e., $E_h(O_2/H_2O, STP, pH\ 7) = 0.82$ V[350]). This would cause the water that is in contact with air, such as the tap water, to have an E_h in the range of ca. 0.4–0.5 V,[351] which may retard or even prohibit the occurrence of the observed reductive process by Skibo to generate the kinamycin-derived quinone methides. Even if such kinamycin-based quinone methides might form under the aerobic condition in the presence of the reductant and catalyst (H_2/Pd-C), their resistance towards air oxidation is not clear. Therefore, the aerobic condition in the real world poses a serious challenge to Skibo's theory.

A common feature among the above three mechanisms, which were proposed by Feldman, Melander and Skibo respectively, is that an initial but essential one-electron or two-electron reduction of the kinamycin's quinone moiety must occur first prior to any further actions. As pointed out earlier, conclusions under both Feldman and Skibo's reductive conditions have certain flaws to be reasonably extended to explain the mode-of-action of kinamycins in real biological systems. On the other hand, Melander did use mild aerobic and physiological conditions (thiols in aqueous buffers at physiological temperatures and pH) in his study, but the work did not provide any chemical evidence to support the mechanistic proposal. In addition, DTT (**4.2**) and GSH (**4.1**) are not only good reductants as Melander realized (i.e., E_h(DTT/DTT-disulfide, pH 7–10) = -0.4 V;[352] E_h(GSH/GSSG,

pH 7) = -0.24 V and E_h(GSH/GSSG, cells/tissues) = -0.26 – -0.15 V[353,354]), but such thiols are also strong nucleophiles and the fact that they co-exist with a good electrophilic site (i.e., the diazo group within the kinamycins) is entirely ignored by Melander. In fact, all these reductive modes-of-action of kinamycins face a very tough argument, as Melander has observed that the strong and bio-significant reductant NADPH is not capable of inducing kinD (**1.1d**) to cleave DNA at all.[307] This result casts doubt in the validity of the various reductive mechanisms for kinamycins, since NADPH is much stronger than GSH (**4.1**) and equivalent to DTT (**4.2**) in terms of reducing power (i.e., E_h(NADPH/NADP$^+$) = -0.4 V), and it is the actual reductant involved in the GSH/GSSG redox cycle in living organisms through a NADPH-dependent reductase.[353] It is even more interesting to notice that, when Melander compared DTT (**4.1**) and GSH (**4.1**) side by side, even at a 10-times higher concentration of DTT (**4.2**) than GSH (**4.1**) under otherwise identical conditions, the much stronger reductant of DTT (**4.2**) with higher concentration demonstrated only marginally better performance of DNA cleavage than the weaker competitor of GSH (**4.1**) at lower concentration.[307] The observed minimal difference in DNA cleavage activity does not seem to be reasonably proportional to the significant difference of redox potentials between these two thiols, if assuming the DNA cleavage by kinamycins indeed occurs initially through the quinone reduction. Not to mention that DTT (**4.2**) is much smaller in size than GSH (**4.1**) thus kinetically, the former is expected to reduce the kinamycins easier and faster, and DTT (**4.2**) also doubles the available reductive sites (–SH group) per molecule when compared to GSH (**4.1**).

More importantly, the observed mass spectrometric evidence from this thesis work (section 4.2.1) strongly disfavours these quinone reduction speculations in the literature. The thiol GSH (**4.1**) used in this mechanistic study was chosen by the Dmitrienko group for its strong nucleophilicity and bio-significance, but the good reducing power of this thiol was also considered. If GSH (**4.1**) preferentially acts as a quinone reductant rather than being a nucleophile for the diazo moiety towards

the kinamycins (Scheme 4-14), then the B-ring quinone of kinF (**1.1f**) might be reduced to the corresponding semi-quinone radical form **4.111** (by following Feldman's one-electron reduction pathway) or dihydroxyquinone form **4.112** (by following Melander/Skibo's two-electron reduction pathway). It is not unreasonable to expect that, based on the structural similarity, these possible initial products derived from kinF (**1.1f**) should be observed as either the protonated or Li^+-complexed ion species under the +ESI-MS conditions involved. However, mass peaks with the expected *m/z* for such ion species (Scheme 4-14) were never observed in this thesis work. Instead, covalently bonded kinF-GSH adduct **4.18** was spectrometrically observed as the corresponding protonated form. This clearly suggests that the first and key step, prior to any later actions of kinamycins, is a nucleophilic attack at the diazo moiety by the thiols rather than quinone reduction despite their good reducing power. Since the (in vitro) mechanistic studies of this thesis work were carried out under aerobic and physiological conditions (see section 4.7 for details) in the presence of a bio-significant thiol, the chemical behaviour of kinamycins observed under such control should be very close to the actual mode-of-action of kinamycins in the real biological systems (in vivo).

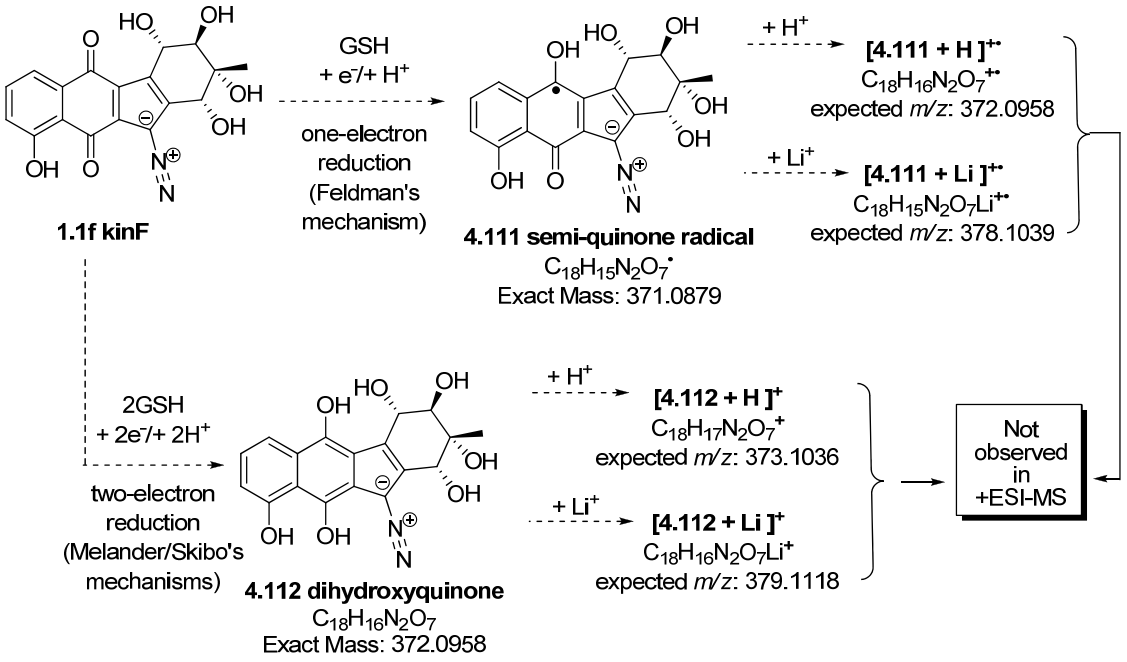

Scheme 4-14. Possible products and +ESI-MS ion species derived from kinF (**1.1f**) by following two quinone reductive activation processes for kinamycins proposed in the literature.

Even though this thesis work does not exclude the possibility that a quinone reductive activation might be involved, the results did suggest that the kinamycin quinone reduction needs some very strong reductant under the physiological and aerobic conditions. This is quite different from observations of kinamycin quinone reduction by certain non-bio-significant/bio-relevant chemical reductants under the abiological/anaerobic conditions, such as the Feldman's and Skibo's discovery. Under the physiological and aerobic conditions, the required power to smoothly reduce the quinone moiety of the kinamycins is definitely beyond the capability of GSH (**4.1**, E_h(cells/tissues) = -0.26 – -0.15 V[353,354]), or even NADPH (E_h = -0.4 V[353]) and DTT (**4.2**, E_h(pH 7–10) = -0.4 V[352]). From a practical point of view, such redox requirement (E_h < -0.4 V) is also beyond the reducing power of many biological systems. For example, blood under low oxygen pressure (55–32 mm Hg, cf.

P_{oxygen}(air) ~ 160 mm Hg) has an E_h of ca. -0.062 – -0.102 V, and even in the complete absence of oxygen, E_h of blood would drop to -0.202 – -0.416 V (depending on the time of equilibrium after deoxygenation),[355] which is at most comparable to the redox potential of NADPH and DTT (**4.2**). Another example is bacteria, some of which are important targets of the kinamycin antibiotics, and the bacteria's range of E_h generally varies from -0.4 V for anaerobes to 0.3 V for aerobes.[356] Thus, it is reasonable to predict that the quinone of kinamycin is unlikely to be reduced in vivo either, particularly under aerobic conditions. Such prediction is also consistent with the literature report that GSH (**4.1**) can not reduce the α-tocopherol quinone **4.113**, under the aerobic and physiological conditions, both in aqueous buffer (pH 7.4) and in rat liver microsome.[357] This quinone **4.113** is in fact the oxidized form of Vitamin E and has a fairly high E_h of -0.48 V at pH 7.[358] It could serve as a model for the B-ring quinone moiety of kinamycin, whose redox potential is not known. In case if one argues that the quinone moiety of kinamycin is fused with two aromatic rings so the tetra-alkylated quinone model **4.113** may not be electronically appropriate, anthraquinones such as **4.114** can be used as an alternative model, which also has a comparable high E_h of -0.527 V at pH 7.[352] Either way, such literature examples are in support of the proposal that reduction of kinamycin quinone does require very strong reducing agents, which are very likely not available in real biological systems. Thus, the reductive modes-of-action for kinamycins are likely not involved in the action of their bioactivity under the physiological conditions.

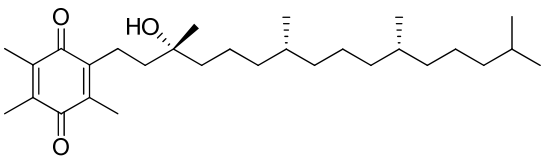

4.113 α-tocopherol quinone (oxidized Vitamin E)

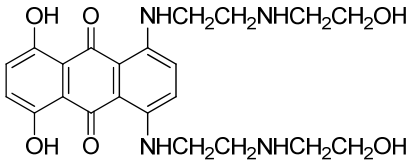

4.114 substituted anthraquinone

4.3 NMR Studies on the Interaction of Kinamycin F and Double-stranded DNA

Upon the collaboration between the Dmitrienko group and the Hasinoff group, weak binding of kinF (**1.1f**) to DNAs had been confirmed by evidence from UV-vis spectroscopy, DNA melting experiments and fluorescence spectroscopy.[241] It was further proposed by Dmitrienko and Hasinoff that the fairly planar structure of kinF (**1.1f**), similar to that of anthracycline antitumor drugs such as doxorubicin and daunomycin, might also be able to intercalate with the DNA base pairs.[241] This hypothesis was supported by some molecular modeling results, as calculations with the docking program GOLD (Genetic Optimisation for Ligand Docking) predicted that kinF (**1.1f**) could intercalate with model DNA at least from a steric point of view (Figure 4-17).[241] The model DNA was deduced from a doxorubicin-DNA X-ray structure (PDB ID: 1DA9) having two doxorubicin molecules bound to the self-complementary DNA of d(TGGCCA), and one doxorubicin was removed to make the space available for docking kinF (**1.1f**) computationally. The D-ring of kinF (**1.1f**) could adopt two different conformations (see section 2.3 for details), and both conformations dock well in the model DNA but in opposite orientations (ca. 180 degree rotation along the long axis of kinF). Figure 4-17 illustrated the simulated result of docking conformer **A** of kinF (**1.1f**) having an equatorial C4-OH into the model DNA, and such intercalation would be stabilized through hydrogen bonding of the C1-OH and C2-OH on the six-membered D-ring of kinF (**1.1f**) to DNA as well as base(π)-stacking. However, the conformer **A** of kinF (**1.1f**) having an equatorial C4-OH, which happens to be the more stable one and also higher in diazonium ion character, scored better than the corresponding C4-axial conformer **B** in the docking simulations.[241]

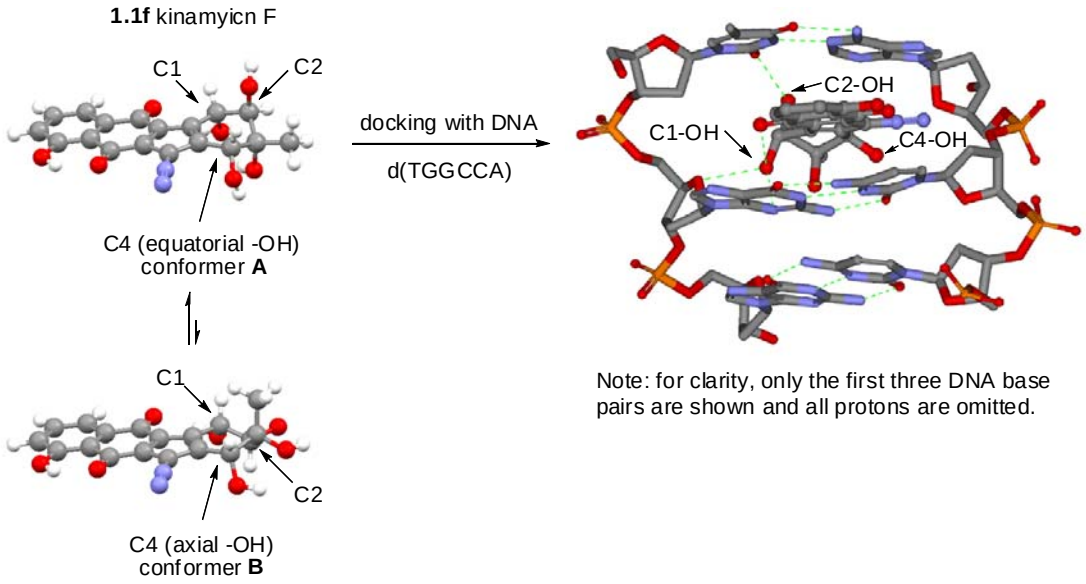

Figure 4-17. Docking of kinF (**1.1f**) into a model DNA d(TGGCCA).[241]

Earlier studies on the cleavage of DNA by kinF (**1.1f**) in the presence of GSH (**4.1**) was performed with large and various DNAs in a very complex plasmid or bioassay,[241] and it was practically impossible to determine the exact spot where the drug (kinamycin) interacts with the DNA under such conditions. Therefore, it was expected that exploration of interactions between kinF (**1.1f**) and a short/simple DNA fragment might be able to pinpoint the specific binding/interacting site. To study the drug-DNA interactions, one of the most powerful and commonly used methods is NMR spectroscopy, since ^{1}H, ^{13}C, ^{15}N and ^{31}P are all present in the DNAs. Changes in the corresponding NMR chemical shifts, coupling constants, splitting patterns and other NMR behaviours in between the free DNA/drug and the DNA-drug complex, which are quite significant in most cases, would be clear indications and precise measurements to reflect such drug-DNA interactions.[359]

In this study, a self complementary double-stranded DNA with the particular sequence of 5'-d(CGTACG) was custom synthesized commercially for the project. This dsDNA was used to react with kinF (**1.1f**) at room temperature in an aqueous solution (H_2O:D_2O (9:1, v/v), 100 mM NaCl,

sodium phosphate buffer, pH 6.2), with a small amount of MeOD-d4 (5% by volume) as the co-solvent. Without the presence of GSH (**4.1**), when kinF (**1.1f**) was mixed with the above dsDNA in a molar ratio of 1:2, neither immediate binding nor slow interaction between the kinF (**1.1f**) and the dsDNA could be observed on the corresponding ^{1}H-NMR spectra (Figure 4-18) when the sample was monitored up to 11 days, since the entire proton signals for both the DNA and kinF (**1.1f**) showed essentially no change at all during the whole process. Upon addition of one equivalent of GSH (**4.1**) to the above aqueous NMR sample ([kinF]:[GSH]:[dsDNA]=1:1:2), a small change in chemical shifts was observed in the ^{1}H-NMR region of 12.5–13.5 ppm (Figure 4-18, bottom spectrum), which corresponded to the hydrogen-bonded imino protons of the DNA bases of guanine (G) and thymine (T). The magnitude of the observed change in chemical shifts (only ca. 0.05 ppm), however, was way less than what would be expected if significant or strong interaction between kinF (**1.1f**) and the dsDNA indeed occur. As a comparison, literature results indicated that binding of various antitumor drugs with DNA even at lower drug to DNA ratio from 1:50 to 1:3 (relative to the 1:2 ratio between kinF (**1.1f**) and DNA used in this study) would cause a significant changes in the chemical shifts for those DNA-imino protons, typically in between 0.1–1 ppm.[360] In addition, the proton signals in the aromatic region for both the kinF (**1.1f**) and DNA bases showed practically no change even after the addition of GSH (**4.1**), which would also suggest that no specific interaction occurred in between kinF (**1.1f**) and this particular DNA. Otherwise some noticeable changes in the chemical shifts of the aromatic protons were very likely to be observed, since intercalation of daunomycin with DNA could lead to about 0.1–0.2 ppm shift for some aromatic protons of both daunomycin and DNA.[361,362]

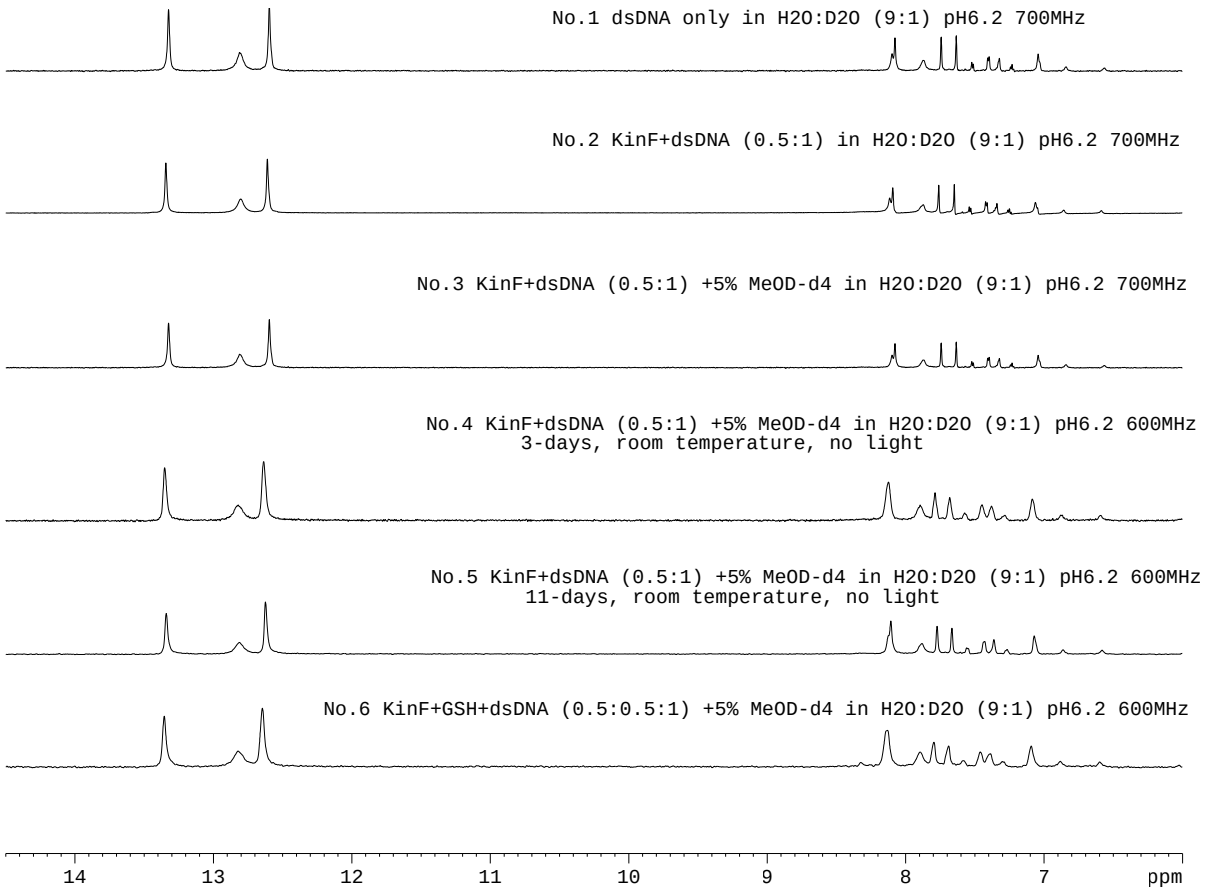

Figure 4-18. Time-resolved NMR spectra of kinF (**1.1f**) and a self complementary dsDNA 5'-d(CGTACG) in aqueous buffer (conditions as marked on each spectrum; for clarity, only the NMR region 6–14 ppm that corresponds to the aromatic and DNA-imino protons is shown).

The above NMR observation, although disappointing, does not necessarily mean that no further experimental and computational attempts should be made. The double-stranded DNA fragments involved in this study (Figure 4-19) such as **4.115** d(TGGCCA) (for modeling) and **4.116** d(CGTACG) (for NMR) did not provide all the possible combinations of having each of the four available DNA-bases (i.e., A, T, C and G) bonded to all other available DNA bases, by which a total of eight different types of spatial cavities in between the two layers of DNA base pairs could be generated. They are marked as (1) to (8) in Figure 4-19. Failure of kinF (**1.1f**) to intercalate/bind with

4.116 would only imply that half of the possible cavities, i.e. (1) to (4) in Figure 4-19, were not suitable for the expected interaction even though some situation such as (2) had been predicted to be feasible by docking simulation. However, double-stranded DNA containing fragments of d(AAG) and d(CCT) such as **4.117** could provide four other possible binding sites (i.e., (5) to (8) in Figure 4-19) that are untested, which may allow the real physical intercalation of DNA by kinF (**1.1f**) to occur. The proposed dsDNA fragment structure such as **4.117** d(AAG···CCT) is not self complementary, which could make its preparation relatively more complicated and difficult. However, simpler and self complementary DNA fragments that can be readily prepared, such as d(AAGCTT), d(CTTAAG), d(GAATTC) and d(TTCGAA) to provide the possible binding site of (5) and (6) as well as d(CCTAGG), d(TCCGGA), d(AGGCCT) and d(GGATCC) to provide the possible binding site of (7) and (8), shall be able to serve as better alternative DNAs to study the interactions with kinF (**1.1f**).

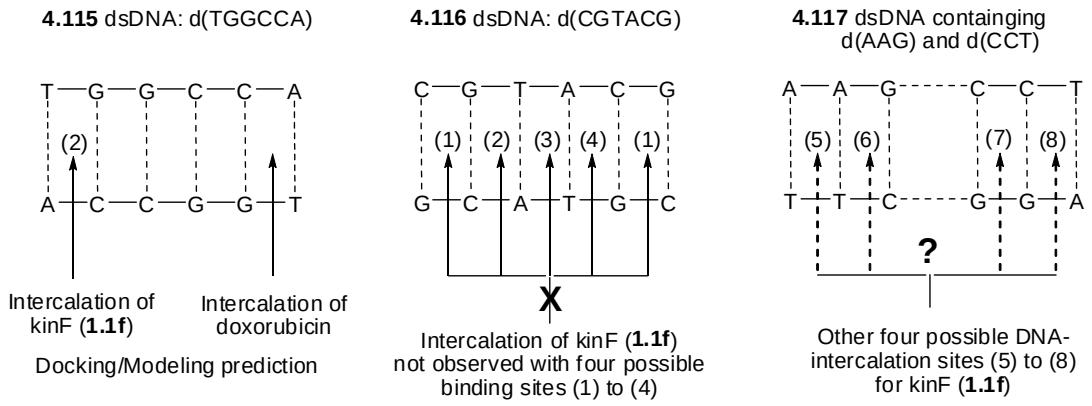

Figure 4-19. Possible binding sites within dsDNA for kinF (**1.1f**).

4.4 Ab initio MO Calculations and Solution IR Studies of Kinamycin F

As described earlier in the thesis (section 2.3), based on NMR spectroscopic observations, the D-ring of kinF (**1.1f**) was found experimentally to adopt two different conformations, and the

corresponding equilibrium showed a clear solvent-dependence, i.e. polar solvent favours the conformation of kinF (**1.1f**) that gives a small NMR coupling constant for the D-ring H1-H2 (Scheme 2-12, section 2.3). However, similar NMR behaviour was never encountered with other kinamycins (either literature results or this work). Therefore, quite extensive computational analyses were also carried out in the Dmitrienko group (this work) in hope that such efforts may revealed the origin of this unusual conformational behavior of kinF (**1.1f**). Since kinF (**1.1f**) possesses the most breadth of antibacterial activity of the kinamycin family, and it may be generated from the other kinamycins by esterase action in vivo to function as the actual bioactive growth inhibitory form of these anticancer agents, it is very interesting and essential to understand the influence of such conformational change on the various properties of the molecule, as this may in turn affect their biological activities to a certain extent.

The kinamycins are quite rigid and flat molecules due to their aromatic ABC-rings, and the only flexible part is the non-aromatic D-ring with four oxygen substituents and a (common) methyl group, which can be considered as a fully substituted cyclohexene ring by itself. Similar to the well-known cyclohexane ring system, the unsubstituted cyclohexene ring would also equilibrate in between two half-chair conformations that interconvert via a boat form, but with a much lower free energy barrier of activation ($\Delta G^{\ddagger}$) of about 5.6 kcal/mol (cf. the corresponding $\Delta G^{\ddagger}$ for cyclohexane is ~ 10.1^{solution} or $10.4^{\text{gas-phase}}$ kcal/mol).[363] For substituted cyclohexenes, the two conformations would normally have certain energy difference depending on the orientation of the substituent(s), i.e. ax. (axial) vs eq. (equatorial). However, the values of the free energy difference between these two conformations (ΔG^{0}, also known as the A-value) are significantly smaller (in general) for the cyclohexene system than those found with the cyclohexane system (Table 4-2).

Table 4-2. A-Values for some substituted cyclohexenes and cyclohexanes.

	ΔG^0 (axial-equatorial) (kcal/mol)*		
Substituent	4-substituted cyclohexene	4-substituted 1,2-di-methyl cyclohexene	Mono substituted cyclohexane
F	0.014[a,b]	-	0.276[a,c], 0.25[d]
Cl	0.20[a,b], 0.31[a,e], -0.02[a,f], 0.19[c,g], 0.23[c,h]	0.38[a,e], 0.06[a,f]	0.528[a,c], 0.52[d]
Br	0.077[a,b], 0.2[a,e]	0.30[a,e]	0.476[a,c], 0.48-0.62[d]
I	-0.016[a,b], 0.16[a,e]	0.20[a,e]	0.468[a,c], 0.46[d]
-C≡N	0.15[a,e], 0.02[a,f], -0.15[i,j], 0.1[i,g]	0.14[a,e], 0.14[a,f]	0.24[a,c], 0.20[i,k], 0.44[i,g]
-OH	0.22[a,e]	0.70[a,e]	1.04[a,l], 0.92-0.97[d]
-OTMS	0.31[a,e]	-	-
-OAc	-	-	0.71[d]
$-OCH_3$	-	-	0.75[d]
$-CH_3$	~ 1[m]	-	1.74[d]
$-CH_2CH_3$	-	-	~1.75[d]
$-CH=CH_2$	> 1.0[m,n]	-	1.7[d]
-CHO	0.5[m,o], 0.26[m,p], 0.44[m,q]	-	-
$-CH_2\bullet$	0.17[a], 0[a] (3-substituted)	-	-

*For a given substrate, the ΔG^0 generally shows small (but noticeable in some cases) dependence on the solvent and temperature; a. Taken from reference[364] (and references therein); b. -160 °C in CD_2=CDCl; c. -80 °C in CS_2; d. Taken from reference[365] (and references therein); e. -145 °C in CF_2Cl_2; f. 145 °C in CHF_2Cl; g. 30 °C in CS_2; h. -60 °C in CS_2; i. Taken from reference[366]; j. 75 °C in DMSO-d6; k. 0 °C in CS_2; l. -83 °C in MeOD-d4; m. Taken from reference[367]; n. -133 °C in CF_2Cl_2-CHF_2Cl (1:1); o. room temperature in $CHCl_3$; p. -167 °C in CHF_2Cl; q. -165 °C in CF_2Cl_2.

There is a lack of literature data of A-values for the cyclohexene ring system. It is then necessary to estimate a few such values based on available data and their correlations (Table 4-2), so that a semi-quantitative conformational analysis could be carried out with the kinamycins. For instance, when comparing kinF (**1.1f**) and kinE (**1.1e**) (Figure 4-20), A-values of 0.70 kcal/mol for -OH, 0.71 kcal/mol for -OAc and 1 kcal/mol for $-CH_3$ are used to estimate the approximate free energy difference between the two D-ring conformer **A** (with an equatorial C4-substituent) and **B** (with an

axial C4-substituent). The corresponding ΔG^0 for kinF (**1.1f**) and kinE (**1.1e**) are both about -0.4 kcal/mol, which would indicate that the conformation **B** is slightly more stable than conformation **A**.

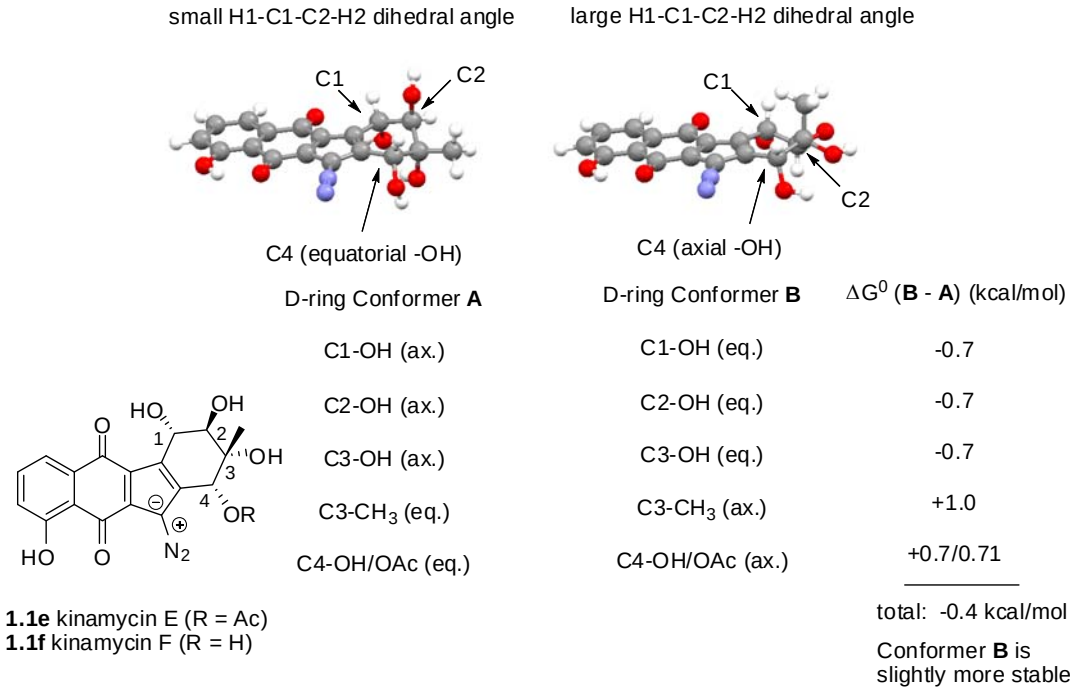

Figure 4-20. Semi-quantitative conformational analysis of kinE (**1.1e**) and kinF (**1.1f**).

Even though the above prediction is consistent with the known facts that (i) compared with the conformation **A**, the conformation **B** possess a significantly larger dihedral angle for the D-ring H1-C1-C2-H2 matching the observed normal NMR coupling constants (6–9 Hz) for all other kinamycins except kinF (**1.1f**) and (ii) the conformation **B** had been confirmed by X-ray crystallographic results of several natural kinamycin derivatives to be the actual situation in the solid state; however, the prediction would be exactly the opposite to what was suggested by the observed NMR results of kinF (**1.1f**). In this case, the conformer **A** of kinF (**1.1f**) is much more favoured by polar solvents, indicating the presence of likely other interacting factors that greatly promote kinF (**1.1f**) to behave differently, which is obviously not covered by the above analysis since it only considered the energy difference caused by variation of the substituents' orientation due to the D-ring conformational

change. The additional interacting factors may include intramolecular hydrogen bonding and possible interactions from the C4-substituent towards the nearby C5-diazo group, both of which can be affected by the D-ring conformation.

Ab initio molecular orbital (MO) calculations, on the other hand, would be able to afford a quantitative and much more precise prediction of the thermodynamics (stability), geometry (bond length and bond angle) and spectroscopic behaviour of the compounds of interest. Gas phase MO calculations (geometry optimization and frequency calculation) of kinF (**1.1f**) carried out using the Gaussian03® program at the RHF/6-31G//6-31G level predict that the corresponding **A**-type conformer (eq. C4-OH) is favored by 0.4 kcal/mol (Table 4-3). A similar computational study of kinE (**1.1e**) reveals an opposite but substantial preference of the **B**-type conformation (ax. C4-OAc) that is favoured by 4.8 kcal/mol (Table 4-3), which is in parallel with the experimental data for this and other kinamycins but in contrast with the conformational preference found for kinF (**1.1f**).

Table 4-3. Gas phase ab initio MO calculations of kinE (**1.1e**) and kinF (**1.1f**).[a]

	E (RHF) (a.u.)[b]		
	Conformation **A**	Conformation **B**	ΔE (**B** - **A**)
kinE (**1.1e**) 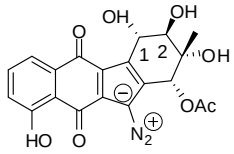	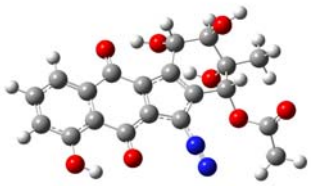 -1473.433862	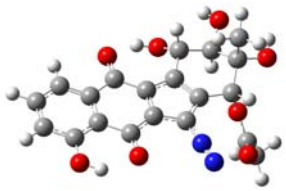 -1473.441514	-0.007652 (-4.8 kcal/mol) Conformer **B** is more stable
kinF (**1.1f**) 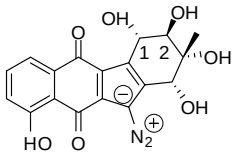	 -1321.773871	 -1321.773242	0.000629 (0.4 kcal/mol) Conformer **A** is more stable

a. Ab initio MO geometry optimization and calculation of vibrational frequencies were performed with Gaussian03® at the RHF/6-31G//6-31G level; b. The E(RHF) (restricted Hartree-Fork energy) was corrected with ZPE (zero-point energy), 1 a.u. = 627.5095 kcal/mol.

Further solution phase MO calculations, employing the PCM (polarizable continuum model) solvation model, showed a preference for the **A**-type conformer of kinF (**1.1f**) increases substantially with the increasing solvent polarity. This is clearly indicated by the concurrent increasing change in free energy of solvation ($\Delta\Delta G_{solvation}$ = 3.4, 5.3 and 12.4 kcal/mol for $CHCl_3$, acetone and DMSO respectively, Table 4-4) between the two conformers, which takes into account the contributions from both the electrostatic and non-electrostatic factors. Unfortunately, similar calculations with kinE (**1.1e**) in identical solvents failed unexpectedly, particularly with its less-favoured conformation **A**, and led to no useful data for comparison (Table 4-4). In addition, the calculated dipole moments for the two conformers of kinF (**1.1f**), in both gas phase and solutions (Table 4-4), also showed a

consistent increasing tendency along with the increasing medium/solvent polarity (as indicated by the corresponding dielectric constant ε). The (much) higher dipole moment was always associated with the conformer **A**, which would also suggest its preference in more polar environment. On the contrary, for kinE (**1.1e**) in gas phase, the more stable conformer **B** (0.7316 Debye) is also much more polar than its competitor conformer **A** (0.2925 Debye).

Table 4-4. Ab initio MO calculations of kinF (**1.1f**) and kinE (**1.1e**) in various solvents.[a]

kinF (**1.1f**): conformation **A** is more stable than **B** by 0.4 kcal/mol (gas phase)			
Solvent	$\Delta G_{solvation}$ (kcal/mol)		$\Delta\Delta G_{solvation}$ (**B** - **A**)[b] (kcal/mol)
	Conformation **A**	Conformation **B**	
$CHCl_3$	-13.53	-10.13	3.4
Acetone	-25.9	-20.62	5.3
DMSO	-30.62	-18.26	12.4
Solvent (ε)	Dipole Moment μ (Debye)		
	Conformation **A**	Conformation **B**	
Gas phase (0)	3.1963	2.1963	
$CHCl_3$ (5)	4.6083	2.7730	
Acetone (21)	5.0711	3.2696	
DMSO (49)	7.9513	3.4780	
kinE (**1.1e**): conformation **B** is more stable than **A** by 4.8 kcal/mol (gas phase)			
Solvent	$\Delta G_{solvation}$ (kcal/mol)		$\Delta\Delta G_{solvation}$ (**B** - **A**) (kcal/mol)
	Conformation **A**	Conformation **B**	
$CHCl_3$	-9.81	-[c]	-
Acetone	-[c]	-17.99	-
DMSO	-[c]	-14.44	-

a. Ab initio MO calculations were performed with Gaussian03® at the RHF/6-31G//6-31G level, PCM (polarizable continuum model) solvation model was used for solution phase modeling; b. Values are rounded to one decimal point; c. MO calculations failed even after several attempts.

Furthermore, it appears that there is some influence from the conformational preferences for D-ring of kinF (**1.1f**) on the diazonium ion character of the diazo group, which can be characterized by

its corresponding IR stretching frequency (and diazo bond length). Ab initio MO calculations overestimate the absolute values for the diazo (and other) stretching frequencies, even after these calculated raw frequency values had already been corrected with an empirical scaling factor (i.e., 0.8929) to account for systematic errors originated from the neglect of electron correlation. However, the significant difference in calculated diazo IR frequency for the two conformers of kinF (**1.1f**), i.e. $\nu_{N\equiv N}$(conformer **A**) = 2206 cm^{-1} and $\nu_{N\equiv N}$(conformer **B**) = 2183 cm^{-1}, is quite surprising.

A solution IR study of kinF (**1.1f**) was carried out in various solvents and the corresponding results, as summarized in Table 4-5, revealed more physical evidence to support the above theoretical predictions. The diazo stretch in the solution IR spectra of kinF (**1.1f**) was observed experimentally (Table 4-5, part II) as two clearly distinguished bands in the very polar and H-bonding solvents such as DMSO (2142 cm^{-1} and 2165 cm^{-1}, $\Delta\nu$ = 23 cm^{-1}) and acetone (2137 cm^{-1} and 2174 cm^{-1}, $\Delta\nu$ = 37 cm^{-1}), which are essentially non-concentration dependent. This is consistent with the proposed co-existence of two conformers of kinF (**1.1f**) having different diazonium ion character in these two solvents. However, in much less polar and non-H-bonding solvents such as MeCN, $CHCl_3$ and CCl_4 (Table 4-5, part I), the corresponding diazo stretching IR signal of kinF (**1.1f**) appeared as essentially one single peak, and the observed frequencies (i.e., 2138–2140 cm^{-1} in MeCN, 2132–2140 cm^{-1} in $CHCl_3$ and 2130 cm^{-1} in CCl_4) are in better agreement with the diazo IR results of kinF (**1.1f**) obtained from the solid-state (i.e., 2142 cm^{-1} in KBr; 2134–2140 cm^{-1} as film on NaCl plate depending on the solvent used to prepare the film), suggesting that the less polar **B**-type conformer of kinF (**1.1f**) with a lower diazo IR frequency predominates in non-polar solvents. The predicted significant preference in polar solvents for conformer **A** of kinF (**1.1f**) is also entirely consistent with the previous NMR findings (i.e., the observed D-ring H1-H2 coupling constant of kinF (**1.1f**) is inversely proportional to the solvent polarity involved, Table 2-4, section 2.3). The more polar conformer **A** of kinF (**1.1f**) has a calculated small dihedral angle of 75° for H1-C1-C2-H2 (close to

90°), which should give a rather small NMR coupling constant as estimated by the Karplus equation. As a comparison, the corresponding dihedral angle is 171° (close to 180°) within the conformer **B**, which shall lead to a normal (large) proton coupling constant.

It is very interesting to notice that in the case of using MeOH as the solvent (Table 4-5, part II), a gradual shift of the diazo IR signal of kinF (**1.1f**) from 2142 cm^{-1} to 2170 cm^{-1} ($\Delta\nu$ = 28 cm^{-1}) was observed upon dilution of the kinF-MeOH solution, which appeared as a broad peak (an intermediate situation in between a single peak and two bands) during the entire shifting process. It is very likely that the two conformers of kinF (**1.1f**) also equilibrate within MeOH, similar to the situation observed with DMSO and acetone. In the mean time, the strong and bidirectional hydrogen bonding capability of MeOH and kinF (**1.1f**), i.e. both species can act inter- and intramolecularly as a H-bond donor and/or acceptor while DMSO/acetone can only behave as a hydrogen bond acceptor, would complicate the various interactions between the solvent (MeOH) and solute (kinF) as well as the appearance of the IR spectra, hence the observed broad diazo IR peak and the concentration-dependent diazo IR shift.

The predicted $\Delta\nu$ of 23 cm^{-1} (in gas phase) with the calculated higher stretching frequency being associated with the conformer **A**, agrees pretty well with the difference between the two solution IR bands observed for the diazo group of kinF (**1.1f**) in solutions ($\Delta\nu$ = 23 cm^{-1} in DMSO and $\Delta\nu$ = 37 cm^{-1} in acetone, Table 4-5). It is also noteworthy that the calculated diazo IR frequencies for the two conformers of kinF (**1.1f**) in DMSO and acetone (Table 4-6), even though giving a smaller calculated $\Delta\nu$ between the two conformers when compared with the experimental values in each case, do show a consistency with the experimental observation that acetone induces larger change in diazo IR frequency than DMSO.

Table 4-5 (part I). Diazo IR frequency of kinF (**1.1f**) in organic solvents.[a]

IR sample No.[b]	[kinF][c]	Solvent	$\nu_{N\equiv N}$ (cm^{-1})[d]
CNIR0037	C_0 Saturated stock solution[e]	CCl_4	2130 (w)
CNIR0041	C_1 Saturated stock solution	$CHCl_3$	2132 (w)
CNIR0042	$0.2C_1$ 5x dilution of stock	$CHCl_3$	2139 (w, br)
CNIR0043	$0.1C_1$ 10x dilution of stock	$CHCl_3$	2137 (w)
CNIR0044	$0.04C_1$ 5x dilution of CNIR0042	$CHCl_3$	2136 (w, noisy)
CNIR0045	$0.02C_1$ 5x dilution of CNIR0043	$CHCl_3$	2135–2140 (very w, noisy)
CNIR0032	C_2 Saturated stock solution	MeCN	2140
CNIR0033	$0.2C_2$ 5x dilution of stock	MeCN	2138
CNIR0034	$0.04C_2$ 25x dilution of stock	MeCN	2139 (w)

a. See section 4.7 for experimental details; b. IR spectra were recorded consecutively in the numeric order as indicated by the sample's No., however, IR results were tabulated and presented in the increasing order of solvent polarity, and for each individual solvent, data were listed in the descending order of substrate concentration; c. The concentration of kinF (**1.1f**) in solutions had no actual values since each stock solution was prepared with a very small amount of kinF (ca. 0.1–0.2 mg or less). In case a saturated stock solution was made, excess kinF (**1.1f**) was mixed with a small volume of solvent and quickly sonicated to ensure complete saturation of the solvent by kinF (**1.1f**). The saturated stock solution was then filtered to remove the undissolved substrate; d. All IR wavenumbers were rounded to the closest integer. w = weak, br = broad; e. solubility of kinF (**1.1f**) in CCl_4 was extremely low and there were still visible and very fine solid particles of kinF (**1.1f**) in the solution even after sonication, which was used directly for the IR study without filtration.

Table 4-5 (part II). Diazo IR frequency of kinF (**1.1f**) in organic solvents.[a]

IR sample No.[b]	[kinF][c]	Solvent	$\nu_{N\equiv N}$ (cm^{-1})[d]	$\Delta\nu$ (cm^{-1})
CNIR0023	$3.0C_3$ 3x concentration of stock	MeOH	2142	-
CNIR0020	C_3 (Stock solution)	MeOH	2142	-
CNIR0021	$0.2C_3$ 5x dilution of stock	MeOH	2148 (w, br)	-
CNIR0027	$0.1C_3$ concentration of CNIR0025	MeOH	2159 (very br)	-
CNIR0025	$0.04C_3$ concentration of CNIR0024	MeOH	2169 (br)	-
CNIR0024	$0.02C_3$ 50x dilution of stock	MeOH	2170 (w, br)	-
CNIR0071	C_4 Saturated stock solution	Acetone	2138 2173	35
CNIR0063	$0.2C_5$ 5x dilution of stock	Acetone	2136 2174	38
CNIR0065	$0.1C_5$ 10x dilution of stock	Acetone	2137 2174	37
CNIR0067	$0.04C_5$ 5x dilution of CNIR0063	Acetone	2135 2174	39
CNIR0069	$0.02C_5$ 5x dilution of CNIR0065	Acetone	2136 2173	37
CNIR0049	C_5 (stock solution)	DMSO	2145 (br)	-
CNIR0050	$0.2C_5$ 5x dilution of stock	DMSO	2142 2165	23
CNIR0052	$0.1C_5$ 10x dilution of stock	DMSO	2142 2165	23
CNIR0054	$0.04C_5$ 5x dilution of CNIR0050	DMSO	2142 2165	23
CNIR0056	$0.02C_5$ 5x dilution of CNIR0052	DMSO	2142 2165	23

Table 4-6. Calculated diazo IR frequency and bond length of kinF (**1.1f**) in gas phase and solutions.[a]

Solvent	Conformer **A** of kinF (**1.1f**)	Conformer **B** of kinF (**1.1f**)	$\Delta\nu_{N\equiv N}$ (cm^{-1})
Gas phase	$\nu_{N\equiv N}$[b]: 2206 cm^{-1}; $d_{N\equiv N}$: 1.098 Å	$\nu_{N\equiv N}$[b]: 2183 cm^{-1}; $d_{N\equiv N}$:1.100 Å	23
$CHCl_3$	$\nu_{N\equiv N}$[b]: 2225 cm^{-1}; $d_{N\equiv N}$: 1.095 Å	$\nu_{N\equiv N}$[b]: 2197 cm^{-1}; $d_{N\equiv N}$:1.098 Å	28 (not observed)
Acetone	$\nu_{N\equiv N}$[b]: 2229 cm^{-1}; $d_{N\equiv N}$: 1.095 Å	$\nu_{N\equiv N}$[b]: 2206 cm^{-1}; $d_{N\equiv N}$:1.097 Å	23 (observed 37)
DMSO	$\nu_{N\equiv N}$[b]: 2216 cm^{-1}; $d_{N\equiv N}$: 1.096 Å	$\nu_{N\equiv N}$[b]: 2210 cm^{-1}; $d_{N\equiv N}$:1.096 Å	6 (observed 23)

a. Ab initio MO geometry optimization and vibrational frequency calculation were performed with Gaussian03® at the RHF/6-31G//6-31G level, PCM (polarizable continuum model) solvation model was used for solution phase modeling; b. Scaled by the scaling factor of 0.8929.

These observations suggest that some specific interaction of the diazo group, which is absent in the D-ring model compound of kinF (**1.1f**) such as the simple aromatic tetrol **2.59** that showed no conformational change in different (NMR) solvents (Table 2-3, section 2.3), might be responsible for the preference for the equatorial orientation of the C4-OH group in kinF (**1.1f**) as observed in its calculated conformation **A**. Further ab initio molecular orbital calculations on simpler models **4.118** (Figure 4-21) led to the initial suggestion that the effect on diazonium ion character may be a consequence of a favorable through space interaction of the C4-O bond dipole with the oppositely polarized C5-N bond dipole of the diazo group, which is enhanced when the two bond dipoles (C4→O/C5←N) are aligned. The triatomic link $-C^{-}-N^{+}\equiv N$ of kinamycins exists within the flat plane as defined by the aromatic ABC-rings, as confirmed by several X-ray works and many MO calculation results from this work. A good alignment between the two nearby polar bonds of C4-O and C5-N would only be achieved if the C4-OH occupies the equatorial orientation, while the axial C4-OH conformer would almost completely lose such energetically beneficial interaction due to the near perpendicular correlation of the C4-substituent with the ring plane and C5-N bond. This is clearly indicated by the calculated small dihedral angle of ca. 36.7° for O-C4-C5-N within conformer **A** of kinF (**1.1f**), relative to a much larger dihedral angle of ca. 60.2° for O-C4-C5-N within conformer **B** of kinF (**1.1f**).

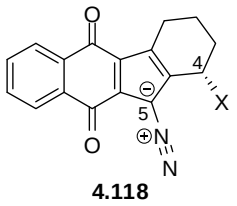

4.118

X (equatorial) =	H	OAc	F	OH
$\nu_{N\text{-}N}$ (cm^{-1})	2104	2123	2158	2173
$d_{N\text{-}N}$ (Å)	1.107	1.105	1.102	1.100

Figure 4-21. Calculated diazo IR stretching frequencies and N≡N bond lengths (RHF/6-31G//6-31G) for the proposed simple kinamycin analogue **4.118** with different equatorial C4-substituents.

However, subsequent MO calculations on isoprekinamycin analogues, which are to be described in Chapter 5, have led to the conclusion that a through-space interaction of an electron-rich heteroatom at C4 with the C5-diazo group might be the major cause of the increase in diazonium ion character. Further discussion is provided in Chapter 5.

The significant influence from a simple D-ring conformational change on the diazonium character of kinF (**1.1f**) might play some important role in the corresponding biological activities of such natural antibiotics, especially when considering the earlier mechanistic studies (section 4.2) indicating the crucial reaction between the bio-significant thiols and kinF (**1.1f**) to involve the very likely attack of the diazo moiety by the sulfur nucleophile. Therefore, the conformer of kinF (**1.1f**) having a diazo group with a higher diazonium ion character and hence higher reactivity, which is favoured by polar solvents, may be the bioactive form.

4.5 Investigation of Intramolecular H-bonds within Diazobenzo[*b*]fluorenes

The common presence of strong intramolecular H-bonds within the diazobenzo[*b*]fluorene type of kinamycins in between their C7-OH and C6-O as well as C1-OH and C11-O is well known. This is characterized by the unusually high NMR chemical shifts of such H-bonded phenolic and alcoholic protons[9] and is supported by some unambiguous evidence from X-ray crystallographic studies.[21]

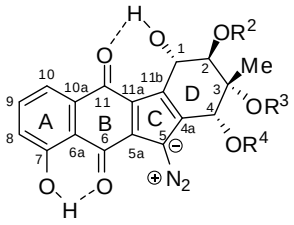

Previous MO calculations carried out by Laufer in the Dmitrienko group (unpublished results) indicate that such intramolecular H-bonding interactions within a diazobenzo[*b*]fluorene structure will increase the diazonium ion character but only to a rather small extent (Table 4-7).[80]

Table 4-7. Calculated diazo IR frequencies and bond lengths of some diazobenzo[*b*]fluorenes.[a]

Compound	$\nu_{N\equiv N}$ (cm^{-1})[b]	$d_{N\equiv N}$ (Å)	Compound	$\nu_{N\equiv N}$ (cm^{-1})[b]	$d_{N\equiv N}$ (Å)
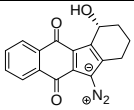 **4.119**	2120	1.105(9)	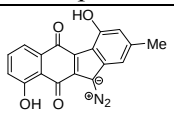 **1.4**	2058	1.111
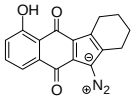 **4.120**	2116	1.106(3)	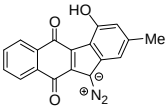 **4.123**	2060	1.111(6)
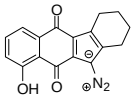 **4.121**	2113	1.106(5)	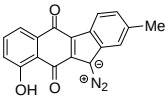 **4.124**	2050	1.112(8)
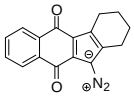 **4.122**	2104	1.107	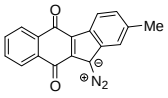 **4.125**	2044	1.113

a. From R. Laufer's thesis,[80] ab initio MO geometry optimization and IR frequencies of the compounds were performed with Gaussian98® at RHF/6-31G//6-31G level; b. Scaled by a scaling factor of 0.8929.

However, one can easily realize that, the two series of model diazobenzo[*b*]fluorene compounds in Laufer's result (Table 4-7) experience the loss of intramolecular H-bonding interaction upon the gradual removal/relocation of hydroxy group(s) (e.g., from **4.119** to **4.122** and from **1.4** to **4.123**–**4.125**). Thus, the concurrent presence of a substituent effect (i.e., replacement of –OHs by –Hs) is unavoidable, and consequently the corresponding change in the calculated diazo IR frequencies

would be an overall result of the combined two effects (i.e., presence/absence of intramolecular H-bonding and substituent effect) that can not be clearly distinguished. Therefore, ab initio MO calculations with two representative natural diazobenzo[*b*]fluorene type of kinamycins (this work), namely the kinD (**1.1d**) and prekinamycin (**1.4**), were carried out with the various possible conformations of these two compounds. While maintaining exactly the same chemical composition and substituent pattern, conformations of both substrates (**1.1d** and **1.4**) that lack the intramolecular H-bond(s) were subjected to the computation. These results, as summarized in Table 4-8 (for **1.1d**) and Table 4-10 (for **1.4**), provide a better understanding and more precise measurement of the neat influence from the intramolecular H-bonding interaction(s) on the diazonium ion character within the diazobenzo[*b*]fluorenes.

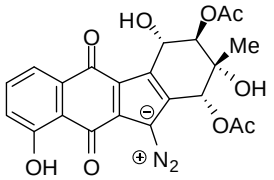

1.1d kinamycin D

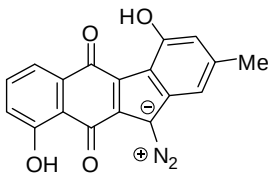

1.4 prekinamycin

Table 4-8. Gas phase MO calculations of kinD (**1.1d**) with different conformations.[a]

Starting geometry of **1.1d** used for MO calculation[b]	Ending geometry of **1.1d** obtained from MO calculation	$\nu_{N\equiv N}$ (cm^{-1})[c] $d_{N\equiv N}$ (Å) E(RHF) (a.u.)[d]
 Starting conformation I	 Ending conformation I	2235 1.095(6) -1625.113881
 Starting conformation II	 Ending conformation II	2230 1.096(0) -1625.093600
 Starting conformation III	 Ending conformation III (identical to I)	2235 1.095(6) -1625.113881
 Starting conformation IV	 Ending conformation IV (identical to II)	2230 1.096(0) -1625.093601

a. Ab initio MO geometry optimization and calculation of vibrational frequencies were performed with Gaussian03® at the RHF/6-31G//6-31G level; b. For kinD (**1.1d**), starting geometry I was modified from the corresponding X-ray results of (+)-α-methylbutryryl kinD (**1.1v**) by adding or removing necessary substituents. Other starting geometries of **1.1d** with intramolecular H-bond(s) missing were obtained upon manual rotation of the phenol or alcohol hydroxy group(s) within the optimized conformation I to "break" the H-bond(s), which were then subjected to MO calculation; c. Scaled by a scaling factor of 0.8929; d. The E(RHF) was corrected with ZPE. 1 a.u. = 627.5095 kcal/mol.

In theory, the C5 partial negative charge of **1.1d** could delocalize, as shown in Scheme 4-15, to either the C6-O (resonance form I) or C11-O (resonance form II) to enhance the corresponding intramolecular A-B ring or B-D ring H-bonding interactions, and the diazonium ion character is simultaneously enhanced due to the decrease of nearby negative charge. However, it can be clearly seen from the above calculation results that the two intramolecular H-bonds within the diazobenzo[*b*]fluorenes are quite different in terms of their effects on the stability and the diazonium ion character of the compound. Relative to the most stable conformation of kinD (**1.1d**) that possesses two intramolecular H-bonds (i.e., conformer I/III), loss of the A-B ring H-bonding interaction between C7-OH and C6-O as in conformation II/IV significantly destabilizes the molecule by 12.7 kcal/mol, but the corresponding diazonium ion character only drops slightly, which is indicated by a concurrent decrease of 5 cm^{-1} in diazo IR frequency. On the other hand, various attempts to "break" the intramolecular B-D ring H-bond between the C1-OH and C11-O all failed (cf. starting and ending conformation I, III and IV, Table 4-8), and the optimized geometry of **1.1d** always ends up with the B-D ring H-bond presenting within the final optimized conformation, regardless of the starting conformation or the status of the A-B ring H-bond. Such observation would suggest that the overall energetic benefit from having a B-D ring H-bond is even larger than the already very strong A-B ring H-bond.

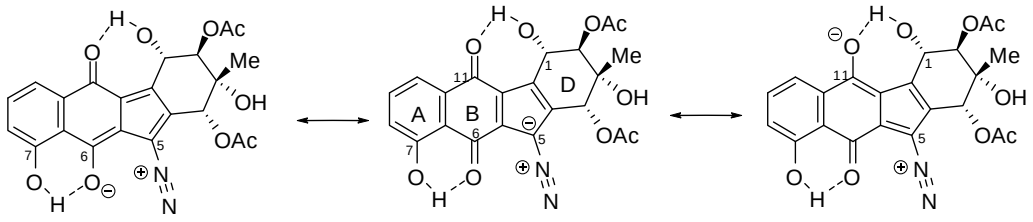

Scheme 4-15. Possible resonance delocalization of C5 negative charge within kinD (**1.1d**).

Although the energy contribution from the B-D ring H-bonding interaction within kinD (**1.1d**) can not be obtained quantitatively, the corresponding influence on the diazonium ion character can be estimated. Obviously, the B-D ring H-bonding interaction within the structure of kinD (**1.1d**) would disappear if the C1-OH group is methylated (i.e., C1-OMe-kinD **4.126**) or acetylated (i.e., C1-OAc-kinD, which is kinC (**1.1c**) indeed). Compounds **4.126** and **1.1c** may represent the situation of kinD (**1.1d**) missing the B-D ring H-bonding interaction and offer some meaningful results for comparison; however, it shall be noted that estimation by this manner would contain some contribution from a substituent effect (i.e., C1-O-**Ac** of **1.1c** vs C1-O-**H** of **1.1d** vs C1-O-**Me** of **4.126**).

MO calculations on the diazo IR frequencies of **1.1c**, **1.1d**, **4.126** and another closely related synthetic analogue **3.176**[24] are summarized in Table 4-9. Even though the calculated absolute values of these diazo IR frequencies are much higher than the corresponding experimental observations, the calculated relative differences between them are in very good agreement with the experimental ones. For example, diazo IR frequencies of **1.1d** and **1.1c** have a calculated difference of 8 cm^{-1} while the experimental difference is 5–7 cm^{-1} (Table 4-9). Comparison between the calculated diazo IR frequencies of **1.1d** (with H-bonded C1-OH, 2235 cm^{-1}), **4.126** (with C1-OMe, 2216 cm^{-1}) and **1.1c** (with C1-OAc, 2227 cm^{-1}) indicates that the influence on the diazonium ion character from the B-D ring H-bond of **1.1d** should be within the range of ca. 8–19 cm^{-1}, since the acetyl group is electron-withdrawing while the methyl is electron-donating when compared to proton. This effect is slightly larger than the corresponding one from the A-B ring H-bond, which reduces the diazo IR frequency by 5 cm^{-1} when the intramolecular A-B ring H-bond is absent (Table 4-8). The noticeable decrease of diazo IR frequency by 11 cm^{-1} from **1.1c** (C1-OAc) to **4.126** (C1-OMe) would suggest a moderate benefit of having some electron-withdrawing factor at the C1 position to enhance the diazonium ion character, presumably through inductive effect that could help to delocalize the C5 negative charge.

Table 4-9. Calculated and experimental diazo IR frequencies of some diazobenzo[*b*]fluorenes.[a]

Compound	$\nu_{N\equiv N}$ (cm^{-1})[b]	$d_{N\equiv N}$ (Å)	Compound	$\nu_{N\equiv N}$ (cm^{-1})[b]	$d_{N\equiv N}$ (Å)
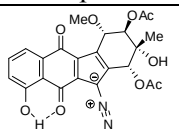 **4.126**	2216	1.097(1)	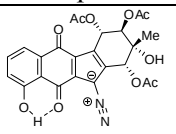 **1.1c**	2227 Expt. 2150[c] Expt. 2148[d]	1.096(3)
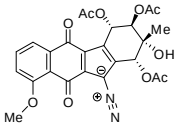 **3.176**	2219 Expt. 2146[e]	1.096(9)	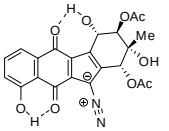 **1.1d** (double H-bonds)	2235 Expt. 2155[f]	1.095(6)
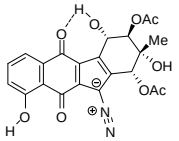 **1.1d** (No A-B ring H-bond)	2230	1.096(0)	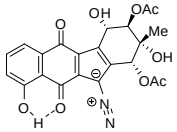 **1.1d** (No B-D ring H-bond)	N/A	N/A
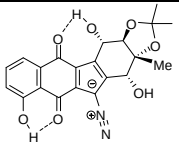 **1.1t**	Expt. 2160[g]	N/A	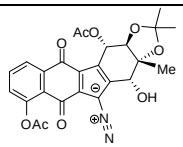 **1.1u**	Expt. 2150[g]	N/A

a. Ab initio MO geometry optimization and vibrational frequencies calculation were performed with Gaussian03® at the RHF/6-31G//6-31G level; b. Scaled by a scaling factor of 0.8929, Expt. refers to experimental IR values; c. Film, from reference[23]; d. Film, from reference[16]; e. Racemic mixture (oil) prepared by total synthesis, IR was measured by means of ATR (attenuated total reflection), from reference[24]; f. In KBr, from reference[78]; g. In KBr, from reference[9].

In addition, compound **3.176** (with C1-OAc and C7-OMe) serves as another good and practical example to demonstrate the effect on the diazonium ion character, either from the double intramolecular H-bonding interactions when compared with **1.1d** (with C1-OH and C7-OH), or from the A-B ring H-bond alone when compared with **1.1c** (with C1-OAc and C7-OH). The calculated decrease of diazo IR frequency are 16 cm^{-1} (**3.176** vs **1.1d**) and 8 cm^{-1} (**3.176** vs **1.1c**) respectively, which are in good agreement with the corresponding experimental values of 9 cm^{-1} (**3.176** vs **1.1d**) and 2–4 cm^{-1} (**3.176** vs **1.1c**). This suggests that the overall combined effect from the double

intramolecular H-bonding interactions on the diazonium ion character within **1.1d** should fall in the range of ca. 8–16 cm^{-1} (theoretical prediction) or 2–9 cm^{-1} (experimental observation). This conclusion is also entirely consistent with (i) the estimated individual H-bonding effect within **1.1d** on its diazonium ion character (i.e., 5 cm^{-1} from the A-B ring H-bond and ~ 8–19 cm^{-1} from the B-D ring H-bond); and (ii) the experimental difference in diazo IR frequencies of 10 cm^{-1} observed for isopropylidenekinamycin C (**1.1t**) and its C1/C7-diacetate **1.1u** (Table 4-9).[9]

When the same MO calculations were carried out with prekinamycin (**1.4**), a diazobenzo[*a*]fluorene but having an aromatic D-ring, the corresponding results (Table 4-10) are even more interesting. The most stable conformation I of **1.4** possessing the double intramolecular H-bonds was used as the starting point, and a gradual loss/breaking of H-bond(s), first with the A-B ring H-bond (conformation II) then the B-D ring H-bond (conformation III) and finally at both H-bonded sites (conformation IV) provided three additional and relatively stable conformations of **1.4** after computation. The stabilities of these conformations decrease in the same consecutive order and the corresponding increase in energy are 12.4, 12.5 and 25.1 kcal/mol, respectively. The last value (25.1 kcal/mol) is very close to the sum of the first two (24.9 kcal/mol), indicating the self-consistency of such MO calculations. The energy contribution of 12.4 kcal/mol due to the presence of the intramolecular A-B ring H-bond of **1.4** is almost identical to the calculated corresponding value for **1.1d** (i.e., 12.7 kcal/mol for its A-B ring H-bond); however, the B-D ring H-bond of **1.4** seems to be much easier to break than that of **1.1d**.

Table 4-10. Gas phase MO calculations of prekinamycin (**1.4**) with different conformations.[a]

Starting geometry of **1.4** used for MO calculation[b]	Ending geometry of **1.4** obtained from MO calculation	$\nu_{N\equiv N}$ (cm^{-1})[c] $d_{N\equiv N}$ (Å) E(RHF) (a.u.)[d]
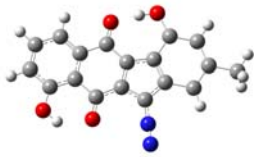 Starting conformation I	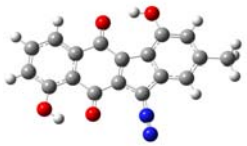 Ending conformation I	2065 1.111 -1095.054362
 Starting conformation II	 Ending conformation II	2071 1.110(5) -1095.034643
 Starting conformation III	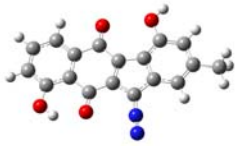 Ending conformation III	2057 1.112 -1095.034486
 Starting conformation IV	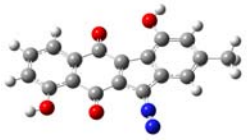 Ending conformation IV	2061 1.111(7) -1095.014427

a. Ab initio MO geometry optimization and vibrational frequency calculation were performed with Gaussian03® at the RHF/6-31G//6-31G level; b. For prekinamycin **1.4**, starting geometries were obtained by modification of other optimized kinamycin conformations upon adding or removing necessary substituents, and its missing of H-bonding was carried out in the same manner as in the case of **1.1d** (see footnote b of Table 4-8); c. The E(RHF) was corrected with ZPE. 1 a.u. = 627.5095 kcal/mol; d. Scaled by a scaling factor of 0.8929.

Even though the different degrees of intramolecular H-bonding interactions within the several conformations of **1.4** have applied an expected effect on the stability of the molecule, the corresponding influence on the diazo IR frequencies is somehow confusing. The highest diazonium ion character of **1.4** (2071 cm^{-1}) comes from the conformation II that lacks A-B ring H-bond only and the lowest diazonium ion character (2057 cm^{-1}) corresponds to the conformation III that lacks the B-D ring H-bond only, while both the most stable conformation I (with A-B and B-D ring H-bonds) and the least stable conformation IV (with no intramolecular H-bonds) possess some middle range diazonium ion characters (2065 and 2061 cm^{-1} respectively). It seems that there is no consistent pattern of correlation in between the diazonium ion character (diazo IR frequency) and the intramolecular H-bonding interactions of **1.4**. Such observations are significantly different from the diazobenzo[*b*]fluorene of kinD (**1.1d**, Table 4-8 and 4-9), whose stabilities and diazonium ion characters would both decrease concurrently with the decrease of intramolecular H-bonding interactions. The maximum overall change in diazo IR frequency of **1.4** having various degrees of H-bond is ca. 14 cm^{-1}, which is comparable to the value (i.e., 8–16 cm^{-1}) estimated for **1.1d**.

Although the exact reasons behind the apparently lack of correlation between the diazonium ion character and the H-bonding interactions within **1.4** are not clear at the moment, such observation might be very likely related with its aromatic D-ring, since all other diazobenzo[*b*]fluorenes such as **1.1d** possesses non-aromatic D-rings. Fusion of the aromatic D-ring of **1.4** with the diazo-containing C-ring forms a significantly larger and better aromatic system, and this increased aromaticity could introduce some additional delocalization of the C5 partial negative charge (onto the aromatic D-ring) that are not available with other diazobenzo[*b*]fluorenes. The C5 partial negative charge of **1.4** may still be delocalized to either of the two carbonyl oxygens (Scheme 4-16) through the resonance enhanced H-bonding interaction like other diazobenzo[*b*]fluorenes such as kinD (**1.1d**) (Scheme 4-15), but its increased CD-ring aromaticity would probably favour less such resonance forms due to

their sabotage of the stable aromatic structure. This situation is similar to the example of pyrrole vs indole. The indole can be considered as a benzene ring fused with the pyrrole that is also aromatic. The increased aromaticity of indole would require a greater conjugation of the nitrogen's lone pair of electrons and made it less available. Therefore, indole (pK_b ~ 17.5) is an even weaker base than pyrrole (pK_b ~ 13.6). Back to the case of prekinamycin (**1.4**), the higher aromaticity of its CD-rings could further offer a few more resonance forms (Scheme 4-16) that are not available in other diazobenzo[*b*]fluorenes having non-aromatic D-rings. These new resonance forms may contribute quite differently depending on the presence/absence of intramolecular H-bonding interaction(s), leading to the observed rather random pattern of the H-bonding effect on the diazonium ion character.

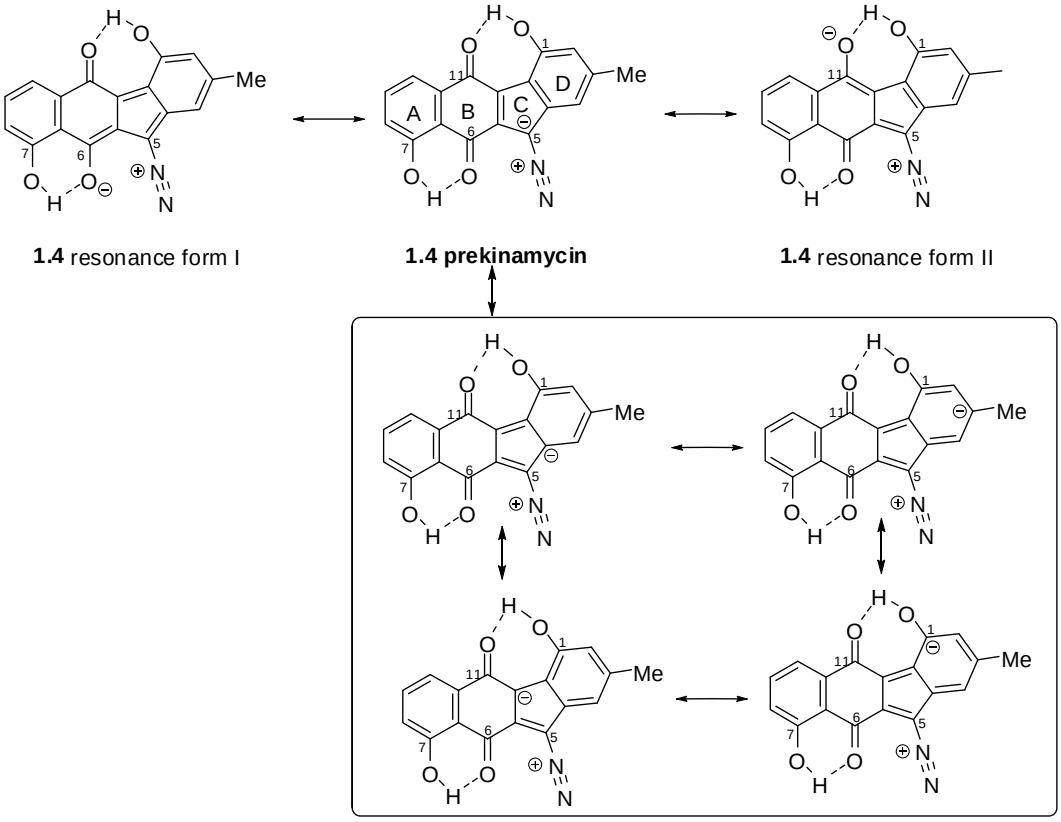

Scheme 4-16. Resonance forms of prekinamycin (**1.4**) to delocalize the C5 negative charge.

A brief conclusion from the above studies of the intramolecular H-bonding interaction within the diazobenzo[*b*]fluorenes is that such interaction is crucial for the stability of the molecule, but the corresponding influence to enhance the diazonium ion character is rather small or even negligible in some cases. It is highly possible that simple diazobenzo[*b*]fluorene analogues of kinamycins and lomaiviticins, which are as (or even more) biologically active as the natural antibiotics, may not require the mandatory presence of such H-bonding interactions.

4.6 Conclusion

In summary, the formation of a covalent adduct between kinF (**1.1f**) and glutathione (GSH**, 4.1**) in experiments that approximate physiological conditions has been demonstrated using ESI-MS methods. The MS/MSMS fragmentation is consistent with the assumption that the kinF-GSH adduct is formed by nucleophilic attack of the thiol group of GSH (**4.1**) on the terminal nitrogen of the diazo group of kinF (**1.1f**). However, the structure of this kinF-GSH adduct still awaits more rigorous analysis by complementary and more powerful spectroscopic methods such as ^{1}H and ^{13}C NMR, which require somewhat larger quantities of the adduct than that could be generated in the present work. Although only a few milligrams of kinF (**1.1f**) were available for this study, recent dramatic improvement in the fermentation method in the Dmitrienko group now provide access to gram quantities of kinF (**1.1f**) and other kinamycins so that further characterization of the adduct will soon be possible.

Whether the kinF-GSH adduct represents a key intermediate in DNA cleavage remains to be established by further experimentation. The possibility that the interaction of the diazo group of kinF with thiol groups in other possible biological targets such as topoisomerase IIα and the serine/threonine kinases such as Akt/PKB is being actively pursued in this group and that of collaborators at the University of Manitoba.

The previously observed D-ring conformational preference of kinF (**1.1f**) in solution by means of NMR, as determined by the solvent polarity, is further confirmed by molecular orbital calculations in solution phase. The apparently simple D-ring conformational change of kinF (**1.1f**) in solution is found, as suggested by consistent results from both experimental IR studies and computational analysis, to be able to significantly alter the diazonium ion character. The conformer of kinF (**1.1f**) having a diazo group with a higher diazonium ion character and hence higher reactivity, which should possess a D-ring with a pseudo-equatorial C4-OH group that is favoured by polar solvents, may be the actual bioactive form. On the other hand, the intramolecular H-bonds, which are commonly present in the diazobenzo[*b*]fluorenes of kinamycins, are found to be crucial for the stability of the molecule but to be much less influential on the corresponding diazonium ion character. Such finding suggests that simple diazobenzo[*b*]fluorene analogues of kinamycins with comparable (or even higher) biological activity as the natural antibiotics may not require the mandatory presence of such intramolecular H-bonds.

4.7 Experimental Details

+ESI-MS studies of kinF reacting with thiols

+ESI-MS studies were performed on a Micromass Q-TOF Ultima Global spectrometer equipped with an atmospheric pressure ionization (API) source (Department of Chemistry, University of Waterloo, Waterloo, Ontario, Canada). HPLC separation was carried out using a Waters HPLC system (Waters 600 controller, Waters Millenium® software) equipped with a Waters 996 photodiode array detector on a reverse phase column (NovaPak® C18 column: 60 Å, 4 μm, 3.9 x 150 mm; Sigma-Aldrich® Vydac 214TP C4 column: 5 μm, 4.6 x 250 mm). A linear gradient of HPLC-eluents specifically developed by Val Goodfellow in the Dmitrienko group for the separation of kinamycin

antibiotics, known as either the "Val Method" (on C18 and C4 column) or "Val Slow Method" (on C18 column) and listed in Table 4-11, was used as the separation conditions.

Table 4-11. HPLC gradient conditions for chromatographic separation of kinamycin antibiotics.

"Val" Method					
Time (min)	Flow rate (mL/min)	Solvent A% (H_2O)	Solvent B% (MeCN)	Solvent C% (10% HOAc)	Solvent D%
0	1.50	94	5	1	0
20	1.50	5	94	1	0
21	1.50	94	5	1	0
"Val Slow" Method					
Time (min)	Flow rate (mL/min)	Solvent A% (H_2O)	Solvent B% (MeCN)	Solvent C% (10% HOAc)	Solvent D%
0	0.25	94	5	1	0
10	0.25	88	11	1	0
11	1.50	88	11	1	0
20	1.50	5	94	1	0
21	1.50	94	5	1	0

A stock MeCN solution of kinF (**1.1f**) and a stock aqueous solution of the thiol with comparable concentrations were prepared separately. KinF (**1.1f**) was prepared from natural kinD (**1.1d**) under the Zemplen deacylation conditions (Chapter 2), and its purity was verified by both NMR and +ESI-MS spectroscopy. Commercial optical grade MeCN (Optima® by EMD) was used directly to prepare the kinF-MeCN solution. Fresh ultra-pure water with a conductivity ≥ 18 MΩ•cm, obtained from a Milli-Q® ultra-pure water system by passing deionized water through a Millipore QPAK® filter, was used to prepare the aqueous thiol solutions and the LiOH/NaOH solutions (for pH adjustment). To minimize the air oxidation of the thiol, the corresponding stock solution was always freshly prepared right before the start of the reaction with kinF (**1.1f**). The LiOH/NaOH solution was added dropwise

under stirring to the aqueous thiol solution, whose pH was monitored with a pH meter until the pH reached the desired value of 7.60. The final concentration of the thiol stock solution was calculated by taking into account the volume of the base solution added for pH adjustment. The mechanistic studies were carried out under aerobic conditions by following the general procedure as shown in Scheme 4-17.

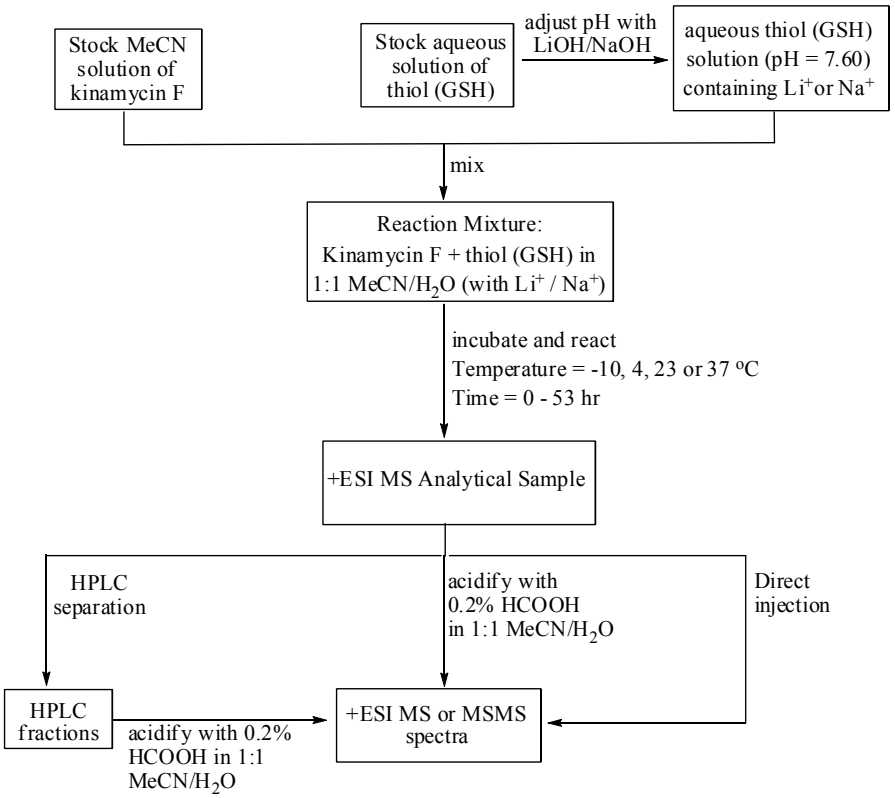

Scheme 4-17. Experimental procedure to study reactions between kinF (**1.1f**) and thiols by +ESI-MS.

Certain volumes of both stock solutions, i.e. the kinF-MeCN solution and the (pH-adjusted) aqueous thiol solution, were pipetted into an Eppendorf® tube. If necessary, an appropriate amount of either MeCN or water was added to the kinF-thiol mixture to maintain a final 1:1 (v/v) ratio of MeCN and H_2O. The Eppendorf® tube containing the reaction mixture was capped and then shaken on an

IKA MS2 minishaker for at least 10 sec at ca. 500–1000 rpm to ensure a thorough mix, which was then allowed to incubate and react at the desired temperature. The Eppendorf® tube containing the reaction mixture was covered with aluminum foil during the entire course of the reaction to minimize any possible photolytic (side) reactions, however, quick tests indicated that even direct exposure of the reaction sample to normal room/day light for several hours applied no observable effect on the obtained mass spectra. After certain time intervals, a sample of the reaction solution was either directly subjected to the +ESI mass spectrometer, or in some cases it was first diluted with excess 0.2% formic acid in 1:1 (v/v) MeCN/H_2O prior to the mass studies. Some reaction samples were also separated first by HPLC and the obtained fractions were acidified with 0.2% formic acid and then subjected the +ESI-MS studies. To ensure a precise analysis of the mass samples without any contamination and undesired interference, prior to the loading of a new sample, the +ESI-MS spectrometer was flushed thoroughly with blank solvent (1:1 MeCN/H_2O) until the obtained mass spectra for the background showed no presence of any left-over kinF (**1.1f**) or thiol from the previous experiment.

IR studies of kinamycin F

All IR spectra of kinF (**1.1f**) in both solution and solid phase were recorded on a Perkin Elmer RX I FT-IR spectrometer without calibration. However, the reading consistency of the IR wavenumber was monitored and verified by periodically checking the instrument with a standard polystyrene film (0.038 mm thick). An excellent matching of the observed IR peaks with the expected standard IR values (± 0.1 cm^{-1} at most) for polystyrene was found consistently. Solution IR spectra were measured with each individual solution sample in a demountable liquid IR cell kit (Aldrich catalog No. Z112003-1KT) with two CaF_2 windows (diameter x thickness: 32 mm x 3 mm) that have a light path of 0.1 mm. All solution IR spectra were recorded with an automatic deduction of both solvent and air background. All solid IR spectra were recorded with an automatic deduction of only the air

background. All IR spectra were recorded with a default resolution of 4.0 cm^{-1} except sample CNIR0046, which was recorded with a resolution of 1.0 cm^{-1}. Most IR spectra were recorded in the default IR range of 4000 to 400 cm^{-1} but some were observed in narrower ranges (2300–2000 or 2200–2000 cm^{-1}) to achieve slightly better quality spectra. Within experimental errors and instrumental resolution, such change in scanning range did not affect the accuracy or consistency of the observed wavenumbers at all. All solvents used were either HPLC grade (MeOH, MeCN, $CHCl_3$ and acetone), Omni® grade (DMSO) or Optima® grade (CH_2Cl_2) expect CCl_4, which was ACS grade.

Ab initio MO calculations of kinamycins

Ab initio MO calculations were carried out with the Gaussian03® (G03) program on either Microsoft Windows®-based PCs (G03 revision B04)[368] or RedHat Enterprise Linux-based workstations (G03 revision C02),[369] and a basis set of RHF/6-31G//6-31G was used for geometry optimization and vibrational frequency calculation. The PCM (Polarizable Continuum Model) solvation model was used for solution phase calculations.

Chapter 5

Chemistry of the Diazobenzo[*a*]fluorene of Isoprekinamycin

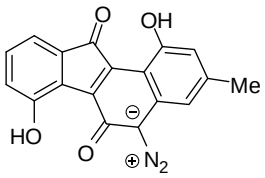

1.5 isoprekinamycin

In the Dmitrienko lab, the availability of isoprekinamycin (**1.5**), initially through bacterial fermentation and later on by means of total synthesis, led to some important discoveries of this molecule that may help to further understand the mode-of-action of the kinamycins. During the course of the present project, the development of synthetic methodology for construction of isoprekinamycin (**1.5**) and other diazobenzo[*a*]fluorene analogues in the Dmitrienko group was underway in parallel with the work related to the diazobenzo[*b*]fluorene types of kinamycins (Chapter 2 and 3). Since interesting results as presented in Chapter 4 were obtained both experimentally (IR) and computationally (MO calculations) for the diazobenzo[*b*]fluorene of kinamycin F (**1.1f**), it was decided that similar studies with the diazobenzo[*a*]fluorene ring system of isoprekinamycin (**1.5**) might be helpful not only in predicting the effect of structure on the reactivity, but also in designing promising analogues.

For simplification purposes, the name "isoprekinamycin" will be abbreviated as "IPK" throughout this chapter and accordingly, the name "prekinamycin" will be abbreviated as "PK". The elemental van der Waals (vdW) radii used in this chapter for discussion are values suggested by CCDC (Cambridge Crystallographic Data Centre, Cambridge, UK).[370] The typical bond lengths used in this chapter for discussion are all taken from March's "Advanced Organic Chemistry".[365] Where a

literature model compound that is used for discussion is taken from the CSD (Cambridge Structural Database, by CCDC), then the corresponding Refcode is given and the original reference can be retrieved accordingly from the CSD.

5.1 Structural Properties of Isoprekinamycin

Previous attempts in both the Gould and the Dmitrienko laboratories over the past many years to crystallize IPK (**1.5**), ever since its discovery in 1989[5,6] (although it was mistakenly considered as the isomeric PK (**1.4**) at the time until the structure was revised in 2000[14]), failed to produce the desired single crystals. However, during the course of this project, an NMR sample of some fairly pure natural IPK (**1.5**), which was isolated from the bacterial fermentation broth by this work, very slowly deposited a dark purple crystalline solid inside the NMR tube. This crystal of IPK (**1.5**) was then subjected to X-ray crystallographic studies and the corresponding results (Figure 5-1, see Appendix D for details),[25] for the very first time, provided not only the ultimate and unambiguous spectroscopic evidence for the assigned structure of IPK (**1.5**)[14] but also some very important geometrical information of this compound that helps to elucidate the diazo activity. At the same time when IPK single crystals became available, synthetic work carried out by Wei Liu in the Dmitrienko group accomplished the total synthesis of a simple IPK-analogue **3.236**, which had an unsubstituted D-ring and an A-ring with methoxy group. Contrary to the problematic IPK (**1.5**), crystallization of **3.236** was very smooth and the corresponding single crystal was also examined by X-ray (Figure 5-1, see Appendix E for details).[25]

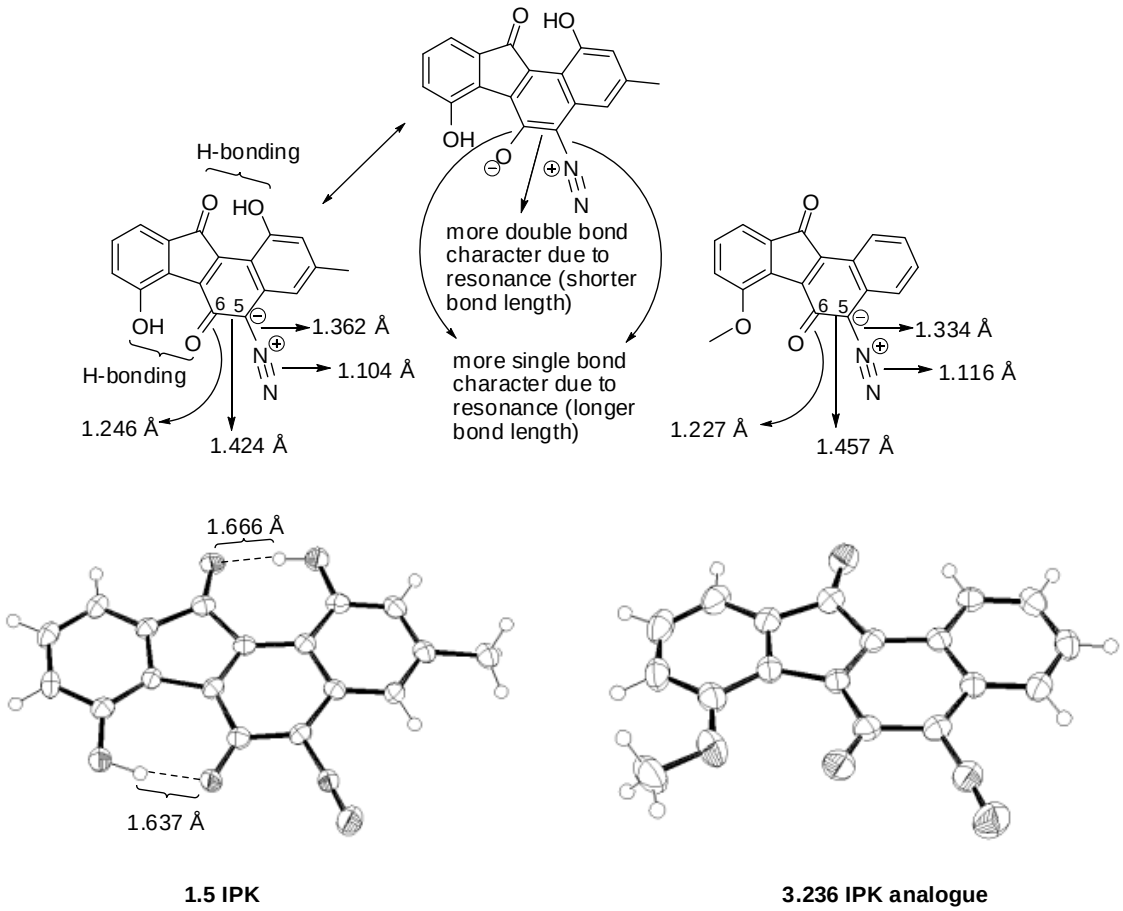

Figure 5-1. ORTEP plots of single crystals of natural IPK (**1.5**) and its synthetic analogue **3.236**.

Comparison of these two kinamycins, both having a diazobenzo[*a*]fluorene skeleton, clearly indicates a significantly increased diazonium ion character in IPK (**1.5**) relative to **3.236** (the experimental diazo IR stretching frequencies are $\nu_{N\equiv N}$ (**1.5**) =2160 cm^{-1} and $\nu_{N\equiv N}$ (**3.236**) = 2096 cm^{-1}), as evidenced by the alternating shorter N-N (1.104 vs 1.116 Å), longer C5-N (1.362 vs 1.334 Å), shorter C5-C6 (1.424 vs 1.457 Å), and longer C6-O (1.246 vs 1.227 Å) bond length. This observation provides solid physical evidence for the previous proposal by the Dmitrienko group, which was solely based on computational prediction at the time, that an increased diazonium ion contribution to the resonance hybrid representing the *o*-quinodiazide functionality exist in IPK (**1.5**) (Figure 5-1).[124] The

presence of strong intramolecular hydrogen bonding interactions within IPK (**1.5**), between the A-ring phenol and C-ring carbonyl group ($d_{C=O\cdots HO}$= 1.637 Å) as well as the D-ring phenol and the B-ring carbonyl group ($d_{C=O\cdots HO}$= 1.666 Å), were also confirmed by the corresponding X-ray results (Figure 5-1). It should be noted that, although hydrogen atom portions are typically not determined by X-ray crystallographic methods, in this case of IPK (**1.5**), the presence of electron density connected with the placement of the phenolic H atoms in the indicated H-bonding arrangement was determined. This intramolecular H-bonding interaction is considered one of the primary factors that significantly enhance the diazonium ion character, which does not apply in the case of IPK-analogue **3.236** due to the lack of appropriate functionalities.

In addition, comparison of the crystal structure of the diazobenzo[*b*]fluorene ring system of IPK (**1.5**) with the diazobenzo[*a*]fluorene skeleton of PK (**1.4**), which was obtained from MO computations since no crystal structure of **1.4** was available, offered some interesting observations. The superimposition of these two isomeric species (Figure 5-2) revealed that, despite the rearranged carbon skeletons, the carbonyl oxygens and diazo nitrogen atoms on the periphery of these two different types of kinamycins align well. This finding would suggest that the diazobenzo[*a*]fluorenes and diazobenzo[*b*]fluorenes might be two variants of the same pharmacophore.[25]

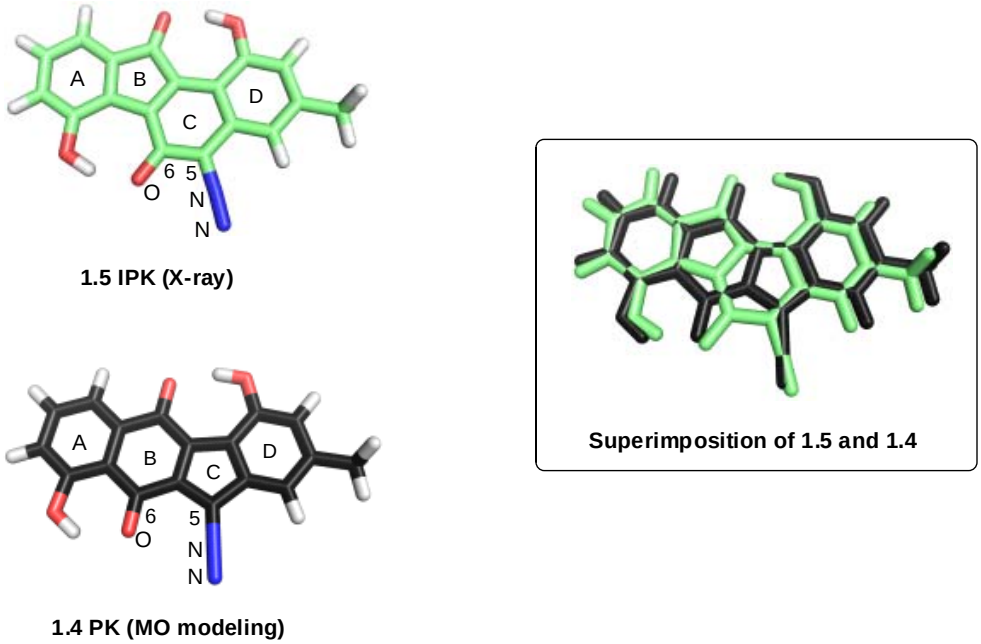

Figure 5-2. Superimposition of the diazobenzo[*a*]fluorene of IPK (**1.5**) and the diazobenzo[*b*]fluorene of PK (**1.4**).

5.2 Computation Studies of the Influence of Structure on the Diazonium Ion Character of Isoprekinamycin Analogues

The successful total synthesis of the diazobenzo[*a*]fluorene of IPK (**1.5**)[25] and some of its simpler analogues,[25,124] using the synthetic procedures developed by the Dmitrienko group (introduced in section 3.2.2), has provided the feasibility of generating various analogues and derivatives of the rare diazobenzo[*a*]fluorene antibiotics. Such analogues may possess better biological activities and drug-like properties than the original natural products. However, the choice of which IPK-analogues should be prepared is not an easy decision to make, since very little is known about the influence on molecular properties when introducing different substituents onto the diazobenzo[*a*]fluorene skeleton. Therefore, it would be valuable if some molecular modeling work could be performed to predict useful and effective IPK-similar structures that are worthy of the effort required for total synthesis.

Previous MO calculations on diazobenzo[*a*]fluorenes in the Dmitrienko group mainly focused on IPK (**1.5**), with a strong interest in the influence on diazonium ion character from intramolecular H-bonding interactions.[80,124] This diazonium ion character of kinamycins has been considered by the Dmitrienko group as a potentially important factor for the observed biological activities of these diazobenzofluorene antibiotics, which is supported by evidence from early work of Laufer[124] in this group and the current work of this thesis (section 4.2). The discovery that different conformations of the diazobenzo[*b*]fluorene kinamycin F (**1.1f**) have different diazonium ion character, which is due to simple D-ring conformational change leading to different orientation of its C4 polar substituent relative to the nearby C5-diazo moiety (section 4.4), also triggered the interest in studying the similar case with the diazobenzo[*a*]fluorenes.

Experimental results obtained in this laboratory have demonstrated that the diazo group of kinamycins can serve as an electrophile with a suitable nucleophilic species such as electron-rich aromatics (Scheme 1-18) or thiols (Scheme 4-2b and 4-3). Such observations have also led to the proposal by this group that nucleophilic addition to the diazo moiety of kinamycins by the DNA/DNA bases (Scheme 1-20a) might be the ultimate mode-of-action of these antibiotics, which is supported by evidence from this thesis work (Chapter 4) under the (near) physiological conditions. However, the possibility of involving a reductive activation of such diazoquinones through single electron transfer can not be completely ruled out (Dmitrienko's proposal, Scheme 1-20b; Feldman's proposal, Scheme 4-7; Melander's proposal, Scheme 4-10; Skibo's proposal, Scheme 4-11). The observation that DNA cleavage by lomaiviticins occurred under reducing conditions seems to partially support the latter idea.[52] Unlike the nucleophilic diazo-addition mechanism, the reductive activation by electron transfer does not require close contact of the reductant with the kinamycins, as long as electron(s) can be freely transferred in between them. Even if the mode-of-action of kinamycins occurs via the electron-reductive pathway, a high diazonium ion character would still

enhance the bioactivities of such diazoquinones. The high electron-demanding nature of the diazo moiety would make the compound more readily to accept electrons and be reduced, especially in the case of kinamycins in which the diazo group is in conjugation with the quinone moiety. It should be noted that, although the Dmitrienko nucleophilic addition mechanism for the kinamycins (section 4.2) would suggest a positive correlation between the diazonium ion character and the biological activity, this does not necessarily mean that kinamycin analogues having diazonium ion character that is much higher than those of the natural products would be practically better drug candidates. Excessively high diazonium ion character of such possible kinamycin analogues, even if successfully synthesized, might cause unwanted biological deactivation or cell damage upon competitive reactions with other available nucleophiles (or reductants) in the system, instead of the occurrence of the desired selective reactions between such highly active kinamycins and the intended biotargets (e.g., DNA of cancer/bacterial cells). In other words, it is crucial to balance the diazo reactivity to achieve a higher biological activity than the natural kinamycins but probably not over-active as those typical aryl diazonium salts. Furthermore, the structural complexity of such kinamycin analogues should be controlled at a reasonable level from the synthetic point of view, when various substituents are to be introduced into (or removed from) the skeletons of benzo[*a*]fluorenes or benzo[*b*]fluorenes to modulate the corresponding diazonium ion character.

The entirely aromatic diazobenzo[*a*]fluorene core of IPK (**1.5**) is significantly flatter and more rigid than the carbon skeleton of the diazobenzo[*b*]fluorene-type kinamycins, such as in kinamycin F (**1.1f**). This flatter geometry is expected to provide a better alignment of its C4-substituent with the C5-diazo group than in the diazobenzo[*b*]fluorenes having an equatorial C4-substituent, thus leading to a possibly stronger interaction between the C5-N_2 and C4-X groups and perhaps a higher diazonium ion character. On the other hand, the expected better alignment between the C4-substituent and the C5-diazo group within the IPK-C4-substituted analogues may be compromised if the C4-substituent

is bulky enough, and unfavourable steric interactions between this C4-substituent with either the C5-diazo group or the C3-methyl group may further affect the corresponding diazonium ion character significantly. In addition, the aromatic D-ring of the diazobenzo[*a*]fluorene would also make the inductive and the resonance effect from the C4-substituent more effective than the C4-substituent on the non-aromatic D-ring of diazobenzo[*b*]fluorene, both of which delocalize the C5 negative charge and consequently enhance the diazonium ion character as well. Last but not least, this C4-position of IPK (**1.5**) is the closest available spot to the C5-diazo group within the molecule, which is expected to be able to apply the maximum influence on the diazonium ion character upon appropriate substitution. Therefore, a series of IPK-C4-substituted analogues such as **5.1**–**5.6** and an IPK-D-ring-quinone analogue **5.7** as shown below were proposed for the study, which cover the common and possible substituents including (saturated and unsaturated) aliphatic groups, halogens, heteroatom-based (S, N and O) functional groups and carbonyl derivatives.

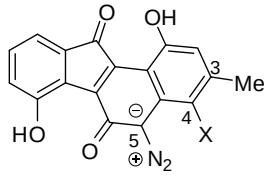

5.1-5.6 IPK-C4-substituted analogues

5.1a X = Me
5.1b X = Et
5.1c X = *n*-Pr
5.1d X = *n*-Bu
5.2a X = vinyl
5.2b X = ethynyl
5.2c X = CN

5.3a X = F
5.3b X = Cl
5.3c X = Br

5.4a X = NH_2
5.4b X = NHCOMe
5.4c X = NO
5.4d X = NO_2

5.5a X = SH
5.5b X = SMe
5.5c X = OH
5.5d X = OMe
5.5e X = O^-
5.5f X = OAc
5.5g X = OSO_2Me
5.5h X = OSO_2PhMe

5.6a X = CHO
5.6b X = COMe
5.6c X = $CONH_2$
5.6d X = CO_2H
5.6e X = CO_2Me
5.6f X = CO_2^-

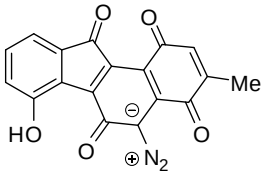

5.7 IPK-D-ring-quinone analogue

Before discussing the modeling results of these proposed IPK-C4-substituted analogues, it is useful to examine a few key structural and electronic features of IPK (**1.5**) and its analogue **3.236** from physical (X-ray) and theoretical (MO calculations) evidence (Table 5-1), which are closely related with their diazonium ion characters. X-ray results of **1.5** and **3.236** (Appendix D and E) revealed that, both C5-diazo groups adopt an almost linear geometry, as indicated by the corresponding bond angles

of C5-N1-N2 (177.6° and 176.3° respectively). Both C5-diazo groups also possess near-perfect coplanarity with each individual aromatic ring plane defined by the benzo[*a*]fluorene carbon skeleton, as indicated by the very small dihedral angle between the diazo moiety and the corresponding aromatic ring plane (< 3° for **1.5** and < 6° for **3.236**). Such experimental observations are consistent with literature X-ray results of many other diazo compounds such as aryl diazonium salts and (aromatic) α-diazoketones.[371] In addition, the computed geometry and the relative values of the diazo IR stretching frequency for these two diazobenzo[*b*]fluorenes (Table 5-1) are also in very good agreement with the experimental findings.

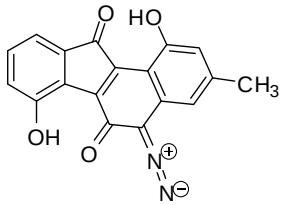

1.5

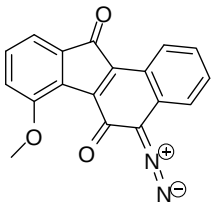

3.236

Table 5-1. Ab initio MO calculations and experimental measurements of IPK (**1.5**) and its simple synthetic analogue **3.236**.

Structure	Optimized geometry	$\nu_{N\equiv N}$ (cm^{-1})[a]	$d_{N\equiv N}$ (Å)	<C-N-N(°)
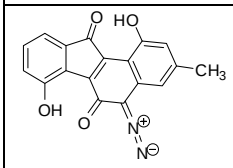 **1.5**	 from X-ray 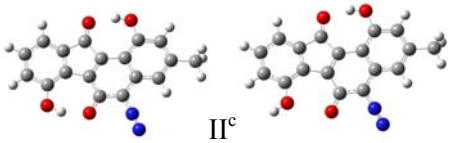 I^b II^c from MO calculation ΔE(II - I) = 17.4 kcal/mol	Expt.: **2160** MO: I. 2139 II. 2084	X-ray: **1.104** MO: I. 1.103 II. 1.108	X-ray: **177.6** MO: I. 176.2 II. 176.1
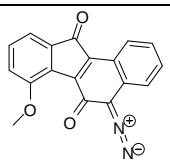 **3.236**	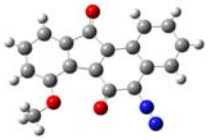 from X-ray 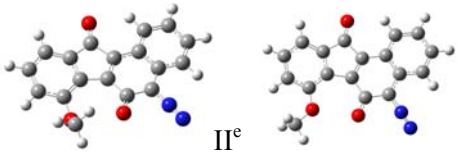 I^d II^e from MO calculation ΔE(II - I) = 2.6 kcal/mol	Expt.: **2099** MO: I. 2081 II. 2068	X-ray: **1.116** MO: I. 1.109 II. 1.110	X-ray: **176.3** MO: I. 176.4 II. 176.2

a. Scaled by a scaling factor of 0.8929 (MO results); b. This geometry was obtained from MO optimization starting from the X-ray structure of **1.5**; c. This geometry was obtained from MO optimization starting from the X-ray structure of **1.5** but the intramolecular A-C ring H-bond was manually broken; d. This geometry was obtained from MO optimization starting from the X-ray structure of **3.236** with no restrictions; e. This geometry was obtained from MO optimization starting from the X-ray structure of **3.236**, but the relative orientation of the A-ring methoxy towards the aromatic ring plane (i.e., dihedral angle between the methoxy group and the flat aromatic A-ring) was fixed, which would otherwise be optimized to conformation I.

Initial MO computation on IPK (**1.5**) provided an intramolecular double H-bonded conformation (conformer I, Table 5-1) as expected, which entirely agrees with the X-ray findings. Similar to the previous MO studies on PK (**1.4**) (section 4.5), various further attempts were also made to "break" the intramolecular H-bonding interactions between the A-C rings and/or B-D rings within IPK (**1.5**). However, only one additional conformation (conformer II, Table 5-1) in which the A-C ring H-bond is missing, was obtained. Failure to find a stable conformation in which the intramolecular B-D ring H-bond is missing would suggest that, the energy benefit from this interaction is even larger than the corresponding contribution from the "breakable" A-C ring H-bond, whose absence in conformer II of **1.5** already destabilizes the molecule dramatically by 17.4 kcal/mol. The absence of A-C ring H-bond within IPK (**1.5**) also causes a large decrease of the diazonium ion character ($\Delta\nu_{N\equiv N}$ = 55 cm^{-1}), suggesting that this intramolecular H-bond is essential for the delocalization of the C5 negative charge and the consequent and significant enhancement of the diazonium ion character (Figure 5-1). This theoretical prediction in fact agrees fairly well with some experimental observations. When the two phenols of IPK (**1.5**) are either acetylated (i.e., IPK-diacetyl ester, **1.5a**) or methylated (i.e., IPK-dimethyl ether, **1.135**) so that both intramolecular H-bonds no longer exist, the observed experimental diazo IR frequencies of these two substrates (i.e., $\nu_{N\equiv N}$ = 2113–2124 cm^{-1}/2119 cm^{-1} for **1.5a**; $\nu_{N\equiv N}$ = 2111–2114 cm^{-1} for **1.135**)[*] are about 40–50 cm^{-1} lower than that of IPK (**1.5**, $\nu_{N\equiv N}$ = 2160 cm^{-1}). This comparison also suggests that, even thought the B-D ring H-bonding is very important for the

[*] Diazo IR frequencies for **1.5a**, which was prepared by acetylation of natural IPK (**1.5**) in the Dmitrienko laboratory, were determined in this thesis work to be 2114 cm^{-1} (CH_2Cl_2 solution), 2113 cm^{-1} ($CHCl_3$ solution) and 2124 cm^{-1} (film). The cause for this observed difference in diazo IR frequency of **1.5a** between solution and solid state is not clear at the moment. Literature work by Gould gave a value of 2119 cm^{-1} (film) for **1.5a**. (5) Seaton, P. J.; Gould, S. J. *J. Antibiot.* **1989**, *42*, 189-197. Diazo IR frequencies for **1.135**, which was prepared by methylation of natural IPK (**1.5**) in the Dmitrienko laborotary, were determined in this thesis work to be 2111 cm^{-1} (CH_2Cl_2 solution), 2114 cm^{-1} ($CHCl_3$ solution) and 2112 cm^{-1} (film). These two substrates could serve as suitable models to examine the influence from intramolecular H-bonding interactions on the diazonium ion character of IPK (**1.5**), even though they do possess small but very likely negligible substituent effect (i.e. –OMe or –OAc vs –OH) on the diazonium ion character.

stability of IPK (**1.5**) molecule, its influence on the diazonium ion character is likely to be rather limited when compared to the A-C ring H-bonding interaction.

Interestingly, in the case of **3.236**, gas phase MO calculations also predicted two possible conformations (Table 5-1) that are apparently only different in the orientation of its A-ring methoxy group. Conformation II of **3.236** with its methoxy group being parallel (coplanar) to the aromatic skeleton was found experimentally by X-ray to be the real situation in its solid state (single crystals), despite its higher energy of 2.6 kcal/mol than that of the conformation I, whose methoxy group is almost perpendicular to the aromatic ring plane. The lower stability of conformation II (in the gas phase) seems to be derived from a unfavourable lone pair electron repulsion between the C7-O and C6-O, which is minimized in conformation I upon simple C7-O bond rotation (Figure 5-3a). In addition, the C7-O/C6-O lone pair electron repulsion within conformation II is expected to disfavour the delocalization of C5 negative charge onto the C6 carbonyl oxygen and thus decreases the diazonium ion character accordingly, which is consistent with the observed decrease in diazo IR frequency from conformation I ($\nu_{N\equiv N}$ = 2081 cm^{-1}) to II ($\nu_{N\equiv N}$ = 2068 cm^{-1}). On the other hand, the real physical packing of **3.236** that employs the more energetic conformation II instead of the more stable conformation I is still explainable. Conformation II is capable of providing closer distance and hence stronger π-π stacking interactions between the aromatic planes of molecules within the crystal (Figure 5-3b), while conformation I's methoxy group being perpendicular to the aromatic ring plane would significantly decrease such beneficial packing interaction.

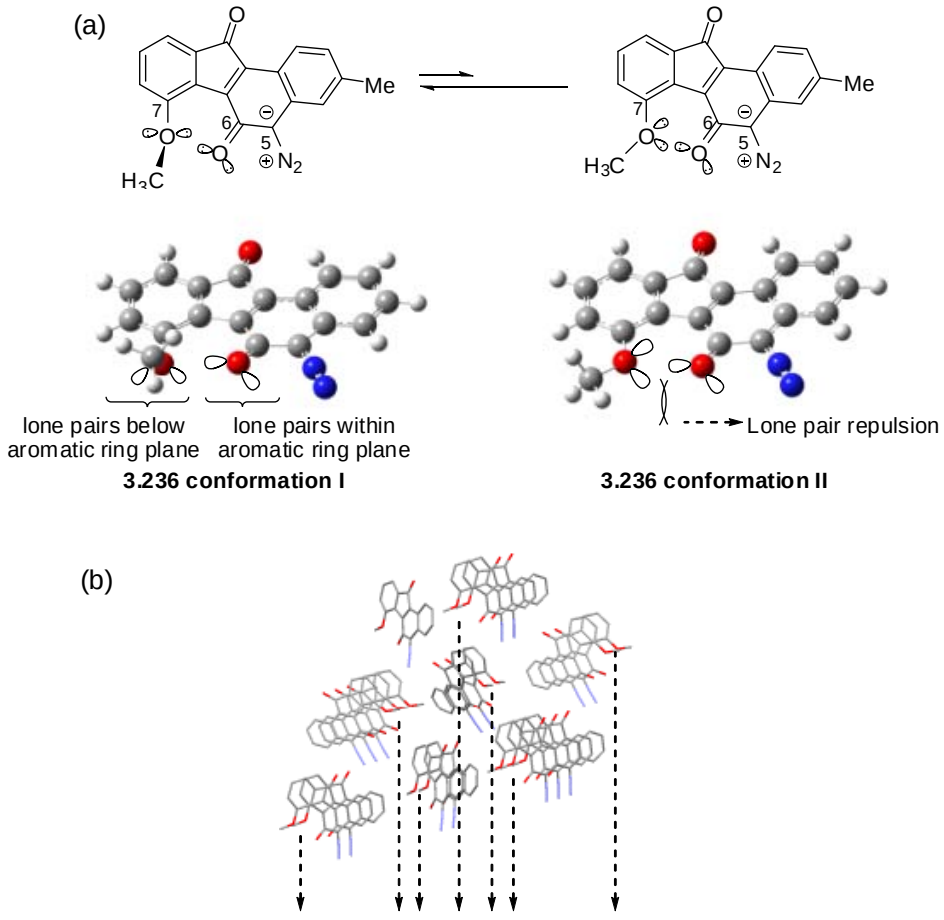

Figure 5-3. (a) Repulsion of lone pair of electrons within IPK analogue **3.236** (conformation II) and (b) π-π stacking of **3.236** (conformation I) in its single crystals.

Within these two diazobenzo[*a*]fluorenes, there seems to exist a through-space and beneficial interaction between the lone pair of electrons of the C6 carbonyl oxygen and the nearby C5-diazo nitrogens. This proposal is necessary in order to explain the small but preferential bending of the C5-N1-N2 bond towards the apparently more crowded C6-carbonyl site instead of the unsubstituted and less hindered C4-H site, which have been observed for both IPK (**1.5**) and **3.236** from the X-ray and computational results (Figure 5-4). One might have expected that the steric repulsion alone between

the C6-oxygen and C5-diazo, when no favourable electronic interactions between them are involved, would have forced the diazo moiety to bend towards the less hindered C4-H site. However, such prediction is opposite to both experimental and theoretical observations for **1.5** and **3.236**. Interestingly, in the optimized conformation of PK (**1.4**), the diazo group is entirely linear with a very slight bending (0.2°) towards the less hindered C4-H site (Figure 5-4).

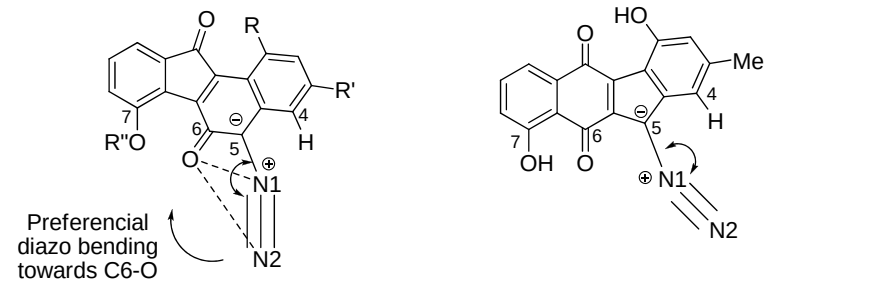

1.5 IPK (R = OH, R' = Me, R' = H)
bond angle (C5-N1-N2) = 177.6 ^{o} (X-ray)
176.2 ^{o} (MO)
3.236 (R = R' = H, R' = Me)
bond angle (C5-N1-N2) = 176.3 ^{o} (X-ray)
176.4 ^{o} (MO)

1.4 PK
bond angle (C5-N1-N2) = 179.8 ^{o} (MO)

Figure 5-4. Different preference of diazo bending within diazobenzo[*a*]- and diazobenzo[*b*]fluorenes.

The difference in diazo bending between IPK (**1.5**) and PK (**1.4**) would suggest a lack of such lone pair electron-diazo interaction within the diazobenzo[*b*]fluorenes in the case of PK (**1.4**). Despite the isomeric and nicely superimposed skeletons of diazobenzo[*a*]- and diazobenzo[*b*]fluorenes (Figure 5-2), the significantly different carbonyl oxygen-diazo distances within these two types of structures are likely the cause of such difference in this intramolecular lone pair-diazo interaction. The computed distances between the C6 carbonyl oxygen and the two diazo nitrogens for PK (**1.4**, $d_{C6=O\cdots N1}$ = 2.904 Å, $d_{C6=O\cdots N2}$ = 3.300 Å) are much longer than the corresponding distances within IPK (**1.5**, $d_{C6=O\cdots N1}$ = 2.635 Å, $d_{C6=O\cdots N2}$ = 3.241 Å) and its analogue (**3.236**, $d_{C6=O\cdots N1}$ =2.615 Å, $d_{C6=O\cdots N2}$ = 3.220 Å,

conformation II).* Judging by the vdW radius of oxygen (r_O = 1.52 Å) and nitrogen (r_N = 1.55 Å), it is reasonable to predict that the diazobenzo[*a*]fluorene system should possess relatively much stronger (C6 carbonyl oxygen) lone pair-diazo interactions than the isomeric diazobenzo[*b*]fluorene system. This through-space lone pair-diazo interaction is expected to partially neutralize the partial positive charge of the diazo moiety and stabilize the molecule. On the other hand, the influence from this lone pair-diazo interaction on the diazonium ion character was not clear initially when this study began. However, later studies (section 5.2.3) revealed that such lone pair-diazo interaction actually favours a higher diazonium ion character.

With the above knowledge in mind, gas phase ab initio MO calculations were carried out with the proposed IPK-C4-substitued analogues **5.1**–**5.6** and the IPK-D-ring-quinone analogue **5.7**. The calculated diazo IR stretching frequencies ($\nu_{N\equiv N}$), N≡N bond lengths ($d_{N\equiv N}$), C5-N1-N2 bond angles (<C-N-N) and the optimized geometries are summarized in the following sections. There are some very interesting predictions that could be made based on these MO calculation results. A C4-substituent on the aromatic D-ring within the flat and rigid diazobenzo[*a*]fluorene skeleton of IPK (**1.5**) is found to apply a quite complex and combined (overall) substitution effect on the corresponding diazonium ion character, which includes inductive effect, resonance effect, dipole-dipole interaction, steric effect and some other unique through-space electronic interactions with the diazo moiety as well, depending on the electronic and steric nature of the C4-substituent involved.

* These computed values are in good agreement with the (C6 carbonyl) oxygen-diazo distances measured from X-ray data of IPK (**1.5**, $d_{C6=O\cdots N1}$ = 2.675 Å, $d_{C6=O\cdots N2}$ = 3.312 Å) and analogue **3.236** ($d_{C6=O\cdots N1}$ =2.636 Å, $d_{C6=O\cdots N2}$ = 3.251 Å, conformation II). Unfortunately, no X-ray data is available for PK (**1.4**).

5.2.1 MO Calculations of IPK-C4-aliphatic Analogues

Introducing an alkyl group at the sp^2-hybridized C4 position of IPK (**1.5**), as summarized in Table 5-2, provides no significant inductive effect, resonance effect or dipole-dipole interaction in favour of the diazonium ion character. Even if these factors were to be considered, polarity and dipole moment of the C4–C bond would oppose a higher diazonium ion character due to the stronger electron-withdrawing ability of the sp^2-C4 than that of the sp^3-carbon of the alkyl substituent (Figure 5-5). The electron-donating nature of the alkyl group (relative to hydrogen) towards the aromatic ring would also counteract the resonance contribution towards a higher diazonium ion character (Figure 5-5).

Table 5-2. Ab initio MO calculations of IPK-C4-alkyl analogues **5.1a**–**5.1d**.

Structure	Optimized geometry	$\nu_{N\equiv N}$ (cm^{-1})[a]	$d_{N\equiv N}$ (Å)	<C-N-N(°)
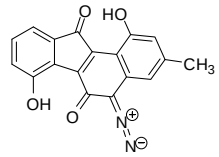 **1.5**	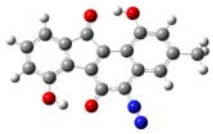	2139	1.103	176.2
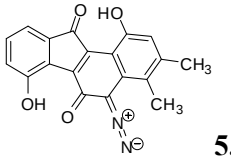 **5.1a**		2129	1.103	170.6
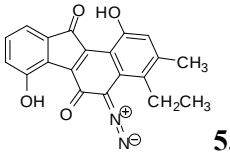 **5.1b**	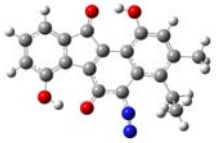	2129	1.103	168.7
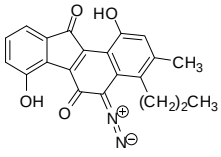 **5.1c**		2128	1.103	168.5
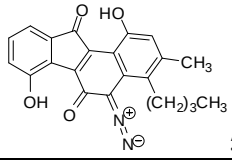 **5.1d**	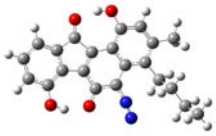	2127	1.103	168.5

a. Scaled by a scaling factor of 0.8929.

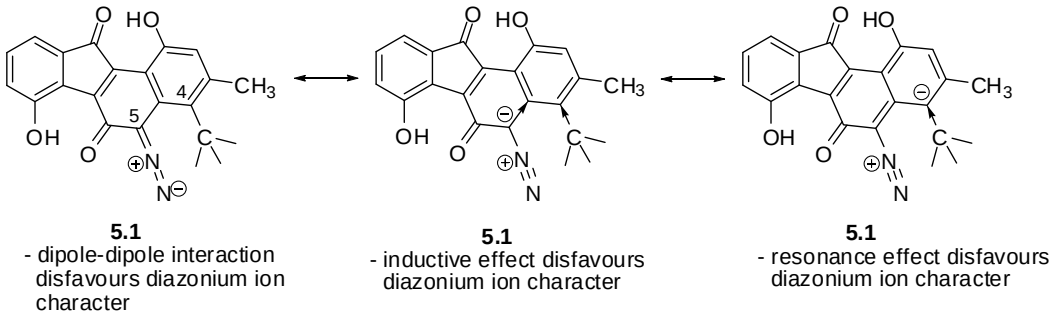

Figure 5-5. Substituent effects on diazonium ion character within IPK-C4-alkyl analogues **5.1**.

Longer alkyl chains at C4, such as Et, *n*-Pr and *n*-Bu groups (i.e., analogues **5.1b**–**5.1d**), have essentially the same overall effect on the diazonium ion character as the methyl group (analogue **5.1a**), partially due to their close electronic nature. On the other hand, the longer alkyl chain could freely stretch out in space without interfering sterically much with either the adjacent C5-diazo or the C3-methyl group. Therefore, the calculated slightly lower diazo IR frequencies of **5.1a**–**5.1d** (C4-alkyl, $\nu_{N\equiv N}$ = 2129–2127 cm^{-1}) than that of **1.5** (C4-H, $\nu_{N\equiv N}$ = 2139 cm^{-1}) is a combined result from mainly the diazonium-unfavourable inductive effect, resonance effect, dipole-dipole interaction and partially from steric repulsion, and the latter distorts the original nearly linear geometry of the C5-N1-N2 triatomic moiety and forces the C5-N1-N2 bond to noticeably bend more towards the C6-carbonyl side, as indicated by the significantly smaller bond angles of ca. 168.5–170.6° than that of **1.5** (176.2°). The introduction of a branched alkyl group such as the isopropyl group results in much geometrical distortion with the C5-diazo group substantially sticking out of the aromatic ring plane in order to avoid the steric clash with the C4-alkyl group. Placing a *t*-butyl group at C4 causes even more severe geometrical distortion with the *t*-butyl group being completely pushed out of the plane of the aromatic D-ring. Neither the IPK-C4-*i*Pr analogue ($\nu_{N\equiv N}$ = 2126 cm^{-1}) nor the IPK-C4-*t*Bu ($\nu_{N\equiv N}$ = 2116 cm^{-1}) analogue is considered to be a feasible synthetic target. However, such results would

suggest that steric repulsion alone from the C4-substituent towards the C5-diazo group would decrease the diazonium ion character, but only in a very limited manner.

Even though the IPK-C4-alkyl substituted analogues **5.1a**–**5.1d** are predicted to have lower diazonium ion character and hence to be less active than the natural IPK (**1.5**), such compounds may serve as useful candidates for mechanistic studies. If the mode-of-action of the kinamycins indeed involves the nucleophilic diazo-addition mechanism (section 4.2) as the Dmitrienko group has proposed and (partially) proved, such IPK analogues are expected to be more difficult to undergo the nucleophilic attack at the C5-diazo group due to the presence of the bulky C4-substituents.

When unsaturated groups such as vinyl, alkynyl and cyano (i.e., sp/sp^2-hybridized carbon atoms) are introduced at the sp^2-C4 position (analogues **5.2a**–**5.2c**), a significant increase of the diazo IR frequency and hence diazonium ion character relative to that of IPK (**1.5**) is observed (Table 5-3).

Table 5-3. Ab initio MO calculations of IPK-C4-carbon (unsaturated) analogues **5.2a**–**5.2c**.

Structure	Optimized geometry	$\nu_{N\equiv N}$ (cm^{-1})[a]	$d_{N\equiv N}$ (Å)	<C-N-N(°)
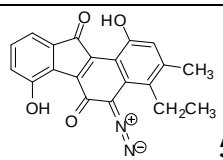 **5.1b**	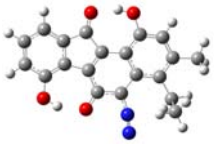	2129	1.103	168.7
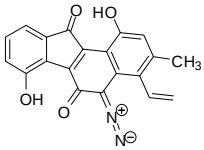 **5.2a**		2159	1.101	171.5
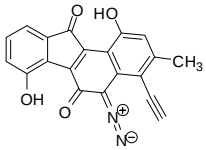 **5.2b**	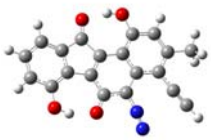	2180	1.099	169.8
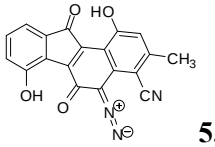 **5.2c**	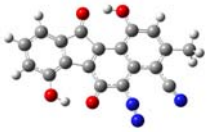	2189 ($\nu_{C\equiv N}$: 2254)	1.098 ($d_{C\equiv N}$:1.149)	169.8

a. Scaled by a scaling factor of 0.8929.

The vinyl substituent (-CH=CH_2) at the C4 position as in the optimized conformation of **5.2a** is found to be oriented with the plane of the C=C bond nearly orthogonal to the aromatic ring plane (Table 5-3 and Figure 5-6). Thus, resonance delocalization of the C5 negative charge by the vinyl group is expected to be minimal, since coplanarity of the C=C bond with the aromatic system is not allowed by steric factors (Figure 5-6). The sp^2 carbon of the vinyl group would be (slightly) more inductively electron-withdrawing when compared with the sp^3 carbon in **5.1b**, and hence (slightly) in favour of a higher diazonium ion character than **5.1b**. However, the favourable influence on diazonium ion character from either the inductive effect or the dipole-dipole interaction should be very small, since the C4-C bond within **5.2a** is not very polar (dipole ~ 0 as both carbons are sp^2-hybridized). Therefore, in order to explain the substantially higher diazo IR frequency of **5.2a** (C4-CH=CH_2, $\nu_{N\equiv N}$ = 2159 cm^{-1}) than that of not only **5.1b** (C4-CH_2CH_3, $\nu_{N\equiv N}$ = 2129 cm^{-1}) but also **1.5** (C4-H, $\nu_{N\equiv N}$ = 2139 cm^{-1}), an intramolecular and through-space interaction between the C4-vinyl group and the C5-diazo moiety seems to be the only other option. This possible vinyl-diazo interaction within **5.2a** is geometrically allowed by the space proximity of its C4-vinyl group to the C5-diazo group (Figure 5-6), since the closest distance between them ($d_{C1'\cdots N1}$ = 2.771 Å) is much shorter than the sum of the corresponding vdW radii (r_N = 1.55 Å, $r_{C\cdot}$= 1.70 Å). More importantly, the vinyl-diazo interaction would also be greatly favoured by the electronic nature of the two participating groups, as the vinyl moiety is fairly rich in π electron density while the diazo group is somewhat electron deficient. The reason(s) why such vinyl-diazo interaction would enhance the diazonium ion character, however, is not very clear at first glance.

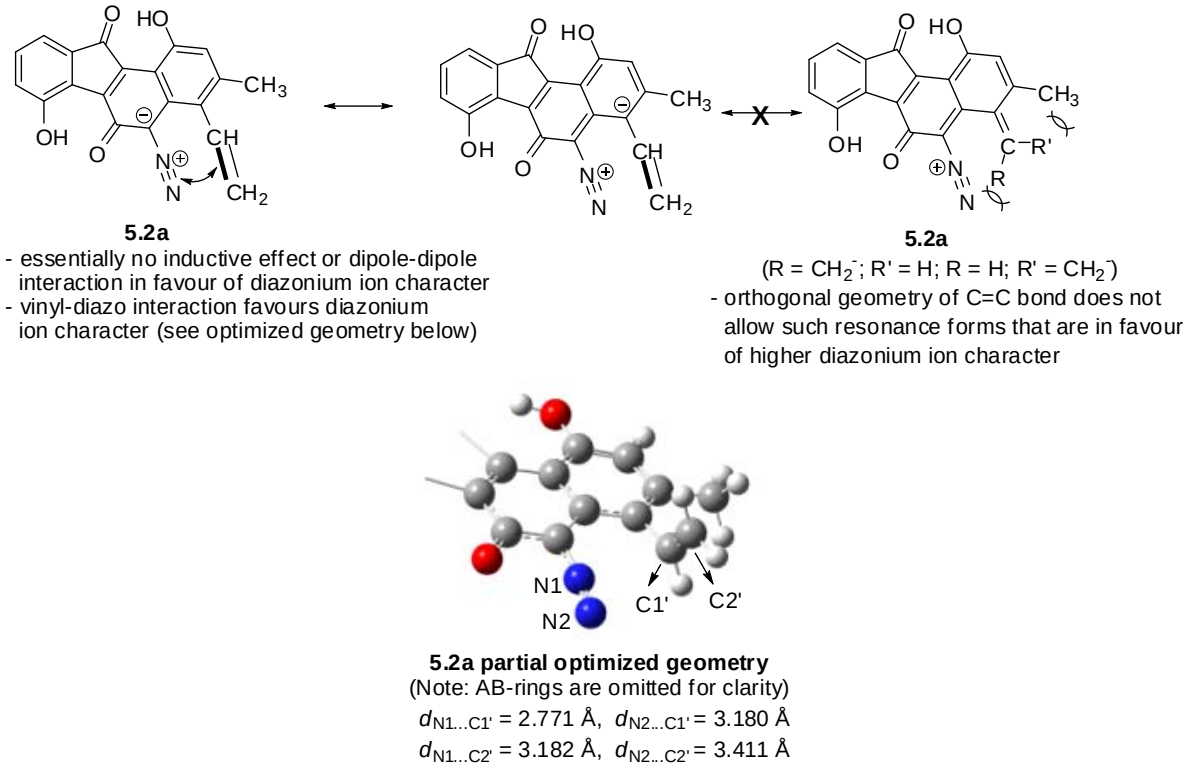

Figure 5-6. Substituent effects on diazonium ion character within IPK-C4-vinyl analogue **5.2a**.

The increase in diazonium ion character is much more pronounced for the IPK-C4-acetylenic structure **5.2b** (C4-C≡CH, $\nu_{N\equiv N}$ = 2180 cm^{-1}). In this case, the slightly higher electronegativity of the sp-hybridized alkynyl carbon than that of the sp^2-hybridized C4-carbon would introduce some inductive effect and dipole-dipole interaction (C4(sp^2)→C(sp)/C5←N1), both in favour of a higher diazonium ion character. At the same time, delocalization of electron density onto the acetylenic linkage to increase the diazonium ion character also becomes feasible (Figure 5-7). The calculated bond length of 1.197 Å for the carbon-carbon triple bond within **5.2b** is significantly longer (more double-bond like) than the typical bond length of ca. 1.18 Å for typical alkynes, consistent with the prediction of resonance delocalization of the C5 partial negative charge favouring the diazonium ion character. In addition, some through-space interaction is also possible between the C4-alkynyl and the

C5-diazo groups, similar to the previous case of **5.2a**. It is expected that, due to the higher electron density on the C4-alkyne (than the C4-alkene of **5.2a**) and the even closer distances between the two linear groups that are now coplanar (Figure 5-7), the acetylene-diazo interaction within **5.2b** should be stronger than the vinyl-diazo interaction within **5.2a**. Switching from the C4-vinyl (**5.2a**) to C4-alkynyl (**5.2b**) group applies positive influence on all the diazonium-affecting interactions (i.e., inductive effect, resonance effect, dipole-dipole interaction and through-space C4/C5 interaction), consistent with the substantial increase of diazo IR frequency from **5.2a** ($\nu_{N\equiv N}$ = 2159 cm^{-1}) to **5.2b** ($\nu_{N\equiv N}$ = 2180 cm^{-1}).

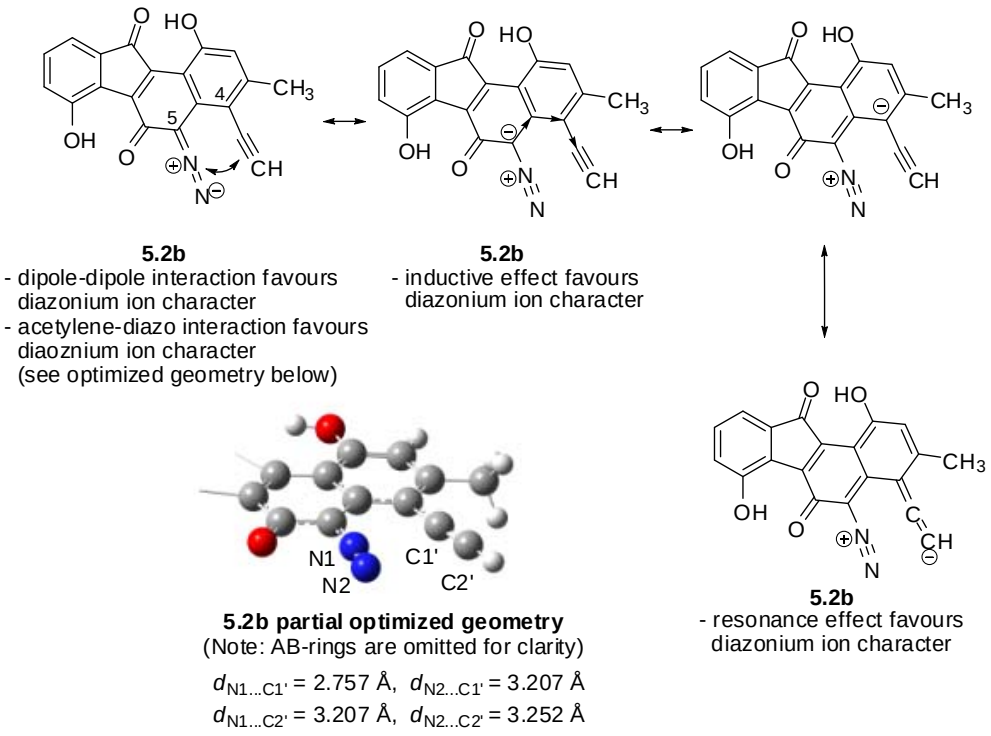

Figure 5-7. Substituent effects on diazonium ion character within IPK-C4-acetylene analogue **5.2b**.

The diazonium ion character increases even more with a cyano substituent at C4 as in structure **5.2c**, which possesses the highest diazo IR frequency of 2189 cm^{-1} among this series of analogues.

Qualitatively, this is consistent with the strong inductive and resonance effects expected from the cyano group to enhance the diazonium ion character (Figure 5-8). The latter effect is evident from the calculated C≡N bond length of 1.149 Å, which is longer than the typical cyano bond length of ca. 1.14 Å as a result of such resonance contribution. In addition, the strong electron-withdrawing capability of the cyano group would cause a highly polar C4-C bond that benefits a strong dipole-dipole interaction (C4(sp^2)→C(sp^3)/C5←N1) to enhance the diazonium ion character (Figure 5-8). Finally, a through-space interaction between the cyano and diazo groups in favour of a higher diazonium ion character that is very similar to such interaction between the alkynyl and the diazo moiety within **5.2b**, is also applicable in the case of **5.2c** (Figure 5-8). Since the sp^3-hybridized C1' within **5.2b** (C4-**C**≡N) is expected to be significantly lower in electron density than that of **5.2a** (C4-**C**≡CH), the cyano-diazo interaction is likely to be weaker than the acetylene-diazo interaction.

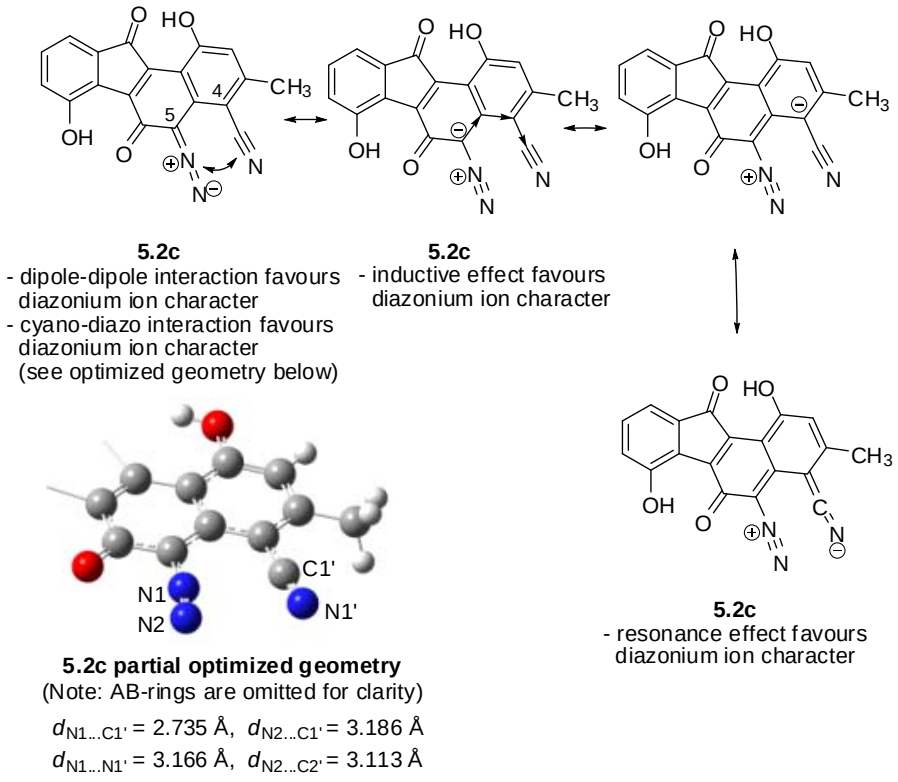

Figure 5-8. Substituent effects on diazonium ion character within IPK-C4-cyano analogue **5.2c**.

Interestingly, despite the much stronger electronegativity of the -C≡N group than that of the -C≡CH group, analogue **5.2c** (C4-C≡N, $\nu_{N\equiv N}$ = 2189 cm^{-1}) is only slightly higher in diazonium ion character than **5.2b** (C4-C≡CH, $\nu_{N\equiv N}$ = 2180 cm^{-1}). This seems to suggest that the inductive effect, dipole-dipole interaction and resonance effect, which would all enhance the diazonium ion character when the C4-substituent is electron-withdrawing, are likely to play a less influencing role on the diazonium ion character than the intramolecular through-space interaction between the C4-π-substituent and the C5-diazo group.

5.2.2 MO Calculations of IPK-C4-halogen Analogues

When halogens such as F, Cl and Br are present at the C4 position (analogues **5.3a**–**5.3c**, Table 5-4), the corresponding diazonium ion characters of such analogues are also greatly enhanced to approximately the same extent as those IPK-C4-carbon (unsaturated) analogues such as **5.2b** (C4-C≡CH) and **5.2c** (C4-C≡N). Within this series of analogues, the diazonium ion character decreases slightly with decreasing electronegativity of the halogen involved.

Table 5-4. Ab initio MO calculations of IPK-C4-halogen analogues **5.3a**–**5.3c**.*

Structure	Optimized geometry	$\nu_{N\equiv N}$ (cm^{-1})[a]	$d_{N\equiv N}$ (Å)	<C-N-N(°)
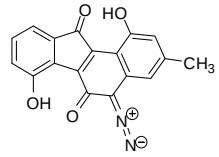 **1.5**	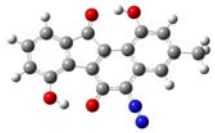	2139	1.103	176.2
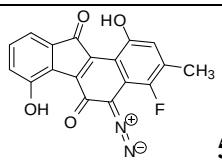 **5.3a**	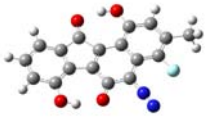	2193	1.09837	174.6
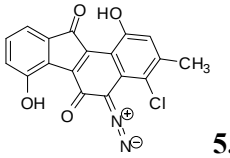 **5.3b**	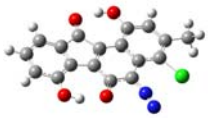	2188	1.09839	169.0
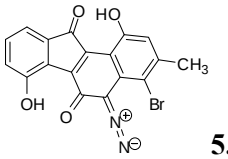 **5.3c**	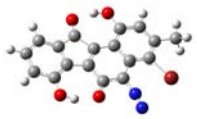	2180	1.099	167.3

* I (iodine) was not examined since it is not covered by the basis set of 6-31G used for MO calculations; a. Scaled by a scaling factor of 0.8929.

The observed influence and tendency of diazonium ion character can be reasonably explained by the strong electron-withdrawing capability of the halogen, which decreases with the increasing atomic number, leading to inductive, resonance and dipole-dipole interactions all favouring a higher diazonium ion character than the unsubstituted parent compound IPK (**1.5**). In addition, the observed clear tendency of decreasing bond angle of C5-N1-N2 in the order of **5.3a** > **5.3b** > **5.3c** is consistent with the increasing size of the C4-halogen atom in the order of F < Cl < Br and hence increasing steric interaction.

Interestingly, the diazonium ion character of **5.3a** (C4-F, $\nu_{N\equiv N}$ = 2193 cm^{-1}) is only modestly higher than the cases of **5.3b** (C4-Cl, $\nu_{N\equiv N}$ = 2188 cm^{-1}) and **5.3c** (C4-Br, $\nu_{N\equiv N}$ = 2180 cm^{-1}), despite the

substantially higher electronegativity of the fluorine atom. One possibility* is that, when compared with the previous IPK-C4-aliphatic analogues (**5.1a**–**5.1d** and **5.2a**–**5.2c**), the enhancement of diazonium ion character in the IPK-C4-halogen compounds may rely more significantly on a favourable dipole-dipole (C4→X/C5←N1) interaction due to the highly polarized C4-halogen bond. The C-F bond has more covalent character than the C-Cl and C-Br bonds, and thus the C-Cl and C-Br bond have higher bond polarity. Therefore, compared to the C4-Cl and C4-Br, the C4-F substituent would enhance the corresponding diazonium ion character significantly more from the inductive and resonance effects but much less from the dipole-dipole interaction. The combined overall result is then the observed (only) slightly higher diazo IR frequency for **5.3a** (C4-F) than that of **5.3b** (C4-Cl) and **5.3c** (C4-Br).

5.2.3 MO Calculations of IPK-C4-nitrogen Analogues

When some nitrogen-based substituents are introduced at the C4 position of IPK (**1.5**), the calculated diazo IR frequencies of such analogues are overall much higher than the parent compound with some more interesting discoveries (Table 5-5).

* Later studies indicate that there is another possibility to explain the rather small difference in diazo IR frequency for the IPK-C4-halogen analogues, which relies more on the very likely (halogen) lone pair-diazo interaction. See section 5.2.3 for detailed discussion.

Table 5-5. Ab initio MO calculations of IPK-C4-nitrogen analogues **5.4a**–**5.4d**.

Structure	Optimized geometry	$\nu_{N\equiv N}$ (cm^{-1})[a]	$d_{N\equiv N}$ (Å)	<C-N-N(°)
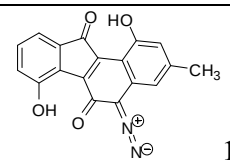 **1.5**	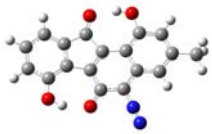	2139	1.103	176.2
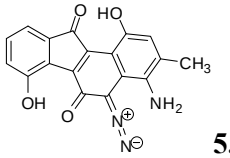 **5.4a**	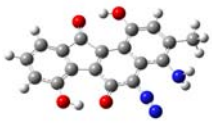	2219	1.096	171.2
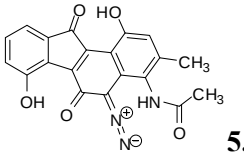 **5.4b**	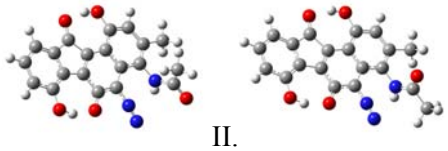 I. s-cis amide II. s-trans amide ΔE(II - I) = 0.12 kcal/mol	I. 2192 II. 2173	I. 1.099 II. 1.100	I. 170.2 II. 170.6
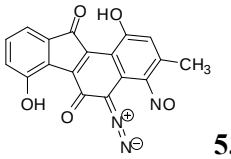 **5.4c**	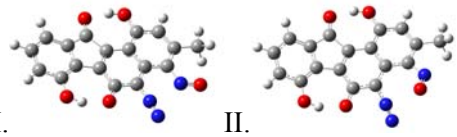 I. II. ΔE(II - I) = 5.0 kcal/mol	I. 2260 II. 2260	I. 1.093 II. 1.093	I. 171.3 II. 172.2
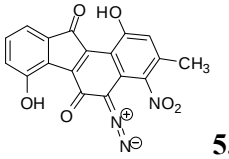 **5.4d**		2218	1.096	171.6

a. Scaled by a scaling factor of 0.8929.

An amine group at the C4 position of IPK (i.e., analogue **5.4a**) causes the corresponding diazo IR frequency to shift to a very high value of 2219 cm^{-1}, which is even substantially higher than the IPK-C4-halogen analogues (**5.3a**–**5.3c**, $\nu_{N\equiv N}$ = 2193–2180 cm^{-1}). In principle, the strong electron(π)-donating nature of the amine group is not expected to bring any significant resonance effect in favour of a higher diazonium ion character. The moderately polar C4→N bond with nitrogen being more electronegative could still provide some but very limited inductive effect and dipole-dipole interaction (C4→NH_2/C5←N1) that benefit the diazonium ion character, when compared to other

more electronegative elements such as the halogens. Therefore, the enormous increase in diazo IR frequency by 90 cm^{-1}, from 2139 cm^{-1} for IPK (**1.5**, C4-H) to 2219 cm^{-1} for **5.4a** (C4-NH_2), must originate predominantly from other interactions of the C4-amine with the diazo moiety besides the above mentioned diazo-influencing factors.

The optimized geometry of **5.4a** shows that the sp^3-hybridized C4-amine nitrogen along with its lone pair of electrons is coplanar with the aromatic ring, and these electrons point in a near orthogonal orientation to the diazo nitrogens (Figure 5-9), particularly the internal N1. As a matter of fact, even if the C4-amine group of **5.4a** adopts different starting orientations with the nitrogen's lone pair of electrons pointing anywhere else instead of the diazo group, the final optimized conformation is always identical to the one shown in Figure 5-9. This suggests the presence of a beneficial and through-space electronic interaction between the C4-amine and C5-diazo groups. The geometric data of **5.4a** provides some further evidence to support this proposed lone pair-diazo interaction (Figure 5-9). The C4-N bond aligns almost perfectly with the C5-N1 bond not only in the same (aromatic) plane but also near parallel to each other, which is indicated by the bond angles of <C5-N1-NH_2 and <C4-NH_2-N1 that are both very close to 90°. Moreover, the distances between the diazo nitrogens and the C4-amino nitrogen ($d_{C4\text{-}N\cdots N1}$ = 2.604 Å; $d_{C4\text{-}N\cdots N2}$ = 3.027 Å) are significantly shorter than the sum of the corresponding vdW radii (r_N = 1.55 Å). The preferential orientation (alignment) of the nitrogen's lone pair of electrons towards the electron-deficient diazo moiety, along with the close enough distance between the nitrogen and the diazo group, suggest the presence of a favourable (nitrogen) lone pair-diazo interaction.

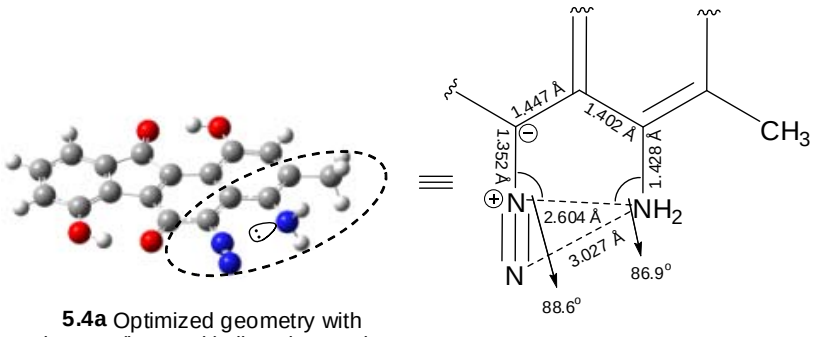

5.4a Optimized geometry with nitrogen (lone pair)-diazo interaction

Figure 5-9. Optimized geometry of IPK-C4-NH_2 analogue **5.4a**.

In addition, the optimized conformation of **5.4a** was further subjected to some single point energy (SPE) calculations, in which the entire optimized conformation was kept unaltered except that the dihedral angle between the C4-amine and the aromatic ring plane was manually set and fixed at 90°, 180° and 270° that deviates from the optimized C4-amine orientation (Figure 5-10). Such manipulation would force the amine-nitrogen's lone pair of electrons to point away and stay far enough from the diazo group, so that the lone pair-diazo interaction should either decrease significantly or even totally vanish. It is found that the optimized conformation of **5.4a** having the nitrogen lone pair-diazo interaction is much more stable than all the rest, which lack such interaction, by at least 8.3 kcal/mol. Therefore, the energy contribution associated with this amine lone pair-diazo interaction should be slightly less than 8.3 kcal/mol, since the optimized conformation of **5.4a** with the 180°-rotated C4-amine (Figure 5-10) might be accompanied with some additional but likely small steric repulsion due to the close distance between the two amine-hydrogens and the diazo group.

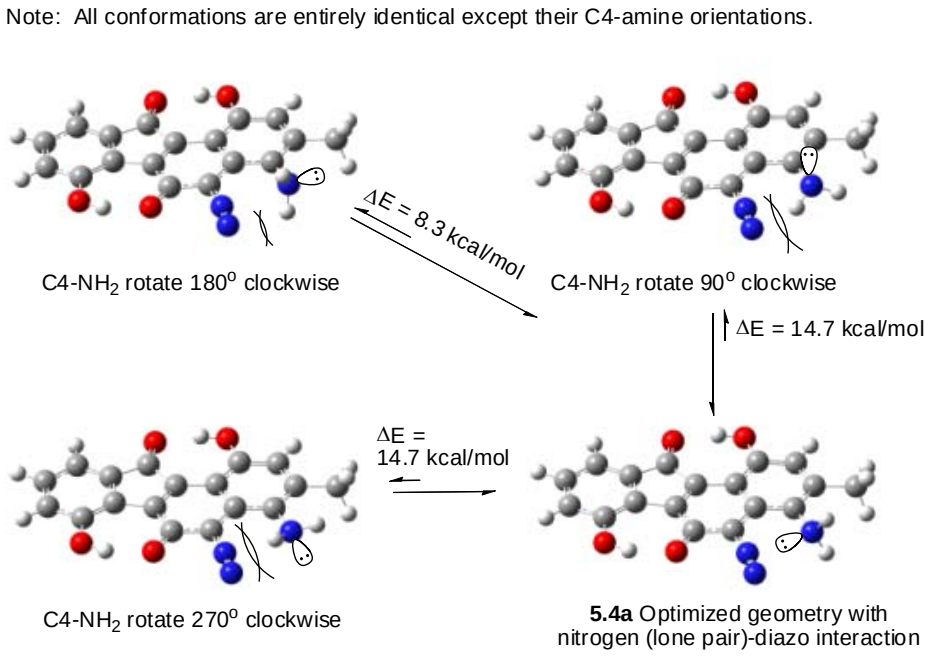

Figure 5-10. SPE calculations of IPK-C4-NH_2 analogue **5.4a**.

In fact, the observation that the C4-amine acts as an electron donor and interacts with the C5-diazo group is consistent with and resembles some similarity to two previous discoveries. First, within **1.5** and **3.236** (section 5.1), the C6 carbonyl oxygen with available lone pair of electrons does interact with the C5-diazo group through space and induce a preferential diazo bending towards the carbonyl oxygen. Second, in the case of **5.2a**–**c** (section 5.2.1), through-space interaction between the C4-vinyl/acetylenic/cyano and C5-diazo group is considered an important factor to be responsible for the corresponding (high) diazonium ion character, while such C4-π-substituents can also be regarded as an electron donor. The nature of this electron donor-diazo interaction is intriguing but not intuitively obvious (see section 5.3 for further discussion). Such an intramolecular lone pair-diazo interaction does, however, lead to a very strongly increased diazonium ion character.

In addition, later studies that are to be discussed next further confirmed the common presence of such lone pair-diazo interaction and its dramatic capability to enhance the diazonium ion character.

Exploring the real physical nature of such electron donor-diazo interaction would be of at least academic interest by itself (section 5.3). On the other hand, and probably more importantly from a practical point of view, this finding may be very useful in the design of diazobenzo[*a*]fluorene type of kinamycin analogues. Apparently, the introduction of an appropriate electron donor at the C4 position is a powerful yet simple strategy to achieve a high diazonium ion character, which may lead to structurally simpler diazobenzo[*a*]fluorene analogues with comparable or even higher bioactivity than the natural IPK (**1.5**).

Moreover, correlation of this finding of lone pair-diazo interaction with the IPK-C4-halogen analogues **5.3a**–**c** (section 5.2.2) would suggest that, the calculated high diazonium ion character of these IPK-C4-halogen analogues are very likely to also have some contribution from the halogen's lone pair electrons interacting with the diazo group. The availability of the multiple lone pairs of electrons on the C4-halogen, along with the halogen's close distance to the diazo group (Figure 5-11) that is significantly shorter than the sum of the corresponding vdW radii (r_F = 1.47 Å, r_{Cl} = 1.75 Å, r_{Br} = 1.85 Å and r_N = 1.55 Å), does permit such beneficial halogen lone pair-diazo interaction electronically and geometrically. In addition, this newly discovered interaction offers a second explanation to the rather small difference in diazo IR frequency for **5.3a**–**c** (section 5.2.2), which does not match well with the significant difference in the halogens' electronegativity. Previously, it was presumed that the dipole-dipole interaction may play an important role that is significant than other interactions in affecting the diazonium ion character of **5.3a**–**c** (section 5.2.2), so that the less polar C4-F bond than C4-Cl and C4-Br bonds was thought to be responsible for its less-than-expected increase (based on electronegativity) in diazo IR frequency. Alternatively, if the halogen lone pair-diazo interaction to enhance the diazonium ion character plays the important role in the case of **5.3a**–**c**, then the very high electronegativity of F is expected to make the fluorine to maintain its lone pair of electrons much better than Cl and Br and hence a smaller increase in diazonium ion character from its

weaker interaction with the diazo group, which partially cancels the higher increase in diazonium ion character from the fluorine's inductive and resonance effects than that from Cl and Br. It should be pointed out that the dipole-dipole and the lone pair-diazo interactions could co-exist since there is no conflict between them. In both cases, the stronger electronegativity of F would make it to contribute less to a higher diazonium ion character than Cl and Br. However, judging by the fact that the lone pair-diazo interaction has a huge capability to enhance the diazonium ion character and much stronger than all the other diazo-affecting interactions as observed in the case of **5.4a**, it is more likely that the (halogen) lone pair-diazo interaction also plays a bigger role than the corresponding dipole-dipole interaction to affect the diazonium ion character even in the cases of **5.3a**–**c**.

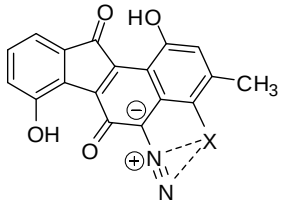

5.3a (X = F) $d_{F...N1}$ = 2.535 Å, $d_{F...N2}$ = 2.904 Å
5.3b (X = Cl) $d_{Cl...N1}$ = 2.849 Å, $d_{Cl...N2}$ = 3.207 Å
5.3c (X = Br) $d_{Br...N1}$ = 2.930 Å, $d_{Br...N2}$ = 3.284 Å

Figure 5-11. Close distances between C4-halogen and C5-diazo group with IPK-C5-halogen analogues **5.3a**–**5.3c** suggesting lone pair-diazo interactions.

It is not surprising that, in the case of analogue **5.4b**, when the electron-withdrawing acetyl group is attached to the C4-amine that significantly decreases the electron density (i.e., availability of lone pair electrons) on the nitrogen atom, the calculated diazo IR frequency drops from 2219 cm^{-1} of **5.4a** to 2192 cm^{-1} of **5.4b**. This reduced diazonium ion character is likely the result of a significantly weaker lone pair interaction from C4 amide-nitrogen of **5.4b** (relative to the C4 amino-nitrogen of **5.4a**) to the C5-diazo group, even though the inductive effect and dipole-dipole interaction favouring a higher diazonium ion character are expected to be slightly enhanced for **5.4b** relative to that of **5.4a**. However, a new situation arises in this case, since the C4-amide could adopt either an *s*-cis or an *s*-

trans conformation that are interconvertible upon a simple rotation of the acetyl group (Table 5-5). Despite the very small energy difference of only 0.12 kcal/mol between these two possible conformations of **5.4b**, the corresponding diazo IR frequency of the *s*-trans species (conformer II, $\nu_{N\equiv N}$ = 2173 cm^{-1}) is significantly lower than the *s*-cis species (conformer I, $\nu_{N\equiv N}$ = 2192 cm^{-1}). Apparently the diazonium ion character is very sensitive to the change in the surrounding electronic environment, even though such variation may not cause any noticeable alteration of the molecule's energy or steric congestion.

The calculations on IPK-C4-nitroso analogue **5.4c** present some other interesting results and two conformers are found as energy minima (Table 5-5). Conformer I, in which the nitroso-nitrogen is close to the diazo group and the nitroso group is coplanar with the aromatic ring, is lower in energy by 5 kcal/mol than conformer II, in which the nitroso-oxygen is close to the diazo group and the nitroso group is skewed to the aromatic ring (Figure 5-12). There is no doubt that the fairly strong electron-withdrawing capability of the nitroso group would introduce inductive, resonance and dipole-dipole interactions in favour of a (significantly) higher diazonium ion character than IPK (**1.5**). It should be noted that the resonance contribution to delocalize the C5 partial negative charge onto the nitroso group is expected to be less significant in conformer II than I, which is due to the skewed geometry of the nitroso group towards the aromatic ring (a torsion of ca. 20º) within the former conformation. The enormous increase of 120 cm^{-1} for the diazo IR frequency (**5.4c** vs **1.5**), however, is well beyond the known influencing capability of the several electronic effects mentioned above. In the case of **5.4c**, the presence of some additional and very strong interactions that enhance and dominate the influence on the diazonium ion character is mandatory. This concern makes even more sense when considering the later result that, introducing the stronger electron-withdrawing nitro group at C4 (i.e., analogue **5.4d**, to be discussed next) in fact induces less increase in diazonium ion character than the nitroso group. Once again the required additional interaction to dramatically

increase the diazonium ion character seems to be a through-space interaction from the nitroso group towards the diazo group, which is clearly different in the two conformers (Figure 5-12).

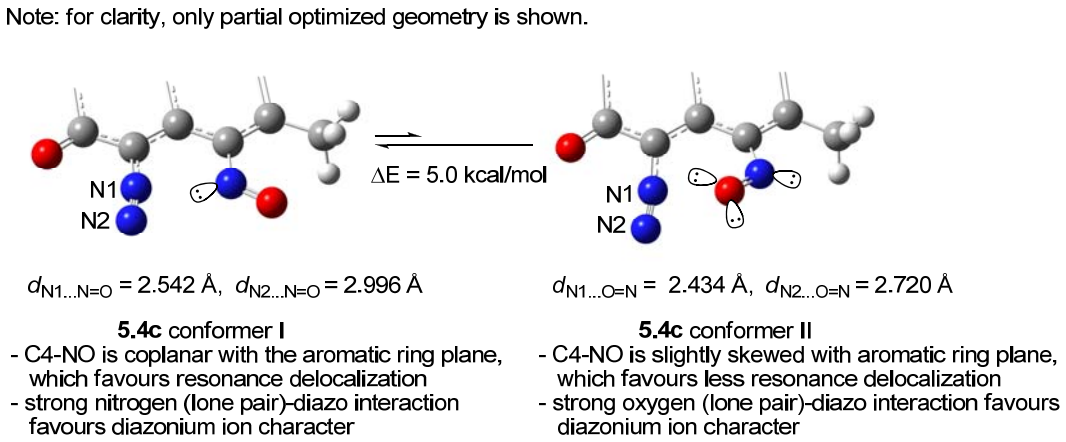

Figure 5-12. Lone pair-diazo interactions within the two conformers of IPK-C4-nitroso analogue **5.4c**.

Within conformer I of **5.4c** (Figure 5-12), a strong lone pair effect from the sp^2-hybridized nitroso-nitrogen (C4-**N**=O) towards the diazo moiety is evident from the following two observations. First, the nitroso-nitrogen stays in very close distance from the two diazo nitrogens ($d_{O=N\cdots N1}$ = 2.542 Å; $d_{O=N\cdots N2}$ = 2.996 Å), which are even significantly shorter than such distances observed for **5.4a** (C4-NH_2, $d_{C4\text{-}N\cdots N1}$ = 2.604 Å; $d_{C4\text{-}N\cdots N2}$ = 3.027 Å) that is found to already have strong (nitrogen) lone pair-diazo interactions. Second, the lone pair of electrons on the nitroso-nitrogen does point to the two diazo nitrogens in an orientation that looks suitable for some orbital interactions. For conformer II of **5.4c** (Figure 5-12), rotation of the C4-nitroso group (from conformer I) leads to a lack of nitroso-nitrogen lone pair-diazo interaction, which is then compensated by a strong through-space nitroso-oxygen lone pair-diazo interaction. The close distance between the nitroso-oxygen and the diazo moiety within conformer II ($d_{N=O\cdots N1}$ = 2.434 Å; $d_{N=O\cdots N2}$ = 2.720 Å), which is also much shorter than the sum of the corresponding vdW radii (r_O = 1.52 Å, r_N = 1.55 Å), not only makes the oxygen lone pair-diazo interaction feasible but also explains the higher energy associated with this conformation

(i.e., from steric repulsion between nitroso-oxygen and the diazo group). Interestingly, the predicted diazonium ion character of the two conformers, as measured by the diazo IR stretching frequency and N≡N bond length, are coincidentally identical. Yet it might be argued that the overall strength of interactions from the nitroso-nitrogen within conformer I and nitroso-oxygen within conformer II towards the diazo group are fortuitously comparable. This coincidentally identical effect is also consistent with a qualitative analysis that the nitroso-nitrogen is a better electron donor but interacting at a longer distance with the diazo moiety than the nitroso-oxygen, both of which are sp^2-hydridized with oxygen being more electronegative.

Although the nitro group is one of the strongest electron-withdrawing substituents available, its presence at the C4 position of IPK (i.e., analogue **5.4d**) has less influence on the diazonium ion character than does the nitroso group. The diazo IR frequency of **5.4d** (C4-NO_2, $\nu_{N\equiv N}$ = 2218 cm^{-1}) is still much higher than IPK (C4-H, $\nu_{N\equiv N}$ = 2139 cm^{-1}) as expected, but the significantly lower effect of the nitro group on diazonium ion character when compared with the nitroso group (**5.4c**, C4-NO, $\nu_{N\equiv N}$ = 2260 cm^{-1}) was at first surprising. Consideration of the various interactions that might influence the diazonium ion character does provide a possible rationalization of the result. On one hand, one would predict that the nitro group would have a stronger inductive and dipole-dipole interactions favouring higher diazonium ion character than the nitroso group. On the other hand, the nitroso group within **5.4c** is able to interact more favourably in a resonance fashion because the plane of the C4-N=O (within either conformer) is much less skewed from planarity than the C4-NO_2 plane within **5.4d**, which possesses a torsion angle of ca. 50º relative to the corresponding aromatic ring plane (Figure 5-13). Also, the through-space interaction with the diazo group of **5.4d** from the lone pair of electrons of one of two nitro-oxygen atoms is evident (Figure 5-13), as the nitro plane tilts so that one nitro-oxygen does get close enough to the diazo moiety. Since the electron density on the oxygen atom of the -NO_2 group is lower than on the oxygen of the –N=O group, and the orientation of the oxygen's

lone pair of electrons towards the diazo moiety within **5.4d** (Figure 5-13) to achieve the lone pair-diazo interaction seems to be less perfect than **5.4c** (Figure 5-12), the through-space interaction to enhance the diazonium ion character is expected to be significantly weaker in the case of **5.4d**. Thus, the difference between the overall effect of the -NO and -NO_2 groups on diazonium ion character may be an indication of the importance of both resonance stabilization and through-space lone pair-diazo interaction.

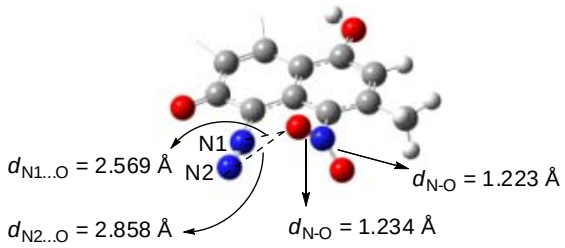

5.4d partial optimized geometry
(Note: AB-ring are omitted for clarity)

Figure 5-13. Optimized (partial) geometry of the IPK-C4-nitro analogue **5.4d**.

There is one more interesting discovery with **5.4d** that is worthy of discussion, which seems to be further supportive to the presence of a through-space interaction from one of the nitro-oxygens to the diazo moiety. The resonance forms of the nitro group would suggest that the two oxygen atoms are equivalent (Figure 5-14), therefore the geometry of the nitro group (especially the two N-O bonds) is not affected significantly by the nature of the moiety to which the nitro group is attached.[372] As indicated by examples in a literature review[372] and structural survey on simple aromatic nitro-substituted compounds (this work) within CSD (version 5.30), bond lengths of the two N-O bonds within the nitro group are in general identical or at least very close to each other. It is noticed that, in the case of **5.4d**, the two N-O bond lengths are in fact quite different (Figure 5-14). The N-O bond (d_{N-O} = 1.234 Å), which is closer to the diazo group with its oxygen that is presumed to interact with

the diazo moiety, is noticeably longer than the other N-O bond ($d_{N\text{-}O}$ = 1.223 Å) that stays far from and hence has no interaction with the diazo moiety. This observation complies with the lone pair-diazo interaction proposal, as the N-O bond is expected to compensate the decrease of electron density on the oxygen due to its partial electron donation to the diazo moiety, and consequently the N-O bond shall be more single bond like and its bond length is extended.

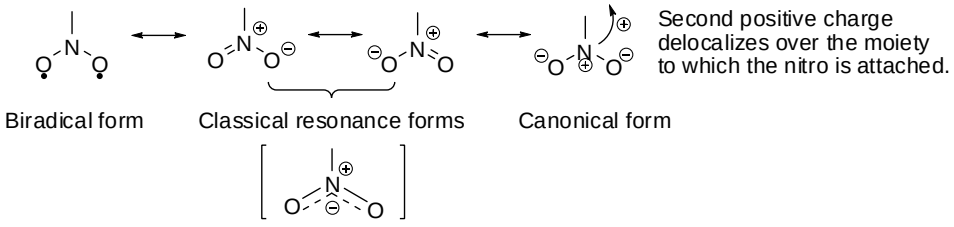

Figure 5-14. Resonance forms of the nitro group.

Comparison of **5.4a** (C4-NH_2, $\nu_{N\equiv N}$ = 2219 cm^{-1}), **5.4c** (C4-NO, $\nu_{N\equiv N}$ = 2260 cm^{-1}) and **5.4d** (C4-NO_2, $\nu_{N\equiv N}$ = 2218 cm^{-1}) based on the above detailed analysis would clearly indicate that, for diazobenzo[*a*]fluorene system, enhancement of the diazonium ion character by C4 electron-withdrawing factor is in general (much) less effective than the presence of a C4 electron-donor that could interact with the C5-diazo group through-space.

5.2.4 MO Calculations of IPK-C4-sulfur/oxygen Analogues

The next series of IPK-C4 analogues are based on sulfur- (Table 5-6) and oxygen-derived (Table 5-7 and 5-8) substituents. With either a thiol (analogue **5.5a**) or methylthiol (analogue **5.5b**) present at the C4 position, the corresponding diazo IR frequencies (i.e., $\nu_{N\equiv N}$ = 2197 cm^{-1} for **5.5a** and $\nu_{N\equiv N}$ = 2198 cm^{-1} for **5.5b**) are essentially the same, and such values are comparable to those of the IPK-C4-halogen analogues (**5.3a**–**c**, $\nu_{N\equiv N}$ = 2193–2180 cm^{-1}).

Table 5-6. Ab initio MO calculations of IPK-C4-sulfur analogues **5.5a**–**b**.

Structure	Optimized geometry	$\nu_{N\equiv N}$ (cm^{-1})[a]	$d_{N\equiv N}$ (Å)	<C-N-N(°)
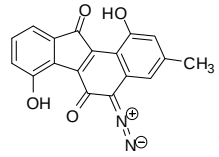 **1.5**	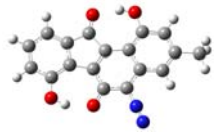	2139	1.103	176.2
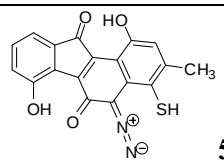 **5.5a**	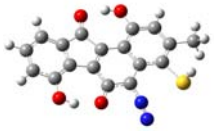	2197	1.0978	168.8
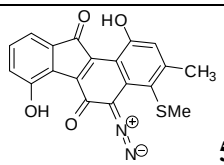 **5.5b**	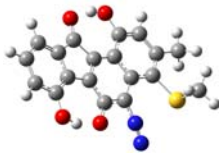	2196	1.0979	169.1

a. Scaled by a scaling factor of 0.8929.

Since sulfur is a much weaker electronegative element than the halogens such as fluorine and chlorine, the observed high level of diazonium ion character of **5.5a** (and **5.5b**) is likely not a result of diazonium-favourable inductive, resonance or dipole-dipole interactions. This would suggest the possibility of the lone pair interaction from sulfur to the diazo to account for the fairly high calculated diazo IR frequencies. Similar to the previous case of **5.4a** (C4-NH_2), optimization of both **5.5a** (C4-SH) and **5.5b** (C4-SMe) with different starting orientations of the sulfur atom always ends up with one of the sulfur's two lone pairs of electrons pointing towards the diazo nitrogens (Figure 5-15). Such geometries would suggest again the presence of beneficial electronic interactions between the sulfur lone pair of electrons and the diazo group. Partial donation of a lone pair of electrons to the diazo group from sulfur would also benefit from its low electronegativity. The high diazonium ion character of **5.5a** and **5.5b** is likely the consequence of such lone pair-diazo interaction. This sulfur lone pair-diazo interaction is further evident from the close distances in between the C4-S and two diazo nitrogens (Figure 5-15), which are significantly shorter than the sum of the corresponding vdW

radii (r_N= 1.55 Å, r_S= 1.80 Å). The long C4-S bonds in both cases (1.849 Å for **5.5a** and 1.842 Å for **5.5b**) would align the sulfur atom approximately to the middle point of the N≡N bond (Figure 5-15), since distances between C5 and the middle point of the N≡N bond are ca. 1.90 Å for both **5.5a** and **5.5b**. Such alignment would probably allow a stronger interaction between the sulfur (lone pair) and the terminal N2 atom than the case of **5.4a** (C4-NH_2), in which the amine aligns mainly with the middle N1 atom (Figure 5-9) due to the shorter C4-N bond (vs the C4-S bond). Similar geometry was in fact observed in the previous case of **5.3c** (C4-Br), in which the extended C4-Br bond ($d_{C4–Br}$ = 1.945 Å) also aligns the bromine atom approximately to the middle point of the corresponding diazo moiety, while distance between C5 and the middle point of the N≡N bond is also ca. 1.90 Å for **5.3c**.

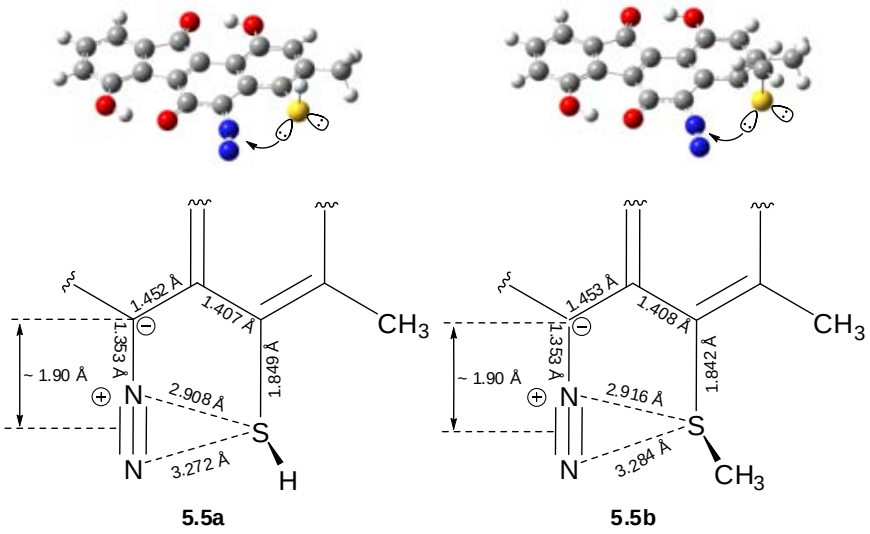

5.5a **5.5b**

Figure 5-15. Optimized geometries of IPK-C4-sulfur analogues **5.5a** (C4-SH) and **5.5b** (C4-SMe).

When substituents such as –OH (analogue **5.5c**) and –OMe (analogue **5.5d**) are introduced at the C4 position (Table 5-7), the corresponding diazo IR frequencies are expected and found indeed to be higher than those of **5.5a** (C4-SH) and **5.5b** (C4-SMe), partially due to the much higher electronegativity of oxygen than sulfur that should strengthen the inductive effect and dipole-dipole

interaction favouring a high diazonium ion character. On the other hand, the significantly smaller size of oxygen than sulfur allows the –OH/–OMe to adopt better orientations than the –SH/–SMe to offer stronger lone pair-diazo interactions in favour of higher diazonium ion character, even though oxygen is a weaker electron donor than sulfur.

Table 5-7. Ab initio MO calculations of IPK-C4-oxygen analogues **5.5c–e**.

Structure	Optimized geometry	$\nu_{N\equiv N}$ (cm^{-1})[a]	$d_{N\equiv N}$ (Å)	<C-N-N(°)
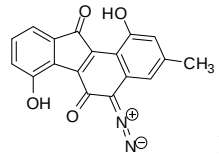 **1.5**	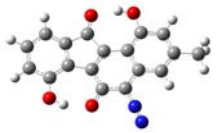	2139	1.103	176.2
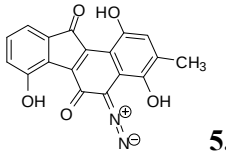 **5.5c**	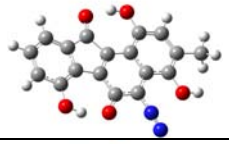	2210	1.097	173.5
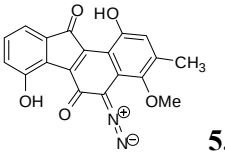 **5.5d**	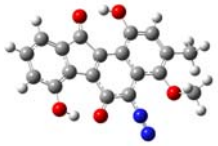	2198	1.098	173.6
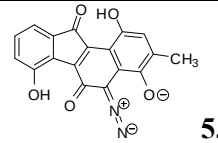 **5.5e**	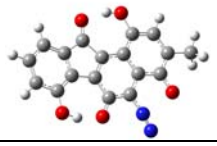	2226	1.095	170.8

a. Scaled by a scaling factor of 0.8929.

Similar to the previous amine/amide (**5.4a**/**5.4b**) and thiol/methylthiol (**5.5a**/**5.5b**) cases, geometry optimization of **5.5c** and **5.5d** also leads to conformations (Table 5-7 and Figure 5-16) with their C4-oxygen's lone pair(s) of electrons pointing towards the diazo moiety regardless of the starting orientations. Once again a lone pair interaction between the C4-oxygen and the C5-diazo group is evident from the optimized geometries of **5.5c** and **5.5b** (Figure 5-16), as the distances between the C4-oxygen and the two diazo nitrogens are significantly shorter than the sum of the corresponding vdW radii (r_N = 1.55 Å, r_O = 1.52 Å) in both cases. There are some interesting and noticeable

difference between the **5.5c** (C4-OH) and **5.5d** (C4-OMe) as to how the corresponding lone pair of electrons of oxygen interact with the diazo moiety. The C4-OH within **5.5c** is coplanar with the aromatic ring in the optimized geometry (Figure 5-16), which makes the oxygen's two lone pairs of electrons both intersect and interact with the diazo moiety. Yet the C4-OMe within **5.5d** can not make the oxygen's both lone pairs of electrons interact with the diazo group simultaneously (Figure 5-16), due to the steric interaction between the C4-methoxy methyl group and the C3-methyl group that forces the methoxy group to adopt a conformation orthogonal to the aromatic ring plane. As a result of this geometry, only one of the two lone pairs of electrons on the methoxy-oxygen could interact with the diazo moiety. The significantly stronger lone pair-diazo interaction within **5.5c** (C4-OH) than **5.5d** (C4-OMe), as determined by the geometry, explains the noticeably lower diazonium ion character of the latter structure (**5.5c**, $\nu_{N\equiv N} = 2210\ cm^{-1}$; **5.5d**, $\nu_{N\equiv N} = 2198\ cm^{-1}$).

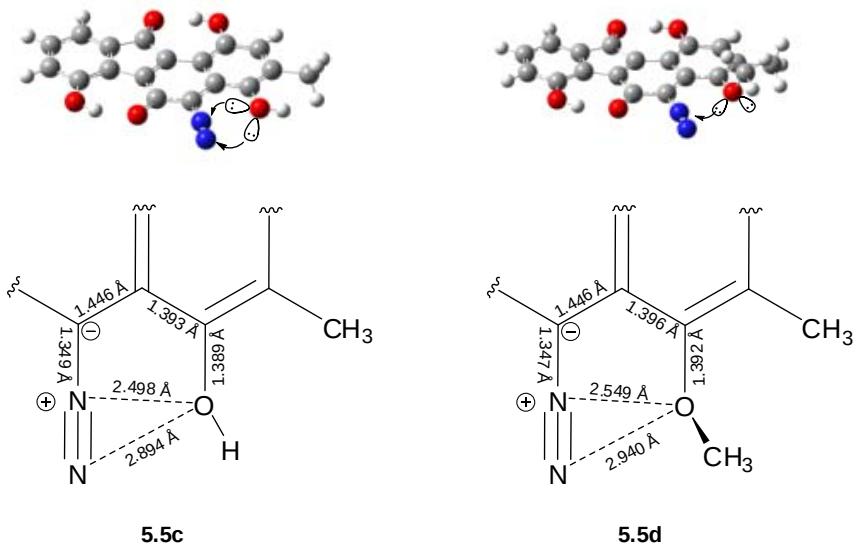

5.5c **5.5d**

Figure 5-16. Optimized geometries of IPK-C4-oxygen analogues **5.5c** (C4-OH) and **5.5d** (C4-OMe).

On the other hand, since methyl is an electron-donating group when compared to hydrogen, the methoxy-oxygen is higher in electron density than the hydroxy-oxygen. If the C3-methyl group within **5.5c** (C4-OH, C3-Me) and **5.5d** (C4-OMe, C3-Me) is replaced by the smallest "substituent" of hydrogen so that the steric interaction between C3/C4 substituents no longer prohibits the free rotation of the C4-moiety to achieve a maximum lone pair-diazo interaction, then a higher diazonium ion character induced by the C4-OMe than C4-OH is expected. In fact, computation of such simpler analogues (i.e., IPK-C4-OH-C3-H **5.8a** and IPK-C4-OMe-C3-H **5.8b**, Figure 5-17) did provide results that are entirely consistent with such a prediction. Without the steric restriction from the nearby C3 group, the C4-OMe within **5.8b** (not including the methyl hydrogens though) is now coplanar with the aromatic ring, similar to the case of **5.5c** (C4-OH, C3-Me) but not possible within **5.5d** (C4-OMe, C3-Me) for steric reasons. Similarly, the C4-OH within **5.8a**, not surprisingly, adopts the beneficial coplanarity with the aromatic ring in the even less crowded environment. Such conformations of **5.8a** and **5.8b** are capable of providing a maximum (oxygen) lone pair-diazo interaction in which both lone pairs of electrons on the oxygen participate. The higher electron density on the methoxy-oxygen within **5.8b** than the hydroxy-oxygen within **5.8a** does lead to a slightly higher diazo IR frequency for the former structure as predicted (**5.8b**, $\nu_{N\equiv N}$ = 2213 cm^{-1}; **5.8a**, $\nu_{N\equiv N}$ = 2211 cm^{-1}). Stronger lone pair-diazo interaction within **5.8b** (C4-OMe, C3-H) than **5.8a** (C4-OH, C3-H) is also evident from the shorter O-N interacting distances that associate with **5.8b** (Figure 5-17), which are correlated in an opposite manner (Figure 5-16) in the case of **5.5d** (C4-OMe, C3-Me) and **5.5c** (C4-OH, C3-Me).

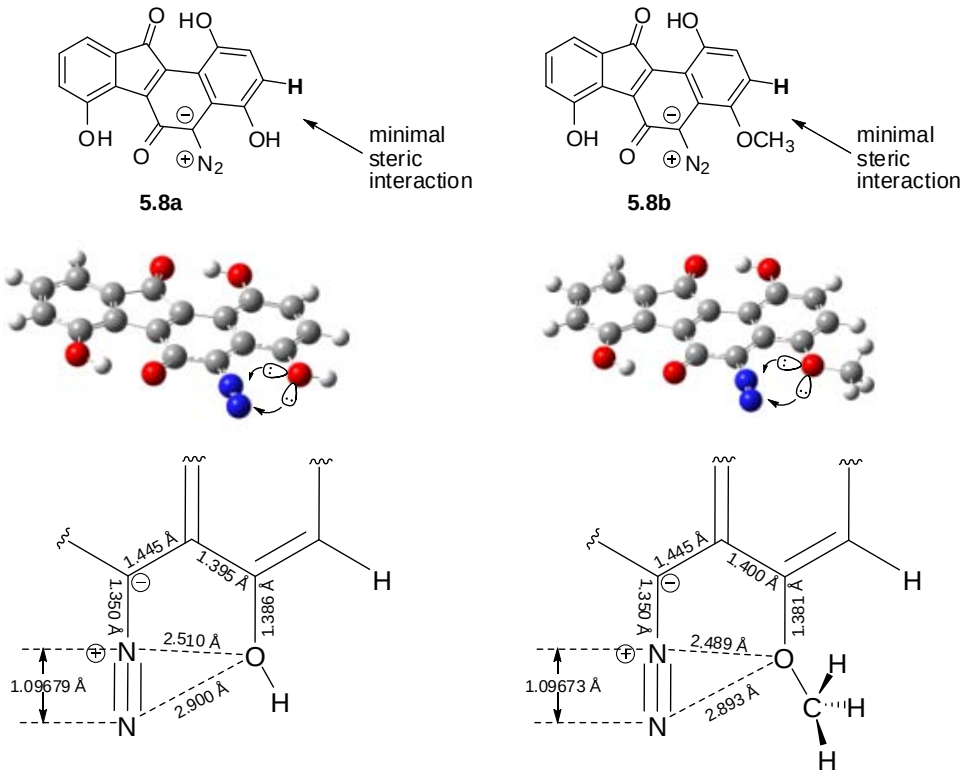

Figure 5-17. Optimized geometries of IPK-C4-OH-C3-H **5.8a** and IPK-C4-OMe-C3-H **5.8b**.

Similar to the previous work on **5.4a** (C4-NH_2) as shown in Figure 5-10, SPE calculations were also performed with **5.5c** (C4-OH) in order to estimate the energy contribution from the (oxygen) lone pair-diazo interaction. Rotation of dihedral angle between the C4-OH group and the aromatic ring plane by 90°, 180° and 270°, while keeping the rest of the optimized conformation unaltered, results in noticeable increase in energy (Figure 5-18). An estimated moderate energy contribution of ca. 4.3 kcal/mol from the (oxygen) lone pair-diazo interaction is obtained when the C4-O is deviated by either 90° or 270° from the optimized orientation (Figure 5-18), however, one needs to realize that, within these two conformations, some lone pair-diazo interaction from one of the two lone pairs of electrons is still feasible due to the geometry. On the other hand, the much higher energy of 26.5 kcal/mol of the conformation having the C4-O deviated by 180° from the optimized orientation

(Figure 5-18) is mainly due to the unfavourable steric repulsion between the hydrogen and diazo moiety even though in this case the beneficial lone pair-diazo interaction completely disappears. Therefore, the energy contribution from the oxygen lone pair-diazo interaction should be in the range of 26.5 kcal/mol >> E > 4.3 kcal/mol. Considering the higher electronegativity of oxygen than that of nitrogen and thus less electron donation and weaker lone pair interaction with the diazo, this electronic energy from oxygen is likely to be lower than the corresponding value of **5.4a** (C4-NH_2, ~ 8.3 kcal/mol). This lone pair effect would still dominate but probably to a lesser extent to affect the diazonium ion character in the case of **5.5c** (C4-OH) than **5.4a** (C4-NH_2), which seems to be consistent with the observed slightly lower diazo IR frequency of **5.5c** ($\nu_{N\equiv N}$ = 2210 cm^{-1}) than that of **5.4a** ($\nu_{N\equiv N}$ = 2219 cm^{-1}).

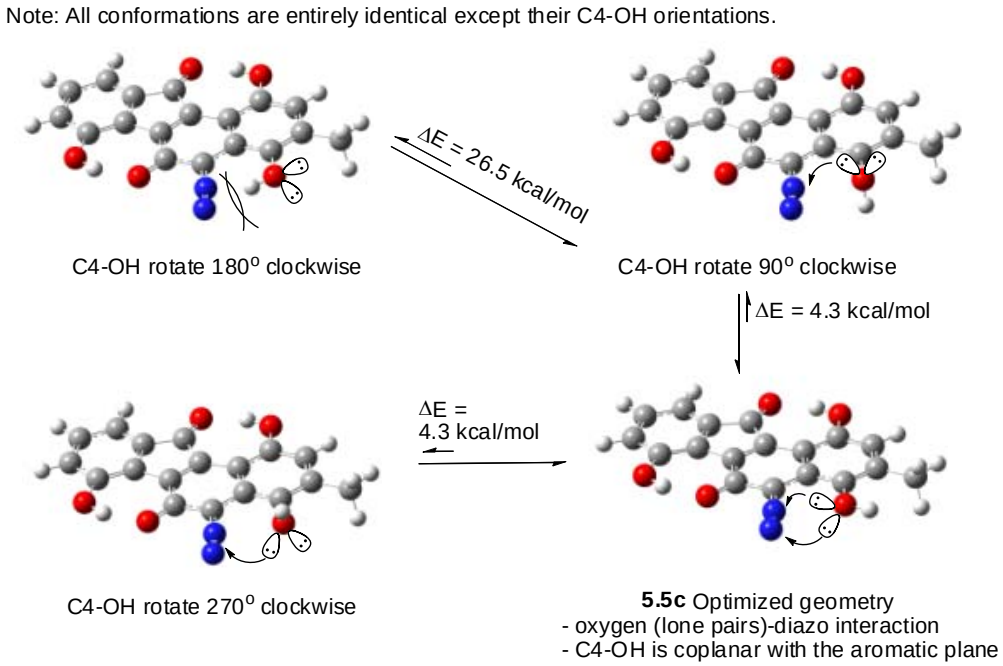

Figure 5-18. SPE calculations of IPK-C4-OH analogue **5.5c**.

The phenolate analogue **5.5e** (C4-O^-) is in fact a variant of **5.5c** (C4-OH) upon simple C4-phenol deprotonation (ionization). This ionization is possible under the physiologically important pHs (7.4 ± 1) due to the moderate acidity of the phenols, whose typical pKa is about 7–10. The resulting even higher diazo IR frequency of **5.5e** (C4-O^-, $\nu_{N\equiv N}$ = 2226 cm^{-1}) than the corresponding neutral form **5.5c** (C4-OH, $\nu_{N\equiv N}$ = 2210 cm^{-1}) is not surprising by now. The negatively charged C4-O^- would definitely provide neither favourable inductive nor resonance effect to delocalize the C5 negative charge to enhance the diazonium ion character. Dipole-dipole interaction in favour of a higher diazonium ion character, however, should still be applicable in this case yet it is expected to be very limited and weaker than the case of **5.5c**. This would once again make the lone pair interaction from the C4-O^- towards the C5-diazo group as the major contributing factor to be responsible for the very high diazonium ion character of **5.5e**. Such lone pair-diazo interaction is further supported by the very close O-N distances ($d_{C4\text{-}O\cdots N1}$ = 2.447 Å, $d_{C4\text{-}O\cdots N2}$ = 2.875 Å) and shall benefit significantly from the very high electron density on the negative C4-oxygen.

Furthermore, the typical bond lengths for $C(sp^2)$–O and $C(sp^2)$=O are 1.34 Å and 1.21 Å respectively, and literature X-ray data of model compounds such as **5.9** (CSD Refcode: TALGOD) and **5.10** (CSD Refcode: MENAQU10) also give similar values (Figure 5-19). Thus, the short C4-O^- bond length of 1.299 Å within **5.5e** would indicate that the resonance delocalization of the phenolic negative charge onto the aromatic D-ring (Figure 5-19) is a significant contribution to the stability of the anion. Consequently the C4-O bond of **5.5e** possesses substantial double-bond character and hence a short bond length. This result is consistent with a corresponding value from the computed results of the anion of **5.10** (Figure 5-19), which possesses significant delocalization of the phenolic negative charge onto the aromatic ring.

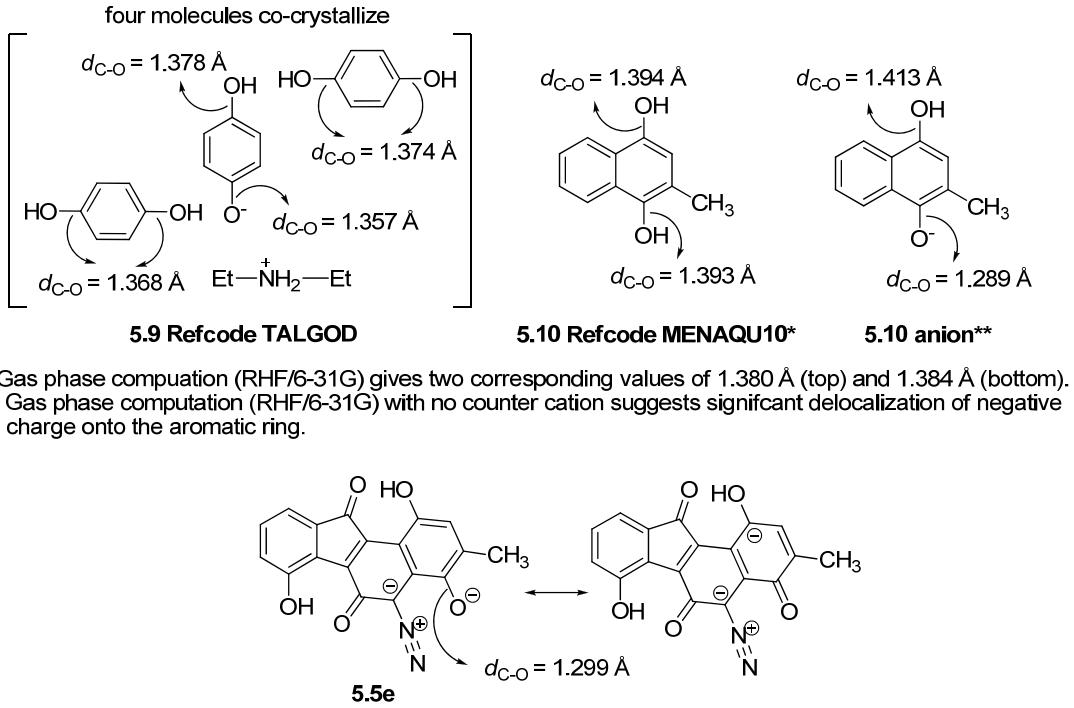

Figure 5-19. Model compounds and resonance forms of IPK-C4-O$^-$ analogue **5.5e**.

Interestingly, when electron-withdrawing groups such as acetyl (analogue **5.5f**), mesyl (analogue **5.5g**) and tosyl (analogue **5.5h**) are attached to the C4-oxygen of **5.5c**, the corresponding diazo IR frequencies show some consistency with the electron-withdrawing ability of such ester groups (Table 5-8).

Table 5-8. Ab initio MO calculations of IPK-C4-oxygen analogues **5.5f**–**h**.

Structure	Optimized geometry	$\nu_{N\equiv N}$ (cm^{-1})[a]	$d_{N\equiv N}$ (Å)	<C-N-N(°)
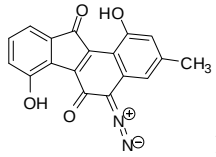 **1.5**	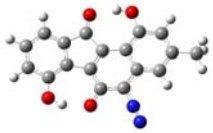	2139	1.103	176.2
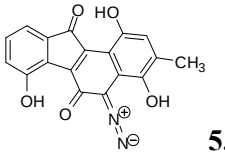 **5.5c**	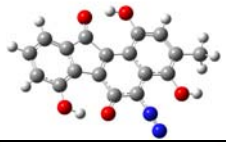	2210	1.097	173.5
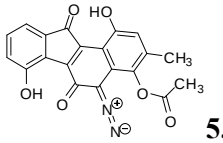 **5.5f**	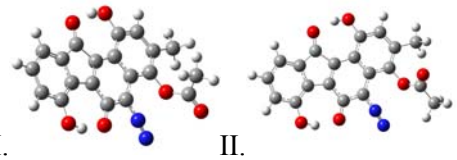 I. II. *s*-cis ester *s*-trans ester ΔE(II - I) = -5.4 kcal/mol	I. 2207 II. 2174	I. 1.097 II. 1.110	I. 173.0 II. 173.0
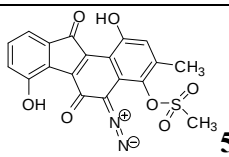 **5.5g**		2219	1.096	173.0
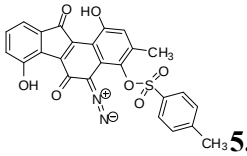 **5.5h**	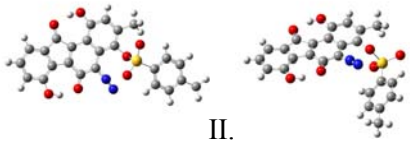 I. II. ΔE(II - I) = 2.1 kcal/mol	I. 2217 II. 2195	I. 1.096 II. 1.098	I. 173.1 II. 173.5
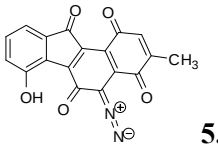 **5.7**		2265	1.093	173.8

a. Scaled by a scaling factor of 0.8929.

The decrease of diazo IR frequency from **5.5c** (C4-OH, $\nu_{N\equiv N}$ = 2210 cm^{-1}) to **5.5f** (C4-OAc, conformer I, $\nu_{N\equiv N}$ = 2207 cm^{-1}) is only 3 cm^{-1}, which is much smaller than the corresponding change ($\Delta\nu_{N\equiv N}$ = 27 cm^{-1}) observed between **5.4a** (C4-NH_2, $\nu_{N\equiv N}$ = 2219 cm^{-1}) and **5.4b** (C4-NHAc, conformer I, $\nu_{N\equiv N}$ = 2192 cm^{-1}). This observation is consistent with the more substantial diminution in electron density at nitrogen in an amide vs in an amine, as a consequence of amide resonance, than

that observed at oxygen in an ester vs an alcohol. Not surprisingly, the acetyl ester **5.5f** also exists as either *s*-cis or *s*-trans conformers that are quite different in energy (|ΔE| = 5.4 kcal/mol, Table 5-8), similar to the previous case of **5.4b** (C4-NHAc) but its *s*-cis and *s*-trans conformers are comparably stable (|ΔE| = 0.12 kcal/mol, Table 5-5). An even larger difference in diazo IR frequencies between the two conformers of **5.5f** ($\Delta\nu_{N\equiv N}$ = 33 cm^{-1}) than the case of **5.4b** ($\Delta\nu_{N\equiv N}$ = 19 cm^{-1}) is observed. There is no good explanation at the moment to rationalize such diazo IR difference between the *s*-cis/*s*-trans conformation for both **5.5f** (C4-OAc) and **5.4b** (C4-NHAc); however, it is interesting to notice that in both cases, the *s*-cis conformer is always associated with a higher diazonium ion character.

When much stronger electron-withdrawing groups such as mesyl (Ms) and tosyl (Ts) are present (analogue **5.5g** and **5.5h**), the (C4-oxygen) lone pair-diazo interaction is expected to decrease more noticeablely. There are, however, two additional and beneficial influencing factors for the diazonium ion character to be considered at the same time. The first one, of less importance, is the enhanced inductive and dipole-dipole interaction from the more electron-withdrawing ester groups (–OMs/–OTs vs –OH) in favour of a higher diazonium ion character. Second, very likely a (much) stronger influencing factor, is the common presence of an electron-rich sp^2-hybridized sulfonyl-oxygen (**O**=S-) within **5.5g** (C4-OMs) and **5.5h** (C4-OTs), which is also located in close proximity to the diazo group besides the C4-oxygen but slightly further away (Table 5-8). For example, within the optimized conformation of **5.5g** (C4-OMs), distances between one of the sulfonyl-oxygens and the diazo moiety ($d_{S=O\cdots N1}$ = 2.985 Å; $d_{S=O\cdots N2}$ =3.029 Å) are longer than the corresponding values for the C4-oxygen/diazo ($d_{C4\text{-}O\cdots N1}$ = 2.637Å; $d_{C4\text{-}O\cdots N2}$ =3.042 Å) but still shorter than the sum of the corresponding vdW radii (r_O = 1.52 Å, r_N = 1.55 Å). Similar to the C4-oxygen, the sulfonyl-oxygen "-S=**O**" is also capable of donating partially its lone pair of electrons to the diazo moiety to enhance the diazonium ion character when geometry allows. The strong lone pair interaction from the C4-X**:** (X =

N, O, S) towards the diazo group due to the close interacting distance can be regarded as a primary effect, while the further but weaker lone pair interaction from the "-S=**O**" towards the diazo moiety (due to the longer interacting distance) is more like a secondary effect. This secondary lone pair-diazo interaction, along with the enhanced inductive effect and dipole-dipole interaction, apparently could override the decreasing influence on the diazonium ion character due to the weakening of the primary lone pair effect from the strong electron-withdrawing –Ms or –Ts group. Therefore, the observed slightly higher diazo IR frequencies for **5.5g** (C4-OMs, $\nu_{N\equiv N}$ = 2219 cm^{-1}) and **5.5h** (C4-OTs, conformer I, $\nu_{N\equiv N}$ = 2217 cm^{-1}) than that of **5.5c** (C4-OH, $\nu_{N\equiv N}$ = 2210 cm^{-1}) are the overall results from the combined influence as discussed above.

In the case of **5.5h** (C4-OTs), it is interesting to find a slightly less stable conformer II than conformer I by ca. 2.1 kcal/mol (Table 5-8 and Figure 5-20). More surprisingly, distances between the C4-oxygen and the diazo nitrogens within conformer II ($d_{C4\text{-}O\cdots N1}$ = 2.581 Å, $d_{C4\text{-}O\cdots N2}$ =2.986 Å) are shorter than the corresponding values from conformer I ($d_{C4\text{-}O\cdots N1}$ = 2.632 Å, $d_{C4\text{-}O\cdots N2}$ = 3.033 Å), yet the former is significantly lower in diazonium ion character. This observation seems to be contradictory to the earlier results at first glance, since for the IPK-C4-X**:** analogues, shorter distances between C4-X**:** and diazo nitrogens would (in principle) correspond to stronger lone pair-diazo interactions and consequently higher diazonium ion character. However, careful examination of the optimized geometries of both conformers of **5.5h** (Figure 5-20) indicates that, the lone pair of electrons on the sp^3-hybridized C4-oxygen within conformer I possesses a much better lone pair-diazo alignment than conformer II. To achieve a maximum of the beneficial electronic interaction, alignment of the interacting orbitals (in an appropriate orientation to overlap) should be of the importance as well as the interaction distance. Therefore, despite the slightly longer C4-oxygen/diazo distances, conformer I is expected to possess a stronger primary lone pair-diazo interaction in favour of a higher diazonium ion character due to the right orientation of the lone pair of electrons. In

addition, conformer I also has one of its sulfonyl-oxygen "-S=**O**" to stay close enough to the diazo moiety to offer additional secondary lone pair-diazo interaction to further enhance the diazonium ion character, while conformer II totally lacks such interaction from either of its two "-S=**O**" oxygens due to their far distance from the diazo group (Figure 5-20). Combination of these two effects might be the cause of the significant difference in diazonium ion character between the two conformers of **5.5h**.

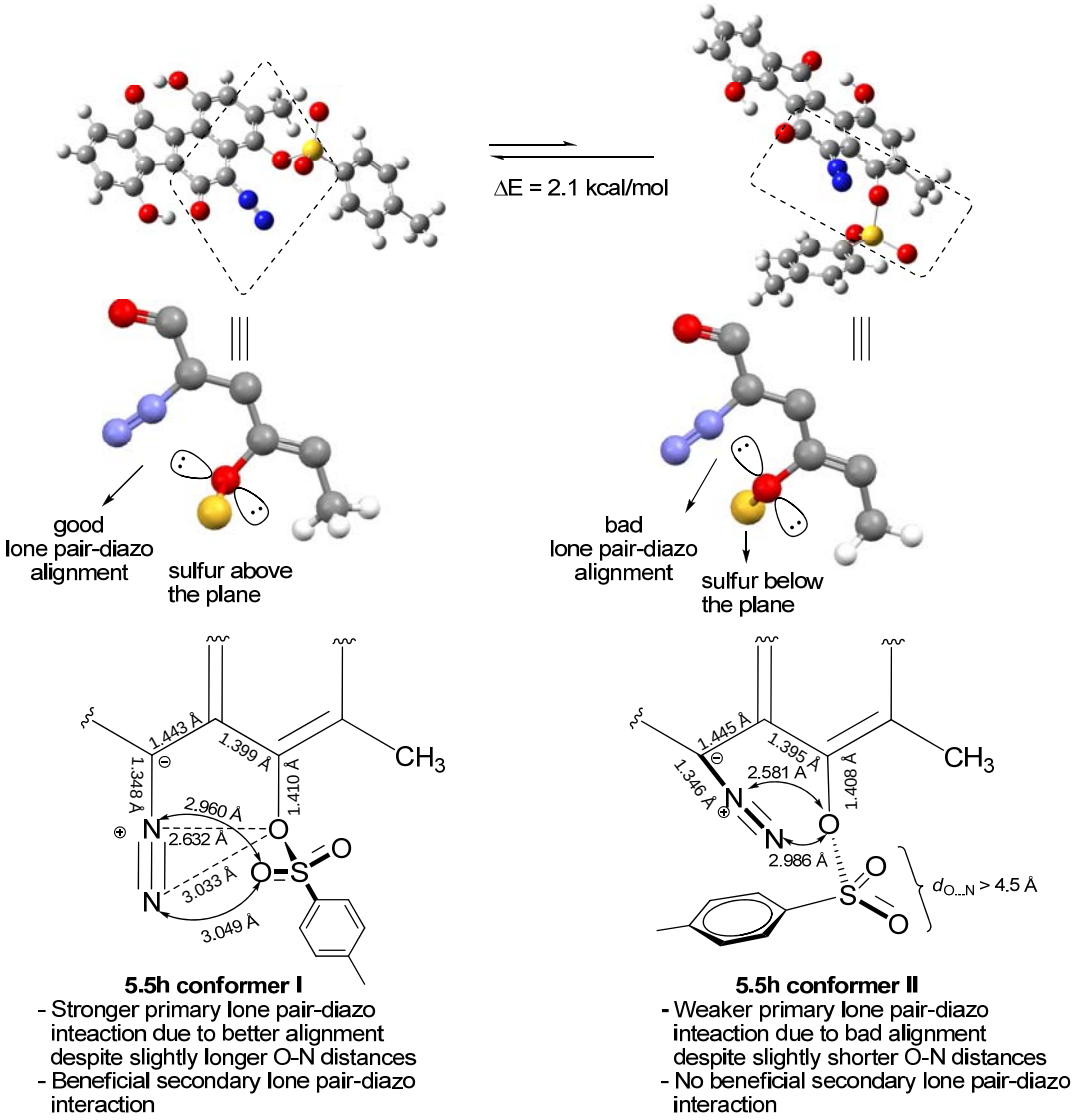

Figure 5-20. Optimized geometries of the two conformers of IPK-C4-tosylate analogue **5.5h**.

Strictly speaking, the IPK-D-ring-quinone analogue **5.7** is no longer an IPK-C4-analogue since it loses the D-ring's aromaticity when two conjugated carbonyl groups are present at C1 and C4. This D-ring quinone system presents a strong resonance stabilization effect owing to the presence of the C1-carbonyl group, which is expected to enhance the diazonium ion character over and above that induced by strong inductive effect and dipole-dipole interaction from the C4-carbonyl group, as described for the IPK-C4 analogues previously (Figure 5-21). However, the very high diazo IR frequency of **5.7** ($\nu_{N\equiv N}$ = 2265 cm^{-1}), which is by far the largest value obtained, might suggest the presence of some other strong interactions to be capable of enhancing the diazonium ion character to such a high level. This can be traced back again to a strong oxygen lone pair-diazo interaction (Figure 5-21), in which the sp^2-hybridized and electron-rich C4 carbonyl oxygen locates close enough to the diazo moiety ($d_{O\cdots N1}$ = 2.579 Å, $d_{O\cdots N2}$ = 2.985 Å, cf. r_N = 1.55 Å, r_O = 1.52 Å) with one of its two lone pairs of electrons pointing towards the electron-deficient diazo nitrogens.

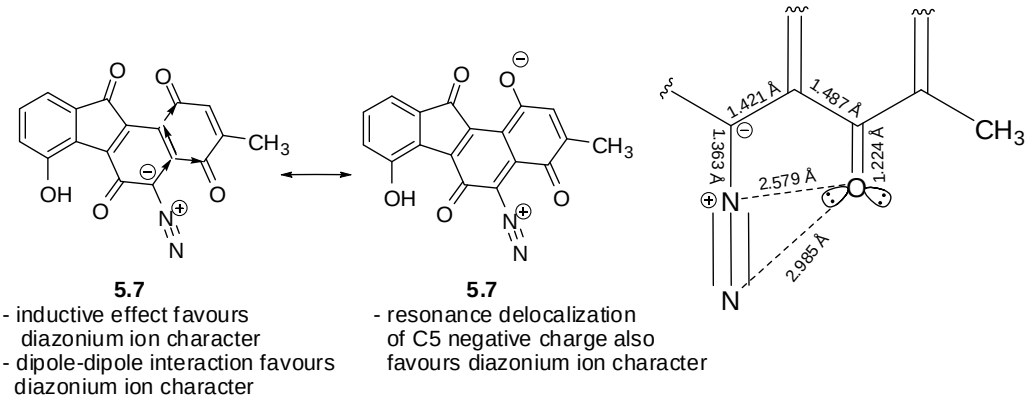

Figure 5-21. Substitution effects within IPK-D-ring-quinone analogue **5.7** on diazonium ion character.

The molecule **5.7** is of particular interest not only because of its unusually high diazonium ion character but also due to its structural simplicity. In principle, **5.7** might be easier to prepare than the other proposed IPK-C4-analogues. For example, a direct and selective D-ring phenol oxidation of

IPK (**1.5**), which is now readily available through either fermentation or synthesis, is apparently the easiest way to achieve the goal. Alternatively, modification of the Dmitrienko synthetic procedure of **1.5** (Scheme 3-36, section 3.2.2) is also feasible. Careful selection of appropriate D-ring phenol protecting group, which should be different from and more easily cleaved than the A-ring phenol protecting group later on, may provide access to an intermediate having a free D-ring phenol while the A-ring phenol is still protected as an ether or ester. It should be possible to selectively oxidize the D-ring of such a compound to the corresponding quinone (as in **5.7**), prior to the introduction of the remaining diazo moiety and deprotection of the A-ring phenol ether or ester.

5.2.5 MO Calculations of IPK-C4-carbonyl Analogues

The last series of IPK-C4-analogues are based on some carbonyl-derived substituents present at the C4 position of IPK (**1.5**). Although the results (Table 5-9 and 5-10) may seem a little bit more complicated than the previous cases, all calculated diazo IR frequencies can be reasonably explained by using the concepts discussed earlier.

Table 5-9. Ab initio MO calculations of IPK-C4-carbonyl analogues **5.6a**–**c**.

Structure	Optimized geometry	$\nu_{N\equiv N}$ (cm^{-1})[a]	$d_{N\equiv N}$ (Å)	<C-N-N(°)
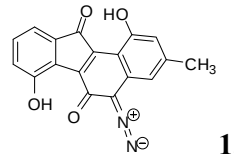 **1.5**	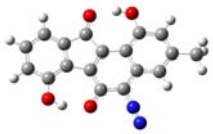	2139	1.103	176.2
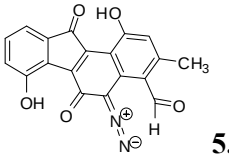 **5.6a**	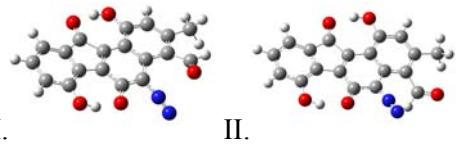 I. II. ΔE(II - I) = 3.6 kcal/mol	I. 2248 II. 2147	I. 1.094 II. 1.102	I. 172.1 II. 171.9
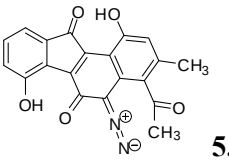 **5.6b**	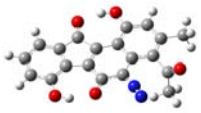	2142	1.102	171.4
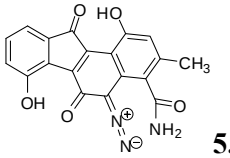 **5.6c**	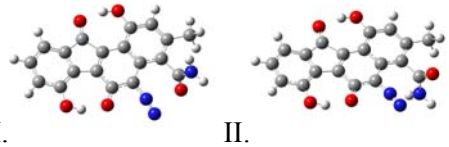 I. II. ΔE(II - I) = 0.06 kcal/mol	I. 2186 II. 2173	I. 1.099 II. 1.100	I. 170.8 II. 171.3

a. Scaled by a scaling factor of 0.8929.

With the simplest carbonyl-based substituent, an aldehyde, introduced at the C4 position (analogue **5.6a**), two C4-conformers of **5.6a** with a significant energy difference of 3.6 kcal/mol are found through geometry optimization (Table 5-9). The major difference between the two conformers is the orientation of the C4-aldehyde group, and the geometry of the aldehyde's C=O double bond of conformer I resembles the previously observed one for **5.2a** (C4-CH=CH_2) and **5.4c** (C4-NO, conformer II). Interestingly, the corresponding diazonium ion character is found to be dramatically affected by the orientation of the aldehyde carbonyl group. When the C=O double bond of the aldehyde is closer to the diazo moiety as in conformer I (Figure 5-22), the presence of a very strong lone pair interaction from the carbonyl oxygen with the diazo moiety is indicated by the geometry data ($d_{HC=O\cdots N1}$ = 2.470 Å, $d_{HC=O\cdots N2}$ = 2.722 Å), while such an effect is completely absent in the case

of conformer II since its aldehyde carbonyl oxygen is too far from the diazo moiety ($d_{HC=O\cdots N1}$ > 3.68 Å) to interact through-space. The structure of **5.6a** would still have inductive and dipole-dipole interactions from the electron-withdrawing C4-CHO group in favour of a higher diazonium ion character, and such effects are expected to be very limited but identical for the two conformers. Contribution to higher diazonium ion character from resonance delocalization is also expected to be small but still comparable between conformer I and II, since the CH=O plane is skewed to the corresponding aromatic ring plane in approximately the same dihedral angle within the two conformers (Figure 5-22). Therefore, the observed enormous difference in diazonium ion character ($\Delta\nu_{N\equiv N}$ = 101 cm^{-1}) between these two conformers of **5.6a** must originate predominantly from the different level of (carbonyl oxygen) lone pair-diazo interactions. Another noteworthy observation is that in the case of conformer I of **5.6a** in which the lone pair-diazo interaction is quite obvious, the interacting lone pair of electrons from oxygen points towards the N1-C5 site rather than the N1-N2 site (Figure 5-22), while all previously observed lone pair-diazo interactions have the interacting lone pair pointing towards the N1-N2 site.

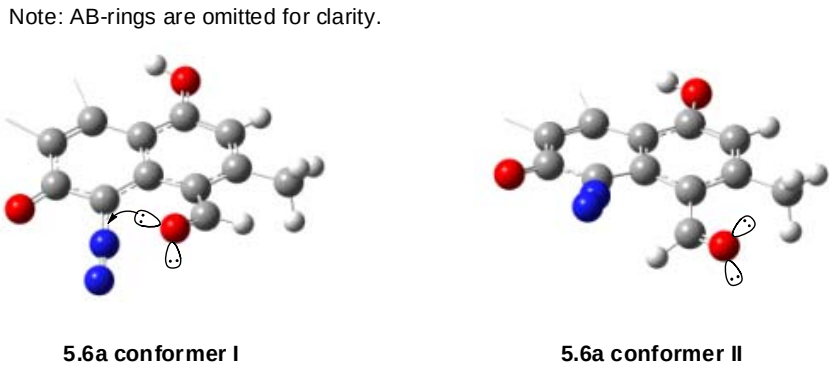

Figure 5-22. Optimized (partial) geometries of the two conformers of IPK-C4-CHO analogue **5.6a**.

In addition, the calculated diazo IR frequency for conformer II of **5.6a** (C4-CHO, $\nu_{N\equiv N}$ = 2147 cm^{-1}), which has no intramolecular lone pair-diazo interaction to greatly enhance the diazonium ion

character, is only slightly higher than the corresponding value of IPK (C4-H, $\nu_{N\equiv N}$ = 2139 cm^{-1}). This small and rather limited increase in diazo IR frequency would clearly suggest (again) that, contributions towards a higher diazonium ion character by inductive effect, resonance effect and dipole-dipole interaction from the C4-substituent are much weaker than the through-space lone pair-diazo interaction, if the latter is present.

It is not surprising to find that, within the lowest energy conformation of IPK-C4-acetyl analogue **5.6b**, the C4-acetyl plane is almost orthogonal to the aromatic skeleton (Table 5-9). The much larger acetyl methyl group within **5.6b** than that of aldehyde hydrogen within **5.6a** would greatly limit the freedom of the C4-substituetnt. The best and probably the only solution for **5.6b** is to adopt the geometry as shown. For **5.6b**, adopting a conformation similar to either of the conformer I or II of **5.6a** is unfavourable, since this would introduce significant steric repulsion between the C4 acetyl methyl group with either the C3-methyl group or the C5-diazo group. Within the optimized conformation of **5.6b**, the carbonyl oxygen not only stays far from the diazo moiety ($d_{MeC=O\cdots N}$ > 3.22 Å), but also the orientation of the carbonyl oxygen is such that its lone pair of electrons can not interact at all with the diazo moiety. The absence of the lone pair-diazo interaction to enhance the diazonium ion character within **5.6b** is similar to the situation observed for conformer II of **5.6a**. The slightly smaller diazo IR frequency of **5.6b** ($\nu_{N\equiv N}$ = 2142 cm^{-1}) than that of **5.6a** (conformer II, $\nu_{N\equiv N}$ = 2147 cm^{-1}) is consistent with the prediction that the C4-carbonyl of **5.6b** (C4-COMe) is less electron-deficient than that of **5.6a** (C4-CHO) since methyl is more electron-donating than hydrogen, which corresponds to slightly weaker inductive, resonance and dipole-dipole interactions and hence a lower diazonium ion character.

The IPK-C4- $CONH_2$ analogue **5.6c** adopts two conformations that are very close in energy (Table 5-9), both of which are very similar to the optimized conformation of **5.6b**, with the carbamide plane nearly orthogonal to the aromatic ring plane (Figure 5-23). Such conformations would obviously

minimize the steric interactions between the carbamide group with both the C5-diazo and C3-methyl groups. The significantly higher diazo IR frequency of **5.6c** (C4-$CONH_2$, $\nu_{N\equiv N}$ = 2173/2186 cm^{-1}) than that of **5.6b** (C4-$COCH_3$, $\nu_{N\equiv N}$ = 2142 cm^{-1}) is expected; initially and apparently it was thought that the carbamide nitrogen within **5.6c** is able to provide a lone pair-diazo interaction that is absent within **5.6b**. However, the existence of a (carbamide nitrogen) lone pair-diazo interaction within **5.6c** is very questionable upon a more detailed examination of the geometry (Figure 5-23), since the distances between the carbamide nitrogen and the two diazo nitrogens (conformer I, $d_{O=C-N\cdots N1/N2}$ > 3.31 Å; conformer II, $d_{O=C-N\cdots N1/N2}$ > 3.11 Å) are in fact larger than the sum of the corresponding vdW radii (r_N = 1.55 Å). In addition, the calculated higher diazo IR frequency for conformer I ($\nu_{N\equiv N}$ = 2186 cm^{-1}) than that of conformer II ($\nu_{N\equiv N}$ = 2173 cm^{-1}) of **5.6c** also does not match well with the observed much longer distances between the carbamide nitrogen and the two diazo nitrogens for conformer I than those of conformer II (Figure 5-23), even if such (nitrogen) lone pair-diazo interaction exists.

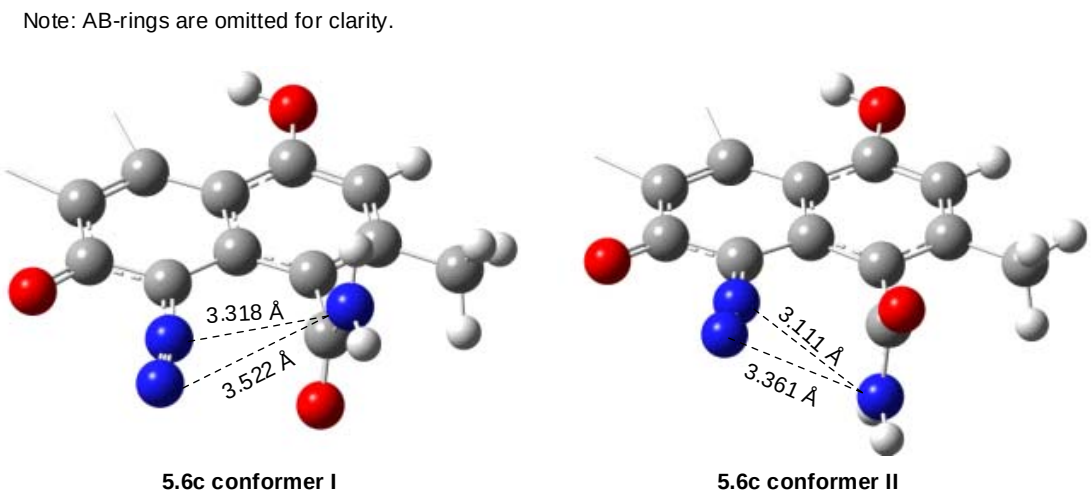

Figure 5-23. Optimized (partial) geometries of the two conformers of IPK-C4-carbamide analogue **5.6c** suggesting no (carbamide-nitrogen) lone pair-diazo interaction.

Instead, the C4 carbamide-carbon actually stays in very close proximity to the diazo nitrogens in both conformers of **5.6c**, and the corresponding distances (Figure 5-24) are significantly shorter than the sum of the vdW radii (r_N= 1.55 Å, r_C= 1.70 Å). It is also found that the lone pair of the carbamide-nitrogen partially delocalizes to the carbonyl group through resonance, which is indicated by the partial double bond character of the carbamide's C-N bond in the optimized geometry (Figure 5-24). This lone pair delocalization would significantly increase the electron density on the carbamide-carbon, which may in turn act as an electron donor to interact with the diazo (particularly the N1) and consequently enhances the diazonium ion character. Such diazonium-enhancing electronic interaction is expected to be noticeablely stronger in conformer I, due to its much better overall alignment between the C5-diazo and C4-carbamide groups than conformer II (Figure 5-24), despite the slightly longer interacting distances. In addition, the good alignment between the C5→N1 and C4←C in conformer I, when compared to the distorted alignment in conformer II, would offer a better dipole-dipole interaction in favour of a higher diazonium ion character.

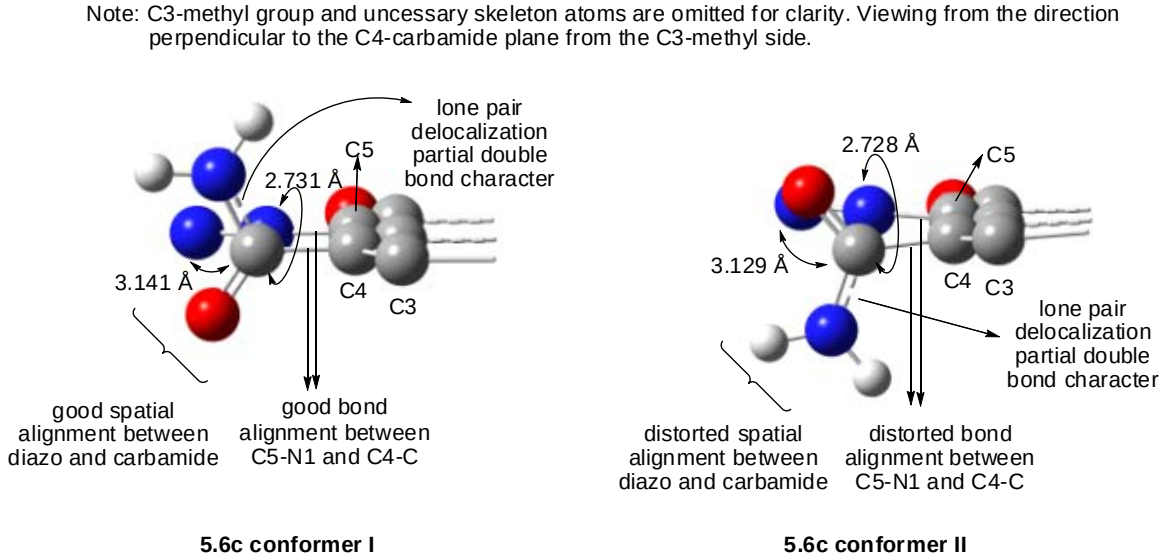

Figure 5-24. Optimized (partial) geometries of the two conformers of IPK-C4-carbamide analogue **5.6c** suggesting interactions between carbamide-carbon and the diazo moiety.

The IPK-C4-carboxylic acid analogue **5.6d** and IPK-C4-acetoxy analogue **5.6e** (Table 5-10) are the most complicated examples among all IPK-C4-analogues examined, since the C4-COOH/COOMe group possesses two geometric variables concurrently, and consequently a maximum of four different but possible conformations may arise from their combination. First, such C4-substituents may possess different orientations as a result of C4-C rotation leading to two possible C4-rotamers. Second, such C4-substituents may also independently adopt two different conformations (i.e., *s*-trans vs *s*-cis acid/ester) due to their C(carbonyl)-O rotation. In fact, geometry optimization of **5.6d** (C4-COOH) does provide all four possible conformers (Table 5-10) with a maximum energy difference of ca. 6.2 kcal/mol among them, which includes two rotamers for each of the *s*-trans and *s*-cis acid as predicted. *S*-cis acids (conformation III and IV of **5.6d**) are obviously higher in energy due to the unfavourable steric repulsion between the hydrogen and the aromatic plane, which is minimized in the corresponding *s*-trans conformations (I and II of **5.6d**). The same but more severe situation also applies to **5.6e** (C4-COOMe) when the small carboxylic proton of **5.6d** (C4-COOH) is replaced by a much bulkier methyl group, and it makes more logical and chemical sense that the observed energy difference among the corresponding conformers of **5.6e** is noticeablely larger (i.e., 8.4 kcal/mol) than that of **5.6d** (6.2 kcal/mol). However, only one stable conformer IV is found with the C4-acetoxy group of **5.6e** being *s*-cis, and absence of another theoretically possible *s*-cis conformer III is not surprising at all. Such a conformer would be strongly disfavoured due to the predictable large steric interaction between its C4-ester methyl group and C3-methyl group, which is expected to be even higher in energy than the already quite unstable conformer IV.

It can be easily recognized that **5.6e** (C4-COOMe) and **5.5f** (C4-OCOMe) are indeed regioisomers that only differ in the order of connectivity of their C4-substituents. However, they behave quite differently from each other in terms of the C4-substitution effect on the diazonium ion character.

Within **5.5f** (C4-OCOMe), the sp^3-hybridized C4-oxygen is always much closer to the diazo group than the sp^2-hybridized carbonyl-oxygen, regardless of orientation of the C4-ester group (Table 5-8). For **5.6e** (C4-COOMe), the sp^3-hybridized methoxy-oxygen and the sp^2-hybridized carbonyl-oxygen could stay at almost identical distances from the diazo moiety if the C4-carbonyl plane is orthogonal to the aromatic ring plane, and the same situation also applies to **5.6d** (C4-COOH) as well. Therefore, rotation of C4-C bond of **5.6e** (and **5.6d**) could lead to an electron-donor competition between these two available but different types of oxygens as to which one preferentially interacts with the diazo moiety. On the other hand, the *s*-trans and *s*-cis conformation could also significantly alter the orientation of the oxygen's lone pair to the diazo group. All these geometrical variations of **5.6d** and **5.6e** are expected and observed to have significant effects on the corresponding diazonium ion characters.

Table 5-10. Ab initio MO calculations of IPK-C4-carbonyl analogues **5.6d**–**f**.

Structure	Optimized geometry	$\nu_{N\equiv N}$ (cm^{-1})[a]	$d_{N\equiv N}$ (Å)	<C-N-N(°)
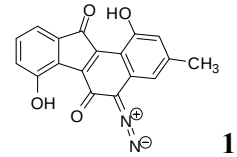 **1.5**	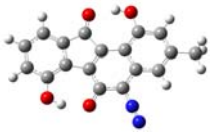	2139	1.103	176.2
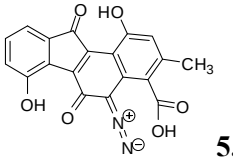 **5.6d**	***s*-trans acid**  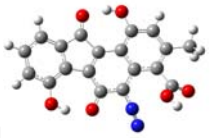 I. II. C=O closer to $-N_2^+$ -OH closer to $-N_2^+$ ΔE(II - I) = 0.06 kcal/mol ***s*-cis acid**  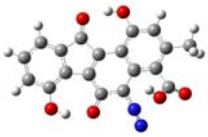 III. IV. C=O closer to $-N_2^+$ -OH closer to $-N_2^+$ ΔE(IV - III) = 0.6 kcal/mol ΔE(IV - I) = 6.2 kcal/mol Stability: I ~ II > III > IV	I. 2221 II. 2182 III. 2209 IV. 2190	I. 1.096 II. 1.099 III. 1.097 IV. 1.098	I. 171.6 II. 172.4 III. 170.6 IV. 171.8
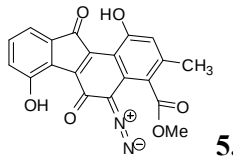 **5.6e**	***s*-trans ester**   I. II. C=O closer to $-N_2^+$ -OMe closer to $-N_2^+$ ΔE(II - I) = -0.17 kcal/mol ***s*-cis ester** 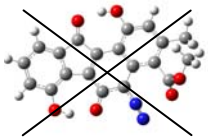  III. IV. C=O closer to $-N_2^+$ -OMe closer to $-N_2^+$ ΔE(IV - I) = 8.4 kcal/mol Stability: II ~ I > IV (> III)	I. 2214 II. 2178 III. N/A IV. 2200	I. 1.096 II. 1.099 III. N/A IV. 1.098	I. 171.6 II. 172.2 III. N/A IV. 171.6
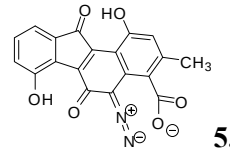 **5.6f**		2275	1.092	171.0

a. Scaled by a scaling factor of 0.8929.

The observed difference in diazo IR frequencies among the conformers for either **5.6d** or **5.6e** can be very well explained solely by the different level of lone pair-diazo interaction involved in each conformation. Other factors such as inductive effect, resonance effect and dipole-dipole interaction have already been shown to have rather limited influence on the diazonium ion character, not to mention that for the conformers of the same compound, such interactions are essentially identical. The oxygen lone pair-diazo interaction within **5.6d** and **5.6e** is determined by the combination of three individual but closely related aspects: (i) the distance between the interacting oxygen atom and the diazo group (i.e., strength of the lone pair-diazo interaction is inversely proportional to the interacting distance); (ii) the orientation of the involved oxygen's lone pair with respect to the diazo group (i.e., poor alignment of the donor's lone pair of electrons with the diazo moiety would significantly decrease the lone pair-diazo interaction even if the interacting distance maybe short enough); and (iii) the choice of the preferential diazo-interacting donor from the concurrent presence of two different types of oxygens both having available lone pairs of electrons. There is something noteworthy in regard to the very last aspect. Generally speaking, for the same element, the availability of the donor's lone pair of electrons is inversely proportional to the electronegativity of the atom as determined by its hybridization state. Therefore, the sp^3-hybridized oxygen should be a better electron source than the sp^2-hybridized oxygen, if they exist individually. However, in the case of a carboxylic acid or ester group when an sp^3-hybridized oxygen and an sp^2-hybridized oxygen are connected simultaneously to an sp^2-hybridized carbon, the situation becomes a little bit complicated. It is well known in organic chemistry that, for carboxylic acids and esters, protonation[373] and formation of intermolecular hydrogen bond[374,375] predominantly occur at the sp^2-hybridized carbonyl oxygen rather than the sp^3-hybridized hydroxy or alkoxy oxygen. This would suggest that, contrary to the hybridization trend, the sp^2-hybridized carbonyl oxygen is a stronger base and better electron donor than the sp^3-hybridized competitor in the solution phase. However, it has been reported that, based on

evidence of (experimental) molecular ionization potentials, protonation of esters in the gas phase should occur at the alkoxy oxygen rather than the carbonyl oxygen yet protonation of carboxylic acids in the gas phase would still occur in the same manner as in the solution phase, i.e. preferentially at the carbonyl oxygen.[376] Since all MO calculations in this study were carried out in the gas phase, it is important for the following discussion to keep in mind that, in the case of carboxylic acid (analogue **5.6d**), the carbonyl-oxygen is a better electron donor than the hydroxy-oxygen; while in the case of the ester (analogue **5.6e**), the alkoxy-oxygen is a stronger donor than the corresponding carbonyl-oxygen.

It can be clearly seen from the optimized four different conformations of **5.6d** (Figure 5-25) that rotation of the C4-C bond would suit only one oxygen at a time from the carboxylic acid to act as an electron donor staying close enough to the diazo moiety, while the remaining oxygen of the carboxylic acid then has to stay far away from the diazo group due to the planar geometry of the carboxylic group. Such conformations could achieve a strong lone pair-diazo interaction that should dominate the influence on the diazonium ion character. Among all four conformers of **5.6d**, even the shortest distances between the "remaining" carboxylic oxygen and the diazo nitrogens (i.e., 3.349 Å and 3.448 Å, conformer IV, Figure 5-25) are still significantly larger than the sum of their vdW radii (r_O= 1.52 Å; r_N= 1.55 Å), thus it is safe to conclude that only the donor oxygen, which is much closer to the diazo moiety, is able to interact through space.

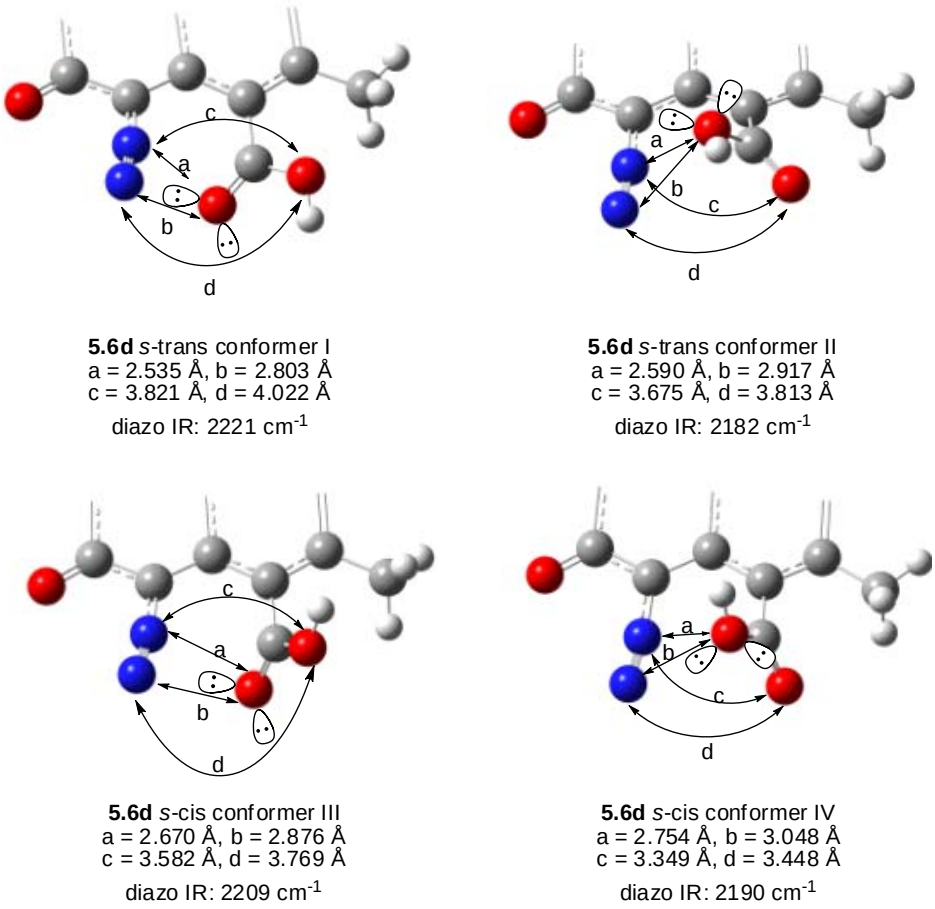

Figure 5-25. Optimized (partial) geometries of the four conformers of IPK-C4-carboxylic acid analogue **5.6d**.

The higher diazo IR frequency and stability of conformer I than the other three conformations of **5.6d** could be attributed exclusively to its very strong (carbonyl-oxygen) lone pair-diazo interaction, which benefits from all three factors discussed earlier: (i) the very close oxygen-diazo interacting distances that are in fact the shortest ones among all conformations; (ii) a good alignment exists between the carbonyl-oxygen's lone pair with the diazo group and (iii) the carbonyl-oxygen is a better electron donor than the hydroxyl-oxygen. The dramatic decrease of diazo IR frequency by almost 40 cm^{-1} from conformer I to conformer II is of no surprise. The hydroxy group of conformer II orientates

in such a manner that its diazo-interacting lone pair of electrons are indeed pointing towards the C5-N1 bond rather than the N1-N2 diazo site. This situation represents a severely compromised diazo-lone pair alignment, which is the worst among all four conformers. In addition, the hydroxyl-oxygen is a weaker donor when compared to the carbonyl-oxygen. Therefore, despite its apparently fairly close O-N interacting distances, which are only slightly longer than those of conformer I but significantly shorter than those of conformer III and IV, conformer II still ends up with the lowest diazo IR frequency. It is also interesting to notice that, in the case of conformer II, the polar O←H bond within the carboxylic acid aligns quite well in parallel with the polar diazo N1→N2 bond at some distances (~ 2.6–3.2 Å). Such observation resembles the known dipole-dipole interaction between C5←N1 and C4→X, suggesting the presence of some additional and energetically beneficial dipole-dipole interaction. However, such interaction itself might be weak as a result of the long distance and its influence on the diazonium ion character is expected to be negligible, since even the much closer and hence stronger dipole-dipole interaction (C5←N1/C4→X) is not able to affect it much.

One can easily identify the geometric similarity between conformer III and I (Figure 5-25) with both of their carbonyl-oxygens as electron donor to stay close to the diazo moiety at comparable distances and lone pair orientations, other than the different orientations of their hydroxy groups (*s*-cis vs *s*-trans). The slightly longer O-N interacting distances within conformer III ($d_{C=O\cdots N1}$ = 2.670 Å, $d_{C=O\cdots N2}$ =2.876 Å) than I ($d_{C=O\cdots N1}$ = 2.535 Å, $d_{C=O\cdots N2}$ = 2.803 Å) are consistent with the corresponding slightly smaller diazo IR frequency of III ($\nu_{N\equiv N}$ = 2209 cm^{-1}) than I ($\nu_{N\equiv N}$ = 2221 cm^{-1}). Even though a shorter O-N interacting distance within conformer III to match that of conformer I may be apparently achievable by a simple and small C4-C rotation clockwise (when viewing from the C5-diazo/C4-acid side), such action would cause large unfavourable steric interaction between the

hydroxy group of this *s*-cis acid and the C3-methyl group that are already close enough and thus prohibited.

For conformer IV, although the corresponding O-N interacting distances ($d_{HO\cdots N1}$ = 2.754 Å, $d_{HO\cdots N2}$ = 3.048 Å) are significantly longer than the other three cases, its diazo IR frequency is surprisingly not the lowest one. Even though the orientation and alignment of its hydroxy-oxygen's lone pair towards the diazo moiety is not as good as those found within conformer I and III, the situation is obviously much better than that of conformer II (Figure 5-25). Since both conformer IV and II have the hydroxyl-oxygen to act as the electron donor and the conformer II even possesses a significantly shorter O-N interacting distances than conformer IV, then the much better lone pair-diazo alignment seems to be the only reason that the conformer IV is still higher in diazonium ion character than conformer II.

Two key conclusions can be made based on the above observations. First, for the same type of lone pair donor (same element having identical hybridization state), orientation of the lone pair electrons and its alignment with the diazo moiety are more important than the interacting distance (within certain limits), as evident from the above comparison between conformer II and IV. Second, if the orientations and alignments of the donor's lone pair towards the diazo are very similar, then the interacting distance becomes the determining factor, as evident from the comparison between conformer I and III. It should be noted that the O-N interacting distance is largely determined by the steric interaction from the C4-substituent with respect to the nearby C3-methyl group (and C5-diazo group yet to a smaller extent), but the contribution to stability from such lone pair-diazo effect can not be ignored at the same time. In other words, the C4-substituent having available electrons to interact with the diazo moiety through space would try to adopt a conformation to simultaneously minimize the steric repulsion but maximize the electron-diazo interaction.

Similar to the above case of **5.6d** (C4-COOH), the differences in diazo IR frequencies among the three conformers of **5.6e** (C4-COOMe) could also be satisfactorily explained with the same rationale based on the different lone pair-diazo interactions involved in these optimized geometries (Table 5-10 and Figure 5-26). Briefly speaking, the much higher diazonium ion character of conformer I ($\nu_{N\equiv N}$ = 2214 cm^{-1}) than II ($\nu_{N\equiv N}$ = 2178 cm^{-1}) is mainly owing to its closer O-N interacting distance (Figure 5-26) and better lone pair-diazo alignment (Table 5-10), even though conformer I has a weaker electron donor (carbonyl-oxygen) than II (alkoxy-oxygen) to interact with the diazo moiety. On the other hand, despite that conformer IV has the longest O-N interacting distance among the three conformers (Figure 5-26), its moderate diazonium ion character ($\nu_{N\equiv N}$ = 2200 cm^{-1}) relative to that of conformer I ($\nu_{N\equiv N}$ = 2214 cm^{-1}) and conformer II ($\nu_{N\equiv N}$ = 2178 cm^{-1}) is noticeable. In the case of comparing conformer IV and I, the disadvantage of having a worse lone pair-diazo alignment within conformer IV than I (Table 5-10), as well as the longer O-N interacting distance, is compensated partially by the stronger electron donor of alkoxy-oxygen within conformer IV than the weaker carbonyl-oxygen as electron donor within conformer I. When the comparison is between conformer IV and II, since both species involve the same alkoxy-oxygen as the electron donor and conformer IV still suffers from the longer O-N interacting distances, the higher diazonium ion character of VI than II shall benefit exclusively from its much better lone pair-diazo alignment (Table 5-10).

It is even more interesting to compare **5.6e** (C4-COOMe) and **5.6d** (C4-COOH) for each of their same type of conformation (Figure 5-26), since this clearly demonstrates the influence on diazonium ion character mainly from a small substituent variation (methyl vs H) rather than a significant conformational change of the whole C4-substituent.

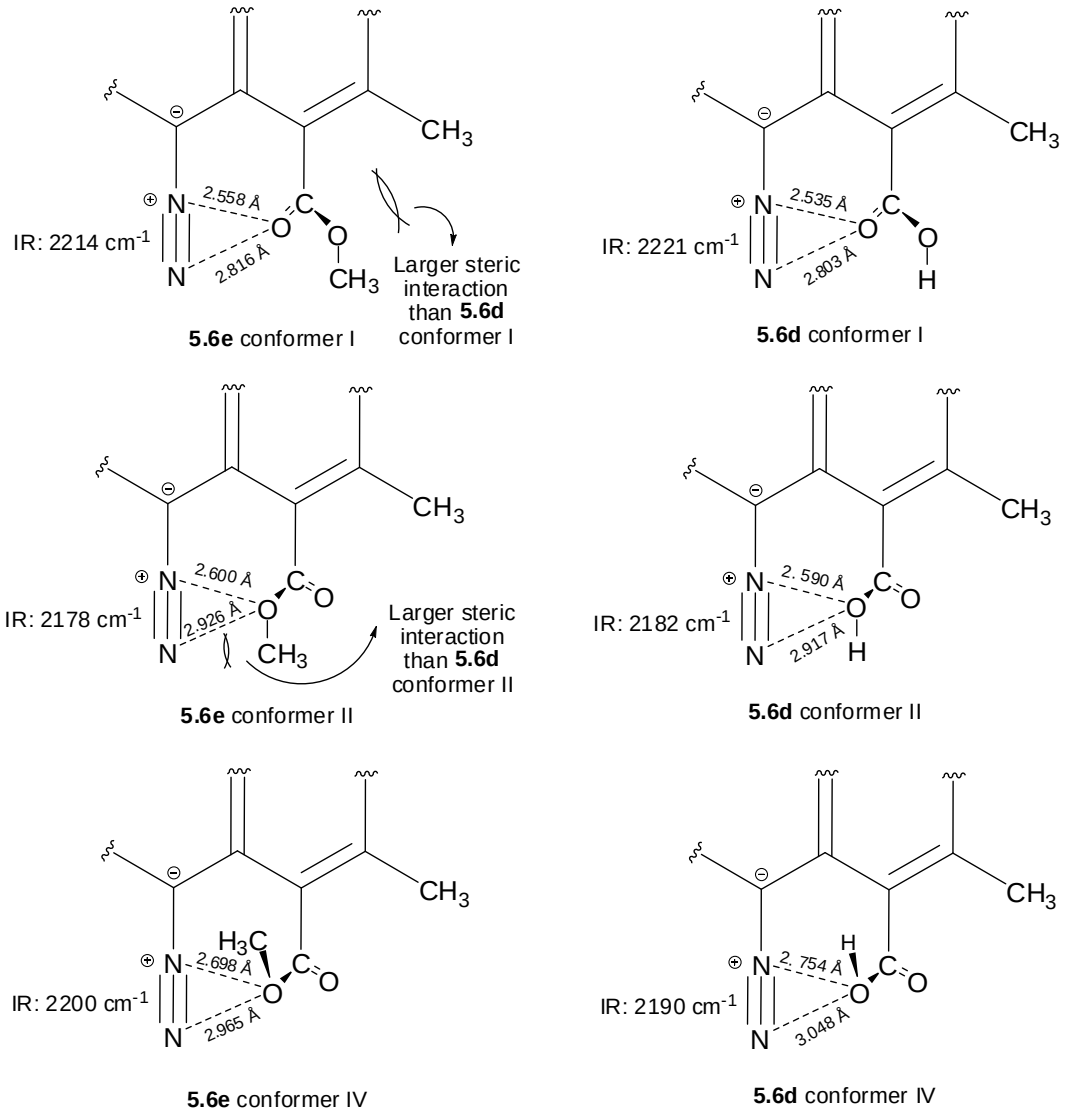

Figure 5-26. Comparison of geometries and diazo IR frequency between similar conformers of IPK-C4-carboxylic acid **5.6d** and IPK-C4-ester **5.6e**.

Since both conformer I of **5.6e** and **5.6d** involve the same type of carbonyl-oxygen as electron donor with very similar lone pair-diazo alignment (Table 5-10), the lower diazo IR frequency for conformer I of **5.6e** ($\nu_{N\equiv N}$ = 2214 cm^{-1}) than that of **5.6d** ($\nu_{N\equiv N}$ = 2221 cm^{-1}) is due to the slightly longer O-N interacting distance within **5.6e** (Figure 5-26), which originates from the larger steric

interaction between its carboxylic-methoxy/C3-methyl groups than the carboxylic-hydroxy/C3-methyl groups within **5.6d**. Similar steric interaction between the C5-diazo and the ester methoxy group causing larger O-N interacting distance is able to explain the smaller diazo IR frequency for conformer II of **5.6e** than **5.6d** (Figure 5-26). The most interesting result comes from the comparison of conformer IV of both structures. In this case, both the ester methyl group of **5.6e** and the hydroxy group of **5.6d** points up to the open space above the aromatic ring (see optimized geometries in Table 5-10 and Figure 5-25), and the steric interaction from the C4-substituent with the C5-diazo moiety and the C3-methyl group is no longer a significant issue. Therefore, the observed diazo IR frequency difference should be mainly a result of change in electron-donating capability of the sp^3-oxygen (alkoxy-oxygen vs hydroxyl-oxygen). The ester methyl group of **5.6e** is expected to increase the electron density of the alkoxy-oxygen to be higher than the hydroxy-oxygen within **5.6d**. The calculated higher diazo IR frequency for conformer IV of **5.6e** ($\nu_{N\equiv N}$ = 2200 cm^{-1}) than **5.6d** ($\nu_{N\equiv N}$ = 2190 cm^{-1}) is completely consistent with the predicted increase of electron density on the sp^3-oxygen due to the presence of ester methyl group within **5.6e**, which shall offer a noticeablely stronger lone pair-diazo interaction and hence a higher diazonium ion character than **5.6d**. This stronger lone pair-diazo interaction is further reflected by the closer O-N interacting distances within **5.6e** ($d_{MeO\cdots N1}$ = 2.698 Å, $d_{MeO\cdots N2}$ = 2.965 Å) than those within **5.6d** ($d_{HO\cdots N1}$ = 2.754 Å, $d_{HO\cdots N2}$ = 3.048 Å), even though the methyl is much bulkier than the proton.

As the last compound within this series, the IPK-C4-carboxylate **5.6f** (C4-COO^-) is just the deprotonated form of the corresponding carboxylic acid **5.6d** (C4-COOH), which at physiological pHs would be in fact in the form of the carboxylate anion rather than the neutral acid. A practical advantage of **5.6d**/**5.6f**, if synthetically available, is that their solubility in aqueous solutions (particularly the bioassay and cells) and common polar organic solvents is expected to be

significantly improved relative to that of IPK (**1.5**).* It can be predicted that, due to the much higher electron density (negative charge) of the carboxylate anion than the neutral acid, **5.6f** (C4-COO^-) shall possess some very strong diazonium ion character that is likely even higher than **5.6d** (C4-COOH, $\nu_{N\equiv N}$ = 2182–2221 cm^{-1}). Indeed, the calculated diazo IR frequency of **5.6f** ($\nu_{N\equiv N}$ = 2275 cm^{-1}) is the highest value among the entire series of IPK-C4-analogues studied.

Delocalization of the carboxylate negative charge evenly in between two identical resonance forms would make the two oxygen atoms equivalent in electron density and hybridization (Figure 5-27). Unlike the previous cases of the carboxylic acid and ester (i.e., **5.6d** and **5.6e**), there is neither a competition of electron donor between the two oxygen atoms within the carboxylic group, nor a choice of an *s*-cis vs *s*-trans conformation any more. Despite the various possible starting geometries attempted, optimization only led to one single conformation as given in Figure 5-27. The optimized conformation for **5.6f** shows several interesting observations. First of all, the O-N interacting distances within **5.6f** ($d_{COO\cdots N1}$ =2.491 Å, $d_{COO\cdots N2}$ = 2.751 Å) are found to be closer than any of the previous examples having (oxygen) lone pair-diazo interactions, not to mention that such distances are a lot shorter than the sum of the corresponding vdW radii (r_O = 1.52 Å, r_N = 1.55 Å). This is entirely consistent with the highest diazo IR frequency associated with the structure of **5.6f**. Second, delocalization of the negative charge within the carboxylate is also evident from the computed two close C-O bond lengths (i.e., 1.263 Å and 1.252 Å), but more interestingly, it is noticed that the C-O bond having its oxygen interacting with the diazo moiety is slightly longer than the other C-O bond that has no interaction with the diazo moiety (Figure 5-27). The same observation was previously encountered with the two N-O bonds within **5.4d** (C4-NO_2) as given in Figure 5-13 (section 5.2.3), and the earlier rationale also applies in the case of **5.6f**. Last but not least, it is quite obvious that

* Solubility of IPK (**1.5**) in all common organic solvents (except CH_2Cl_2) and water is very low, and this physical property greatly limits the research and practial application of IPK (**1.5**) as a potential drug candidate.

rotation of the C4-C bond (Figure 5-27) would further shorten the O-N interacting distances and enhance the lone pair-diazo interaction and consequently the diazonium ion character, although one needs to realize that there is also some unfavourable steric interaction between the carboxylic group and the diazo moiety that associates and increases with such C4-C rotation. On the other hand, the C4-C rotation shall be prohibited by the increasing steric repulsion from the C3-methyl group towards the carboxylic oxygen, which does not interact with the diazo moiety but stays close to the C3-methyl group. Therefore, it is expected that replacement of the C3-methyl group by hydrogen shall remove the steric limit on C4-C rotation and an even stronger lone pair-diazo interaction might be achieved. This prediction is in fact confirmed later on (see section 5.2.6 for details).

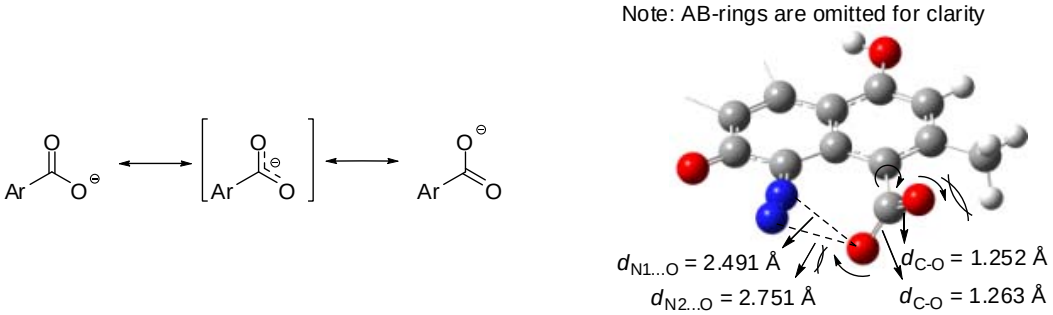

(a) resonance forms of carboxylate

(b) partial optimized geometry of **5.6f**

Figure 5-27. (a) Resonance of (aromatic) carboxylate anion and (b) optimized (partial) geometry of IPK-C4-carboxylate analogue **5.6f**.

5.2.6 Design of Simple Diazobenzo[*a*]fluorene Analogues

All of the above computational results (section 5.2.1–5.2.5) reveal the potential importance of the C4-substituents on the diazonium ion character of IPK, or diazobenzo[*a*]fluorene in general. The key discovery is that the through-space electronic interaction with the C5-diazo group from the C4-substituent, which partially donates electrons (if available) to the diazo moiety when it stays at close

enough distance with appropriate orientation, applies dramatic influence on the corresponding diazonium ion character. Future research in the area of kinamycin could benefit significantly from such a finding. With the predicted much higher diazonium ion character than the natural antibiotic of IPK (calc. $\nu_{N\equiv N}$ = 2139 cm^{-1}; expt. $\nu_{N\equiv N}$ = 2160 cm^{-1}), IPK-C4-analogues such as **5.2c** (C4-CN, $\nu_{N\equiv N}$ = 2189 cm^{-1}), **5.4a** (C4-NH_2, $\nu_{N\equiv N}$ = 2219 cm^{-1}), **5.5c**/**5.5e** (C4-OH/O^-, $\nu_{N\equiv N}$ = 2210/2226 cm^{-1}), **5.6a** (C4-CHO, $\nu_{N\equiv N}$ = 2248/2147 cm^{-1}), **5.7** (IPK-D-ring-quinone, $\nu_{N\equiv N}$ = 2265 cm^{-1}) and **5.6d**/**5.6f** (C4-COOH/COO^-, $\nu_{N\equiv N}$ = 2182–2221/2275 cm^{-1}) are some promising target molecules to prepare to explore the influence of diazonium ion character on biological activity.

From a synthetic point of view, the above mentioned several analogues are also closely related in a general chemical sense. For example, interconversion in between IPK (**1.5**), **5.5c** (C4-OH) and **5.7** (IPK-D-ring-quinone) through oxidation/reduction, and functional group transformations in between **5.2c** (C4-CN), **5.6d** (C4-COOH, from **5.2c** upon hydrolysis of C4-CN) and **4.66** (C4-CHO, from **5.6d** upon reduction of C4-COOH) are all possible. Nevertheless, compounds such as **5.2c** (C4-CN) and **5.7** (IPK-D-ring-quinone) are worthy of some particular attention since they have the potential to be easily transformed into other IPK-C4-analogues while their own syntheses do not seem to be very difficult. Of course the real synthetic efforts towards such IPK-C4-analogues, by modifying the Dmitrienko synthetic route, are probably more complicated than stated above, since the involvement of extra protection/deprotection steps, unforeseen difficulties in preparing the corresponding starting materials, and managing the high reactivities of (diazo-containing) advanced intermediates and final target molecules are possible.

The power of having appropriate C4-substituents to enhance the diazonium ion characters offers some further flexibility to design and prepare (much) simpler diazobenzo[*a*]fluorene analogues, which can still possess high enough diazonium ion character. Simplifying the structure of diazobenzo[*a*]fluorenes would make the corresponding synthetic work more concise and efficient.

For example, judging by its electronic nature, the C3-methyl group on the D-ring of these diazobenzo[*a*]fluorenes is expected to be non-critical to the diazo group's properties by itself, and it is probably better to be removed since the electron-donating nature of the methyl group is not expected to favour a higher diazonium ion character. However, it has already been shown that the C3-methyl group can apply significant steric restraints on the C4-substituent, and consequently may affect the diazonium ion character to a significant extent indirectly. Another example is the intramolecular H-bonding between the C1-OH and C10-O as well as the C7-OH and C6-O within such IPK-C4-analogues. It has been found experimentally (undisclosed results from this work) and computationally (by earlier work of Laufer from the Dmitrienko group[124]) that these intramolecular H-bonding interactions are essential for the high diazonium ion character of IPK (**1.5**). However, these H-bonds also seem to be apparently the origin for IPK's (**1.5**) poor solubility,[*] which is a practical issue that would significantly decrease the efficiency and value of such IPK-C4-analogues to be used as drug candidates. Therefore, removal of these functional groups (i.e., C3-methyl, C1-OH or C7-OH) from the diazobenzo[*a*]fluorenes would cause certain (decreasing) effects on the diazonium ion character, which is hoped to be counteracted to a greater extent by the installation of an appropriate C4-substituent that interacts electronically with the C5-diazo moiety. This hypothesis of designing simpler diazobenzo[*a*]fluorene analogues with high enough diazonium ion character can be clearly illustrated by the results to be discussed next. Table 5-11 presents the calculated diazo IR frequencies of some simpler diazobenzo[*a*]fluorene analogues derived from IPK (**1.5**), and results for those simpler structures derived from or **5.6f** (IPK-C4-COO^-) are given in Table 5-12.

[*] IPK analogue **3.236** without the double intramolecular H-bonds, which is due to the lack of appropriate functional groups, has much better solubility than IPK (**1.5**) in all common organic solvents and even aqueous solutions.

Table 5-11. Ab initio MO calculations of some simpler IPK-based diazobenzo[*a*]fluorene analogues.

Structure	Optimized geometry	$\nu_{N\equiv N}$ (cm^{-1})[a]	$d_{N\equiv N}$ (Å)	<C-N-N(°)
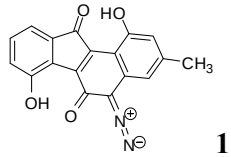 **1.5**		Expt. IR: **2160** MO: 2139	X-ray: **1.104** MO: 1.103	X-ray: **177.6** MO: 176.2
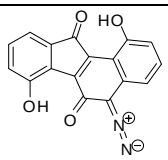 **5.11**	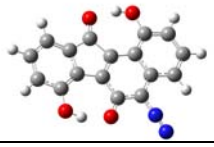	2138	1.103	176.3
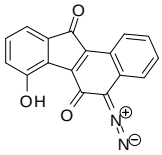 **5.12**		2124	1.105	176.4
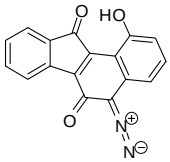 **5.13**	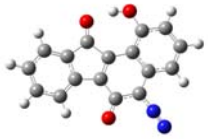	2100	1.107	176.2
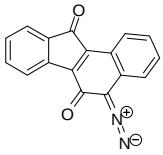 **1.123**[b]	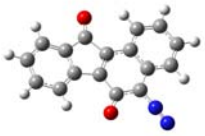	Expt. IR[c]: **2105** MO: 2086	MO: 1.108	MO: 176.4

a. Scaled by a scaling factor of 0.8929 (MO results); b. This compound was synthesized by Laufer from the Dmitrienko group[124]; c. Experimental IR frequency observed with **1.123** as film.[124]

Table 5-12. Ab initio MO calculations of some simpler **5.6f**-based diazobenzo[*a*]fluorene analogues.

Structure	Optimized geometry	$\nu_{N\equiv N}$ (cm^{-1})[a]	$d_{N\equiv N}$ (Å)	<C-N-N(°)
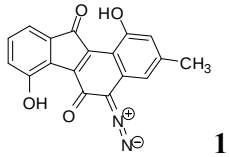 **1.5**		2139	1.103	176.2
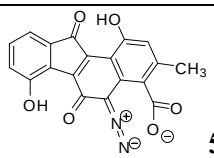 **5.6f**		2275	1.092	171.0
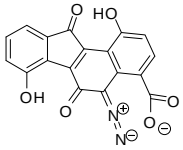 **5.14**		**2291**	**1.0908**	**169.8**
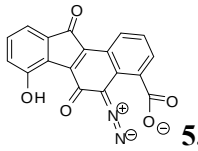 **5.15**		2285	1.0912	169.9
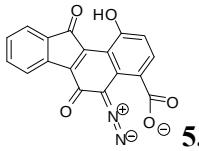 **5.16**		2254	1.093	170.1
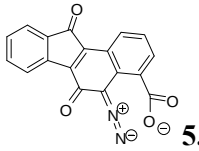 **5.17**		2247	1.094	170.2

a. Scaled by a scaling factor of 0.8929.

In the series of IPK(**1.5**)-based simpler analogues (Table 5-11), initial replacement of C3-methyl group of IPK (**1.5**) by hydrogen (i.e., analogue **5.11**) causes a decrease of only 1 cm^{-1} in the diazo IR frequency, consistent with the earlier prediction that this C3-methyl group is of very little importance towards the diazonium ion character when diazo-interacting C4-substituent is not present. Further substituent replacement within the structure of **5.11**, first the C1-OH replaced by hydrogen (analogue **5.12**), then C7-OH (analogue **5.13**) and eventually both C1/C7-OHs (analogue **1.123**) replaced by

hydrogens show a gradual and significant decrease of their diazo IR frequencies (Table 5-11). This trend can be well explained by the gradual diminution of intramolecular H-bonding interactions that delocalize the C5 partial negative charge to enhance the diazonium ion character. Another comparison is made between **5.13** and one of the optimized conformations of IPK (**1.5**, conformation II, Table 5-1), since both structures have intramolecular B-D ring H-bonding interaction, and both of them also lack the intramolecular A-C ring H-bonding interaction yet in two different manners (Figure 5-28). The lack of A-C ring H-bond within **5.13** is due to the complete absence of C7-OH group, while for conformer II of IPK (**1.5**), the C7-OH is present but does not participate in the H-bonding. The noticeably higher diazo IR frequencies of **5.13** ($\nu_{N\equiv N}$ = 2100 cm^{-1}) than conformer II of **1.5** ($\nu_{N\equiv N}$ = 2084 cm^{-1}) would suggest that, when the C7-OH is not involved in the intramolecular H-bonding interaction, it would act as a strong electron-donating group to increase the electron density of the A-ring and consequently disfavour the delocalization of the C5 negative charge and reduce the diazonium ion character. This comparison also suggests that, incorporation of strong electron-donating substituent(s) onto the A-ring of the diazobenzo[*a*]fluorene structure is another method to lower the diazonium ion character, if the A-ring electron-donating group(s) forms no intramolecular H-bond(s) with either the C6=O or C11=O.

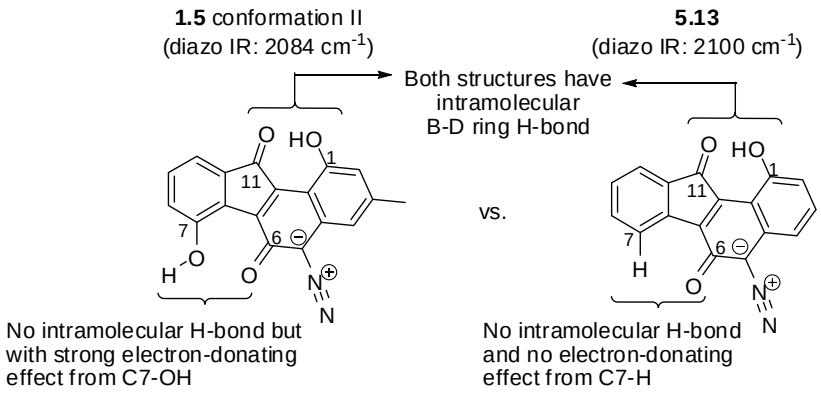

Figure 5-28. Comparison between IPK (**1.5**) and a simpler analogue **5.13**.

The results become even more interesting in the case of **5.6f** (C4-COO^-), when its C3-methyl, C1-OH and C7-OH groups are replaced by hydrogen(s) stepwise (Table 5-12). The absence of the C3-methyl group from the structure of **5.6f** (i.e., analogue **5.14**, $\nu_{N\equiv N}$ = 2291 cm^{-1}) causes a fairly large increase in diazonium ion character ($\Delta\nu_{N\equiv N}$ = 16 cm^{-1}) from the starting structure **5.6f** ($\nu_{N\equiv N}$ = 2275 cm^{-1}). This observation is contrary to the previous situation of almost identical diazo IR frequencies for IPK (**1.5**) and its simpler methyl-missing analogue **5.11** (IPK-C3-H), but entirely consistent with the significantly shorter O-N interacting distances within **5.14** ($d_{COO\cdots N1}$ = 2.386 Å, $d_{COO\cdots N2}$ = 2.670 Å) than those within **5.6f** ($d_{COO\cdots N1}$ = 2.491 Å, $d_{COO\cdots N2}$ = 2.751 Å) as shown in Figure 5-29. Such positive influence on diazonium ion character has been previously predicted (see Figure 5-27 and related text in section 5.2.5), since the C3-methyl group is an obvious steric obstacle for the C4-carboxylate when the latter tries to get closer to the C5-diazo group as much as possible to achieve the maximum lone pair-diazo interaction. Therefore, only after the replacement of C3-methyl group by hydrogen, the C4-carboxylate is then free from the steric limitation by the C3-substituent and rotation of C4-C bond to achieve the maximum lone pair-diazo interaction becomes possible. This is clearly indicated by the observation that, the large torsion angle of ca. 51º between the C4-carboxylic plane and the aromatic ring plane within **5.6f** becomes a much smaller torsion angle of only ca. 24º within **5.14** (Figure 5-29). It should be noted that the diazo IR frequency of 2291 cm^{-1} for **5.14** is the most diazonium-like diazobenzo[*a*]fluorene analogue so far (Note: Such a high diazonium ion character of **5.14** is comparable to the typical aryl diazonium salts, which have experimental diazo IR frequencies of ca. 2230–2300 cm^{-1}.[377,378]) Similar to the IPK (**1.5**) and its simpler analogues (Table 5-11), the stepwise change in substituent (Table 5-12) in the order of **5.6f**, **5.14** (C3-Me of **5.6f** replaced by H), **5.15** (C1-OH of **5.14** replaced by H), **5.16** (C7-OH of **5.14** replaced by H) and **5.17** (both C1-OH and C7-OH of **5.14** replaced by Hs) shows the same tendency of gradual decreasing diazo IR

frequencies. This can be once again attributed to the gradual loss of the intramolecular H-bonding interactions.

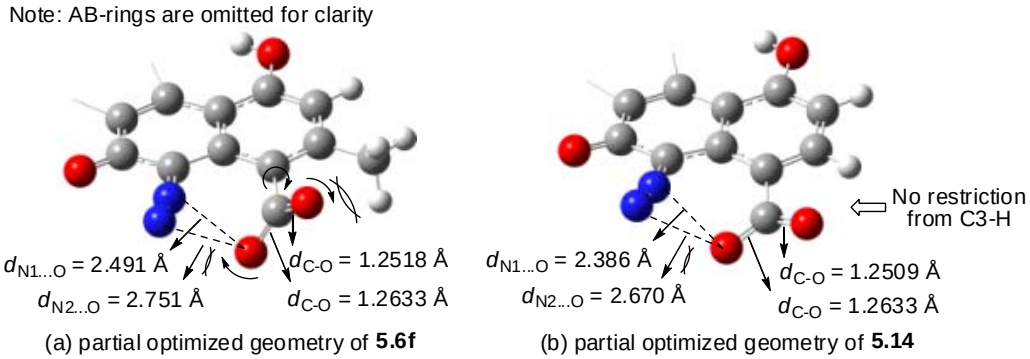

Figure 5-29. Comparison of optimized (partial) geometries of analogues **5.14** and **5.6f**.

It is also interesting to realize that compounds **5.12/5.13** (Table 5-11) and **5.14/5.15** (Table 5-12) are two pairs of regioisomers, respectively. The common presence of an A-C ring H-bond but absence of a B-D ring H-bond within **5.12** and **5.14**, is the origin of their higher diazonium ion characters than the corresponding regioisomer of **5.13** and **5.15**, which both possess the B-D ring H-bond but lack the A-C H-bond. Such comparison would suggest that the A-C ring H-bond is more important than the B-D ring H-bond to maintain a high diazonium ion character, which is consistent with a similar prediction made for IPK (**1.5**) earlier (see Table 5-1 and related text in the introduction part of section 5.2 for details).

Structure **5.17**, which has the weakest diazonium ion character among the **5.6f**-derived analogues (Table 5-12), shows a diazo IR frequency of 2247 cm^{-1} that is still much higher than compound **1.123** (calc. $\nu_{N\equiv N}$ = 2086 cm^{-1}; expt. $\nu_{N\equiv N}$ = 2105 cm^{-1}), and **1.123** is in fact a C4-unsubstituted version of **5.17**. When a C4-carboxylate is introduced into the structure of **1.123** leading to analogue **5.17**, the observed dramatic enhancement of the diazonium ion character is of no surprise due to the strong carboxylic lone pair-diazo interaction. In addition, analogue **5.17** is expected to be able to solve the

known low solubility issue of compound **1.123** in both aqueous solutions and organic solvents.[80,124] More importantly, structure **5.17** is a good example to support the hypothesis for designing simpler diazobenzo[*a*]fluorene analogues as mentioned at the beginning of this section (section 5.2.6). The appropriate selection of C4-substituent, which strongly and electronically interacts with the diazo moiety, can override the decreasing effect on the diazonium ion character from the (complete) removal of other substituents within the diazobenzo[*a*]fluorene. Such structural simplification of diazobenzo[*a*]fluorene while maintaining a high diazonium ion character shall greatly simplify the corresponding total synthesis. The fairly high diazo IR frequency of **5.17** further triggered some interests in modeling the complete stripped-down diazobenzo[*a*]fluorene structure **1.123** with minimal presence of diazo-influencing substituent, i.e. a single substituent at either the C4 or C2 position, in hoping to find very simple diazobenzo[*a*]fluorene structures with high enough diazonium ion character as suitable synthetic targets. Choices of the substituent at C4- or C2-position of **1.123** were kept essentially the same as those IPK-C4-analogues but with small variations. The corresponding results (Table 5-13) of these two series of compounds, i.e. **1.123**-C4-analogues and **1.123**-C2-analogues are summarized below and reveal some more interesting discoveries.

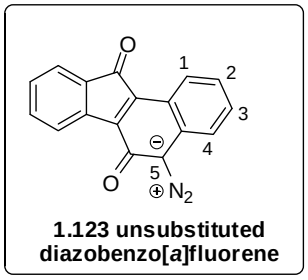

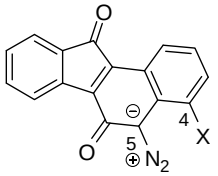
1.123-C4-analogue

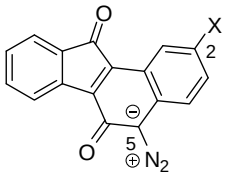
1.123-C2-analogue

Table 5-13. Calculated diazo IR stretching frequency of C4- and C2- analogues of **1.123**.

C4 substituent X	$\nu_{N\equiv N}$ (cm^{-1})[a]		C2 substituent X	$\nu_{N\equiv N}$ (cm^{-1})[a]
X = CH_3	2080	Lower diazonium ion character	X = O^-	1977
X = H (**1.123**)	2086		X = COO^-	2056
X = Br	2130	↑	X = NH_2	2060
X = Cl	2136.9	↑	X = OMe	2067
X = CN	2137.4	↑	X = OH	2070
X = SH	2141[b]	IPK (**1.5**) ← 2139 cm^{-1}	X = CH_3	2081
X = F	2143	↓	X = H (**1.123**)	2086.2
X = OH	2157.2	↓	X = F	2086.4
X = OMe	2157.6	↓	X = Br	2092.5
X = CF_3	2160	↓	X = Cl	2092.9
X = OCF_3	2161	↓	X = SH	2095
X = NH_2	2166	↓	X = OCF_3	2098
X = O^-	2177	↓	X = COOMe	2104
X = $COCF_3$	2183	↓	X = CN	2105
X = COMe	2192.2	↓	X = COOH	2106.2
X = COOMe	2192.5[b]	↓	X = COMe	2106.6
X = NO	2192.8[b]	↓	X = CF_3	2108
X = NO_2	2192.9	↓	X = NO	2115
X = COOH	2194[b]	Higher diazonium ion character	X = $COCF_3$	2117.2
X = COO^- (**5.17**)	2247		X = NO_2	2117.9

a. Scaled by a scaling factor of 0.8929. The IR frequencies are listed in ascending order; b. Multiple diazo IR frequencies are available due to the multiple possible conformations; however, only the diazo IR frequency of the most stable conformation is used in this table for ranking.

First of all, judging by the calculated diazo IR stretching frequencies (Table 5-13), there are a number of **1.123**-C4-analogues that possess higher diazonium ion character than the natural antibiotic of IPK (**1.5**, $\nu_{N\equiv N}$ = 2139 cm^{-1}) and are suitable as potential synthetic targets. On the other hand, even the highest diazo IR frequency of **1.123**-C2-analogues (C2-NO_2, $\nu_{N\equiv N}$ = 2117.9 cm^{-1}) is still significantly lower than that of IPK (**1.5**, $\nu_{N\equiv N}$ = 2139 cm^{-1}), which makes none of this C2-series structures a promising synthetic candidate. However, it is very interesting to realize the totally different trends of change in diazo IR frequency as a function of the substituent observed for the **1.123**-C4-analogues and **1.123**-C2-analogues (Table 5-13). The **1.123**-C4-analogues demonstrate very similar substitution effects as the IPK-C4-analogues, and lone pair-diazo interaction dominates the influence on the diazonium ion character whenever available. Therefore, both (strong) electron-donating and electron-withdrawing substituents, as long as this C4-moiety contains heteroatom(s) with available lone pair(s) that could stay close enough to the C5-diazo group, lead to high diazonium ion character. However, diazo IR frequencies of the **1.123**-C2-analogues indicate that their diazonium ion characters are proportional to the electron-withdrawing capability of the C2-substituent. Since the C2-substituent is far from the C5-diazo group, it can no longer provide a dipole-dipole interaction or lone pair-diazo interaction to affect the diazonium ion character yet such interactions must be considered in the cases of C4-substitution. Instead, the C2-substituent is only able to apply inductive and resonance effects through the aromatic D-ring to influence the diazonium ion character, but at a much further distance than the C4-substituent and hence weaker (in general). Obviously, an electron-withdrawing C2-substituent would favour the delocalization of the C5 partial negative charge, either inductively or through resonance, to enhance the diazonium ion character. Another noticeable difference, as one can predict, is that variations of the substituent's conformation no longer affects the diazonium ion character in the cases of the **1.123**-C2-analogues, but it is still applicable to some

1.123-C4-analogues that are very similar to the corresponding IPK-C4-analogues (see footnote b of Table 5-13).

The current work offers a systematic computation and analysis of various diazo-affecting interactions within the diazobenzo[*a*]fluorenes upon possible substitution. Structures of some IPK-C4-analogues and simpler diazobenzo[*a*]fluorene analogues, with predicted diazo IR frequencies (much) higher than the natural IPK (**1.5**), are proposed for future synthetic projects. Whether or not such proposed target molecules are higher in biological activity than the natural IPK (**1.5**), as a result of their higher diazonium ion character, remains to be established. It is also hoped that such target molecules involve smoother and easier syntheses, especially for those rather simple structures such as the **1.123**-C4-analogues, by taking advantage of the two established synthetic procedures towards the diazobenzo[*a*]fluorenes from the Dmitrienko group (section 3.2) that have already led to the successful total synthesis of IPK (**1.5**) [25]and **1.123**.[124].

5.3 Theoretical Analysis of Interaction of Proximal Electron Rich Heteroatoms with Diazonium Groups

The mechanistic studies of kinamycin F (**1.1f**), from chemical evidence for nucleophilic thiol addition to diazo and spectroscopic/computational evidence of diazo IR frequency as described in Chapter 4, have demonstrated that the diazo group in diazobenzo[*b*]fluorenes is indeed diazonium-like. This is consistent with an earlier suggestion by the Dmitrienko group that the chemical properties of the diazo group in the diazobenzo[*a*]fluorene of IPK (**1.5**) are also more like those of aryl diazonium ions rather than those of typical diazo groups, based on chemical evidence for nucleophilic naphthol addition to diazo and computational evidence of diazo IR frequency.[124] Therefore, it is appropriate to compare the discussion presented above (section 5.2), particularly the

discovered and unexpected lone pair-diazo interactions, with discussions in the literature concerning the interactions of aryl diazonium groups with proximal electron rich functional groups.

In the early 1990s, X-ray crystallographic studies by Wallis, Easton and Dunitz revealed that, within the 8-substituted-naphthalene-1-diazonium cations **5.18** (Figure 5-30), the presence of a proximal group such as $(N^+–)O^-$, MeS, Me_2N and NO_2 to the diazonium moiety causes a deviation of the diazo group geometry from C-N-N linearity such that the terminal nitrogen (N_β) is bent away from the proximal group, yet the distances between the proximal group's electron-rich heteroatom (O, S or N) and the internal nitrogen (N_α) of the diazonium group are close enough (i.e., shorter than the sum of the corresponding vdW radii) to warrant some (apparently) attractive interactions.[379] They suggested that this observed phenomenon of the diazonium moiety distortion by the proximal group is reminiscent of related interactions of proximal electron rich groups with carbonyl groups, which was likened to the generally accepted Bürgi-Dunitz model for the interaction of nucleophiles with ketones and aldehydes where the intramolecular interaction is considered to be an "incipient nucleophilic attack" (INA) as shown in the example **5.19** (Figure 5-30) that leads to distortion of the C=O group involving partial pyramidalization of the carbonyl group carbon atom.[380]

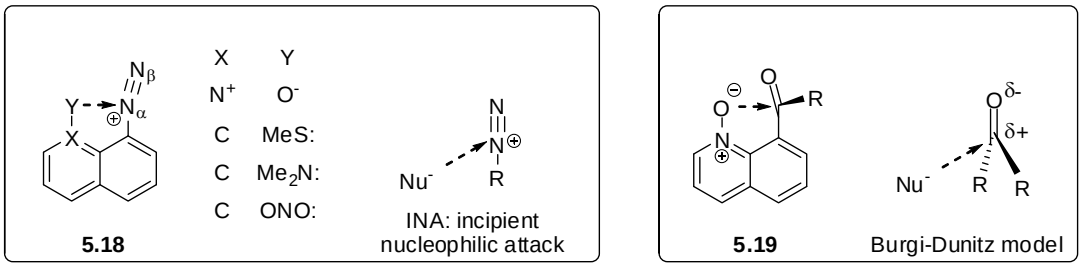

Figure 5-30. Intramolecular electron-rich proximal group interacting with the diazonium moiety within the 8-substituted-naphthalene-1-diazonium cations **5.18** and the corresponding Bürgi-Dunitz/INA model of **5.19**.

Later on, however, Glaser and coworkers presented an alternative interpretation[381] that challenges the basic assumptions and validity of the intuitively appealing "arrow-pushing" explanation provided by Wallis, Easton and Dunitz[379] for the neighbouring group interactions within aryl diazonium ions. They pointed out that the INA model, also known as the N_α–attraction model (Figure 5-31), assumes that the formal positive charge on the internal nitrogen (N_α) of the diazonium ion group implied in the Lewis structure is an accurate representation of the true electronic character of the group. The Glaser group pointed out that, in reality, the electronic character of the diazonium ion group is better represented as in the diagram below (Figure 5-31), with overall partial positive charge associated with both the carbon atom and the terminal nitrogen (N_β) but with partial negative charge, rather than positive charge, associated with the internal nitrogen (N_α). The Glaser group also suggested that the electron-rich proximal group interacts with the diazonium ion in a 1,3-bridging fashion, with attractive interactions of the electron rich site with the carbon and terminal nitrogen (N_β) of the diazonium ion and a repulsive interaction with the electron rich internal nitrogen (N_α).

Figure 5-31. The INA (N_α–attraction) model vs the 1,3-bridging attraction model for diazonium ion.

In support of their alternate interpretation, Glaser and Horan present X-ray crystallographic data for the diazonium ion **5.20** and its conjugate base **5.21** in which the distortions of the diazonium ion similar to those noted by the Dunitz group are evident.[381]

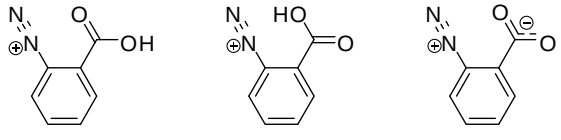

5.20a **5.20b** **5.21**

A computational analysis of the two rotamers of the acid, **5.20a** and **5.20b**, and of the conjugate base **5.21** at the RHF/6-31G* level reproduced the geometry observed experimentally relatively well and also provided insight into the nature of the electronic interactions of the proximal groups with the diazonium ion.[381] The ab initio MO analysis results were then employed as input into a calculation of the electrostatic interaction energy between the atoms in the diazonium ion and the proximal electron rich groups. The analysis involved a model in which the electrostatic interaction energy between two atoms (ESI_{ij}) was considered to be the sum of a Coulomb energy (CC_{ij}) arising from interaction between the atomic charges, an energy term (CD_{ij}) arising from interaction of the atomic charge on each atom with the atomic dipole at each other atom, a dipole-dipole interaction (DD_{ij}), a quadrupole-atomic charge interaction (QC_{ij}), a quadrupole-dipole interaction (QD_{ij}) and a quadrupole-quadrupole interaction (QQ_{ij}), therefore, $ESI_{ij} = CC_{ij} + CD_{ij} + DD_{ij} + QC_{ij} + QD_{ij} + QQ_{ij}$. This analysis leads to a clear demonstration that the interaction of the proximal group with the diazonium ion cannot be interpreted via the INA model that depends on the assumption of partial positive charge on the internal nitrogen (N_α) of the diazonium ion group. The computed model for **5.20a** (Figure 5-32) is entirely consistent with the 1,3-bridging attraction model (Figure 5-31), and brings to light an attractive interaction of the electron rich internal nitrogen (N_α) of the diazonium ion group with the partially positively charged carbonyl carbon atom bearing the electron rich carbonyl oxygen atom of the proximal group. This attractive interaction contributes to the tendency of the diazonium ion to be distorted from linearity so as to increase the favourable interaction of the internal nitrogen (N_α) with this carbonyl carbon atom, but at the same time increasing somewhat the interaction of this nitrogen atom (N_α) to the electron rich site of the proximal group as suggested in Figure 5-32.

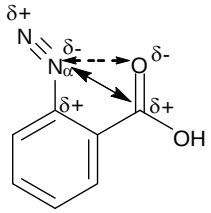

5.20a

Figure 5-32. Computed model of **5.20a** in consistent with the 1,3-bridging attraction model.

Glaser also pointed out that the 1,3-bridging interaction parallels the interaction of alkali metal ions with an allyl anion but in a polarity reversed sense.[381] In such complexes the metal ion forms a 1,3-bridge to the terminal electron-rich sites of the anion and, by doing so, is positioned such that the cation is closer to the central carbon atom of the anion that is somewhat electron deficient. The geometry that arises is a compromise that balances all the attractive and repulsive electronic interactions. In the diazonium ion case, a related balance of multiple electronic attractive and repulsive interactions leads to the counterintuitive distortion of the diazonium ion group such that the electron rich internal nitrogen is brought closer to the electron rich site in the proximal group.

Although the diazo group in the IPK and in the kinamycin systems is not quite a diazonium ion, it seems reasonable to suggest interactions of the type pointed out by Glaser and Horan, in their analysis of diazonium ion interactions with proximal electron rich groups, contribute to the distortions of the diazo group suggested by the ab initio MO calculations presented above for the IPK analogues. In the case of kinamycin F (**1.1f**) where a preference for the conformation shown below has been demonstrated experimentally (see Chapter 2) and computationally (see Chapter 4), the enhanced diazonium ion character may be a consequence of the through space 1,3-bridging interaction of the electron rich pseudo-eq. C4-OH group with the C5-diazo group with attractive (solid double headed arrow) and repulsive interactions (single headed dashed arrow) analogous to those suggested by Glaser for the aryldiazonium ions.

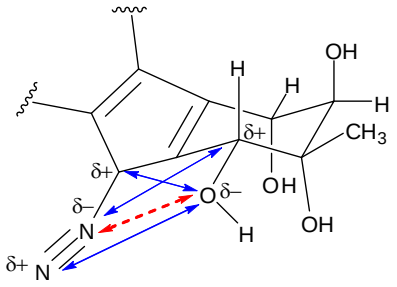

Figure 5-33. Analysis of the kinamycin F (**1.1f**) conformer having pseudo-eq. C4-OH group by using the 1,3-bridging attraction model of Glaser.

Application of Glaser's electrostatic interaction analysis method to the IPK systems should be explored in future to evaluate the importance of the 1,3-attractive interaction in determining the properties of the diazo group in the substituted IPK analogues.

5.4 Conclusion

In summary, this study has provided a number of insights into the potential influence of substituents on the diazonium ion character of the diazo group within the diazobenzo[*a*]fluorene ring system found in isoprekinamycin (IPK, **1.5**). X-ray crystallographic analysis of IPK (**1.5**) and a synthetic analogue **3.236** lacking intramolecular H-bonding clearly shows that the diazonium ion character in IPK (**1.5**) is substantially enhanced by the presence of such intramolecular H-bonds.

Ab initio molecular orbital calculations indicate that, within the diazobenzo[*a*]fluorenes, the C4-substituent can interact with the C5-diazo group so as to substantially increase the diazonium ion character. Particularly effective in this regard are C4-functional group with heteroatom(s) bearing lone pairs of electrons (e.g., $–NH_2$), which must locate geometrically close enough and in an appropriate orientation toward the C5-diazo moiety. Although the precise nature of such lone pair interaction with the diazo group that results in a substantial increase in diazonium ion character

remains to be elucidated, there is good reason to believe that a through-space bonding interaction of the lone pair orbitals with the π-bonding orbital of the diazo group, which is orthogonal to the rest of the π-system, might contribute significantly to the discovered effect. This can be clearly demonstrated by one of the molecular orbitals for the IPK-C4-NH_2 analogue **5.4a** as shown in Figure 5-34. This predicted effect, which is by no means intuitively obvious, forms the basis for synthetic experiments being pursued by others in this group. It is hoped that such efforts may be able to not only test the predictions presented in this chapter experimentally but also to determine if such alteration of diazonium ion character influences the biological activity of these compounds in a beneficial way.

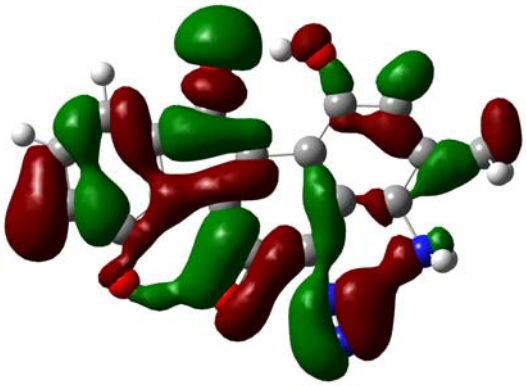

Figure 5-34. Computed MO orbital of IPK-C4-NH_2 analogue **5.4a** suggesting possible lone pair-diazo interactions.

5.5 Experimental Details

Refer to section 4.7 for details regarding the ab initio MO calculations of the diazobenzo[*a*]fluorene type of kinamycins and related analogues.

Chapter 6

Conformational Studies of Lomaiviticins

6.1 MO Calculations for Lomaiviticin A and B

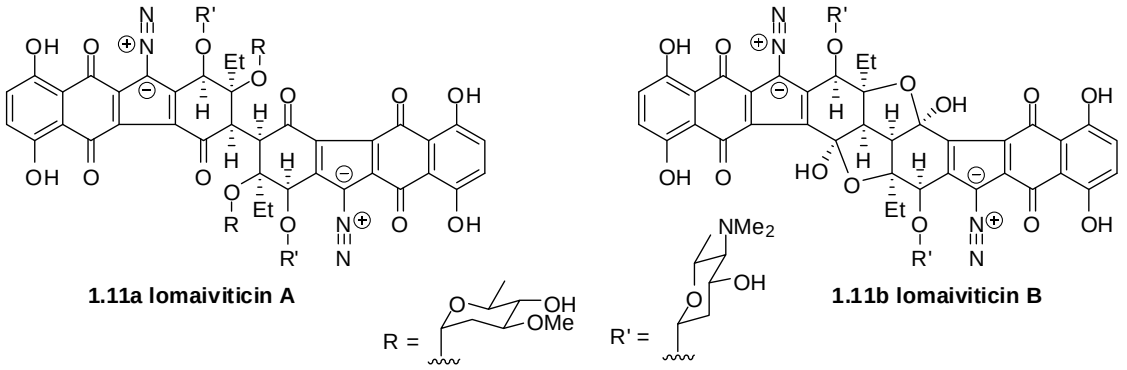

As introduced in Chapter 1, the lomaiviticins (**1.11a**/**b**) are natural dimeric analogues of the kinamycins isolated from *Micromonospora lomaivitiensis* almost a decade ago by He and co-workers at Wyeth Pharmaceuticals, which is now part of Pfizer.[52] The connectivity and the relative stereochemistry of the polyketide-derived core of the lomaiviticins were determined based on detailed spectroscopic analysis[52] and comparison with spectroscopic data for the better understood kinamycins.[21,22] The absolute stereochemistry of the dimeric diazobenzo[*b*]fluorene core remains unknown but has been assumed to be that of the kinamycins for which anomalous dispersion X-ray crystallographic data exists.[9] The relative stereochemistry within each of the two carbohydrate components attached to the D-ring of lomaiviticins via glycosidic linkages was established spectroscopically; however, the absolute configurations of the sugars are also unknown.

The very high potency of lomaiviticins as anticancer agents in vitro[52] has created high interest in gaining access to sufficient quantities for more detailed studies. Although the Wyeth group was able to obtain small amounts of lomaiviticins from the natural source, the fermentation approach has

proven to be highly variable such that only milligram quantities of these natural products have ever been isolated. As a consequence of the inability to have access to multigram quantities of these compounds, the Wyeth group has not mounted a full medicinal chemistry program around these compounds and, in fact, disclosed their structures without filing a patent.[382] The Wyeth group has made efforts to isolate all of the genes for the biosynthetic pathway with the hope that these might be used for more efficient heterologous expression in another bacterium and that the substrate specificities of the enzymes of the biosynthetic pathway might be altered to allow for biosynthesis of structural analogues.[382] Elsewhere, much interest has arisen in synthetic organic chemistry groups in total synthesis of these structurally complex compounds.[157-159]

In the Dmitrienko group, it was felt that a better understanding and some valuable insight of the three dimensional structure and the diazonium ion character of the lomaiviticins might be obtained by computational molecular modeling, even if there is no direct access to these natural products at the moment. In addition, results from such modeling studies might help to design simpler analogues with anticancer activities comparable to those of the lomaiviticins. Due to the structural complexity of the lomaiviticins, it was decided that the compounds would be analyzed computationally in a step-wise fashion as follows:

1) Conformational analysis of the two carbohydrate components of lomaiviticins, namely the methyl glycoside form of α-L-oleandrose (**6.1**) and the β-D-*N*,*N*-dimethylpyrrolosamine (**6.2**). The methyl group (bolded in the structures shown below) represents the aglycon skeleton within the lomaiviticins to which these sugars are attached.

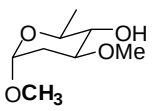

6.1 methyl glycoside of α-L-oleandrose

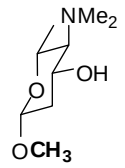

6.2 methyl glycoside of β-D-*N*,*N*-dimethylpyrrolosamine

2) Analysis of the conformational preferences of the polyketide-derived portion of the monomeric core **6.3** of the lomaiviticins, which is in fact a diazobenzo[*b*]fluorene, with a C2-methyl group representing the other half of the dimer and with the two carbohydrates at C3 and C4 also simplified as methyl groups.

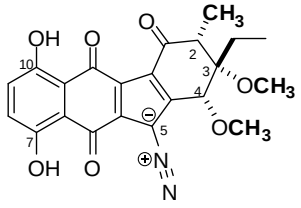

6.3 Monomeric core of lomaiviticin A

3) Attachment of the optimized carbohydrate components (**6.1** and **6.2** from step 1) to the optimized monomeric models (**6.3** from step 2) via glycosidic linkages assuming a specific absolute configuration for the aglycone and the carbohydrates.

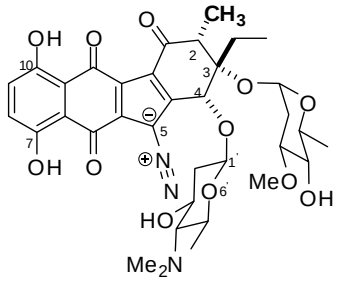

6.4 Monocore of lomaiviticin A with two sugars

4) Exploration of the conformational preferences of the aglycone of lomaiviticin A **6.5** (i.e., a dimeric diazobenzo[*b*]fluorene core) with methyls representing the carbohydrates, by attachment of the various possible conformations of two monomers (i.e., **6.4**).

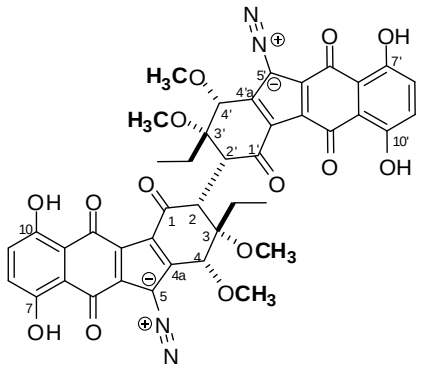

6.5 Dimeric core of lomaiviticin A

5) Conformational study of the full structures of lomaiviticin A (**1.11a**) and lomaiviticin B (**1.11b**), which can be constructed through either linking of two monomers containing the carbohydrates (**6.4** from step 3) or attaching appropriate carbohydrates (**6.1** and **6.2** from step 1) to the dimeric core (**6.5** from step 4).

This series of analyses constitutes a complex computational problem which is not as yet complete. However, the progress that has been made in pursuit of a full computational description of the lomaiviticins has revealed some interesting intramolecular interactions between the diazo group and the carbohydrate component at C4, which may influence the reactivity of the diazo group and in turn impact the behaviour of these natural products with biological targets in vivo.

The progress made in each of the five sequential analyses listed above is described below.

6.1.1 Conformational Analysis of the Carbohydrates of Lomaiviticins

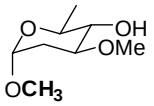

6.1 methyl glycoside of α-L-oleandrose

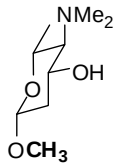

6.2 methyl glycoside of β-D-*N*,*N*-dimethylpyrrolosamine

The two types of carbohydrates within lomaiviticin A (**1.11a**) were concluded to be C3/C3'α-oleandrose and C4/C4' β-*N*,*N*-dimethylpyrrolosamine, respectively.[52] The relative stereochemistry within each of these two sugars was established solely from the observed NMR homonuclear coupling constants and comparison with literature results for the corresponding carbohydrates (i.e., α-oleandrose and β-pyrrolosamine), yet their absolute configurations were not determined.[52] The existence of the glycosidic linkages between the carbohydrates and the lomaiviticin core of carbon skeleton, either in the α- or β-manner, was determined exclusively by the NMR data with no further need of other spectroscopic evidence.

When this computational work started, however, it was noticed that there are a few obvious but previously ignored flaws with the reported structures of the carbohydrates within lomaiviticins. The two sugar units of either the C3/C3' α-oleandrose or the C4/C4' β-*N*,*N*-dimethylpyrrolosamine were concluded to be entirely identical, since only one set of NMR signals (both ^{1}H and ^{13}C) was observed for each type of carbohydrate.[52] Within the published chemical drawing of lomaiviticin A (Figure 6-1),[52] however, the two supposedly identical sugar units are illustrated with apparently opposite absolute stereochemical configurations, in which the oleandrose at C3 is shown as an α-L-sugar while the one at C3' is given as an α-D-sugar, and similarly the carbohydrate at C4 is shown as a β-D-sugar while the corresponding one at C4' is demonstrated as a β-L-sugar. The same stereochemical problem

was also found with the two C4/C4' β-*N*,*N*-dimethylpyrrolosamines within the published structure of lomaiviticin B (**1.11b**).[52]

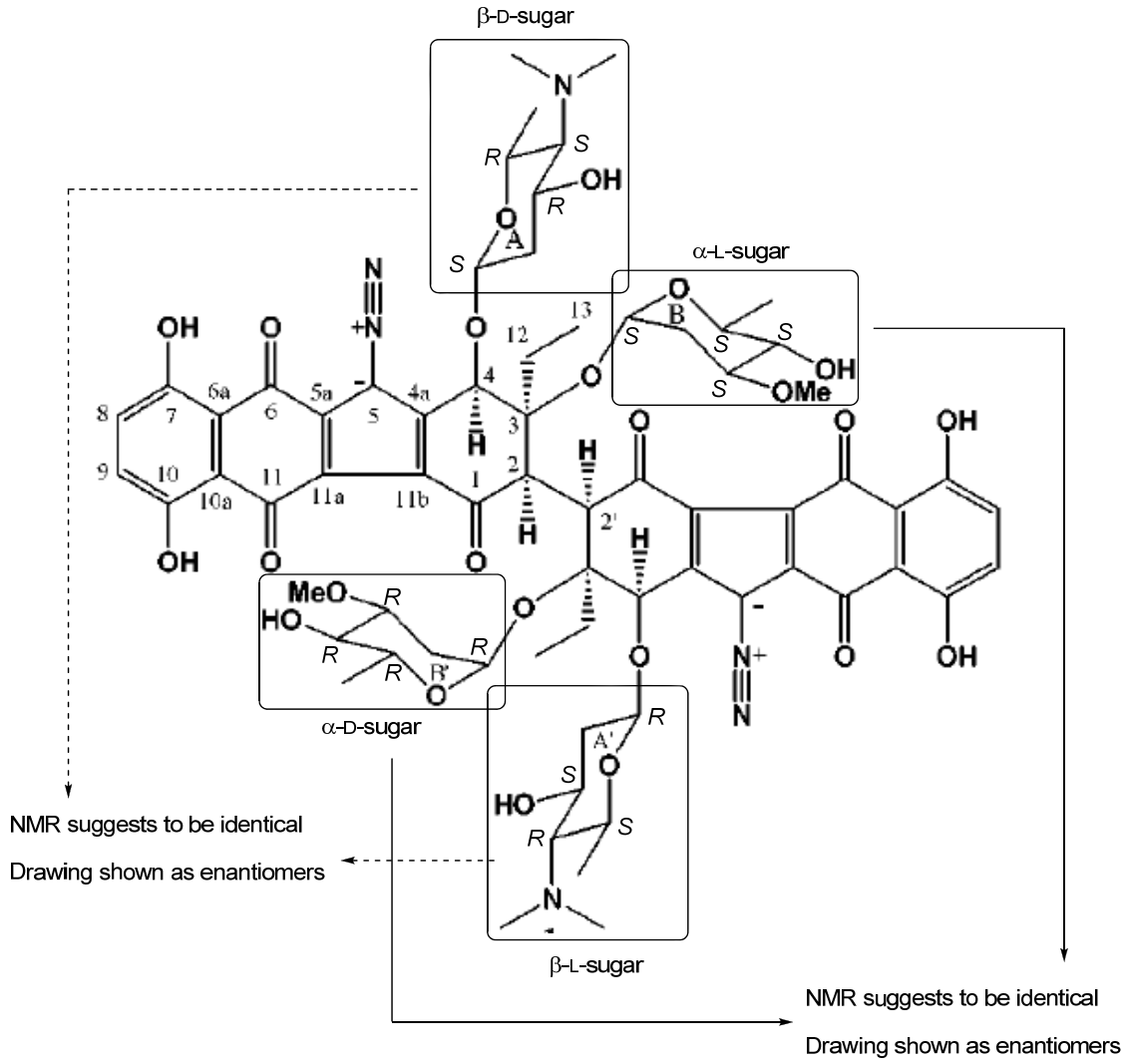

Figure 6-1. Published literature drawing of lomaiviticin A (**1.11a**) from the original reference[52] with no alteration except the added stereochemical labels (*R*/S) for carbohydrates.

Although the above mentioned errors in the published drawing of lomaiviticins may be regarded as a simple editorial issue, it does serve to point out that the experimental data of lomaiviticins does not define the absolute configuration of the carbohydrate components. The NMR data of lomaiviticins

requires symmetry in the dimer and, if assuming that the kinamycin-like core structure has the same absolute configuration in the two halves of the dimer, the symmetry of lomaiviticins must be C_2 (at least on average). Thus, the absolute configurations of the two C3/C3' oleandrose-derived components must either both be of the L- or both be of the D-configuration. Likewise the two C4/C4' pyrrolosamine-derived components must either both be of the D- or both be of the L-configuration. The uncertainty of the absolute stereochemistry of these carbohydrates would complicate the situation, since the experimental data can be reasonably accommodated by any of the four stereoisomeric possibilities for lomaiviticin A (**1.11a**) as follows: C3/C3'-α-L-sugars and C4/C4'-β-D-sugars, C3/C3'-α-D-sugars and C4/C4'-β-L-sugars, C3/C3'-α-L-sugars and C4/C4'-β-L-sugars or C3/C3'-α-D-sugars and C4/C4'-β-D-sugars. For lomaiviticin B (**1.11b**), the absence of carbohydrates at C3/C3' simplifies its stereoisomeric possibilities to two options, either C4/C4'-β-D-sugars or C4/C4'-β-L-sugars.

Ideally, the absolute configuration of the carbohydrates in the lomaiviticins should be determined through rigorous experimental methods. In the absence of such information, however, some consideration of the structures of biosynthetically related polyketide-derived antibiotics from other *Actinomycetes/Streptomyces* species is instructive. For example, oleandomycin (**6.6**, Scheme 6-1a) is an antibiotic produced by *Streptomyces antibioticus*, whose polyketide-derived macrolide core contains two carbohydrate components attached by glycosidic linkages. One of these sugar units is L-oleandrose (cf. dTDP-activated L-oleandrose **6.14**, Scheme 6-1a), which is proposed to be also a component of lomaiviticins. The other carbohydrate component in oleandomycin is D-desosamine (cf. dTDP-activated D-desosamine **6.19**, Scheme 6-1a), which is in fact isomeric with the *N*,*N*-dimethylpyrrolosamine of lomaiviticins. A very interesting biosynthetic pathway (Scheme 6-1a) has been proposed whereby both the D-desosamine component and the L-oleandrose component of oleandomycin (**6.6**) are derived from the same bioprecursor D-glucose-6-phosphate (**6.7**).[383] The key

to the ability of producing both L-series and D-series carbohydrate derivatives from the same D-series precursor in the case of oleandomycin (**6.6**) is the existence of a common C4-keto intermediate **6.9**. This D-sugar is then converted enzymatically to either **6.19** (a D-sugar) or **6.14** (a L-sugar), and epimerization at C3 and C5 catalyzed by an appropriate enzyme (from **6.11** to **6.12**) plays a critical role in the D- to L- transformation. It is reasonable to suggest that a related and similar biosynthetic pathway (Scheme 6-1b) may exist in *Micromonospora lamaivitiensis*, the *Actinomycete* species that produces lomaiviticins, providing on one hand a L-oleandrose intermediate **6.14**, on the other hand, a D-*N,N*-dimethylpyrrolosamine derivative **6.23**, both of which are activated by dTDP for *O*-glycosylation of the hydroxyl groups on the D-ring of lomaiviticins.

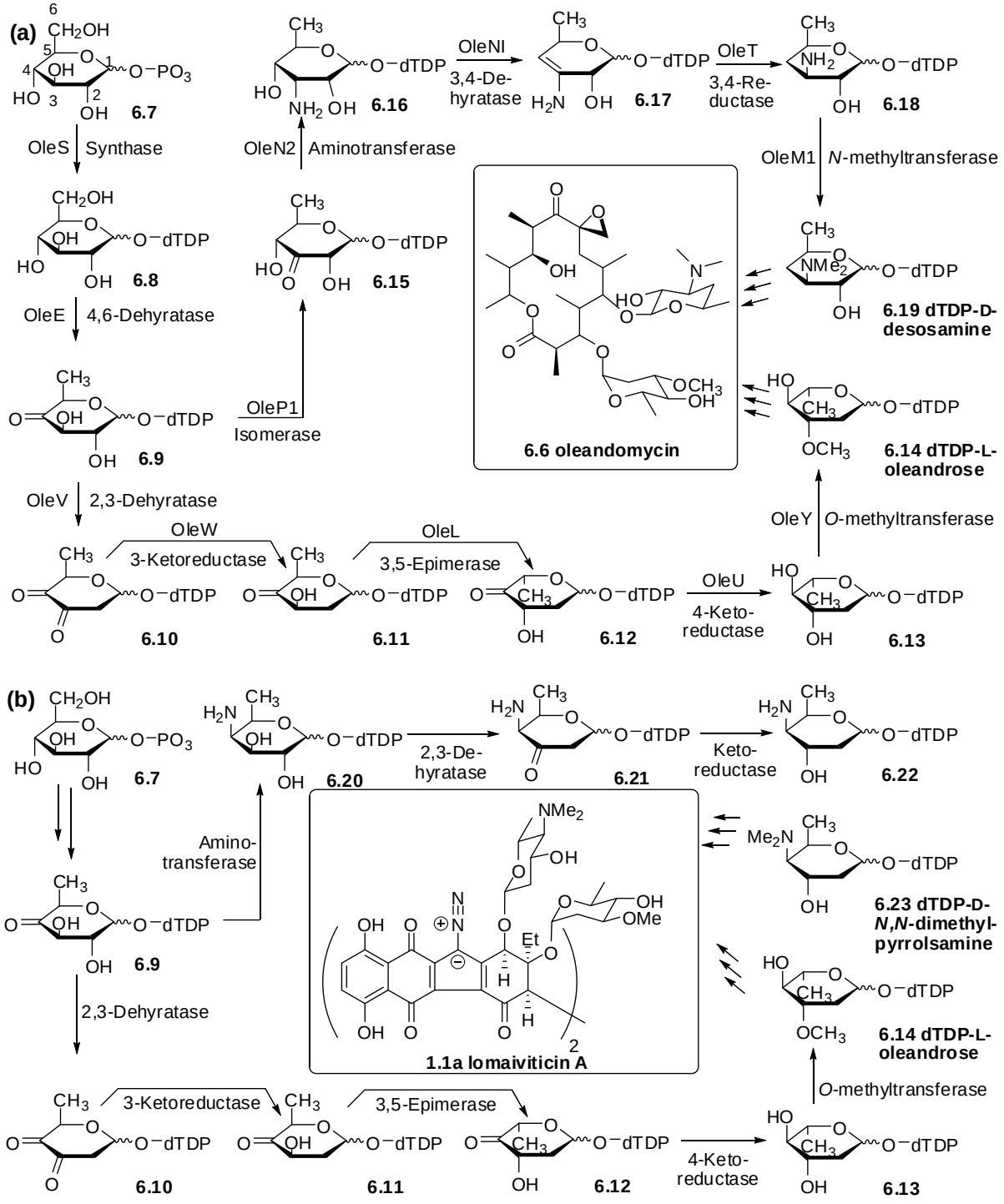

Scheme 6-1. Proposed (a) literature biosynthetic pathways of L-oleandrose and D-desosamine component of oleandomycin (**6.6**) and (b) hypothetic pathways of biosynthesis for L-oleandrose and D-*N*,*N*-dimethylpyrrolosamine of lomaiviticins by this work.

Thus, the computational analysis of the conformational properties of lomaiviticin A (**1.11a**) were carried out based on the assumption that the carbohydrate components consist of L-oleandrose, attached via a glycosidic linkage to the oxygen at C3 and C3', and D-*N*,*N*-dimethylpyrrolosamine, attached via a glycosidic linkage to the oxygen at C4 and C4'. MO calculations at the RHF/6-31G level on both methyl glycoside forms of carbohydrates α-L-oleandrose (**6.1**) and β-D-*N*,*N*-dimethylpyrrolosamine (**6.2**), produced the optimized geometries as shown in Figure 6-2. The obtained results are used directly in the later construction of the lomaiviticin-related structures. Not surprisingly, both species have an obvious and beneficial intramolecular H-bonding interaction (between the C-**OH** and adjacent C-**O**Me within **6.1**, $d_{O\text{-}H\cdots O}$ = 2.423 Å, <O-H-O = 102.1º; and between the C-**OH** and adjacent C-**N**Me_2 within **6.2**, $d_{O\text{-}H\cdots N}$ = 2.377 Å, <O-H-N = 108.4º).

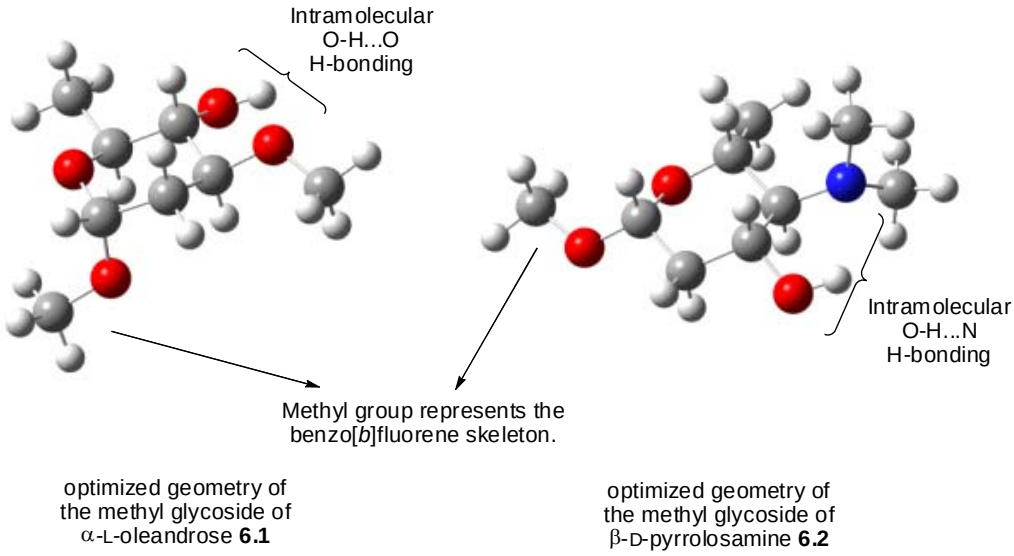

Figure 6-2. Optimized geometries of the methyl glycoside of α-L-oleandrose **6.1** and the methyl glycoside of β-D-*N*,*N*-dimethylpyrrolosamine **6.2**.

6.1.2 Conformational Preferences of the Monomeric Diazobenzo[*b*]fluorene Core of Lomaiviticins

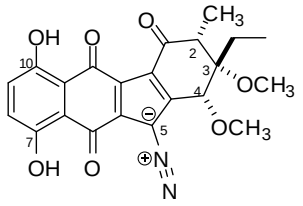

6.3 Monomeric core of lomaiviticin A

The structure of the monomeric core of lomaiviticin A (**1.11a**) was initially approximated, with the C3 and C4 sugar units being simplified as two methyl groups and another methyl placed at C2 to represent the other diazobenzo[*b*]fluorene core of the dimer. This simplified monomeric core model **6.3** is essentially a diazobenzo[*b*]fluorene that matches the same type of skeletons within the kinamycins, yet with three distinctive differences. The first one is the presence of an extra hydroxy group at C10 in the lomaiviticins, besides the common C7-OH that exists in all natural kinamycins and lomaiviticins. In principle, this additional C10-OH should lead to a strong intramolecular H-bonding interaction with the nearby C11 carbonyl oxygen, which may further help to delocalize the C5 partial negative charge and enhance the diazonium ion character. Unfortunately, no direct spectroscopic evidence for such intramolecular H-bonding interactions (i.e., significant downfield chemical shifts of the phenolic proton due to H-bonding that are commonly observed with kinamycins) is available, since the ^{1}H-NMR spectra of lomaiviticins was acquired in MeOD-d4.[52] The second difference lies in the non-aromatic D-ring, in which an sp^{2}-hydridized ketone carbonyl carbon is located at the C1 position of **6.3** (and **1.11a**) while all other natural diazobenzo[*b*]fluorene of kinamycins contain an sp^{3}-hydridized C1-carbon with either a hydroxy or ester substituent. The flatness of the C1-carbonyl within **6.3** (and **1.11a**) may restrain the conformation of its six-membered

cyclohexenyl D-ring to a greater extent when compared with the kinamycins, but the D-ring is still capable of adopting at least two possible conformations (i.e., two half chairs). On the other hand, the strong electron-withdrawing capability of the C1-carbonyl group is predicted to be beneficial towards a higher diazonium ion character. The last difference also originates from the D-ring but at its C3 position, **6.3** possesses an ethyl group while all other diazobenzo[*b*]fluorenes of kinamycins have a slightly smaller methyl substituent. Even though the difference in electronic effect between the C3-Et and the C3-Me group is expected to be negligible, the steric interaction is probably going to play a much bigger role, especially in the case of lomaiviticins, since their dimeric structures would provide significantly less spacial flexibility.

The non-aromatic D-ring of **6.3** is capable of adopting two different half chair conformations, similar to those of other diazobenzo[*b*]fluorene type of kinamycins (section 2.3 and 4.4). Between the two possible D-ring conformations of **6.3**, the one that matches the D-ring of most kinamycins (i.e., C4-OMe in a pseudo-axial orientation) will be called the "normal D-ring", while the other conformation (i.e., C4-OMe in a pseudo-equatorial orientation) will be named as the "flipped D-ring" since it can be obtained from the former upon a simple ring flip. In addition, both the C7-OH and C10-OH of **6.3** adopt a conformation favouring the intramolecular H-bonding interaction, since previous experience on simple diazobenzo[*b*]fluorene type of kinamycins has already demonstrated the significant importance of such H-bonds towards the stability of the molecule and their (limited) benefit towards a higher diazonium ion character (section 4.5). The structure of **6.3** possessing the two different D-ring conformations was then subjected to geometry optimization and frequency calculation, and the corresponding results are listed in Table 6-1. The MO calculations predict that, for the monomeric core **6.3**, the conformer having a "flipped D-ring" is not only slightly more stable than the one with a "normal D-ring" by 0.92 kcal/mol, but it also has a significantly higher diazo IR frequency ($\Delta\nu$ = 19 cm^{-1}) and hence higher diazonium ion character than the competitor.

Table 6-1. Comparison of the two D-ring conformers of the monocore model **6.3**.[a]

Optimized conformation of **6.3**[b]	E(RHF) (a.u.)[c]	$\nu_{N\equiv N}$[d] (cm^{-1})
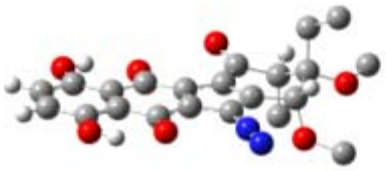 normal D-ring (pseudo-ax. C4-OMe)	-1476.528437	2174
 flipped D-ring (pseudo-eq. C4-OMe)	-1476.529905	2193

a. Ab initio MO geometry optimization and vibrational frequency calculation were performed with Gaussian03® at the RHF/6-31G//6-31G level; b. Protons on the D-ring ethyl and methyl groups are omitted for clarity; c. The E(RHF) was corrected with ZPE, 1 a.u. = 627.5095 kcal/mol; d. Scaled with a scaling factor of 0.8929.

This calculated energetic preference and higher diazonium ion character of **6.3** with "flipped D-ring" than the "normal D-ring" can be explained by using the previous arguments to rationalize the similar observations with kinamycin F (**1.1f**) (section 4.4). The free energy difference between the two conformers of **6.3**, when estimated by using the corresponding A-values of the D-ring substituents (i.e., 0.75 kcal/mol for $-OCH_3$, 1 kcal/mol for $-CH_3$ and ~ 1 kcal/mol for $-CH_2CH_3$ from Table 4-2), is ca. 2 kcal/mol. This empirical value is quite consistent with the MO predicted energy difference of ca. 0.92 kcal/mol, suggesting that the major influence leading to the slightly different stabilities of the two conformers of **6.3** should come from the simple conformational change of its D-ring. As in the case of kinamycin F (**1.1f**) (section 4.4), **6.3** with a "flipped D-ring" present a dipole-

dipole interaction between the C4-O bond and the C5-N bond that is expected to enhance the diazonium ion character. At this stage, it is not clear if the simplification of the lomaiviticin structure (i.e., replacing half of the very bulky dimeric core of lomaiviticin A and the sugar units with the much smaller methyl groups) is responsible for the calculated rather small energy difference between the two conformers of **6.3**. It is possible that more complicated lomaiviticin-related structure with dramatically increased steric factors introduced onto the D-ring might experience much greater energy difference and conformational preference in between their corresponding D-ring conformers.

6.1.3 Conformational Preference of the Lomaiviticin Monocore Containing Sugars

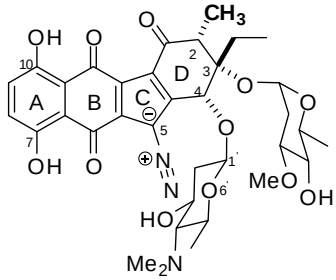

6.4 Monocore of lomaiviticin A with two sugars

With the optimized geometries of both the C3/C4-carbohydrates (section 6.1.1) and the monomeric diazobenzo[*b*]fluorene core of lomaiviticin A **6.3** (section 6.1.2) available, the next logical step was to attach the carbohydrate units to each of the two conformers of the monocore **6.3** (normal vs flipped D-ring), via the corresponding α- or β-glycosidic linkage as suggested by the NMR data of lomaiviticin A (**1.11a**). To construct this bigger monocore of lomaiviticin A **6.4** that now contains the two sugar components as in the natural product, it was obvious that a few necessary methyl groups from the optimized structures of **6.1**/**6.2** and **6.3**, which were used to represent the bigger substituents, had to be chopped off and the remaining pieces were to be merged with minimal

modification on the optimized bond length and bond angle of the two C-O-C glycosidic linkages; however, there were some additional factors that had to be carefully considered.

The C3-α-oleandrose within **6.4** is in a less-hindered environment than the C4-β-pyrrolosamine and can rotate rather freely. The predictable influence on the conformation of the core from this C3-sugar is not major but some obvious steric repulsion with the nearby C2-methyl, C3-ethyl and C4-sugar. However, the C4-β-pyrrolosamine is expected to have much less conformational freedom than its C3 neighbor since it has to stay in a crowded and concave space, whose boundary is defined by the C2-methyl, C3-ethyl, C3-sugar and C5-diazo groups, as well as the planar C-ring. A reasonable starting geometry of **6.4** can be constructed by attaching the optimized sugar **6.2** at the C4 position with the sugar's ring plane either orthogonal (diagram (a) in Figure 6-3) or parallel (diagram (b) in Figure 6-3) to the aromatic diazobenzo[*b*]fluorene ring plane, which are the two extreme situations of possible conformations. Interestingly, MO optimization always forced a rotation, if necessary, of the C4-carbohydrate so that its ring plane ends up with a near orthogonal orientation relative to the aromatic ring plane, which is expected as this should minimize the steric repulsion of the C4-sugar from at least the C5-diazo and C3-sugar. In addition, this preferred orthogonal correlation between the two planes would further create two possibilities of conformation, since the cyclic C4-sugar ring is unsymmetric along the C1'-O (the one attached to C4) bond/axis and thus the oxygen that attaches to the anomeric carbon (i.e., O6') may be close (diagram (c) in Figure 6-3) or far (diagram (d) in Figure 6-3) from the C5-diazo group. If O6' and the diazo group stay in close enough proximity, the available lone pair of electrons on the former may provide some favourable intramolecular through-space interactions towards the diazo moiety, similar to the earlier observations with the diazobenzo[*a*]fluorenes of some IPK-C4-analogues (Chapter 5). This possible oxygen-diazo interaction is also encountered previously in the optimized geometries of some other diazobenzo[*b*]-fluorene type of kinamycins such as kinamycin E (**1.1e**, Table 4-3, section 4.4) and kinamycin D

(**1.1d**, Table 4-8, section 4.5), in which the carbonyl oxygens of their C4-acetoxy groups (i.e., -C4-O-(C=**O**)-CH_3) seem to always preferentially point towards the C5-diazo nitrogens at some rather short distances (ca. 2.7–2.9 Å, shorter than the sum of the corresponding vdW radii). The structural similarity between the -C4-O-C1'(H)-**O6'**- of **6.4** and the -C4-O-C(=**O**)- of **1.1d**/**1.1e** would imply that such oxygen-diazo interaction may well exist in the case of lomaiviticins and related structures. Similar to kinamycins and compound **6.3**, the non-aromatic D-ring of **6.4** is also capable of adopting either the normal (pseudo-ax. C4-O-sugar) or flipped (pseudo-eq. C4-O-sugar) conformation, which has to be considered together. In the end, MO optimization provided a total of four stable conformers of **6.4** as summarized in Table 6-2.

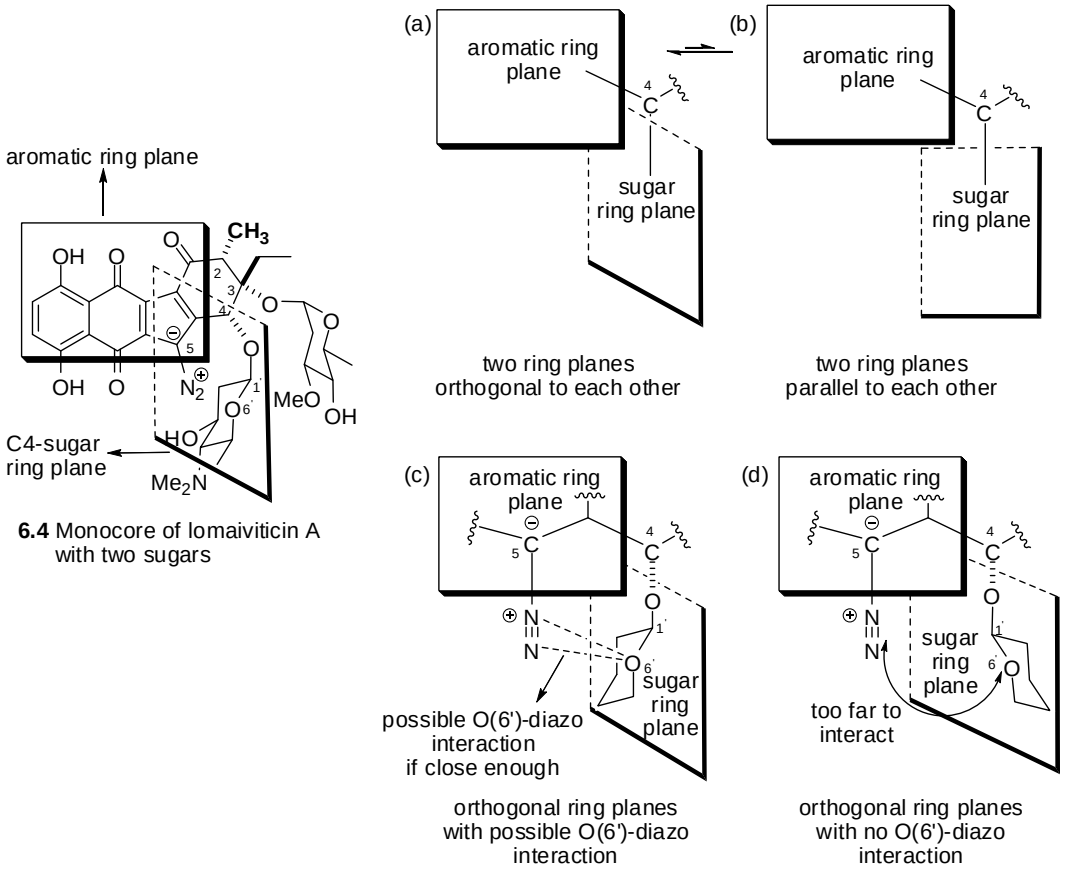

Figure 6-3. Possible conformations of **6.4** based on its D-ring conformation and C4-sugar orientation.

Table 6-2. Optimized geometries of the monocore of lomaiviticin A with two sugars **6.4**.[a]

Optimized conformations of **6.4**[b]	E(RHF) (a.u)[c]	$\nu_{N\equiv N}$ (cm^{-1})[d]	$d_{O6'\cdots N1}/d_{O6'\cdots N2}$ (Å)
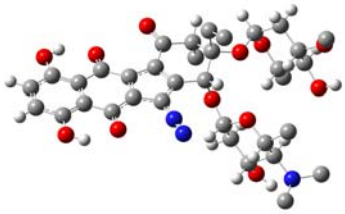 conformer I (normal D-ring)	-2410.138023	2150	4.085/4.135
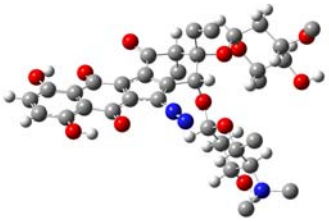 conformer II (normal D-ring)	-2410.138045 ΔE^e = -0.014 kcal/mol	2175	3.211/3.219
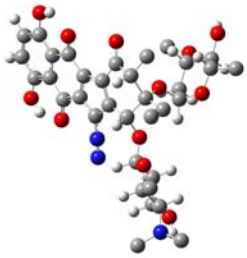 conformer III (flipped D-ring)	-2410.148218 ΔE^e = -6.40 kcal/mol[e]	2162	4.568/4.695
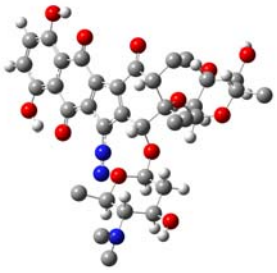 conformer IV (flipped D-ring)	-2410.149376 ΔE^e = -7.12 kcal/mol[e]	2198	2.921/2.985

a. Ab initio MO geometry optimization and calculation of vibrational frequencies were performed with Gaussian03® at the RHF/6-31G//6-31G level; b. Unimportant protons of D-ring substituents were omitted for clarity; c. All E(RHF) were corrected with ZPE, 1 a.u. = 627.5095 kcal/mol; d. Scaled by a scaling factor of 0.8929; e. Relative to conformer I, the least stable conformation.

For both the normal and the flipped D-ring conformation of **6.4**, two conformations with different C4-sugar orientation towards the corresponding C5-diazo group were obtained. Comparison of the energies, geometries and diazo IR frequencies of these conformers (Table 6-2) has revealed several important aspects of the molecule. First, the stability of the four conformers of **6.4** increases in the order of I < II < III < IV, in which the two conformers I and II having normal D-rings are significantly less stable than the other two conformers III and IV having flipped D-rings. This tendency of change in energy due to variation of D-ring conformation is entirely consistent with the previous example of **6.3** but the absolute value is much higher (i.e., ~ 6–7 kcal/mol for **6.4** vs 0.92 kcal/mol for **6.3**), indicating that the much larger sugar units of **6.4** (than the corresponding methyl groups of **6.3**) have applied significantly larger steric effect on the stability of the molecule, depending on the axial or equatorial orientation of the carbon-sugar bonds. However, when the D-ring of **6.4** adopts the particular "normal" or "flipped" conformation, the energy differences between the two conformers that are only slightly different with the orientation of their C4-sugars (i.e., I vs II or III vs IV, Table 6-2), which can be judged by the distance between the C4-sugar's ring-oxygen (O6') and the diazo moiety, are indeed very small (~ 0.01–0.7 kcal/mol). In fact, the distances between the O6' and the two diazo nitrogens vary significantly among the four conformers (i.e., ~ 2.9–4.7 Å). The vdW radius of oxygen (r_O = 1.52 Å) and nitrogen (r_N = 1.55 Å), along with the optimized geometries (Table 6-2), would suggest that conformer II and IV (particularly the latter one) possess some fairly strong intramolecular oxygen-diazo interactions as predicted earlier, since their O6'-N distances ($d_{O6'\cdots N1/N2}$ = 2.9–3.2 Å) are shorter or at least comparable to the sum of the corresponding vdW radii. Conformer I and III, however, completely lack such an interaction since their O6' is too far away from the corresponding diazo group ($d_{O6'\cdots N1/N2}$ = 4.1–4.7 Å). The presence of this oxygen-diazo interaction, which is very similar to the previous observations of some IPK-C4-analogues having diazonium-favouring electron donor-diazo interactions (Chapter 5), shall be the main reason for the

much higher diazonium ion characters of conformer II ($\nu_{N\equiv N}$ = 2175 cm^{-1}) and IV ($\nu_{N\equiv N}$ = 2198 cm^{-1}) than that of conformer I ($\nu_{N\equiv N}$ =2150 cm^{-1}). Of course in the case of both conformer III and IV having flipped D-rings, their diazonium ion characters shall also be partially attributed to the presence of the diazonium-favouring dipole-dipole interactions between their C4-O and C5-N bonds, which are not available within conformer I and II having normal D-rings. However, the enhancement of diazonium ion character by dipole-dipole interaction is significantly smaller than the oxygen-diazo interaction. This conclusion is strongly supported by the following comparisons: (i) oxygen-diazo interaction causes a large increase of diazo IR frequency by 25cm^{-1} from conformer I ($\nu_{N\equiv N}$ = 2150 cm^{-1}) having long O6'-diazo distance to conformer II ($\nu_{N\equiv N}$ = 2175 cm^{-1}) having short O6'-diazo distance, both of which have no C4→O/C5←N dipole-dipole interactions; (ii) the observed even larger diazo IR frequency increase of 36 cm^{-1} from conformer III ($\nu_{N\equiv N}$ = 2162 cm^{-1}) to conformer IV ($\nu_{N\equiv N}$ = 2198 cm^{-1}) shall be mainly due to the oxygen-diazo interaction that presents in conformer IV but not III, since these two conformers have almost identical C4→O/C5←N dipole-dipole interactions (dipole-related bond lengths, distance between bonds and dihedral angles are essentially the same for conformer III and IV); and (iii) the moderate diazo IR frequency increase of 12 cm^{-1} from conformer I ($\nu_{N\equiv N}$ = 2150 cm^{-1}) to conformer III ($\nu_{N\equiv N}$ = 2162 cm^{-1}) is the result of a C4→O/C5←N dipole-dipole interaction, which presents in conformer III ("flipped" D-ring) but not conformer I ("normal" D-ring), since neither conformation possesses the oxygen-diazo interaction due to the large distance of their O6' from the corresponding diazo group.

Within the above optimized four conformations of **6.4** (Table 6-2), the C4-sugar ring plane always adopts an orthogonal correlation with the aromatic diazobenzo[*b*]fluorene plane (near perpendicular in cases of conformer I, II and III). It is quite obvious that even a small variation of the C4-sugar's orientation in the space may significantly affect its interactions with the nearby C5-diazo group and C3-sugar as a result of changes in interacting distances, both electronically (e.g., the possible oxygen-

diazo interaction) and sterically (e.g., steric repulsion with C3-sugar). However, such (small) conformational deviation may not necessarily cause significant increase in the overall energy of the molecule (e.g., conformer I vs II or conformer III vs IV). To ensure that the obtained geometries are indeed the (local) energy minimum and no other possible and stable conformations are missing, a torsion scan was performed with each of the four conformers of **6.4** along the dihedral angle of C4-O-C1'-O6'. Starting with each of the optimized conformers of **6.4**, the corresponding dihedral angle of C4-O-C1'-O6' was rotated 10° stepwise until a full circle (360°) is achieved while the remaining (optimized) part of the molecule was kept intact. For each conformation generated during the torsion scan, the corresponding single point energy (SPE) was calculated and plotted as a function of the dihedral angle (Figure 6-4). This obtained dependence of SPE on the orientation of the C4-sugar clearly indicates that the four geometries obtained (Table 6-2) are indeed the energy minima. Despite its strong enhancement of the diazonium ion character, energetically, the oxygen-diazo interaction within **6.4** is only slightly beneficial (< 1 kcal/mol). This observation is similar to the previous findings with the diazobenzo[*a*]fluorenes of some IPK-C4-analogues (such as IPK-C4-NH_2 **5.4a** and IPK-C4-OH **5.5c**, section 5.2), but the latter ones have significantly higher energy contribution from the corresponding electron donor-diazo interactions (i.e., 8.3 and > 4.3 kcal/mol for **5.4a** and **5.5c** respectively).

The above discovered interaction between the C4-sugar and C5-diazo group, and the corresponding effect on the diazonium ion character within the simple model compound **6.4**, is expected to be present also in the more complicated structures of lomaiviticins. This might influence the reactivity of the diazo group and in turn impact the biological behaviour of such natural products.

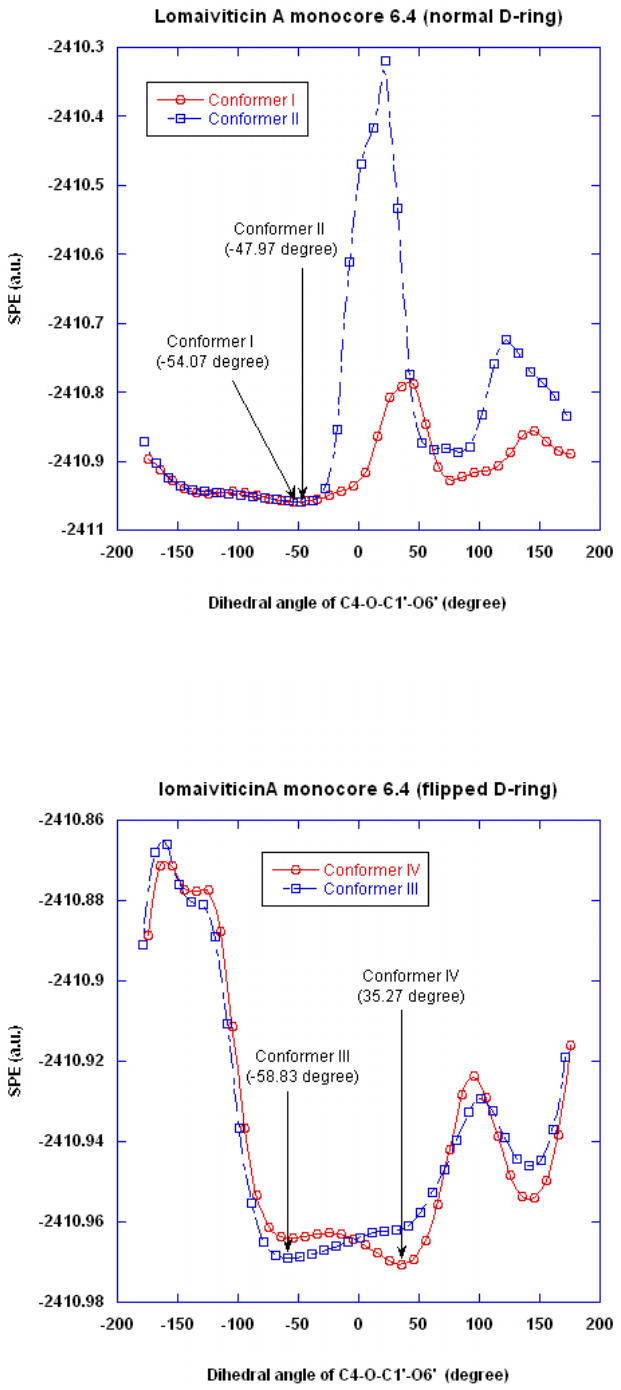

Figure 6-4. SPE of each conformer of **6.4** as a function of the dihedral angle of C4-O-C1'-O6'.

6.1.4 Conformational Preference of the Dimeric Core of Lomaiviticins

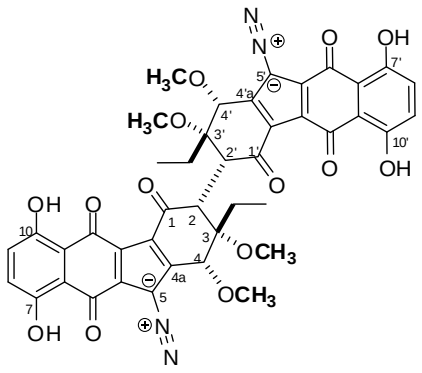

6.5 Dimeric core of lomaiviticin A

Within the previous simple monocore model compounds such as **6.3** (section 6.1.2) and **6.4** (section 6.1.3), half of the dimeric diazobenzo[*b*]fluorene core of lomaiviticin A (**1.11a**) is simplified as a C2-methyl group. A significant drawback of such a simplification is that the C2-methyl group does not provide a close imitation of the steric situation within the lomaiviticins. The C2-C2' single bond linkage between the two D-rings of diazobenzo[*b*]fluorenes within lomaiviticins is one of the unique structural features of these natural products, and initial studies of the corresponding influence on the conformation was thought to be better performed starting with the simplified dimeric species **6.5**, which is in fact a trimmed lomaiviticin A (**1.11a**) with its four sugar units substituted by methyl groups.

To construct the appropriate starting geometries of **6.5**, the optimized conformation of **6.3** was used as the essential building block. Even though the C2-methyl group of **6.3** could be easily chopped off and two such units then joined to afford **6.5**, there were two additional conformational factors that needed to be considered. The first one is obviously the D-ring conformation, since each D-ring within **6.5** may adopt the one of the two possible conformations (i.e., "normal" vs "flipped") and the two D-rings could behave independently. Therefore, three different conformational possibilities could arise

from such combinations, i.e. “normal-normal”, “normal-flipped” and “flipped-flipped” D-rings. The second concern is that when attaching two units of the optimized **6.3** (with its C2-methyl group removed) together, the C2-C2’ bond linkage has to be orientated in an appropriate manner to minimize obvious and unfavourable steric interactions. The basic organic principle of preferring a staggered rather than eclipsed correlation in between the (six) substituents attached to the two vicinal carbons >C-C< (as in the simplest example of such, e.g., ethane) was used as a logical criterion to produce some possible starting geometries of **6.5**. Since the three substituents on C2 (and C2’) of **6.5** are all different from each other, three staggered conformations along the >C2-C2’< bond had to be considered. Therefore, combination of the various possible conformations of the D-rings and along the C2-C2’ linkage would lead to at least nine (3 x 3) different starting geometries of **6.5** to be subjected to the MO calculations (Figure 6-5). It can be realized from these simplified drawing of **6.5** that, some of the conformations (e.g., conformer I and VII) might in principle possess a C_2 symmetry, which is indicated by the experimental observation for natural lomaiviticins.

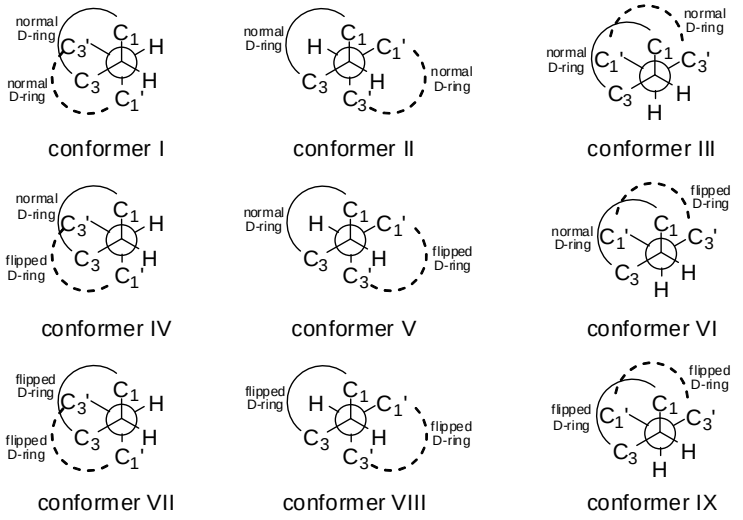

Figure 6-5. Schematic diagram of the nine possible starting geometries for **6.5**.

The geometry optimization and IR frequency calculations of the above nine different starting conformations of **6.5** were carried out at the RHF/6-31G//6-31G level as usual. The corresponding optimized conformations are given in Figure 6-6. The calculated Hartree-Fock energy, diazo IR stretching frequencies and some geometric data for the nine conformers are summarized in Table 6-3, which are tabulated in the descending order of the conformers' stability.

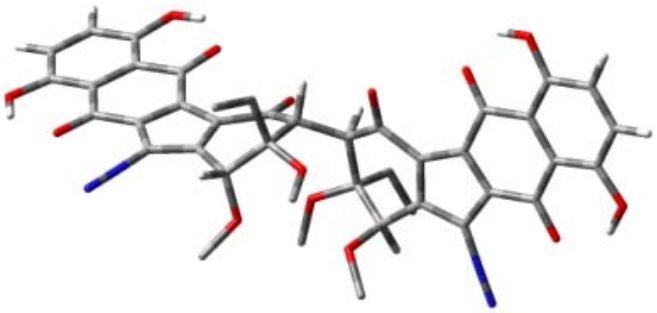

conformer I

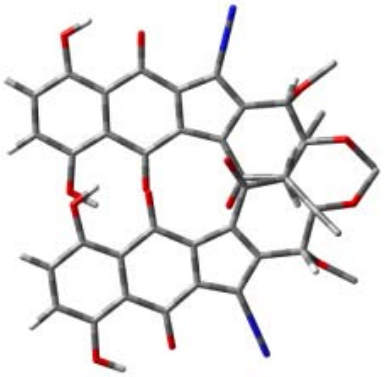

Conformer II
(two parrallel ring planes)

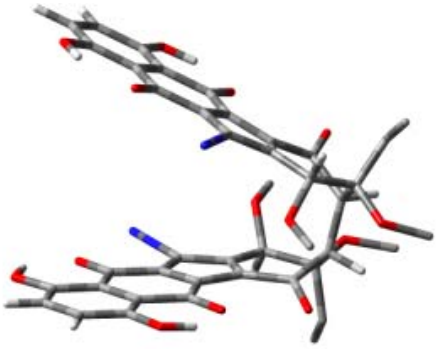

Conformer III

Figure 6-6 (part I). Optimized conformer I–IX of lomaiviticin model compound **6.5** (Refer to Appendix F (Figure F1–9) for a more detailed conformation diagram displayed in multiple viewing angles. Due to the structural complexity, the molecule of **6.5** is displayed in "Tube" format instead of the previous "Ball and Stick" format. For further clarity, all hydrogens on the D-ring C4/C4'-OMe methyl groups and C3/C3'-Et groups are omitted).

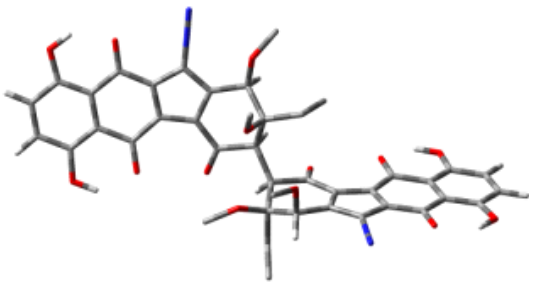

Conformer IV

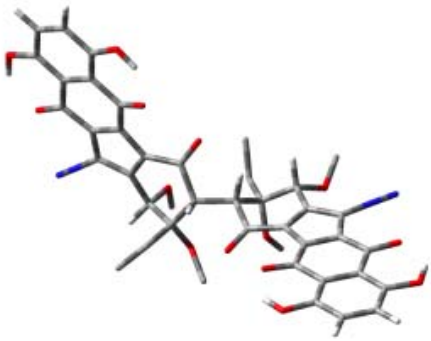

Conformer V

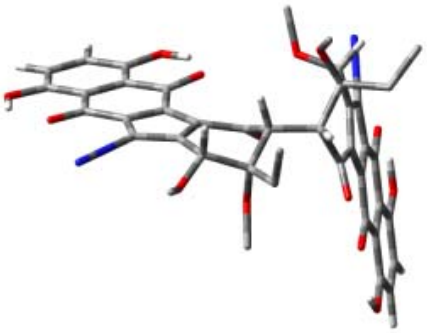

Conformer VI

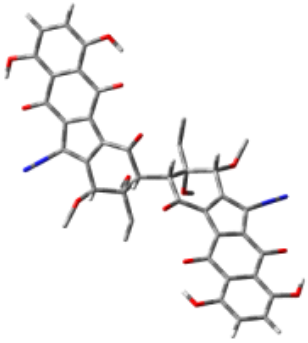

Conformer VII

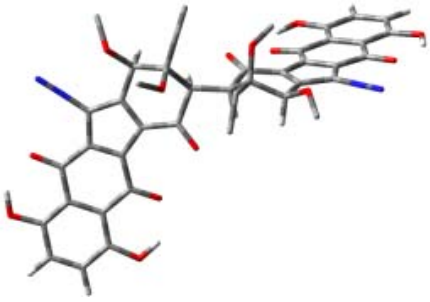

Conformer VIII

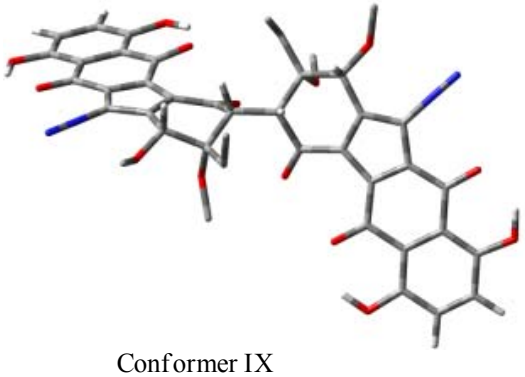

Conformer IX

Figure 6-6 (part II). Optimized conformer I–IX of lomaiviticin model compound **6.5** (Refer to Appendix F (Figure F1–9) for a more detailed conformation diagram).

Table 6-3. Summary of some calculated physical properties of the nine possible conformers of **6.5**.

Conformer of **6.5** (D-rings)[a]	E (RHF) (a.u.)[b] ΔE (kcal/mol)[c]	$\nu_{N\equiv N}$ (cm^{-1})[d] <O-C4-C4a-C5 (°)[e]	C2-C2' conformation[f]	$d_{C2\text{-}C2'}$ (Å)
Conformer VII (flipped-flipped)	-2873.923413 0	2207/2208 21.8/21.8	near Eclipsed	1.575
Conformer VIII (flipped-flipped)	-2873.919512 2.45	2199/2200 26.8/26.8	Eclipsed	1.572
Conformer II (normal-normal)	-2873.915437 5.01	2168/2171 62.2/62.2	Eclipsed	1.587
Conformer VI (normal-flipped)	-2873.910056 8.38	2167/2177 68.4/34.2	Staggered	1.558
Conformer III (normal-normal)	-2873.906928 10.34	2182/2184 61.6/61.6	Staggered	1.577
Conformer V (normal-flipped)	-2873.905350 11.33	2159/2200 85.1/29.5	near Eclipsed	1.571
Conformer IV (normal-flipped)	-2873.904530 11.85	2181/2206 70.8/21.5	Staggered	1.575
Conformer IX (flipped-flipped)	-2873.904206 12.05	2192/2193 30.9/30.9	Staggered	1.554
Conformer I (twist-boat-twist-boat)[g]	-2873.881362 26.39	2143/2145 86.8/86.8	Staggered	1.570

a. All final optimized geometries except conformer I (see footnote g) adopt the same type of D-ring conformations as in the corresponding starting geometry, i.e. a starting conformation with "normal-normal" D-rings would give an optimized one also having "normal-normal D-rings", and so on; b. All E(RHF) were corrected with ZPE, 1 a.u. = 627.5095 kcal/mol; c. Relative to the most stable conformer (i.e., conformer VII); d. Scaled by a scaling factor of 0.8929; e. Each conformer has two of such dihedral angles (i.e., <O-C4-C4a-C5 and <O-C4'-C4a'-C5'); f. Refer to Appendix F (Figure F1–9) for details regarding the C2-C2' conformation; g. Conformer I started with "normal-normal" D-rings but ended with "twist-boat-twist-boat" D-rings.

There are several important and interesting findings based on the above modeling results. First, each of the nine starting conformations of **6.5** led to a corresponding optimized geometry after MO calculations (Figure 6-6 and Appendix F). Since previous experience with **6.3**, **6.4** and kinamycin F (**1.1f**) has already indicated the energetic benefit when their D-rings adopt the "flipped" conformation, it is not surprising that the final two most stable (preferred) conformations of **6.5** are derived from conformer VII and VIII, which both have "flipped-flipped" D-rings. However, the third (conformer II) and the fourth (conformer VI) most stable conformers of **6.5** have "normal-normal" D-rings and "normal-flipped" D-rings respectively, suggesting that the conformation of the D-rings is not the sole factor that dominates the stability of the molecule. On the other hand, the particular starting conformation I with "normal-normal" D-rings was twisted by the Gaussian03® program during the geometry optimization, and the corresponding two final D-rings were found to both exist in twist-boat conformation (Figure 6-6 and Figure F-1) rather than either the "normal" or "flipped" half-chair conformation. Since the twist-boat conformation is an intermediate in the transition between two half-chairs and thus much higher in energy, it is not surprising that conformer I with its two twist-boat D-rings, which is indeed a true local energy minimum, is the least stable one among the nine possible conformations. The energy difference of conformer I relative to the most stable one (conformer VII) is so high (i.e., 26.39 kcal/mol) that, with no hesitation, this very unstable species can be excluded from the possible conformations of **6.5**. Yet conformer I may serve as a theoretically possible intermediate during the conformational change of **6.5**, particularly when its D-ring(s) is interconverting between the "normal" and "flipped" half-chair conformations. In theory, thermodynamic interconversions between these conformers (except conformer I) is possible, since some of such conformational equilibria only require a small change in overall energy through either a simple/small rotation along the C2-C2' bond (e.g., VII↔VIII, ΔE = 2.45 kcal/mol; V↔IV, ΔE = 0.52 kcal/mol), or a combination of the C2-C2' bond rotation along with a single/double cyclohexene ring

inversion (e.g., VI↔III↔V, ΔE_{III-VI} = 1.96 kcal/mol, ΔE_{V-III} = 0.99 kcal/mol). However, the very unstable conformer I, if indeed acting as the actual conformational intermediate, would suggest that such conformational changes are kinetically impossible under standard (room temperature) conditions. More importantly, when judging by the calculated energy difference, the ca. 5 kcal/mol between the conformer II (3rd most stable conformation) and the most stable conformer VII would already indicate that contributions from any conformers with even higher energy are completely negligible, and conformation VII and VIII of **6.5** shall dominate. One could also easily realize that, many of the above eight conformations of **6.5** (Figure 6-5 and Appendix F), such as conformations III, V and VI, are not physically possible for lomaiviticin A (**1.11a**), since the four D-ring methoxy groups within **6.5** are already very close to each other (as well as the two ethyl groups) and leave no further room to accommodate the much bulkier sugar units of **1.11a**.

Another interesting observation from these optimized geometries of **6.5** is the relatively long C2-C2' bond. The calculated bond lengths for this dimeric linkage within the two most stable conformers of **6.5** are 1.575 and 1.572 Å (Table 6-3), while the typical C-C single bond length is only ca. 1.54 Å. As a further comparison with some other simple models for the C2-C2' linkage of lomaiviticin A (**1.11a**), the computed (at the RHF/6-31G level) C-C bond lengths for the dimeric linkage of 2,3-dimethylbutane $(CH_3)_2$>CH–CH<$(CH_3)_2$ and 1,1'-dicyclohexane C_6H_{11}–C_6H_{11} are 1.552 Å and 1.554 Å respectively, which are longer than the typical C-C bond length but still significantly shorter than the C2-C2' bond of **6.5**. The significantly extended C2-C2' bond within **6.5** is a natural response of the molecule to minimize the repulsive interactions (steric congestion) between the six substituents attached to the carbon linkage. In fact, literature results indicate that extra long single carbon-carbon bond (> 1.6 Å) have been experimentally observed when large enough steric congestion exists,[384] therefore, the calculated C2-C2' bond length of ca. 1.57 Å of **6.5** seems to be fairly reasonable given the surrounding steric congestion. It is expected that, in the case of lomaiviticins when the much

bulkier D-ring sugar units are present, the corresponding C2-C2' bond length might be comparable to (if not longer than) the current calculated values of **6.5**. On the other hand, the proposed preference of staggered conformation along the C2-C2' linkage is only retained in five cases (out of nine), and apparently some near eclipsed conformations along the C2-C2' linkage are even lower in energy than those similar but staggered conformers (note that the three most stable conformers of **6.5** all have eclipsed or near eclipsed conformations along their C2-C2' bonds, refer to Appendix F for the detailed illustration of the staggered/eclipsed C2-C2' correlation), which could benefit significantly from this extended C2-C2' bond.

In addition, conformer II (Figure 6-6 and Figure F-2) is found to be unique since its two flat aromatic planes of diazobenzo[*b*]fluorene skeleton are parallel to each other, and the distance between them is ca. 3.15 Å (Figure F-2). Such a distance is comparable to the rise of base pair (ca. 3.3–3.4 Å) along the double-helix axis within B-DNA, which is the most common DNA conformation in vivo. This coincidental distance similarity would suggest that a double-intercalation between the conformer II of **6.5** and DNA might be geometrically possible, and some docking simulations in this regard would be intriguing. It is also very interesting to notice the likely presence of some π-π interactions in the case of conformer III (Figure 6-6 and Figure F-3), whose two aromatic ring planes stay fairly close to each other and its two aromatic C-rings within the two diazobenzo[*b*]fluorenes align well (one on top of the other when viewed from the C2-C2' axis).

The symmetric dimer structure of **6.5** is in principle expected to adopt a C_2 symmetry as do the lomaiviticins. The rotation flexibility and freedom of the substituents on the two D-rings of **6.5**, even though quite limited, have made none of the optimized conformation of **6.5** to truly possess a C_2 symmetry (by strict definition). Examination of the optimized conformers having the same type of D-rings (e.g., conformer I having "normal-normal" D-rings and conformer VII having "flipped-flipped" D-rings), however, indicates that they are very close to C_2 symmetric species.

The conformation of the two D-rings within **6.5** is found to have quite a dramatic influence on the diazonium ion character of the corresponding diazo groups (Table 6-3). When both D-rings adopt the same type of conformation, the individual diazonium ion character of the two diazo groups are essentially the same. However, when the two D-rings adopt different conformation (i.e., one D-ring is "normal" while the other D-ring is "flipped"), the two diazo groups show substantial differences between their diazonium ion characters. In all cases, the "flipped" D-ring having a C4(C4')-OMe group in pseudo-equatorial position is found to always associate with a (much) higher diazo IR frequency than the "normal" D-ring having a pseudo-axial C4(C4')-OMe (Table 6-3), and a clear trend is that the diazo IR frequency is inversely related to the corresponding dihedral angle in between the C4/C4'-OMe and the attached aromatic ring plane (i.e., <O-C4-C4a-C5 or <O-C4'-C4a'-C5'), which also serves as a good indication for the D-ring conformation (i.e., the D-ring is a "flipped" one if this dihedral angle is < 35° but a "normal" one if the dihedral angle is > 60°). The flipped D-ring(s) of **6.5** offers a much better alignment between the polar C4-O (C4'-O) bond and the C5-N (C5'-N) bond and consequently a stronger dipole-dipole interaction favouring a higher diazonium ion character, which is entirely consistent with the earlier findings with kinamycin F (**1.1f**, section 4.4) and other simple lomaiviticin model compounds such as **6.3** (section 6.1.2) and **6.4** (section 6.1.3).

Finally, the calculated dipole moments of the nine conformers of **6.5** vary significantly between 5.9–13.3 Debye depending on the conformation involved, yet it is not expected to play any significant role at the moment since all MO calculations were carried out in the gas phase. However, the different polarities of this molecule based on its different conformations may be of certain importance when the equilibria between these conformations are to be considered in solution phase.

6.1.5 Conformational Preference of Lomaiviticin A and B

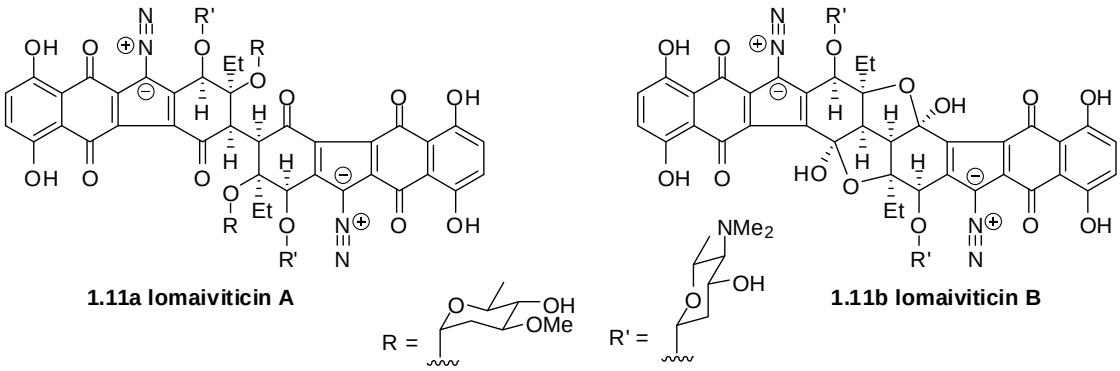

The last step in this series of computational studies is to build and optimize the complete structure of lomaiviticin A (**1.11a**) and B (**1.11b**). Obviously there are two different construction pathways to achieve the same goal: (i) by taking advantage of the optimized conformers of the lomaiviticin core model compound **6.5** (section 6.1.4), and replacement of methyl groups with appropriate sugar units such as **6.1** and **6.2** (section 6.1.1) affords some starting conformations of the natural product; (ii) by using the previously obtained conformations of simpler lomaiviticin monocore model compound **6.4** (section 6.1.3) that contains the carbohydrate components, and combination of two such molecules will also produce the desired starting geometry.

As indicated earlier, despite the higher structural/chemical similarity between **6.5** and **1.11a** (the only difference between them is their D-ring oxygenated substituents, i.e. methyls of **6.5** vs sugar units of **1.11a**), practical building of the appropriate and reasonable starting conformations of **1.11a** from optimized **6.5** (pathway i) within GaussView®, the graphic control interface for Gaussian03®, and the consequent MO calculations were found to be very problematic, mainly due to the rather limited space around the dimeric D-ring structure that restricts the orientation of the much larger sugars. These initial unsuccessful attempts, however, suggested that the real possible conformations of the natural lomaiviticin A (**1.11a**) should be fairly limited when compared to its simpler model **6.5**.

Later, the modeling work on **1.11a** was performed more smoothly by joining two molecules of **6.4** at their C2 positions (pathway ii), originally occupied by a methyl group to represent the bigger C2-fluorene substituent. Since the D-ring of **6.4** is also capable of adopting either the "normal" or "flipped" conformation, the starting geometry of **1.11a** was then constructed having either "normal-normal" D-rings, "normal-flipped" D-rings or "flipped-flipped" D-rings by using the previously optimized **6.4** with either type of D-ring. Furthermore, within each starting conformation of **1.11a**, the C4/C4' amino sugar was kept in the same orientation as in the optimized **6.4** so that the sugar's ring oxygen O6', the one that is bonded to the sugar's anomeric carbon, stays in close proximity to the C5/C5' diazo group, since modeling results of **6.4** had already suggested the significant benefits on molecular energy (stability) and the corresponding diazonium ion character by doing so. While the C3/C3' sugars within the starting conformations of **1.11a** were given more flexibility during the construction of the molecule to better accommodate the very crowded environment. The same modeling practice was also carried out with lomaiviticin B (**1.11b**), whose starting conformations having three different situations of D-rings were also built from the previously optimized structures of **6.4**.

Even though this is still an ongoing investigation that requires some further work to complete, the present results are enough to draw some significant conclusions. For lomaiviticin A (**1.11a**), four conformations having either the "normal-normal" or "flipped-flipped" D-rings (in fact two for each type of D-rings) were obtained after extensive attempts of conformational optimization. However, all efforts to achieve conformations of **1.11a** containing the "normal-flipped" D-rings failed. Such failure should not be a major concern since literature spectroscopic data (NMR) suggest the natural lomaiviticin A (**1.11a**) to exist as a C_2 symmetric dimer,[52] which would obviously require the molecule to possess two (identical) D-rings of the same type. In other words, both D-rings within a stable conformation of **1.11a** shall be either "normal" or "flipped" but not a mixed "normal-flipped"

situation. Interestingly and similar to the previous model compound **6.5** (section 6.1.4), an unusual conformation of **1.11a** having the "twist-boat-flipped" D-rings was also obtained from the optimization, which might serve as the other possible key intermediate (besides a conformation containing the "normal-flipped" D-rings) for the conformational changes of this molecule. These modeling results of **1.11a** are given in Figure 6-7 and summarized in Table 6-4 (tabulated in descending order of conformers' stability).

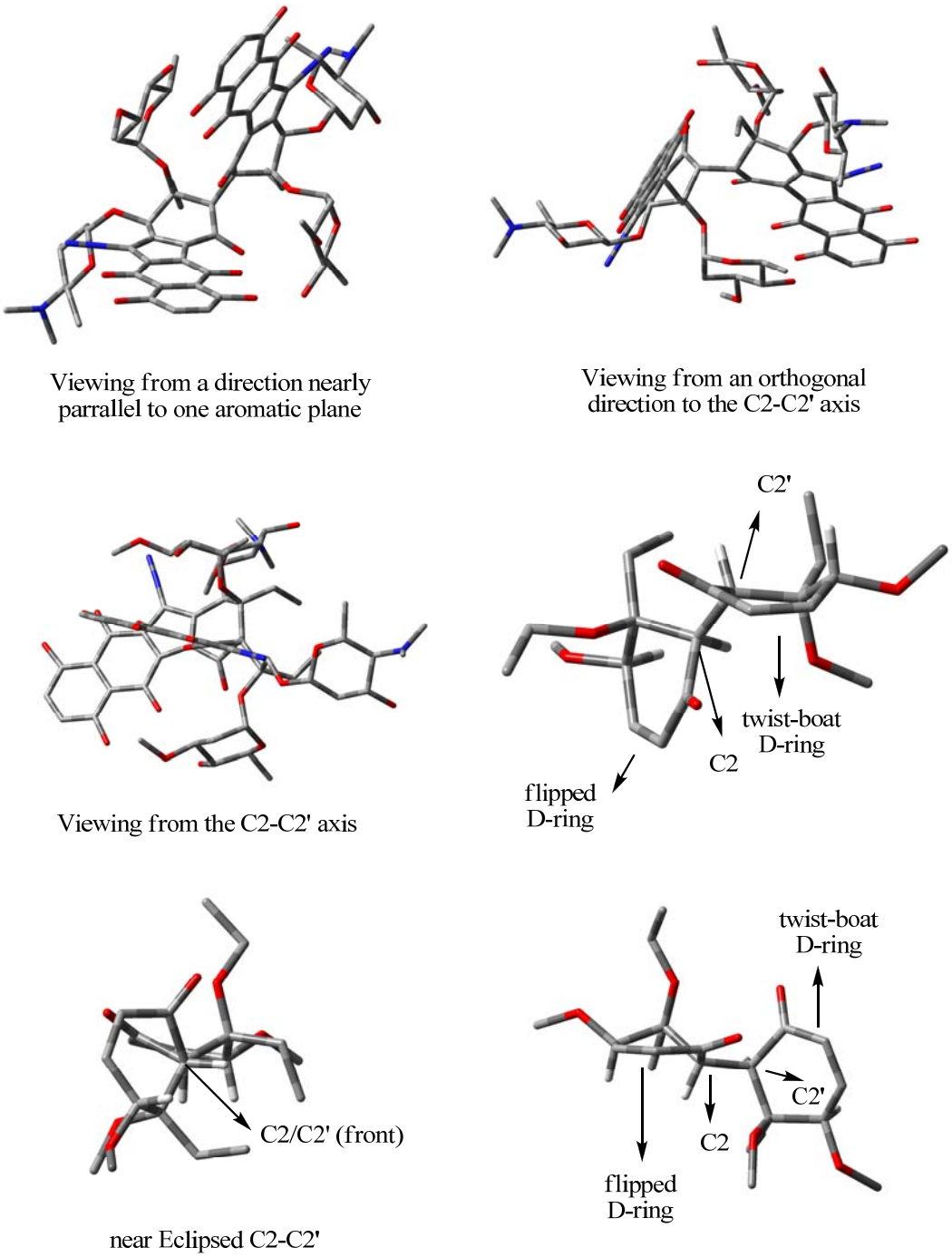

Figure 6-7a. Optimized conformer I of lomaiviticin A (**1.11a**). For further clarity, all hydrogens within the molecule are omitted. The partial dimeric D-ring structures, however, show some critical hydrogens including the C2/C2' and C4/C4'-Hs, and this "display rule" also applies to the rest.

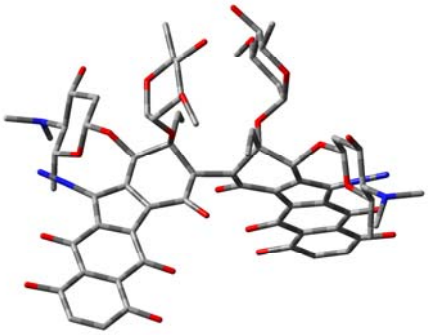

Viewing from an orthogonal direction to the C2-C2' axis

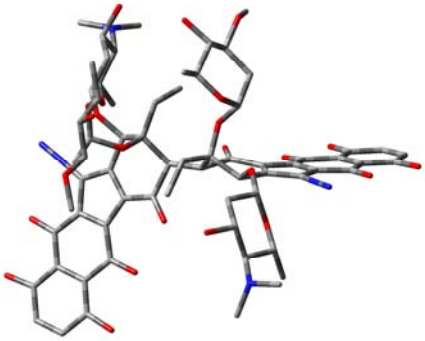

Viewing from a direction nearly parrallel to one aromatic plane

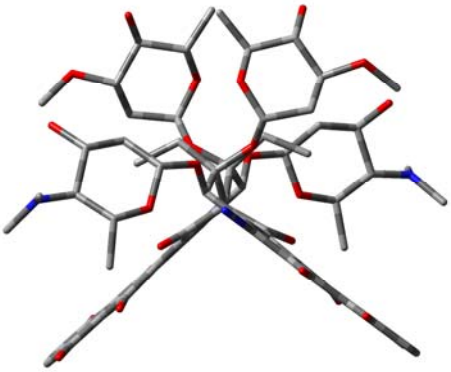

Viewing from the C2-C2' axis

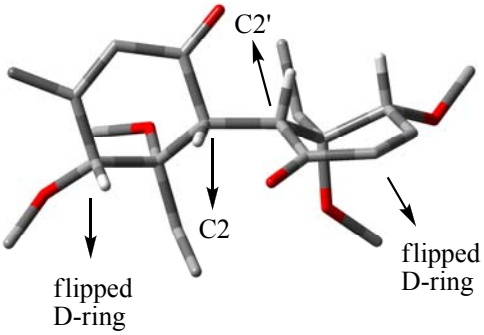

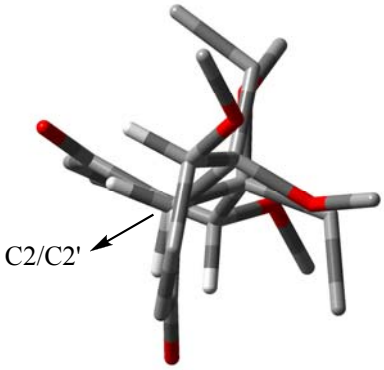

Eclipsed C2-C2'

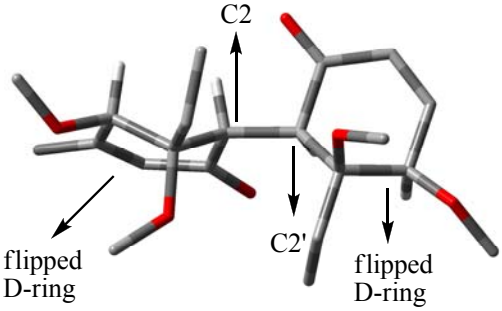

Figure 6-7b. Optimized conformer II of lomaiviticin A (**1.11a**).

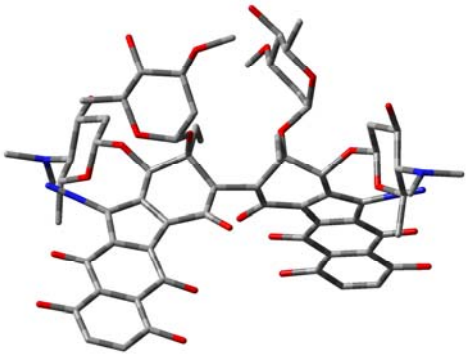

Viewing from an orthogonal direction to the C2-C2' axis

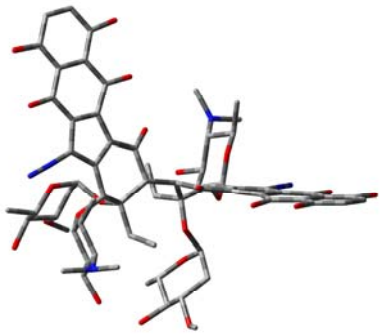

Viewing from a direction nearly parrallel to one aromatic plane

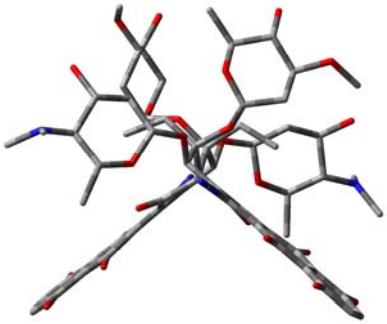

Viewing from the C2-C2' axis

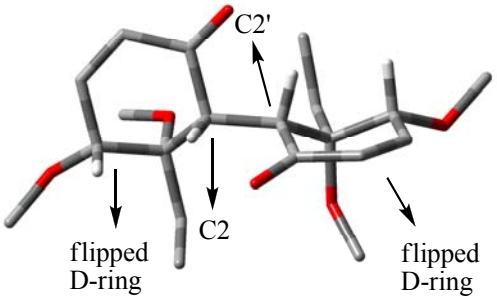

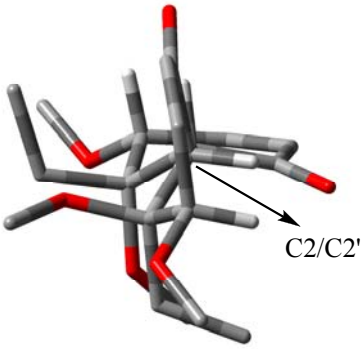

Eclipsed C2-C2'

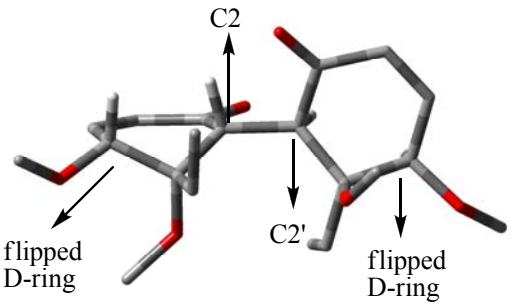

Figure 6-7c. Optimized conformer III of lomaiviticin A (**1.11a**).

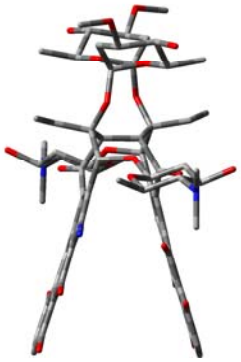

Viewing from an orthogonal direction to the C2-C2' axis

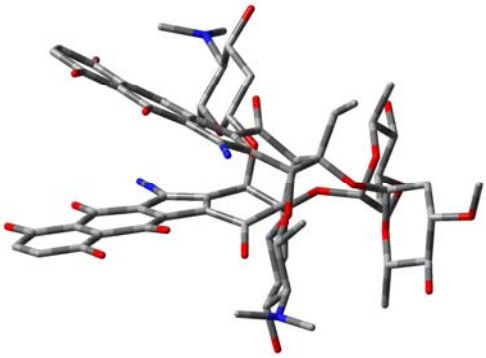

Viewing from a direction nearly parrallel to one aromatic plane

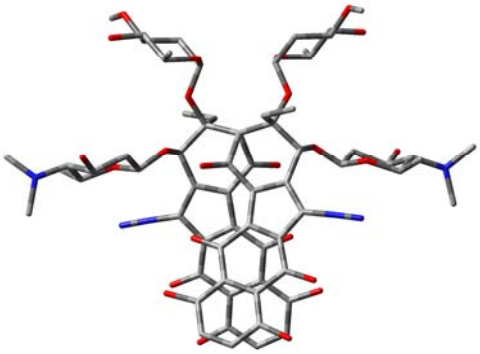

Viewing from the C2-C2' axis

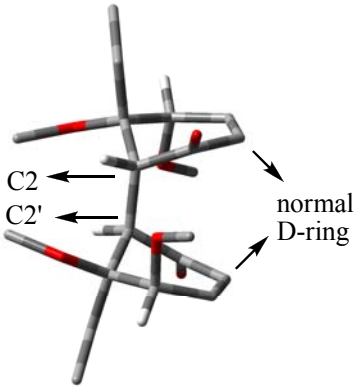

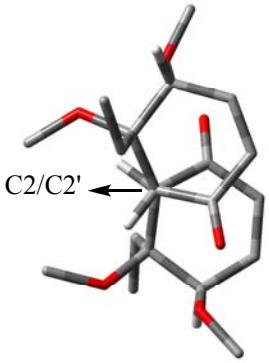

near Eclipsed C2-C2'

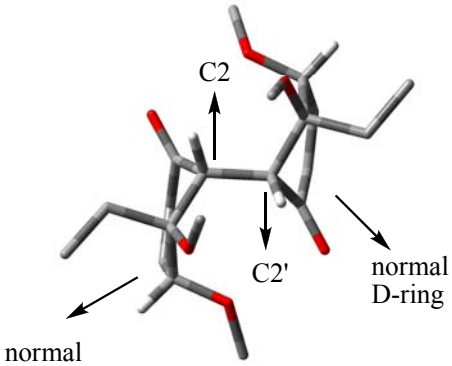

Figure 6-7d. Optimized conformer IV of lomaiviticin A (**1.11a**).

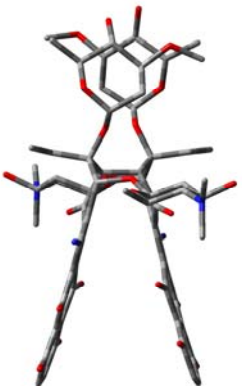

Viewing from an orthogonal direction to the C2-C2' axis

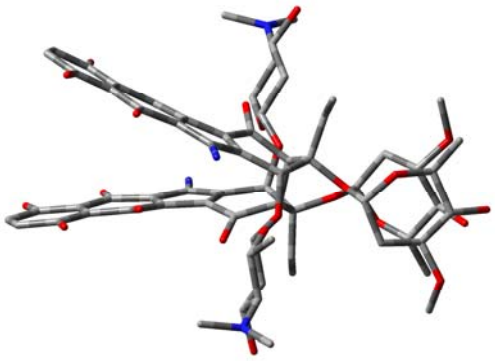

Viewing from a direction nearly parrallel to one aromatic plane

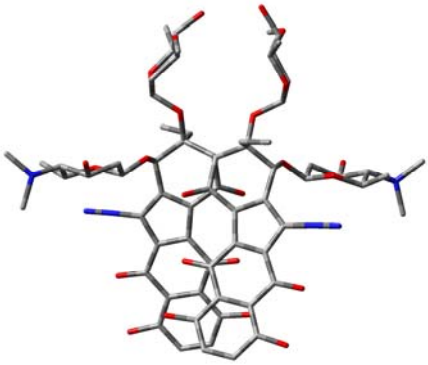

Viewing from the C2-C2' axis

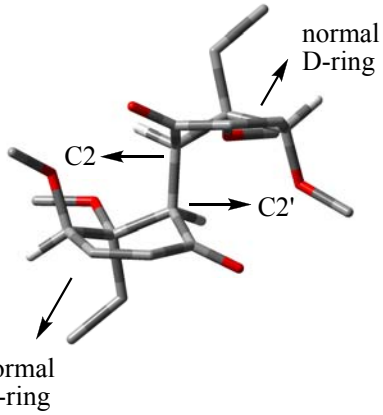

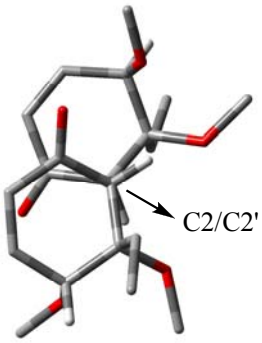

Eclipsed C2-C2'

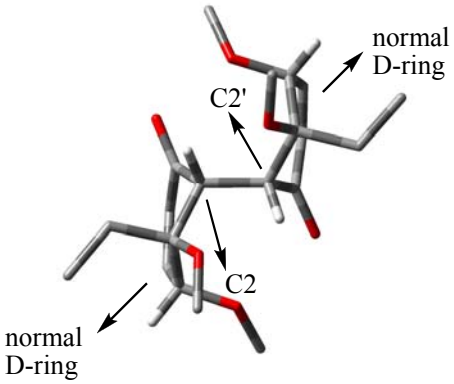

Figure 6-7e. Optimized conformer V of lomaiviticin A (**1.11a**).

Table 6-4. Summary of some calculated physical properties of the possible conformations of **1.11a**.

Conformer of **1.11a** (D-rings)[a]	E (RHF) (a.u.)[b] ΔE (kcal/mol)[c]	$\nu_{N\equiv N}$ (cm^{-1})[d] <O-C4-C4a-C5 (°)[e]	C2-C2' conformation	$d_{C2\text{-}C2'}$ (Å)
Conformer V (normal-normal)	-4742.72165161 0	N/A 86.9/86.7	Eclipsed	1.572
Conformer I (twist-boat-flipped)[f]	-4742.71652412 3.22	failed 17.2 (twist-boat) /37.3 (flipped)	near Eclipsed	1.566
Conformer II (flipped-flipped)	-4742.69837153 14.39	N/A 27.4/27.4	Eclipsed	1.578
Conformer IV (normal-normal)	-4742.69763559 15.07	2186/2186 83.7/83.7	near Eclipsed	1.575
Conformer III (flipped-flipped)	-4742.69015339 19.77	N/A 31.1/25.5	Eclipsed	1.582

a. All final geometries except conformer I (see footnote f) adopt the same type of D-ring conformations as in the corresponding starting geometry, i.e. a starting conformation with "normal-normal" D-rings would give an optimized one also having "normal-normal" D-rings, and so on; b. All E(RHF) were not corrected with ZPE since it was not available from MO calculations due to the lack/failure of frequency calculations, 1 a.u. = 627.5095 kcal/mol; c. Relative to the most stable conformer (i.e., conformer V); d. Scaled by a scaling factor of 0.8929. "N/A" means that no frequency calculation was performed while "failed" indicates that the frequency calculation was carried out but terminated due to errors; e. Similar to the cases of **6.5**, each conformer of lomaiviticin A (**1.11a**) also has two of such dihedral angles (i.e., <O-C4-C4a-C5 and <O-C4'-C4a'-C5') due to the symmetric dimer structure, which is a good indication for the D-ring conformation (dihedral angle < 40° indicates "flipped" D-ring and dihedral angle > 80° corresponds to "normal" D-ring); f. Conformer I started with "flipped-flipped" D-rings but ended with "twist-boat-flipped" D-rings.

Some very interesting observations and useful conclusions could be made based on these computational results of lomaiviticin A (**1.11a**). First of all, the chances to find other stable conformations of **1.11a** besides the above five (Figure 6-7 and Table 6-4) are judged to be extremely small. The availablity of fewer conformations of lomaiviticin A (**1.11a**) than the model compound **6.5** (nine conformations) is expected, since the four bulky sugars within **1.11a** would definitely take more

space along the D-rings, which is already very crowded even in the case of **6.5**. This dramatically limits the conformational freedom of the dimeric skeleton as well as the sugars themselves. Second, the obtained conformations of **1.11a** resemble some characteristics of those previously observed for **6.5** (section 6.1.4). For example, all conformers of **1.11a** along the C2-C2' axis possess a (near) eclipsed rather than staggered conformation for the six C2/C2' substituents (Figure 6-7 and Table 6-4), as previously observed with the three most stable conformations of **6.5** (Figure 6-6 and Appendix F). The C2-C2' bond lengths within **1.11a** (i.e., 1.566–1.582 Å), as predicted earlier, are also closely comparable to the ones found within **6.5** (i.e., ~ 1.57 Å). Third, to satisfy the C_2 symmetry requirement of lomaiviticin A (**1.11a**) as suggested by its spectroscopic data, among the five conformational candidates, the obviously unsymmetric conformer I (Figure 6-7a) and III (Figure 6-7c) can be immediately ruled out. The remaining conformers II (Figure 6-7b), IV (Figure 6-7d) and V (Figure 6-7e) are all essentially near C_2 symmetric, especially when the dimeric diazobenzo[*b*]fluorene skeletons (including the skeletons of the corresponding four carbohydrates) of these conformations are examined for symmetry. However, the much higher energy of conformer II and IV than V (i.e., ~ 14–15 kcal/mol) would suggest that the last species is the only reasonable conformation of **1.11a** to be considered.

Interestingly, the most stable and near C_2 symmetric conformation V of **1.11a** adopts the "normal-normal" D-rings. This is in contrast to the structurally very similar dimer **6.5** and other simpler model species (i.e., **6.3** and **6.4**) studied earlier, which all have the "flipped" D-ring(s) within their most stable conformations. This apparent preference for "normal-normal" D-ring of lomaiviticin A (**1.11a**) can be traced to some unique structural features and beneficial interactions within the conformation V as illustrated in Figure 6-8.

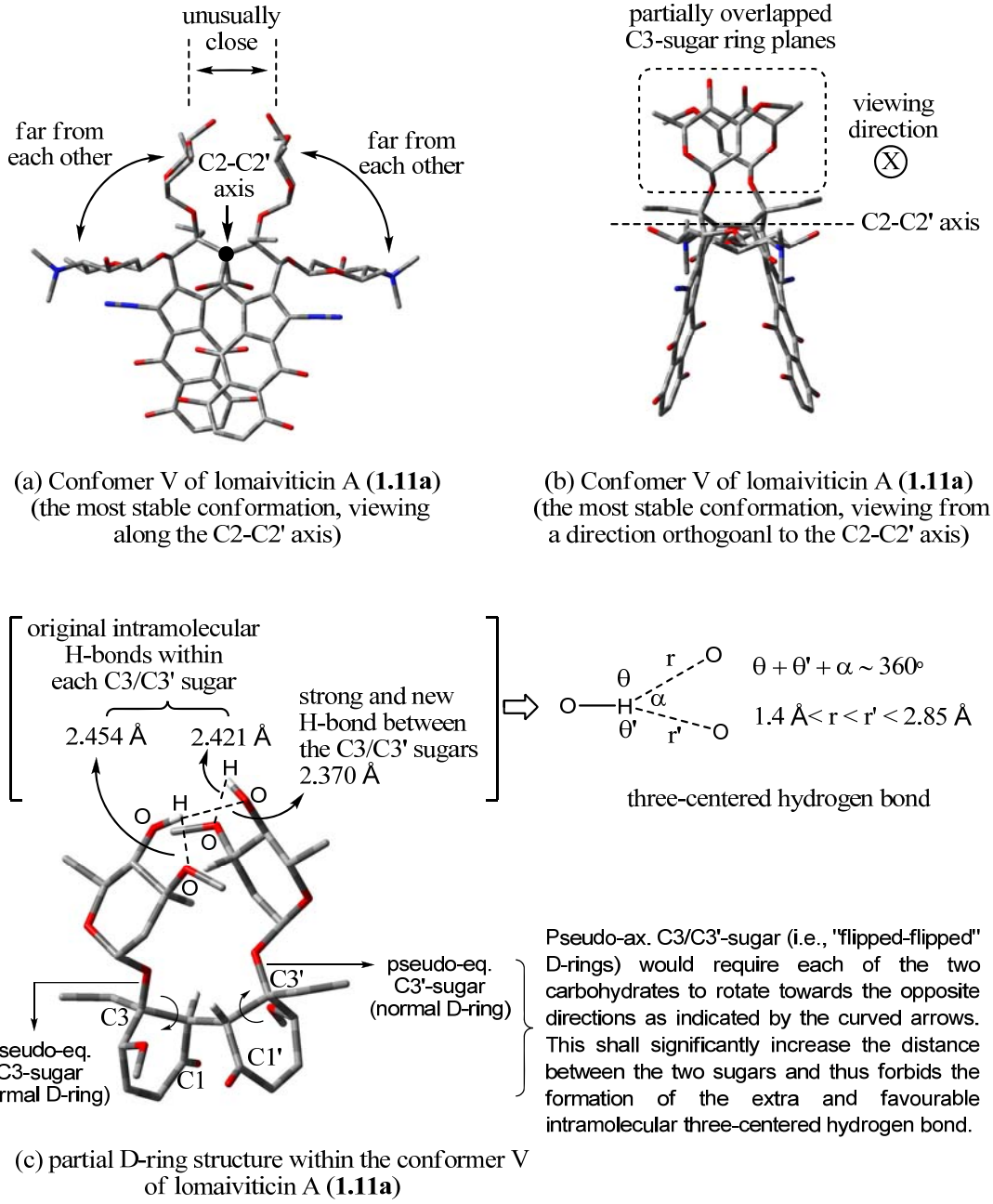

(a) Confomer V of lomaiviticin A (**1.11a**) (the most stable conformation, viewing along the C2-C2' axis)

(b) Confomer V of lomaiviticin A (**1.11a**) (the most stable conformation, viewing from a direction orthogoanl to the C2-C2' axis)

(c) partial D-ring structure within the conformer V of lomaiviticin A (**1.11a**)

Figure 6-8. Structural features within conformer V of lomaiviticin A (**1.11a**) favouring the "normal-normal" D-rings.

The energy increase of molecule of **1.11a**, upon adopting the "normal" D-ring conformation instead of the anticipated and more stable "flipped" D-ring conformation, is expected to be totally compensated and eventually exceeded by the combination of the following several energetically beneficial interactions.

First, the two C3/C3' sugars within conformer V are unusually close to each other in a face-to-face manner (diagram (a) in Figure 6-8), which are partially overlapped when viewed from the direction orthogonal to the sugar's ring plane (diagram (b) in Figure 6-8). Apparently and sterically, it is expected that the two C3/C3' sugars of **1.11a** would extend out in space and stay as far as possible from each other in order to minimize the steric interaction between them, and such predicted geometries are observed indeed with other optimized conformations of **1.11a** (e.g., II–IV, Figure 6-7b–6-7d). This "abnormal" case of conformation V, however, indicates the presence of some other favourable interactions that are at least strong enough to overcome the steric energy penalty from having two very closely situated C3/C3' sugars. Besides the already existing intramolecular H-bonding interactions within each C3/C3' sugar (i.e., intramolecular H-bond interaction between the –OH and the vicinal –OMe at an –OH···O< distance of ca. 2.42–2.45 Å, diagram (c) in Figure 6-8), closer examination of conformation V suggests the existence of a new and strong intramolecular H-bonding interaction between the two hydroxyl groups of the two C3/C3' sugars, which is clearly indicated by the significantly shorter distance of only 2.37 Å between the (C3-sugar)–O–H···O(H)–(C3'-sugar) (diagram (c) in Figure 6-8). Formation of this new and extra intramolecular H-bond would demand the two C3/C3' sugars to stay at a close enough distance, and, as illustrated in diagram (c) of Figure 6-8, only the pseudo-equatorial orientation for both C3/C3' sugars (i.e., the "normal-normal" D-rings) would be able to comply with the H-bond geometry (distance) requirement; while C3/C3' sugars having pseudo-axial orientation (i.e., the "flipped-flipped" D-rings) would cause these two carbohydrates to stay too far away from each other to gain this extra stabilization effect. In

addition, this intramolecular H-bond situation around the C3/C3' sugars within the conformer V of **1.11a** shall now be considered as a three-centered (bifurcated) hydrogen bond (diagram (c) in Figure 6-8), which are rather common both intermolecularly and intramolecularly (to a lesser extent) among crystal structures of simple sugars and amino acids.[385,386] The three-centered hydrogen bond has been estimated, based on a structural survey, to be energetically comparable to the most common two-centered hydrogen bonds (-O–H···O-).[386] Another literature work on **6.24**, a diaryl amide with two nearby interacting methoxy groups has found, both experimentally and computationally, that an intramolecular three-centered hydrogen bond in this partially rigidified structure significantly enhances its stability due to a positive cooperativity between the two two-centered components of the three-centered hydrogen bonding interaction.[387,388] Therefore, it is likely that the three-centered hydrogen bond interaction observed within the conformation V of **1.11a** is one of the significant energetic contributors to the preference for this geometry. On the other hand, the presence of multiple oxygen atoms and nearby hydrogen atoms (attached to carbon) in close proximity within these two very close C3/C3' sugars might also lead to weak but possible and multiple C-H···O hydrogen bonding interactions,[389] which could further stabilize the conformation.

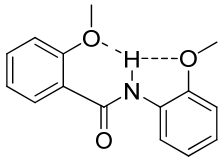

6.24 diaryl amide with strong three-centered intramolecular hydrogen bonding interactions

Second, as an added bonus for stability when compared with others, the conformation V of **1.11a** should also benefit decreased steric repulsion between the two adjacent sugars at C3 and C4 (as well C3' and C4'), as a result of to the now larger space and further distance between them caused by the closer correlation between the C3 and C3' sugars.

Assuming that the conformer V is indeed not only the most stable conformation for lomaiviticin A (**1.11a**) in the gas phase but also in solution phase, it is necessary to consider the very likely protonation of the dimethylamino group(s) of the C4/C4'-sugars under (near) physiological pH (~ 7.4), in which its biological activities were studied. The pKa values of the two dimethylamino groups within the two C4/C4'-sugars of lomaiviticin A (**1.11a**) are unknown, but they are expected to be comparable to a typical tertiary organic amine such as NMe_3 (pKa ~ 9.8). Despite the many measured pKa and proposed models for predicting pKa of various simple aminosugars, literature data on the basicity of 4-aminosugars is rather limited.[390-392] The only known example, to the best of the author's knowledge, is a UDP-4-aminosugar **6.25** that has a measured pKa of 9.5 ± 0.4 for its C4 amino group.[393] In addition, estimation of the pKa of the methylated model aminosugar **6.2** by using the (online) program "ALOGPS 2.1"[394,395] also gave a predicted pKa value of 8.70, which is fairly consistent with the above analysis and literature example.

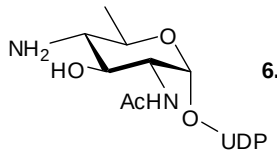

6.25 UDP-4-aminosugar

Since the two amino nitrogens of lomaiviticin A (**1.11a**) stay very far away from each other even though they co-exist within the same molecule, it is reasonable to assume that each of them would behave independently. Therefore, both dimethylamino groups of **1.11a** should be almost fully protonated under physiological pH (~ 7.4) when considering the estimated range of pKa (~ 8.70–9.80). It is of considerable practical meaning to determine whether such double protonation would significantly alter the conformation of the molecule or not. The study was carried out by manually adding a proton at each of the two amino nitrogen sites of the most stable conformation V of lomaiviticin A (**1.11a**). The double protonated structure [**1.11a** + H + H]$^{2+}$ was then subjected to the

same geometry optimization as before. The final results, as given in Figure 6-9 (diagram (a) vs (b), neutral **1.11a** vs double protonated **1.11a**), clearly indicate that such protonation does not apply any significant alteration to the overall conformation of the molecule. The most obvious change caused by the protonation, as one would expect, is that the intramolecular hydrogen bonding interactions within the C4/C4'-sugar vary from the $–Me_2N\cdots H–O–$ in the neutral molecule to the $–Me_2N^+H\cdots O(H)–$ in the double protonated species, since hydrogen bonding of the latter type is significantly stronger than the former one. Of course, it would be of even greater interest to examine the influence of such protonation on the diazonium ion character (diazo IR frequency) of the molecule, which is currently in progress in the Dmitrienko group. However, the diazonium ion character of **1.11a** is not expected to be affected dramatically upon such protonation, since the protonated sites are too far away from the corresponding diazo moiety to apply any significant electronic effects, either inductively or through space, or steric effects.

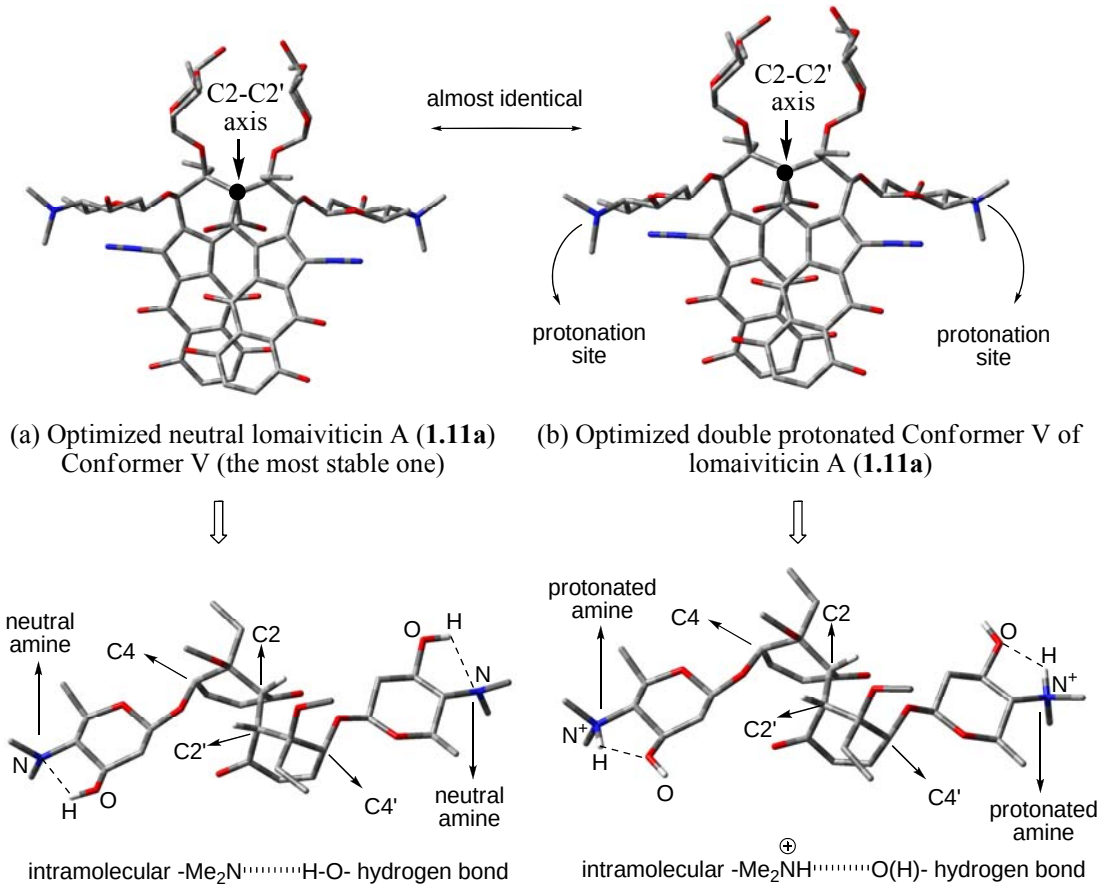

(a) Optimized neutral lomaiviticin A (**1.11a**) Conformer V (the most stable one)

(b) Optimized double protonated Conformer V of lomaiviticin A (**1.11a**)

(c) Partial structure from (a)*

(d) Partial structure from (b)*

* For clarity, only the dimeric D-rings with C4/C4'-sugars are shown and C3/C3'-sugars are omitted. All hydrogens except C2/C2'-H and those involved in the intramolecular hydrogen bonding are omitted.

Figure 6-9. Comparison of the optimized conformations of the double protonated and neutral lomaiviticin A (**1.11a**).

For lomaiviticin B (**1.11b**), after extensive optimization of various possible conformations, only one single conformation having the "flipped-flipped" D-rings (Figure 6-10) was obtained. All efforts to achieve stable conformations of **1.11b** containing either the "normal-flipped" D-rings or the "normal-normal" D-rings failed. The former situation is once again of very little importance, since just like lomaiviticin A (**1.11a**), spectroscopic evidence suggest this slightly simpler derivative **1.11b** also exists as a symmetric dimer with two identical D-rings.[52] Although the obtained conformation of **1.11b** (Figure 6-10) is not considered to possess a C_2 symmetry by the Gaussian03® program, one can easily recognize the near C_2 symmetry that lies in the main skeleton of this conformation. The "C_2 symmetry axis" would be in the middle point of and orthogonal to the C2-C2' bond within the first structure shown in Figure 6-10, which is also perpendicular to the paper plane that the C2-C2' bond lies in.

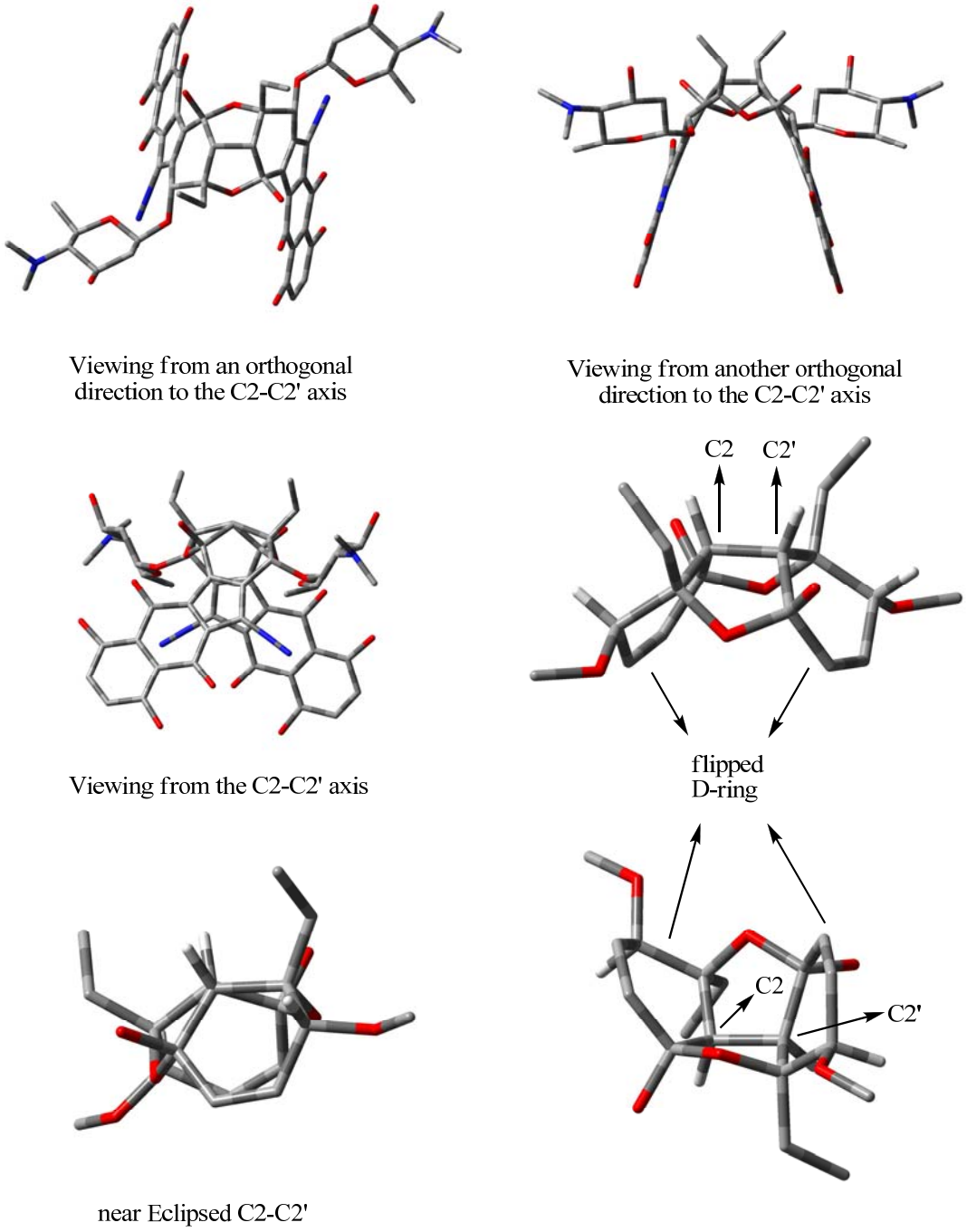

Figure 6-10. Optimized conformation of the lomaiviticin B (**1.11b**) having "flipped-flipped" D-rings.

The preference of "flipped-flipped" D-rings rather than "normal-normal" D-rings for lomaiviticin B (**1.11b**), which is different from the lomaiviticin A (**1.11a**) but consistent with other model compounds (i.e., **6.3**–**6.5**), can be explained by the following rationale. Formation of the double intramolecular hemiketals within lomaiviticin B (**1.11b**) requires not only the loss of two C3/C3'-sugars (very likely through hydrolysis) leading to C3/C3' free hydroxyl groups, but also a close distance between this tertiary alcohol at C3' (or C3) with the corresponding C1 (or C1') carbonyl carbon. Only the "flipped" D-ring would be able to offer a close enough distance since its C3-OH (or C3'-OH) exists in an axial orientation, which seems to be the best possible position to facilitate the formation of the saturated furan ring and produce the hemiketal. As labeled in Figure 6-11, the significantly longer C-O-C bond lengths within the two 5-membered furan rings than the other similar C-O-C bonds within the molecule (i.e., 1.425/1.442 Å vs 1.411/1.438 Å) clearly indicate the difficulty to form such a concave and cyclic structure. If the C3/C3'-OH is part of a "normal" D-ring instead, the corresponding equatorial orientation of this tertiary alcohol as well as the corresponding axial C1/C1'-O bond (which exists in equatorial orientation in a "flipped" D-ring) would stay much further away from each other and make it practically impossible to carry out the same construction of the hemiketal. In addition, this "flipped-flipped" D-rings of lomaiviticin B (**1.11b**) would provide the added benefit of having the equatorial C4/C4'-O(sugar) bond to align much better (than the axial C4/C4'-O bond within a "normal" D-ring) with the C5/C5'-diazo bond, leading to favourable dipole-dipole interactions that lower the energy and enhance the diazonium ion character. As a supportive evidence, the unusual and possible conformation of lomaiviticin A (**1.11a**) having the "twist-boat-flipped" D-rings is only ca. 3 kcal/mol higher in energy than its most stable conformation with the "normal-normal" D-rings, suggesting that switching from normal D-ring (of **1.11a**) to flipped D-ring (of **1.11b**) may not be difficult at least thermodynamically, especially when such conformational

conversion is accompanied and partially driven by the chemical transformation (loss of C3/C3'-sugars and formation of hemiketals) at the mean time.

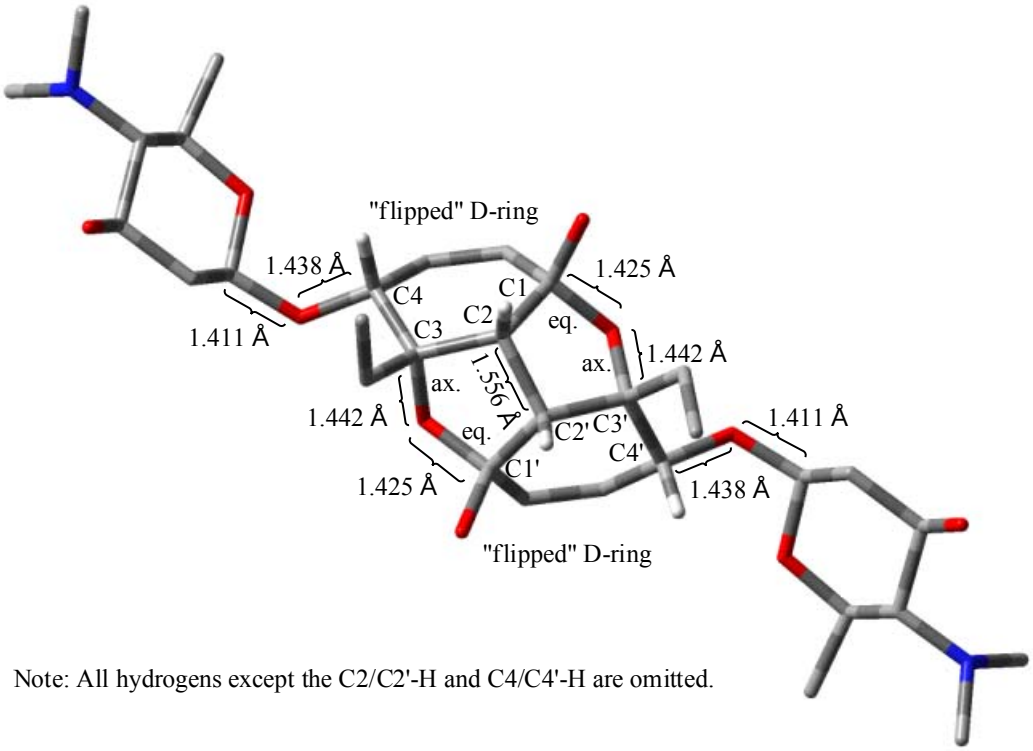

Figure 6-11. Detailed geometric information of partial structure from the optimized conformation of lomaiviticin B (**1.11b**) with "flipped-flipped" D-rings.

Even though it is slightly premature at the moment to completely exclude the possibility of lomaiviticin B (**1.11b**) to adopt the "normal-normal" D-rings, the above analysis would suggest that such a possibility is extremely low. In addition, fusion of the two saturated furan rings with the two adjacent D-rings, which are part of the rigid diazobenzo[*b*]fluorene system, completely locks the entire skeleton of the molecule (not including the C4/C4'-sugars though) and restrains the orientation

of the D-ring substituents greatly in space. Therefore, if there exist other possible/stable conformations of lomaiviticin B (**1.11b**), they are very likely dealing with mainly (if not only) small variation of the two C4-sugars' position when compared to the stable conformation shown in Figure 6-10.

Finally, the uncertainty of the absolute stereochemistry of the carbohydrate components of lomaiviticins, as discussed in section 6.1.1, is worthy of some further consideration. The lack of both C3/C3' sugars within lomaiviticin B (**1.11b**) due to the formation of intramolecular bishemiketals seems to affect the biological activities to a minimal extent, since lomaiviticin A (**1.11a**) and B (**1.11b**) possess almost identical DNA cleavage capability.[52] This observation would suggest that the C3/C3' sugars are not essential components of the molecule to account for its biological activity, thus the sugar's absolute stereochemistry would be of even less importance. On the other hand, the C4/C4' sugars are probably more involved in the biological activities of lomaiviticins, partially due to the fact that this carbohydrate stays in the close proximity of the C5/C5'-diazo group and could significantly enhance the diazonium ion character upon taking up an appropriate conformation (section 6.1.3). The mode-of-action of the lomaiviticins is presumably similar to the kinamycins, as suggested by the Dmitrienko group based on the evidence discussed in Chapter 4. Yet the absolute stereochemistry of these C4/C4'-sugars is probably of less importance as well, since both enantiomers of the C4/C4'-sugar are expected to have the same type and same degree of influence on the nearby linear and achiral diazo group. In the mean time, one should not underestimate the very possible and potential usefulness of these sugar units from some other points of view. The presence of the sugar moiety within the lomaiviticins could, in principle, improve the solubility of the compounds in the aqueous biological systems and help the molecule to diffuse through the cell membrane, which may be practically crucial to their potent activities. Therefore, it is believed that the absolute stereochemistry

of these sugars is not as important as the mere presence of such carbohydrates within lomaiviticins towards their biological activities.

With no further available information on the absolute stereochemistry of the carbohydrates within lomaiviticins, current MO calculations assuming the C3/C3' sugars as α-*L*-oleandrose and the C4/C4' sugars as β-*D*-pyrrolosamine, which are the same as what had been shown in the original work from the Wyeth group, should be a reasonable starting point. Even if later spectroscopic evidence may prove the absolute stereochemistry of the carbohydrate component of lomaiviticins to be otherwise, the computed conformations of lomaiviticins can be easily modified to reflect such possible changes, which are not expected to pose significant influence on the overall conformation and diazonium ion character of these natural antibiotics. It has been noticed that two very recent works regarding the total synthesis of the lomaiviticin carbohydrate components (or similar analogues) have been reported by the Herzon's group[396] and Shair's group,[397] yet none of these results have realized or offered any further information to clarify the absolute stereochemistry problem of such sugars.

In summary, the above successful computation of stable conformation(s) of lomaiviticins has provided the first study of its kind in this area of kinamycins and related diazobenzo[*b*]fluorenes. The results could be the important basis for future in-depth mechanistic studies regarding these natural products and their biological activities, and may be of great help in designing simpler but efficient analogues of kinamycins and lomaiviticins.

6.2 Vibrational Circular Dichroism Spectra of Kinamycins

The vibrational optical activity (VOA) is the response of a molecule to circularly polarized radiation, and VOA in the IR region is more commonly known as the vibrational circular dichroism (VCD).[398,399] A chiral molecule would behave differently toward the left and right circularly polarized (IR) radiation, which is in fact an electromagnetic wave with chirality. Thus, the VCD technique is

very effective to study chirality (absolute configuration) and distinguish between enantiomers/diastereomers in a non-destructive manner,[400] yet it receives much less attention from most organic chemists than it really deserves. As an added bonus feature and particularly related to this study, VCD is also extremely useful in determining conformation in solution, since even a rather small change in conformation of the same molecule would lead to an apparent and significant difference of the corresponding VCD spectrum.[401] When compared with other traditional methods for studying stereochemistry, chirality and conformation, VCD requires neither physical separation of stereoisomers/conformers (vs chiral chromatography), nor very complicated/expensive equipment (vs X-ray or NMR), additional reagents (e.g., chiral NMR shift reagent) or procedures (e.g., growth of single crystal for X-ray). Most VCD cases simply involve an acquisition of the spectrum, which is very similar to a routine IR experiment, along with an electronic structure calculation that is performed through computational methods with a software package such as Gaussian®. Then a comparison between the experimental and the simulated VCD spectra should be able to determine the stereochemistry of interest. Such practice offers a further and unique advantage when dealing with an inseparable mixture of two or more stereoisomers/conformers. Theoretical VCD spectrum of each individual stereoisomer/conformer can be calculated rather accurately, and mathematical treatment with the experimental spectrum based on these predicted individual VCD spectrum can provide, in principle, a good estimation of the distribution of each species presents. The less common availability of commercial VCD instruments and the lack of practical molecular modeling study among the general organic community, however, are probably the two main reasons for the rather limited applications of VCD in organic chemistry so far, although they have been growing in recent years.

With no direct access to a VCD spectrometer by the Dmitrienko group at the moment, studies were focused on the VCD calculations of the kinamycins and lomaiviticins. Previous NMR, IR and theoretical studies on kinamycin F (**1.1f**) in different solvents (section 2.3 and 4.4) have already

suggested an equilibrium between its two D-ring conformers, which is affected dramatically by the solvent polarity. The simulated VCD spectra of kinamycin F (**1.1f**) in various media (gas phase and solutions) showed that the corresponding two conformers, with the only structural difference in their D-ring conformation (i.e., "normal" D-ring vs "flipped" D-ring), would lead to distinctively different VCD spectra as illustrated in Figure 6-12a (**1.1f** with a "normal" D-ring) and Figure 6-12b (**1.1f** with a "flipped" D-ring). On the other hand, for each individual conformer, the media (gas phase vs non-polar solvent $CHCl_3$ vs polar solvent acetone) also shows some (solvent) effects on the calculated VCD spectra, which involves mainly the shift of peaks and variation of signal intensities due to the change in environmental polarity, but the major spectrum pattern persists fairly well. Since kinamycin F (**1.1f**) is readily available in the Dmitrienko laboratory through chemical transformation of other and more abundant natural kinamycins produced by bacterial fermentation, possible collaborations with other research laboratories having a VCD spectrometer in the near future would definitely lead to a quick and hopefully quantitative analysis of the conformational preference of kinamycin F (**1.1f**) in solution.

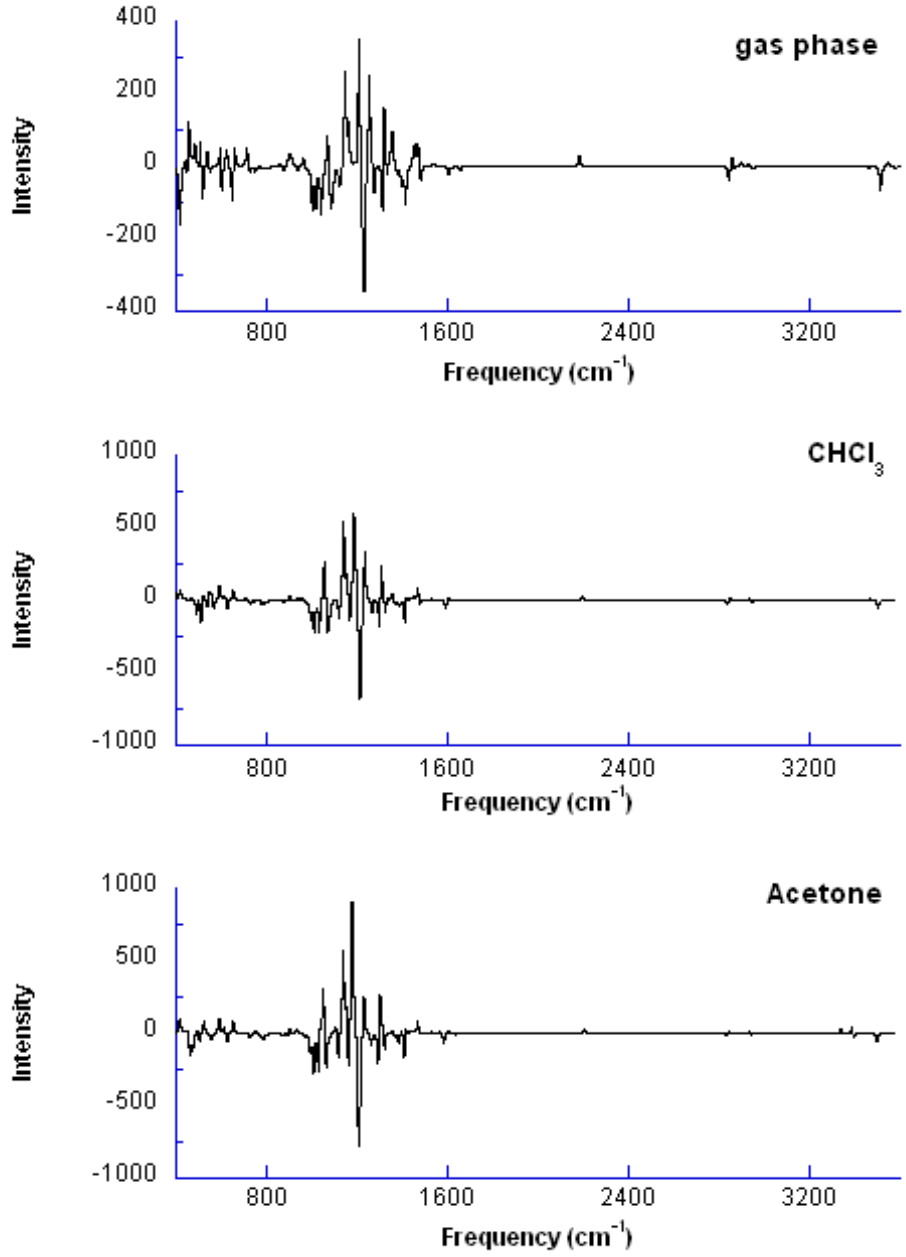

Figure 6-12a. Computed VCD spectra of kinamycin F (**1.1f**) with a "normal" D-ring at RHF/6-31G level in different medium. (Note: 1. IR frequencies were corrected with a scaling factor of 0.8929; 2. PCM model was used for solution calculations.)

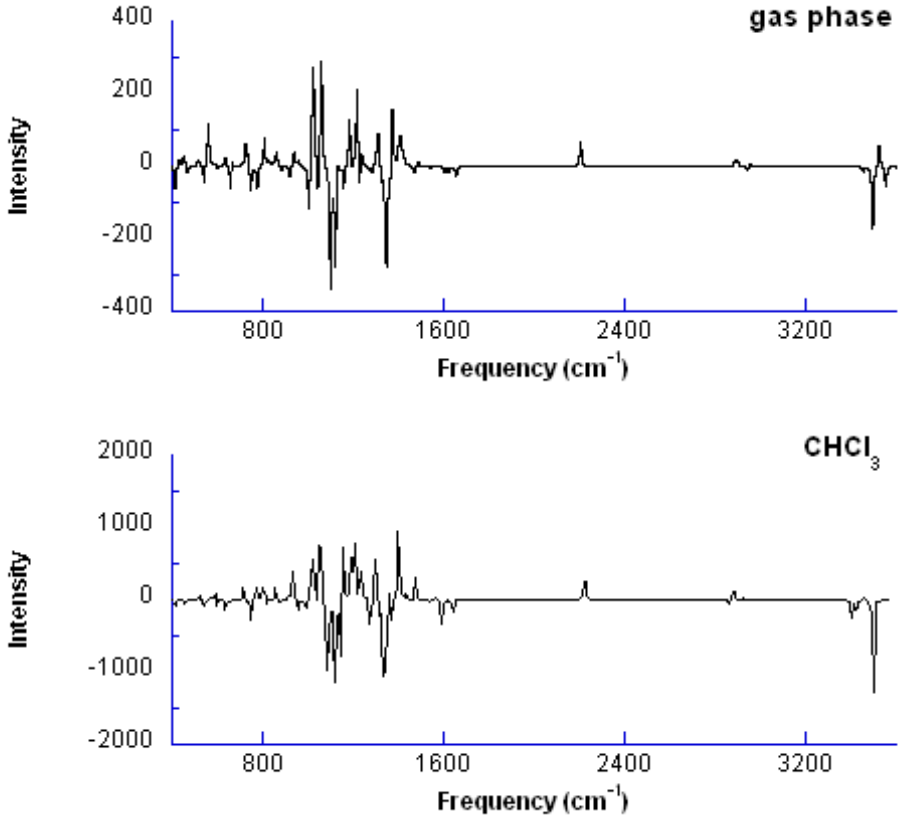

Figure 6-12b. Computed VCD spectra of kinamycin F (**1.1f**) with a flipped D-ring at RHF/6-31G level in different medium. (Note: 1. IR frequencies were corrected with a scaling factor of 0.8929; 2. PCM model was used for solution calculations; 3. Calculation in acetone failed.)

The benefit of using the VCD technique to determine the unknown absolute stereochemistry and conformation of lomaiviticins would be very significant, especially when considering the computational results of lomaiviticins discussed in the previous section of this chapter. There are only very few possible (reasonable) conformations for these complex natural products (section 6.1.5), and the corresponding VCD spectrum for every single one of them can be calculated in principle. If the experimental VCD spectra of lomaiviticins become available in the future (the Wyeth group who

discovered lomaiviticins still possesses a small amount of these natural products[382]), comparison with simulated VCD spectra could offer valuable and detailed understanding of these unique natural products. However, preliminary attempts on calculation of lomaiviticins' VCD spectra did suggest that, compared to the simpler monomeric diazobenzo[*b*]fluorene of kinamycins, the large number of atoms and complicated structures of lomaiviticins requires significantly much more computational resources to be devoted to the simulation, particularly in solutions. For example, when a Linux workstation equipped with dual Intel Xeon® dual-core processors @ 2.33 GHz (4 CPUs) and 8 GB of memory is solely dedicated to such computation, calculation of VCD spectra for kinamycin F (**1.1f**) would take hours (gas phase) or up to several days (solution phase) to finish, but structures like lomaiviticins would cost weeks if not months of computation time on the same hardware platform and calculations in solutions seem to be more problematic with these bigger molecules. Further work in this regard is currently being pursued in the Dmitrienko group as a continuation of the study presented above.

6.3 Conclusion

In summary, a systematic application of ab initio molecular orbital calculations has led to the identification of the most likely conformations for lomaiviticin A (**1.11a**) and B (**1.11b**) in the gas phase. In the case of lomaiviticin A (**1.11a**), the D-ring of the diazobenzo[*b*]fluorene system takes up a conformation that differs from the favoured conformation of the D-ring of kinamycin F (**1.1f**), and that orients the C-4 oxygen substituent in a pseudo-axial orientation. This conformation resembles that of the majority of other kinamycins.

The possibility is raised that that these models could serve as the basis for further calculations of the VCD spectra of lomaiviticins, which might be used for comparison with experimental VCD spectra in order to confirm the validity of the computationally derived structures including the

assumed absolute configuration, if sufficient quantities of the lomaiviticins are made available by the Wyeth (now Pfizer) research group. It is hoped that these computed three dimensional structures will serve to guide the design of simpler, more accessible molecules with biological activities comparable to those of the natural lomaiviticins.

Appendix A. Summary of Antibiotic Activities of Natural Kinamycins in The Literature[4,6-10,18,52]

Table A-1. Antimicrobial activities of natural kinamycins: diazobenzo[*b*]fluorene with D-ring having four oxygenated substituents.[a]

Test organism (gram-positive bacteria)* (gram-negative bacteria)**	Minimum inhibitory concentration (MIC, μg/mL)													
	Kin A **1.1a**	Kin B **1.1b**	Kin C **1.1c**	Kin D **1.1d**	Kin E **1.1e**	Kin F **1.1f**	Kin G **1.1g**	Kin H **1.1h**	Kin I **1.1i**	Kin K **1.1k**	FL-120A **1.1m**	FL-120C **1.1n**	FL-120C' **1.1o**	FL-120D' **1.1p**
Bacillus subtilis PCI-219 (ATCC 6633)*	0.024 <0.01	0.012 <0.01	0.19	0.012 <0.01	< 0.01	0.078 <0.01	0.39	0.20		< 0.01				
Bacillus anthracis (ATCC 14578)*	0.19	0.012	0.19	0.024 0.05							0.01	0.02		
Bacillus cereus (ATCC 11778)*											0.25	0.03	0.03	0.1
Bacillus circulans OSU2	0.2	5.0		0.05	0.02	0.05				0.05				
Clostridium tetani (ATCC 10779)*				0.2							0.1	0.39		
Corynebacterium diphtheriae (ATCC 27011)*				0.1							0.2	0.1		
*Enterococcus faecium**									4.0					
Listeria monocytogenes (ATCC 15313)*				0.1							0.78	0.1		
Micrococcus luteus PCI 1001 (ATCC 9341)*	1.0	0.2		5.0	1.0	1.0	0.78	0.78		1.0				
Mycobacterium (smegmatis) (ATCC 607)*	25	6.25	6.25	6.25		1.56	3.12	3.12						
*Sarcina lutea**			0.78	0.024		0.39								
*Staphylococcus albus**	0.024	0.012	0.39	0.024										

Table A-1. Antimicrobial activities of natural kinamycins: diazobenzo[*b*]fluorene with D-ring having four oxygenated substituents (continued).[a]

Test organism (gram-positive bacteria)* (gram-negative bacteria)**	Minimum inhibitory concentration (MIC, μg/mL)													
	Kin A **1.1a**	Kin B **1.1b**	Kin C **1.1c**	Kin D **1.1d**	Kin E **1.1e**	Kin F **1.1f**	Kin G **1.1g**	Kin H **1.1h**	Kin I **1.1i**	Kin K **1.1k**	FL-120A **1.1m**	FL-120C **1.1n**	FL-120C' **1.1o**	FL-120D' **1.1p**
Staphylococcus aureus (ATCC 25923)*	1.0	0.2		1.0	0.2	0.2			0.06	0.2				
Staphylococcus aureus FDA 209P (ATCC 6538P)*	0.78	0.012	0.78	0.024 0.03		0.024	0.78	0.39			0.05	0.01	0.01	0.03
Staphylococcus aureus SM-(R)*	1.56	0.006	0.39	0.024										
Staphylococcus aureus Smith*							0.78	0.39						
*Staphylococcus epidermidis**									0.06					
Streptococcus haemolyticus (Cook)*	100	12.5	12.5	50										
Streptococcus haemolyticus (NY-5)*	1.56	3.15	12.5	12.5										
Streptococcus haemolyticus (S-8)*	6.25	6.25	12.5	12.5										
Streptocossus faecalis (ATCC 29212)*	1.0	0.2		0.2	0.2					0.2				

Table A-1. Antimicrobial activities of natural kinamycins: diazobenzo[*b*]fluorene with D-ring having four oxygenated substituents (continued).[a]

Test organism (gram-positive bacteria)* (gram-negative bacteria)**	Minimum inhibitory concentration (MIC, μg/mL)													
	Kin A **1.1a**	Kin B **1.1b**	Kin C **1.1c**	Kin D **1.1d**	Kin E **1.1e**	Kin F **1.1f**	Kin G **1.1g**	Kin H **1.1h**	Kin I **1.1i**	Kin K **1.1k**	FL-120A **1.1m**	FL-120C **1.1n**	FL-120C' **1.1o**	FL-120D' **1.1p**
Streptococcus pneumoniae (ATCC 6303) *				0.1							0.39	0.78		
Streptococcus pneumoniae PARK*									0.06					
*Streptococcus pyogenes**									0.06					
*Aspergillus niger***	> 100	> 100	> 100	> 100										
Brucella abortus (ATCC 11192)**				0.78							0.39	1.56		
*Candida albicans***	> 100	> 100	> 100	> 100										
Escherichia coli NIHJ (ATCC 10536)**	> 100	3.12 5.0	100	12.5 25	25	0.78 25	> 50	> 50		5.0				
Escherichia coli (ATCC 25922)**											> 50	> 50	50	12.8
Francisella tularensis (ATCC 29684)**				0.78							0.78	0.39		
Haemophilus influenzae (ATCC 19418)**				6.25					> 128		> 50	6.25		
Klebsiella pneumoniae (*K. pneumoniae* "A"AD) (ATCC 13883)**	> 100	12.5 5.0	100	25 3.13	5.0	12.5 5.0				5.0	> 50	> 50		

Table A-1. Antimicrobial activities of natural kinamycins: diazobenzo[*b*]fluorene with D-ring having four oxygenated substituents (continued).[a]

Test organism (gram-positive bacteria)* (gram-negative bacteria)**	Minimum inhibitory concentration (MIC, μg/mL)													
	Kin A **1.1a**	Kin B **1.1b**	Kin C **1.1c**	Kin D **1.1d**	Kin E **1.1e**	Kin F **1.1f**	Kin G **1.1g**	Kin H **1.1h**	Kin I **1.1i**	Kin K **1.1k**	FL-120A **1.1m**	FL-120C **1.1n**	FL-120C' **1.1o**	FL-120D' **1.1p**
*Neisseria gonorrhoeae*** (ATCC 23050)	50	12.5	> 100	50 0.02							0.1	0.13		
Penicillium chrysogenum Q-176**	50	> 100	> 100	12.5										
Proteus vulgaris OSU1**		5.0		5.0										
Proteus vulgaris OX-19**	> 100	12.5	> 100	6.25	25					25				
Pseudomonas aeruginosa (ATCC 25619)**	>100	>100		25	25	25				25				
Pseudomonas aeruginosa (ATCC 27853)**				> 50							> 50	> 50	> 50	> 50
Pseudomonas aeruginosa A3**							> 25	> 25						
Pseudomonas aeruginosa P-1**	> 100	> 100	> 100	> 100										
Pseudomonas aeruginosa P-2**	> 100	> 100	> 100	> 100		> 100								
Pseudomonas sp. 258**									> 128					
*Saccharomyces sake***	> 100	> 100	> 100	> 100										

Table A-1. Antimicrobial activities of natural kinamycins: diazobenzo[*b*]fluorene with D-ring having four oxygenated substituents (continued).[a]

Test organism (gram-positive bacteria)* (gram-negative bacteria)**	Minimum inhibitory concentration (MIC, μg/mL)													
	Kin A **1.1a**	Kin B **1.1b**	Kin C **1.1c**	Kin D **1.1d**	Kin E **1.1e**	Kin F **1.1f**	Kin G **1.1g**	Kin H **1.1h**	Kin I **1.1i**	Kin K **1.1k**	FL-120A **1.1m**	FL-120C **1.1n**	FL-120C' **1.1o**	FL-120D' **1.1p**
*Salmonella enteritidis gaertnerii***	> 100	> 100	> 100	> 100										
*Salmonella paratyphi A***	> 100	> 100	> 100	25										
Salmonella sp. 514**									> 128					
*Salmonella typhimurium***			6.25	2.5		6.25								
Salmonella typhi (ATCC 6539)**				6.4							> 50	> 50	> 50	6.4
Salmonella typhi T-63**							> 50	> 50						
Salmonella typhosa 901 W**	> 100	6.25	> 100	12.5										
Serratia marcescens (ATCC 13880)**	> 100	> 100		5.0	100	25	> 50	> 50	> 128					
*Shigella dysenteriae***	> 100	25	> 100	25										
*Shigella sonnei***			> 100	25		1.56								
Vibrio cholerae (ATCC 14035)**				0.78							> 50	1.56		
*Vibrio comma***	> 100	0.19	25	12.5										
Vibrio comma Inaba 904**	50	0.09												

a. All MIC values and ATCC numbers are taken from the corresponding original reference where the activities were directly measured and reported. When two MIC values are available, this would indicate that two individual measurements have been performed by different laboratories.

Table A-2. Antimicrobial activities of natural kinamycins: diazobenzo[*b*]fluorenes and diazobenzo[*a*]fluorene with D-ring being aromatic, or having epoxide or ketone functionalities.[a]

Test organism (gram-positive bacteria)* (gram-negative bacteria)**	Minimum inhibitory concentration (MIC, μg/mL)					
	FL-120B **1.2a**	FL-120B' **1.2b**	Ketoanhydrokina-mycin **1.3**	Prekinamycin **1.4**	Isoprekinamycin **1.5**	Lomaiviticin A/B **1.11a/1.11b**
Bacillus anthracis (ATCC 14578)*	0.01					
Bacillus cereus (ATCC 11778)*	1.6	0.05				
Bacillus circulans OSU2*			5.0		5.0	
Clostridium tetani (ATCC 10779)*	0.2					
Corynebacterium diphtheriae (ATCC 27011)*	0.2					
*Enterococcus faecium**						6-25 ng/spot
Listeria monocytogenes (ATCC 15313)*	0.39					
Micrococcus luteus PCI 1001 (ATCC 9341)*			1.0		5.0	
Staphylococcus aureus (ATCC 25923)*			1.0		5.0	6-25 ng/spot
Staphylococcus aureus FDA 209P (ATCC 6538P)*	0.4	0.01				

Table A-2. Antimicrobial activities of natural kinamycins: diazobenzo[*b*]fluorenes and diazobenzo[*a*]fluorene with D-ring being aromatic, or having epoxide or ketone functionalities (continued).[a]

Test organism (gram-positive bacteria)* (gram-negative bacteria)**	Minimum inhibitory concentration (MIC, μg/mL)					
	FL-120B **1.2a**	FL-120B' **1.2b**	Ketoanhydrokina-mycin **1.3**	Prekinamycin **1.4**	Isoprekinamycin **1.5**	Lomaiviticin A/B **1.11a/1.11b**
Streptocossus faecalis (ATCC 29212)*			1.0		10	
Streptocossus pneumoniae (ATCC 6303)**	0.78					
Brucella abortus (ATCC 11192)**	0.2					
Escherichia coli NIHJ (ATCC 10536)**			5.0		> 25	
Escherichia coli (ATCC 25922)**	> 50	50				
Francisella tularensis (ATCC 29684)**	0.39					
Haemophilus influenzae (ATCC 19418)**	25					
Klebsiella pneumoniae (*K. pneumoniae* "A"AD) (ATCC 13883)**	> 50		5.0		> 25	
Neisseria gonorrhoeae (ATCC 23050)**	0.02					

Table A-2. Antimicrobial activities of natural kinamycins: diazobenzo[*b*]fluorenes and diazobenzo[*a*]fluorene with D-ring being aromatic, or having epoxide or ketone functionalities (continued).[a]

Test organism (gram-positive bacteria)* (gram-negative bacteria)**	Minimum inhibitory concentration (MIC, μg/mL)					
	FL-120B **1.2a**	FL-120B' **1.2b**	Ketoanhydrokina-mycin **1.3**	Prekinamycin **1.4**	Isoprekinamycin **1.5**	Lomaiviticin A/B **1.11a/1.11b**
Proteus vulgaris OSU1**			5.0		> 25	
Pseudomonas aeruginosa (ATCC 25619)**			25		> 25	
Pseudomonas aeruginosa (ATCC 27853)**	> 50	> 50				
Salmonella typhi (ATCC 6539)**	> 50	> 50				
Serratia marcescens (ATCC 13880)**			25		> 25	
Vibrio cholerae (ATCC 14035)**	> 50					

Table A-3. Antimicrobial activities of semi-synthetic kinamycins.[a]

Test organism (gram-positive bacteria)* (gram-negative bacteria)**	Minimum inhibitory concentration (MIC, μg/mL)				
	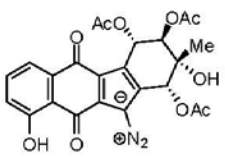 **1.1c**[b]	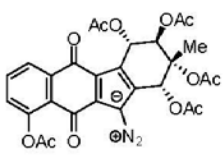 **1.1q**	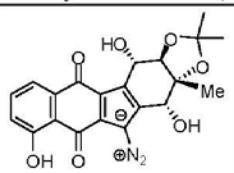 **1.1t**	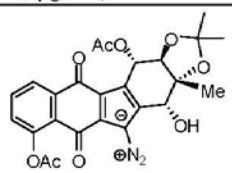 **1.1u**	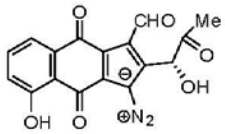 **1.1w**[c]
Bacillus subtilis PCI-219 (ATCC 6633)*	0.024	1.25	0.31	25	1.25
Mycobacterium (smegmatis) (ATCC 607)*	> 100	> 100	12.5	> 100	0.78
*Sarcina lutea**	0.78	1.56	0.012	2.5	0.012
Staphylococcus aureus FDA 209P (ATCC 6538P)*	0.024	1.56	0.024	5.0	0.024
Escherichia coli NIHJ (ATCC 10536)**	> 100	> 100	25	> 100	6.25
Klebsiella pneumoniae (K. pneumoniae "A"AD) (ATCC 13883)**	> 100	> 100	50	> 100	0.39
Pseudomonas aeruginosa P-2**	> 100	> 100	> 100	> 100	> 100
*Salmonella typhimurium***	6.25	6.25	2.5	10	100
*Shigella sonnei***	> 100	> 100	25	50	0.78

b. For comparison purpose, activities of natural kinamycin C (**1.1c**) are listed here.

c. **1.1w** is no longer a diazobenzo[*b*]fluorene type of analogue of the kinamycins but it still possesses the core functionalities and very significant biological activity.

Appendix B. X-ray Crystallographic Structure of Epoxy Diester 2.30

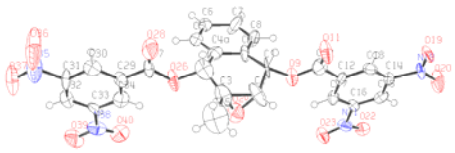

Table B-1. Crystal data and structure refinement for epoxy diester **2.30**

Empirical formula	C25H16N4O13
Formula weight	580.42
Cell measurement temperature	200(1) K
Wavelength	0.71073 Å
Crystal system, space group	Monoclinic, C_2
Unit cell dimensions	a = 29.621(4) Å alpha = 90.00 deg. b = 5.5479(7) Å beta = 95.328(4) deg. c = 15.0615(18) Å gamma = 90.00 deg.
Volume, Z	2464.4(5) $Å^3$, 4
Density	1.564 g/cm^3
Absorption coefficient	0.130 mm^{-1}
F(000)	1192
Crystal size	0.50 mm × 0.052 mm × 0.026 mm
2θ range for data collection	2.74° to 24.84°
Limiting indices	-31 < h < 31, -5 < k < 5, -16 < l < 15
Reflections collected / unique	4779 / 2961 [$R_{(int)}$ = 0.0750]
Completeness to θ = 24.84°	99.8 %
Absorption correction	None
Refinement method	Full-matrix least-squares on F^2
Data / restraints / parameters	2961 / 0 / 376
Goodness-of-fit on F^2	1.591
Final R indices [I>2σ(I)]	R1 = 0.0983, wR2 = 0.1555
R indices (all data)	R1 = 0.1217, wR2 = 0.1618
Largest diff. peak and hole	0.356 and -0.285 e-.$Å^{-3}$

Table B-2. Atomic coordinates (x 10^4) and equivalent isotropic displacement parameters (Å^2 x 10^3) for **2.30**. U_{eq} is defined as one third of the trace of the orthogonalized U_{ij} tensor.

	x	y	z	U_{eq}
C(1)	1704(3)	200(20)	6577(5)	44(3)
C(2)	1902	-721	5780	68(3)
C(3)	1564(4)	690(20)	4940(7)	62(3)
C(4)	1094(4)	30(20)	4988(7)	65(3)
C(4A)	1025(3)	1910(20)	5689(6)	45(2)
C(5)	678(3)	3580(30)	5613(6)	57(3)
C(6)	597(3)	5140(30)	6237(6)	61(3)
C(7)	908(3)	5230(30)	7035(7)	78(4)
C(8)	1255(3)	3670(20)	7112(6)	51(3)
C(8A)	1329(3)	1970(20)	6446(6)	42(3)
C(10)	2226(3)	170(20)	7913(6)	48(3)
C(12)	2619(3)	1510(20)	8395(6)	35(2)
C(13)	2782(3)	510(20)	9214(5)	40(2)
C(14)	3135(3)	1650(20)	9671(5)	36(2)
C(15)	3333(3)	3800(20)	9383(6)	41(3)
C(16)	3152(3)	4634(19)	8579(5)	30(2)
C(17)	2808(3)	3560(20)	8069(6)	39(2)
C(25)	1712(5)	-2480(30)	4245(9)	143(6)
C(27)	541(3)	260(20)	3688(6)	47(3)
C(29)	393(3)	1740(20)	2906(6)	44(3)
C(30)	-9(3)	1040(20)	2405(6)	48(3)
C(31)	-138(3)	2320(20)	1632(6)	46(3)
C(32)	78(3)	4370(20)	1377(6)	43(3)
C(33)	467(3)	5020(20)	1905(6)	43(3)
C(34)	616(3)	3720(20)	2664(6)	52(3)
N(18)	3348(3)	390(20)	10488(4)	45(2)
N(21)	3362(3)	6788(18)	8205(5)	45(2)
N(35)	-563(4)	1600(20)	1072(8)	90(4)
N(38)	710(3)	7158(19)	1673(6)	54(2)
O(9)	2079(2)	1303(15)	7148(4)	48(2)
O(11)	2090(2)	-1748(17)	8125(4)	68(2)
O(19)	3169(2)	-1391(16)	10729(4)	47(2)
O(20)	3685(3)	1300(19)	10876(4)	82(3)
O(22)	3645(2)	7854(15)	8733(4)	44(2)
O(23)	3252(2)	7398(16)	7457(4)	54(2)
O(24)	1909(2)	1185(17)	5073(4)	68(2)
O(26)	919(2)	1162	4121(4)	62(2)
O(28)	346(2)	-1470(20)	3949(4)	78(3)

Table B-2 (continued). Atomic coordinates (x 10^4) and equivalent isotropic displacement parameters ($Å^2$ x 10^3) for **2.30**. U_{eq} is defined as one third of the trace of the orthogonalized U_{ij} tensor.

	x	y	z	U_{eq}
O(36)	-765(4)	70(20)	1338(7)	191(7)
O(37)	-648(3)	2550(20)	371(5)	103(3)
O(39)	599(3)	8069(18)	941(5)	83(3)
O(40)	1018(2)	7928(17)	2185(5)	63(2)
H(1)	1591	-1211	6905	53
H(2)	2147	-1966	5846	81
H(4)	907	-1426	5097	78
H(5)	485	3608	5073	68
H(6)	341	6173	6166	73
H(7)	867	6360	7494	93
H(8)	1460	3724	7635	61
H(13)	2652	-904	9438	48
H(15)	3573	4603	9725	50
H(17)	2702	4196	7502	47
H(25X)	1540	-3987	4278	215
H(25Y)	2037	-2819	4365	215
H(25Z)	1653	-1788	3647	215
H(30)	-185	-270	2589	57
H(32)	-33	5286	870	51
H(34)	880	4240	3020	62

Table B-3. Bond lengths and bond angles for **2.30**.

	Length [Å]		Length [Å]
C1-O9	1.472(9)	C32-C33	1.385(12)
C1-C8A	1.478(12)	C33-C34	1.386(12)
C1-C2	1.478(9)	C33-N38	1.449(13)
C2-O24	1.502(9)	N35-O37	1.187(11)
C2-C3	1.539(11)	N35-O36	1.191(13)
C3-C4	1.458(15)	N38-O40	1.216(9)
C3-O24	1.461(13)	N38-O39	1.230(9)
C3-C25	1.536(17)		
C4-O26	1.497(11)		Angle [°]
C4-C4A	1.511(13)	O9-C1-C8A	108.7(7)
C4A-C5	1.382(13)	O9-C1-C2	106.4(6)
C4A-C8A	1.386(11)	C8A-C1-C2	118.1(6)
C5-C6	1.315(14)	C1-C2-O24	111.4(6)
C6-C7	1.446(12)	C1-C2-C3	112.7(5)
C7-C8	1.338(13)	O24-C2-C3	57.4(5)
C8-C8A	1.412(12)	C4-C3-O24	117.2(9)
O9-C10	1.349(10)	C4-C3-C25	123.1(11)
C10-O11	1.192(11)	O24-C3-C25	108.4(11)
C10-C12	1.510(12)	C4-C3-C2	120.9(8)
C12-C17	1.377(12)	O24-C3-C2	60.0(6)
C12-C13	1.398(11)	C25-C3-C2	110.4(10)
C13-C14	1.353(11)	C3-C4-O26	109.0(9)
C14-C15	1.417(12)	C3-C4-C4A	114.6(9)
C14-N18	1.502(10)	O26-C4-C4A	105.2(9)
C15-C16	1.358(11)	C5-C4A-C8A	118.3(9)
C16-C17	1.355(11)	C5-C4A-C4	123.6(9)
C16-N21	1.482(11)	C8A-C4A-C4	118.1(9)
N18-O19	1.193(10)	C6-C5-C4A	124.4(9)
N18-O20	1.217(10)	C5-C6-C7	118.2(10)
N21-O23	1.193(8)	C8-C7-C6	118.3(11)
N21-O22	1.249(8)	C7-C8-C8A	122.7(9)
O26-C27	1.339(10)	C4A-C8A-C8	117.9(9)
C27-O28	1.205(12)	C4A-C8A-C1	121.2(9)
C27-C29	1.467(13)	C8-C8A-C1	120.9(7)
C29-C34	1.351(12)	C10-O9-C1	118.2(7)
C29-C30	1.405(11)	O11-C10-O9	123.6(9)
C30-C31	1.388(12)	O11-C10-C12	125.1(9)
C31-C32	1.378(13)	O9-C10-C12	110.8(9)
C31-N35	1.502(12)	C17-C12-C13	121.6(8)

Table B-3 (continued). Bond lengths and bond angles for **2.30**.

	Angle [°]		Angle [°]
C17-C12-C10	123.8(8)	O26-C27 C29	110.9(10)
C13-C12-C10	114.6(8)	C34-C29 C30	119.4(9)
C14-C13-C12	116.8(8)	C34-C29-C27	123.7(9)
C13-C14-C15	124.0(8)	C30-C29-C27	116.8(9)
C13-C14-N18	116.5(9)	C31-C30-C29	117.6(9)
C15-C14-N18	119.3(8)	C32-C31-C30	123.8(9)
C16-C15-C14	114.8(8)	C32-C31-N35	116.8(9)
C17-C16-C15	124.7(8)	C30-C31-N35	119.1(9)
C17-C16-N21	117.3(8)	C31-C32-C33	116.0(9)
C15-C16-N21	117.8(8)	C34-C33-C32	121.5(9)
C16-C17-C12	118.0(8)	C34-C33-N38	119.7(10)
O19-N18-O20	124.4(8)	C32-C33-N38	118.7(9)
O19-N18-C14	117.9(8)	C29-C34-C33	121.3(10)
O20-N18-C14	117.6(9)	O37-N35-O36	124.9(12)
O23-N21-O22	125.1(8)	O37-N35-C31	118.6(11)
O23-N21-C16	120.0(8)	O36-N35-C31	116.1(11)
O22-N21-C16	114.9(7)	O40-N38-O39	123.2(9)
C3-O24-C2	62.6(6)	O40-N38-C33	119.7(9)
C27-O26-C4	118.3(8)	O39-N38-C33	117.0(10)
O28-C27 O26	122.9(9)		
O28-C27-C29	126.1(9)		

Appendix C. X-ray Crystallographic Structure of Epoxy Diester 2.31

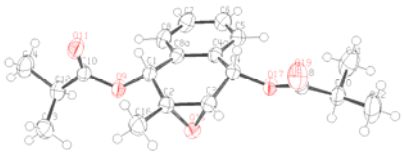

Table C-1. Crystal data and structure refinement for epoxy diester **2.31**.

Empirical formula	$C_{19}H_{24}O_5$	
Formula weight	332.38	
Cell measurement temperature	200(2) K	
Wavelength	0.71073 Å	
Crystal system, space group	Triclinic, P_1	
Unit cell dimensions	a = 9.2389(8) Å b = 10.0480(9) Å c = 10.7755(9) Å	alpha = 110.302(2) deg. beta = 97.268(2) deg. gamma = 106.443(2) deg.
Volume, Z	871.27(13) $Å^3$, 2	
Density	1.267 g/cm^3	
Absorption coefficient	0.091 mm^{-1}	
F(000)	356	
Crystal size	0.38 mm × 0.28 mm × 0.20 mm	
2θ range for data collection	2.08° to 27.88°	
Limiting indices	$-12 < h < 12$, $-13 < k < 13$, $-14 < l < 14$	
Reflections collected / unique	9304 / 4163 [$R_{(int)}$ = 0.0351]	
Completeness to θ = 27.88°	99.9 %	
Absorption correction	None	
Refinement method	Full-matrix least-squares on F^2	
Data / restraints / parameters	4163 / 0 / 223	
Goodness-of-fit on F^2	1.164	
Final R indices [I>2σ(I)]	R1 = 0.0426, wR2 = 0.0963	
R indices (all data)	R1 = 0.0490, wR2 = 0.0986	
Largest diff. peak and hole	0.337 and -0.205 e-.$Å^{-3}$	

Table C-2. Atomic coordinates (x 10^4) and equivalent isotropic displacement parameters ($Å^2$ x 10^3) for **2.31**. U_{eq} is defined as one third of the trace of the orthogonalized U_{ij} tensor.

	x	y	z	U_{eq}
C(1)	5155(1)	3009(1)	3380(1)	32(0)
C(2)	5374(1)	1942(1)	4020(1)	33(0)
C(3)	4525(1)	1789(1)	5049(1)	33(0)
C(4)	3460(1)	2658(1)	5440(1)	30(0)
C(4A)	2813(1)	3091(1)	4341(1)	30(0)
C(5)	1431(1)	3396(1)	4336(1)	36(0)
C(6)	863(2)	3878(2)	3388(2)	42(0)
C(7)	1668(2)	4056(2)	2426(2)	47(0)
C(8)	3031(2)	3749(2)	2415(1)	41(0)
C(8A)	3622(1)	3263(1)	3366(1)	32(0)
C(10)	6426(1)	3302(1)	1633(1)	32(0)
C(12)	6364(2)	2553(2)	142(1)	39(0)
C(13)	7091(2)	1331(2)	-58(2)	48(0)
C(14)	7173(2)	3720(2)	-377(2)	57(0)
C(16)	6899(2)	1684(2)	4056(2)	47(0)
C(18)	2296(2)	1895(2)	7061(1)	35(0)
C(20)	753(2)	1086(2)	7249(1)	42(0)
C(21)	-284(2)	2009(2)	7267(2)	68(1)
C(22)	928(2)	765(3)	8515(2)	77(1)
O(9)	5294(1)	2420(1)	1984(1)	37(0)
O(11)	7356(1)	4498(1)	2432(1)	48(0)
O(15)	4029(1)	608(1)	3688(1)	37(0)
O(17)	2145(1)	1757(1)	5751(1)	34(0)
O(19)	3496(1)	2591(1)	7917(1)	54(0)
H(1)	6013	4011	3896	38
H(3)	5049	1564	5783	39
H(4)	4047	3604	6276	36
H(5)	873	3271	4994	43
H(6)	-78	4086	3397	51
H(7)	1283	4389	1772	56
H(8)	3576	3872	1748	50
H(12)	5246	2056	-383	47
H(13X)	8189	1799	450	72
H(13Y)	7018	812	-1032	72
H(13Z)	6533	596	279	72
H(14X)	6705	4508	-196	85
H(14Y)	7053	3224	-1363	85
H(14Z)	8284	4181	93	85

Table C-2 (continued). Atomic coordinates (x 10^4) and equivalent isotropic displacement parameters ($Å^2$ x 10^3) for **2.31**. U_{eq} is defined as one third of the trace of the orthogonalized U_{ij} tensor.

	x	y	z	U_{eq}
H(16X)	6967	1054	4565	71
H(16Y)	7759	2661	4505	71
H(16Z)	6966	1168	3120	71
H(20)	252	94	6442	50
H(21X)	166	2975	8068	102
H(21Y)	-1321	1449	7309	102
H(21Z)	-371	2201	6434	102
H(22X)	1616	175	8478	115
H(22Y)	-96	188	8566	115
H(22Z)	1380	1724	9325	115

Table C-3. Bond lengths and bond angles for **2.31**.

	Length [Å]		Angle [°]
C1-O9	1.4500(14)	O15-C2-C1	115.73(10)
C1-C2	1.5051(17)	C3-C2-C1	117.89(10)
C1-C8A	1.5078(17)	C16-C2-C1	115.83(11)
C2-O15	1.4426(14)	O15-C3-C2	59.53(7)
C2-C3	1.4622(17)	O15-C3-C4	116.38(10)
C2-C16	1.5011(18)	C2-C3-C4	120.82(10)
C3-O15	1.4432(15)	O17-C4-C3	109.67(9)
C3-C4	1.4976(16)	O17-C4-C4A	107.25(9)
C4-O17	1.4492(13)	C3-C4-C4A	113.96(10)
C4-C4A	1.5075(16)	C8A-C4A-C5	119.39(11)
C4A-C8A	1.3941(16)	C8A-C4A-C4	120.67(10)
C4A-C5	1.3954(17)	C5-C4A-C4	119.86(10)
C5-C6	1.3796(18)	C6-C5-C4A	120.92(12)
C6-C7	1.382(2)	C5-C6-C7	119.71(12)
C7-C8	1.379(2)	C8-C7-C6	119.94(12)
C8-C8A	1.3944(18)	C7-C8-C8A	121.11(12)
O9-C10	1.3533(14)	C4A-C8A-C8	118.93(11)
C10-O11	1.1971(15)	C4A-C8A-C1	120.75(11)
C10-C12	1.5052(18)	C8-C8A-C1	120.24(11)
C12-C14	1.5204(19)	C10-O9-C1	117.70(9)
C12-C13	1.525(2)	O11-C10-O9	123.21(11)
O17-C18	1.3547(14)	O11-C10-C12	125.96(11)
C18-O19	1.1928(16)	O9-C10-C12	110.81(10)
C18-C20	1.5051(18)	C10-C12-C14	110.66(12)
C20-C22	1.507(2)	C10-C12-C13	109.05(11)
C20-C21	1.507(2)	C14-C12-C13	111.84(12)
		C2-O15-C3	60.89(7)
	Angle [°]	C18-O17-C4	117.32(9)
O9-C1-C2	108.58(10)	O19-C18-O17	123.01(12)
O9-C1-C8A	108.51(10)	O19-C18-C20	126.85(12)
C2-C1-C8A	114.99(10)	O17-C18-C20	110.13(11)
O15-C2-C3	59.58(7)	C18-C20-C22	112.37(13)
O15-C2-C16	115.11(11)	C18-C20-C21	109.01(12)
C3-C2-C16	120.43(11)	C22-C20-C21	111.45(13)

Appendix D. X-ray Crystallographic Structure of Isoprekinamycin (1.5)

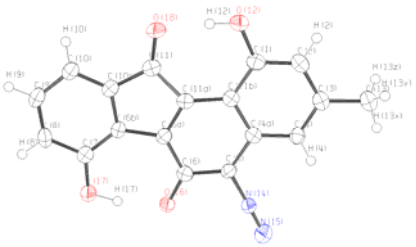

Table D-1. Crystal data and structure refinement for isoprekinamycin **1.5**

Empirical formula	C18H10N2O4
Formula weight	318.28
Cell measurement temperature	180(2) K
Wavelength	0.71073 Å
Crystal system, space group	Monoclinic, P2_1/c
Unit cell dimensions	a = 4.8053(5) Å alpha = 90.00 deg. b = 14.6913(16) Å beta = 91.020(3) deg. c = 18.927(2) Å gamma = 90.00 deg.
Volume	1336.0(2) $Å^3$
Z, Calculated density	4, 1.582 g/cm^3
Absorption coefficient	0.115 mm^{-1}
F(000)	656
Crystal size	0.66 mm × 0.056 mm × 0.034 mm
2θ range for data collection	1.75° to 25.02°
Limiting indices	-5 < h < 5, -17 < k < 17, -22 < l < 21
Reflections collected / unique	7057 / 2344 [$R_{(int)}$ = 0.0664]
Completeness to θ = 25.02°	99.2 %
Absorption correction	None
Refinement method	Full-matrix least-squares on F^2
Data / restraints / parameters	2344 / 0 / 226
Goodness-of-fit on F^2	1.186
Final R indices [I>2σ(I)]	R1 = 0.0598, wR2 = 0.0993
R indices (all data)	R1 = 0.0847, wR2 = 0.1051
Largest diff. peak and hole	0.304 and -0.194 e-.$Å^{-3}$

Table D-2. Atomic coordinates (x 10^4) and equivalent isotropic displacement parameters ($Å^2$ x 10^3) for **1.5**. U_{eq} is defined as one third of the trace of the orthogonalized U_{ij} tensor.

	x	y	z	U_{eq}
C(1)	7070(6)	7872(2)	2655(2)	30(1)
C(2)	9012(6)	7503(2)	2212(2)	32(1)
C(3)	9753(5)	6579(2)	2247(1)	28(1)
C(4)	8528(5)	6038(2)	2745(1)	28(1)
C(4A)	6527(5)	6390(2)	3197(1)	25(1)
C(5)	5147(6)	5832(2)	3711(2)	27(1)
C(6)	2987(6)	6092(2)	4176(2)	28(1)
C(6A)	2321(5)	7048(2)	4121(1)	26(1)
C(6B)	238(5)	7538(2)	4545(1)	25(1)
C(7)	-1521(5)	7274(2)	5082(1)	28(1)
C(8)	-3223(6)	7949(2)	5378(2)	32(1)
C(9)	-3213(6)	8833(2)	5146(2)	34(1)
C(10)	-1471(6)	9098(2)	4597(2)	31(1)
C(10A)	219(5)	8444(2)	4319(1)	27(1)
C(11)	2286(5)	8548(2)	3750(1)	28(1)
C(11A)	3580(5)	7621(2)	3645(1)	25(1)
C(11B)	5715(5)	7329(2)	3162(1)	25(1)
O(12)	6582(5)	8778(1)	2570(1)	39(1)
C(13)	11847(6)	6194(2)	1746(2)	35(1)
N(14)	5897(4)	4941(2)	3765(1)	28(1)
N(15)	6449(5)	4215(2)	3827(1)	44(1)
O(16)	1798(4)	5550(1)	4577(1)	37(1)
O(17)	-1746(4)	6431(1)	5347(1)	38(1)
O(18)	2816(4)	9261(1)	3447(1)	37(1)
H(2)	9874	7883	1873	38
H(4)	9050	5416	2784	33
H(8)	-4421	7786	5752	39
H(9)	-4394	9268	5359	41
H(10)	-1464	9705	4425	37
H(13X)	11992	5535	1816	53
H(13Y)	13665	6477	1838	53
H(13Z)	11247	6321	1258	53
H(12)	5260(60)	8983(19	2872(16)	44(10)
H(17)	-520(80)	6010(30)	5090(20)	93(14)

Table D-3. Bond lengths and bond angles for **1.5**.

	Length [Å]		Angle [°]
C(1)-O(12)	1.361(3)	C(2)-C(3)-C(13)	120.3(2)
C(1)-C(2)	1.377(4)	C(3)-C(4)-C(4A)	120.9(3)
C(1)-C(11B)	1.416(4)	C(4)-C(4A)-C(11B)	121.2(2)
C(2)-C(3)	1.404(4)	C(4)-C(4A)-C(5)	122.1(2)
C(3)-C(4)	1.374(4)	C(11B)-C(4A)-C(5)	116.7(2)
C(3)-C(13)	1.505(4)	N(14)-C(5)-C(6)	114.0(2)
C(4)-C(4A)	1.397(4)	N(14)-C(5)-C(4A)	118.2(2)
C(4A)-C(11B)	1.435(3)	C(6)-C(5)-C(4A)	127.8(2)
C(4A)-C(5)	1.444(4)	O(16)-C(6)-C(5)	123.6(2)
C(5)-N(14)	1.362(3)	O(16)-C(6)-C(6A)	124.2(2)
C(5)-C(6)	1.424(4)	C(5)-C(6)-C(6A)	112.3(2)
C(6)-O(16)	1.246(3)	C(11A)-C(6A)-C(6)	122.8(2)
C(6)-C(6A)	1.445(3)	C(11A)-C(6A)-C(6B)	111.4(2)
C(6A)-C(11A)	1.379(4)	C(6)-C(6A)-C(6B)	125.8(2)
C(6A)-C(6B)	1.481(4)	C(7)-C(6B)-C(10A)	119.3(2)
C(6B)-C(7)	1.390(4)	C(7)-C(6B)-C(6A)	133.4(2)
C(6B)-C(10A)	1.398(4)	C(10A)-C(6B)-C(6A)	107.4(2)
C(7)-O(17)	1.340(3)	O(17)-C(7)-C(6B)	125.9(2)
C(7)-C(8)	1.408(4)	O(17)-C(7)-C(8)	116.7(2)
C(8)-C(9)	1.371(4)	C(6B)-C(7)-C(8)	117.4(2)
C(9)-C(10)	1.401(4)	C(9)-C(8)-C(7)	122.3(3)
C(10)-C(10A)	1.369(4)	C(8)-C(9)-C(10)	120.4(3)
C(10A)-C(11)	1.486(4)	C(10A)-C(10)-C(9)	117.2(3)
C(11)-O(18)	1.222(3)	C(10)-C(10A)-C(6B)	123.4(3)
C(11)-C(11A)	1.512(3)	C(10)-C(10A)-C(11)	128.0(2)
C(11A)-C(11B)	1.451(3)	C(6B)-C(10A)-C(11)	108.6(2)
N(14)-N(15)	1.104(3)	O(18)-C(11)-C(10A)	125.1(2)
		O(18)-C(11)-C(11A)	128.4(3)
		C(10A)-C(11)-C(11A)	106.5(2)
	Angle [°]	C(6A)-C(11A)-C(11B)	123.7(2)
O(12)-C(1)-C(2)	115.5(2)	C(6A)-C(11A)-C(11)	106.1(2)
O(12)-C(1)-C(11B)	123.4(2)	C(11B)-C(11A)-C(11)	130.2(2)
C(2)-C(1)-C(11B)	121.1(2)	C(1)-C(11B)-C(4A)	116.4(2)
C(1)-C(2)-C(3)	121.7(2)	C(1)-C(11B)-C(11A)	126.9(2)
C(4)-C(3)-C(2)	118.7(2)	C(4A)-C(11B)-C(11A)	116.7(2)
C(4)-C(3)-C(13)	121.0(2)	N(15)-N(14)-C(5)	177.6(3)

Appendix E. X-ray Crystallographic Structure of Isoprekinamycin Analogue 3.236

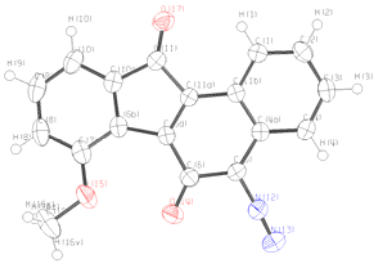

Table E-1. Crystal data and structure refinement for isoprekinamycin analog **3.236**.

Empirical formula	C18H10N2O3
Formula weight	302.28
Cell measurement temperature	180(2) K
Wavelength	0.71073 Å
Crystal system, space group	Orthorhombic, $Pna2_1$
Unit cell dimensions	a = 19.6350(16) Å alpha = 90.00 deg. b = 4.6545(4) Å beta = 90.00 deg. c = 14.8606(12) Å gamma = 90.00 deg.
Volume, Z	1358.13(19) $Å^3$, 4
Density	1.478 g/cm^3
Absorption coefficient	0.103 mm^{-1}
F(000)	624
Crystal size	0.24 mm × 0.11 mm × 0.11 mm
2θ range for data collection	2.07° to 28.02°
Limiting indices	-24 < h < 25, -6 < k < 6, -19 < l < 19
Reflections collected / unique	9029 / 1707 [$R_{(int)}$ = 0.0464]
Completeness to θ = 28.02°	100.0 %
Absorption correction	None
Refinement method	Full-matrix least-squares on F^2
Data / restraints / parameters	1707 / 1 / 210
Goodness-of-fit on F^2	1.044
Final R indices [I>2σ(I)]	R1 = 0.0344, wR2 = 0.0656
R indices (all data)	R1 = 0.0414, wR2 = 0.0673
Largest diff. peak and hole	0.158 and -0.162 e-.$Å^{-3}$

Table E-2. Atomic coordinates (x 10^4) and equivalent isotropic displacement parameters ($Å^2$ x 10^3) for **3.236**. U_{eq} is defined as one third of the trace of the orthogonalized U_{ij} tensor.

	x	y	z	U_{eq}
C(1)	-246(1)	805(4)	2184(2)	32(1)
C(2)	-620(1)	-1272(4)	1748(2)	38(1)
C(3)	-470(1)	-2009(4)	866(2)	39(1)
C(4)	51(1)	-672(4)	410(2)	36(1)
C(4A)	438(1)	1458(4)	840(2)	30(1)
C(5)	984(1)	2979(4)	413(1)	33(1)
C(6)	1386(1)	5326(4)	785(1)	33(1)
C(6A)	1236(1)	5799(4)	1740(2)	29(1)
C(6B)	1573(1)	7761(4)	2400(2)	33(1)
C(7)	2131(1)	9627(5)	2362(2)	41(1)
C(8)	2317(1)	11128(5)	3144(2)	49(1)
C(9)	1964(1)	10809(5)	3934(2)	52(1)
C(10)	1406(1)	8988(5)	3984(2)	44(1)
C(10A)	1225(1)	7525(4)	3214(2)	34(1)
C(11)	658(1)	5458(4)	3104(1)	32(1)
C(11A)	712(1)	4365(4)	2154(1)	28(1)
C(11B)	289(1)	2214(4)	1741(1)	28(1)
N(12)	1154(1)	2327(4)	-432(1)	41(1)
N(13)	1330(1)	1849(5)	-1130(2)	60(1)
O(14)	1790(1)	6697(3)	323(1)	48(1)
O(15)	2470(1)	9880(4)	1567(1)	60(1)
C(16)	2976(1)	12049(6)	1477(2)	65(1)
O(17)	232(1)	4848(3)	3667(1)	43(1)
H(1)	-350	1287	2790	39
H(2)	-984	-2204	2053	45
H(3)	-730	-3454	573	46
H(4)	148	-1189	-194	43
H(8)	2696	12396	3125	59
H(9)	2104	11844	4454	62
H(10)	1157	8760	4528	53
H(16X)	2781	13917	1639	97
H(16Y)	3136	12108	852	97
H(16Z)	3360	11615	1876	97

Table E-3. Bond lengths and bond angles for **3.236**.

	Length [Å]		Angle [°]
C1-C2	1.377(3)	C2-C1-C11B	120.5(2)
C1-C11B	1.403(3)	C1-C2-C3	120.3(2)
C2-C3	1.387(3)	C4-C3-C2	120.8(2)
C3-C4	1.375(3)	C3-C4-C4A	119.9(2)
C4-C4A	1.403(3)	C4-C4A-C11B	119.68(19)
C4A-C11B	1.414(3)	C4-C4A-C5	123.5(2)
C4A-C5	1.434(3)	C11B-C4A-C5	116.77(18)
C5-N12	1.334(3)	N12-C5-C4A	119.46(19)
C5-C6	1.457(3)	N12-C5-C6	113.06(19)
C6-O14	1.227(2)	C4A-C5-C6	127.44(18)
C6-C6A	1.466(3)	O14-C6-C5	121.83(19)
C6A-C11A	1.374(3)	O14-C6-C6A	126.4(2)
C6A-C6B	1.495(3)	C5-C6-C6A	111.77(18)
C6B-C10A	1.392(3)	C11A-C6A-C6	120.79(19)
C6B-C7	1.400(3)	C11A-C6A-C6B	109.49(18)
C7-O15	1.360(3)	C6-C6A-C6B	129.72(19)
C7-C8	1.403(4)	C10A-C6B-C7	117.9(2)
C8-C9	1.372(4)	C10A-C6B-C6A	107.80(18)
C9-C10	1.389(4)	C7-C6B-C6A	134.3(2)
C10-C10A	1.378(3)	O15-C7-C6B	118.1(2)
C10A-C11	1.481(3)	O15-C7-C8	123.3(2)
C11-O17	1.216(2)	C6B-C7-C8	118.6(2)
C11-C11A	1.504(3)	C9-C8-C7	121.6(2)
C11A-C11B	1.438(3)	C8-C9-C10	120.7(2)
N12-N13	1.116(3)	C10A-C10-C9	117.4(2)
O15-C16	1.423(3)	C10-C10A-C6B	123.8(2)
		C10-C10A-C11	127.3(2)
		C6B-C10A-C11	108.93(19)
		O17-C11-C10A	126.4(2)
		O17-C11-C11A	128.0(2)
		C10A-C11-C11A	105.68(19)
		C6A-C11A-C11B	125.40(19)
		C6A-C11A-C11	108.00(18)
		C11B-C11A-C11	126.60(19)
		C1-C11B-C4A	118.88(19)
		C1-C11B-C11A	123.80(19)
		C4A-C11B-C11A	117.31(18)
		N13-N12-C5	176.3(2)
		C7-O15-C16	119.0(2)

Appendix F. Optimized and Possible Conformations of Lomaiviticin Model Compound 6.5

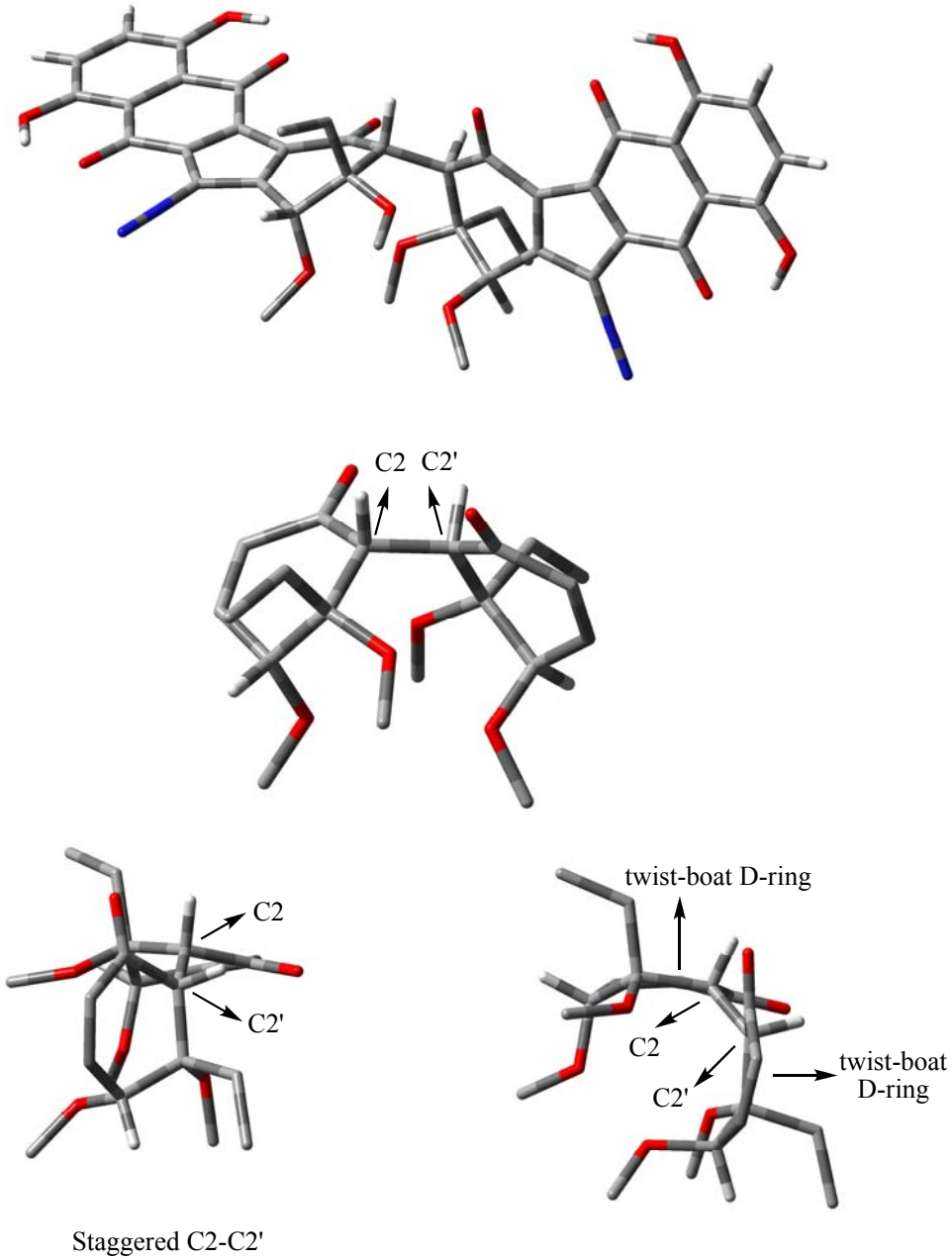

Figure F-1. Optimized conformer I of lomaiviticin model compound **6.5**.

Viewing from the C2-C2' axis

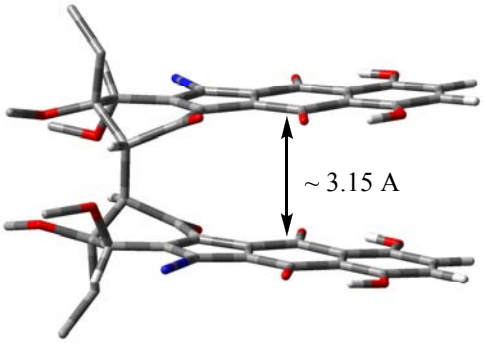

Viewing from an orthogonal direction
to the C2-C2' axis (parrellel aromatic planes)

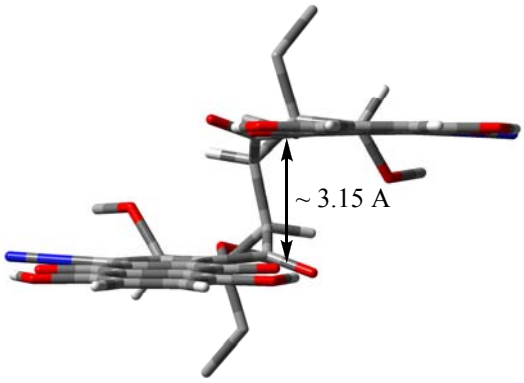

Viewing from another orthogonal direction
to the C2-C2' axis (parrellel aromatic planes)

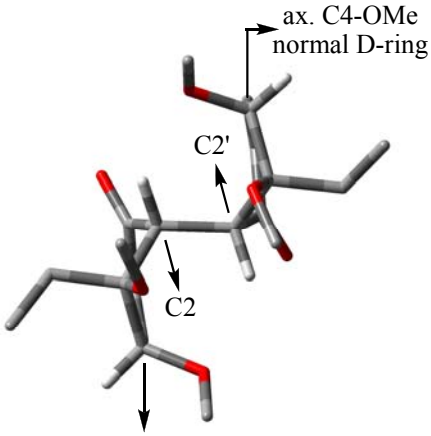

ax. C4-OMe
normal D-ring

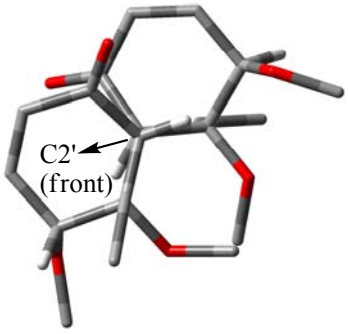

Eclipsed C2-C2'

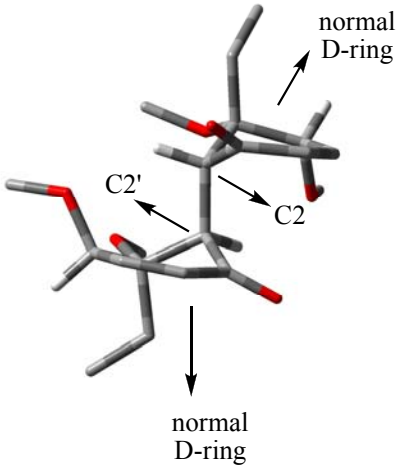

Figure F-2. Optimized conformer II of lomaiviticin model compound **6.5**.

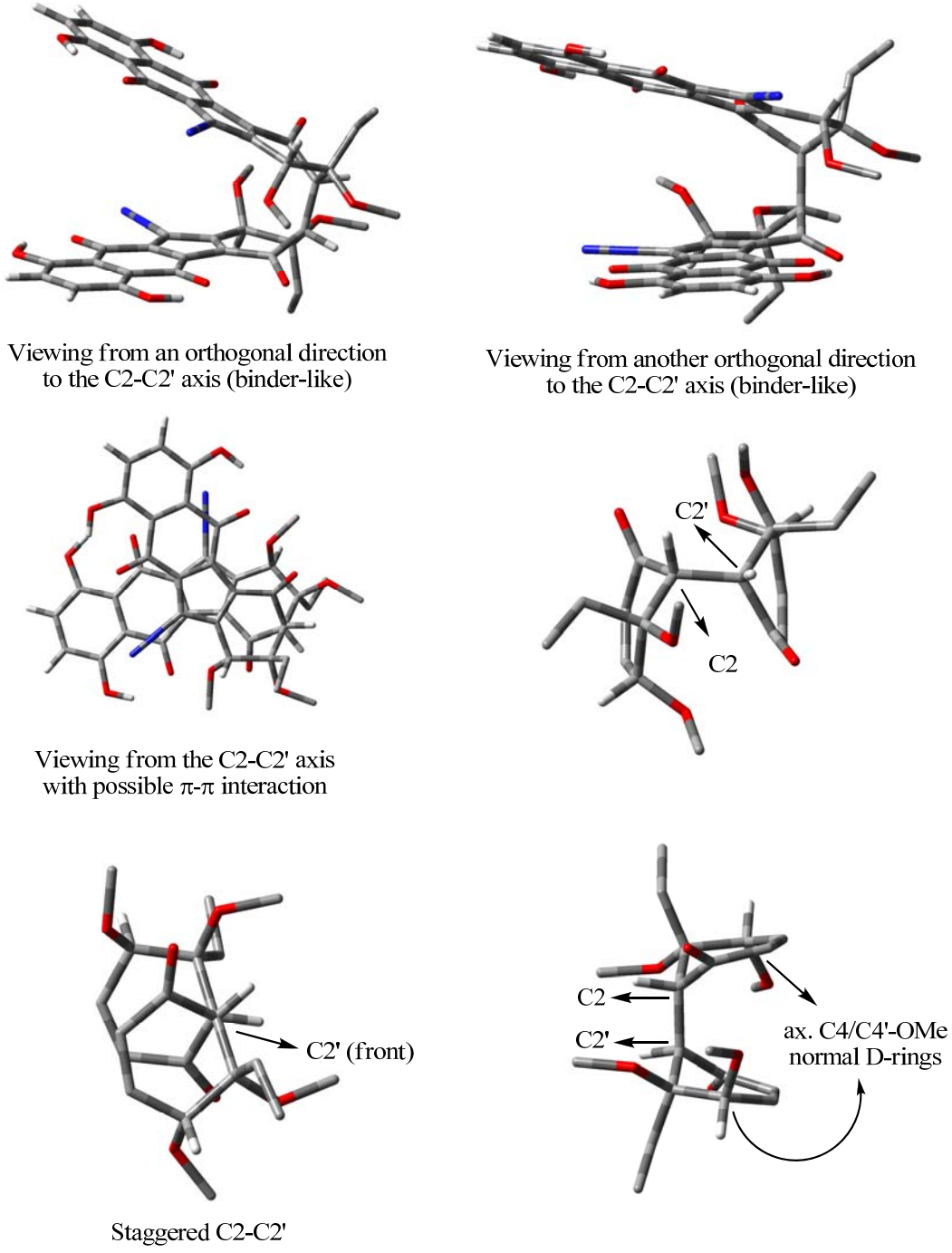

Figure F-3. Optimized conformer III of lomaiviticin model compound **6.5**.

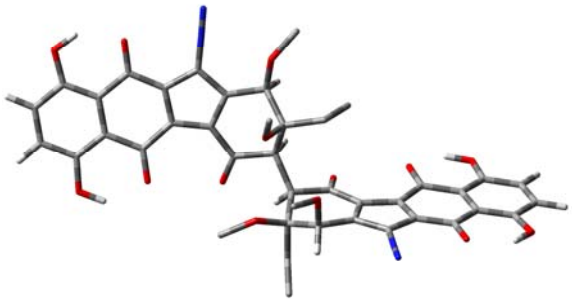

Viewing from an orthogonal direction to the C2-C2' axis

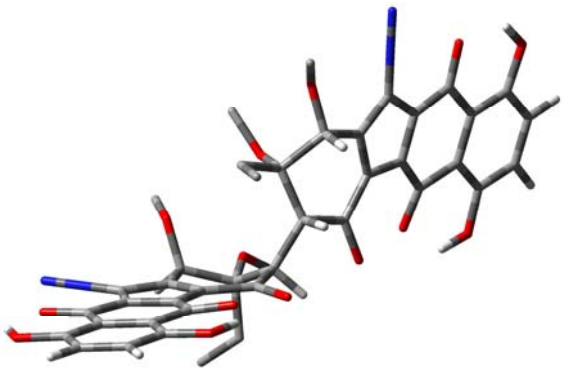

Viewing from another orthogonal direction to the C2-C2' axis

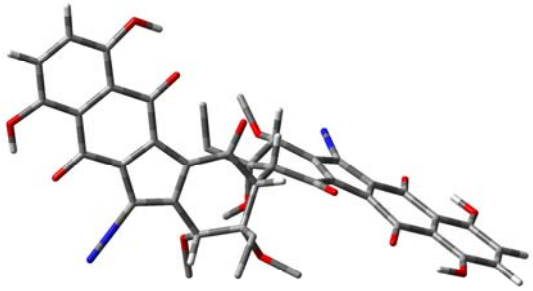

Viewing from the C2-C2' axis

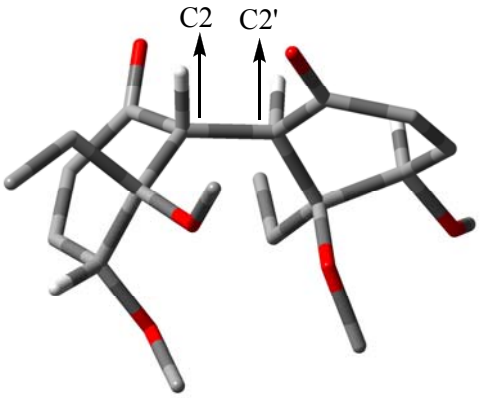

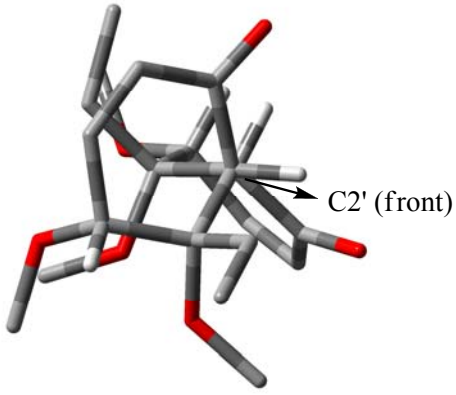

Staggered C2-C2'

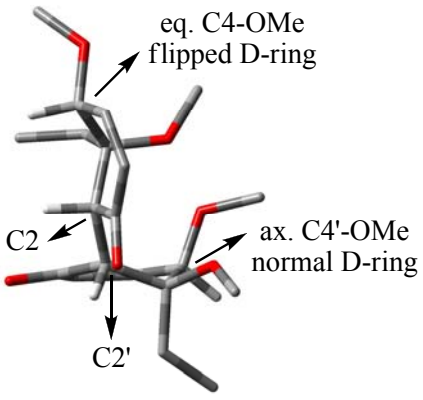

Figure F-4. Optimized conformer IV of lomaiviticin model compound **6.5**.

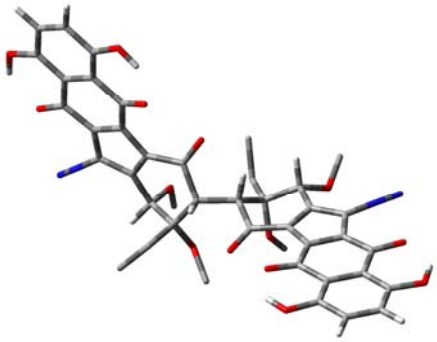

Viewing from an orthogonal direction to the C2-C2' axis

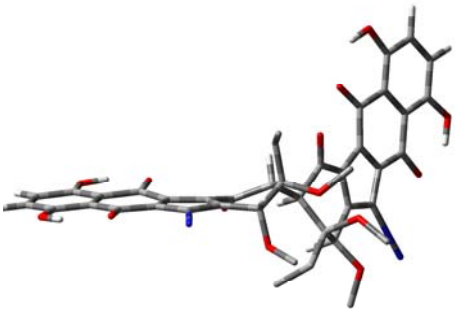

Viewing from a direction nearly parallel to one aromatic plane

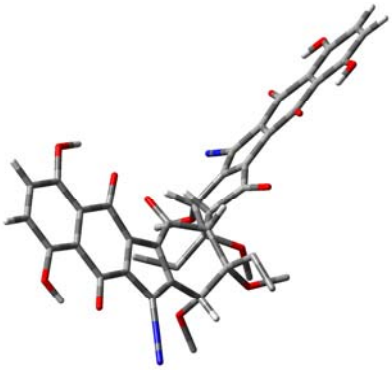

Viewing from the C2-C2' axis

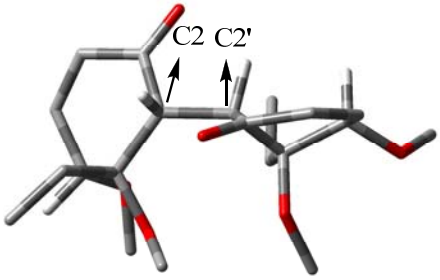

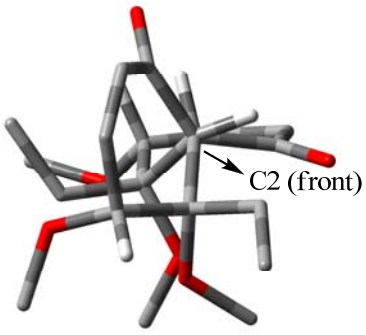

near Eclipsed C2-C2'

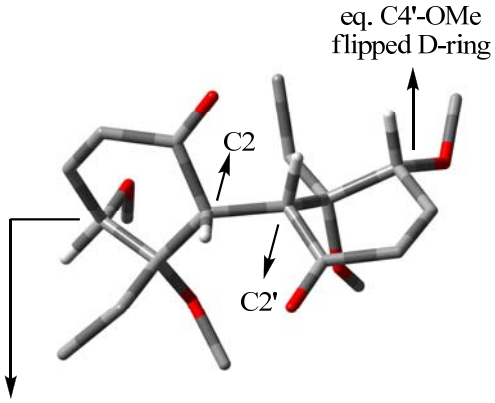

Figure F-5. Optimized conformer V of lomaiviticin model compound **6.5**.

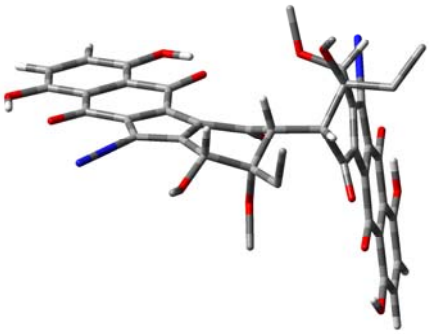

Viewing from an orthogonal direction to the C2-C2' axis

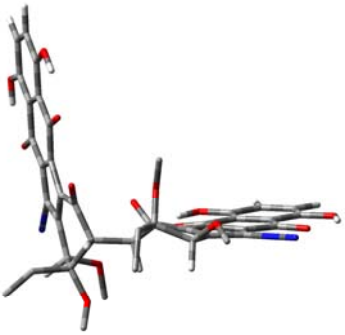

Viewing from another orthogonal direction to the C2-C2' axis

Viewing from the C2-C2' axis

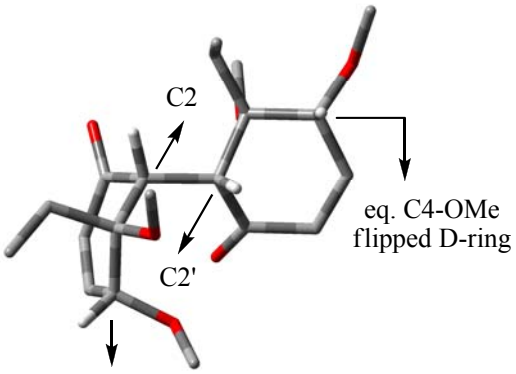

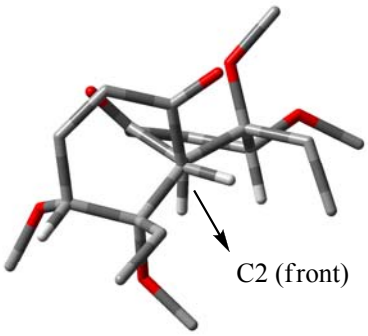

Staggered C2-C2'

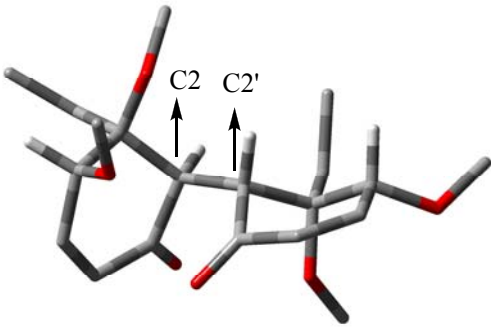

Figure F-6. Optimized conformer VI of lomaiviticin model compound **6.5**.

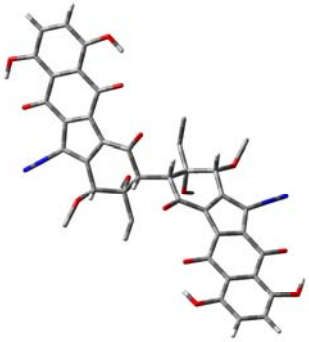

Viewing from an orthogonal direction to the C2-C2' axis

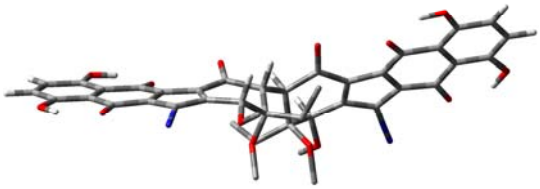

Viewing from a direction nearly parallel to one aromatic plane

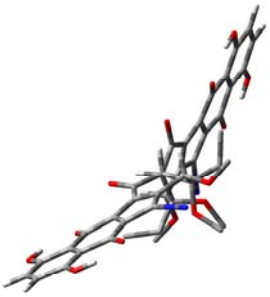

Viewing from the C2-C2' axis (butterfly-like, near C_2 symmetry)

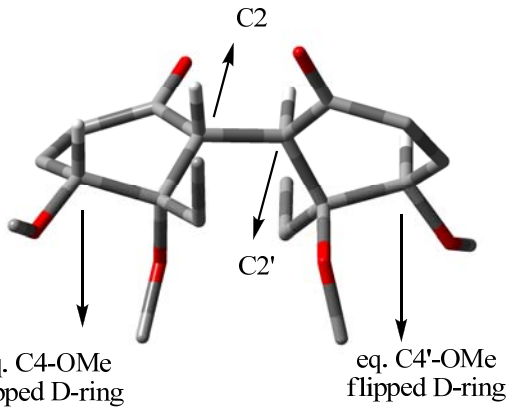

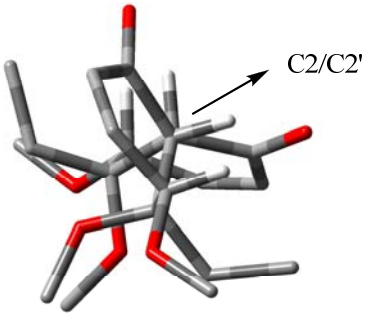

near Eclipsed C2-C2'

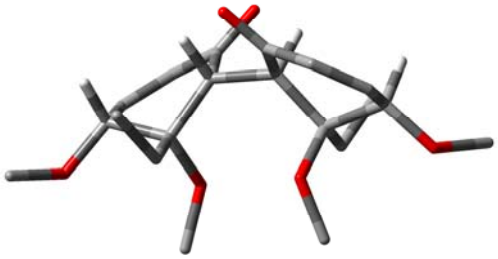

Figure F-7. Optimized conformer VII of lomaiviticin model compound **6.5**.

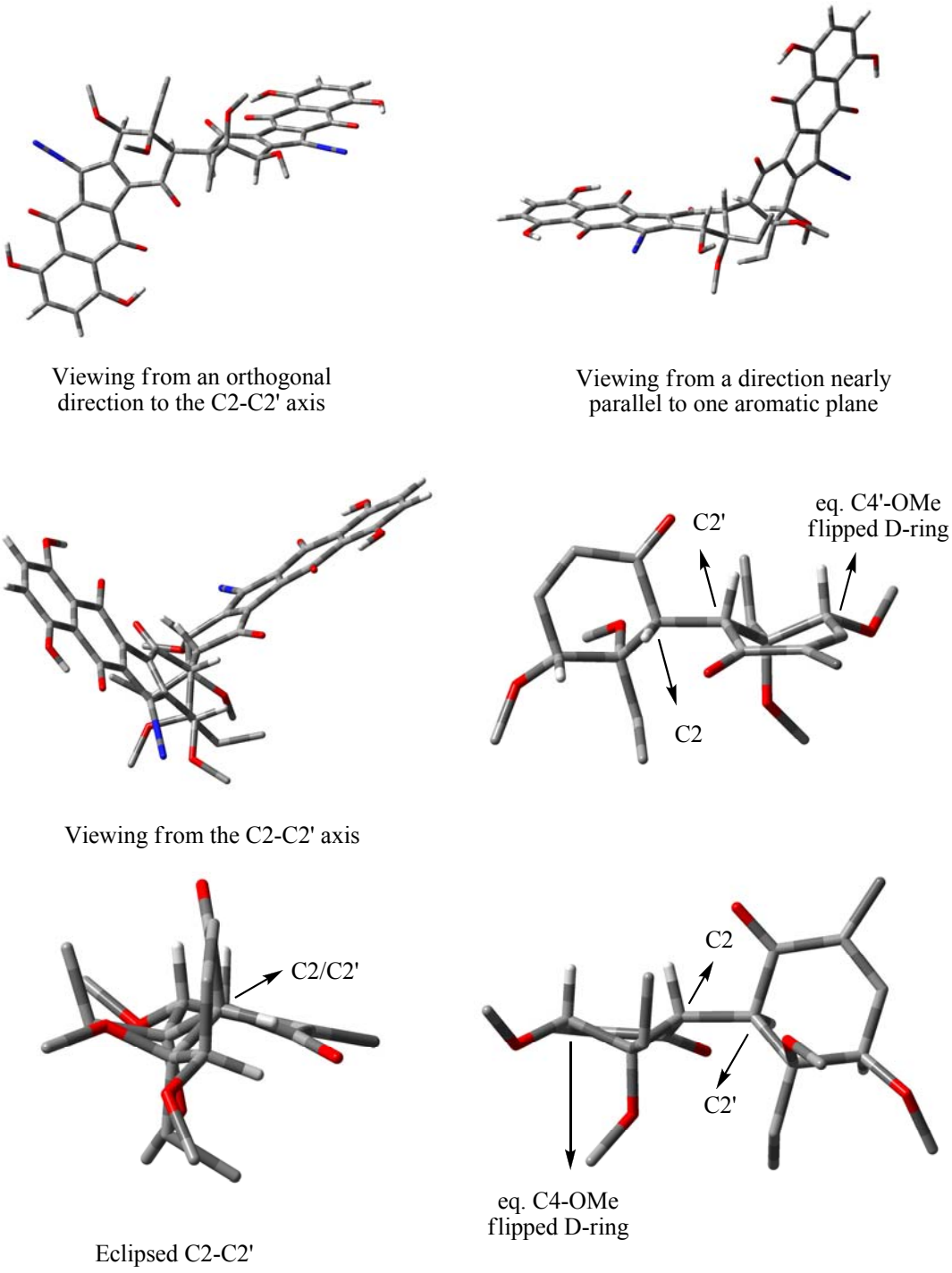

Figure F-8. Optimized conformer VIII of lomaiviticin model compound **6.5**.

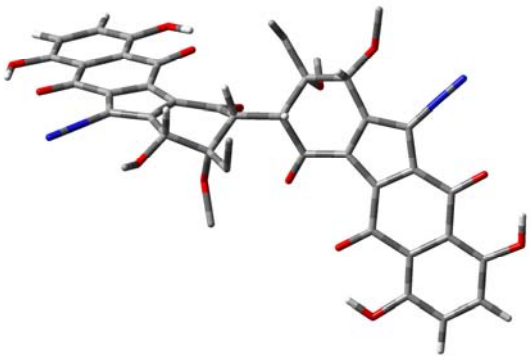

Viewing from an orthogonal direction to the C2-C2' axis

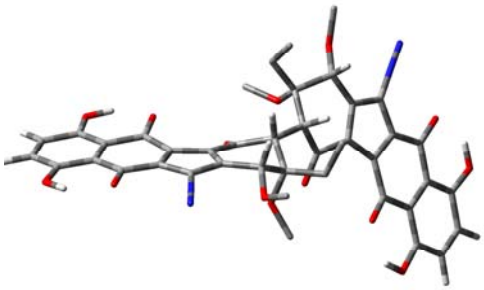

Viewing from a direction nearly parallel to one aromatic plane

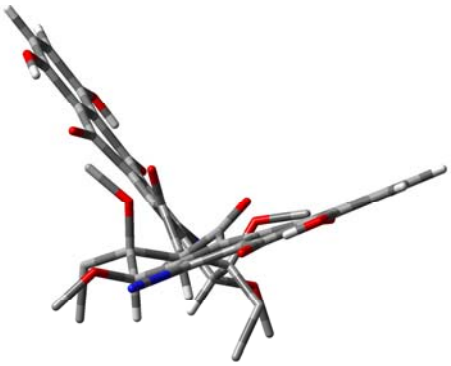

Viewing from the C2-C2' axis

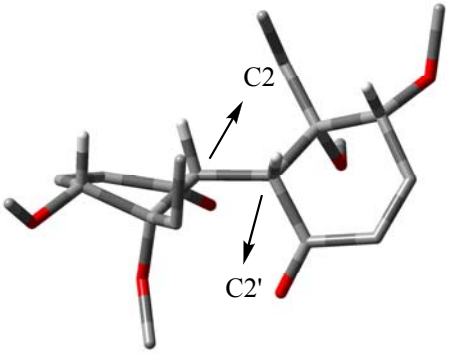

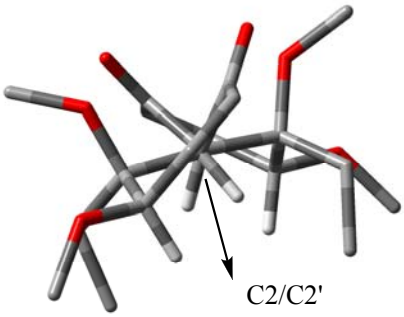

Staggered C2-C2'

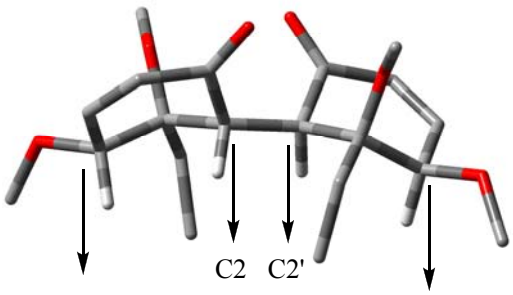

eq. C4-OMe flipped D-ring

eq. C4'-OMe flipped D-ring

Figure F-9. Optimized conformer IX of lomaiviticin model compound **6.5**.

References

(1) Sarker, S. D.; Nahar, L. In *Chemistry For Pharmacy Students*; John Wiley & Sons Ltd.: Sussex, 2007, p 283-370.

(2) Borders, D. B. In *Kirk-Othmer Encylopedia of Chemical Technology*; John Wiely & Sons, Inc.: 2007.

(3) Hopwood, D. A. *Streptomyces in Nature and Medicine. The Antibiotic Makers*; Oxford University Press Inc.: New York, 2007.

(4) Ito, S.; Matsuya, T.; Omura, S.; Otani, M.; Nakagawa, A.; Takeshima, H.; Iwai, Y.; Ohtani, M.; Hata, T. *J. Antibiot.* **1970**, *23*, 315-317.

(5) Seaton, P. J.; Gould, S. J. *J. Antibiot.* **1989**, *42*, 189-197.

(6) Cone, M.; Seaton, P. J.; Halley, K. A.; Gould, S. J. *J. Antibiot.* **1989**, *42*, 179-188.

(7) Isshiki, K.; Sawa, T.; Naganawa, H.; Matsuda, N.; Hattori, S.; Hamada, M.; Takeuchi, T.; Oosono, M.; Ishizuka, M.; Yang, Z.; Zhu, B.; Xu, W. *J. Antibiot.* **1989**, *42*, 467-468.

(8) Smitka, T. A.; Bonjouklian, R.; Perun, T. J. J.; Hunt, A. H.; Foster, R. S.; Mynderse, J. S.; Yao, R. C. *J. Antibiot.* **1992**, *45*, 581.

(9) Omura, S.; Nakagawa, A.; Yamada, H.; Hata, T.; Furusaki, A.; Watanabe, T. *Chem. Pharm. Bull.* **1973**, *21*, 931-940.

(10) Young, J.-J.; Ho, S.-N.; Ju, W.-M.; Chang, L.-R. *J. Antibiot.* **1994**, *47*, 681-687.

(11) Lin, H.-C.; Chang, S.-C.; Nan-Li, W.; Chang, L.-R. *J. Antibiot.* **1994**, *47*, 675-680.

(12) Cone, M. C.; Hassan, A. M.; Gore, M. P.; Gould, S. J.; Borden, D. B.; Alluri, M. R. *J. Org. Chem.* **1994**, *59*, 1923-1924.

(13) Gould, S. J.; Chen, J.; Cone, M. C.; Gore, M. P.; Melville, C. R.; Tamayo, N. *J. Org. Chem.* **1996**, *61*, 5720-5721.

(14) Proteau, P. J.; Li, Y.; Chen, J.; Willianson, R. T.; Gould, S. J.; Laufer, R. S.; Dmitrienko, G. I. *J. Am. Chem. Soc.* **2000**, *122*, 8325-8326.

(15) Gould, S. J. *Chem. Rev.* **1997**, *97*, 2499-2510.

(16) Nicolaou, K. C.; Li, H.; Nold, A. L.; Pappo, D.; Lenzen, A. *J. Am. Chem. Soc.* **2007**, *129*, 10356-10357.

(17) Gould, S. J.; Melville, C. R.; Cone, M. C.; Chen, J.; Carney, J. R. *J. Org. Chem.* **1997**, *62*, 320-324.

(18) Omura, S.; Nakagawa, A.; Yamada, H.; Hata, T.; Furusaki, A.; Watanabe, T. *Chem. Pharm. Bull.* **1971**, *19*, 2428-2430.

(19) Furusaki, A.; Matsui, M.; Watanabe, T.; Omura, S.; Nakagawa, A.; Hata, T. *Isr. J. Chem.* **1972**, *10*, 173-187.

(20) Hata, T.; Omura, S.; Iwai, Y.; Nakagawa, A.; Otani, M.; Ito, S.; Matsuya, T. *J. Antibiot.* **1971**, *24*, 353-359.

(21) Gould, S. J.; Tamayo, N.; Melville, C. R.; Cone, M. C. *J. Am. Chem. Soc.* **1994**, *116*, 2207-2208.

(22) Mithani, S.; Weeratunga, G.; Taylor, N. J.; Dmitrienko, G. I. *J. Am. Chem. Soc.* **1994**, *116*, 2209-2210.

(23) Lei, X.; Porco, J. A. J. *J. Am. Chem. Soc.* **2006**, *128*, 14790-14791.

(24) Kumamoto, T.; Kitani, Y.; Tsuchiya, H.; Yamaguchi, K.; Seki, H.; Ishikawa, T. *Tetrahedron* **2007**, *63*, 5189-5199.

(25) Liu, W.; Buck, M.; Chen, N.; Shang, M.; Taylor, N. J.; Asoud, J.; Wu, X.; Hasinoff, B. B.; Dmitrienko, G. I. *Org. Lett.* **2007**, *9*, 2915-2918.

(26) Woo, C. M.; Lu, L.; Gholap, S. L.; Smith, D. R.; Herzon, S. B. *J. Am. Chem. Soc.* **2010**, *132*, 2540-2541.

(27) Ehrlich, J.; Coffey, G. L.; Fisher, M. W.; Hillegas, A. B.; Kohberger, D. L.; Machamer, H. E.; Rightsel, W. A.; Roegner, F. R. *Antibiotics & Chemotherapy* **1956**, *6*, 487-497.
(28) Dion, H. W.; Fusari, S. A.; Jakubowski, Z. L.; Zora, J. G.; Bartz, Q. R. *J. Am. Chem. Soc.* **1956**, *78*, 3075-3077.
(29) Stock, C. C.; reilly, H. C.; Buckley, S. M.; Clarke, D. A.; Rhoads, C. P. *Nature* **1954**, *173*, 71-72.
(30) Ehrlich, J.; Anderson, L. E.; Coffey, G. L.; Hillegas, A. B.; Knudsen, M. P.; Koepsell, H. J.; Kohberger, D. L.; Oyaas, J. E. *Nature* **1954**, *173*, 72.
(31) Bartz, Q. R.; Elder, C. C.; Frohardt, R. P.; Fusari, S. A.; Haskell, T. H.; Johannessen, D. W.; Ryder, A. *Nature* **1954**, *173*, 72-73.
(32) Fusari, S. A.; Frohardt, R. P.; Ryder, A.; Haskell, T. H.; Johannessen, D. W.; Elder, C. C.; Bartz, Q. R. *J. Am. Chem. Soc.* **1954**, *76*, 2878-2881.
(33) Fusari, S. A.; Haskell, T. H.; Frohardt, R. P.; Bartz, Q. R. *J. Am. Chem. Soc.* **1954**, *76*, 2881-2883.
(34) Moore, J. A.; Dice, J. R.; Nicolaides, E. D.; Westland, R. D.; Wittle, E. L. *J. Am. Chem. Soc.* **1954**, *76*, 2884-2887.
(35) Nicolaides, E. D.; Westland, R. D.; Wittle, E. L. *J. Am. Chem. Soc.* **1954**, *76*, 2887-2891.
(36) Hata, T.; Umezawa, I.; Iwai, Y.; Katagiri, M.; Awaya, J.; Komiyama, K.; Oiwa, R.; Atsumi, K. *J. Antibiot.* **1973**, *26*, 181-183.
(37) Satoh, K.; Komiyama, K.; Kitao, C.; Iwai, Y.; Atsumi, K.; Oiwa, R.; Katagiri, M.; Umezawa, I.; Omura, S.; Hata, T. *J. Antibiot.* **1974**, *27*, 620-625.
(38) Pittillo, R. F.; Hunt, D. E. In *Antibiotics I. Mechanism of Action*; Gottlieb, D., Shaw, P. D., Eds. New York, 1967, p 481-493.
(39) Lee, M. D.; Fantini, A. A.; Kuck, N. A.; Greenstein, M.; Testa, R. T.; Borders, D. B. *J. Antibiot.* **1987**, *40*, 1657-1663.
(40) Kameyama, T.; Takahashi, A.; Matsumoto, H.; Kurasawa, S.; Hamada, M.; Okami, Y.; Ishizuka, M.; Takeuchi, T. *J. Antibiot.* **1988**, *41*, 1561-1567.
(41) Takahashi, A.; Nakamura, H.; Daishiro Ikeda; Naganawa, H.; Toshiyuki Kameyama; Kurasawa, S.; Okami, Y.; Takeuchi, T.; Iitaka, Y. *J. Antibiot.* **1988**, *41*, 1568-1574.
(42) Nishimura, M.; Nakada, H.; Nakajima, H.; Hori, Y.; Ezaki, M.; Goto, T.; Okuhara, M. *J. Antibiot.* **1989**, *42*, 542-548.
(43) Nishimura, M.; Nakada, H.; Takase, S.; Akira Katayama; Goto, T.; Tanaka, H.; Hashimoto, M. *J. Antibiot.* **1989**, *42*, 549-552.
(44) Nishimura, M.; Nakada, H.; Kawamura, I.; Mizota, T.; Shimomura, K.; Nakahara, K.; Goto, T.; Yamaguchi, I.; Okuhara, M. *J. Antibiot.* **1989**, *42*, 553-557.
(45) McGuire, J. N.; Wilson, S. R.; Rinehart, K. L. *J. Antibiot.* **1995**, *48*, 516-519.
(46) Varley, L. M.; Moody, C. J. *Synthesis* **2008**, 3601-3604.
(47) Singh, P. D.; Johnson, J. H.; Aklonis, C. A.; O'Sullivan, J. *J. Antibiot.* **1986**, *39*, 1054-1058.
(48) Nihei, Y.; Hasegawa, M.; Suzuki, K.; Yamamoto, S.; Hanada, M.; Furumai, T.; Fukagawa, Y.; Oki, T. *J. Antibiot.* **1993**, *46*, 900-907.
(49) Imae, K.; Nihei, Y.; Oka, M.; Yamasaki, T.; Konishi, M.; Oki, T. *J. Antibiot.* **1993**, *46*, 1031-1033.
(50) Shomura, T.; Gomi, S.; Ito, M.; Yoshida, J.; Tanaka, E.; Amano, S.; Watabe, H.-o.; Ohuchi, S.; Itoh, J.; Sezaki, M. *J. Antibiot.* **1987**, *40*, 732-739.
(51) Gomi, S.; Ohuchi, S.; Sasaki, T.; Itoh, J.; Sezaki, M. *J. Antibiot.* **1987**, *40*, 740-748.
(52) He, H.; Ding, W.; Bernan, V. S.; Richardson, A. D.; Ireland, C. M.; Greenstein, M.; Ellestad, G. A.; Carter, G. T. *J. Am. Chem. Soc.* **2001**, *123*, 5362-5363.
(53) Seaton, P. J.; Gould, S. J. *J. Am. Chem. Soc.* **1987**, *109*, 5282-5284.

(54) Volkmann, C.; Rossner, E.; Metzler, M.; Zahner, H.; Zeeck, A. *Liebigs Ann.* **1995**, 1169-1172.
(55) Shin-ya, K.; Furihata, K.; Teshima, Y.; Hayakawa, Y.; Seto, H. *Tetrahedron Lett.* **1992**, *33*, 7025-7028.
(56) Gould, S. J.; Melville, C. R. *Bioorg. Med. Chem. Lett.* **1995**, *5*, 51-54.
(57) Cone, M. C.; Melville, C. R.; Gore, M. P.; Gould, S. J. *J. Org. Chem.* **1993**, *58*, 1058-1061.
(58) Gould, S. J.; Hong, S.-T.; Carney, J. R. *J. Antibiot.* **1998**, *51*, 50-57.
(59) Carney, J. R.; Hong, S.; Gould, S. J. *Tetrahedron Lett.* **1997**, *38*, 3139.
(60) Aoyama, T.; Zhao, W.; Kojima, F.; Muraoka, Y.; Naganawa, H.; Takeuchi, T. *J. Antibiot.* **1993**, *46*, 1471-1474.
(61) Meselhy, M. R.; Kadota, S.; Tsubono, K.; Hattori, M.; Nambaa, T. *Tetrahedron* **1994**, *50*, 3081-3098.
(62) Meselhy, M. R.; Nishimoto, E.; Akao, T.; Hattori, M. *J. Tradit. Med.* **2001**, *18*, 58-63.
(63) Akiyama, T.; Harada, S.; Kojima, F.; Takahashi, Y.; Imada, C.; Okami, Y.; Muraoka, Y.; Aoyagi, T.; Takeuchi, T. *J. Antibiot.* **1998**, *51*, 553-559.
(64) Schneider, K.; Nicholson, G.; Ströbele, M.; Baur, S.; Niehaus, J.; Fiedler, H.-P.; Süssmuth, R. D. *J. Antibiot.* **2006**, *59*, 105-109.
(65) Baur, S.; Niehaus, J.; Karagouni, A. D.; Katsifas, E. A.; Chalkou, K.; Meintanis, C.; Jones, A. L.; Goodfellow, M.; Ward, A. C.; Beil, W.; Schneider, K.; Süssmuth, R. D.; Fiedler, H.-P. *J. Antibiot.* **2006**, *59*, 293-297.
(66) Gould, S. J.; Melville, C. R. *Tetrahedron Lett.* **1997**, *38*, 1473.
(67) Iwai, Y.; Omura, S. *J. Antibiot.* **1982**, *35*, 123-141.
(68) Short, J. M.; Paradkar, A.; Varoglu, M.; Mathur, E. J.; Organization, W. I. P., Ed.; Diversa Co. (CA, USA): USA, 2003, p 47.
(69) Sato, Y.; Geckle, M.; Gould, S. J. *Tetrahedron Lett.* **1985**, *26*, 4019-4022.
(70) Sato, Y.; Gould, S. J. *Tetrahedron Lett.* **1985**, *26*, 4023-4026.
(71) Seaton, P. J.; Gould, S. J. *J. Am. Chem. Soc.* **1988**, *110*, 5912-5914.
(72) Duthaler, R. O.; Fonster, H. G.; Roberts, J. D. *J. Am. Chem. Soc.* **1978**, *100*, 4974-4979.
(73) Dmitrienko, G. I.; Nielsen, K. E.; Steingart, C.; Ming, N. S.; Willson, J. M.; Weeratunga, G. *Tetrahedron Lett.* **1990**, *31*, 3681.
(74) Echavarren, A. M.; Tamayo, N.; Paredes, M. C. *Tetrahedron Lett.* **1993**, *34*, 4713-4716.
(75) Echavarren, A. M.; Frutos, O. d. *Tetrahedron Lett.* **1997**, *38*, 7941-7942.
(76) Hauser, F. M.; Zhou, M. *J. Org. Chem.* **1996**, *61*, 5722.
(77) Sato, Y.; Gould, S. J. *J. Am. Chem. Soc.* **1986**, *108*, 4625-4631.
(78) Ajisaka, K.; Takeshima, H.; Omura, S. *J. Chem. Soc., Chem. Commun.* **1976**, 571-572.
(79) Gould, S. J.; O'Hare, T.; Seaton, P.; Soodsma, J.; Tang, Z. *Bioorg. Med. Chem.* **1996**, *4*, 987.
(80) Laufer, R., Ph.D. thesis, University of Waterloo, 2002.
(81) LaRue, T. A. *Lloydia* **1977**, *40*, 307-321.
(82) Walton, K.; Coombs, M. M.; Walker, R.; Ioannides, C. *Mutat. Res., Fundam. Mol. Mech. Mutagen.* **1997**, *381*, 131-139.
(83) Walton, K.; Coombs, M. M.; Catterall, F. S.; Walker, R.; Ioannides, C. *Carcinogenesis* **1997**, *18*, 1603-1608.
(84) Parry, R. J.; Li, W. *J. Chem. Soc., Chem. Commun.* **1994**, 995-996.
(85) Walton, K.; Coombs, M. M.; King, L. J.; Walker, R.; Ioannides, C. *Nutri. Can.* **2000**, *37*, 55-64.
(86) Gonzalez-Lopez, J.; Martinez-Toledo, M. V.; Pozo, C.; Rodelas, B.; Gomez, M. A.; Hontoria, E. *Trends Soil Sci.* **2004**, *3*, 91-97.
(87) Suzuki, T. *Genes Environ.* **2006**, *28*, 48-55.

(88) Omura, S.; Tanaka, H.; Oiwa, R.; Nagai, R.; Koyama, Y.; Takahashi, Y. *J. Antibiot.* **1979**, *32*, 978-984.
(89) Tanaka, Y.; Sugoh, M.; Ji, W.; Iwabuchi, J.; Yoshida, H.; Omura, S. *J. Antibiot.* **1995**, *48*, 720-724.
(90) Khdour, O.; Skibo, E. B. *Org. Biomol. Chem.* **2009**, *7*, 2140-2154.
(91) Moore, H. W. *Science* **1977**, *197*, 527-532.
(92) Moore, H. W.; Czerniak, R. *Med. Res. Rev.* **1981**, *1*, 249-280.
(93) Rajski, S. R.; Williams, R. M. *Chem. Rev.* **1998**, *98*, 2723-2795.
(94) Griffiths, J.; Murphy, J. A. *J. Chem. Soc., Chem. Commun.* **1992**, 24-26.
(95) Kizil, M.; Yilmaz, E. I.; Pirinccioglu, N.; Aytekin, C. *Turk. J. Chem.* **2003**, *27*, 539-544.
(96) Augusto, O. *Free Rad. Bio. Med.* **1993**, *15*, 329-336.
(97) Zollinger, H. *Diazo Chemistry I: Aromatic and Heteroaromatic Compounds*; VCH: New York, 1994.
(98) Reszka, K. J.; Chignell, C. F. *Chem.-Biol. Interact.* **1995**, *96*, 223-234.
(99) Gannett, P. M.; Lawson, T.; MIller, M.; Thakkar, D. D.; Lord, J. W.; Yau, W.-M.; Toth, B. *Chem.-Biol. Interact.* **1996**, *101*, 149-164.
(100) Chin, A.; Hung, M.-H.; Stock, L. M. *J. Org. Chem.* **1981**, *46*, 2203-2207.
(101) Hung, M.-H.; Stock, L. M. *J. Org. Chem.* **1982**, *47*, 448-453.
(102) McLick, J.; Bauer, P. I.; Hakam, A.; Kun, E. *Biochemistry* **1987**, *26*, 2226-2231.
(103) Koepke, S. R.; Kroeger-Koepke, M. B.; Michejda, C. J. *Chem. Res. Toxicol.* **1990**, *3*, 17-20.
(104) Lawson, T.; Gannett, P. M.; Yau, W.-M.; Dalal, N. S.; Toth, B. *J. Agric. Food Chem.* **1995**, *43*, 2627-2635.
(105) Gannett, P. M.; Powell, J. H.; Rao, R.; Shi, X.; Lawson, T.; Kolar, C.; Toth, B. *Chem. Res. Toxicol.* **1999**, *12*, 297-304.
(106) Gannett, P. M.; Ye, J.; Ding, M.; Powell, J.; Zhang, Y.; Darian, E.; Daft, J.; Shi, X. *Chem. Res. Toxicol.* **2000**, *13*, 1020-1027.
(107) Kikugawa, K.; Kato, T.; Takeda, Y. *Mutat. Res.* **1987**, *177*, 35-43.
(108) Furihata, C.; Yamakoshi, A.; Matsushima, T.; Kato, T.; Kikugawa, K. *Mutagenesis* **1988**, *3*, 299-301.
(109) Kikugawa, K.; Kato, T.; Takeda, Y. *Chem. Pharm. Bull.* **1989**, *37*, 1600-1603.
(110) Kikugawa, K.; Kato, T. *Food Chem. Toxic.* **1988**, *26*, 209-214.
(111) Kikugawa, K.; Kato, T.; Kojima, K. *Mutat. Res.* **1992**, *1*, 65-75.
(112) Kato, T.; Kojima, K.; Hiramoto, K.; Kikugawa, K. *Mutat. Res.* **1992**, *268*, 105-114.
(113) Kato, T.; Tadokoro, N.; Tsutsui, M.; Kikugawa, K. *Mutat. Res.* **1991**, *249*, 243-254.
(114) Hiramoto, K.; Inoue, M.; Maeda, K.; Kato, T.; Kikugawa, K. *Jpn. J. Toxicol. Environ. Health* **1994**, *40*, 414-421.
(115) Hiramoto, K.; Kato, T.; Kikugawa, K. *Mutat. Res., Fundam. Mol. Mech. Mutagen.* **1994**, *306*, 153-163.
(116) Hiramoto, K.; Kaku, M.; Sueyoshi, A.; Fujise, M.; Kikugawa, K. *Chem. Res. Toxicol.* **1995**, *8*, 356-362.
(117) Hiramoto, K.; Kaku, M.; Kato, T.; Kikugawa, K. *Chem.-Biol. Interact.* **1995**, *94*, 21-36.
(118) Hiramoto, K.; Fujino, T.; Kikugawa, K. *Mutat. Res., Environ. Mutagen.* **1996**, *360*, 95-100.
(119) Kato, T.; Kikugawa, K. *Food Chem. Toxic.* **1992**, *30*, 617-626.
(120) Hiramoto, K.; Yasuhara, Y.; Sako, K.-i.; Aoki, K.; Kikugawa, K. *Biol. Pharm. Bull.* **2003**, *26*, 1129-1134.
(121) Arya, D. P.; Jebaratnam, D. J. *J. Org. Chem.* **1995**, *60*, 3268-3269.
(122) Eppley, H. J.; Lato, S. M.; Ellington, A. D.; Zaleski, J. M. *Chem. Commun.* **1999**, 2405-2406.

(123) Kraft, B. J.; Eppley, H. J.; Huffman, J. C.; Zaleski, J. M. *J. Am. Chem. Soc.* **2002**, *124*, 272-280.
(124) Laufer, R. S.; Dmitrienko, G. I. *J. Am. Chem. Soc.* **2002**, *124*, 1854-1855.
(125) Cain, J. C. *The Chemistry And Technology of The Diazo-compounds*; 2nd ed.; Oxford: London, 1920.
(126) Porai-Koshits, B. A. *Russ. Chem. Rev.* **1970**, *39*, 283-289.
(127) Regitz, M.; Mass, G. *Diazo Compounds: Properties and Synthesis* Academic Press: New York, 1986.
(128) Zollinger, H. *Diazo Chemistry II: Aliphatic, Inorganic and Organometallic Compounds*; VCH: New York, 1995.
(129) Kostuch, A.; Urban, A.; Tomasik, P. *ARKIVOC* **2000**, 181-185 and references therein.
(130) McDowell, L. J.; Khodae, M. M.; Bethell, D. *Org. Biomol. Chem.* **2003**, *1*, 995.
(131) Pearson, R. G. *Chemical Hardness*; WILEY-VCH: New York, 1997.
(132) Silverstein, R. M.; Webster, F. X. *Spectrometric Identification of Organic Compounds*; 6th ed.; John Wiley & Sons: New York, 1998.
(133) Kobayashi, K.; Takeuchi, H.; Seko, S.; Suginome, H. *Helv. Chim. Acta* **1991**, *74*, 1091-1094.
(134) O'Sullivan, P. J.; Moreno, R.; Murphy, W. S. *Tetrahedron Lett.* **1992**, *33*, 535-538.
(135) Hu, H.-Y.; Liu, Y.; Ye, M.; Xu, J.-H. *Synlett* **2006**, 1913-1917.
(136) Poumaroux, A.; Bouaziz, Z.; Fillion, H.; Domard, M.; Giraud, J.; Petavy, A.-F. *Chem. Pharm. Bull.* **1999**, *47*, 643-646.
(137) Itoigawa, M.; Kashiwada, Y.; Ito, C.; Furukawa, H.; Tachibana, Y.; Bastow, K. F.; Lee, K.-H. *J. Nat. Prod.* **2000**, *63*, 893-897.
(138) Bernardo, P. H.; Chai, C. L. L.; Guen, M. L.; Smith, G. D.; Waring, P. *Bio. Med. Chem. Lett.* **2007**, *17*, 82-85.
(139) Hopkingson, A. C.; Lee-Ruff, E.; Maleki, M. *Synthesis* **1986**, 366-371.
(140) Trost, B. M.; Walchli, R. *J. Am. Chem. Soc.* **1987**, *109*, 3487-3488.
(141) Bestmann, H. J. *Pure & Appl. Chern.* **1980**, *52*, 771-788.
(142) Streitwieser-Jr., A.; Brown, S. M. *J. Org. Chem.* **1988**, *53*, 904-906.
(143) Krogh, E.; Wan, P. *Can. J. Chem.* **1990**, *68*, 1725-1731.
(144) Gore, M. P.; Gould, S. J.; Weller, D. D. *J. Org. Chem.* **1991**, *56*, 2289-2291.
(145) Gore, M. P.; Gould, S. J.; Weller, D. D. *J. Org. Chem.* **1992**, *57*, 2774-2783.
(146) Mohri, S.-i.; Stefinovic, M.; Snieckus, V. *J. Org. Chem.* **1997**, *62*, 7072-7073.
(147) Koyama, H.; Kamikawa, T. *J. Chem. Soc., Perkin Trans. 1* **1998**, 203-209.
(148) Williams, W.; Sun, X.; Jebaratnam, D. *J. Org. Chem.* **1997**, *62*, 4364-4369.
(149) Qabaja, G.; Jones, G. B. *Tetrahedron Lett.* **2000**, *41*, 5317-5320.
(150) Qabaja, G.; Jones, G. B. *J. Org. Chem.* **2000**, *65*, 7187-7194.
(151) Mal, D.; Hazra, N. K. *Tetrahedron Lett.* **1996**, *37*, 2641-2642.
(152) Hauser, F. M.; Rhee, R. P. *J. Org. Chem.* **1978**, *43*, 178-180.
(153) Birman, V. B.; Zhao, Z.; Guo, L. *Org. Lett.* **2007**, *9*, 1223-1225.
(154) Ana Martinez, J. C.; Barcia, A. M. E.; Fernandez, F.; Gonzalez, L.; Estevez, J. C.; Estevez, R. J. *Tetrahedron Lett.* **2007**, *48*, 2147-2149.
(155) Rodríguez, D.; Castedo, L.; Domínguez, D.; Saá, C. *Tetrahedron Lett.* **1999**, *40*, 7701-7704.
(156) Atienza, C.; Mateo, C.; Frutos, O. d.; Echavarren, A. M. *Org. Lett.* **2001**, *3*, 153-155.
(157) Nicolaou, K. C.; Denton, R. M.; Lenzen, A.; Edmonds, D. J.; Li, A.; Milburn, R. R.; Harrison, S. T. *Angew. Chem. Int. Ed.* **2006**, *45*, 2076-2081.
(158) Nicolaou, K. C.; Nold, A. L.; Li, H. *Angew. Chem. Int. Ed.* **2009**, *48*, 1-5.
(159) Krygowski, E. S.; Murphy-Benenato, K.; Shair, M. D. *Angew. Chem. Int. Ed.* **2008**, *47*, 1680-1684.

(160) Buck, M., M.Sc. thesis, University of Waterloo, 2003.
(161) Liu, W., Ph.D. thesis, University of Waterloo, 2009.
(162) Yu, M.; Danishefsky, S. J. *J. Am. Chem. Soc.* **2008**, *130*, 2783-2785.
(163) Kumamoto, T.; Tabe, N.; Yamaguchi, K.; Ishikawa, T. *Tetrahedron Lett.* **2000**, *41*, 5693-5697.
(164) Kumamoto, T.; Tabe, N.; Yamaguchi, K.; Yagishita, H.; Iwasa, H.; Ishikawa, T. *Tetrahedron* **2001**, *57*, 2717-2728.
(165) Chen, N.; Carriere, M. B.; Laufer, R. S.; Taylor, N. J.; Dmitrienko, G. I. *Org. Lett.* **2008**, *10*, 381-384.
(166) Fieser, L. F.; Campbell, W. P.; Fry, E. M.; Marshall D. Gates, J. *J. Am. Chem. Soc.* **1939**, *61*, 3216-3223.
(167) Masahiko, T.; Fujii, H.; Oshima, K.; Utimoto, K. *Tetrahedron* **1995**, *51*, 679-686.
(168) Carriere, M. B., M.Sc. thesis, University of Waterloo, 1998.
(169) Akbulut, N.; Balci, M. *J. Org. Chem.* **1988**, *53*, 3338.
(170) Rucker, G.; Horster, H.; Gajewski, W. *Synth. Commun.* **1980**, *10*, 623.
(171) Masahiko, T.; Hideaki, F.; Oshima, K.; Utimoto, K. *Tetrahedron* **1995**, *51*, 679-686.
(172) Preusch, P. C.; Smalley, D. M. *Free Rad. Res. Comms.* **1990**, *8*, 401-415.
(173) Preusch, P. C.; Suttie, J. W. *J. Org. Chem.* **1983**, *48*, 2291-2293.
(174) Schneider, C. *Synthesis* **2006**, 3919-3944.
(175) Cavelier, F.; Yim, A.-M. *Org. Prep. Proced. Int.* **1998**, *30*, 103-106.
(176) O'Brien, D. F. *J. Org. Chem.* **1968**, *33*, 262-265.
(177) Nan, F.; Chen, X.; Xiong, Z.; Li, T.; Li, Y. *Synth. Commun.* **1994**, *24*, 2319-2324.
(178) Kido, F.; Abe, T.; Yoshikoshi, A. *J. Chem. Soc., Chem. Commun.* **1986**, 590.
(179) Isobe, M.; Kitamura, M.; Goto, T. *Tetrahedron Lett.* **1981**, *22*, 239-242.
(180) Phillips, R. E.; Soulen, R. L. *J. Chem. Ed.* **1995**, *72*, 624-625.
(181) Loken, B.; Kaufmann, S.; Rosenkranz, G.; Sondheimer, F. *J. Am. Chem. Soc.* **1956**, *78*, 1738-1741.
(182) Kamano, Y. *Chem. Pharm. Bull.* **1969**, *17*, 1711-1719.
(183) Baraldi, P. G.; Barco, A.; Benetti, S.; Ferretti, V.; Pollini, G. P.; Polo, E.; Zanirato, V. *Tetrahedron* **1989**, *45*, 1517-1532.
(184) Naruta, Y.; Nishigaichi, Y.; Maruyama, K. *J. Org. Chem.* **1988**, *53*, 1192-1199.
(185) Urones, J. G.; Basabe, P.; Lithgow, A. M.; Marcos, I. S.; Jimenez, A.; Diez, D.; Gomez, A.; White, A. J. P.; Williams, D. J.; Simmonds, M. S. J.; Blaney, W. M. *Tetrahedron* **1995**, *51*, 2117-2128.
(186) Urones, J. G.; Basabe, P.; Marcos, I. S.; Jimenez, A.; Lithgow, A. M.; Lopez, M.; Moro, R. F.; Gomez, A. *Tetrahedron* **1994**, *50*, 10791-10802.
(187) Confalone, P. N.; Pizzolato, G. *J. Org. Chem.* **1990**, *55*, 5520-5525.
(188) Isaacs, N. S.; Neelakantan, K. *Can. J. Chem.* **1968**, *46*, 1043-1046.
(189) Ponser, G.; Rogers, D. Z. *J. Am. Chem. Soc.* **1977**, *99*, 8208-8214.
(190) Kakiuchi, H.; Iijima, T. *Tetrahedron* **1980**, *36*, 1011-1016.
(191) Girdhar, N. K.; Ishar, M. P. S.; Kumar, R.; Singh, R.; Singh, G. *Tetrahedron* **2001**, *57*, 7199-7204.
(192) Rampalli, S.; Chaudhari, S. S.; Akamanchi, K. G. *Synthesis* **2000**, 78-80.
(193) Riego, J.; Costa, A.; SAA, J. M. *Chem. Lett.* **1986**, 1565-1568.
(194) Liu, Y.-j.; Chu, T.-y.; Engel, R. *Synth. Commun.* **1992**, *22*, 2367-2371.
(195) Mohammadpoor-Baltork, I.; Tangestaninejad, S.; Mirkhani, V. *Synth. Commun.* **2000**, *30*, 2365-2374.
(196) Montalban, A. G.; Wittenberg, L.-O.; McKillop, A. *Tetrahedron Lett.* **1999**, *40*, 5893-5896.

(197) Hanzlik, R. P.; Leinwetter, M. *J. Org. Chem.* **1978**, *43*, 438-440.
(198) Nambu, Y.; Endo, T. *Tetrahedron Lett.* **1990**, *31*, 1723-1726.
(199) Iranpoor, N.; Tarrian, T.; Movahedi, Z. *Synthesis* **1996**, 1473-1476.
(200) Salehi, P.; Seddighi, B.; Irandoost, M.; Behbahani, F. K. *Synth. Commun.* **2000**, *30*, 2967-2973.
(201) Iranpoor, N.; Adibi, H. *Bull. Chem. Soc. Jpn.* **2000**, *73*, 675-680.
(202) Kalita, B.; Barua, N. C.; Bezbarua, M. S.; Bez, G. *Synlett* **2001**, 1411-1414.
(203) Righi, G.; Pescatore, G.; Bonadies, F.; Bonini, C. *Tetrahedron* **2001**, *57*, 5649-5656.
(204) Bonini, C.; Righi, G. *Tetrahedron* **1992**, *48*, 1531-1538.
(205) Constantino, M. G.; Jr., V. L.; Aragão, V. *Molecules* **2001**, *6*, 770-776.
(206) Iranpoor, N.; Zeynizadeh, B. *Synth. Commun.* **1999**, *29*, 1017-1024.
(207) Ghelfi, F.; Grandi, R.; Pagnoni, U. M. *J. Chem. Res. (S)* **1988**, 200-201.
(208) Armstrong, R. N. In *Comprehensive Natural Products Chemistry*; Poulter, C. D., Ed.; Elsevier Science: New York, 1999; Vol. 5, p 51-70.
(209) Iranpoor, N.; Baltork, I. M. *Synth. Commun.* **1990**, *20*, 2789-2797.
(210) Iranpoor, N.; Zardaloo, F. S. *Synth. Commun.* **1994**, *24*, 1959-1969.
(211) Iranpoor, N.; Baltork, I. M. *Tetrahedron Lett.* **1990**, *31*, 735-738.
(212) Iranpoor, N.; Tamami, B.; Niknam, K. *Can. J. Chem.* **1997**, *75*, 1913-1919.
(213) Zwan, M. C. V.; Hartner, F. W. *J. Org. Chem.* **1978**, *43*, 2655-2657.
(214) Mall, T.; Stamm, H. *J. Org. Chem.* **1987**, *52*, 4812-4817.
(215) Honda, T.; Mizutani, H. *Heterocycles* **1998**, *48*, 1753-1757.
(216) Caron, M.; Sharpless, K. B. *J. Org. Chem.* **1985**, *50*, 1557-1560.
(217) Chong, J. M.; Sharpless, K. B. *J. Org. Chem.* **1985**, *50*, 1560-1563.
(218) Akira, K.; Taira, T.; Hasegawa, H.; Sakuma, C.; Shinohara, Y. *Drug Metab. Dispos.* **1998**, *26*, 457-464.
(219) Evans, D. A.; Chapman, K. T.; Carreira, E. M. *J. Am. Chem. Soc.* **1988**, *110*, 3560-3578.
(220) Thompson, H.; Wolfrom, M. L.; Whistler, R. L., Wolfrom, M. L., BeMiller, J. N., Eds.; Academic Press: New York, 1963; Vol. 2, p 215-220.
(221) Barrett, A. G. M.; Braddock, D. C. *Chem. Commun.* **1997**, 351-352.
(222) Ranu, B. C.; Dutta, P.; Sarkar, A. *Tetrahedron Lett.* **1998**, *39*, 9557.
(223) Ma, J.; Chan, T. H. *Tetrahedron Lett.* **1998**, *39*, 2499.
(224) Li, W.-D. Z.; Ma, B.-C. *Org. Lett.* **2005**, *7*, 271-274.
(225) Arai, S.; Oku, M.; Miura, M.; Shioiri, T. *Synlett* **1998**, 1201-1202.
(226) Arai, S.; Tsuge, H.; Oku, M.; Miura, M.; Shioiri, T. *Tetrahedron* **2002**, *58*, 1623-1630.
(227) Baba, N.; Oda, J. i.; Kawaguchi, M. *Agric. Biol. Chem.* **1986**, *50*, 3113-3117.
(228) Pluim, H.; Wynberg, H. *J. Org. Chem.* **1980**, *45*, 2498-2502.
(229) Wynberg, H. *Chimia* **1976**, *30*, 445-451.
(230) Dwyer, C. L.; Gill, C. D.; Ichihara, O.; Taylor, R. J. K. *Synlett* **2000**, 704-705.
(231) Colonna, S.; Manfredi, A.; Annunziata, R.; Gaggero, N.; Casella, L. *J. Org. Chem.* **1990**, *55*, 5862-5866.
(232) Colonna, S.; Manfredi, A. *Tetrahedron Lett.* **1986**, *27*, 387-390.
(233) Colonna, S.; Gaggero, N.; Manfredi, A.; Spadoni, M.; Casella, L.; Carrea, G.; Pasta, P. *Tetrahedron* **1988**, *44*, 5169-5178.
(234) Colonna, S.; Manfredi, A.; Annunziata, R.; Spadoni, M. *Tetrahedron* **1987**, *43*, 2157-2164.
(235) Harigaya, Y.; Yamaguch, H.; Onda, M. *Heterocycles* **1981**, *15*, 183-185.
(236) Porter, M. J.; Skidmore, J. *Chem. Commun.* **2000**, 1215--1225.
(237) Berkessel, A.; Guix, M.; Schmidt, F.; Neudorfl, J. M.; Lex, J. *Chem. Eur. J.* **2007**, *13*, 4483-4498.

(238) Barfield, M.; Johnston, M. D. J. *Chem. Rev.* **1972**, *73*, 53-73.
(239) Desjardins, M.; Lallemand, M.-C.; Freeman, S.; Hudlicky, T.; Abboud, K. A. *J. Chem. Soc., Perkin Trans. 1* **1999**, 621-628.
(240) Orsini, F.; Pelizzoni, F. *Tetrahedron: Asymmetry* **1996**, *7*, 1033.
(241) O'Hara, K. A.; Wu, X.; Patel, D.; Liang, H.; Yalowich, J. C.; Chen, N.; Goodfellow, V.; Adedayo, O.; Dmitrienko, G. I.; Hasinoff, B. B. *Free Rad. Bio. Med.* **2007**, *43*, 1132-1144.
(242) Gottlieb, H. E.; Kotlyar, V.; Nudelman, A. *J. Org. Chem.* **1997**, *62*, 7512-7515.
(243) Weeratunga, G.; Prasad, G. K. B.; Dilley, J.; Taylor, N. J.; Dmitrienko, G. I. *Tetrahedron Lett.* **1990**, *31*, 5713-5716.
(244) Hasinoff, B. B.; Wu, X.; Yalowich, J. C.; Goodfellow, V.; R., L.; Adedayo , O.; Dmitrienko, G. I. *Anti-Cancer Drugs* **2006**, *17*, 825-837.
(245) Mithani, S., Ph.D. thesis, University of Waterloo, 1996.
(246) Jacobsen, N.; Torssell, K. *Liebigs Ann. Chem.* **1972**, *763*, 135-147.
(247) Jacobsen, N.; Torssell, K. *Acta Chem. Scand.* **1973**, *27*, 3211-3216.
(248) Kirmse, W. *Eur. J. Org. Chem.* **2002**, 2193-2256.
(249) Baumbach, B.; Bendig, J.; Nagel, T.; Dubsky, B. *J. Prakt. Chem.* **1991**, *333*, 625-635.
(250) Bendig, J.; Sauer, E.; Polz, K.; Schopf, G. *Tetrahedron* **1992**, *48*, 9207-9216.
(251) Sus, O.; Steppan, H.; Dietrich, R. *Justus Liebigs Ann. Chem.* **1958**, 20-25.
(252) Trost, B. M.; Kinson, P. L. *J. Am. Chem. Soc.* **1975**, *97*, 2438-2449.
(253) Presset, M.; Coquerel, Y.; Rodriguez, J. *J. Org. Chem.* **2009**, *74*, 415-418.
(254) Patra, A.; Ghorai, S. K.; De, S. R.; Mal, D. *Synthesis* **2006**, 2556-2562.
(255) Acheson, R. M. *Acc. Chem. Res.* **1971**, *4*, 177-186 and references therein.
(256) Jung, M. E.; Jung, Y. H. *Tetrahedron Lett.* **1988**, *29*, 2517.
(257) Rizzacasa, M. A.; Sargent, M. V. *J. Chem. Soc. Perkin Trans. 1* **1991**, *1991*, 841-844.
(258) Kitani, Y.; Morita, A.; Kumamoto, T.; Ishikawa, T. *Helv. Chim. Acta* **2002**, *85*, 1186-1195.
(259) Heinzman, S. W.; Grunwell, J. R. *Tetrahedron Lett.* **1980**, *21*, 4305-4308.
(260) Jung, M. E.; Hagenah, J. A. *J. Org. Chem.* **1983**, *48*, 5359-5361.
(261) Johnstone, R. W.; Rose, M. *Tetrahedron* **1979**, *35*, 2169-2173.
(262) Tschesche, R.; Korte, F. *Chem. Ber.* **1951**, *84*, 77-83.
(263) Bateman, L.; Cunneen, J. I.; Koch, H. F. *J. Chem. Soc.* **1950**, 3045-3051.
(264) Bateman, L.; Cunneen, J. I.; Koch, H. F. *J. Chem. Soc.* **1950**, 3051-3056.
(265) Dupont, M. G.; Dulou, R.; Defay, M. N. *Bull. Soc. Chim. Fr.* **1943**, *16*, 310-314.
(266) Smith, J. G.; Dibble, P. W.; Sandborn, R. E. *J. Org. Chem.* **1986**, *51*, 3762-3768.
(267) Bringmann, G.; Pabst, T.; Henschel, P.; Michel, M. *Tetrahedron* **2001**, *57*, 1269-1275.
(268) Abike, A.; Mesamune, S. *Tetrahedron Lett.* **1992**, *33*, 5517-5518.
(269) Cannon, J. G.; Koble, D. L. *J. Med. Chem.* **1980**, *23*, 750-754.
(270) Ripin, D. H.; Evans, D. A.; http://evans.harvard.edu/pdf/evans_pKa_table.pdf: 2005.
(271) Kodama, H.; Katsuhira, T.; Nishida, T.; Hino, T.; Tsubata, K.; WIPO, Ed. Japan, 2001; Vol. WO 01/83421 A1.
(272) Orito, K.; Hatakeyama, T.; Takeo, M.; Suginome, H. *Synthesis* **1995**, 1273-1277.
(273) Greene, T. W.; Wuts, P. G. M. *Protective Groups in Organic Synthesis*; 3rd ed.; John Wiley & Sons: New York, 1999.
(274) Sorrell, T. N.; Ellis, D. J. *J. Org. Chem.* **1985**, *50*, 5765-5769.
(275) Majewski, M.; Bantle, G. *Tetrahedron Lett.* **1989**, *30*, 6653-6656.
(276) Majewski, M.; Irvine, N. M.; Bantle, G. W. *J. Org. Chem.* **1994**, *59*, 6697-6702.
(277) Yonezawa, S.; Komurasaki, T.; Kawada, K.; Tsuri, T.; Fuji, M.; Kugimiya, A.; Haga, N.; Mitsumori, S.; Inagaki, M.; Nakatani, T.; Tamura, Y.; Takechi, S.; Taishi, T.; Ohtani, M. *J. Org. Chem.* **1998**, *63*, 5831-5837.

(278) Ali, Y.; Hussain, M. *Carbohydrate Res.* **1979**, *69*, 311-315.
(279) Webster, K. T.; Eby, R.; Schuerch, C. *Carbohydrate Res.* **1983**, *123*, 335-340.
(280) Ritter, T.; Stanek, K.; Larrosa, I.; Carreira, E. M. *Org. Lett.* **2004**, *6*, 1513-1514.
(281) Mei, T.-S.; Giri, R.; Maugel, N.; Yu, J.-Q. *Angew. Chem. Int. Ed.* **2008**, *47*, 5215-5219.
(282) Deng, C.-L.; Guo, S.-M.; Xie, Y.-X.; Li, J.-H. *Eur. J. Org. Chem.* **2007**, 1457-1462.
(283) Suau, R.; Najera, F.; Rico, R. *Tetrahedron* **2000**, *56*, 9713-9723.
(284) Davis, F. A.; Reddy, G. V.; Chen, B.-C.; Kumar, A.; Haque, M. S. *J. Org. Chem.* **1995**, *60*, 6148-6153.
(285) Lampkins, A. J.; Abdul-Rahim, O.; Li, H.; Castellano, R. K. *Org. Lett.* **2005**, *7*, 4471-4474.
(286) Bradsher, C. K.; Beavers, D. J.; Little, E. D. *J. Am. Chem. Soc.* **1954**, *76*, 948.
(287) Bradsher, C. K.; Little, E. D.; Beavers, D. J. *J. Am. Chem. Soc.* **1956**, *78*, 2153-2156.
(288) Sperber, N.; Papa, D.; Schwenk, E. *J. Am. Chem. Soc.* **1948**, *70*, 3091-3094.
(289) Moss, R. A.; Bracken, K.; Emge, T. J. *J. Org. Chem.* **1995**, *60*, 7739-7746.
(290) Luo, F.-T.; Jeevanandam, A. *Tetrahedron Lett.* **1998**, *39*, 9455-9456.
(291) Xu, Y.-C.; Lebeau, E.; Walker, C. *Tetrahedron Lett.* **1994**, *35*, 6207-6210.
(292) Kaestle, K. L.; Anwer, M. K.; Audhya, T. K.; Goldstein, G. *Tetrahedron Lett.* **1991**, *32*, 327-330.
(293) Browden, E. *J. Am. Chem. Soc.* **1938**, *60*, 645-647.
(294) Leon, A. A.; Daub, G.; Silverman, I. R. *J. Org. Chem.* **1984**, *49*, 4544-4545.
(295) Hwang, J. P.; Prakash, G. K. S.; Olah, G. A. *Tetrahedron* **2000**, *56*, 7199-7203 and references therein.
(296) Grassie, N. *J. Polym. Sci.:Poly. Chem. Ed.* **1973**, *11*, 2287-2294.
(297) Premasagar, V.; Palaniswamy, V. A.; Eisenbraun, E. J. *J. Org. Chem.* **1981**, *46*, 2974-2976.
(298) Cho, H.; Matsuki, S. *Heterocycles* **1996**, *43*, 127-131.
(299) Sharma, A. K.; Amin, S.; Kumar, S. *Polycyclic Aromatic Compounds* **2002**, *22*, 277-288.
(300) Seganish, W. M.; DeShong, P. *Org. Lett.* **2006**, *8*, 3951-3954.
(301) Loev, B. *Chem. Ind.* **1964**, 193-194.
(302) Berenyi, S.; Csutoras, C.; Gyulai, S.; Rusznyak, G. *Synth. Commun.* **2001**, *31*, 1987-1992.
(303) Kamal, A.; Laxman, N.; Ramesh, G. *Bio. Med. Chem. Lett.* **2000**, *10*, 2059-2062.
(304) Simons, J., B.Sc. thesis, University of Waterloo, 2009.
(305) Etomi, N.; Kumamoto, T.; Nakanishi, W.; Ishikawa, T. *Beils. J. Org. Chem.* **2008**, *4*, http://www.beilstein-journals.org/bjoc/content/pdf/1860-5397-4-15.pdf.
(306) Simplicio, P. D.; Franconi, F.; Frosalı, S.; Giuseppe, D. D. *Amino Acids* **2003**, *25*, 323-339.
(307) Ballard, T. E.; Melander, C. *Tetrahedron Lett.* **2008**, *49*, 3157-3161.
(308) Galm, U.; Hager, M. H.; Lanen, S. G. V.; Ju, J.; Thorson, J. S.; Shen, B. *Chem. Rev.* **2005**, *105*, 739-758.
(309) Gredicak, M.; Jeric, I. *Acta Pharm.* **2007**, *57*, 133-150.
(310) Takita, T.; Muraoka, Y.; Yoshika, T.; Fujii, A.; Maeda, K.; Umezawa, H. *J. Antibiot.* **1972**, *25*, 755-758.
(311) Lloyd, R. S.; Haidle, C. W.; Robberson, D. L.; Dodsom-Jr., M. L. *Current Microbio.* **1978**, *1*, 45-50.
(312) Mirabelli, C. K.; Huang, C.-H.; Fenwick, R. G.; Crooke, S. T. *Antimicrob. Agents Chemother.* **1985**, *27*, 460-467.
(313) Nicolaou, K. C.; Smith, A. L.; Yue, E. W. *Proc. Natl. Acad. Sci.* **1993**, *90*, 5881-5888.
(314) Smith, A. L.; Nicolaou, K. C. *J. Med. Chem.* **1996**, *39*, 2103-2117.
(315) Baker, J. R.; Woolfson, D. N.; Muskett, F. W.; Stoneman, R. G.; Urbaniak, M. D.; Caddick, S. *Chembiochem* **2007**, *8*, 704-717.

(316) Edo, K.; Saito, K.; Mtsuda, Y.; Akiyama-murai, Y.; Mizugaki, M.; Koide, Y.; Ishida, N. *Chem. Pharm. Bull.* **1991**, *39*, 170-176.
(317) Kobayashi, S.; Hori, M.; Wang, G. X.; Hirama, M. *J. Org. Chem.* **2006**, *71*, 636-644.
(318) Teplyakov, A.; Obmolova, G.; Wilson, K.; Kuromizu, K. *Eur. J. Biochem.* **1993**, *213*, 737-741.
(319) Lee, M. D.; Manning, J. K.; Williams, D. R.; Kuck, N. A.; Testa, R. T.; Borders, D. B. *J. Antibiot.* **1989**, *42*, 1070-1087.
(320) Golik, J.; Dubay, G.; Groenewold, G.; Kawaguchi, H.; Konishi, M.; Krishnan, B.; Ohkuma, H.; Saitoh, K.-i.; Doyle, T. W. *J. Am. Chem. Soc.* **1987**, *109*, 3464-3466.
(321) Konishi, M.; Ohkuma, H.; Tsuno, T.; Oki, T. *J. Am. Chem. Soc.* **1990**, *112*, 3715-3716.
(322) Shiomi, K.; Iinuma, H.; Naganawa, H.; Hamada, M.; Hattori, S.; Nakamura, H.; Takeuchi, T. *J. Antibiot.* **1990**, *43*, 1000-1005.
(323) Zhang, Y.-c.; Abula, A.-g.; Yang, X.-p. *World Notes on Antibiotics* **2008**, *29*, 20-23 and references therein.
(324) Jones, R. R.; Bergman, R. G. *J. Am. Chem. Soc.* **1972**, *94*, 66-67.
(325) Snell, J. M.; Weissbeger, A. *J. Am. Chem. Soc.* **1939**, *61*, 450-453.
(326) Lyons, J. M.; Thomson, R. H. *J. Chem. Soc.* **1953**, 2910-2915.
(327) Bolton, J. L.; Trush, M. A.; Penning, T. M.; Dryhurst, G.; Monks, T. J. *Chem. Res. Toxicol.* **2000**, *13*, 135-160.
(328) Price, C. C.; Tsunawaki, S. *J. Org. Chem.* **1963**, *28*, 1867-1867.
(329) Chan, J. K.; Anderson, B. M. *J. Biol. Chem.* **1975**, *250*, 67-72.
(330) Paulson, G. D.; Feil, V. J. *Xenobiotica* **1990**, *20*, 81-89.
(331) Barbero, M.; Degani, I.; Diulgheroff, N.; Dughera, S.; Fochi, R.; Migliaccio, M. *J. Org. Chem.* **2000**, *65*, 5600-5608.
(332) Podhradsky, D.; Drobnica, L.; Kristina, P. *Cell Mol. Life Sci.* **1979**, *35*, 154-155.
(333) Pirie, N. W.; Pinhey, K. G. *J. Biol. Chem.* **1929**, *84*, 321-333.
(334) Nesbett, F. B.; Ames, A. *Anal. Biochem.* **1963**, *5*, 452-457.
(335) Bagiyan, G. A.; Koroleva, I. K.; Soroka, N. V.; Ufimtsev, A. V. *Russ. Chem. Bull. Ind. Ed.* **2003**, *52*, 1135-1141.
(336) Wang, S. S.-S.; Hung, Y.-T.; Lin, Y.-C. *Bioprocess Biosyst. Eng.* **2009**, *32*, Epub ahead of print.
(337) Fan, Y.; Schreiber, E. M.; Giorgianni, A.; Yalowich, J. C.; Day, B. W. *Chem. Res. Toxicol.* **2006**, *19*, 937-943.
(338) Mallet, C.; Waters Corporation: 2004, p 82.
(339) Vessecchi, R.; M. Crotti, A. E.; Guaratini, T.; Colepicolo, P.; Galembeck, S. E.; Lopes, N. P. *Mini-Rev. Org. Chem.* **2007**, *4*, 75-87.
(340) O'Hara, K. A.; Dmitrienko, G. I.; Hasinoff, B. B. *Chem.-Biol. Interact.* **2010**, Publication Date (Web): January 15 2010. DOI: 10.1016/j.cbi.2010.01.013
(341) Heerding, D. A.; Safonov, I. G.; Verma, S. K. In *Ann. Rep. Med. Chem.*; Macor, J. E., Ed. New York, 2007; Vol. 42, p 365-373.
(342) Toral-Barza, L.; Zhang, W.-G.; Huang, X.; McDonald, L. A.; Salaski, E. J.; Barbieri, L. R.; Ding, W.-D.; Krishnamurthy, G.; Hu, Y. B.; Lucas, J.; Bernan, V. S.; Cai, P.; Levin, J. I.; Mansour, T. S.; Gibbons, J. J.; Abraham, R. T.; Yu, K. *Mol. Cancer Ther.* **2007**, *6*, 3028-3038.
(343) Salaski, E. J.; Krishnamurthy, G.; Ding, W.-D.; Yu, K.; Insaf, S. S.; Eid, C.; Shim, J.; Levin, J. I.; Tabei, K.; Toral-Barza, L.; Zhang, W.-G.; McDonald, L. A.; Honores, E.; Hanna, C.; Yamashita, A.; Johnson, B.; Li, Z.; Laakso, L.; Powell, D.; Mansour, T. S. *J. Med. Chem.* **2009**, *52*, 2181-2184.

(344) Hanks, S. K.; Hunter, T. *FASEB J.* **1995**, *9*, 576-596.
(345) Feldman, K. S.; Eastman, K. J. *J. Am. Chem. Soc.* **2005**, *127*, 15344-15345.
(346) Feldman, K. S.; Eastman, K. J. *J. Am. Chem. Soc.* **2006**, *128*, 12562-12573.
(347) Arya, D. P. In *Topics in Heterocyclic Chemistry 02 Heterocyclic Antitumor Antibiotics*; Lee, M., Ed.; Springer: 2006; Vol. 2, p 129-152.
(348) Kopke, T.; Zaleski, J. M. *Anti-Cancer Agents in Med. Chem.* **2008**, *8*, 292-304.
(349) Zeng, W.; Ballard, T. E.; Tkachenko, A. G.; Burns, V. A.; Feldheim, D. L.; Melander, C. *Bioorg. Med. Chem. Lett.* **2006**, *16*, 5148-5151.
(350) Sawyer, D. T. In *Oxygen Chemistry*; Oxford University Press: New York, 1991, p 19-50.
(351) Cvetković, V. S.; Purenović, J. M.; Jovićević, J. N. *Appl. Clay Sci.* **2008**, *38*, 268-278.
(352) Wardman, P. *J. Phys. Chem. Ref. Data* **1989**, *18*, 1637-1755.
(353) Jones, D. P. In *Methods in Enzymology*; Sies, H., Packer, L., Eds.; Academic Press: New York, 2002; Vol. 348, p 93-112.
(354) Nkabyo, Y. S.; Gu, L. H.; Jones, D. P.; Ziegler, T. R. *J. Nutr.* **2006**, *136*, 1242-1248.
(355) Grosz, H. J.; Farmer, B. B. *Nature* **1967**, *213*, 717-718.
(356) Brown, H. M.; Emberger, O. In *Microbial Ecology of Foods*; I.C.M.S.F., Ed.; Academic Press Inc.: New York, 1980; Vol. 1, p 112-125.
(357) Haaften, R. I. M. v.; Evelo, C. T. A.; Haenen, G. R. M. M.; Bast, A. *Biochem. Pharmco.* **2001**, *61*, 715-719.
(358) Lien, E. J.; Ren, S.; Bui, H.-h.; Wang, R. *Free Rad. Bio. Med.* **1999**, *26*, 285-294.
(359) Lane, A. N. In *Methods in Enzymology. Drug-Nucleic Acid Interactions*; Chaires, J. B., Waring, M. J., Eds.; Academic Press: New York, 2001; Vol. 340, p 252-281.
(360) Feigon, J.; Denny, W. A.; Leupin, W.; Kearns, D. R. *J. Med. Chem.* **1984**, *27*, 450-465.
(361) Barthwal, R.; Sharma, U.; Srivastava, N.; Jain, M.; Awasthi, P.; Kaur, M.; Barthwal, S. K.; Govil, G. *Eur. J. Med. Chem.* **2006**, *41*, 27-39.
(362) Evstigneev, M. P.; Khomich, V. V.; Davies, D. B. *Eur. Biophys. J.* **2006**, *36*, 1-11.
(363) Anet, F. A. L.; Freedberg, D. I.; Storer, J. W.; Houk, K. N. *J. Am. Chem. Soc.* **1992**, *114*, 10969-10971.
(364) Anet, F. A. L. In *Conformational Analysis of Cyclohexenes, Cyclohexadienes, and Related Hydroaromatic Compounds*; Rabideau, P. W., Ed.; VCH: New York, 1989, p 1-45.
(365) Smith, M. B.; March, J. *March's Advanced Organic Chemistry Reactions, Mechanisms, and Structure*; 5th ed.; John Wiley & Sons Inc.: New York, 2001.
(366) Aycard, J.-P.; Bodot, H.; Garnier, R.; Lauricella, R.; Pouzard, G. *Org. Mag. Res.* **1970**, *2*, 7-18.
(367) Concepcion, R. V.; Breeyear, J. J.; Jewett, J. G.; Bushweller, C. H. *J. Phys. Org. Chem.* **1998**, *11*, 84-90.
(368) Frisch, M. J.; Trucks, G. W.; Schlegel, H. B.; Scuseria, G. E.; Robb, M. A.; Cheeseman, J. R.; J. A. Montgomery, J.; Vreven, T.; Kudin, K. N.; Burant, J. C.; Millam, J. M.; Iyengar, S. S.; Tomasi, J.; Barone, V.; Mennucci, B.; Cossi, M.; Scalmani, G.; Rega, N.; Petersson, G. A.; Nakatsuji, H.; Hada, M.; Ehara, M.; Toyota, K.; Fukuda, R.; Hasegawa, J.; Ishida, M.; Nakajima, T.; Honda, Y.; Kitao, O.; Nakai, H.; Klene, M.; Li, X.; Knox, J. E.; Hratchian, H. P.; J. B. Cross; Adamo, C.; Jaramillo, J.; Gomperts, R.; Stratmann, R. E.; Yazyev, O.; Austin, A. J.; Cammi, R.; Pomelli, C.; Ochterski, J. W.; Ayala, P. Y.; Morokuma, K.; Voth, G. A.; Salvador, P.; J. J. Dannenberg; Zakrzewski, V. G.; Dapprich, S.; Daniels, A. D.; Strain, M. C.; Farkas, O.; Malick, D. K.; Rabuck, A. D.; Raghavachari, K.; Foresman, J. B.; Ortiz, J. V.; Cui, Q.; Baboul, A. G.; Clifford, S.; Cioslowski, J.; Stefanov, B. B.; Liu, G.; Liashenko, A.; Piskorz, P.; Komaromi, I.; Martin, R. L.; Fox, D. J.; Keith, T.; Al-Laham, M. A.; Peng, C. Y.;

Nanayakkara, A.; Challacombe, M.; Gill, P. M. W.; Johnson, B.; Chen, W.; Wong, M. W.; Gonzalez, C.; Pople, J. A.; Gaussian, Inc.: Pittsburgh PA, 2003.
(369) Frisch, M. J.; Trucks, G. W.; Schlegel, H. B.; Scuseria, G. E.; Robb, M. A.; Cheeseman, J. R.; J. A. Montgomery, J.; Vreven, T.; Kudin, K. N.; Burant, J. C.; Millam, J. M.; Iyengar, S. S.; Tomasi, J.; Barone, V.; Mennucci, B.; Cossi, M.; Scalmani, G.; Rega, N.; Petersson, G. A.; Nakatsuji, H.; Hada, M.; Ehara, M.; Toyota, K.; Fukuda, R.; Hasegawa, J.; Ishida, M.; Nakajima, T.; Honda, Y.; Kitao, O.; Nakai, H.; Klene, M.; Li, X.; Knox, J. E.; Hratchian, H. P.; Cross, J. B.; Adamo, C.; Jaramillo, J.; Gomperts, R.; Stratmann, R. E.; Yazyev, O.; Austin, A. J.; Cammi, R.; Pomelli, C.; Ochterski, J. W.; Ayala, P. Y.; Morokuma, K.; Voth, G. A.; Salvador, P.; Dannenberg, J. J.; Zakrzewski, V. G.; Dapprich, S.; Daniels, A. D.; Strain, M. C.; Farkas, O.; Malick, D. K.; Rabuck, A. D.; Raghavachari, K.; Foresman, J. B.; Ortiz, J. V.; Cui, Q.; Baboul, A. G.; Clifford, S.; Cioslowski, J.; Stefanov, B. B.; Liu, G.; Liashenko, A.; Piskorz, P.; Komaromi, I.; Martin, R. L.; Fox, D. J.; Keith, T.; Al-Laham, M. A.; Peng, C. Y.; Nanayakkara, A.; Challacombe, M.; Gill, P. M. W.; Johnson, B.; Chen, W.; Wong, M. W.; Gonzalez, C.; Pople, J. A.; Gaussian, Inc.: Wallingford CT, 2004.
(370) http://www.ccdc.cam.ac.uk/products/csd/radii/; CCDC (Cambridge Crystallographic Data Centre): and references therein, Cambridge, UK, 2010.
(371) Allen, F. H. *Acta Cryst.* **1995**, *B51*, 378-381.
(372) Exner, O.; Krygowski, T. M. *Chem. Soc. Rev.* **1996**, 71-75.
(373) Scudder, P. H. In *Electron Flow in Organic Chemistry*; John Wiley & Sons: New York, 1992, p 77-88.
(374) Levchenko, A. I.; Sukach, Y. A.; Panasenko, B. F.; Levchenko, T. A. *J. Appl. Spectrosc.* **1977**, *26*, 71-74.
(375) Besseau, F.; Laurence, C.; Berthelot, M. *J. Chem. Soc. Perkin Trans. 2* **1994**, 485-489.
(376) Levitt, L. S.; Widing, H. F.; Levitt, B. W. *Can. J. Chem.* **1973**, *51*, 3963-3965 and references therein.
(377) Aroney, M.; Fevre, R. J. W. L.; Werner, R. L. *J. Chem. Soc.* **1954**, 276.
(378) Tabei, K.; Ito, C. *Bull. Chem. Soc. Jpn.* **1968**, *41*, 514-515.
(379) Wallis, J. D.; Easton, R. J. C.; Dunitz, J. D. *Helv. Chim. Acta.* **1993**, *76*, 1411-1424.
(380) Burgi, H. B.; Dunitz, J. D.; Shefter, E. *J. Am. Chem. Soc.* **1973**, *95*, 565-5067.
(381) Glaser, R.; Horan, C. J. *Can. J. Chem.* **1996**, *74*, 1200-1214.
(382) Personal communication from Dr. Guy Carter (Wyeth) to Dr. Gary I. Dmitrienko.
(383) Aguirrezabalaga, I.; Olano, C.; Allende, N.; Rodriguez, L.; Brana, A. F.; Mendez, C.; Salas, J. A. *Antimicrob. Agents Chemother.* **2000**, *44*, 1266-1275.
(384) Kaupp, G.; Boy, J. *Angew. Chem. Int. Ed.* **1997**, *36*, 48-49.
(385) Jeffrey, G. A.; Maluszynska, H. *Int. J. Quantum Chem.: Quantum Bio. Symp.* **1981**, *8*, 231-239.
(386) Jeffrey, G. A.; Mitra, J. *Acta Cryst.* **1983**, *B39*, 469-480.
(387) Parra, R. D.; Zeng, H.; Zhu, J.; Zheng, C.; Zeng, X. C.; Gong[, B. *Chem. Eur. J.* **2001**, *7*, 4352-4357.
(388) Parra, R. D.; Gong, B.; Zeng, X. C. *J. Chem. Phys.* **2001**, *115*, 6036-6041.
(389) Desiraju, G. R. *Acc. Chem. Res.* **1996**, *29*, 441-449.
(390) Inouye, S. *Chem. Pharm. Bull.* **1968**, *16*, 1134-1137.
(391) Barlow, C. B.; Gutheie, R. D.; Prior, A. M. *Carbohydrate Res.* **1969**, *10*, 481-485.
(392) Blasko, A.; Bunton, C. A.; Bunel, S.; Ibarra, C.; Moraga, E. *Carbohydrate Res.* **1997**, *298*, 163-172.
(393) Olivier, N. B.; Imperiali, B. *J. Biol. Chem.* **2008**, *283*, 27937-27946.

(394) Tetko, I. V.; Gasteiger, J.; Todeschini, R.; Mauri, A.; Livingstone, D.; Ertl, P.; Palyulin, V. A.; Radchenko, E. V.; Zefirov, N. S.; Makarenko, A. S.; Tanchuk, V. Y.; Prokopenko, V. V. *J. Comput. Aid. Mol. Des.* **2005**, *19*, 453-463.
(395) VCCLAB *Virtual Computational Chemistry Laboratory*, http://www.vcclab.org, **2005**.
(396) Gholap, S. L.; Woo, C. M.; Ravikumar, P. C.; Herzon, S. B. *Org. Lett.* **2009**, *11*, 4322-4325.
(397) Morris, W. J.; Shair, M. D. *Org. Lett.* **2009**, *11*, 9-12.
(398) Dukor, R. K.; Nafie, L. A. In *Encyclopedia of Analytical Chemistry: Instrumentation and Applications*; Meyers, R. A., Ed.; Wiley: Chichester, 2000, p 662-676.
(399) Vargek, M.; Freedman, T. B.; Nafie, L. A. *Raman Spectrosc.* **1997**, *28*, 627.
(400) Freedman, T. B.; Cao, X.; Nafie, L. A.; Solladie-Cavallo, A.; Jierry, L.; Bouerat, L. *Chirality* **2004**, *16*, 467.
(401) Stephens, P. J.; Devlin, F. J. *Chirality* **2000**, *12*, 172-179.